XXIII Congreso de Física Estadística
FisEs'22

Libro de Resúmenes

Book of Abstracts

Zaragoza, 12 – 14 de mayo de 2022

XXIII Congreso de Física Estadística

FisEs'22

Libro de Resúmenes

Book of Abstracts

Zaragoza, 12 – 14 de mayo de 2022

La Reunión de Física Estadística se viene celebrando, con intervalos de año y medio, desde 1987, año en el que tuvo lugar la primera edición en Barcelona. Desde el año 1996 esta reunión es conocida también como FisEs. Con FisEs'22 se cumplirán, por tanto, 35 años de reuniones.

Ha sido organizada siempre por distintos grupos de investigación, repartidos por toda la geografía nacional, reuniendo a investigadores y a conferenciantes invitados de primera talla mundial.

En torno a FisEs se creó, en el año 2001, el Grupo Especializado de Física Estadística y No Lineal (GEFENOL), dentro del marco de la Real Sociedad Española de Física. Su principal objetivo es promover la Física Estadística y No Lineal en España y el intercambio científico y académico entre los grupos que investigan en estas disciplinas.

En Mayo de 2020 se iba a celebrar el congreso FisEs'20 en Zaragoza, pero la pandemia COVID-19 obligó a cancelarlo. La iniciativa se retomó en 2022.

Reuniones de Física Estadística previas

I	Congreso de Física Estadística ’87	Barcelona, mayo de 1987
II	Congreso de Física Estadística ’88	Palma de Mallorca, septiembre de 1988
III	Congreso de Física Estadística ’90	Badajoz, mayo de 1990
IV	Congreso de Física Estadística ’91	Gijón, septiembre de 1991
V	Congreso de Física Estadística ’93	El Escorial, mayo de 1993
VI	Congreso de Física Estadística ’94	Sevilla, septiembre de 1994
VII	Congreso de Física Estadística FisEs’96	Zaragoza, mayo de 1996
VIII	Congreso de Física Estadística FisEs’97	Getafe, septiembre de 1997
IX	Congreso de Física Estadística FisEs’99	Santander, mayo de 1999
X	Congreso de Física Estadística FisEs’00	Santiago de Compostela, sep. de 2000
XI	Congreso de Física Estadística FisEs’02	Tarragona, mayo de 2002
XII	Congreso de Física Estadística FisEs’03	Pamplona, septiembre de 2003
XIII	Congreso de Física Estadística FisEs’05	Madrid, mayo de 2005
XIV	Congreso de Física Estadística FisEs’06	Granada, septiembre de 2006
XV	Congreso de Física Estadística FisEs’08	Salamanca, mayo de 2008
XVI	Congreso de Física Estadística FisEs’09	Huelva, septiembre de 2009
XVII	Congreso de Física Estadística FisEs’11	Barcelona, mayo de 2011
XVIII	Congreso de Física Estadística FisEs’12	Palma de Mallorca, septiembre de 2012
XIX	Congreso de Física Estadística FisEs’14	Ourense, mayo de 2014
XX	Congreso de Física Estadística FisEs’15	Badajoz, septiembre de 2015
XXI	Congreso de Física Estadística FisEs’17	Sevilla, mayo de 2017
XXII	Congreso de Física Estadística FisEs’18	Madrid, septiembre de 2018

Comité organizador

- Francho Bauzá Mingueza
- Sergio Faci Lázaro
- Fernando Falo Forniés
- Alessandro Fiasconaro
- Jesús Gómez Gardeñes
- Pedro J. Martínez Ovejas
- Juan José Mazo Torres (coordinador)
- Hugo Pérez Martínez
- Adriana Reyna Lara
- Alejandro Sáinz Agost
- David Soriano Paños
- Pablo Valgañón Ruiz

Comité científico

- Enrique Abad (Universidad de Extremadura)
- Rosa María Benito (Universidad Politécnica de Madrid)
- Javier Burguete (Universidad de Navarra)
- Mario Castro (Universidad Pontificia de Comillas)
- Álvaro Dominguez (Universidad de Sevilla)
- Pablo Ignacio Hurtado (Universidad de Granada)
- Cristina Massoller (Universitat Politècnica de Catalunya)
- Juan José Mazo (Universidad Complutense de Madrid)
- Alberto Pérez Muñuzuri (Universidad Santiago de Compostela)
- David Reguera (Universitat de Barcelona)
- Miguel Ángel Rubio (Universidad Nacional de Educación a Distancia)
- Tomás Sintes Olives (Universitat de les Illes Balears)

Celebración

Facultad de Medicina de la Universidad de Zaragoza,
C/ Domingo Miral, s/n

Comidas en el Hospital Clínico Universitario

PROGRAMA DEL CONGRESO

Hora	Jueves 12 de mayo
08:15 – 09:00	Inscripción
09:00 – 09:15	Inauguración
09:15 – 9:45	**Homenaje en recuerdo de Luis Rull y Luis Pesquera**
9:45 – 10:30	**I-01: Mario Floría:** The HCO model of social norm violation and punishment
10:30 – 10:45	**O-01: Eva G Noya:** Diseño de cuasicristales icosaédricos mediante enlaces
10:45 – 11:15	Café
11:15 – 11:45	**I-O2: Marta Sales:** Using inference for recommendation and to obtain models from data: is data always good enough?
11:45 – 12:00	**O-02: Raúl A Rica:** Brownian dynamics of levitated nanoparticles
12:00 – 12:15	**O-03: Gonzalo Manzano:** Survival and extreme statistics of work, heat, and entropy production in steady-state heat engines
12:15 – 12:45	**I-03: Javier Buceta:** The 3D Structure of Epithelia Monolayers: Biology meets Math and Physics
13:00 – 15:00	Comida
15:00 – 16:30	**Presentación de pósteres**
16:00 – 16:30	Café
16:30 – 17:15	**I-04: Francisco Chinesta:** Physics-based & Data-driven models: the winning team
17:15 – 17:30	**O-04: Nerea Alcázar-Cano:** The role of hydrodynamics in the diffusion of passive tracers in random networks
17:30 – 17:45	**O-05: AdriánAguirre-Tamaral:** A complexity theory approach to the origin of life: towards the first RNA replication
17:45 – 18:00	**O-06: L. F. Seoane:** Games in rigged economies
18:00 – 18:15	**O-07: Iñaki Echeverría:** Spontaneous emergence of counterclockwise vortex motion in assemblies of pedestrians roaming within an enclosure
18:15 – 19:15	**Concurso Tesis en 3 Minutos**

Hora	Viernes 13 de mayo
09:00 – 9:45	**I-05: Carmen Miguel:** Collective motion and consensus decision-making in social animal groups
9:45 – 10:00	**O-08: Pau Clusella:** Complex spatiotemporal oscillations emerging from transverse instabilities in large-scale brain networks
10:00 – 10:15	**O-09: Miguel Ángel López Castaño:** Diffusion in a two-dimensional chiral fluid
10:15 – 10:30	**O-10: Isabel Serra:** The Brevity Law as a Scaling Law, and the Origin of Zipf's Law for Word Frequencies as a Mixture from Different Lengths
10:30 – 10:45	**O-11: Diego Escribano:** Chimpanzees organize their social relationships like humans
10:45 – 11:15	Café
11:15 – 11:45	**I-06: Ester Lázaro:** Virus adaptation to low host density
11:45 – 12:00	**O-12: Javier Galeano:** Can Statistical Physics Help You Win an Olympic Medal...in Badminton?
12:00 – 12:15	**O-13: Guillerme Vilhena:** Tuning the Dynamics of Life: One Chemical Moiety at a Time
12:15 – 12:45	**I-07: Felipe Blas:** Simulación de hidratos de dióxido de carbono
13:00 – 15:00	Comida
15:00 – 16:30	**Presentación de pósteres**

16:15 – 16:45	Café
16:45 – 17:30	**I-08: Ernesto Estrada:** What makes a network “complex”?
17:30 – 17:45	**O-14: Rafael Díaz-Hernández:** Jamming of Hard-Spheres through the Lens of Constrained Optimization
17:45 – 18:00	**O-15: Beatriz Barreales:** Kinetic roughening of coffee-ring interfaces
18:00 – 18:15	**O-16: Miguel Ruíz-García:** Learning inter-particle interactions and active forces from particle trajectories
18:15 – 18:30	**O-17: Jaime Iranzo:** How genetic parasites persist despite the purge of natural selection
18:30 – 18:45	**O-18: S. Cloux:** Validación de un modelo Lagrangiano para el transporte de macroplásticos usando palillos de batea en la Ría de Arousa

Hora	Sábado 14 de mayo
09:00 - 9:45	**I-09: Ralf Metzler** Beyond Brownian motion: from data to models
9:45 - 10:00	**O-19: Juan Fernández-Gracia:** Inferring Generalized Lotka-Volterra parameters from logitudinal microbial data
10:00 - 10:15	**O-20: Jordi Ignés-Mullol:** Selection rules and scaling regimes in active nematic turbulence
10:15 - 10:45	**I-10: Carmen Molina:** Why are cell populations maintained via multiple intermediate compartments?
10:45 - 11:15	Café
11:15 - 11:45	**I-11: Andrés Santos:** Mpemba effect in driven gases: Are the thermal and entropic criteria equivalent?
11:45 - 12:00	**O-21: Jasper van der Kolk:** A geometry-induced topological phase transition in random graphs
12:00 - 12:15	**O-22: M. Isabel García de Soria:** Auto-difusión en un gas de esferas duras cuasi-bidimensional
12:15 - 12:30	**O-23: Arturo Moncho-Jordá:** Controlling the structure, phase behavior and dynamics of soft colloids by active interaction switching
12:30 - 12:45	Clausura

Luis Pesquera González

En primer lugar, quiero agradecer al comité del Fises el encargo de dedicar unas palabras de recuerdo a nuestro colega Luis Pesquera, recientemente fallecido en Santander y uno de los fundadores de este congreso.

Luis Pesquera acabó su licenciatura en Física en la Universidad de Valladolid en 1975, tras una brillante carrera (fue Premio Daza y Valdés al mejor expediente nacional en Ciencias) e, inmediatamente, se incorporó al equipo de Emilio Santos en Valladolid, con quien comenzaría su tesis doctoral. Entre los años 1977-1980 Luis desarrolló su tesis en la Universidad Paris VI, merced a una beca francesa que a duras penas le permitía sobrevivir. Eran tiempos difíciles para la ciencia en España. Lee su tesis francesa bajo la dirección de Pierre Claverie y la tesis española bajo la de Emilio Santos.

En esta tesis, enfocada a establecer fundamentos de la electrodinámica estocástica como un primer paso hacia una aproximación clásica de la mecánica cuántica, Luis tuvo que aprender y poner a punto diversas técnicas para el tratamiento de procesos estocásticos, que aplicaría durante los siguientes años a muchos sistemas físicos. En el año 1981 se incorporó al grupo de Emilio Santos que acababa de instalarse en Santander, donde ya desarrollaría toda su carrera profesional. Es profesor adjunto (ahora titular) en 1985 y catedrático en 1991, siempre en el área de Física Teórica.

En el año 1984 Luis organizó una Escuela Internacional bajo los auspicios de la Menéndez Pelayo, titulada “Stochastic Processes Applied to Physics”, que resultó ser el preludio de los congresos Fises. Ahí nos conocimos muchos de los que a nivel nacional nos reuniríamos unos años más tarde en lo que sería el primer Congreso Fises y a nivel internacional los que luego, al cabo de los años, serían nuestros colaboradores o nuestros referees, que al fin y al cabo es otra forma de colaboración. Merece la pena mencionarlos, pues alguno también ha fallecido: Chris Van der Broeck y Hannes Risken. Todos los que estuvimos en esa escuela recordamos la ilusión y alegría de ese encuentro.

Tres años más tarde, en 1987, apareció una circular convocando a una reunión de colegas interesados en la Física Estadística. El texto de la convocatoria es muy ilustrativo. Está en la página del Fises y merece la pena leerlo porque sería el germen de un congreso autoorganizado y mucho más robusto de lo que nunca llegamos a pensar: el ahora llamado Fises. En esa convocatoria se lee: “Un grupo de personas…” Ese grupo, compuesto inicialmente por Maxi San Miguel, Luis Pesquera, José María Sancho y yo, intentábamos aglutinar al mayor número de colegas posible. Luis fue una pieza fundamental, como promotor y ejecutor,

porque tenía ese don. Luis tenía una fabulosa memoria, era persistente en extremo, y le gustaba facilitar la vida a los demás. Estas cualidades le permitían enfrentarse al laberinto burocrático con muchas probabilidades de éxito, cosa que todos los de su alrededor aprovechábamos. Cuántas veces habré yo dicho: "Pídeselo a Luis, si él no lo consigue, dalo por imposible". Por eso a Luis le caían tareas de gestión en tiempos difíciles. Fue director del Departamento de Física Moderna durante la etapa de transición a Instituto Mixto y, años después, director del Instituto de Física de Cantabria (IFCA) durante la fase de consolidación y construcción del nuevo edificio, sede actual del Instituto.

En el aspecto docente, Luis era un todo terreno. En la Universidad impartió clases en todo tipo de asignaturas tanto teóricas como prácticas experimentales. Dirigió seis tesis Doctorales. Fue coordinador de los estudios de postgrado en Ciencias durante los años 2009-2013. Algunos de los que estáis aquí le recordaréis como profesor en los cursos de doctorado que organizábamos en Santander durante la década de los 90 y que, en mi opinión, fueron de gran utilidad para los físicos estadísticos de esa generación. También fueron el germen de posteriores cursos de interés para nuestros estudiantes.

Aunque ahora no es el momento para hablar en detalle de los logros científicos de Luis, sí que hay que señalar su curiosa trayectoria que supuso la transformación de un teórico puro y duro en cuya tesis se pueden contar 350 fórmulas, eso sí, escritas a mano como la época imponía, en un experimental de la fotónica que en el año 2005 crea, junto a Ángel Valle, un laboratorio de Comunicaciones Ópticas en el IFCA y es firmante de un *Nature* donde se prueban las comunicaciones ópticas basadas en sincronización sobre el anillo del espacio olímpico de Atenas.

Esta transformación es gradual. Comenzó los primeros años con aplicaciones de procesos estocásticos a distintos sistemas físicos (reactores nucleares, láseres, medios desordenados, reacciones químicas), colaborando con destacados miembros de esta comunidad (Maxi San Miguel, José María Sancho, Aurora Hernández-Machado, Emilio Hernández, Pere Colet). Después se centró más específicamente en sistemas ópticos, trabajando sobre todo en dinámica nolineal de láseres de semiconductor, elaborando proyectos TIC coordinados, primero con Palma y después incluyendo a Ignacio Esquivias de la Politécnica de Madrid. Posteriormente trabajó en aplicaciones a sistemas de comunicaciones ópticas y procesamiento de información (en proyectos europeos como el PHOCUS en colaboración con Claudio Mirasso del IFISC). Estos eran ya temas más especializados y fuera de la física estadística, publicando en revistas del IEEE y participando en congresos de ingeniería como el CLEO. La etapa experimental de Luis (desde el 2005) fue una auténtica sorpresa para los que le conocíamos y para él muy gratificante, pues nos llegó a comunicar más tarde el alto grado de satisfacción que sentía cuando, por una parte, reproducían con fórmulas algunos extraños hechos experimentales que a veces observaban en el laboratorio o, al revés, los experimentos que se clavaban a las predicciones teóricas. Verlo para creerlo.

Yo compartí con él los primeros años de nuestra carrera investigadora. Recuerdo con emoción nuestras aventuras por medio mundo, cuando viajábamos de congreso en congreso. Nuestras preciosas y valiosas horas de pizarreo científico. La alegría que nos produjo saber que otros españoles (Maxi y José María) trabajaban como nosotros en procesos estocásticos. La decepción del Congreso de Reactores Nucleares en Valencia, donde los más jóvenes nos doblaban en edad. Las risas al ver en un periódico que nuestro libro recién publicado estaba en la estantería de Hawking. Una amistad que duró más de 40 años. Y justo ahora que ya nos estábamos retirando…

Quiero finalmente reproducir aquí el mensaje que Maxi envió a la lista Fises el día de su muerte. Es lo que sentimos los que disfrutamos de su amistad y trabajamos con él:

"Siempre le recordaremos por su gran humanidad e inteligencia, honestidad, sinceridad, curiosidad y entrega. La comunidad Fises es parte de su legado."

Miguel Ángel Rodríguez Díaz

Luis Felipe Rull Fernández

Agradezco sinceramente al comité organizador del FisEs la oportunidad que se me ha brindado de realizar este breve homenaje a la figura de mi mentor, amigo y colega **Luis Felipe Rull Fernández**, Catedrático Emérito de Universidad en el departamento de Física Atómica, Molecular y Nuclear (FAMN) de la Universidad de Sevilla, quien falleció repentinamente el pasado día 14 de febrero en Sevilla.

Licenciado en Ciencias, Sección Físicas, por la Universidad de Sevilla en 1971, se doctoró en dicha Universidad en enero de 1976 bajo la dirección de Juan de la Rubia Pacheco. Realizó una estancia postdoctoral entre 1981 y 1982 en la Universidad de Copenhague (Dinamarca), donde colaboró con S. Toxvaerd y varias estancias breves en el grupo de K. E. Gubbins de la Universidad de Cornell (EEUU) entre los años 1986 y 1988. Profesor Adjunto Numerario desde 1979, en 1983 pasó a ser Profesor Titular de Universidad en la Universidad de Sevilla y en 1995 tomó posesión como Catedrático de Universidad en el área de Física Teórica del departamento de FAMN de la Universidad de Sevilla. Tras su jubilación en 2019, fue nombrado Profesor Emérito por la Universidad de Sevilla, posición que disfrutó hasta su fallecimiento.

Luis fue un pionero en el campo de la simulación por ordenador en España. Comenzó su carrera científica programando con tarjetas perforadas que aún atesoraba en su despacho, y fue testigo del vertiginoso desarrollo en el área de la computación científica hasta llegar a los supercomputadores de alta capacidad de computación de la actualidad. Su amplia actividad investigadora, que se plasmó en multitud de publicaciones y colaboraciones con diversos grupos nacionales e internacionales, se desarrolló en esta área, principalmente en su aplicación al estudio de las propiedades termodinámicas, de transporte y diagramas de fases de líquidos simples y complejos, especialmente cristales líquidos, dentro del ámbito de la Física Estadística. Entre sus muchos méritos, cabe destacar que fue miembro del *board* de la Sección de Líquidos de la Sociedad Europea de Física entre 1996 y 2000 y que fue miembro del equipo editorial de las revistas *Molecular Physics* y *Molecular Simulation.* A pesar de encontrarse cerca de su retiro definitivo, seguía disfrutando con la Ciencia que siempre le divirtió hacer. En los últimos tiempos se interesó en el uso de las técnicas de la Física Estadística en otros ámbitos más aplicados. Así, participaba en un proyecto donde se investigaba la incidencia de accidentes cardiovasculares en pacientes de ictus en Andalucía a partir de los datos registrados en el Servicio Andaluz de Salud.

Fue un miembro activo en la comunidad FisEs. Así, Luis participó en el primer congreso de Fisica Estadística de Barcelona en 1987. Coorganizó, junto a José Manuel Casado, la VI Reunión de Física Estadística FisEs'94 en Sevilla. También formó parte del comité organizador del FisEs'17 que volvió a organizarse en Sevilla el año 2017. Asimismo, codirigió la NATO-ASI y Enrico Fermi *Summer School "Observations and Predictions of Phase Transitions in Complex Fluids"* de 1994 en Varenna (Italia), en la que participaron varios miembros de la comunidad de FisEs.

Además de su actividad investigadora, tuvo una importante actividad docente en las titulaciones de Física y Matemáticas de la Universidad de Sevilla, actividad que continuó desarrollando hasta el último momento, así como de gestión. Fue Decano de la Facultad de Física entre los años 1984 y 1989, miembro del Claustro Universitario entre 1985 y 2000 y miembro del Consejo Social de la Universidad de Sevilla entre 1986 y 1989. Además, hay que resaltar su compromiso con el avance de la investigación científica en España. En este sentido, además de participar en múltiples paneles de expertos y evaluación científicos a lo largo de su dilatada carrera, asesoró a grupos de todo el espectro político en temas relacionados con la Universidad y la Ciencia. Asimismo, presidió la Asociación para el Avance de la Ciencia y Tecnología en España (AACTE) entre los años 2001 y 2003. En todos estos ámbitos siempre mantuvo una postura independiente, crítica y coherente con sus ideas, que defendió vehementemente, aunque mostrándose abierto en todo momento al debate constructivo.

Los que lo conocimos coincidimos en destacar su gran corazón y generosidad. Muchos colegas nacionales y extranjeros con los que trabajó se sentían literalmente como en casa cuando le visitaban, desvelándoles los encantos de Sevilla. Inició en el campo de la Física Estadística a muchos investigadores (entre los que me encuentro), contagiándonos su entusiasmo por la ciencia y proporcionándonos todos los medios en su mano para nuestro progreso en el ámbito científico. Y aunque no le solía gustar viajar, guardo buenos recuerdos de las reuniones y congresos a los que fuimos juntos. A aquellos que trabajamos estrechamente con él nos deja una huella indeleble.
Siempre te llevaremos con cariño en nuestro recuerdo y corazones.
Descansa en paz.

José Manuel Romero Enrique

CONTENIDOS

CONFERENCIAS INVITADAS

The HCO model of social norm violation and punishment

Mario Floría
Departamento de Física de la Materia Condensada y BIFI, Universidad de Zaragoza

We analyze the population dynamics of social-norm-violating (corrupt) behaviors when social punishment is present, with the use of a simple compartmental model where social agents can be in three possible states: *honesty, corruption and ostracism* (social isolation), wherefrom the name HCO.

Most of the litterature on modeling corruption is framed in either classical or evolutionary game theory. At least in the simplest game-theoretical settings, the *honest versus corrupt* behavioral dilemma is somewhat identified with the *cooperator versus defector* strategic dilemma, which has become the standard interpretation of the two-person-two-strategies normal form of games (Prisoner's dilemma, Stag-hunt, etc.) or group games (Public goods). Nonetheless, the generalization to $n \geq 3$ strategies is needed if punishment (the hallmark of norm violation) has to be introduced in a stronger way than a mere penalty in the benefit received by wrongdoers. Besides, the incorporation of social ingredients eventually relevant through payoff matrix coefficients easily leads to the practical difficulties posed by a large parametric space and strategic space that often render impractical a desirable thorough analysis of model computations.

The HCO model [1] adopts a different, almost minimalistic approach, where norm-violating behavior is not assumed to be a greedy strategy in a population game dynamics, but a simpler formal entity: an infectious state. The transitions from honesty to corruption and from corruption to ostracism are modeled as pairwise interactions, i.e. honest agents can imitate corrupt peers while corrupt individuals pass to ostracism due to the delation by honest acquaintances. These *corruption and delation flows* are assigned transition probabilities that are functions of the local environmental states. Individuals in the state of ostracism do not interact and transit to the honest state at a constant rate.

On top of this basic modeling framework one can easily incorporate different social ingredients in order to analyze their relevance and effects into the stationary states of the social dynamics, by e.g. incorporating additional compartmental flows or judiciously modifying the transition probability functions. The structure (network) of agents' contacts can be chosen at will.

After introducing the HCO model and presenting results (obtained through stochastic simulations and different approximations) that incorporate a variety of social ingredients (e.g. warning to wrongdoers [1], social intimidation [2], among others), I will discuss an interesting extension of the model, where two different "gangs of corruption" are allowed to compete each other [3].

[1] Dan Lu, F. Bauzá, D. Soriano-Paños, J. Gómez-Gardeñes, and L.M. Floría, , Phys. Rev. E **101**, 02336 (2020).

[2] F. Bauzá, D. Soriano-Paños, J. Gómez-Gardeñes, and L.M. Floría, Chaos **30**, 063107 (2020).

[3] H. Pérez-Martínez, F. Bauzá, D. Soriano-Paños, J. Gómez-Gardeñes, and L.M. Floría (submitted).

Using inference for recommendation and to obtain models from data: Is data always good enough?

Marta Sales[1]
[1] Universitat Rovira i Virgili, Tarragona (Spain)

I will talk about two different problems that share a common behavior: a transition between a desired inference outcome and a less desirable one. My first example example will be that of recommender systems (or bipartite graphs with multi-valued edges) and the use of node attributes (such as gender of a user and the genre of a movie) to increase prediction accuracy of unobserved ratings. My second example will be that of obtaining models from data using a Bayesian inference framework in the presence of noise. I will discuss how adata attributes are not always useful to make recommendations in the same way that increasing the noise in the data will prevent us from finding the model that generated the data. I will also discuss that if we increase the importance of the attributes or the noise, we observe a transition between a regime in which we only see the data and a regime in which we only see the attributes or models that are compatible with noise.

The 3D Structure of Epithelia Monolayers: Biology meets Math and Physics

Javier Buceta
Institute for Integrative Systems Biology (I2SysBio),
CSIC-UV, C/ Catedrático Agustín Escardino Benlloch, 9 46980, Paterna (Valencia), Spain

Building and shaping tissues and organs relies on the ability of cells to efficiently pack together and regulate their interactions. Over the last years we have been working on the physical and mathematical aspect of this problem. Our contributions include the understanding of the role of cell size for regulating the signalling noise [1], the interplay of mechanical properties and patterning to achieve shape remodeling [4], the interaction between different cell populations [5], the development of tissue simulation codes for mechanobiology experiments [3], and the 3D organization of epithelial cells [2, 6]. As for the latter topic, we have shown that epithelial cells display a previously undescribed geometrical shape when tissues are subjected to bending (curvature): the scutoid (Fig. 1).

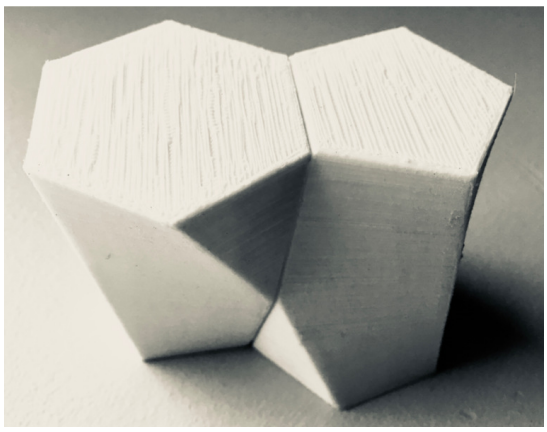

Fig. 1. Scutoids are novel shapes that allow epithelial cells to pack efficiently (from an energetic viewpoint) in tissues subjected to bending or folding.

The scutoidal shape allows cells to pack minimizing their energy and this discovery has opened the door to a deeper understanding of morphogenesis. Yet, further consequences of this new paradigm in terms of the 3D cellular organization have remained elusive. Recently, we have addressed this problem using a combination of experiments, mathematical analyses, computer simulations, and biophysical approaches. In that context we have shown that the thickness and curvature of epithelial tissues are linked to the cellular connectivity via energetic cues. This principle explains how the topological and physical constraints inherent to living matter contribute to build functional complex shapes and lead to the self-organization of tissues.

[1] Javier Buceta. Finite cell-size effects on protein variability in Turing patterned tissues. *Journal of the Royal Society, Interface*, 14(133):20170316, 2017.

[2] Pedro Gómez-Gálvez, Pablo Vicente-Munuera, Antonio Tagua, Cristina Forja, Ana M Castro, Marta Letrán, Andrea Valencia-Expósito, Clara Grima, Marina Bermúdez-Gallardo, Óscar Serrano-Pérez-Higueras, Florencia Cavodeassi, Sol Sotillos, María D Martín-Bermudo, Alberto Márquez, Javier Buceta, and Luis M Escudero. Scutoids are a geometrical solution to three-dimensional packing of epithelia. *Nature communications*, 9(1):2960, 2018.

[3] Oriol Canela-Xandri, Samira Anbari, and Javier Buceta. TiFoSi: an efficient tool for mechanobiology simulations of epithelia. *Bioinformatics*, 36(16):4525, 2020.

[4] Samira Anbari and Javier Buceta. Self-sustained planar intercalations due to mechanosignaling feedbacks lead to robust axis extension during morphogenesis. *Scientific Reports*, 10(1):10973, 2020.

[5] Carla Prat-Rojo, Philippe-Alexandre Pouille, Javier Buceta, and Enrique Martin-Blanco. Mechanical coordination is sufficient to promote tissue replacement during metamorphosis in *Drosophila*. *The EMBO Journal*, 39(3), 2020.

[6] Pedro Gómez-Gálvez, Pablo Vicente-Munuera, Samira Anbari, Javier Buceta, and Luis M. Escudero. The Complex Three-Dimensional Organization of Epithelial Tissues. *Development*, 148(1):dev195669, 2021.

Physics-based & Data-driven models: the winning team

Francisco Chinesta[1] and Elías Cueto[2],
[1] ESI Group Chair @ Arts et Métiers Institute of Technology, París, France
[2] ESI Group Chair @ I3A, University of Zaragoza, Zaragoza, Spain

In the previous industrial revolution, virtual twins emulating a physical system were considered as the major protagonists of simulation-based engineering. This type of twin was usually based on numerical, yet static, models that were used, often separately and independently, in designing, manufacturing and testing complex systems and their components. They were, however, not expected to accommodate or assimilate data. The reason is that the characteristic time of standard simulations was, and still is even today, not compatible with the real-time responses needed when prediction are required in-operation, as nowadays needed in the context of connected systems.

The subsequent generation of twins, called digital twins, allows real-time decision making by using powerful data analytics, machine learning and artificial intelligence on the abundant collected data. Thus, predictive and operative maintenance, and data-based control can be possible. However, creating a data-based model from scratch is expensive and sometimes requires too much data that can be difficult or even impossible to collect. Moreover, in science and engineering decisions and designs must be certified, and for that, the employed rationale explained, a real issue for nowadays artificial intelligence based procedures.

Hence, a hybrid paradigm seems more pertinent. Hybrid twins also include predictions from physics-based models. However, persistent and biased deviations from the physical measurements are now interpreted as ignorance about some hidden physics taking place, and thus provide an opportunity to learn on-the-fly. Hybrid Twins embrace physics-based models (that should accommodate real-time queries) and "deviation data-driven models", the last intended to fill the gaps on inherent epistemic ignorance in the physics-based model.

Thus, the "Hybrid" framework allows combining data and models, mathematical physics and artificial intelligence. On the other hand, it allows operating with a more consequent and reasonable amount of data (within the so-called smart-data paradigm), because it serves to model the gap more than creating the models from scratch. Finally, as soon as engineering systems are certified from the physics-based model, the data-driven model of the deviation (ignorance) serves for improving prediction, and can be viewed as a bonus or surplus.

Data was present in industry from the very beginning. However, it has served traditionally for calibrating models and for validating designs. These data contributed to generate knowledge enabling the training of experts. Today, new technologies facilitate massive data acquisition that in most cases remain without analysis. This is often due to the lack of appropriate tools for treating that data at the required rates, or simply to the inadequacy of these techniques for extracting the hidden knowledge behind data.

Today the industrial reality is large. For example, testing machines used for calibrating material models produce vast amounts of data (X-tomography, Microscopy, Laser velocimetry, ...) in particular in form of sequence of images or time-series. On the other hand, production machines provide, in general, much less data, because in most of cases its acquisition is very expensive, in some cases technologically challenging, and often simply impossible.

Thus, the main three factors associated to data collected in industry concern (i) quantity, (ii) characteristic time of the response, and (iii) data quality (noise or bias).

Our framework concerns the hybrid paradigm in which data (within an engineered artificial intelligence framework) will enrich models exhibiting limited accuracy, and models should help data to become smarter, by informing what data, at what scale, where and when it should be collected.

Model enrichment is based on the use of the gap between measurements and model predictions. The interest of using a model is twofold; first, it allows moving faster on a solid foundation, and second, the better are the models, the smaller are the deviations, implying an almost linear or slightly nonlinear behavior, both making possible their approximation from few data, instead of the vast amount of data needed for creating a model from the scratch.

The hybrid paradigm can be expressed as: *Reality = First order physics-based model, manipulated from the tools of applied mathematics and computer science PLUS a data-driven correction learned on-the-fly, based on data manipulated from adequate (engineered) artificial intelligence techniques.*

This framework makes it possible operating in both, the big-data limit as well as in the scarce-data limit, and both must accommodate with the characteristic time of the industrial process. When data is abundant and we proceed offline, the use of deep-learning is an excellent candidate. However, when data is very scarce and the data-driven model must adapt in time very fast, other techniques able to operate in those circumstances could and should be considered, analyzed, developed, improved and tested on real use cases.

In the industrial context, AI has six major axes: (i) visualizing multidimensional data; (ii) classifying data; (iii) modeling the input / output relationship enabling quantitative predictions – the art of modeling –; (iv) certifying those predictions; (v) explaining them, that is, extracting knowledge from the available data, and (vi) apply them in production (taking advantage of the online adaptation –hybrid twin paradigm–) and training final users and students on the use of AI techniques for adding value to industrial technology.

[1] F. Chinesta, E. Cueto, E. Abisset, J.L. Duval and K. El Khaldi, *Virtual, Digital and Hybrid Twins: A New Paradigm in Data-Based Engineering and Engineered Data*, Archives of Comput. Meth. in Engrg., **27**, 105-134 (2020).

Collective motion and consensus decision-making in social animal groups

M. Carmen Miguel[1,2]
[1] Departament de Física de la Matèria Condensada, Universitat de Barcelona, Martí i Franquès 1, 08028 Barcelona, Spain
[2]Universitat de Barcelona Institute of Complex Systems (UBICS), Universitat de Barcelona, Barcelona, Spain

Collective motion usually refers to the coordinated motion exhibited by groups of social animals and its a beautiful example of self-organization in natural far-from-equilibrium systems. It is observed in a broad range of living systems, from bacterial colonies to the spectacular form of wildebeest herds crossing deserts in Africa, huge fish schools running away coordinately from predators, and even in human crowds.

Real animals percieve a broad variety of social and environmental stimuli and, probably, perform complex stochastic decision-making processes to eventually coordinate their behavior, since coordination and cooperation are often crucial to their survival and reproductive success. Despite the rich ethological diversity, the ubiquity of collective behavior in very disparate systems suggests the existence of some underlying principles that transcends the peculiarities of individual animals and species.

As statistical physicists, our current understanding of collective animal behavior is thus largely based on models that, quite often, consider self-propelled identical agents that obey similar interaction rules. Indeed, statistical models, such as the celebrated Vicsek model, have shown that simple rules for local interaction among individuals can generate coordinated behavior like that found in natural systems. Using these models, or more coarse-grained descriptions, physicist have established several analogies between collective motion and more traditional physics disciplines such as collective phenomena, phase transitions and rheology.

Following this statistical physics approach, we will first discuss some modeling results where we apply common statistical physics techniques to characterize collective motion in social animal systems. Then, since our research group is currently working to validate some of our modeling hypothesis and results by using empirical data obtained from the observation of schools of black neon tetra swimming in a lab tank, we will also discuss some empirical results along with our modeling efforts to describe the collective behavior of real fish schools.

Social relationships, for instance, characterize the interactions that occur within social species and may have an important impact on collective animal motion. By incorporating interactions mediated by an empirically motivated scale-free topology that represents a heterogeneous pattern of social contacts, we observe thatthe degree of order of the model is strongly affected by network heterogeneity.

We also examine avalanching behavior (behavioral cascades) in the collective motion of groups where a single individual has a long range orientational contagion effect over the rest ofindividuals. Behavioral changes at the individual level, which may by transmitted to the group, are well documented in the literature and can trigger intermittent avalanche-like behavior. The results obtained appear to be in qualitative agreement with experimental results characterizing collective motion in schooling fish (see Fig. 1). Yet, more empirical data are needed to obtain a better understanding of the reorientations patterns in confined systems.

Speed acts as a modulator of collective ordering, which makes sense from an adaptive perspective. Responding to speed variations requires minimum perception and cognitive abilities, and it functions as a mechanism to transfer information fast and efficiently. We find that individual fish speeds, compatible with a burst-and-coast behavior, are synchronized at the global level, resulting in a quasi-periodic oscillation pattern of speed over time. Changes in global polarization are positively correlated with changes in average speed with a characteristic time lag, and both quantities tend to oscillate with the same effective period.

Collective motion implies collective decision-making, a process which occurs daily in the lives of many group living animals. Understanding how consensus is reached, understanding who, if any, has any influence and the mechanisms by which information and preferences are integrated, poses a fundamental challenge in this research field. We finally discuss modeling results of consensus decision-making to understand the effects of animal interdependencies for the case of information pooling. Some of these results are also studied experimentally in a swarm of kilobots, mini-robots that are able to detect each other and exchange simple messages within a given distance, especially well suited to study the process of collective decision making.

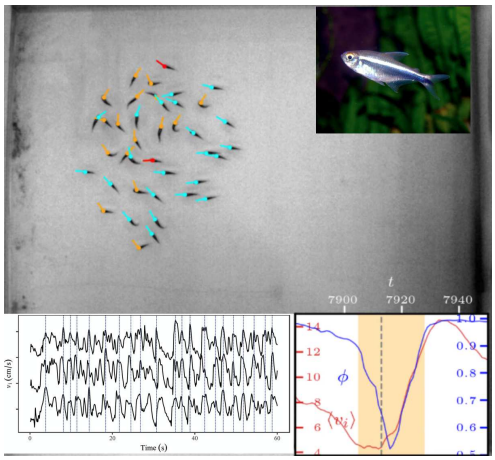

Fig. 1. School of 40 black neon tetra in a laboratory tank. Bottom insets: Fish speed in time. Average speed (red line) and polarization (blue line) in the course of an avalanche.

Virus adaptation to low host density

Ester Lázaro[1] and Mara Laguna[1]
[1] Centro de Astrobiología (CSIC-INTA), Madrid (Spain)

One of the most relevant factors affecting viral propagation is the density of accessible hosts, which determines the number of virus-host contacts and, consequently, the probability of new infections. The lower the host density, the longer the virus spends in the external environment between successive infections, thus increasing its probability of degradation due to physical-chemical variables. There should be a critical host density separating sustained propagation from extinction. In the latter situation, the virus is under a selective pressure to fix survival strategies under limited host availability. The study of these strategies is important from an evolutionary viewpoint, and it can significantly affect the epidemiological properties of a given virus, potentially turning local outbreaks into endemic propagation. In this work we have carried out an evolution experiment in which the bacteriophage Qβ , a virus with an RNA genome that infects Escherichia coli was propagated in the presence of suboptimal host concentrations at either 37 °C (optimal temperature) or 43 °C (suboptimal temperature). As other RNA viruses, Qβ replicates with very high error rate (between 10^-4 and 10^-6 errors per copied nucleotide) and has a quasispecies population structure.

Our results showed that the minimal host concentration compatible with sustained propagation of the virus depends on temperature. After a certain number of generations, all lineages propagated at suboptimal host concentration and optimal temperature selected a mutation in a minor capsid protein whose phenotypic effect was to favor the entry of the virus into the cell, with no significant effects on other parameters characterizing the infectious cycle. In contrast to this, Qβ adaptation to suboptimal host density at 43 °C took place through a different mutation, located in the virus protein involved in virus adsorption to the bacteria and also in virus release to the external environment once a progeny has been produced. Whereas at optimal temperature the time period that the virus remains within the bacteria was not modified, at 43 °C it was significantly longer. As a consequence, the virus spends less time in the external medium, a behavior similar to that shown by viruses that infect hyperthermophile microorganisms in nature. Although it is difficult to extrapolate our results to more complex situations, as it could be the spread of epidemics in the human population, they provide support for the idea that containment measures based on the reduction of contacts between people (the equivalent to reducing the number of hosts in our system) constitute a selective pressure that may lead to adaptive changes in viruses.

Simulación de hidratos de dióxido de carbono

F. J. Blas
Laboratorio de Simulación Molecular y Química Computacional,
CIQSO-Centro de Investigación en Química Sostenible y Departamento de Ciencias Integradas,
Universidad de Huelva, 21006 Huelva

Los hidratos de dióxido de carbono (CO_2) son compuestos de inclusión no estequiométricos de enorme importancia desde la perspectiva del cambio climático, transporte y almacenamiento de este gas de efecto invernadero. Desde un punto de vista teórico, los mecanismos cinéticos y termodinámicos que controlan la nucleación de hidratos de CO_2 dependen críticamente de la energía libre interfacial hidrato – agua [1, 2]. Únicamente existen en la literatura dos medidas experimentales indirectas de la energía libre interfacial hidrato – agua [3, 4], debido a la dificultad para la determinación experimental de energías libres interfaciales sólido-líquido. En este trabajo se utiliza una combinación de modelos moleculares sencillos pero realistas, TIP4P/ice (agua) [5] y TraPPE (CO_2) [6], y la extensión de la metodología *Mold Integration* [7, 8] para determinar la energía libre del hidrato mediante simulación por primera vez en la literatura [9]. El uso de principios fundamentales de la Termodinámica y la Mecánica Estadística y la definición termodinámica de la energía interfacial, permite obtener un valor consistente de la energía libre interfacial del hidrato de CO_2 con resultados experimentales disponibles en la literatura. Esta metodología abre un nuevo camino para la determinación de energías libres interfaciales de fases sólidas complejas en condiciones de coexistencia mediante principios fundamentales.

[1] E. D. Sloan y C. A. Koh, *Clathrate Hydrates of Natural Gases*, 3ª Edición, CRC PRess, New York, (2008).

[2] Z. M. Aman y C. A. Koh, *Interfacial phenomena in gas hydrate systems*, Chem. Soc. Rev. 45 1678 (2016).

[3] T. Uchida, T. Ebinuma, S. Takeya, J. Nagao y H. Narita, *Effects of pore sizes on dissociation temperatures and pressures of methane, carbon dioxide, and propane hydrates in porous media*, J. Phys. Chem. B **106**, 802 (2002).

[4] R. Anderson, M. Llamedo, B. Tohihi y R. W. Burgass, *Experimental measurement of methane and carbon dioxide clathrate hydrate equilibria in mesoporous silica*, J. Phys. Chem. B **107**, 3507 (2003).

[5] J. L. F. Abascal, E. Sanz, R. G. Fernández y C. Vega, *A potential model for the study of ices and amorphous water: TIP4P/ice*, J. Chem. Phys. **122** 2345111 (2005).

[6] J. J. Potoff y J. I. Siepmann, *Vapor – liquid equilibria of mixtures containing alkanes, carbon dioxide, and nitrogen*, AIChE J. **47** 1676 (2001).

[7] J. R. Espinosa, C. Vega y E. Sanz, *The mold integration method for the calculation of the crystal – fluid interfacial free energy from simulations*, J. Chem. Phys. **141** 1347091 (2014).

[8] J. R. Espinosa, C. Vega y E. Sanz, *Ice – water interfacial free energy for the TIP4P, TIP4P/2005, TIP4P/ice, and MW models as obtained from the mold integration technique*, J. Phys. Chem. C **120** 8068 (2016).

[9] J. Algaba, E. Acuña, J. M. Míguez, B. Mendiboure, I. M. Zerón y F. J. Blas, *Simulation of the Carbon Dioxide Hydrate-Water Interfacial Energy*, submitted to J. Colloid Interface Sci. (2022).

What makes a network "complex"?

Lucas Lacasa[1], Ernesto Estrada[1]
[1]Institute of Cross-Disciplinary Physics and Complex Systems (IFISC), UIB-CSIC, Palma de Mallorca

The advent of Network Science was precipitated by an urgent need to decipher simple mechanisms that could explain the formation and growth of natural and man-made networks. The large-scale structural patterns of these networks systematically deviate from stylized models such as random networks or lattices in a variety of ways, which include the existence of phenomena like "small-worldness" (SW) and "scale-freeness" (SF) (see [1] and refs. therein). Although these mechanisms explain some of the structural properties of real-world networks they also open intriguing questions. For instance, it is easy to see that the SW mechanism reduces mean path length simply by creating shortcuts, making enhanced connectivity overly dependent –and thus, fragile– on them. Likewise, SF-like networks are robust against random node removal but highly fragile against selected removal of highly connected nodes (hubs). It turns out that an optimal (geodesic) navigation of SW and SF networks tends on average to "overuse" both shortcuts or hubs, making these the first candidates to experience jamming, a property that induces a failure cascade which can severely harm the macroscopic network's function.

Here we investigate the microscopic structure of SW and SF networks and discovered that both mechanisms generate topological bypasses connecting pairs of nodes, which facilitates the network communication beyond the topological shortest paths. We model the dynamics on the network by using the time-dependent Schrödinger equation with a tight-binding (TB) Hamiltonian $\mathcal{H}$. Then, the real-time propagator $e^{-it\mathcal{H}/\hbar}$ is mapped into the thermal propagator $e^{-\beta\mathcal{H}}$, where β is the inverse temperature of a thermal bath in which the network is submerged to. After setting appropriately the TB parameters we get that $\mathcal{H} = -A$, such that we define

$$\xi_{vw}(\beta) := \langle \psi_v - \psi_w | \, e^{\beta A} \, | \psi_v - \psi_w \rangle \,, \qquad (1)$$

which accounts for the *resistance* offered by the network to the displacement of the particle from the node v to the node w at inverse temperature β. We proved that $\xi_{vw}(\beta)$ is a square Euclidean distance between the pair of nodes v and w [2].

Further we define a walk-based network entropy, which accounts for the structural ordering of the network produced by the emergence of walks among pairs of nodes. Using it, we shown that both mechanisms, SW and SF, increase network entropy as a result of rocketting the choices that the particle has to navigate between every pair of nodes (see Fig. 1). Therefore, a particle navigating between a pair of nodes v and w can go through the topological shortest path (SP) connecting it or via some of the alternative bypasses created by the SW and SF mechanisms. We assume that the particle will "select" such a path that minimizes the thermal resistance between the two nodes. Based on $\xi_{vw}(\beta)$ we obtain the energy ϵ that a particle needs to travel between a given pair of nodes using a given path that connects them. The path for which the particle needs minimum energy among all which connect a pair of nodes is named the thermally resistive shortest paths (TRSP).

We investigate when the TRSP is favored over the SP for the navigation between pairs of nodes in a network created by the Watt-Strogatz (WS) SW mechanism as well as by the Barabási-Albert (BA) SF one. The results are illustrated in Fig. 1. We can see that the change of the net energy factor ϵ exhibits a non-monotonic shape as a function of the rewiring probability p in the so-called small-world regime. In fact, our measure detects a minimum for $p \approx 0.15$ at which, on average, traveling through the TRSP is energetically much more favorable than traveling through the SP. We call this probability the "good navigational point" (GNP) of the network, p_{GNP}. This is also observed in panel (b) for the BA model. Observe that ϵ is again non-monotonic with a minimum close to $\langle k \rangle \approx 11$, i.e. BA model for which $\langle k \rangle_{\text{GNP}} \approx 11$. Finally, we show how this property influences dynamical processes (synchronization and diffusion) taken place on the networks and investigate the existence of such bypasses in several real-world networks. Therefore we conclude that:

"*a network is complex when its structure is sufficiently rich in walks connecting pairs of nodes as for TRSP emerge as alternative routes that avoid SP and through-hubs navigation, which therefore increases network robustness against jamming*".

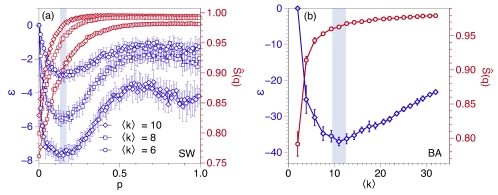

Fig. 1. Normalized communicability entropy $\hat{S}(q)$ (red) and net energy factor ϵ (blue) vs.: (a) the rewiring probability p for WS networks with $N = 250$ nodes and different average degree $\langle k \rangle$, or (b) the mean degree $\langle k \rangle$ of a BA model with $N = 250$ nodes. The shaded area highlighting the minimum of ϵ marks the network Good Navigational Point.

[1] E. Estrada, *The Structure of Complex Networks. Theory and Applications* (Oxford University Press, Oxford, 2011).

[2] E. Estrada, T*he communicability distance in graphs*. Lin. Algebra Appl. **436**, 4317-4328 (2012)

Beyond Brownian motion: from data to models

Ralf Metzler[1]
[1]Institut for Physics & Astronomy, University of Potsdam, 14476 Potsdam-Golm, Germany

After a brief historical introduction to Brownian motion I will address recent experimental and simulations results on diffusive transport in complex systems, ranging from dynamics in single molecules, motion of molecules and tracers in living biological cells, to ants and birds. Data-science methods help us in identifying different physical processes encoded in experimental records and to extract physical parameters. I will provide an overview over different approaches and their performance in the context of diffusive motion.

Why are cell populations maintained via multiple intermediate compartments? LA-UR-22-22540

Flavia Feliciangeli[1], Hanan Dreiwi[1], Grant Lythe[1], Martín López-García[1], Mario Castro[2], and Carmen Molina-París[3,1]
[1] School of Mathematics, University of Leeds, UK
[2] Instituto de Investigación Tecnológica, Universidad Pontificia Comillas, Madrid, Spain
[3] Theoretical Division, Los Alamos National Laboratory, Los Alamos, USA

Abstract There exist in nature many examples of cellular populations with a compartmental structure. For instance, T cell progenitors (thymocytes) in the thymus follow a structured journey of development. During this journey, they divide, die and differentiate [1]. Naive T cells in lymph nodes follow a structured journey of antigen-induced activation. During this journey, they divide, die and differentiate (to become effector and memory T cells) [2].

In this talk I introduce a mathematical compartmental model to characterise the structured journey of cellular populations, making use of a branching process approach. I discuss two cases: that of a single compartment, and that of multiple compartments (Figure 1). Each cellular compartment has its specific sets of rules (probabilities of division, differentiation and death) and function (Figure 2). I shall consider four types of single-cell events in compartment c ($1 \leq c \leq C$):

- **Symmetric division**, $p_b(c)$: both daughter cells remain in compartment c.
- **Asymmetric division**, $p_a(c)$: one daughter cell remains in compartment c and the other moves to compartment $c+1$.
- **Death**, $p_d(c)$: a cell in compartment c dies.
- **Exit**, $p_e(c)$: a cell in compartment c moves to compartment $c+1$.

Each cell in compartment c obeys the same rules and cells are independent; this allows us to make use of the theory of branching processes. The study is restricted to a time-independent analysis (Figure 1). We restrict ourselves to counting cells and ignore inter-event times; that is, we ignore the total time taken for progeny to disappear from all intermediate compartments and exit from the last one. We assume $p_b < p_d + p_e$, so that *extinction* is the ultimate fate of the population of intermediate cells. For the case $C = 1$ and arbitrary C intermediate compartments between progenitor and product cells, we are interested in the following two random variables : the total number of product cells from a single progenitor cell, and the number of divisions that separates each cell from the progenitor, so that we can classify cells by generation. These random variables are studied with first step arguments and probability generating functions.

Results We consider the maintenance of a population of *product* cells from *progenitor* cells via one or more intermediate compartments. We calculate the distribution of $\mathcal{R}$, the number of product cells per progenitor, and its mean, N. We also consider the random variable $\mathcal{G}$, the generation number of a randomly-selected product cell, and its mean, D. Thus, D is the mean age of the product cell population, measured in number of generations from the progenitor.

If $C = 1$, a large ratio of product cells to progenitors can only be achieved at the cost of the product cell population being dominated by large families of cells descended from individual progenitors, and large number of divisions separating product cells from progenitors. These undesirable features can be avoided if there are multiple intermediate compartments. A sequence of compartments is, in fact, an efficient way to maintain a product cell population from a progenitor population, avoiding excessive clonality and minimising the number of rounds of division *en route*.

I shall discuss the case when $p_a = 0$, but the results can be generalised to the case when asymetric division events are present ($p_a \neq 0$). For the symmetric case, we may express all single compartment quantities in terms of N and D.

$$p_b = \frac{1}{2}\frac{D}{D+1}, \text{ and } p_e = \frac{N}{D+1}.$$

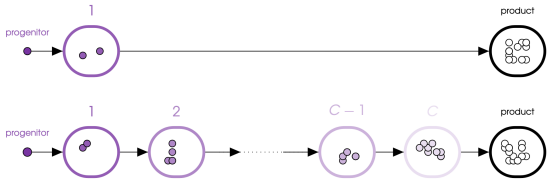

Fig. 1. A single intermediate compartment ($C = 1$). Multiple intermediate compartments ($C \geq 2$). From a single progenitor, how many cells exit a single compartment? From a single progenitor, how many cells exit a sequence of C different compartments?

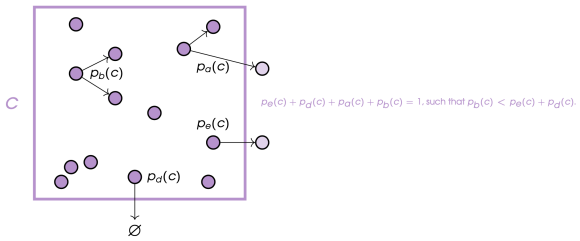

Fig. 2. Each cell in compartment c: same rules and independence ⇒ branching process.

[1] Klein, Kyewski, Allen and Hogquist. *Positive and negative selection of the T cell repertoire: what thymocytes see (and do not see)*. Nature Reviews Immunology 2014.

[2] Farber, Yudanin and Restifo. *Human memory T cells: generation, compartmentalization and homeostasis*. Nature Reviews Immunology 2014.

Mpemba effect in driven gases: Are the thermal and entropic criteria equivalent?

Andrés Santos[1,2], Alberto Megías[1] and Antonio Prados[3]
[1]Departamento de Física, Universidad de Extremadura, E-06006 Badajoz, Spain
[2]Instituto de Computación Científica Avanzada (ICCAEx), Universidad de Extremadura, E-06006 Badajoz, Spain
[3] Física Teórica, Universidad de Sevilla, Apartado de Correos 1065, E-41080 Sevilla, Spain

The response to an excitation in a complex condensed matter system may depend on its entire history and not only on the instantaneous value of the macroscopic state variables, thus signaling the breakdown of a purely macroscopic description due to memory effects.

The so-called Mpemba effect [1] is a counterintuitive memory phenomenon according to which, given two samples of a fluid, the initially hotter one may cool more rapidly than the initially cooler one. Although initially reported in the case of water [2, 3], its existence for that liquid is still questioned [4].

In this talk, the system chosen to reveal the feasibility of the Mpemba effect is a gas of elastic hard spheres coupled to a fluid reservoir via a nonlinear drag force plus a white-noise stochastic force [5]. The associated (spatially uniform) Enskog–Fokker–Planck equation for the one-body velocity distribution function $f(\mathbf{v},t)$ is

$$\partial_t f(\mathbf{v},t)-\partial_{\mathbf{v}}\cdot\left\{\zeta(v)\left[\mathbf{v}+\frac{k_BT_b}{m}\partial_{\mathbf{v}}\right]\right\}f(\mathbf{v},t)=J[\mathbf{v}|f,f],$$

where $J[\mathbf{v}|f,f]$ is the Boltzmann–Enskog collision operator, $\zeta(v)=\zeta_0\left(1+\gamma mv^2/k_BT_b\right)$ is the velocity-dependent drag coefficient (γ measuring the degree of nonlinearity), and T_b is the temperature of the background fluid.

The study is addressed by minimal descriptions based on kinetic theory (basic and extended Sonine approximations), the theoretical predictions being numerically confirmed by the direct simulation Monte Carlo (DSMC) method and by event-driven molecular dynamics (EDMD) [6].

A direct test of the Mpemba effect consists of checking whether or not the (kinetic) temperature $T(t)=\frac{m}{3}\langle v^2\rangle$ of two independent samples A and B cross each other; this defines the *thermal* criterion. An alternative *entropic* criterion, on the other hand, is based on the possible crossover of the relative entropy $\mathcal{D}(t)=\langle\ln[f(\mathbf{v},t)/f^{\text{eq}}(\mathbf{v})]\rangle$, where $f^{\text{eq}}(\mathbf{v})$ is the equilibrium distribution.

As will be discussed in the talk, if the Mpemba effect takes place during the kinetic stage of the relaxation to equilibrium, it is possible to find the thermal effect but not the entropic one (see Fig. 1 for an illustration), or vice versa (see Fig. 2 for an illustration). As observed in Figs. 1 and 2, an excellent agreement between simulation data and the minimal kinetic-theory description exists.

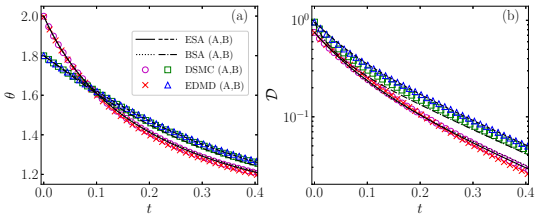

Fig. 1. Relaxation of (a) the scaled temperature $\theta(t)\equiv T(t)/T_b$ and (b) the relative entropy $\mathcal{D}(t)$ for two samples A and B initially prepared with $(\theta_A^0,\theta_B^0)=(2,1.8)$ and $(a_{2A}^0,a_{2B}^0)=(0.5,-0.35)$, where a_2 represents the excess kurtosis. Here, $\zeta_0=1$, $\gamma=0.1$, and the unit of time is the equilibrium mean free time.

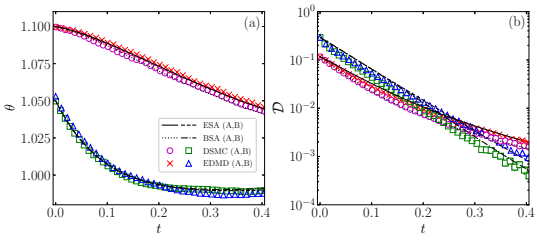

Fig. 2. Same as in Fig. 1, except that the initial conditions are $(\theta_A^0,\theta_B^0)=(1.1,1.05)$ and $(a_{2A}^0,a_{2B}^0)=(-0.35,0.5)$.

[1] Z. Lu and O. Raz, Proc. Natl. Acad. Sci. USA **114**, 5083 (2017).

[2] W. D. Ross (ed.), The Works of Aristotle (Oxford Clarendon Press, Oxford, UK, 1931), Vol. 3, p. 1059.

[3] E. B. Mpemba and D. G. Osborne, Phys. Educ. **4**, 172 (1969).

[4] H. C. Burridge and P. F. Linden, Sci. Rep. **6**, 37665 (2016).

[5] A. Santos and A. Prados, Phys. Fluids **32**, 072010 (2020).

[6] A. Megías, A. Santos, and A. Prados, arXiv:2201.13130.

COMUNICACIONES ORALES

Diseño de cuasicristales icosaédricos mediante enlaces direccionales

Eva G. Noya[1], Chak K. Wong[2], Pablo Llombart[1] and Jonathan P. K. Doye[2]
[1]Instituto de Química-Física Rocasolano, Consejo Superior de Investigaciones Científicas, CSIC, Calle Serrano 119, 28006, Madrid
[2]Physical and Theoretical Chemistry Laboratory, Department of Chemistry, University of Oxford, South Parks Road, Oxford OX1 3QZ, Reino Unido

Los cuasicristales icosaédricos (IQC) son materiales ordenados pero que carecen de periodicidad en cualquier dirección del espacio. Aunque los IQC fueron los primeros cuasicristales que se descubrieron[1], hasta la fecha solo se han observado experimentalmente en aleaciones metálicas[2], pero no en otro tipo de materiales. Por el contrario, en sistemas blandos se han identificado cuasicristales con otras simetrías (por ejemplo, dodecagonal)[3, 4, 5]. En este trabajo, introducimos una nueva clase de IQCs construidos a partir de partículas coloidales con interacciones direccionales que podrían producirse experimentalmente utilizando partículas de origami de ADN[6]. Nuestra estrategia conduce a sistemas modelo que se ensamblan de forma robusta en el cuasicristal diana mediante enlaces direccionales. La aplicabilidad del método de diseño se ilustra para IQCs de tipo primitivo y centrado en el cuerpo. La clave del método de diseño radica en imponer geometrías de las interacciones de las partículas que favorezcan la propagación del orden icosaédrico, aunque esto conduzca a que no todas las partículas sean capaces de formar todos los enlaces posibles. Además de proporcionar sistemas modelo con los que explorar el comportamiento de los IQCs, nuestro método abre una posible ruta para la contrucción de materiales cuasicristalinos funcionales.

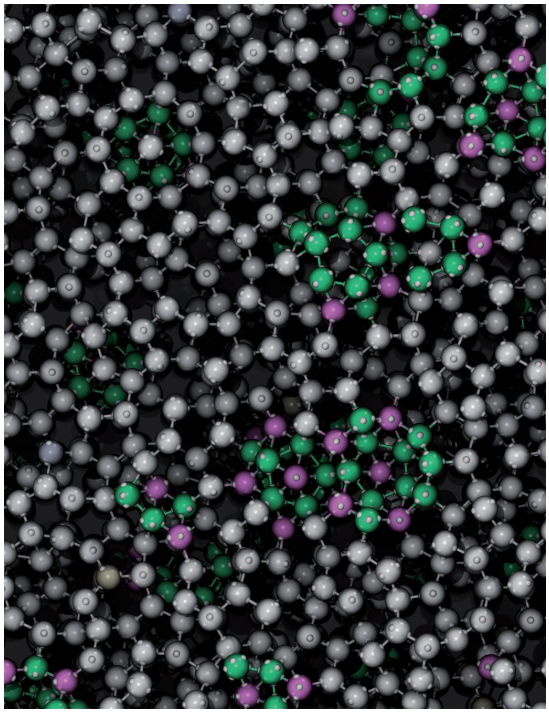

Fig. 1. Cuasicristal icosaédrico obtenido a partir de partículas con interacciones direccionales.

[1] D. Shechtman, I. Blech, D. Gratias, y J. W. Cahn, *Metallic phase with long-range orientational order and no translational symmetry*, Phys. Rev. Lett. **53**, pp. 1951–1953 (1984).

[2] H. Takakura, C. P. Gómez, A. Yamamoto, M. D. Boissieu, y A. P. Tsai, *Atomic structure of the binary icosahedral Yb-Cd quasicrystal*, Nat. Mater., **6**, pp. 58–63 (2007).

[3] X. Zeng, *et al.*, *Supramolecular dendritic quasicrystals*, Nature, **428**, pp. 157–160 (2004).

[4] A. Haji-Akbari, *et al.*, *Disordered, quasicrystalline and crystalline phases of densely packed tetrahedra*, Nature, **462**, pp. 773–777 (2009).

[5] T. Dotera, *Quasicrystals in soft matter*, Isr. J. Chem., **51**, pp. 1197–1205 (2011).

[6] E. G. Noya, C. K. Wong, P. Llombart y E. G. Noya, *How to design an icosahedral quasicrystal through directional bonding*, Nature, **596**, pp. 367–371 (2021).

Brownian dynamics of levitated nanoparticles

Raúl A. Rica[1,2]
[1]Universidad de Granada, Departamento de Física Aplicada, 18071, Granada (Spain)
[2]Universidad de Granada, Nanoparticles Trapping Laboratory, 18071, Granada (Spain)

Micro and nanoparticles can be individually manipulated by different trapping mechanisms, among which optical tweezers and Paul traps are the most extended approaches. Trapped particles are subject to Brownian motion due to collisions with water or gas molecules, depending on the dispersing medium. Once trapped, the particles can be driven out of equilibrium under the action of external fields, giving rise to a very rich dynamics. In this talk, we will discuss some of our work with trapped nanoparticles dispersed in different media, including water, air and vacuum (see Fig. 1) [1, 2, 3, 4, 5]. We will demonstrate that an exquisite control over the dynamics that can be achieved by using state-of-the-art instrumentation, thanks to the sensitivity over position and forces that these provide.

In particular, we will present recent experimental results demonstrating the occurrence of stochastic resonance [3] and the Kovacs effect [6] on the dynamics of a single levitated nanoparticle.

Fig. 1. Picture of a single nanodiamond (size = 100 nm) levitated by a Paul trap. The distance between the conical electrodes is 1.5 mm. The bright spot is due to the scattering of a laser beam focused at the position of the nanoparticle.

[1] I.A. Martínez, E. Roldán, D. Petrov, and R.A. Rica, *Adiabatic processes realized with a trapped brownian particle*, Phys. Rev. Lett. **114**, 120601 (2015).

[2] I.A. Martínez, E. Roldán, D. Petrov, J.M. Parrondo, and R.A. Rica, *Brownian Carnot engine*, Nat. Phys. **12**, 67 (2016).

[3] F. Ricci, R.A. Rica, M. Spasenović, J. Gieseler, L. Rondin, L. Novotny, and R. Quidant., *Optically levitated nanoparticle as a model system for stochastic bistable dynamics*, Nat. Commun. **8**, 15141 (2017).

[4] G.P. Conangla, R.A. Rica,and R. Quidant., *Extending vacuum trapping to absorbing objects with hybrid paul-optical traps.*, Nano Lett. **8**, 6018 (2020).

[5] G.P. Conangla, D. Nwaigwe, J. Wehr, and R.A. Rica, *Overdamped dynamics of a Brownian particle levitated in a Paul trap.*, Phys. Rev. A **101**, 053823 (2020).

[6] A. Militaru, A. Lasanta, M. Frimmer, L.L. Bonilla, L. Novotny, and R.A. Rica, *Kovacs memory effect with an optically levitated nanoparticle.*, Phys. Rev. Lett **127**, 130603 (2021).

Survival and extreme statistics of work, heat, and entropy production in steady-state heat engines

Gonzalo Manzano[1], and Édgar Roldán[2]
[1]Institute for Cross-Disciplinary Physics and Complex Systems IFISC (UIB-CSIC),
Campus Universitat Illes Balears, E-07122 Palma de Mallorca, Spain
[2]International Centre for Theoretical Physics ICTP, Strada Costiera 11, I-34151, Trieste, Italy

In small systems, fluctuations play a prominent role, often pushing systems far away from equilibrium. As a consequence, they are of crucial importance for the performance and robustness of microscopic motors, heat engines and refrigerators, where the work extracted, the heat dissipated, and the efficiency over a finite time, become stochastic quantities that can be described within the framework of stochastic thermodynamics. However, it remains an open, active area of research to derive universal "survival" statistics (e.g. the probability to remain below or above a given threshold) of fluctuating physical quantities in steady-state nonequilibrium processes and in particular those performing some useful thermodynamic task. More precisely, it is relevant to study extreme and survival statistics of the work extracted by microscopic heat engines, of the heat dissipated into the environment, or the peaks in the consumption of chemical fuel driving a molecular machine, since they can shed new light on the function and properties of such systems. In this context, some important questions are: (i) are there universal bounds on the statistics of entropy production maxima and minima during a prescribed interval? (ii) what is the survival probability for the work or heat not to exceed or fall below a certain threshold value? (iii) what is the "optimal" threshold that guarantees a prescribed value of the survival probability for the work extracted by a stationary heat engine?

In this talk, based on reference [1], I will discuss some novel insights about the above questions. First, I will show how to derive universal inequalities for the cumulative distribution of the finite-time maximum and minimum of stochastic entropy production and their averages in generic nonequilibrium stationary states. These nonequilibrium relations entail a new development of martingale theory for entropy production [2, 3, 4] and substantially extend and generalize previous results on entropy production minima statistics [4]. Then I will show how to apply these results to bound the survival statistics of the work extracted and the heat dissipated by steady-state engines permanently coupled to two heat baths at cold $T_{\rm c}$ and hot $T_{\rm h}$ temperatures. Interestingly, we obtain time-dependent thresholds $w_{\pm}(\tau)$ that allow us to bound the extreme fluctuations of the stochastic work and heat with a given confidence level, for a time interval $[0,\tau]$. The main results are tested with numerical simulations of a stochastic photoelectric device, as illustrated in Fig. 1.

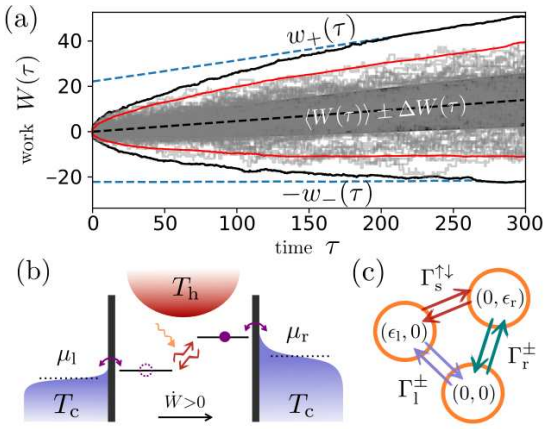

Fig. 1. **(a)** Illustration of work extreme fluctuations and the optimal threshold bounds $w_{\pm}(\tau)$ for its maxima (upper black and red solid lines) and minima (bottom black and red solid lines) developed by a photoelectric device during the interval $[0,\tau]$ as a function of τ. Gray thin lines represent the stochastic work extracted (in $k_{\rm B}T$ units) for a sample of 100 trajectories. The solid lines are optimal thresholds $w_+(\tau)$ (top) and $w_-(\tau)$ (bottom) for a confidence value of 99% ($\alpha = 0.01$, black lines), and 90% ($\alpha = 0.1$, red lines). The average work output $\langle W(\tau)\rangle$ (black dashed line) and its standard deviation $\Delta W(\tau)$ (dark shadow area) are also shown for comparison. The blue dashed lines are linear optimal asymptotic thresholds for $\alpha = 0.01$. **(b)** Photoelectric device composed by two (single-level) quantum dots transporting electrons between their respective fermionic reservoirs at temperature $T_{\rm c}$ against a chemical potential difference ($\mu_{\rm r} \geq \mu_{\rm l}$) powered by photons at temperature $T_{\rm h}$ from a hot source. **(c)** Energetic states of the device and relevant rates producing transitions between them (simultaneous occupancy of the two dots is avoided by Coulomb repulsion).

[1] G. Manzano, and É. Roldán, *Survival and extreme statistics of work, heat, and entropy production in steady-state heat engines*, arXiv: 2109.03260 (2021) — accepted in Phys. Rev. E.

[2] G. Manzano, D. Subero, O. Maillet, R. Fazio, J. P. Pekola, and É. Roldán, *Thermodynamics of Gambling Demons*, Phys. Rev. Lett. **126** 080603 (2021).

[3] G. Manzano, R. Fazio, and É. Roldán, *Quantum Martingale Theory and Entropy Production*, Phys. Rev. Lett. **122** 220602 (2019).

[4] I. Neri, É. Roldán, and F. Jülicher, *Statistics of Infima and Stopping Times of Entropy Production and Applications to Active Molecular Processes*, Phys. Rev. X **7**, 011019 (2017).

The role of hydrodynamics in the diffusion of passive tracers in random networks

Nerea Alcázar-Cano[1], and Rafael Delgado-Buscalioni[1,2]
[1]Departamento de Física Teórica de la Materia Condensada, Universidad Autónoma de Madrid
[2]Condensed Matter Physics Center (IFIMAC)

The first natural consequence of the extra reduction in mobility near a wall induced by hydrodynamic interactions (HI) is to decrease the diffusion coefficient. While this statement is true, the role of HI in the diffusion of tracer particles in random media presents other many unexpected faces, some of them still not fully explored. The present study highlights the role of the network structure: we have considered randomly distributed polymeric fibers, cubic networks formed by randomly placed mutually orthogonal rods (Fig. 1 (a) and (b), respectively), and irregular thicker walls formed by colloidal gels. We unveil the relevance of both HI and the obstacle configuration by analysing the "history" of the particle diffusion, evidenced in the van Hove distribution $P(\Delta, t)$ of the tracer jumps Δ after a lag time t.

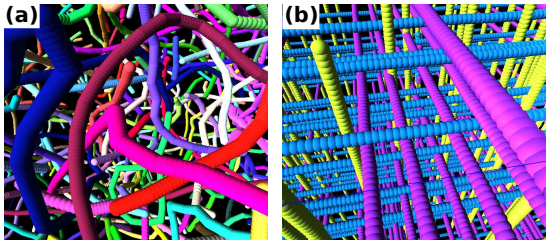

Fig. 1. Pictorial representation of two of our random obstacles structures: (a) polymeric fibrers, and (b) cubic networks.

The details of $P(\Delta, t)$ at long times (or long jumps) subtly depend on the networks structure. We encounter Gaussian tails for $P(\Delta, t)$ in the polymeric network and colloidal gels, while exponential tails in the cubic structure (Fig. 2). Interestingly, all these different behaviours are exclusively due to differences in their *spatial* heterogeneity (the structures are static) [1, 2].

Focusing on hydrodynamics, we find consistently similar hydrodynamic effects in the tracer diffusion across all the random structures considered. As expected, at short times, the probability of small jumps is larger if HI are included (added friction). However at longer times, we observe that the diffusion coefficient of mobile particles in simulations including hydrodynamic interactions (HI) become gradually similar to that of purely Brownian walkers (BD). This HI-induced enhancement of diffusion at long times is more clearly observed close to the critical percolation threshold, i.e., when particles diffuse along single (or very few) fractal paths traversing the system. Our findings suggest that the origin of the HI-induced enhancement of single-particle diffusion at long times is the anisotropy in the perpendicular and longitudinal tracer mobility close to the obstacle structure. HI induces a faster longitudinal diffusion along the paths, compared with diffusion perpendicular to the obstacle "walls" [3].

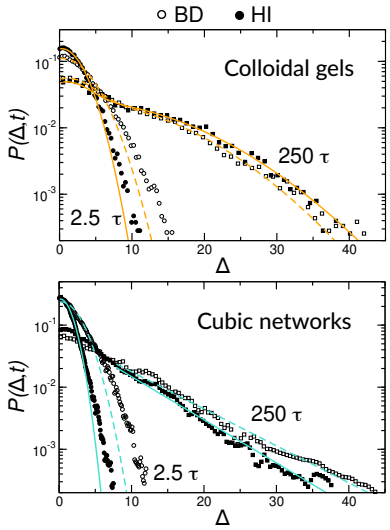

Fig. 2. Displacement probability distribution $P(\Delta, t)$ for a tracer close to the percolation thershold in colloidal gels and cubic networks. Open and filled markers indicate BD and HI simualtions, respectively. Lines correspond to different fits: normal distribution ar short-time interval ($t = 2.5\tau$), and the combination of two Gaussian in colloidal gels and exponetial tails in cubic networks at long lag time ($t = 250\tau$).

[1] Miotto, J. M., Pigolotti, S., Chechkin, A. V. & Roldán-Vargas, S., *Length scales in Brownian yet non-Gaussian dynamics*, Phys. Rev. X **11**, 031002 (2021).

[2] Skaug, M. J., Wang, L., Ding, Y. & Schwartz, D. K., *Hindered nanoparticle diffusion and void accessibility in a three-dimensional porous medium*, ACS Nano **9**, 21482156 (2015).

[3] Alcázar-Cano, N. & Delgado-Buscalioni, R., *Hydrodynamics induce superdiffusive jumps of passive tracers along critical paths of random networks and colloidal gels*, Soft Matter, DOI: 10.1039/D1SM01713F (2022).

A complexity theory approach to the origin of life: towards the first RNA replication

Aguirre-Tamaral. A, Briones. C, and Aguirre. J
Centro de Astrobiología (INTA-CSIC), 28850 Torrejón de Ardoz, Madrid, Spain

The work we present here combines the mathematical modeling of complex systems with the RNA biochemistry to study an open question of critical importance in astrobiology: how the first RNA replication took place on the early Earth.

A hypothesis for the origin of life strongly supported by experimental data is the "*RNA world*", which suggests that life was originated in an environment in which RNA molecules were able to self-replicate (through RNA ribozymes). However, the minimum size for an RNA polymerase ribozyme is ∼165 nt [1], 3-4 times longer than what is attainable through abiotic, random polymerization of activated ribonucleotides [2]. This limitation could be solved if a modular evolution of RNA was achieved [3, 4]. In this model, the RNA ribozyme appeared thanks to a stepwise process, in which (*i*) short ($<$ 40 nt) RNA molecules polymerized abiotically from single ribonucleotides, (*ii*) folded into their minimum free energy structure, (*iii*) some of them were endowed with RNA ligase activity and catalyzed the assembly of larger RNA molecules, (*iv*) generated a functional RNA ribozyme.

However, such a hypothesis leads to the difficulty of obtaining many identical copies of a specific RNA sequence, a critical requirement for the emergence of effective RNA replication. This is the challenge that we want to address. Therefore, we developed a computational model to study the possible first template-dependent replication of RNA molecules located in an adequate environment of the early Earth (e.g. the interphase aqueous solution-clay, Fig. 1A). Our model simulations allowed us to study RNA replication under different environmental conditions (β, Fig. 1B) and to analyze the RNA copy fraction over time (Fig. 1C). Finally, our model can be used as an *in silico* tool to identify and study how the efficiency of the RNA replicative phenomenology depends on the parameters of the system, such as the template RNA length, size of genetic alphabet, strength of chemical bonds and probability of rupture, environmental conditions, etc.

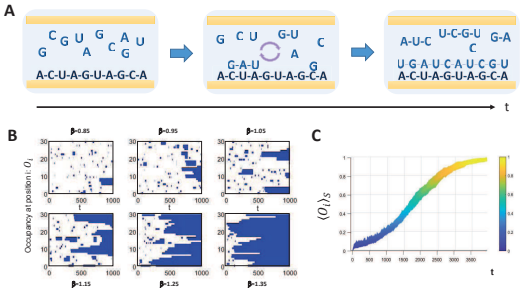

Fig. 1. A) Diagram of a nucleotide pool at a clay-aqueous interface in the early Earth and how a template RNA molecule, located on the clay surface, is replicated. B) Evolution of the copy of an RNA molecule, of length 30 nt, for different environmental conditions (β). C) Average RNA copy fraction over time.

[1] F. Wachowius, P. Holliger, *Non-Enzymatic Assembly of a Minimized RNA Polymerase Ribozyme*, Chem. Systems. Chem. **6**, e1900004 (2019).

[2] W.Huang, J.P.Ferris, *One-Step, Regioselective Synthesis of up to 50-mers of RNA Oligomers by Montmorillonite Catalysis*, J. Am. Chem. Soc. **128** :89148919 (2006).

[3] C.Briones, M.Stich, and SC.Manrubia, *The dawn of the RNA World: toward functional complexity through ligation of random RNA oligomers*, RNA **15**, 743749 (2009).

[4] C.Briones, M.Stich, and SC.Manrubia, *A model for the modular evolution of RNA addressing open questions on the origin of life*, Orig. Life Evol. Biosph. **40**, 427430 (2010).

Games in rigged economies

Seoane LF[1,2,3],
[1]Departamento de Biología de Sistemas, Centro Nacional de Biotecnología (CSIC), C/ Darwin 3, 28049 Madrid, Spain.
[2]Grupo Interdisciplinar de Sistemas Complejos (GISC), Madrid, Spain.
[3]Instituto de Física Interdisciplinar y Sistemas Complejos IFISC (CSIC-UIB), Palma de Mallorca, Spain.

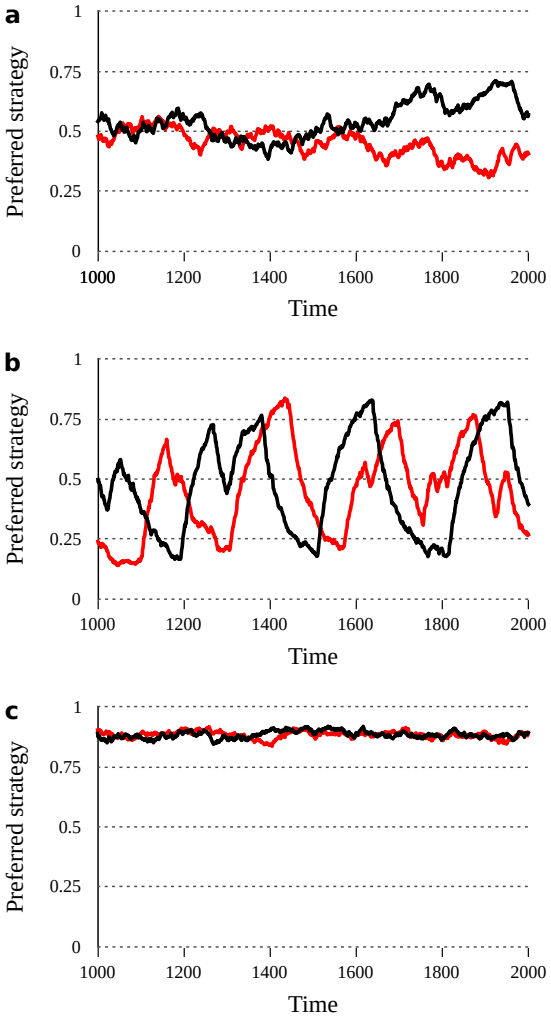

Fig. 1. **Three regimes with increased 'rigging' of** 2 **economic games**. **a** With little intervention, economic DOF are minority games. As agents attempt to play the minority option, an evolving population splits itself equally between the two strategies available. **b** Intermediate 'rigging' prompts structured fluctuations: each game is temporarily manipulated in a direction or the other. **c** Large 'rigging' turns economic DOF into majority games, which the population agrees to play and rig in the same direction.

Modern economies evolved from simpler human exchanges into very convoluted systems. Today, a multitude of aspects can be regulated, tampered with, or left to chance; these are economic degrees of freedom (DOF) which together shape the flow of wealth.

Economic actors can exploit them, at a cost, and bend that flow in their favor [1]. If intervention becomes widespread, microeconomic strategies of different actors can collide or resonate, building into macroeconomic effects. How viable is a rigged economy? How do growing economic complexity and wealth affect it?

Here we capture essential elements of 'rigged economies with a simple model [2]. Nash equilibria of payoff matrices in tractable cases show how increased intervention turns economic DOF from minority into majority games through a dynamical phase. These stages are reproduced by agent-based simulations of our model (Figure 1), which allow us to explore scenarios out of reach for payoff matrices.

Increasing economic complexity is then revealed as a mechanism that spontaneously defuses cartels or consensus situations. But excessive complexity enters abruptly into a regime of large fluctuations that threaten the systems viability. This regime results from non-competitive efforts to intervene the economy coupled across DOF, becoming unpredictable. Thus high economic complexity can result in negative spillover from non-competitive actions. Simulations suggest that wealth must grow faster than linearly with complexity to avoid this large fluctuations regime and keep economies viable in the long run.

Our model provides testable conclusions and phenomenological charts to guide policing of rigged economies. We discuss the recent, real-world case of the Game Stop short-squeeze, in which multiple economic actors got coordinated through social media to invest in allegedly undervalued stocks. This resulted in an emergent upset of the stock market and still-ongoing investigations of market manipulation.

[1] D. Wolpert and J. Grana. *How Much Would You Pay to Change a Game before Playing It?*, Entropy **21**(7), p.686 (2019).

[2] L. F. Seoane. *Games in Rigged Economies*, Phys. Rev. X **11**(3), p.031058 (2021).

Spontaneous emergence of counterclockwise vortex motion in assemblies of pedestrians roaming within an enclosure

Iñaki Echeverría-Huarte[1], Alexandre Nicolás[2], Raúl Cruz Hidalgo[1], Angel Garcimartín[1] and Iker Zuriguel[1]
[1]Departamento de Física y Mat. Apl., Facultad de Ciencias, Universidad de Navarra, E-31080 Pamplona, Spain
[2]Institut Lumière Matière, CNRS Universitè Claude Bernard Lyon 1 & Universitè de Lyon, F-69622, Villeurbanne, France.

Over the last few years, the study of active matter has brought to light surprising results concerning the emergence of collective patterns. Among them, a particularly interesting one is the formation of vortices, present from macroscopic scales (fish schools [1]) to microscopic ones (colloids [2] or bacteria [3]). Although the basics for the origin of these structures have been studied in detail, little attention has been paid so far to the direction of rotation. This manuscript addresses this issue by presenting experimental results of a crowd roaming within an enclosure: A vortex-like structure spontaneously emerges and, even more strikingly, the vortex always rotates counterclockwise (see Figs.1a-b).

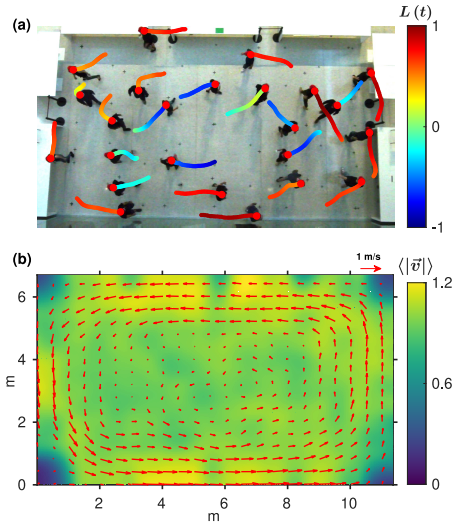

Fig. 1. In (a), snapshot of an experiment with 24 pedestrians. The tails show the instantaneous angular momentum $L_i(t)$ for each agent over the last 1.5 seconds. They have been coloured according to the colorbar on the right. In (b), average velocity modulus field $\langle|\vec{v}|\rangle$ for the same experiment (in m/s). The value of $\langle\vec{v}\rangle$ is indicated by red arrows (as reference, the one on the top right corresponds to 1 m/s).

In order to quantify the collective rotation of the system, we use the normalized angular momemtum:

$$L(t) = \frac{1}{N}\sum_{i=1}^{N}\frac{\vec{r}_i(t)\times\vec{v}_i(t)}{|\vec{r}_i(t)|} \qquad (1)$$

where N is the total number of people within the stage, $\vec{v}_i$ the velocity of pedestrian i, and $\vec{r}_i$ its position (with the origin at the centre of the arena). The analysis of this descriptor will eventually confirm that, regardless of the experimental condition, the symmetry-breaking is always present in the system (Fig.1a).

Finally, for the purpose of revealing the physical origin of this unexpected phenomenon, we put forward a minimal numerical model of self-propelled particles. Thus, the motion of each agent will be determined by a self-propulsion force with no preferential direction of motion and two repulsive forces; one against particles and the other between the agents and the walls (the latter with a dissipative term inspired by the observation of higher densities near the walls).

After replicating the same experimental conditions, we demonstrate the fundamental role that both, the density of agents and their dissipative interaction with the walls, play in the formation of vortices (blue dots in Fig.2). Additionally, for the particular case of pedestrians, we justify that the symmetry-breaking presented in the system could be triggered by the turning preference of right-handed people (the majority in our experiment) to turn leftwards when facing a wall. Incorporating this new feature in the particles' movement by means of a new turning force, the main experimental results are reproduced, particularly the permanent rotation of the system in the counterclockwise direction (orange dots in Fig.2).

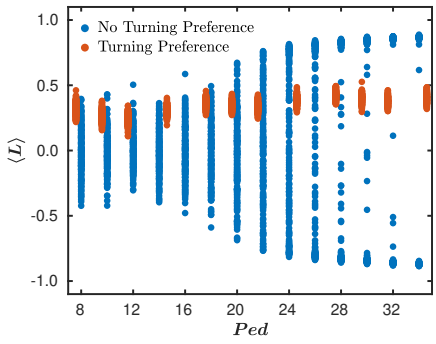

Fig. 2. Bifurcation diagram of the temporal average of $L(t)$ obtained for different number of simulated pedestrians inside the arena. Blue dots correspond to simulations where the turning preference mechanism is not included. In orange, the turning preference is activated. Both models include a dissipative interaction with the walls.

[1] J. Gautrais, C. Jost and G. Theraulaz, *Key behavioural factors in a self-organised fish school model*, Annales Zoologici Fennici **45**, 415-428 (2008).

[2] A. Bricard et al. *Emergent vortices in populations of colloidal rollers*, Nat. Commun. **6**, (2015).

[3] H. Wioland, F. Woodhouse, J. Dunkel, J. Kessler and R. Goldstein, *Confinement Stabilizes a Bacterial Suspension into a Spiral Vortex*, Phys. Rev. Lett. **110**, (2013).

Complex spatiotemporal oscillations emerging from transverse instabilities in large-scale brain networks

Pau Clusella[1], and Jordi Garcia-Ojalvo[1]
[1] Department of Experimental and Health Sciences, Universitat Pompeu Fabra, Barcelona Biomedical Research Park, Barcelona, Spain

The interplay between neurons in the brain produces collective rhythmic behavior at multiple frequencies and spatial resolutions. This oscillatory activity is fundamental for proper cognitive function, and displays a plethora of spatiotemporal phenomenology in recorded signals. Recent advances on neuroimaging allow for representing the brain's inner organization as a complex network in which each node is a well-defined brain region composed of densely interconnected neurons, and edges across nodes represent pairwise interactions across distant regions. Combining neural-mass models (NMM) with connectomics data, one can create large-scale brain models whose dynamical properties reflect the principles underlying macroscopic neural activity. Nonetheless, many aspects about the mechanisms through which large-scale brain models reproduce spatiotemporal brain dynamics are still unknown.

In this work we uncover the onset of irregular spatiotemporal dynamics in a simple large-scale brain model. The model consists of 90 brain regions connected through a complex network obtained from tractography data. The activity of each brain area is governed by the dynamics of a Jansen-Rit NMM [1]. In close analogy to pattern-formation mechanisms in reaction-diffusion systems, we show that the coupling among brain regions alone is enough to spontaneously destabilize an underlying synchronized state, thereby generating complex oscillatory behavior.

Our analysis relies on a suitable normalization on the incoming input of each brain region and consists of two parts. First, we show that the network possesses an invariant homogeneous manifold, i.e., a set of states in which the behavior of each node is identical across all brain regions. These states are described by a self-coupled version of the NMM used for the evolution of each brain region. Bifurcation analysis of this low-dimensional system reveals how the different parameters modify the onset of synchronized oscillatory states within the homogeneous manifold. Second, we employ the Master Stability Function formalism [2] to investigate the stability of the homogeneous states to heterogeneous perturbations, i.e., perturbations that are transversal to the uniform dynamics of the system. According to this technique, the growth rate of any perturbation can be decomposed as a function of the structural connectivity eigenmodes, thereby providing a direct relation between topology and dynamics.

The combination of these two steps provides a comprehensive bifurcation diagram of the system in which the synchronized oscillatory solution turns out transversally unstable in a large region of the parameter space (see Fig 1a). Numerical simulations reveal that this instability gives raise to complex spatiotemporal dynamics, including travelling waves, multistability, and high-dimensional chaos. We study the synchronization and propagation properties of these regimes (see Fig 1b), and show that their complexity increases by reducing the external input of the system.

In order to extend our model to a more realistic setup, next we perform extensive numerical simulations of the unnormalized version of the system. The outcome reveals that irregular oscillations emerge through a mechanism similar to that of the simplified formulation, but differ on how the patterns synchronize and travel across the network. Finally, we also apply the same analysis to investigate the emergence of irregular spatiotemporal activity using a next-generation NMM [3]. Overall, our work reveals that transverse instabilities are an ubiquitous mechanism for the onset of irregular spatiotemporal oscillations in large-scale brain networks.

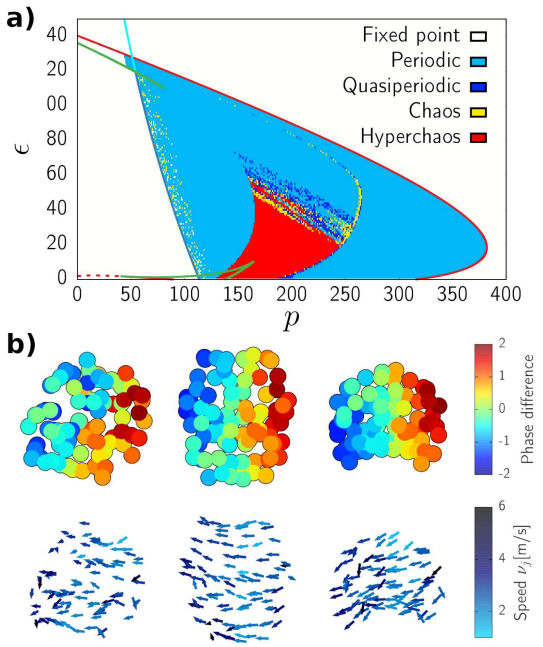

Fig. 1. (a) Bifurcation diagram of the system as obtained from the bifurcation analysis (continuous lines) and numerical simulations (colored regions). Parameters ϵ and p correspond to the coupling strength and external subcortical input respectively. (b) Travelling waves in the large-scale brain model. The top figures show the phase difference between brain regions (three different views of same snapshot). The bottom panels show the direction and speed of propagation.

[1] B. H. Jansen and V. G. Rit, Biol. Cybern. **73**, 357–366 (1995).

[2] L. M. Pecora and T. L. Carroll, Phys. Rev. Lett. **80**, 2109 (1998).

[3] E. Montbri, D. Paz, and A. Roxin, Phys. Rev. X **5**, 021028 (2015).

Diffusion in a two-dimensional chiral fluid

Miguel Ángel López-Castaño[1], Alejandro Márquez Seco[1], Alicia Márquez Seco[1], Álvaro Rodríguez-Rivas[3] and Francisco Vega Reyes[1,3]

[1]Departamento de Física, Universidad de Extremadura, 06071, Badajoz, Spain

[2]Department of Physical, Chemical and Natural Systems, Pablo de Olavide University, 41013, Sevilla, Spain

[3] Instituto de Computación Científica Avanzada (ICCAEx), Universidad de Extremadura, 06071, Badajoz, Spain

Active matter typically sustains a steady energy exchange between its constituents and the surrounding medium. This yields a rich and complex non-equilibrium phenomenology; for instance, collective motion may emerge, sometimes with peculiar features such as chirality [1, 2]. We analyze in this experimental work the diffusive properties of a two-dimensional active chiral fluid composed of air-fluidized spinners. In particular, we show that diffusion is an antisymmetric tensor, the off-diagonal elements corresponding to a new diffusion coefficient that we term here as *odd diffusion*.

$$\mathcal{D} = \begin{bmatrix} D & -D^{\mathrm{odd}} \\ D^{\mathrm{odd}} & D \end{bmatrix} \tag{1}$$

We also show that the control parameter is the fluid flow (global) vorticity $\overline{\omega}$, that appears as a consequence of chirality, $\omega = (1/2)\epsilon_{ij}\partial_i u_j$, where ϵ_{ij} is the 2D Levi-Civita symbol and $\mathbf{u}$ is the fluid flow field. As we can see, this parameter governs the evolution of diffusive coefficients in the fluid. Very surprisingly, the same fluid can be (with the same particle density) either super-diffusive, sub-diffusive or diffusive.

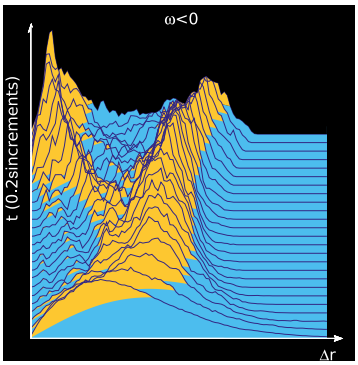

Fig. 1. This figure shows the time evolution of the distribution function of the mean squared displacements, which governs diffusive behavior in the chiral fluid. In orange and blue, regions above and under a gaussian distribution, respectively. Packing fraction $\phi = 0.45$, global vorticity $\overline{\omega}$ is negative in this series of experiments.

Strikingly as well, and for steady chiral flow, diffusion in the fluid slowly ages, as the distribution function of the mean squared displacements vs. time shows in Figure 1.

We demonstrate that D^{odd} is indeed experimentally measurable (we use a modified Green-Kubo relationship). Moreover, the diffusion coefficients D, D^{odd} data vs. the control parameter $\overline{\omega}$ collapse for all densities, as universal curves, as the analysis of experimental data yields in Figure 2.

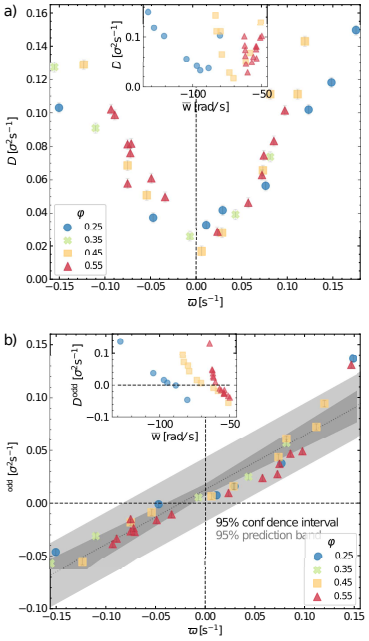

Fig. 2. Diffusion coefficients vs. global mean vorticity $\overline{\omega}$ for several experiment with different densities (packing fraction ϕ) (each denoted with a different symbol and color, see figure legend) (a) Diffusion coefficient D. (b) Odd diffusion D^{odd} coefficient

The experimental set-up, the rich diffusive behavior and the consequences for a number of important and complex biological processes will be discussed in more detail at the conference.

We acknowledge funding from the Government of Spain (AEI) and Junta de Extremadura through projects No. PID2020-116567GB-C22) and GR21091 respectively. A.R.-R. also acknowledges financial support from Conserjera de Transformacin Econmica, Industria, Conocimiento y Universidades (Junta de Andalucía) through post-doctoral grant no. DC 00316 (PAIDI 2020), co-funded by the EU Fondo Social Europeo (FSE).

[1] M. A. López-Castaño and A. Márquez Seco and A. Márquez Seco and A. Rodríguez-Rivas and F. Vega Reyes (2022), Chirality transitions in a system of active flat spinners. Preprint: arXiv:2105.02850.

[2] Hargus, C., Epstein, J. M., & Mandadapu, K. K. (2021). Odd Diffusivity of Chiral Random Motion. Physical Review Letters, 127(17), 178001

The Brevity Law as a Scaling Law, and the Origin of Zipf's Law for Word Frequencies as a Mixture from Different Lengths

Isabel Serra[1] and Álvaro Corral[1,2,3]
[1]Centre de Recerca Matemàtica, Edifici C, Campus Bellaterra, E-08193 Barcelona, Spain
[2]Departament de Matemàtiques, Facultat de Ciències, Universitat Autònoma de Barcelona, E-08193 Barcelona, Spain
[3]Complexity Science Hub Vienna, Josefstädter Straβe 39, 1080 Vienna, Austria

An important body of quantitative linguistics is constituted by a series of statistical laws about language usage. Despite the importance of these linguistic laws, some of them are poorly formulated, and, more importantly, there is no unified framework that encompasses all them. This communication presents a new perspective to establish a connection between different statistical linguistic laws.

Characterizing each word (word type) by two random variables – length ℓ (in number of characters) and absolute frequency n – we show that the corresponding bivariate joint probability distribution shows a rich and precise phenomenology, with the type-length and the type-frequency distributions, $f(\ell)$ and $f(n)$, as its two marginals, and the conditional distribution of frequency at fixed length $f(n|\ell)$ providing a clear formulation for the brevity-frequency phenomenon.

The type-length distribution turns out to be well fitted by a gamma distribution (much better than with the previously proposed lognormal), and the conditional frequency distributions at fixed length display power-law-decay behavior with a fixed exponent a $\alpha \simeq 1.4$ and a characteristic-frequency crossover that scales as an inverse power $\delta \simeq 2.8$ of length, which implies the fulfillment of a scaling law analogous to those found in the thermodynamics of critical phenomena.

As a by-product, we find a possible model-free explanation for the origin of Zipfs law, which should arise as a mixture of conditional frequency distributions governed by the crossover length-dependent frequency.

We explore this issue using all English books in the Standardized Project Gutenberg Corpus [1], which comprises more than 40,000 books in English, with a total number of tokens equal to 2,016,391,406 and a total number of types of 2,268,043. We disregard types with absolute frequency $n < 10$. Figures 1 shows the marginal distribution of frequency n.

Indeed, a statistical analysis shows that the conditional distributions $f(n|\ell)$ can be described in terms of a scaling law, $f(n|\ell) = \ell^{\delta\alpha} g(\ell^{\delta} n)$, for $5 \leq \ell \leq 14$, with the scaling function verifying $g(x) \propto 1/x^{\alpha}$ for small arguments x, see Fig. 2. This scaling law constitutes a new quantitative version of the brevity law in language. The marginal distribution of frequencies arises from the mixture of conditional distributions, $f(n) = \int_{\ell_1}^{\ell_2} f(n|\ell) f(\ell) d\ell$. Substituting the scaling law, and assuming a contant $f(\ell)$ we obtain, for small n, $f(n) \propto 1/n^{\alpha}$. However, for large n, we obtain $f(n) \propto 1/n^{\alpha+\delta^{-1}}$. Substituting the empirical values of α and δ we get a value of 1.79, not far from the ideal Zipf's value (around 2 ± 0.2).

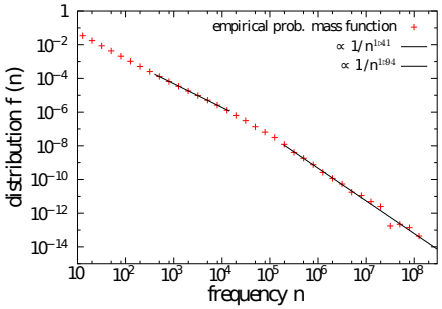

Fig. 1. Marginal probability mass function $f(n)$ of type frequency. The power-law fits yield exponents $\alpha = 1.41$ and $\beta = 1.94$.

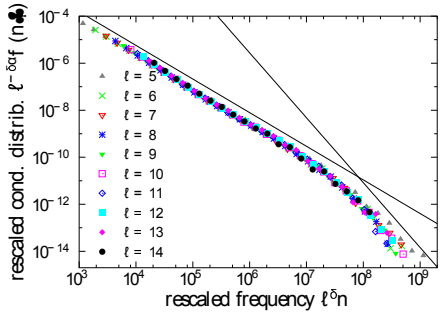

Fig. 2. Rescaled $f(n|\ell)$ as a function of rescaled frequency n for different values of word length ℓ. The good data collapse is the signature of the fulfiment os a scaling law. Two decreasing power laws with exponents 1.43 and 2.76 are shown as straight lines, for comparison.

The main part of these results have been published in Ref. [2].

[1] M. Gerlach and F. Font-Clos, Entropy **22**, 126 (2020).

[2] A. Corral and I. Serra, Entropy **22**, 224 (2020).

Chimpanzees organize their social relationships like humans

D. Escribano,[1] V. Doldán-Martelli,[1] K.A. Cronin,[2] D.B.M. Haun,[3] E.J.C. van Leeuwen,[4] J.A. Cuesta,[1,5] and A. Sánchez[1,5]

[1]Grupo Interdisciplinar de Sistemas Complejos (GISC), Universidad Carlos III de Madrid, 28911 Leganés, Spain
[2]Lester E. Fisher Center for the Study and Conservation of Apes, Lincoln Park Zoo, 60614 Chicago, IL, USA
[3]Max Planck Institute for Evolutionary Anthropology, 04103 Leipzig, Germany
[4]Behavioural Ecology and Ecophysiology Group, Department of Biology, University of Antwerp, 2610 Wilrijk, Belgium
[5]Instituto de Biocomputación y Física de Sistemas Complejos (BIFI), Universidad de Zaragoza, 50018 Zaragoza, Spain

Numerous studies reveal that the way humans organize their social relationships exhibits distinctive organizational patterns, which are related to each person's cognitive capacity. As this capacity is not infinite but limited, there is a restriction on the number of relationships an individual can maintain at the same time (famously called Dunbar's number and estimated to be of the order of 150). Additionally, personal networks show a layered structure where each layer corresponds to relationships of different emotional closeness. The size of the layers (typically 5, 15, 50 and 150) exhibits scaling and the intensity of its associated links decreases outwards.

To formalize mathematically the connection between the layered structure of personal networks and the variable effort required for each relationship, a simple resource allocation model was proposed [1]. This model is based on two widely accepted assumptions: the capacity that an individual can invest in social relationships is finite, and different intensities of relationships carry a different cost. A maximum entropy approach including these two constraints yields a one-parameter probability distribution describing the expectation that a given relationship lies in a specific layer, which is in very good agreement with real life observations. In fact, the theory even predicted that when the cognitive capability is very large or the possible friends are only a few, all of them should be in the first layer of very good friends (so called inverted regime), and this was empirically verified *a posteriori*, providing much support for the model.

In spite of this success, this model in [1] treats relationships as discrete categories, and some features that may be used to determine the strength of a relationship, such as time spent together, do not fit this description. For this reason, the original model has been recently extended [2] to study the structure of social relationships when the resources invested in them take continuous values. The probability distribution of this new approach is governed only by one parameter, called η, which is the equivalent in the continuous case to the scaling ratio between consecutive layers in the discrete one. This parameter presents a typical value of $\eta \sim 6$ for several real-life datasets [2], indicating a characteristic feature on how humans organize their social relationships.

By means of this continuous formalism, here we show for the first time evidence that a similar organization of relationships arises in non-human primates, namely in chimpanzees. We use grooming data extracted from over four years of observations of four groups of chimpanzees living in the Chimfunshi Wildlife Orphanage in Zambia, taking grooming as a proxy of the effort devoted to pairwise relationships. Our results confirm that the time chimpanzees devote to grooming other individuals is generally well described by the continuous probability distribution predicted by the model. Thus, every chimpanzee is characterized by a value of the η parameter, and much as in the case of human relationships, typical values of η are close to 6. Furthermore, our results show that the group size influences the organization of their social relationships. In groups consisting of about 10 chimpanzees, the parameter η has a value closer to 0 for most individuals. This indicates an excess of strong relationships compared to the standard situation described by Dunbar's circles—the kind of behavior identified in [1] as the inverted regime, and arising in the same circumstances. In contrast, for larger groups of tenths of individuals, the normal hierarchical structure of the personal network emerges again, and the mean value of the parameter is comparable to the result obtained for humans at the population level.

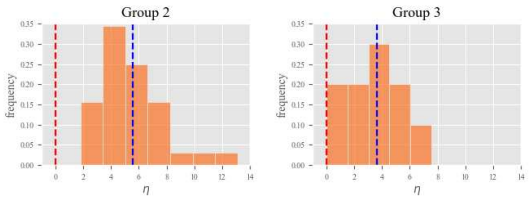

Fig. 1. Histograms of values of η found in a large group (left, $N = 32$) and in a small group (right, $N = 10$) of Chimfunshi chimpanzees. The red dashed line represents the value $\eta = 0$ and the blue one the mean value for each group.

The conclusions of our analysis are twofold: On the one hand, the results provide an indirect confirmation that grooming is indeed indicative of the closeness of a relationship, i.e., it is akin to a measurement of "friendship" among chimpanzees. On the other hand, our analyses confirm the existence of similar social signatures for both humans and chimpanzees, and reveal that they both arise as a consequence of allocating a limited amount of some resource (cognitive capacity) into items (social relationships) with different costs. Therefore, these results should be fairly general and verifiable with data from many other animal species.

[1] I. Tamarit, J.A. Cuesta, R.I.M. Dunbar, and A. Snchez. Cognitive resource allocation determines the organization of personal networks. Proc. Nat'l. Acad. Sci. USA **115**, 8316-8321 (2018).

[2] I. Tamarit, A. Snchez, and J.A. Cuesta. Beyond Dunbar circles: a continuous description of social relationships and resource allocation. Sci. Rep. **12**, 2287 (2022).

Can Statistical Physics Help You Win an Olympic Medal...in Badminton?

Javier Galeano[1], Miguel-Ángel Gomez[2], Fernando Rivas[3] and Javier M. Buldú[4]
[1]Grupo de Sistemas Complejos,UPM
[2]Departamento de CC. Sociales de la Actividad Física, del Deporte y del Ocio, INEF,UPM
[3] Federación Española de Bádminton
[4] Grupo de Sistemas Complejos and GISC, Universidad Rey Juan Carlos

Badminton is one of the most popular sports in the world, with more than 200 million players [1]. The factors for winning a point in badminton are multiple, revealing the complexity of the sport [2]. In particular, badminton is a high-speed sport characterized by high-intensity actions interspersed by periods of effort and pause. Research has widely described the statistical aspects of the temporal structure of badminton matches [1, 3]: (i) the match duration is about 4565 minutes; (ii) the average duration of a point is approximately nine seconds; (iii) the number of strokes per point is about 810. Additionally, other studies have focused their attention on understanding the differences between these parameters when considering the context, such as gender, modalities, or situational variables (number of sets, intervals of play, quality of opponent, etc.) [4, 5].

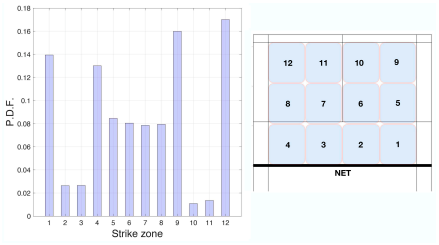

Fig. 1. In the left plot, we have the probability distribution function (PDF) showing the percentages of strokes performed in the 12 predefined zones of the court (see the right plot for the location of each zone).

The aim of the current study [6] was twofold: (i) to investigate the distribution of the strike positions of badminton players while quantifying the corresponding standard entropy and using an alternative metric (spatial entropy) related to winning and losing points and random positions; and (ii) to evaluate the standard entropy of the receiving positions.

With the datasets of 259 badminton matches, we focused on the positions of players strokes and the outcome of each point. First, we identified those regions of the court from which hits were most likely to be struck. Second, we computed the standard entropy of stroke positions, and then the spatial entropy, which also considers the order and clustering of the hitting locations in a two-dimensional Euclidean

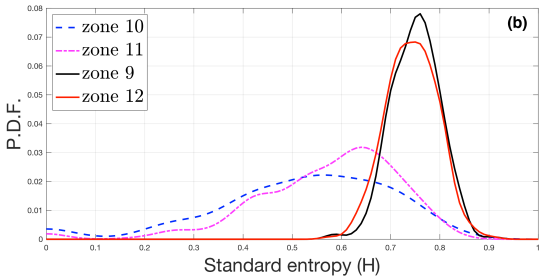

Fig. 2. PDF of the receiving entropy for the most different zones: 9, 10, 11, 12.

space. Both entropy quantifiers revealed high uncertainty in the striking position; however, specific court locations (i.e., the four corners) are preferred over the rest (see Figure 1). When the outcome of each point was taken into account, we observed that the hitting patterns with lower entropy were associated with higher probabilities of winning points. On the contrary, players striking from more random positions were more prone to losing the points (see Fig. 2).

[1] Phomsoupha, M. and Laffaye, G. *The Science of Badminton: Game Characteristics, Anthropometry, Physiology, Visual Fitness and Biomechanics*, Sport. Med. **45**, 473 (2015).

[2] Cohen, C., Texier, B.D., Qur, D., and Clanet, C. *The physics of badminton* New J. Phys. **17** (2015).

[3] Torres-Luque, G.; Fernndez-Garca, .I.; Blanca-Torres, J.C.; Kondric, M.; Cabello-Manrique, D. *Statistical differences in set analysis in badminton at the RIO 2016 Olympic games* Front. Psychol. **10**, (2019).

[4] Gomez, M..; Rivas, F.; Connor, J.D.; Leicht, A.S.*Performance differences of temporal parameters and point outcome between elite mens and womens badminton players according to match-related contexts.* Int. J. Environ. Res. Public Health 2019, **16**, 18, (2019)

[5] Gomez, M.A.; Leicht, A.S.; Rivas, F.; Furley, P. *Long rallies and next rally performances in elite mens and womens badminton.* PLoS ONE **15**, 1, (2020).

[6] Galeano, J.; Gomez, M-A.; Rivas, F.; Buld, J.M. *Entropy of Badminton Strike Positions*. Entropy, **1** (2021).

Tuning the Dynamics of Life: One Chemical Moiety at a Time

J.G. Vilhena[1,2]
[1] Universidad Autónoma de Madrid
[2]IFIMAC - Condensed Matter Physics Center
guilhermevilhena@gmail.com

Life is inherently a non-equilibrium process whereby *the jiggling and wiggling of atoms*, functional building blocks (nucleic-acids and proteins) realize complex tasks in a synchronized manner far exceeding the ones anticipated from their structure alone. In this talk, I selected two examples that portray how bio-molecular vibrations can be harnessed in different biological processes. Firstly we show how a single oxygen atom differentiating dsDNA from dsRNA can completely alter their unwinding dynamics (pivotal in DNA/cell replication). Then, we unveil how DNA sequence is not only a chemical code but also a physical one, thus capable regulating different biological processes. [1, 2, 3, 4, 5, 6] In the second part of the talk, we focus on electron-transport processes occurring in proteins [8, 9, 10, 11, 12, 13] pivotal in several biological processes (photosynthesis, respiration,). In particular, we show how single point mutations provide the means to finely regulate molecular vibrations of the protein matrix surrounding the active redox-active site, thus giving the means to control/regulate charge-transport processes at single-protein level. Overall, these results showcase how vibrations at the molecular level are inextricably connected to different biological functions and conversely how such processes may be tuned/regulated through carefully designed molecular substitutions.

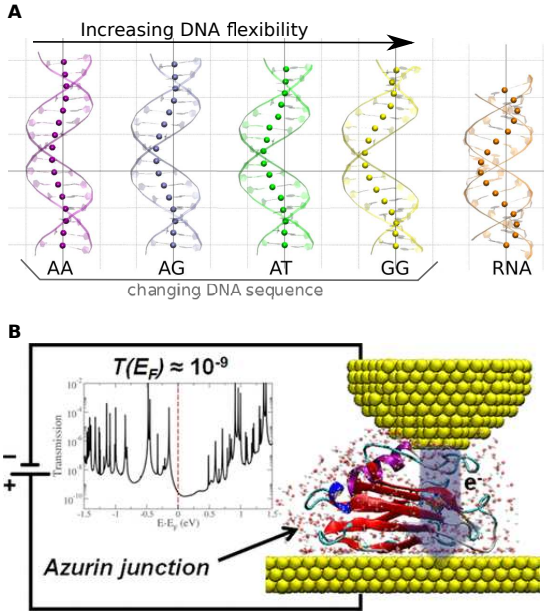

Fig. 1. Tuning the mechanics of DNA and single proteins. **A)** Schematic representation of how DNA sequence modulates structure and consequently its flexibility. **B)** Model of a bio-molecular junctions whose conductance properties can be tweaked via single point mutations.

[1] Proceedings of the National Academy of Sciences **114** (27), 7049 (2017).

[2] Physical Review Letters **122** (4), 048102 (2019).

[3] Nanoscale **11**, 21471 (2019).

[4] Nucleic Acids Research **48** (9), 5024 (2020).

[5] Nucleic Acids Research **48** (22), 12917 (2020).

[6] ACS Sensors **6** (2), 553 (2021).

[7] Quarterly Reviews of Biophysics **54**, E8 (2021).

[8] Journal of the American Chemical Society **139**, 15337 (2017).

[9] Physical Chemistry Chemical Physics **20**, 30392 (2018).

[10] Biomolecules **9**, 506 (2019).

[11] Biomolecules **9**, 611(2019).

[12] Journal of Physical Chemistry C **125** , 1693 (2021)

[13] Applied Sciences **11**, 3732 (2021)

Jamming of Hard-Spheres through the Lens of Constrained Optimization

Claudia Artiaco[1], Rafael Díaz Hernández Rojas[2], Giorgio Parisi[2,3], and Federico Ricci-Tersenghi[2,3]
[1]Department of Physics, KTH Royal Institute of Technology, Stockholm 106 91, Sweden
[2]Dipartimento di Fisica, Sapienza Università di Roma, Piazzale Aldo Moro 5, 00185 Rome, Italy
[3]INFN, Sezione di Roma1, and CNR-Nanotec, unità di Roma, Piazzale Aldo Moro 5, 00185, Rome, Italy

It has recently been discovered that jamming criticality of spheres-based models defines a broad universality class. Yet, computational techniques to produce jammed packings are still somewhat limited. Moreover, most of available methods are based on energy minimization algorithms, and are therefore designed for soft-spheres configurations. Naturally, generating a critical jammed packing of strictly hard-spheres (HS) is more complicated due to the singular interaction between such type of particles.

Here, we present the CALiPPSO algorithm[1], that allows to accurately reach the jamming point of HS configurations through a series of linear optimization problems. Within our approach, the exact, non-convex optimization problem associated to HS jamming is replaced by a sequence of simpler linear problems. Nevertheless, in all cases the non-overlapping constraints imposed by the HS interaction are strictly satisfied.

Importantly, we prove that upon convergence our algorithm produces a stable, well defined jammed state of HS, that corresponds to a (possibly local) optimum of the exact problem. We also show that our method allows to easily construct the full network of contact forces from the Lagrange multipliers associated to the non-overlapping constraints.

This new framework to tackle the jamming problem of HS as a constrained optimization problem also leads to a proxy of the entropy function of HS configurations. Given that entropy is the relevant thermodynamic potential for this type of systems, our approach yields a more precise description of the free-energy landscape. We further exploit this analogy to explore how the vibrational modes of HS can be studied using a cost function derived from the exact jamming optimization problem.

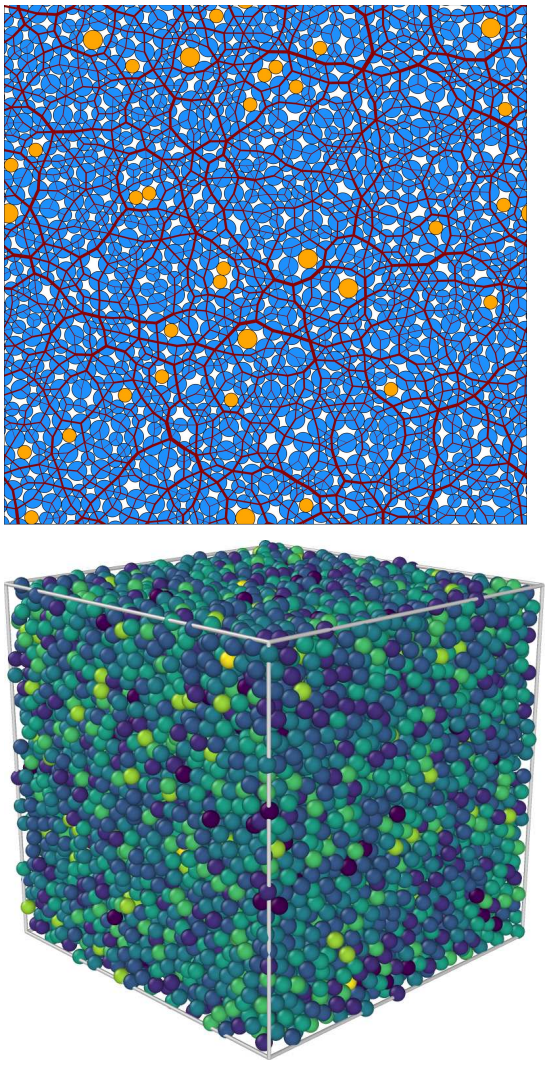

Fig. 1. Top panel: Bidisperse jammed packing of $N = 1024$ disks, showing the full network of contacts and rattlers highlighted in orange. The forces magnitude are indicated by the thickness of the lines. Bottom panel: Monodisperse jammed packing of $N = 16384$ spheres, coloured according to their number of contacts. Lighter particles have more contacts, while the darkest are rattlers, which do not have any force bearing contacts.

[1] C. Artiaco, R. Díaz Hernández Rojas, G. Parisi and F. Ricci-Tersenghi, *CALiPPSO: A linear programming algorithm for jamming hard spheres*, arXiv (2022).

Kinetic roughening of coffee-ring interfaces

B. G. Barreales[1], J. J. Meléndez[1,2], R. Cuerno[3], and J. J. Ruiz-Lorenzo[1,2,4]
[1]Departamento de Física, Universidad de Extremadura, 06006 Badajoz, Spain
[2]Instituto de Computación Científica Avanzada de Extremadura (ICCAEx), Universidad de Extremadura, 06006 Badajoz, Spain
[3] Departamento de Matemáticas and Grupo Interdisciplinar de Sistemas Complejos (GISC), Universidad Carlos III de Madrid, 28911 Leganés, Spain
[4] Instituto de Biocomputación y Física de los Sistemas Complejos (BIFI), 50018 Zaragoza, Spain

Consider a drop of a liquid with suspended particles which evaporates on a solid substrate. During this process, the suspended solid particles are dragged by capillary flow to the edges of the drop, giving rise to a characteristic ring-like pattern. We have all observed this phenomenon in the coffee blots created at the bottom surface of the cup when there is some coffee left on it; this is why it is called the coffee-ring effect [1]. Formed patterns are complex and may be studied in the context of critical phenomena and universality classes. Here, we have studied the coffee-ring effect as a non-equilibrium growth process.

As shown in [1], the ring-like pattern can be sensitively altered by changes in the morphology of the suspended particles. In particular, when their eccentricity is large enough, the ring disappears. To mimic this effect, we have used a discrete model of patchy colloids [2, 3] with strong and weak bonds, that recreate the anisotropic colloids. The parameter $r_{\rm AB}$ controls the affinity of two distinct patches (A and B), and the morphology of the aggregates depends on this ratio, as shown in Fig. 1. Thus, the model reproduces the different growth behaviours depending on particle shape: large values of $r_{\rm AB}$ corresponds to spherical colloids and decreasing values of $r_{\rm AB}$ to increasing colloids eccentricities.

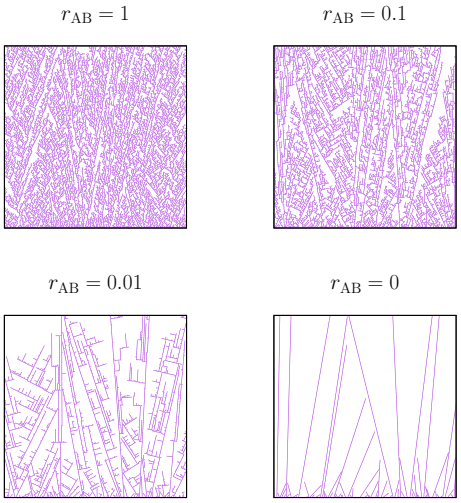

Fig. 1. Morphology of the aggregates calculated for several $r_{\rm AB}$ values (i.e., colloid eccentricities).

We have performed extensive numerical simulations for $r_{\rm AB} \in [0, 1]$. We appreciate a distinctive behaviour of the system for $r_{\rm AB} = 0$, when only AA bonds form. This means that secondary branches do not occur; as a result, the front stops when some branches reach the system boundary.

By studying the surface roughness and the correlation length for different values of $r_{\rm AB}$, we have computed the critical exponents characterising front fluctuations for coffee-ring aggregates. Our results (see Table 1) seem compatible with the quenched Kardar-Parisi-Zhang (QKPZ) universality class exponents $\beta = 0.63$, $z = 1.01$ and $\alpha = 0.63$.

$r_{\rm AB}$	β	z	α
1	0.55(2)	1.06(6)	0.64(4)
0.1	0.64(2)	1.05(11)	0.69(6)
0.01	0.691(14)	1.00(4)	0.89(4)
0.001	0.690(14)	1.13(12)	0.72(7)
0.0001	0.609(10)	1.0(3)	0.74(18)

Table 1. Critical exponents the evaporating drop. Into brackets, the errors estimated by the jackknife procedure.

The height-difference correlation function $C_2(r,t)$ shows anomalous scaling behavior. The collapse of the correlation function using the QKPZ exponents (Fig. 2) fits to $x^{-2\alpha'}$ for $x \ll 1$, with $x = r/t^{1/z}$ and $\alpha' = \alpha - \alpha_{\rm loc} \neq 0$. This allows us to measure the $\alpha_{\rm loc}$ exponent. The nature of the anomalous scaling may be clarified by the structure factors $S(q,t)$ analysis. This shows a systematic shift upwards with time and scales with the wave vector as $S(q,t) \sim q^{-(2\alpha_{\rm loc}+1)}$, which evidences intrinsic anomalous scaling.

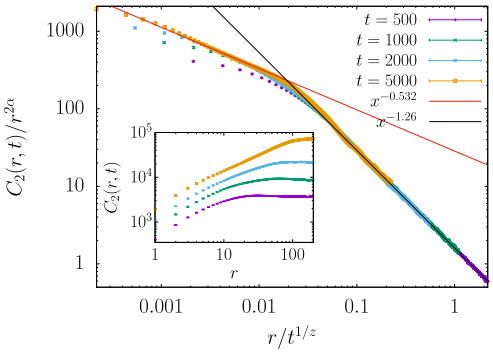

Fig. 2. Collapse of $C_2(r,t)$ for $r_{\rm AB} = 0.001$ at different times. Solid lines are the fits for $x \leq 0.01$ and $x \geq 0.1$ at $t = 5000$. Inset: $C_2(r,t)$ vs. r plot.

[1] P. J. Yunker, T. Still, M. A. Lohr, and A. G. Yodh, Nature **476**, 308 (2011).

[2] C. S. Dias, N. A. Araújo, and M. M. Telo Da Gama, Eur. Phys. Lett. **107**, 56002 (2014).

[3] C. S. Dias, P. J. Yunker, A. G. Yodh, N. A. Araújo, and M. M. Telo Da Gama, Soft Matter **14**, 1903 (2018).

Learning inter-particle interactions and active forces from particle trajectories

Miguel Ruiz-Garcia[1], Miguel Barriuso Gutierrez[2], Lachlan Alexander[3], Dirk Aarts[3], Luca Ghiringhelli[4], and Chantal Valeriani[2]
[1]Universidad Carlos III de Madrid
[2]Universidad Complutense de Madrid
[3]Oxford University
[4]NOMAD Laboratory at the Fritz Haber Institute and Humboldt University

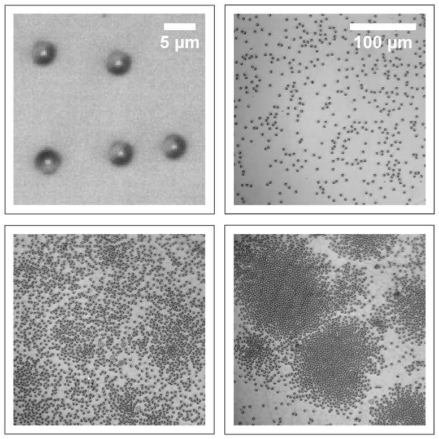

Fig. 1. Motility-induced phase separation in experiment. Panel (a) shows electrophoretic Janus particles when an electric field (E) is applied. They rise to maximise the magnitude of their induced dipoles. Panels (b), (c) and (d) display snapshots of systems in different conditions. Panel (b) shows a system which is too dilute to phase separate ($\phi = 0.10$, $E = 727$). Panel (c) shows a system with an activity that is too low to phase separate ($\phi = 0.29$, $E = 181$). Panel (c) shows a system which phase separates ($\phi = 0.29$, , $E = 363$).

Active particles exhibit complex collective phenomena that emerges from their local interactions.To model such systems, one would usually propose some inter-particle interactions and active forces, simulate the dynamics of a system with many individual elements and finally compare the results with experiments via, for instance, an order parameter. However, not only choosing one order parameter might introduce a bias, but also it is difficult to assess how well the model describes the experimental system. In our work we suggest a completely different approach. What if we could learn the inter-particle interactions and the active forces directly from the data? We propose a machine learning scheme that optimizes the interactions between particles and the active forces to predict the correct particle dynamics. After training the network, one can extract both passive and active interactions between particles and use them (analytically or numerically) to make new predictions or unravel dynamical features of experiments of active particles.

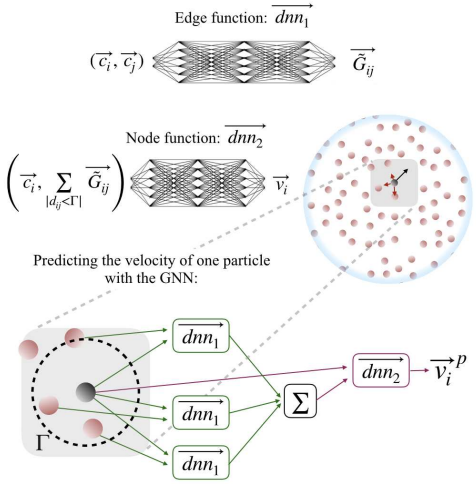

Fig. 2. Predicting the dynamics of active particles with a Graph Neural Network (GNN) while learning the functional form of the inter-particle interactions and the active forces. Our GNN is formed by a node function $\vec{dnn}_1$ and an edge function $\vec{dnn}_2$. Both, $\vec{dnn}_1$ and $\vec{dnn}_2$, are deep neural networks that take the particle coordinates $\vec{c_i}$, the diagrams shown in the figure are just for visualization. After training, the output of $\vec{dnn}_2$, $\vec{v_i}^p$, will be the predicted velocity for particle i. The bottom diagram shows how the GNN is applied to one particle. Applying the GNN to all particles in the system (the graph) provides all the predicted velocities. During the learning process the internal parameters of $\vec{dnn}_1$ and $\vec{dnn}_2$ are optimized so that all the $\vec{v_i}^p$ resemble the real velocities and we can extract the forces present in the system.

How genetic parasites persist despite the purge of natural selection

Jaime Iranzo[1,2], José A. Cuesta[2,3,4], Susanna Manrubia[4,5] and Eugene V. Koonin[6]
[1]Centro de Biotecnología y Genómica de Plantas, UPM-INIA, Pozuelo de Alarcón, Madrid, Spain.
[2]Instituto de Biocomputación y Física de Sistemas Complejos (BIFI), Universidad de Zaragoza, Spain.
[3]Departamento de Matemáticas, Universidad Carlos III de Madrid, Leganés, Madrid, Spain.
[4]Grupo Interdisciplinar de Sistemas Complejos (GISC), Madrid, Spain
[5]Centro Nacional de Biotecnología (CSIC), Madrid, Spain.
[6]National Center for Biotechnology Information (NCBI, NLM, NIH), Bethesda, USA.

Mobile genetic elements, such as transposons, plasmids, and viruses, are ubiquitous in cellular life forms. Although the selfish nature of these genetic elements is undeniable, the actual cost that they impose on their host and the mechanisms by which they counteract natural selection remain unclear. We combined mathematical models and comparative genomics to disentangle the roles of selection, horizontal gene transfer, gene duplication, and gene loss on the spread and persistence of mobile genetic elements (Figure 1). By quantifying the mean contribution of transposons, conjugative plasmids, prophages, and toxin-antitoxin modules to the fitness of microbial hosts, we provide evidence that these genetic elements are deleterious at evolutionary timescales [1]. Moreover, the transfer rates experienced by selfish genetic elements exceed the minimum rates required for their long-term survival (Figure 2), which fully characterizes these elements as parasites [2].

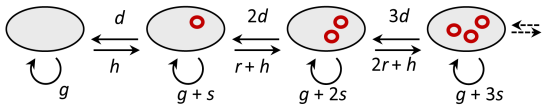

Fig. 1. Copy number dynamics of a family of mobile genetic elements in a population of hosts. Gray ovals represent host genomes, small circles indicate the parasite copy number. Mobile genetic elements are subject to gene duplications at rate r (per copy), loss at rate d (per copy), horizontal transfer at rate h, and host-level selection, with selection coefficient s. Adapted from [2].

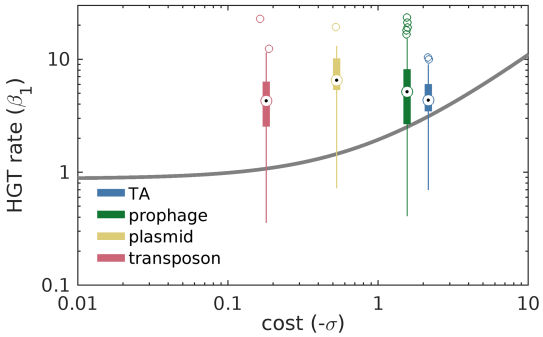

Fig. 2. Critical value of the intra-population horizontal gene transfer (HGT) rate required for long-term persistence of genetic parasites, as a function of the parasite cost. Both the HGT rate and the fitness cost are normalized by the loss rate, such that $\beta = h/d$ and $\sigma = s/d$. The boxplots indicate the empirical HGT rates of different classes of mobile genetic elements inferred from comparative genomics. Adapted from [2].

[1] J. Iranzo, J.A. Cuesta, S. Manrubia, M.I. Katsnelson and E.V. Koonin, *Disentangling the effects of selection and loss bias on gene dynamics*, PNAS **114**, E5626 (2017).

[2] J. Iranzo and E.V. Koonin, *How genetic parasites persist despite the purge of natural selection*, EPL **122**, E5626 (2018).

Validación de un modelo Lagrangiano para el transporte de macroplásticos usando palillos de batea en la Ría de Arousa

S.Cloux[1], S. Allen-Perkins[2], H. de Pablo[3] D. Garaboa-Paz[1] P. Montero[2] and V. Pérez-Muuzuri[1]
[1]CRETUS, Grupo de Física no Lineal, Facultad de Física, Universidad de Santiago de Compostela.
[2]INTECMAR, Instituto Tecnolóxico para o Control do Medio Mariño de Galicia, Vilagarcía de Arousa.
[3]MARETEC, Instituto Superior Técnico, Universidade de Lisboa, Portugal

El crecimiento poblacional en todo el mundo y la mala gestión de los residuos plásticos hacen que estos cuerpos lleguen a los mares y océanos, convirtiéndose en un problema mundial de grandes dimensiones [1]. Una vez que los plásticos llegan a alta mar comienzan un largo periodo de degradación, pasando de un estado macro (plásticos cuyo diámetro es superior a 0,5 cm) a un estado micro (diámetro inferior a 0,5 cm). Los microplásticos se extienden por los océanos, entrando en la cadena alimentaria de las especies marinas y, posteriormente, en la de los seres humanos. Por lo tanto, es importante detener el problema en la macroescala. En este trabajo se valida un modelo computacional lagrangiano (www.mohid.com) que ha sido desarrollado recientemente para seguir el movimiento de los macroplásticos en los mares y océénos. Esta validación se realiza a escala regional, en la Ría de Arousa [2], una de las rás más importantes para el cultivo del mejillón en el noroeste de Espaa. Durante el cultivo de mejillones en bateas, se liberan un tipo de palillos de plástico flotantes.

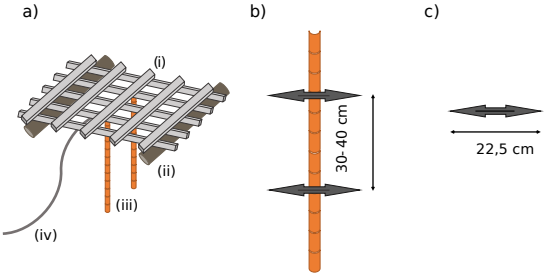

Fig. 1. Esquema de la dispoción de las bateas para el cultivo de mejillón. a) Muestra la estructura flotante de madera (i,ii), las cuerdas donde se cultivan los mejillones (iii) y el anclaje al fondo (iv); b) muestra la disposición vertical de los palillos a lo largo de la cuerda y c) las dimensiones del palillo.

En este estudio [3] se han evaluado estos palillos como trazadores lagrangianos para así comparar los resultados de acumulación del modelo con los datos de acumulación recogidos en las playas gallegas. De los 23 segmentos segmentos de playa inicialmente muestreados, nos quedamos con los contajes en 18 zonas representativas repartidas entre la ría y la Illa de Arousa (ver Figura 2). Inicialmente, se comprobó la influencia del viento en la distribución espacial de las acumulaciones dadas por el modelo. Por otro lado, se encontraron resultados similares para las tendencias

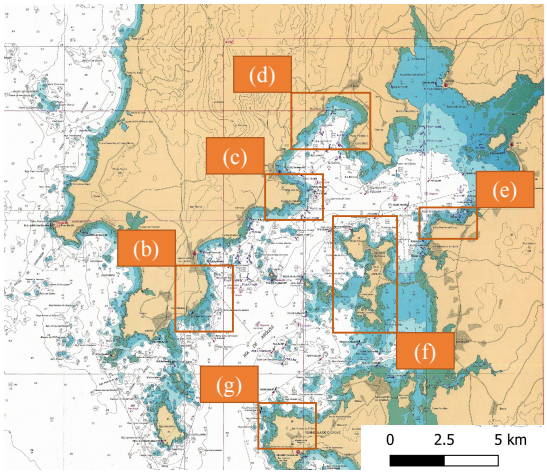

Fig. 2. Carta de navegación donde se sealan las 6 areas de estudio en las que se encuentran los segmentos de costan que se van a estudiar.

de acumulación a lo largo de todo el periodo total con respecto a los datos recogidos en playa, mientras que la representación mensual presenta algunas discrepancias. Estas diferencias pueden atribuirse a situaciones sinópticas particulares, a la mala reproducción de la línea de costa o a la propia orientación de la zona de estudio con respecto a la zona intermareal con respecto a la dinámica intermareal.

[1] Rangel-Buitrago, Nelson and Williams, Allan and Costa, Monica F and de Jonge, Victor, *Curbing the inexorable rising in marine litter: An overview*, Ocean & Coastal Management Volume 188, 2020, 105133, ISSN 0964-5691, https://doi.org/10.1016/j.ocecoaman.2020.105133.

[2] Rosón, G., Pérez, F. F., Alvarez-Salgado, X. A., Figueiras, F. G. *Variation of both thermohaline and chemical properties in an estuarine upwelling ecosystem: Ria de arousa: I. Time evolution* Estuarine, Coastal and Shelf Science, Volume 41, Issue 2, 1995, Pages 195-213, ISSN 0272-7714, https://doi.org/10.1006/ecss.1995.0061.

[3] Cloux, Sara and Allen-Perkins, Silvia and de Pablo, Hilda and Garaboa-Paz, Daniel and Montero, Pedro and Pérez-Muñuzuri, Vicente, *Validation of a Lagrangian Model for Large-Scale Macroplastic Tracer Transport Using Mussel-Peg in Nw Spain (Ría De Arousa)*, Science of Total Enviroment Volume 822, 2022, 153338, ISSN 0048-9697, https://doi.org/10.1016/j.scitotenv.2022.153338.

Inferring Generalized Lotka-Volterra parameters from longitudinal microbial data

Somaye Sheykhali[1], Juan Fernández-Gracia[1], Carlos J. Melián[1], Xabier Irigoien[2], Carlos M. Duarte[3] and Víctor M. Eguíluz[1]
[1]Instituto de Física Interdisciplinar y Sistemas Complejos IFISC (CSIC-UIB), Palma, Spain
[2]AZTI Tecnalia, Pasaia, Spain
[3]Red Sea Research Center (RSRC) and Computational Bioscience Research Center (CBRC), King Abdullah University of Science and Technology, Thuwal, Saudi Arabia

Microorganisms like bacteria, archaea and other eukaryotic cells coexist in large and complex ecosystems. Actually, microbial communities form the largest and more diverse ecosystems on the planet. The interactions among their individuals are diverse, encompassing predation, mutualism, comensalism, amensalism or competition. Measuring these interactions in direction and strength at a large scale is a challenging process that requires a combination of data analysis and modeling. Furthermore, the dynamic nature of the abundances of different species of microorganisms cannot be ignored to present a sound theory on microbial interactions.

Data. We use experimental data that reported the OTU relative abundance – operational taxonomic units, which are quasi-equivalent to a species definition – every day for a period of 20 days in 5 different experiments, with 2 replicates for each. So, for each OTU i we have the relative abundance x_i^t for each $t = 1d, \ldots, 20d$.

Model. We will assume a Generalized Lotka-Volterra model to fit the data. The choice of this model is motivated by the power-law variation in OTU abundances, which suggests a multiplicative process. Other features of longitudinal microbial relative abundance point also to this kind of model [1]. The model is defined by the following system of non-linear ordinary differential equations

$$\frac{1}{x_i}\frac{d}{dt}x_i = a_i + \sum_{j=1}^{N} \beta_{ij} x_j, \qquad (1)$$

where N is the total number of OTUs considered. They consist of a local growth term and an interaction term that encodes the effect of other OTU abundances on the self abundance of one OTU. The particular values of β_{ij} as compared to βji let us define different types of interaction (see Tab. 1).

$\beta_{ij}\beta_{ji}$	$\beta_{ij} + \beta_{ji}$	Interaction type
< 0	–	Predation
> 0	> 0	Mutualism
	< 0	Competition
0	> 0	Comensalism
	< 0	Amensalism
	0	Neutral

Table 1. Different interaction types depending on the values of the interaction matrix $\boldsymbol{\beta}$.

Parameter estimation. In order to estimate the best parameters that fit the data we minimize χ^2 assuming the model in Eq. (1). We assume that the fitting is to $\frac{1}{x_i}\frac{dx_i}{dt}$, which is approximated by $W_i^t = \frac{x_i^t - x_i^{t-1}}{x_i^{t-1}}$ from the data. The result of this minimization has the solution

$$a_i = \langle W_i \rangle - \beta_{ij}\langle x_j \rangle \quad \text{and} \quad \beta_{ij} = \Omega_{ik} C^{-1}_{kj}, \qquad (2)$$

where $\Omega_{ij} = \langle W_i x_j \rangle - \langle W_i \rangle \langle x_j \rangle$, C^{-1}_{kj} are the elements of the inverse of the covariance matrix ($C_{ij} = \langle x_i x_j \rangle - \langle x_i \rangle \langle x_j \rangle$) and the operator $\langle \cdot \rangle$ denotes the average over all time points. This fitting procedure is made in steps by adding first the interactions that reduce most χ^2 and later the best model is selected based on the AIC (Akaike information criterion). This methodology avoids overfitting of the data and produces sparse interaction matrices $\boldsymbol{\beta}$.

Results. The results of the fitting procedure let us explore the parameters that best fit the data. We find that the fixed points defined by these parameters do not correspond to feasible configurations of the model. We also explore the different types of interactions that are present in the system. As can be seen in Fig. 1 neutral and non-reciproval (commensalist and amensalist) dominate, while reciprocal interactions account for a small percentage of the interactions. These results are statistically significant when compared to randomizations of the interaction matrices.

Discussion. The fitted model reveals thus the intrinsic growth rates and the interaction network among OTUs. The estimated parameters imply fixed points that are not feasible, pointing to the fact that the dynamics might be operating around more complex attractors. The interaction types that dominate the results are non-reciprocated. These type of interactions have been mostly ignored in the modeling literature and deserve more attention for a proper description of microbial ecosystems.

Acknowledgements. We aknowledge funding from grant PID2020-114324GB-C22 funded by MCIN/AEI/10.13039/501100011033.

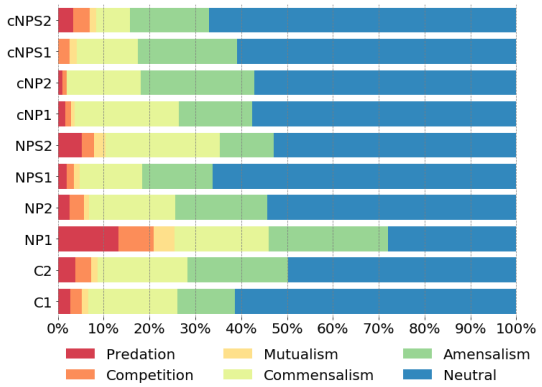

Fig. 1. Percentage of each type of interaction for the different experiments in the dataset.

[1] J. Grilli, *Macroecological laws describe variation and diversity in microbial communities*, Nat. Comm. **11**, 4743 (2020).

Selection rules and scaling regimes in active nematic turbulence

Berta Martínez-Prat[1,2], Jordi Ignés-Mullol[1,2], and Francesc Sagués[1,2]
[1]Departament de Ciència de Materials i Química Física, Universitat de Barcelona
[2]Institute of Nanoscience and Nanotechnology, Universitat de Barcelona

Active systems are composed of self-propelled entities that feature novel emergent spatiotemporal phenomena through collective interactions [1]. During the past few years it has been found that many unbound active systems self-organize into a regime called active turbulence where the self-sustained flows feature an intrinsic vortex size [2]. This has been observed in systems as diverse as bacterial baths, epithelial tissues, and active gels made of cytoskeleton proteins. In all these situations, the emergent scales are intrinsic, that is, they are not determined by external parameters such as the system size.

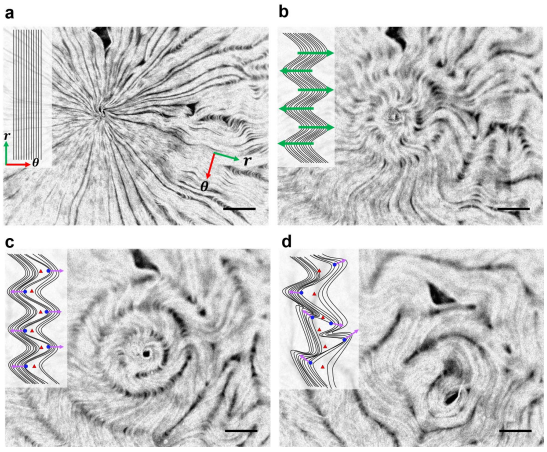

Fig. 1. Route to active turbulence in an active nematic. The radially-aligned configuration in (a) is unstable, and a cascade of defect proliferation, with well-defined wavelength, leads to the steady-state turbulence regime. Scalebars in the fluorescence micrographs are 100μm.

The pathway to such an ubiquitous state has remained elusive until recently. In our studies [3] using a kinesin/tubulin active nematic, we have revealed that the intrinsic length and time scales of active turbulence can be attributed to a pattern-forming instability, in much the same spirit as we rationalize the self-organized dissipative structures that are observed in classical convection (Rayleigh-Benard) or reaction-diffusion (Turing) systems. In our experiments, we report the onset of the turbulent regime as it develops from a well-aligned preparation of active cytoskeleton proteins (Fig. 1). The process is demonstrated to enforce a genuine pattern-selection mechanism that proceeds through a hierarchical cascade of instabilities.

We have further explored the analogy between classical and active turbulence, which has remained unclear, since, until now, experiments had not revealed whether this so-called active turbulence is characterized by universal scaling laws like in classic turbulence. Using the same active nematic material at the interface between an aqueous and an oil phase, and by analyzing the spectra of kinetic energy, we find two scaling laws that had been predicted by theory, and we reveal a new scaling law that results from the coupling between the active and the passive fluids (Fig. 2). This reveals the fundamental role of external dissipation in active turbulence.

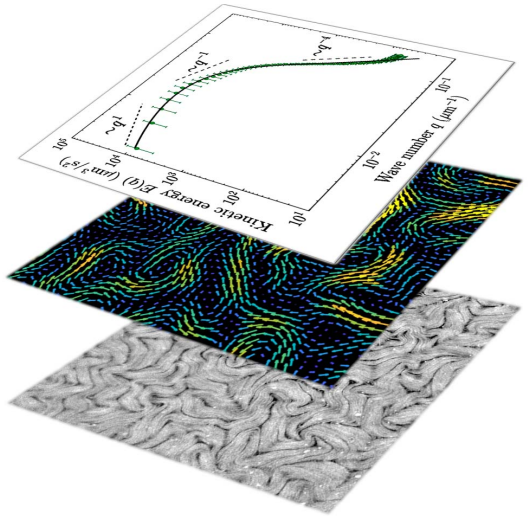

Fig. 2. Scaling regimes in active turbulence with external dissipation, as revealed from the kinetic energy spectrum extracted from the velocity distribution of an active nematic.

[1] M.C. Marchetti, *et al.*, *Hydrodynamics of soft active matter*, Rev. Mod. Phys. **85**, 1143 (2013).

[2] A. Doostmohammadi *et al.*, *Active nematic*s, Nat. Commun. **9**, 3246 (2018).

[3] B. Martínez-Prat, J. Ignés-Mullol, J. Casademunt, and F. Sagués, *Selection mechanism at the onset of active turbulence*, Nat. Phys. **15**, 362 (2019).

[4] B. Martínez-Prat, *et al.*, *Scaling Regimes of Active Turbulence with External Dissipation*, Phys. Rev. X **11**, 031065 (2021).

A geometry-induced topological phase transition in random graphs

Jasper van der Kolk[1,2], M. Ángeles Serrano[1,2,3] and Marián Boguñá[1,2]
[1]Dep. de Física de la Matèria Condensada, Universitat de Barcelona, Martí i Franquès 1, E-08028 Barcelona
[2]Universitat de Barcelona Institute of Complex Systems (UBICS), Universitat de Barcelona, Barcelona
[3]Institució Catalana de Recerca i Estudis Avançats (ICREA), Passeig Lluís Companys 23, E-08010 Barcelona

Recently, network geometry [1] has become a hot research field in network science. Latent geometric spaces underlying real complex networks provides the simplest explanation to many of their observed topological properties, including degree distribution, smallworldness, clustering, community structure, etc. The key topological property within the geometric framework is clustering—the tendency of the network to form cycles of length three—due to the triangle inequality in the latent geometry. Interestingly, in geometric models clustering undergoes a phase transition between a geometric phase with finite clustering coefficient in the thermodynamic limit and a non-geometric phase where the clustering coefficient is zero.

Despite the fact that the transition was known from our previous works [2], its nature was completely unclear. In this work [3], we analyze this transition in detail and show that it has a quite peculiar behavior. Upon mapping the network ensemble to a system of noninteracting fermions (corresponding to the links in the network) at temperature β^{-1}, we show analytically and confirm numerically that

1. there is no symmetry breaking at the critical point β_c. In fact, the transition is a topological one between two different orderings of chordless cycles (which can be regarded as topological defects) in the network. It is then similar to other topological phase transitions like the BKT transition [4, 5].

2. However, unlike in the BKT transition, both the free energy and entropy of the system diverge at the critical point in the thermodynamic limit. This is a very exotic behavior as in standard systems entropy only diverges at infinite temperature.

3. The scaling behavior of clustering at the transition is anomalous. Right at the critical point clustering decays logarithmically with the system size, and it decays as a power of the system size below the critical point. This is at odds with standard continuous phase transitions, where one observes power law decay at the critical point and faster decay below the critical point.

4. This scaling suggests that the effective size of the system is not given by the number of nodes N but by its logarithm $\ln N$. We then propose a finite size scaling ansatz with $\ln N$ instead of N that is confirmed by both the direct numerical integration as numerical simulation of the problem (Fig. 1).

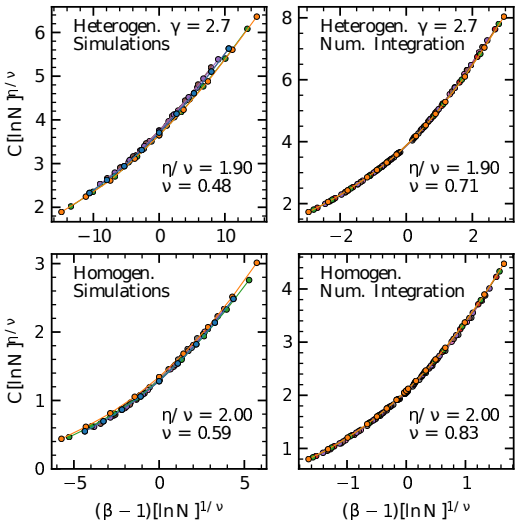

Fig. 1. Data collapse based on the finite size scaling ansatz $C(\beta, N) = [\ln N]^{-\frac{\eta}{\nu}} f((\beta-\beta_c)[\ln N]^{\frac{1}{\nu}})$ for heterogeneous networks with $\gamma = 2.7$ (top row) and homogeneous networks (bottom row). Left column correspond to numerical simulations with sizes in the range $N \in (5 \times 10^2, 10^5)$, whereas the right column is obtained from numerical integration in the range $N \in (5 \times 10^5, 10^8)$.

We also show that real networks with temperatures around and below the critical point are widespread, and therefore justify the practical importance of these findings.

[1] M. Boguñá, I. Bonamassa, M. De Domenico, S. Havlin, D. Krioukov and M. A. Serrano, Nature Reviews Physics **3**, 1 (2021)

[2] M. A. Serrano, D. Krioukov and M. Boguñá, Physical Review Letters **100**, 078701 (2008)

[3] J. van der Kolk, M. A. Serrano and M. Boguñá, (2021) arXiv:2106.08030 [physics.soc-ph]

[4] V. Berenzinskii, Sov. Phys. JETP **32**, 493 (1971)

[5] J. M. Kosterlitz and D. J. Thouless, Journal of Physics C: Solid State Physics **6**, 1181 (1973)

Auto-difusión en un gas de esferas duras cuasi-bidimensional

M. I. García de Soria[1,2], J. J. Brey [1,2], and P. Maynar[1,2]
[1]Física Teórica, Universidad de Sevilla, Apartado de Correos 1065, E-41080, Sevilla, Spain
[2]Institute for Theoretical and Computational Physics. Universidad de Granada, E-18071, Granada, Spain

Se considera un sistema de esferas duras fuertemente confinado entre dos placas plano-paralelas cuya distancia es menor que dos veces el diámetro de las partículas. De esta forma, las partículas no pueden pasar unas por encima de otras y el sistema puede considerarse cuasi-bidimensional. En este trabajo, estudiamos el proceso de auto-difusión cuando el sistema se observa desde arriba o desde abajo a partir de una ecuación tipo Boltzmann-Lorentz donde el término de collisiones está convenientemente modificado para tener en cuenta el efecto del confinamiento extremo. A partir del método de Chapmann-Enskog, la ecuación de difusión en el plano es derivada obteniendo una expresión explícita para el coeficiente de difusión como función de los parámetros del sistema (en particular de la separación de las placas). Las predicciones teóricas son comparadas con resultados de simulación de Dinámica Molecular, obteniendo un acuerdo excelente [1].

[1] J. J. Brey, M. I. García de Soria, and P. Maynar, *Self-diffusion in a quasi-two-dimensional gas of hard spheres*, Phys. Rev. E **101**, 012102 (2020).

Controlling the structure, phase behavior and dynamics of soft colloids by active interaction switching

Michael Bley[1], Pablo I. Hurtado[2,3], Joachim Dzubiella[1,4], and Arturo Moncho-Jordá[3,5],
[1]Physikalisches Institut, Albert-Ludwigs-Universität Freiburg, Hermann-Herder Straße 3, D-79104 Freiburg, Germany.
[2]Departamento de Electromagnetismo y Física de la Materia, Universidad de Granada, Campus Fuentenueva S/N, 18071 Granada, Spain.
[3]Institute Carlos I for Theoretical and Computational Physics, Universidad de Granada, Campus Fuentenueva S/N, 18071 Granada, Spain.
[4]Research Group for Simulations of Energy Materials, Helmholtz-Zentrum Berlin für Materialien und Energie, D-14109 Berlin, Germany.
[5]Departamento de Física Aplicada, Universidad de Granada, Campus Fuentenueva S/N, 18071 Granada, Spain.

We explore the microstructure and phase behavior of confined soft colloids which can actively switch their interactions at a predefined kinetic rate. For this, we employ a Reactive Dynamical Density Functional Theory (R-DDFT) and reactive Brownian-Dynamics computer simulations (R-BD), and study the effect of a two-state switching of the size of colloids interacting with a Gaussian pair potential in the nonequilibrium steady state. The switching rate interpolates between a near-equilibrium binary mixture at low rates and a nonequilibrium monodisperse liquid for large rates, strongly affecting the one-body density profiles, adsorption, and pressure at confining walls. Importantly, we show that sufficiently fast switching impedes the phase separation of an (in equilibrium) unstable liquid, allowing the control of the degree of mixing and condensation and local microstructuring in a cellular confinement by tuning the switching rate [1, 2].

Our results also demonstrate that switching activity significantly modifies the non-equilibrium dynamics and diffusion coefficients of the individual particles, leading to a crossover from short to long times, with a regime for intermediate times showing anomalous diffusion [3]. In addition, the self-part of the van Hove function has a Gaussian form at short and long times, but becomes non-Gaussian at intermediates ones, having a crossover between short and large displacements. The corresponding self-intermediate scattering function shows the two-step relaxation patters typically observed in soft materials with heterogeneous dynamics such as glasses and gels. We also introduce a phenomenological Continuous Time Random Walk (CTRW) theory to understand the heterogeneous diffusion of this system. R-DDFT results are in excellent agreement with R-BD simulations and the analytical predictions of CTRW theory, thus confirming that R-DDFT constitutes a powerful method to investigate not only the structure and phase behavior, but also the dynamical properties of non-equilibrium active switching colloidal suspensions.

[1] A. Moncho-Jordá and J. Dzubiella, *Controlling the Microstructure and Phase Behavior of Confined Soft Colloids by Active Interaction Switching*, Phys. Rev. Lett **125**, 078001 (2020).

[2] M. Bley, J. Dzubiella, and A. Moncho-Jordá, *Active binary switching of soft colloids: stability and structural properties*, Soft Matter **17**, 7682 (2021).

[3] M. Bley, P.I. Hurtado, J. Dzubiella, and A. Moncho-Jordá *Active interaction switching controls the dynamic heterogeneity of soft colloidal dispersions*, Soft Matter **18**, 397 (2022).

COMUNICACIONES

POSTER

Dynamics of conjugation in the Bacillus subtilis plasmid pLS20

Saúl Ares[1], Victoria Doldán-Maretlli[2], Wilfried J. J. Meijer[3] and Christian Cortés[2]
[1] Centro Nacional de Biotecnología, Calle Darwin 3, Madrid-España
[2] Universidad Carlos III de Madrid, Avenida de la Universidad 30, Leganes - España
[3]Spanish National Research Council (CSIC) Madrid, Spain

Bacterial conjugation is one of the horizontal gene transfer processes in which a donor bacterium transfers its conjugative plasmid to a recipient bacterium to become, for example, resistant to an antibiotic. Several experimental studies carried out in recent years have shown that three proteins are involved in the regulation of the conjugation genes present in the pLS20 conjugative plasmid of Bacillus subtilis. In this case, the main promoter that enables conjugation is repressed by a regulatory protein, called RcopLS20, that induces the formation of a DNA loop. However, an anti-repressor of RcopLS20, which enables activation of the conjugation promoter, called RappLS20, is inactivated by a plasmid-encoded signaling peptide, Phr*pLS20. This peptide needs to be exported out of the cell to be modified into its active form and is therefore a quorum-sensing signal that allow cells to receive information from their environment. With the aim of deepen the understanding of this system, this work proposes a mathematical model, using a system of differential equations, which describes the dynamics between the concentration of the conjugative gene and the proteins involved during the conjugation process, contrasted with experimental data.

[1] Itaya, M., Sakaya, N., Matsunaga, S., Fujita, K., and Kaneko, S. *Conjugational transfer kinetics of pLS20 between Bacillus subtilis in liquid medium*. Bioscience, Biotechnology, and Biochemistry, 70(3):740742 (2006).

[2] Meijer, W. J. J., Boer, D. R., Ares, S., Alfonso, C., Rojo, F., Luque-Ortega, J. R., and Wu, L. J. *Multiple layered control of the conjugation process of the Bacillus subtilis plasmid pLS20*. Frontiers in Molecular Biosciences, 8:98 (2021).

Interaction between SARS-CoV-2 virus and human skin

Marc Domingo[1], and Jordi Faraudo[1]
[1] Institut de Ciencia de Materials de Barcelona (ICMAB-CSIC), Campus de la UAB, E-08193 Bellaterra, Barcelona, Spain

The novel coronavirus SARS-CoV-2 emerged in December 2019 as a human pathogen[1] that caused the COVID-19 disease world pandemic. Therefore, it is clear that emerging infectious diseases caused by coronaviruses must be seen as a major threat to human health.

The transmission of respiratory viruses in general (including coronaviruses and SARS-CoV-2 in particular) involves the expiratory emission of virus-containing aerosols and droplets[2] which may infect other individuals via direct or indirect mechanisms. The direct mechanism involves inhalation of aerosols or the deposition of emitted droplets on mucosal surfaces (e.g. mouth, eyes). Indirect transmission may occur through physical contact with virus containing aerosols and droplets deposited onto materials (exposed surfaces of common objects such as furniture or electronic gadgets, textiles, protective equipment,) and byself inoculation of virus into the mouth.

The possibility of contamination of human skin by infectious virions plays an important role in indirect transmission of respiratory viruses but little is known about the fundamental physico-chemical aspects of the virus-skin interactions. In the case of coronaviruses, the interaction with surfaces (including the skin surface) is mediated by their large glycoprotein spikes that protrude from (and cover) the viral envelope.

We perform all atomic simulations between the SARS-CoV-2 spike glycoprotein and human skin models[3]. We consider an oily skin covered by sebum and a clean skin exposing the stratum corneum as seen in Figure 1. The simulations show that the spike tries to maximize the contacts with stratum corneum lipids, particularly ceramides, with substantial hydrogen bonding. In the case of oily skin, the spike is able to retain its structure, orientation and hydration over sebum with little interaction with sebum components. Comparison of these results with our previous simulations of the interaction of SARS-CoV-2 spike with hydrophilic and hydrophobic solid surfaces[4], suggests that the soft or hard nature of the surface plays an essential role in the interaction of the spike protein with materials.

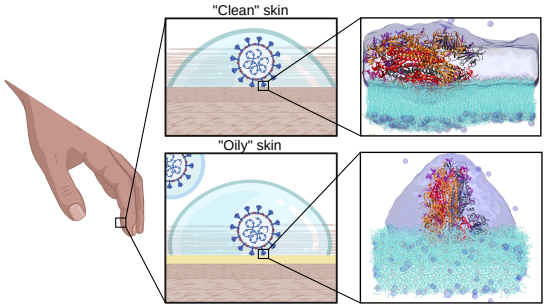

Fig. 1. Scheme of the interaction between SARS-CoV-2 spike glycoprotein and human skin models. The "oily" skin model is covered by sebum and the "clean" skin model exposes the outermost layer of the skin (Stratum Corneum). Reprinted from M. Domingo and J. Faraudo, Soft Matter, **17**, 9457 (2021). Licenced under CC BY-NC 3.0 [5].

Acknowledgements

This work was supported by the Spanish Ministry of Science and Innovation through Grant No. RTI2018-096273-B-I00, the Severo Ochoa Grant No. CEX2019-000917-S for Centres of Excellence in RD awarded to ICMAB and the FPI grant PRE2020-093689 awarded to M. D. We thank the CESGA supercomputing center for computer time and technical support at the Finisterrae supercomputer. M. D. is enrolled in the Material Sciences PhD program of the Universitat Autonoma de Barcelona.

[1] A. E. Gorbalenya et al., Nat Microbiol **5**, 536544 (2020).

[2] S. Asadi et al., Sci. Rep., **10**, 15665 (2020).

[3] M. Domingo and J. Faraudo, Soft Matter, **17**, 9457-9468, (2021).

[4] D. C. Malaspina and J. Faraudo, Biointerphases, **15**, 051008, (2020).

[5] https://creativecommons.org/licenses/by-nc/3.0/

Studying NaCl crystal nucleation from aqueous solutions

C. P. Lamas[1,2], J. R. Espinosa[3], M. M. Conde[4], J. Ramírez[4], P. Montero de Hijes[1], E. G. Noya[2], C. Vega[1], and E. Sanz[1]
[1]Departamento de Química Física (Unidad de I+D+i asociada al CSIC)
[2]Instituto de Química Física Rocasolano, Consejo Superior de Investigaciones Científicas, CSIC, Calle Serrano 119, 28006 Madrid, Spain
[3] Maxwell Centre, Cavendish Laboratory, Department of Physics, University of Cambridge, Cambridge CB3 0H3, United Kingdom
[4] Departamento de Ingeniería Química Industrial y Medio Ambiente, Escuela Técnica Superior de Ingenieros Industriales, Universidad Politécnica de Madrid, 28006, Madrid, Spain

The Seeding method is an approximate approach to investigate nucleation that combines molecular dynamics simulations with classical nucleation theory. This technique has been successfully implemented in a broad range of nucleation studies in the recent years. However, its accuracy is subject to the arbitrary choice of the order parameter threshold used to distinguish liquid-like from solid-like molecules [2]. We revisit here the crystallisation of NaCl from a supersaturated brine solution and show that consistency between Seeding [1] and rigorous methods like Forward Flux Sampling [3] or spontaneous crystallisation [1, 3, 4], is achieved by following a mislabelling criterion to select such threshold (i. e. equalling the fraction of mislabelled particles in the bulk parent and nucleating phases) [5]. This work supports the use of Seeding to obtain fast and reasonably accurate nucleation rate estimates and the mislabelling criterion as one giving the relevant cluster size for classical nucleation theory in crystallisation studies (see Fig. 1).

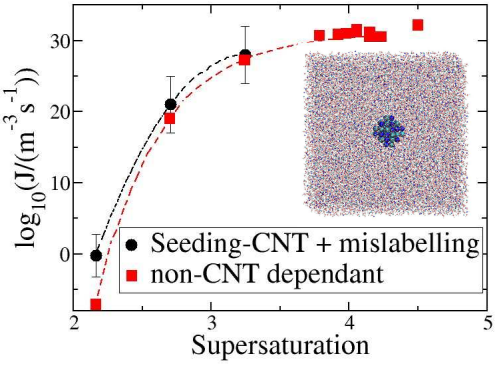

Fig. 1. Decimal logarithm of the nucleation rate vs. supersaturation, obtained with the seeding technique and mislabelling criterion (black circles)[1], and with non classical nucleation theory methods (red squares) [1, 3, 4].

[1] C. P. Lamas, J. R. Espinosa, M. M. Conde, J. Ramírez, P. Montero de Hijes, E. G. Noya, C. Vega and E. Sanz *Homogeneous nucleation of NaCl in supersaturated solutions*, Phys. Chem. Chem. Phys. **23.47**, 26843-26852 (2021).

[2] N. E. Zimmermann, B. Vorselaars, J. R. Espinosa, D. Quigley, W. R. Smith, E. Sanz, C. Vega and B. Peters *NaCl nucleation from brine in seeded simulations: Sources of uncertainty in rate estimates*, J. Chem. Phys. **148**, 222838 (2018).

[3] H. Jiang, A. Haji-Akbari, P.G. Debenedetti and A.Z. Panagiotopoulos *Forward flux sampling calculation of homogeneous nucleation rates from aqueous NaCl solutions*, J. Chem. Phys. **144.3**, 044505 (2018).

[4] G. Lanaro, and G. N. Patey *Birth of NaCl crystals: Insights from molecular simulations*, J. Phys. Chem. B **120.34**, 9076-9087 (2016).

[5] J. R. Espinosa, C. Vega, C. Valeriani and E. Sanz *Seeding approach to crystal nucleation*, J. Chem. Phys. **148**, 034501 (2016).

Efecto de la interacción entre huéspedes en la evolución de virus que pueden mutar

Javier López Pedrares[1,2] and Alberto Pérez Muñuzuri[1,2],
[1] CITMAga, 15782 Santiago de Compostela, España.
[2]Grupo de Física No Lineal, Facultad de Física, Univ. de Santiago de Compostela 15782 Santiago de Compostela, España.

Los seres humanos formamos auténticas redes complejas de interacción que han cambiado mucho en los últimos siglos. El efecto de estas redes puede marcar un punto clave en el desarrollo de una pandemia. Estudiar cómo afecta la topología de la red, en la que nos encontramos, a la evolución de la competencia viral marca un paso a seguir para el desarrollo y prevención de nuevas epidemias que puedan surgir.

Los modelos matemáticos de competición viral acoplados a modelos epidemiológicos mediante redes de interacción permiten estudiar los tipos de infecciones que perdurarán en el tiempo. La evolución viral se produce en largas escalas de tiempo, que permiten la mutación de las especies para poder sobrevivir. Es clave observar que especies aparecerán en el tiempo para poder desarrollar medidas de contención y sanitarias frente estas nuevas cepas virales y cómo las especies que sobreviven pueden venir determinadas por el tipo de red de interacción de los huéspedes.

Dynamics and clogging of colloidal monolayers magnetically driven through a heterogeneous landscape

Sergi G. Leyva,[1,2], Ralph L. Stoop,[1],Ignacio Pagonabarraga,[1,2,3], and Pietro Tierno[1,2,4]
[1]Departament de Física de la Matèria Condensada, Universitat de Barcelona, Barcelona, Spain
[2]Universitat de Barcelona Institute of Complex Systems (UBICS), Universitat de Barcelona, 08028 Spain
[3]CECAM, Centre Européen de Calcul Atomique et Moléculaire, École Polytechnique Fédérale de Lasuanne, Batochime, Avenue Forel 2, 1015 Lausanne, Switzerland
[4]Institut de Nanociència i Nanotecnologia, IN^{2}UB, Universitat de Barcelona, Barcelona, Spain

Typically, clogging is usually characterised through its average velocity in all sort of systems: Pedestrian evacuation, silo discharge of granular media, a collectivity of particles driven through an obstacle landscape, among others. When the average speed decreases to zero, the system is considered to be clogged. However, this approach is partial, as it only allows to characterise a fully clogged state where there is no flow of particles, or unclogged state where there is a flow of particles. Recent works [1] show that a more detailed study of the flow distribution of particles through a bottleneck reveals an intermediate regime of abnormal flow. Such abnormal flow has a certain probability of being occluded for a indefinite period of time. The abnormal flow regime can be characterised by the complementary cumulative distribution function (CCDF) of the difference of passing times (t_p) of particles through a constriction, which exhibits a power law distribution that decays as $t_p^{-\alpha}$, with α the characteristic decay exponent.

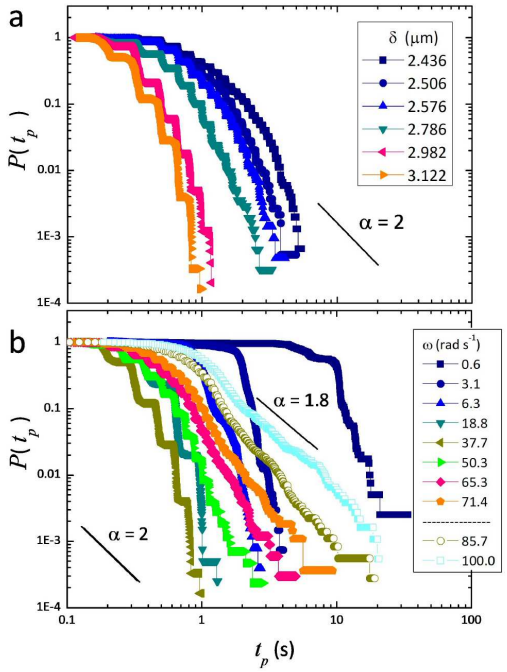

Fig. 1. Cumulative distribution function (CDF) of passing particles trough a constriction. Different colors show a) varying the constriction width and b) varying the frequency.

In this work, we use this approach to characterise a colloidal, microscale system. We combine experiments and numerical simulations to investigate the emergence of clogging in a system of interacting paramagnetic colloidal particles driven against a disordered landscape of larger obstacles. We consider a single aperture in a landscape of immobile silica particles which are irreversibly attached to the substrate. We use an external rotating magnetic field to generate a traveling wave potential which drives the magnetic particles against these obstacles at a constant and frequency tunable speed. Experimentally we find that the particles display an intermittent dynamics with power law distributions at high frequencies. We reproduce these results by using numerical simulations and show that clogging in our system arises at large frequency, when the particles desynchronize with the moving landscape. Further, we use the model to explore the hidden role of flexibility in the obstacle displacements and the effect of hydrodynamic interactions between the particles. We also consider numerically the situation of a straight wall and investigate the range of parameters where clogging emerges in such case. Our work provides a robust method to identify clogging in generical, soft-matter driven systems. [2].

[1] I. Zuriguel *et al.*, *Clogging transition of many-particle systems flowing through bottlenecks*, Sci. Reports **4**, 7324 (2014)

[2] Sergi G. Leyva, Ralph L. Stoop, P. Tierno, I. Pagonabarraga *Dynamics and clogging of colloidal monolayers magnetically driven through a heterogeneous landscape* , Soft Matter, 2020, **16**, 6985-6992

[3] A. V. Straube, and P. Tierno Europhys. Lett., **103**, 28001, (2013)

Personal network structure predicts migrants' cultural backgrounds

José Luís Molina,[1] Juan Ozaita,[2] Ignacio Tamarit,[2] Angel Sánchez,[2,3] Christopher McCarty,[5] and H. Russell Bernard[5,6]
[1]GRAFO-Department of Social and Cultural Anthropology, Universitat Autnoma de Barcelona
[2]Grupo Interdisciplinar de Sistemas Complejos (GISC), Departamento de Matemáticas, Universidad Carlos III de Madrid
[3]Institute for Biocomputation and Physics of Complex Systems (BIFI), Universidad de Zaragoza
[4]Department of Anthropology, University of Florida
[5]School of Human Evolution and Social Change, Arizona State University

In the study of societies from an antropological point of view, culture and social structure have long been considered as two separate phenomena. However, in the 1960's the study of cultural manifestations as a complex product of society emerged. One of these approaches, the so-called Grid/Group theory [1], describes a society as defined by two dimensions, a *group* dimension, characterized by the connections between members (i.e., by the network structure), and a *grid* dimension, characterized by the distribution of social roles, often identified with cultural variables [2].

In this work, we provide for the first time empirical support for the Grid/Group theory. We draw on the idea that individuals are characterized by a "social signature," i.e., a specific manner to allocate their limited cognitive capabilities to relationships with others [3] that is stable in time. We then hypothesize that it is possible to find such a correlate at the same-culture aggregate level, i.e., a "cultural signature." To validate this hypothesis, we used a dataset of personal networks from migrants in USA and Spain (Fig. 1 shows an example of these networks). Specifically, using the country of origin as a proxy for the diverse languages or other cultural institutions, we study the correlation with personal network structural measures, such as closeness, clustering, betweenness, average degree, or assortativity. We understand this problem as a inference/prediction problem, hypothesizing that the social structure around an ego may be a good predictor for its nationality.

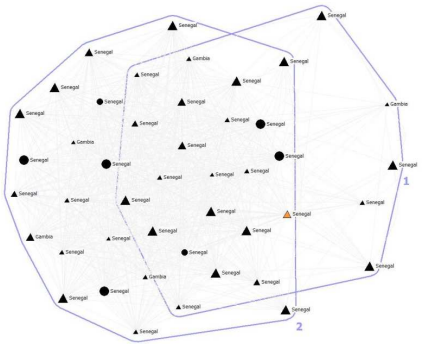

Fig. 1. Personal network of a Senegambian migrant in Spain with 45 alters (ego is not represented in the drawing)

We used three different prediction methods to try and answer this question: a multinomial logistic regression, a random forest algorithm and an artificial neural network. Results from these techniques are in good agreement and provide support for the idea that it is possible to predict the country of origin from network measures reliably, with a 50% improvement in accuracy over the best alternative model. Furthermore, clear interpretability of the results in the case of the random forest comes from looking at the SHAP values [4]. Using SHAP combined with the coefficients of the multinomial logistic regression, we can extract correlations between the nationality of subjects and a characteristic range of network measures, which turns out to be different for nationals of different countries. The range of the distribution of SHAP values is related to the relevance of the predictor, and the correlation can be obtained when the range of the magnitude (in this case a range of colors) and the range of SHAP values show a good concordance. As an example, Fig. 2 shows the distribution of SHAP values according to their relevance in the argentinean subpopulation (Fig. 2). High SHAP values are related to larger probabilities of belonging to the class, so in this case that low average degree and high clustering are correlated with being argentinian.

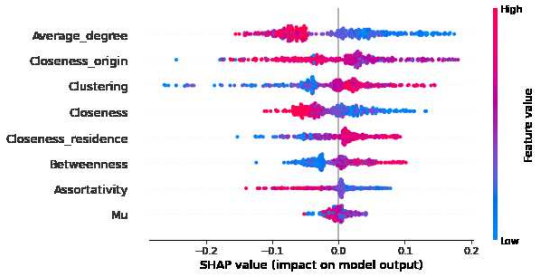

Fig. 2. SHAP values, or contribution from the different network structural measures, on the prediction of the nationality in the case of argentinians.

In conclusion, our analysis shows that it is possible to infer not just their country of origin but also that each of them exhibit a particular combination of network measures compared with others. This finding is relevant theoretically because it suggests how to overcome the duality of culture and structure and support the Grid/Group analytical framework. In addition, our results suggest that personal networks can be conceived as samples of the social structures that frame the group dimension, capturing the effects of cultural institutions (the grid dimension) in the alter-alter matrix of interactions.

[1] Douglas, M. *Natural Symbols: Explorations in Cosmology* (Routledge, 1996).

[2] Rayner, S. and Gross, J. L. *Measuring Culture: A Paradigm for the Analysis of Social Organization* (Columbia University, 1985).

[3] Dunbar, R. The anatomy of friendship. Trends Cog. Sci. **22**, 32-51 (2018).

[4] Lundberg, S. M. and Lee, S.-I. *Advances in Neural Information Processing Systems 30* (Curran Associates, 2017).

Phenotypic-dependent variability and the emergence of tolerance in bacterial populations

Jose MC Mateu[1], Matteo Sirecci[2], and Miguel Angel Muñoz[2]
[1]Grupo Interdisciplinar de Sistemas Complejos (GISC),
Departamento de Matemáticas, Universidad Carlos III de Madrid, Leganes, Spain
[2]Departamento de Electromagnetismo y Física de la Materia and
Instituto Carlos I de Física Teórica y Computacional. Universidad de Granada. Granada, Spain

Ecological and evolutionary dynamics have been historically regarded as unfolding at broadly separated timescales. However, these two types of processes are nowadays well-documented to intersperse much more tightly than traditionally assumed, especially in communities of microorganisms. Advancing the development of mathematical and computational approaches to shed novel light onto eco-evolutionary problems is a challenge of utmost relevance.

With this motivation in mind, here we scrutinize recent experimental results showing evidence of rapid evolution of tolerance by lag in bacterial populations that are periodically exposed to antibiotic stress in laboratory conditions. In particular, the distribution of single-cell lag timesi.e., the times that individual bacteria from the community remain in a dormant state to cope with stressevolves its average value to approximately fit the antibiotic-exposure time. Moreover, the distribution develops right-skewed heavy tails, revealing the presence of individuals with anomalously large lag times. Here, we develop a Markov individual-based stochastic model for phenotypic adaptation that mimicks the actual demographic processes of the experimental setup. Individuals are characterized by a single phenotypic trait: their intrinsic lag time, which is transmitted with variation to the progeny. The model –in a version in which the amplitude of phenotypic variations grows with the parents lag time– is able to reproduce quite well the key empirical observations

Mathematically models such as our are described by a Master equation ruling the time evolution of the joint probability-distribution functions for the whole set of all particles. However, as it is often the case for such many-particle Master equations, it is hard to handle analytically in an exact way. Thus, in order to gain quantitative understanding beyond purely computational analyses, here we develop an approximationwhich becomes exact in the limit of infinitely large population sizes, that allows us to derive a macroscopic (or mean-field) description of the stochastic model in terms of the probability density of finding an individual at any given phenotypic state, (i.e. the one-particle probability density):

$$\begin{aligned} \partial_t \phi(\tau,t) &= \eta(t)\left[f(\tau,t)-\bar{f}(t)\right]\phi(\tau,t) \\ &- (\eta(t)+1)\Big[\partial_\tau \theta(\tau) f(\tau,t)\phi(\tau,t) \\ &- \frac{1}{2}\partial_\tau^2 \sigma^2(\tau) f(\tau,t)\phi(\tau,t)\Big] \end{aligned} \quad (1)$$

this equation is *a generalization of the celebrated continuous-time Crow-Kimura* equation of population genetics, also called selection-mutation equation. In particular, notice that the dynamics of the probability density is exposed to the combined action of the process of selection (first term in previous equation) and mutation, as specified by the drifts (the second and third line). This type of equations, combining replicator dynamics with Fokker-Planck type of terms.

Even if the model does not account for all the biological mechanisms (e.g., genetic changes) in a detailed wayi.e., it is a phenomenological one it sheds light onto the eco-evolutionary dynamics of the problem and can be helpful to design strategies to hinder the emergence of tolerance in bacterial communities. From a broader perspective, this work represents a benchmark for the mathematical framework designed to tackle much more general eco-evolutionary problems, thus paving the road to further research avenues.

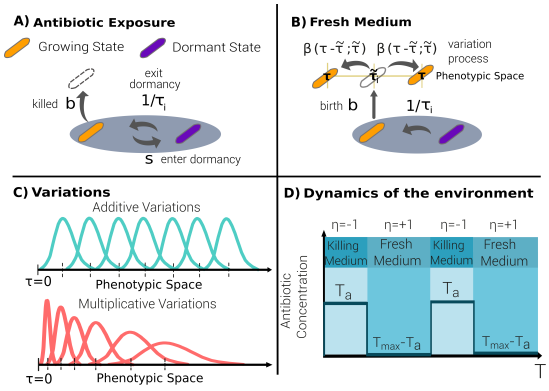

Fig. 1. **Sketch of the main ingredients of the individual-based stochastic model**. Each individual bacterium (i) is characterized by its phenotypic state, lag time τ_i and experiences demographic processes. **(A)** In the presence of antibiotics, bacteria can stochastically switch between the dormant and the growing state (at transition rates s and $1/\tau_i$, respectively); growing individuals can also attempt reproduction (at a "birth" rate b) and be immediately killed by the action of antibiotics (as bactericidal antibiotics usually act during duplication attempts). **(B)** In the fresh medium, dormant bacteria can wake up at a rate $1/\tau_i$, that depends on their intrinsic (phenotypic) lag time; on the other hand, growing cells can reproduce asexually by duplication; the resulting offspring inherit the characteristic time scale with some variation, as specified by a function β. **(C)** Two possible types of variation functions β: in the additive case (top), the standard deviation is constant, i.e. independent of the initial state τ_i, while in the multiplicative case (bottom) the standard deviation is assumed to grow linearly with the parent's lag time τ_i. **(D)** Sketch of the environmental variation, alternating periodically between antibiotic exposure (time T_a) and a fresh medium ($T_{max} - T_a$).

Sampling rare trajectories using stochastic bridges

Javier Aguilar[1], Joseph W. Baron[1], Tobias Galla[1] and Raúl Toral[1]
[1] Instituto de Física Interdisciplinar y Sistemas Complejos IFISC (CSIC-UIB), Campus UIB, 07122 Palma de Mallorca, Spain.

The most uncommonly occurring events in stochastic systems are often the most consequential. Instances where this unlikely-yet-important combination occurs include fade-outs of epidemics, the extinction of species in ecology, the dynamics of biological switches, large fluctuations in chemical reactions and the detection or prediction of rare natural disasters such as earthquakes, storms or heavy rains. The broad range of these applications justifies the considerable recent effort expended on developing sampling algorithms for rare events in models of stochastic phenomena.

We present a new method that constructs an ensemble of stochastic trajectories that are constrained to have fixed start and end points (so-called stochastic bridges). We then show that by carefully choosing a set of such bridges and assigning an appropriate statistical weight to each bridge, one can focus more processing power on the rare events of a target stochastic process while faithfully preserving the statistics of these rare trajectories.

Given a target process defined by the transition probabilities $P(x', t+\delta t|x, t)$ and initial condition $x(t=0) = x_0$, the key components of the algorithm are: 1) build an associate process with transition probabilities

$$\tilde{P}(x', t-\delta t|x, t) = P(x, t|x', t-\delta t)\frac{P(x', t-\delta t|x_0, 0)}{P(x, t|x_0, 0)}. \quad (1)$$

Where $P(x, t|x_0, 0)$ is the probability of the target process to be in state x at time t given the initial condition $x(t=0) = x_0$. By construction, the rates in Eq. (1) will generate the stochastic bridges backwards in time. 2) Once the ensemble of bridges is generated with Eq. (1), we recover the statistics of the target process thanks to the relation

$$\mathcal{P}(\mathcal{T}) = \tilde{\mathcal{P}}(\mathcal{T})P\left(x_{_T}, T|\, x_0, 0\right). \quad (2)$$

With $\mathcal{P}(\mathcal{T})$ and $\tilde{\mathcal{P}}(\mathcal{T})$ the probabilities of sampling a particular path $\mathcal{T}$ with the target and associated process respectively. We can apply the same ideas to any Markov process irrespectively to the continuous or discrete nature of the time and the states. See details of the method in [1].

Our approach does not require the noise in the model to be weak, and it generates uncorrelated and unbiased transition paths. Having access to the ensemble of stochastic paths unveils the whole statistical description of the transition between meta-stable states, making it possible to obtain entire distributions of first-passage times or other characteristics in simulations. For example, in Fig. 1, we show the use the stochastic bridges to sample extinction paths and their statistics in the Susceptible-Infected-Susceptible (SIS) model.

We envisage that the method that we have developed will have applications in myriad systems where sampling rare events is important. We imagine that it can also be used as a numerical aid to intuit when the WKB method will be accurate and useful. The approach presented here can also be extended to sample stochastic trajectories constrained to pass through more than two desired points.

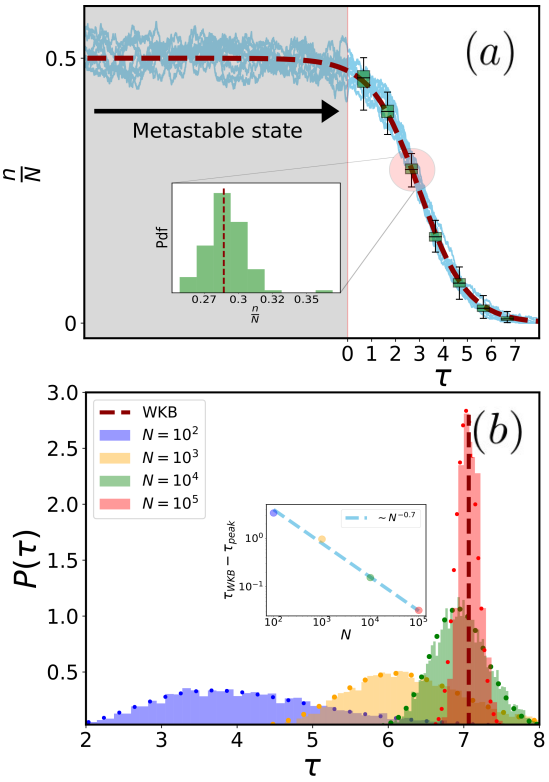

Fig. 1. Extinction paths for the SIS model ($\beta = 2, \gamma = 1$). (a) Paths leading to extinction from a common starting point $\frac{n}{N} = 1 - \frac{\gamma}{\beta} = 0.5$ to $n = 0$ for $N = 10^3$. The WKB instanton is shown as a dashed line. The time $\tau = 0$ corresponds to the point where the WKB instanton crosses $n/N = 0.48$. Boxes indicate the median and first quartiles, and error bars the observed range of the ensemble of stochastic paths. The inset shows the distribution of n/N at time $\tau = 2.8$. (b) Distribution of transition times for extinction trajectories from the quasi-stationary state towards the absorbing state. Dots show fits to log-normal distributions. The inset shows that the modes τ_{peak} of these fits approach the value predicted from the WKB instanton, with $|\tau_{\text{WKB}} - \tau_{\text{peak}}| \sim N^{-0.7}$.

[1] Aguilar, J., Baron, J. W., Galla, T., and Toral, R., *Sampling rare trajectories using stochastic bridges*,rXiv preprint arXiv:2112.08252 (2021).

Random geodesics and the boundary of KPZ

I.A. Domenech[1], D. Villarrubia Moreno[1], J. Rodríguez-Laguna[2], P. Córdoba-Torres[1]and S.N. Santalla[3]
[1]Dpto. Física Matemática y de Fluidos, UNED, Spain.
[2]Dpto. Física Fundamental, UNED, Spain.
[3]Dpto. Física & GISC, Universidad Carlos III de Madrid, Spain.

Metric geometry has a large number of applications in physics. Specifically, random metric spaces present useful methods to obtain effective descriptions of a large number of phenomena showing fluctuations with a geometric origin. For example, thermal fluctuations of important biophysical objects such as fluid membranes. In the context of random metric spaces, a model of interest is given by first-passage percolation (FPP), which was originally introduced as a model of fluid through a random medium.

The FPP model is defined as follows. Given an undirected discrete lattice, we place a non-negative random variable τ_e on each nearest-neighbor edge, which is interpreted as a passage time. The collection $\{\tau_e\}$ is assumed to be independent and identically distributed, with common distribution F. The main objects of interest are the shortest-time paths between any pair of lattice nodes, also called geodesics, and the balls $B(T)$, i.e. the set of nodes which can be reached in a time less than the passage time T. This ball has been studied on the context of random metrics showing, under some circumstances, the exponents corresponding to the Kardar-Parisi-Zhang universality class (KPZ) [1].

These geometric properties were studied by our group in the context of a discrete space using the FPP model [2]. Two types of planar lattices have been considered: regular lattices and disordered lattices. For the regular case we considered square lattices and we studied the fluctuations of the times of arrival to points along the axis and the diagonal directions. For the axis direction, we can observe a pre-asymptotic regime while in the diagonal direction this pre-asymptotic regimen is not present. In order to understand this difference, the concept of geodesic degeneracy is introduced, i.e. the number of geodesics joining the given points in absence of noise. Afterwards, an analogous analysis was done on *Delaunay lattices* as a relevant example of disordered lattices. In both types of lattices, a complete characterization of the scaling behavior has been performed with the study of the lateral deviation of the geodesics, defined as the Euclidean distance from its middle point to the straight line joining the end points. This morphological property is related to the correlation length to the underlying surface. Finally, a complete characterization of the fluctuations of the arrival times and the geometry of the geodesics was performed, allowing us to conjecture that the FPP model belongs to the KPZ universality class under some mild conditions, as supported by our numerical results.

Subsequently, the relevance of the lateral deviation on the emergence of the KPZ universality class has been studied. In order to do that, we have set up an artificial constraint for the lateral desviation of the ensemble of geodesics, by imposing a curved boundary on the underlying manifold, with intention of proving the stability of the KPZ universality class (Fig.1).

This study has been done for the diagonal direction, showing the relevance of the geodesic degeneracy in the pre-asymptotic regime which we can find in the axis. Moreover, our numerical experiments suggest a continuous deformation of the scaling exponents and the arrival time distribution as our boundary constraints more and more the space allowed for the geodesics, thus proving that KPZ scaling is lost when the geodesics are not given enough lateral space.

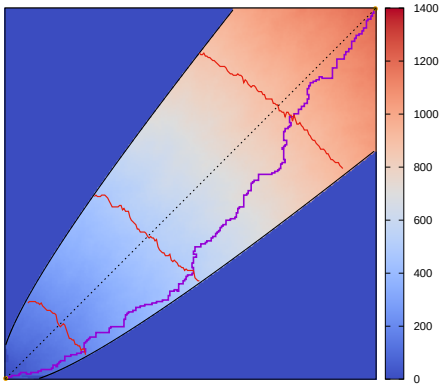

Fig. 1. A geodesic along the diagonal direction of a square lattice under a boundary constraint of the form $f(x) \propto r^{\alpha}$. Differents colors represent different arrival times, and some isochrones can be observed.

[1] Silvia N Santalla et al 2015 *New J. Phys.* **17** 033018

[2] Pedro Córdoba-Torres et al *J. Stat. Mech.* (2018) 063212

Time and space generalized diffusion equation on graph/networks

Fernando Díaz-Díaz[1] and Ernesto Estrada [1]
[1]Institute of Cross-Disciplinary Physics and Complex Systems, IFISC (UIB-CSIC), 07122 Palma de Mallorca, Spain

Random walks and diffusion are one of the most relevant research areas of statistical physics, due to the wide range of phenomena that show a diffusive behavior. Nevertheless, many real systems violate the predictions of standard diffusion, because of the presence of phenomena such as long range interactions or kinetic traps. This *anomalous diffusion* can be identified by looking at the time scaling of magnitudes such as the height of the maximum of the pdf (f_{max}) or the Full Width at Half Maximum (FWHM). In particular, given that f_{max} usually follows a power law ($f_{max} \propto t^{-\gamma}$), exponents $\gamma < 0.5$ can be identified with subdiffusive systems and exponents $\gamma > 0.5$ with superdiffusive ones.

Several tools have been derived to analyze anomalous diffusion, many of them based on continuous time random walks (CTRW) and fractional diffusion equations [1]. However, most of these approaches neglected the networked structure of many of these systems. To overcome this limitation of previous models, we proposed in [2] a generalized diffusion equation for networks, using Caputo time-fractional derivatives and d-path Laplacian operators [3, 4]. As a result, we obtained a simple equation with a fractional derivative parameter α and a nonlocal hopping parameter s. We analytically proved that the solution of this equation is able to recreate diffusive, subdiffusive and superdiffusive scenarios, and found the parameter regimes where the different types of anomalous diffusion appear (figure 1). We also performed computational simulations that qualitatively agree with our analytical predictions (figure 2).

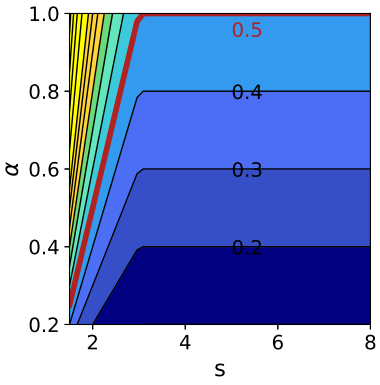

Fig. 1. *Contour plot of the analytical prediction of the exponent γ of the maximum of the pdf as a function of the two parameters of the generalized diffusion equation (α and s). Values below $\gamma = 0.5$ correspond to subdiffusion and above $\gamma = 0.5$ correspond to superdiffusion.*

As as example of the utility of our model, we studied the diffusion of proteins along a DNA chain, which is known to exhibit sub- and superdiffusive behaviors [5]. The DNA chain structure can be modelled as a path graph with long-range interactions, and the diffusing proteins can be modelled as particles with time-varying average jump lengths. We find that an alternancy of sub- and superdiffusion allows the proteins to explore more carefully certain regions of the DNA with a faster global exploration. This could represent an advancement in the understanding of protein-DNA interactions.

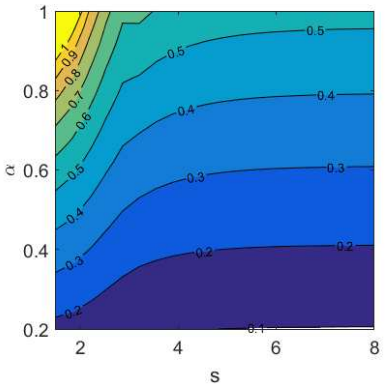

Fig. 2. *Contour plot of the exponent γ of the maximum of the pdf obtained by performing numerical simulations, as a function of the two parameters of the generalized diffusion equation (α and s). Values below $\gamma = 0.5$ correspond to subdiffusion and above $\gamma = 0.5$ correspond to superdiffusion.*

Proofs and fully detailed explanations of our work can be found in Ref. [2].

[1] R. Metzler and J. Klafter, *The random walks guide to anomalous diffusion: a fractional dynamics approach*, Physics Reports, vol. 339, pp. 177, Dec. 2000.

[2] F. Díaz-Díaz and E. Estrada, *Time and space generalized diffusion equation on graph/networks*, Chaos, Solitons and Fractals, vol. 156, p. 111791, Mar. 2022.

[3] E. Estrada, *Path Laplacian matrices: Introduction and application to the analysis of consensus in networks*, Linear Algebra and its Applications, vol. 436, pp. 33733391, May 2012.

[4] E. Estrada, E. Hameed, N. Hatano, and M. Langer, *Path Laplacian operators and superdiffusive processes on graphs*. I. One-dimensional case, Linear Algebra and its Applications, vol. 523, pp. 307334, June 2017. arXiv: 1604.00555.

[5] J. Gorman and E. C. Greene, *Visualizing one-dimensional diffusion of proteins along DNA*, Nature structural and molecular biology, vol. 15, no. 8, pp. 768774, 2008.

Emergence and suppression of chaos in coupled starlike networks of damped driven pendula

Ricardo Chacón[1] and Pedro J. Martínez[2]
[1]Depto. de Física Aplicada, E.I.I., Univ. de Extremadura, Badajoz and
Instituto de Computación Científica Avanzada (ICCAEx), Univ. de Extremadura, Badajoz, Spain.
[2]Depto. de Física Aplicada, E.I.N.A., Univ. de Zaragoza, Zaragoza , Spain and
Instituto de Nanociencia y Materiales de Aragón (INMA), CSIC-Univ. de Zaragoza, Zaragoza , Spain

The emergence and suppression of chaos in a complex network of driven damped pendula which consists of two starlike networks coupled by a single link is investigated in the case where only the two hubs are subject to impulse-induced control. We found distinct chaos-control scenarios depending upon whether the connectivity strategy between the starlike networks is hub to hub, hub to leave or leave to leave. We provide an explanation of their underlying physical mechanisms as well as the main characteristics of such chaos-control scenarios. Our findings may be seen as a contribution to an intermediate step to the long-term goal of controlling chaos in scale-free networks of damped-driven nonlinear systems.

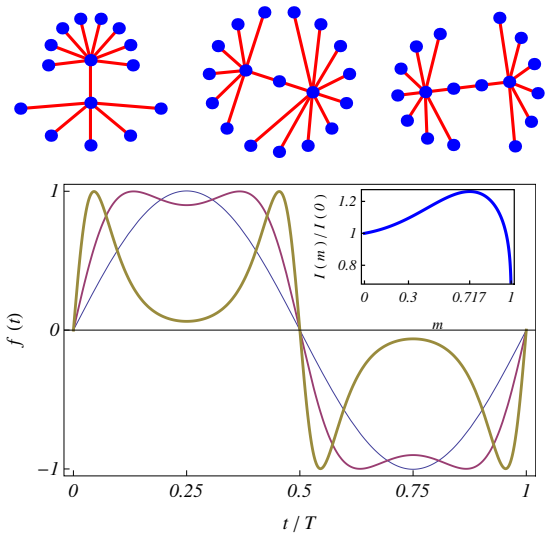

Fig. 1. Top: Schematic representations of three examples of networks of networks, each of which consists of two starlike networks connected by a single interlink: hub-to-hub, hub-to-leave, and leave-to-leave, respectively, from left to right. Bottom: Parametric excitation function $f(t) = N(m)sn[4K(m)t/T; m]dn[4K(m)t/T; m]$ vs t/T for m = 0 (thin line), m = 0.717 (medium line), and m = 0.999 (thick line). The inset shows the normalized impulse vs the shape parameter.

[1] S. P. Cornelius, W. L. Kath, and A. E. Motter, Nat. Commun. 4, 1942 (2013).

[2] R. Chacón, A. Martínez García-Hoz, and J. A. Martínez, Phys. Rev. E 95, 052219 (2017).

Brownian dynamics simulations of the B-cell activation

Miguel García[1] and Mario Castro[1]
[1]Instituto de Investigación Tecnológica (IIT), Universidad Pontificia Comillas, Madrid, Spain

The binding between B cell receptors (BCRs) and their ligands is a fundamental step in the B cell activation. This binding consists of a series of states and processes which include: diffusion, orientation and molecular binding [1] (see Fig.1).

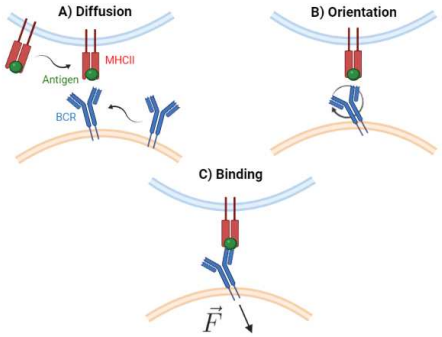

Fig. 1. **Three steps of binding**. **a)** Membrane diffusion, **b)** Orientation and **c)** Molecular binding.

Once the bond is formed, it is mechanically stressed by tensile forces coming from the environment and the internal reorganization of the cell membrane. Interestingly, it has been observed in many biological systems that the applied force changes the bond mean lifetime. Naively, one could expect that the larger the force, the shorter the time (as the two molecules are *pulled* away). This mechanism is called slip-bond unbinding. However, it has been empirically observed that for some systems, the opposite happens (at least for small tensions). This is called catch-bond mechanism, and it has been reported in a wide variety of systems, from elastic fibers to T-cells [2].

Microscopically, the three steps in Fig. 1 are stochastic in nature due to thermal fluctuations at the protein level. In this work, we model all those previous processes as Brownian motions, either in a cell membrane (diffusion), extracellular space (orientation), or a potential landscape (binding rupture). Using Montecarlo simulations, we investigate the so-called "Two-pathways model" of the catch bond [3] and

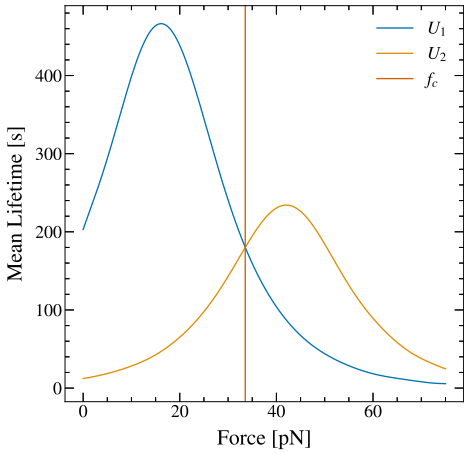

Fig. 2. **Catch behavior of two bonds**. In solution ($f = 0$), the affinity of one bond is much greater than the other. As from a critical force (f_c), the rank in the affinity of both bonds is interchanged.

reproduce the orientation and catch bond dynamics. We find that the affinity of two BCRs with an antigen can drastically change if it is measured in solution (absence of force, $f = 0$) or in a cell-to-cell set up as in physiological conditions (see Fig.2).

Our results highlight the dangers of uncontrolled in-vitro experiments to rank the affinity of antibodies as those experiments are unable to capture the true underlying kinetic rates and, thus, can mislead the quest to find specific therapeutic treatments based on antibodies.

[1] J. Faro, M. Castro, and C. Molina-París, *A unifying mathematical framework for experimental TCR-pMHC kinetic constants*, Scientific Reports, 7 **1** (2017).

[2] O. V. Prezhdo, Y. V. Pereverzev, *Theoretical Aspects of the Biological Catch Bond*, Accounts of Chemical Research, **42** (6) (2009).

[3] V. K. Gupta, *Brownian dynamics simulation of catch to slip transition over a model energy landscape*, J. Biological Systems, **24** (2016).

Terminal heterocyst differentiation in the *Anabaena patA* mutant as a result of post-transcriptional modifications and molecular leakage

Pau Casanova-Ferrer[1,2], Saúl Ares[2] and Javier Muñoz-García[1]

[1] Departamento de Matemáticas and Grupo Interdisciplinar de Sistemas Complejos (GISC), Universidad Carlos III de Madrid, 28911 Leganés, Spain
[2] Departamento de Biología de Sistemas, Centro Nacional de Biotecnología, CNB-CSIC, 28049 Madrid, Spain

The *Anabaena* genus is a model organism of filamentous cyanobacteria whose vegetative cells can differentiate under nitrogen-limited conditions into a type of cell called heterocyst. These heterocysts lose the possibility to divide and are necessary for the colony because they can fix and share environmental nitrogen. In order to distribute the nitrogen efficiently, heterocysts are arranged to form a quasi-regular pattern whose features are maintained as the filament grows. Recent efforts have allowed advances in the understanding of the interactions and genetic mechanisms underlying this dynamic pattern. However, the main role of the *patA* and *hetF* genes are yet to be clarified; in particular, the *patA* mutant forms heterocysts almost exclusively in the terminal cells of the filament. In this work [1], we investigate the function of these genes and provide a theoretical model (Fig.1) that explains how they interact within the broader genetic network, reproducing their knock-out phenotypes in several genetic backgrounds, including a nearly uniform concentration of HetR along the filament for the *patA* mutant. Our results suggest a role of *hetF* and *patA* in a post-transcriptional modification of HetR which is essential for its regulatory function. In addition, the existence of molecular leakage out of the filament in its boundary cells is enough to explain the preferential appearance of terminal heterocysts, without any need for a distinct regulatory pathway (Fig.2).

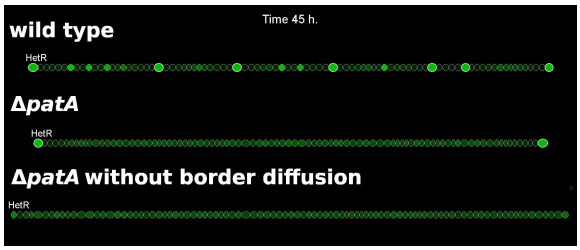

Fig. 2. Computational HetR profiles in filaments of wild-type, patA, and patA with no inhibitor leakage from the terminal cells.

[1] P. Casanova-Ferrer, S. Ares, J. Muñoz-Garca. *Terminal heterocyst differentiation in the Anabaena patA mutant as a result of post-transcriptional modifications and molecular leakage*. bioRxiv, doi:10.1101/2021.12.20.473559 (2021).

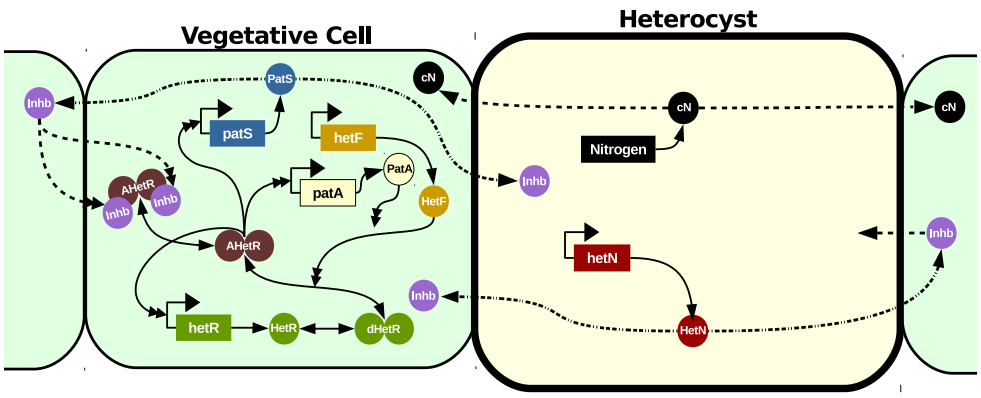

Fig. 1. **Mechanistic Model.** The vegetative cells are represented with a soft green background while the heterocyst has a soft yellow background and a thicker cell wall. Genes are represented in rectangles and proteic elements with circles. The dimers are represented with two attached circles and can be inactivated (in green), activated (in brown), and activated and inhibited (in brown with two attached purple inhibitors). Solid lines represent production (with only one simple arrowhead), transformations (with a simple arrowhead in both ends), and interactions (with a double arrowhead). Dashed lines represent inter-cellular traffic and dashed-doted lines represent a transformation when exported to a neighboring cell.

New insights into self–phoresis

Alvaro Domínguez
Universidad de Sevilla
dominguez@us.es

The notion of phoresis describes the motion of a particle in a fluid due to an externally imposed gradient (in chemical composition, in temperature, in electric potential,...) *and in the absence of a net force or torque*: therefore, the particle's momentum is balanced by the momentum of the flow in the ambient fluid, and the particle is not dragged, but it *swims* instead. Phoresis is a long known phenomenon that can be described in the context of linear–response theory. For instance, in the particular case of chemiophoresis, i.e., of phoresis driven by an external gradient $(\nabla n)_{\rm ext}$ in the concentration of a solute in the ambient fluid, the phoretic velocity $\mathbf{V}$ of the particle can be obtained as

$$\mathbf{V} = \mathcal{L}_{\rm lin} \, (\nabla n)_{\rm ext},$$

for a sufficiently small gradient over the scale of the particle size, in terms of the phoretic coefficient $\mathcal{L}_{\rm lin}$ given by a Green–Kubo expression.

A closely related phenomenology is observed for self–phoretic particles, which have attracted much attention in the last years as physical realization of artificial swimmers. In this case, the particle's surface is catalytically active, so that it induces a gradient $(\nabla n)_{\rm act}$ in the chemical composition of the ambient fluid. Thus, the experimental observations involving self–phoretic particles are customarily addressed as an instance of phoresis in an activity-induced gradient,

$$\mathbf{V} = \mathcal{L}_{\rm lin} \, (\nabla n)_{\rm act}.$$

However, an additional role of the particle's chemical activity has been recently identified, namely, as responsible for a specific *activity–induced response*, so that one has to write

$$\mathbf{V} = (\mathcal{L}_{\rm lin} + \mathcal{L}_{\rm act}) \, [(\nabla n)_{\rm ext} + (\nabla n)_{\rm act}]$$

in the more general scenario, where $\mathcal{L}_{\rm act}$ is the activity–induced contribution to the phoretic coefficient. We will describe the theoretical framework behind this result and argue that the piece $\mathcal{L}_{\rm act}$ could actually be as large as $\mathcal{L}_{\rm lin}$ in realistic configurations, disproving the claim that "self–phoresis is phoresis in a self–induced gradient". We will also discuss possible experimental realizations aimed at controlling the relative importance of the two different contributions to the phoretic response.

[1] A. Domínguez, M. N. Popescu, C. M. Rohwer, S. Dietrich, *Self–Motility of an Active Particle Induced by Correlations in the Surrounding Solution*, Phys. Rev. Lett. **125**, 268002 (2020); doi: 10.1103/PhysRevLett.125.268002

Regimes of intermittence in numerical ensembles of poorly-mixed chemical oscillators

Alejandro Carballosa[1,2] and Alberto P. Muñuzuri[1,2]
[1]Group of Nonlinear Physics, Faculty of Physics, University of Santiago de Compostela, 15782 Santiago de Compostela, Spain
[2]CITMAga, 15782 Santiago de Compostela, Spain

In this work we present a set of numerical results obtained from simulating a large ensemble of chemical oscillators that interact via a chemically active medium following the dynamics of the Belousov Zhabotinsky reaction, a paradigm for oscillating and synchronization phenomena. In well-mixed conditions, the stationary dynamic behaviors observed for this kind of oscillators usually range from full-synchronization (FS), oscillation death (OD) and super-synchronization (SS) [1], which refers to a phase and amplitude locking of the oscillators with the surrounding solution that couples them (which is another oscillator itself). In unmixed systems, the usual observed behavior is that of spiral waves [2] and in non-locally coupled oscillators there has been reported the possibility of chimera states [3]. Here, we direct our focus to a low, poorly-mixed diffusive configuration that corresponds better with a more realistic situation, as perfect mixing is almost never achieved. In the simulations, the oscillators are spatially distributed and are allowed to interact locally with a limited number of other oscillators that lie within a small interaction radius. Figure 1 presents a summary of our results, which are presented and analyzed in detail in [4].

We observed that in the edge of the phase transitions to the previously reported dynamical states, a certain degree of irregularity and intermittence appears. To our extent, these behaviors are yet not found in experimental realizations, and we believe that they could be of highly physical interest. First, in the transition from FS to SS, we present three different situations, showed in panels a), b) and c) of the Figure XX. Panel a) represent the time series of a small set of out-of-phase oscillators. This state is characterized by a synchronization loss caused by the existence of multiple synchronization waves across the system, which only phase locks the oscillators in the wavefront. Panel b) corresponds to a slightly higher coupling, right after the phase transition, and shows a double peak oscillation that only experiment a small sub-ensemble of the oscillators, while the rest remain super-synchronized with the solution and performing single large oscillations. Panel c) represents the averaged time series of all the oscillators in the system, showing a synchronized intermittence between the two dynamical states. There is a coexistence of large amplitude, low frequency oscillations that correspond to the SS state, followed by several low amplitude, high frequency oscillations characteristic from the FS state. This behavior was found to be persistent in time with no underlying patterns in the number of small oscillations that occur after a large oscillation or in the time-occurrence of the latter.

Secondly, in the transition from SS to OD, panel d) shows a similar behavior to the one in panel c), but with an abrupt cease of oscillating activity of all the ensemble right after the large amplitude synched oscillation. In the transition from FS to OD, and only in a situation of zero mixing, we found spatial clusters of oscillatory activity while the rest of oscillators underwent oscillation death. Panels e) and f) show the time series of oscillators with different amplitude and the spatial visualization of the oscillating cluster.

In summary, all the states briefly described above correspond to poor-mixing configurations that are likely to be experimentally observed, either with chemical or with other kind of biological oscillators. The extrapolation of these results to real examples might help to understand other collective behaviors in nature.

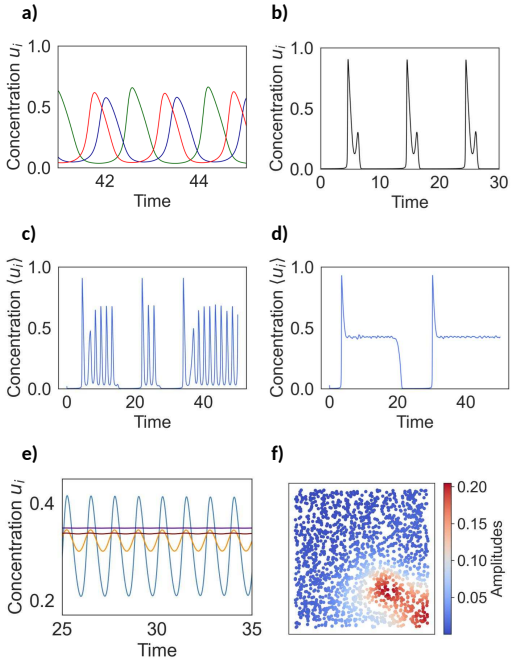

Fig. 1. Intermittence regimes found in the phase transitions from FS to SS (a-c), from SS to OD (d) and from FS to OD (e). Panel f) represents the spatial visualization of the amplitudes in panel e). More details in [4].

[1] G. Ghoshal, A. P. Muñuzuri and J. Prez-Mercader, Sci Rep, 6, 19186 (2016)

[2] M. R. Tinsley, A. F. Taylor, Z. Huang and K. Showalter, PRL, 102, 15, 158301 (2009)

[3] S. Nkomo, M. R. Tinsley and K. Showalter, PRL, 110, 24, 244102 (2013)

[4] A. Carballosa and A.P. Muñuzuri, Submitted (2022)

Mapping of First-Passage Percolation into bond percolation under extreme disorder

D. Villarrubia-Moreno[1,5], I. Álvarez-Domenech [2,5], J. Rodríguez-Laguna[3], S. N. Santalla [4,5] and P. Córdoba-Torres [2]
[1] Dpto. Matemáticas, Universidad Carlos III de Madrid, Spain.
[2] Dpto. Física Matemática y de Fluidos, Universidad Nacional de Educación a Distancia, Spain.
[3] Dpto. Física Fundamental, Universidad Nacional de Educación a Distancia, Spain.
[4] Dpto. Física, Universidad Carlos III de Madrid, Spain.
[5] Grupo Interdisciplinar de Sistemas Complejos (GISC).

Geometry on random manifolds presents both applied and fundamental interest, with applications ranging from the physics of polymers and membranes to quantum gravity. It was recently shown that, in the case of random surfaces which are flat in average and with short-range correlations in the curvature, geodesics present fractal structure, governed by exponents corresponding to the Kardar-Parisi-Zhang universality class (KPZ). When the manifold is discretized the problem is called First-Passage Percolation (FPP).

The FPP model consists of an undirected lattice where a link-time t is assigned randomly to each edge between neighboring nodes. Link-times are independent and identically distributed positive random numbers with common cumulative distribution function $F(t)$. The principal object of study in FPP are geodesics, i.e. the minimal-time paths joining pairs of nodes, and balls $B(T)$ given by the set of nodes which can be reached from the origin in a time less than the passage time T. When the lattice structure is smooth, the ball $B(T)$ grows linearly with T and has a non-random asymptotic shape. However when the probability function is properly tuned to introduce a high level of noise in the link-time distribution, the shape of the ball becomes completely irregular (Fig.1).

In a previous work [1] we analyzed the statistical properties of arrival times to FPP in weak-disorder regime and we showed a crossover between Gaussian and KPZ universality, with the crossover length decreasing as the disorder grows. In this work [2] we have gone one step further by considering the strong-disorder regime, where a new characteristic length appears below which the model displays bond-percolation universality class. In our work we provide a thorough characterization of the bond-percolation phase reproducing its critical exponents through a scaling analysis of the balls, for three different distributions: Weibull, Pareto and Log-Normal. The key to do this is the continuous mapping of the FPP passage time T into the occupation probability p of the bond-percolation problem:

$$p = F(T). \tag{1}$$

The behavior of the new characteristic length can be explained from the properties of the link-time distribution. Moreover, the interplay between the correlation length intrinsic to percolation and this new characteristic length determines the crossover between initial percolation-like growth and asymptotic KPZ scaling. We also provide a first study of the behavior of this interplay.

As long as the new characteristic length stays above the correlation length intrinsic to percolation, we were allowed to observe percolation-like growth in FPP models. But when the correlation length of percolation overtakes the FPP characteristic length, the model starts to develop KPZ scaling.

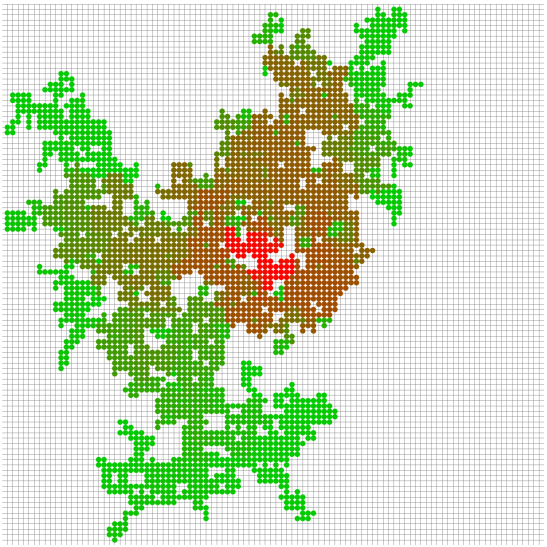

Fig. 1. Geodesic ball from First-Passage Percolation under strong disorder. Different colors represent different values of the passage time T; they correspond to different steps of the ball's growth.

[1] P. Córdoba-Torres, S. N. Santalla, R. Cuerno and J. Rodríguez-Laguna, *Kardar-Parisi-Zhang universality in first passage percolation: the role of geodesic degenerancy*, J. Stat. Mech 063212 (2018).

[2] D. Villarrubia, I. A. Domenech, S. N. Santalla, J. Rodríguez-Laguna and P. Córdoba-Torres, *First-Passage Percolation under extreme disorder: From bond percolation to Kardar-Parisi-Zhang universality*, Phys. Rev. E **101**, 062124 (2020).

Pareto-optimal trade-off: gambling in horse races and growing bacteria

L. Dinis[1], J. Unterberger[2], and D. Lacoste[3]
[1]GISC - Grupo Interdisciplinar de Sistemas Complejos and Dpto. de Estructura de la Materia, Física Térmica y Electrónica, Universidad Complutense de Madrid, 28040 Spain
[2] Institut Elie Cartan, UMR CNRS 7502, Université de Lorraine, BP 239 F-54506 Vandoeuvre-lès-Nancy Cedex, France
[3] Gulliver Laboratory, UMR CNRS 7083, PSL Research University, ESPCI, 10 rue Vauquelin, F-75231 Paris Cedex 05, France

Developed in 1956 by Bell Labs scientist John Kelly, *Kelly's criterion* applied the newly created field of information theory to gambling and investment [1]. Largely popularized in books [2], this criterion allows a gambler (or investment fund) to fix what proportion of bankroll should be risked on a given bet. It essentially exploits side information to maximize the expected geometric growth rate of a capital. Although ensuring optimal growth rate, Kelly's criterion turns out to be risky, giving rise to large fluctuations in the growth rate.

In many situations, one may consider a possible trade-off between the expected growth and the risk involved, seeking for example to minimize the variance while maximizing the gain, and defining and efficient border in the region of possible strategies. A related idea was introduced in finance by Markowitz [3] under the name of mean-variance analysis as a way to mitigate risk, which in Gaussian models is described by the variance of assets or volatility.

We have studied such efficient border or Pareto front in the original Kelly's horse race problem, finding a trade-off between the average growth rate and its fluctuations [4]. Figure 1 represents the computed fronts for a specific game with 3 horses. We have also found an uncertainty relation between average growth and its standard deviation, resembling those found in Stochastic Thermodynamics [5, 6]. This relation in horse races constrains gambling strategies and imposes a minimal level of risk associated to a certain growth rate, a *no risk no gain* type of bound.

A related idea is found in growing populations, for instance, of monoclonal bacterial colonies subject to fluctuating environments and with stochastic phenotypic switching. Phenotypic switching is usually understood as a bet-hedging strategy to protect the colony against environmental fluctuations. We have analyzed a simple model of two randomly switching phenotypes subjected to two stochastically switching environments, and found similar trade-off curves. Building on these Pareto fronts, our simulations of the dynamics suggest a close connection between the long term variance of the growth rate and the extinction probability, indicating that it may be beneficial for a population to accept a reduction of its short-term reproductive success in exchange for longer-term risk reduction [7].

Bet-hedging is an important topic in biology, associated to a number of phenomena such as species polymorphism, antibiotics resistance of bacteria or the resistance of cancer cells to anti-cancer drugs, and more generally to the phenomenon of cell variability and adaptation by the immune system.

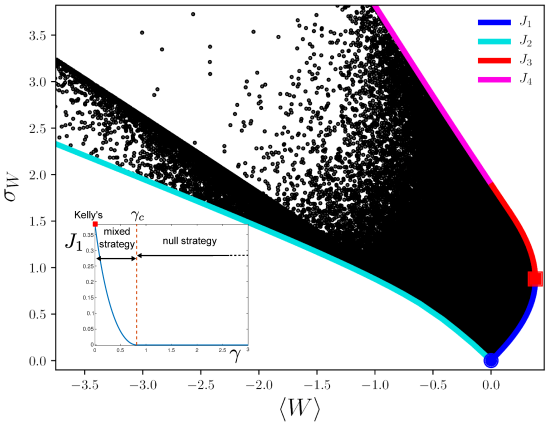

Fig. 1. Pareto borders for 3 horses obtained by simulated annealing built with different utility functions J_1, J_2, J_3 and J_4 (colored solid lines), together with a cloud of points generated by randomly choosing bets satisfying all relevant constraints. Inset: $J_1 = \langle W \rangle - \gamma \sigma_W$ versus γ along the trade-off branch (*i.e.* on the dark blue border) showing the transition from a mixed strategy to a strategy of variance minimization. $\langle W \rangle$ and σ_W stand for the average capital growth rate and its variance, respectively.

[1] J. L. Kelly. A New Interpretation of Information Rate. *Bell System Technical Journal*, 35(4):917–926, 1956.

[2] William Poundstone. *Fortune's Formula: The Untold Story of the Scientific Betting System that Beat the Casinos and Wall Street*. Hill & Wang, 2005.

[3] Harry Markowitz. Portfolio Selection. *The Journal of Finance*, 7(1):77–91, 1952.

[4] L. Dinis, J. Unterberger and D. Lacoste Phase transitions in optimal betting strategies. *Europhys. Lett.* **131**, *60005 (2020)*

[5] Andre C. Barato and Udo Seifert. Thermodynamic Uncertainty Relation for Biomolecular Processes. *Physical Review Letters*, 114(15):158101, April 2015.

[6] Todd R. Gingrich, Jordan M. Horowitz, Nikolay Perunov, and Jeremy L. England. Dissipation Bounds All Steady-State Current Fluctuations. *Physical Review Letters*, 116(12):120601, March 2016.

[7] L. Dinis, J. Unterberger and D. Lacoste. Pareto-optimal trade-off for phenotypic switching of populations in a stochastic environment. *Submitted*

Liquid crystalline patterns of exotic symmetries in monolayers of vertically vibrated granular particles

Yuri Martínez-Ratón[1] and Enrique Velasco[2]

[1]Grupo Interdisciplinar de Sistemas Complejos (GISC), Departamento de Matemáticas, Escuela Politécnica Superior, Universidad Carlos III de Madrid, Avenida de la Universidad 30, E-28911, Leganés, Madrid, Spain.

[2]Departamento de Física Teórica de la Materia Condensada, Insituto de Física de la Materia Condensada (IFIMAC) and Instituto de Ciencia de Materiales Nicolás Cabrera, Universidad Autónoma de Madrid, E-28049, Madrid, Spain.

Monolayers of millimetre-sized metallic particles confined into thin cavities and subject to periodic vertical agitation form a variety of fluid patterns with orientational order that resemble those found in molecular and colloidal liquid crystals. This is remarkable given that these systems are driven by dissipative forces. Within some reasonable windows of experimental parameters one can identify different patterns, including nematic and smectic, which could be understood in terms of classical statistical mechanics of hard bodies. In particular, low aspect ratio cylinders project as rectangles and may form uniaxial and tetratic nematic phases [1]. The latter exhibits four-fold symmetry, possesses two equivalent directors and corresponds to the two-dimensional analogue of the three- dimensional cubatic phase.

We have experimented with more general metallic particles, consisting of prisms with different transverse shapes: equilateral triangles (see Fig. 1), right-angle triangles, etc. In the first case the exotic triatic phase, with six-fold symmetry and three equivalent directors, is excited. Even more remarkable, geometric frustration caused by confinement in cavities that are not compatible with the intrinsic symmetry of the fluid causes topological defects to arise [2]. These defects seem to abide by the same topological rules as standard liquid crystals. Our findings can be understood with the help of simulations of hard particles subject to thermal equilibrium.

Overall, we believe that these experimental systems may be used with advantage to explore many features of two-dimensional liquid crystals, including formation of phases with exotic symmetries, effect of confinement in cavities of different geometries, and formation of topological defects and their nature and interactions.

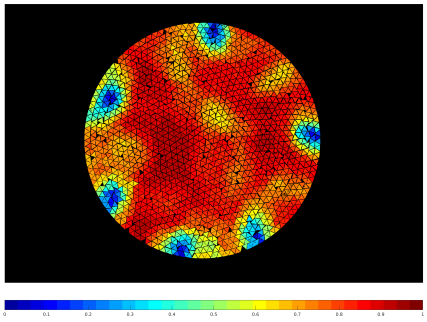

Fig. 1. False colour field of triatic order parameter, showing the formation of a triatic phase and six topological defects that restore the global symmetry of the system, broken by confinement of the six-fold symmetric fluid in a cicular cavity.

[1] M. González-Pinto, F. Borondo, Y. Martínez-Ratón and E. Velasco , Soft Matter, **13**, 2571 (2017).

[2] M. González-Pinto, J. Renner, D. de las Heras, Y. Martínez-Ratón and E. Velasco, New J. Phys. **21**, 033002 (2019). (2019).

El atasco como una transición de fase

A. Garcimartín[1], R. Caitano [1], B. V. Guerrero [1], R. E. R. González [2], and I. Zuriguel[1]
[1] Depto. de Física y Mat. Apl., Facultad de Ciencias, Universidad de Navarra, E-31080 Pamplona, Spain
[2] Laboratório de Sistemas Complexos e Universais, Departamento de Física,
Universidade Federal Rural de Pernambuco, Recife-PE, CEP 52171-900, Brasil

Los flujos de partículas sólidas presentan una característica, y es que pueden atascarse (cosa que suele suceder, por ejemplo, en una angostura o en un orificio). Para deshacer el atasco, con frecuencia se recurre a vibraciones. Si son lo suficientemente intensas, estas vibraciones pueden restablecer el flujo. En este proceso tan general, pueden darse dos casos en el límite de tiempos muy largos: o bien el atasco domina (y el número de partículas por unidad de tiempo tiende a cero), o bien el flujo promedio es mayor que cero.

Esta situación se asemeja a una transición de fase, donde el parámetro de control debe estar relacionado con la intensidad de la vibración, y el parámetro de orden con el flujo medio. En este trabajo se presentan algunos resultados experimentales con los que se describe la transición entre un sistema atascado y un sistema que fluye en el lenguaje de las transiciones de fase. El dispositivo experimental consiste en un silo bidimensional lleno de granos esféricos de diámetro l, con un orificio de tamaño D en la base [1], siendo D la longitud del orificio dividido por el diámetro del grano. A la zona de la base cercana al orificio se la perturba con una vibración sinusoidal de amplitud A y frecuencia angular ω. Grabamos con una cámara de vídeo el orificio de salida, y mediante análisis de imágenes se determina si en cada instante están cayendo granos o no. De esa manera se obtiene una serie temporal con tiempos de flujo t_f e intervalos donde el flujo se interrumpía, de duración t_a.

Para comenzar, partimos de una observación relativa a los flujos intermitentes (en los cuales el sistema está a veces fluyendo y a veces no). La distribución de los tiempos de flujo (t_f) es exponencial, mientras que la distribución de los intervalos en los que el flujo se interrumpe (t_a) presenta una cola potencial. Los parámetros de estas distribuciones dependen de la intensidad de la vibración. El punto clave es que $\langle t_f \rangle$ siempre converge, por ser una distribución exponencial; pero $\langle t_a \rangle$ puede diverger, si el exponente de la ley de potencias es suficientemente pequeño. Se puede definir entonces

$$\Phi = \frac{\langle t_f \rangle}{\langle t_f \rangle + \langle t_a \rangle}$$

que es la fracción de tiempo durante la cual el sistema está fluyendo. Si $\langle t_a \rangle$ diverge, $\Phi \to 0$. Tomaremos esa cantidad, Φ, como parámetro de orden (pues es cero en el sistema atascado, y mayor que cero en el caso de que fluya, aunque sea de manera intermitente).

Como parámetro de control, tras explorar varias posibilidades, escogimos

$$S = \frac{A\omega}{\sqrt{gl}}$$

porque todos los experimentos con idéntico valor de S, aun para distintas frecuencias o amplitudes de la vibración, proporcionan el mismo Φ. Por tanto, S es un buen parámetro de control.

Para cada experimento, hallamos Φ, y encontramos S_c (el valor de S para el que se anula Φ). Si se representa Φ en función de la supercriticalidad $\frac{S-S_c}{S_c}$ para diferentes tamaños de orificio D, se obtiene el gráfico mostrado en la Figura 1. Aunque el ruido de nuestros datos no permite un ajuste preciso, la curva es compatible con un exponente crítico $1/2$. Por otro lado, el diagrama de fases en el espacio S – D viene definido por los valores de S_c, que separan la fase atascada de la que no lo está (Figura 1). Es posible que el término fase no sea riguroso en este contexto, pero se ha propuesto como marco para entender de manera genérica este fenómeno [2].

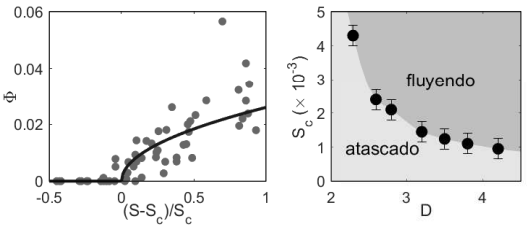

Fig. 1. *Izquierda*: El parámetro de orden Φ en función de la supercriticalidad $\frac{S-S_c}{S_c}$, para diferentes tamaños del orificio. La curva sólida corresponde a $\Phi = \left(\frac{S-S_c}{S_c}\right)^{1/2}$ *Derecha*: el diagrama de fases.

[1] R. Caitano, B.V. Guerrero, R. E. R. González, I. Zuriguel, and A. Garcimartín, Phys. Rev. Lett. **127**,148002 (2021).

[2] I. Zuriguel, D. R. Parisi, R. C. Hidalgo, C. Lozano, A. Janda, P. A. Gago, J. P. Peralta, L. M. Ferrer, L. A. Pugnaloni, E. Clément, D. Maza, I. Pagonabarraga, and A. Garcimartín, Scientific Reports **4**, 7324 (2014).

Experimental and CFD numerical study of hopper discharges.

David Méndez-Esteban[1], RC Hidalgo[1] and Diego Maza[1]
[1]Dpto. de Física y Matemática Aplicada
Facultad de Ciencias, Universidad de Navarra, Spain.

In this work, we numerically examine granular flows in silos and hoppers using Computational Fluid Dynamics (CFD). In particular, we use constitutive models implemented in a commercial software package (ANSYS Fluent[9]) and employ them to simulate the discharge process. The analysis is focused on the velocity and density fields at the silo exit, and the numerical protocol is validated, comparing with experimental data of mass flow rates. In addition, we test the results inside of them at different heights to check if we obtain Gaussian profiles.

Accurate correlations predicting the mass flow rate in granular hoppers and silos have been introduced accounting the discrete nature of the flowing material [1, 2, 8]. On the contrary, R & D factories and technical offices use continuous models to analyze the most used hopper and silo devices. Such algorithms seem to work very well if a wide series of control parameter are tuning adequately, so they require an extensive experimental calibration.

We use a continuous model based in the KTGF theory [4, 5, 6], including a specific procedure to describe densely packed systems, i.e., taking into account the frictional behavior [7] of the material. By means of this tool we analyze the relationship between the hopper angle and the discharge mass flow rate in conical hoppers. Adjusting the simulation parameters feed-backing the code with experimental results, we develop an accurate calibration procedure, which can be employed in both, simplified lab conditions and industrially relevant systems.

Furthermore, we also explore the role of the outlet aperture. We find that the former numerical approach captures the main features of the granular flux through orifices, such as the velocity and density profiles. Importantly, the results show as the systems dynamics near the hopper exit determines the discharge rate.

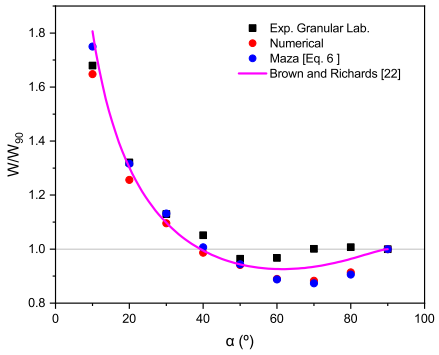

Fig. 1. Comparative Evolution of normalized mass flow rate, $\frac{W}{W_{\alpha=90}}$,Brown and Richards theory and experimental results, for different hopper angles, α.

[1] Beverloo, W. A. and Leniger, H. A. and Van de Velde, J. *The flow of granular solids through orifices*, Chemical Engineering Science (1961).

[2] Mankoc, C. and Janda, A. and Arévalo, R. and Pastor, J. M. and Zuriguel, I. and Garcimartín, A. and Maza, D. *The flow rate of granular materials through an orifice* (Granular Matter, 2007).

[3] Janda, A. and Zuriguel, I. and Maza, D. *Flow rate of particles through apertures obtained from self-similar density and velocity profiles* (Physical Review Letters, 2012).

[4] Gidaspow, D. *Multiphase Flow and Fluidization: Continuum and Kinetic Theory Descriptions* (Physical Elsevier Science, 1992).

[5] Lun, C. K. K. and Savage, S. Br and Jeffrey, D. J. and Chepurniy, N. *Kinetic theories for granular flow: inelastic particles in Couette flow and slightly inelastic particles in a general flowfield* (Journal of Fluid Mechanics, 1984).

[6] Johnson, P. C. and Jackson, R. *Frictional–collisional constitutive relations for granular materials, with application to plane shearings* (Journal of Fluid Mechanics, 1987).

[7] Schaeffer, D. G. *Instability in the evolution equations describing incompressible granular flow* (Journal of Differential Equations,1987).

[8] Brown, R. L. *Minimum energy theorem for flow of dry granules through apertures* (Nature,1961).

[9] ANSYS, Inc. *ANSYS Fluent Theory Guide* (ANSYS Help System,2018).

Modelling parasite-induced marine diseases of immobile hosts

Àlex Giménez-Romero[1], Federico Vázquez[1,2], Cristobal López[1], and Manuel A. Matías[1]
[1] Instituto de Física Interdisciplinar y Sistemas Complejos, IFISC (CSIC-UIB), Campus UIB E-07122 Palma de Mallorca, Spain
[2] Instituto de Cálculo, FCEyN, Universidad de Buenos Aires and CONICET, Buenos Aires, Argentina

Marine infectious diseases are more prevalent in recent times due to climate change and other anthropogenic pressures, posing a substantial threat to marine ecosystems and the conservation of their biodiversity [1]. An important subset of marine organisms are sessile, for which the most common mechanism for disease transmission is direct contact with waterborne parasites. Only recently, some deterministic compartmental models have been proposed to describe this kind of epidemics, being these models based on non-spatial descriptions where space is homogenised and parasite mobility is not explicitly accounted for [2]. These models have been able to describe experimental data in some specific situations, and thus are a good start point to develop more complex models. Indeed, in realistic situations epidemic transmission is conditioned by the spatial distribution of hosts and the parasites mobility patterns. Thus, the interplay between these factors is expected to have a crucial effect in the evolution of the epidemic, so calling for a explicit description of space.

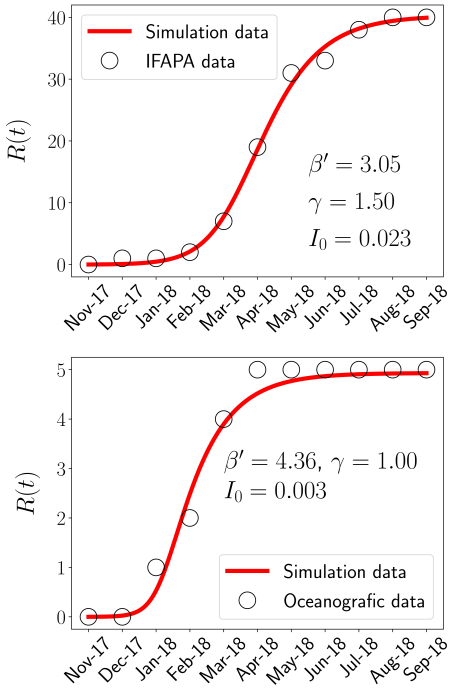

Fig. 1. Model fit using two experimental data sets of the mass mortality event of *Pinna nobilis*.

First, we built a mean-field spatially-homogeneous compartmental model and performed and extensive analytical study [3]. As a result, we were able to show that the model has an exact reduction via a conserved quantity and an approximate one that yields the original SIR model with effective coefficients. The model and its reductions were validated with experimental data of the mass mortality event of *Pinna nobilis* [4] (Fig. 1).

Then, we develop a spatially-explicit individual-based version of the model [5]. We investigate the impact of spatial disease transmission, performing extensive numerical simulations and analytical approximations. Specifically, the effects of parasite mobility into the epidemic threshold and the temporal evolution of the epidemic are assessed. We show that larger values of pathogen mobility have two main implications: more severe epidemics, as the number of infections increases, and shorter time-scales to extinction. Moreover, an analytical expression for the basic reproduction number of the spatial model, $\tilde{R}_0$, is derived as function of the non-spatial counterpart, R_0, which characterises a transition between a disease-free and a propagation phase, in which the disease propagates over a large fraction of the system. This allows to determine a phase diagram for the epidemic model as function of the parasite mobility and the basic reproduction number of the non-spatial model (Fig. 2).

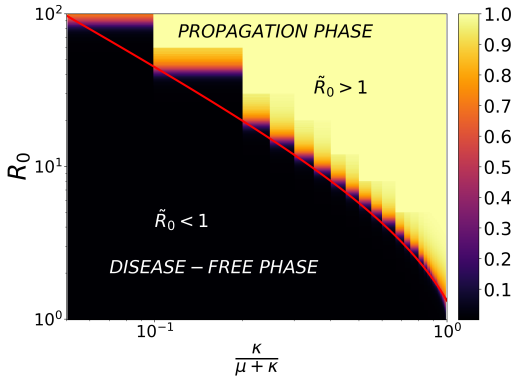

Fig. 2. Phase diagram showing the transition between the the disease-free phase and the propagation phase for several values of the parasite mobility and R_0. The colour code represents the density of dead individuals in the final state of the epidemic computed by the average over 1000 realisations.

[1] K. D. Lafferty et al., Annual Review of Ecology, Evolution, and Systematics **35**, 31-54 (2004).

[2] G. Bidegain et al., Fisheries Research **186**, 82-93 (2017)

[3] À. Giménez-Romero et al., Ecol. Modell. **459** (2021)

[4] García March et al., Biol. Cons. **243** (2020)

[5] À. Giménez-Romero et al., *Spatial effects in parasite induced marine diseases of immobile hosts*, bioRxiv

Global risk predictions for Pierces disease of grapevines

Àlex Giménez-Romero[1], Javier Galván[1], Marina Montesinos[2], Joan Bauzà[3], Martin Godefroid[4], Alberto Fereres[4], José J. Ramasco[1], Manuel A. Matías[1] and Eduardo Moralejo[2]

[1]Instituto de Fsica Interdisciplinar y Sistemas Complejos, IFISC (CSIC-UIB), Campus UIB E-07122 Palma de Mallorca, Spain
[2]Tragsa, Passatge Cala Figuera 6, 07009 Palma de Mallorca, Spain
[3] Departamento de Geografía, Universidad de las Islas Baleares, Campus UIB, 07122 Palma de Mallorca, Spain
[4] Instituto de Ciencias Agrarias, Consejo Superior de Investigaciones Científicas, ICA-CSIC, 28006 Madrid, Spain

The clonal lineage of the bacterium *Xylella fastidiosa* (Xf) responsible for Pierce's disease (PD)[1] poses a threat to viticulture worldwide [2]. Although this vector-transmitted disease has remained mainly restricted to the United States, recent introductions on the islands of Majorca (Spain) and Taiwan have raised concerns about the risk of spreading worldwide [3]. To assess this risk, here we build a climate-driven epidemiological model that simulates PD progression (Fig. 1). The model considers the temperature-dependent infection process based on a 3-year inoculation assay and assume local disease propagation when climatic conditions are favourable. The model was successfully validated with spatiotemporal data of the PD distribution in the United States yielding a remarkable ∼90% accuracy. Thereafter the model was applied to the main winegrowing regions worldwide, specially focusing in Europe as a case study based on the distribution of the main vector, *Philaenus spumarius*.

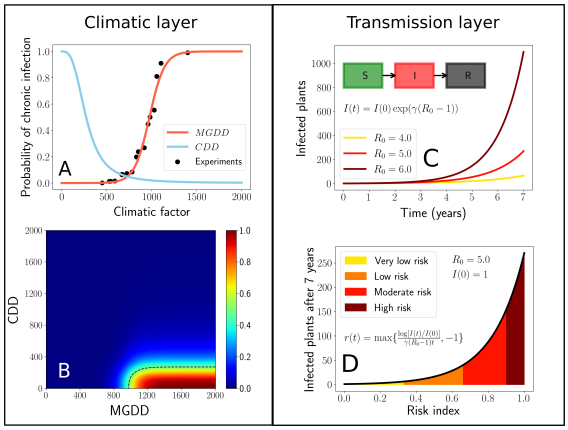

Fig. 1. Climatic and transmission layers composing the epidemiological model. A) Relationship between the likelihood of infection and temperature-related metrics(*CDD* and *MGDD*). Black dots depict the 3-y inoculation assay. (**B**) Combined ranges of $MGDD$ and CDD on the likelihood of developing chronic infection. (**C**) Transmission layer of the dynamic equation. (**D**) Relationship between risk index and the number of infected plants.

Our model simulation reveals that most wine-quality producing areas in China, Europe, Argentina, Chile, South Africa, and Australia currently thrive in non-risk or transient-risk zones (Fig. 2). To a lesser extent, epidemic-risk zones with low to moderate risk indices appear in coastal zones such as Mallorca and Apulia, where Xf outbreaks have been already detected. The European case shows how models assuming a vector heterogeneous distribution yield lesser extended epidemic-risk zones than previous risk maps. Overall, a global expansion of PD epidemic-risk zones is projected for 2050, although with low increase in risk indices. Our study highlights the importance of considering climate variability and an invasive criterion to obtain precise risk maps for plant health decision-making.

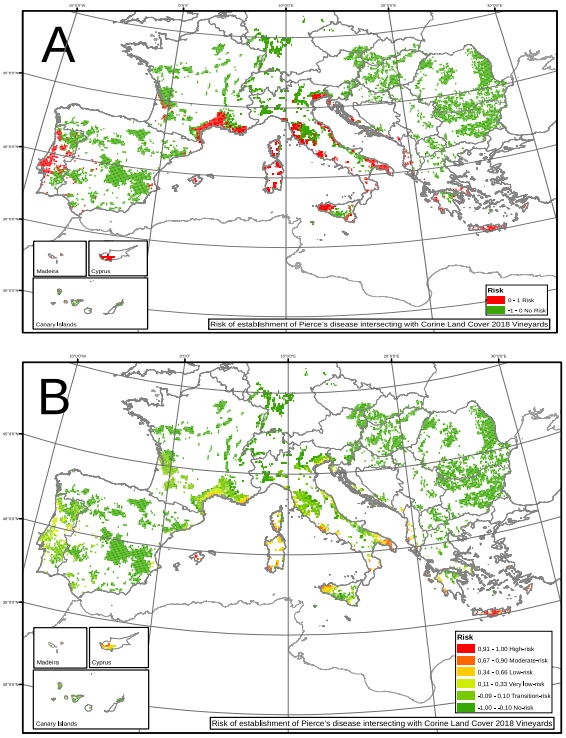

Fig. 2. Climate-driven risk map for PD establishment under a baseline $R_0 = 5$ scenario in Europe. (A) Binray risk map. (B) Risk map divided in severity indices.

[1] Davis, M. J., Purcell, A. H. and Thomson, S. V., Science **199**, 75-77 (1978)

[2] Hopkins, D. L. and Purcell, A. H., Plant Disease **86**, 1056-1066 (2014).

[3] Moralejo, E. et al., Plant Pathology **109**, 222-224 (2019).

On the mean square displacement of intruders in freely cooling granular gases

E. Abad [1], S. B. Yuste[2], and V. Garzó[2]

[1]Departamento de Física Aplicada, Instituto de Computación Científica Avanzada (ICCAEx), Universidad de Extremadura, 06800 Mérida (Spain),

[2]Departamento de Física, Instituto de Computación Científica Avanzada (ICCAEx), Universidad de Extremadura, Avda. de Elvas s/n, 06006 Badajoz (Spain)

We compute the mean square displacement (MSD) of intruders immersed in a freely cooling granular gas composed of inelastic smooth hard spheres ("grains") [1]. In general, intruders and grains are assumed to have different mechanical properties, implying that non-equipartition of energy must be accounted for in the computation of the diffusion coefficient D. In the hydrodynamic regime, the time decay of the granular temperature T of the cooling gas is known to be dictated by Haff's law [2]; the concomitant decay of the intruder's collision frequency entails a time decrease of D. Explicit knowledge of this time dependence allows us to determine the MSD by integrating the corresponding diffusion equation.

Previous studies have found a logarithmic time dependence of the MSD in the limit cases when intruders and grains are mechanically equivalent [selfdiffusion] (see e.g. [3, 4]) or when the intruder's mass is much larger than that of the grains [Brownian limit] (see [5]). We find that the logarithmic time dependence of the MSD extends beyond the two aforementioned cases, and holds in all spatial dimensions for arbitrary values of the mechanical system parameters (Euclidean spatial dimension d, intruder-grain mass ratio m_0/m , intruder-grain diameter ratio σ_0/σ, and the respective coefficients α_0 and α of normal restitution for intruder-grain collisions and grain-grain collisions). The ultraslow type of diffusion observed here (slower than any power-law in time) is due to the energy loss in every collision, as opposed to other systems where it arises from the spatial disorder of the medium.

Beyond the self-diffusion and Brownian cases, we carry out a comprehensive study of the MSD dependence on the mechanical system parameters. For a proper choice of the latter, interesting features emerge from our analysis, such as a non-monotonic dependence of the MSD on the restitution coefficients and on the intruder-hard sphere mass ratio (see Fig. 1). To understand the observed behaviour, we analyze in detail the properties of the intruder's ballistic displacements inside the granular gas.

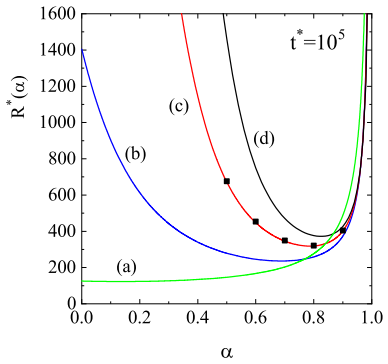

Fig. 1. Plot of the MSD scaled with the squared mean free path ℓ^2 of the three-dimensional granular gas $R^* \equiv \langle|\Delta \mathbf{r}|^2\rangle/\ell^2$ as a function of the coefficient of normal restitution $\alpha = \alpha_0$ for $\sigma_0/\sigma = 2$ and four different values of the mass ratio: $m_0/m = 1/2$ (a), $m_0/m = 5$ (b), $m_0/m = 8$ (c), and $m_0/m = 10$ (d). The symbols refer to the results obtained from Monte Carlo simulations for $m_0/m = 8$. All the curves refer to the same value $t^* = 10^5$ of the scaled time $t^* \equiv \nu(0)^{-1}t$, where $\nu(0)$ is the initial value of the average grain-grain collision frequency and t denotes physical time.

[1] E. Abad, S. B. Yuste, and V. Garzó, arXiv:2112.06541v1.

[2] V. Garzó, *Granular Gaseous Flows* (Springer, Cham, 2019).

[3] J. J. Brey, M. J. Ruiz-Montero, D. Cubero, and R. García-Rojo, *Self-diffusion in freely evolving granular gases*, Phys. Fluids **12**, 876–883 (2000).

[4] A. S. Bodrova, A. V. Chechkin, A. G. Cherstvy, and R. Metzler, *Quantifying non-ergodics dynamics of force-free granular gases*, Phys. Chem. Chem. Phys. **17**, 21791–21798 (2015).

[5] J. J. Brey, M. J. Ruiz–Montero, R. García–Rojo, and J. W. Dufty, *Brownian motion in a granular gas*, Phys. Rev. E **60**, 7174–7181 (1999).

Relaxation of a one-dimensional bead-string model

S. B. Yuste[1], E. Abad[2] and A. Baumgaertner[3]
[1]Departamento de Física, Instituto de Computación Científica Avanzada (ICCAEx),
Universidad de Extremadura, Badajoz (Spain)
[2]Departamento de Física Aplicada, Instituto de Computación Científica Avanzada (ICCAEx),
Universidad de Extremadura, Mérida (Spain)
[3]University of Duisburg-Essen, Faculty of Physics (Germany)

The one-dimensional (1d) bead-spring model, or 1d Rouse model, consists of N monomers (beads) subject to thermal fluctuations and connected by massless springs. Monomers can thus be viewed as impenetrable random walkers (RWs) interacting through a nearest-neighbour harmonic potential. Here we consider a similar model in which the beads are connected by *strings* rather than by springs. Therefore, our model can be viewed as a modified 1d Rouse model where the harmonic potential is replaced by an extremely soft-hard potential: the square well. Note that the beads (RWs) can diffuse freely in 1d, except for the fact that they cannot cross nor separate from one another beyond a certain distance Δ (Δ is the string length or, equivalently, the width of the square-well). We are primarily interested in studying how this system relaxes to its equilibrium state.

It should be noted that our model progressively approaches a standard single-file model (with finite N) the larger Δ or the smaller t becomes; in fact, for $\Delta^2/(4Dt) \to \infty$ (where D is the RW diffusion constant), our model is just the single file model .

In order to obtain an approximate expression for the N-particle positional pdf, we make the following factorization ansatz:

$$p(x_1,\ldots,x_N,t;\Delta) = A\prod_{i=1}^{N} G(x_i,t)\prod_{i=1}^{N-1} R(x_{i+1}-x_i,\Delta)$$

where A is the normalization constant, $G(x,t|x_0,t=0)$ denotes the free-particle Green function (gaussian distribution) and $R(x,\Delta)$ is the rectangular (hat) function of width Δ: $R(x,\Delta)=1$ for $0<x<\Delta$ and $R(x,\Delta)=0$ elsewhere. The exclusion effects arising from the square well potential are accounted for by the hat function. For $\Delta\to\infty$, this ansatz becomes identical with the one used by Aslangul [1] to study the single-file model with a finite RW number N. Reduction of $p(x_1,\ldots,x_N,t;\Delta)$ by repeated integration yields the pdf for the position x_i of the i-th RW. It turns out that it is possible to find approximate expressions for such pdfs and for the corresponding moments as power series of $\delta\equiv\Delta/(4Dt)^{1/2}$. We subsequently compare the dynamics of the beads predicted by our model (and their corresponding collective "polymer" dynamics) with the outcome of MC simulations. Our simulations show that, starting from a fully compressed polymer or a fully stretched polymer, the relaxation of the polymer length L is well described by a Kohlrausch-Williams-Watts (KWW) law for short and intermediate times, at less for not too large values of N (see Fig. 1). However, for very long times, our ansatz predicts that the L-relaxation to its equilibrium state follows the inverse power law $1/t$, which is in full contrast with the exponential decay exhibited by the 3d Rouse model. On the other hand, once the system has attained the equilibrium state, the diffusion constant of each bead (and thus of the polymer as a whole) can be shown to scale as $1/N$, as it is also the case in the 3d Rouse model [2]. It is possible to estimate the full equilibrium pdf for the polymer length L by counting the number of microstates compatible with the equilibrium state. We have also found that the bead-string polymer is Hookean in the sense that the force required to change the equilibrium value of L by an amount of x is proportional to x. The elastic constant turns out to be proportional to Δ and, as in the 3d Rouse model, inversely proportional to N.

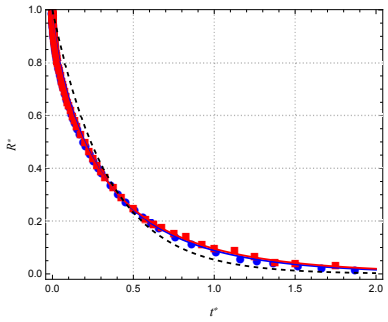

Fig. 1. Relaxation of the scaled relative polymer length $R^*\equiv|L(t)-L_{\rm eq}|/|L(0)-L_{\rm eq}|$ as a function of time $t^*=t/\tau$ with $\tau=\Delta^2/(4D)$. We consider both a fully compressed (circles) and a fully stretched (squares) initial condition. Solid lines represent a KWW relaxation law, $\exp(t/t_R)^\beta$, with $\beta\approx 3/4$ and $t_R\approx 1/3$ for both initial conditions. The dashed line is an exponential fit.

[1] Cl. Aslangul,*Classical diffusion of N interacting particles in one dimension: General results and asymptotic laws*, Europhysics Letters, **44** (3) 284–289 (1998).

[2] M. Rubinstein and R. H. Colby, *Polymer Physics* (OUP Oxford, 2003).

Iberian oak decline ("seca") caused by *Phytophthora cinnamomi*: A spatiotemporal analysis incorporating the effect of host heterogeneities at landscape scale

E. Cardillo[1], E. Abad [2], and S. Meyer[3]
[1]Institute of Cork, Wood and Charcoal, Centro de Investigaciones Científicas y Tecnológicas de Extremadura, Mérida, Spain,
[2]Departamento de Física Aplicada, Instituto de Computación Científica Avanzada (ICCAEx),
Universidad de Extremadura, Mérida, Spain,
[3] Institute of Medical Informatics, Biometry, and Epidemiology,
Friedrich-Alexander-Universität Erlangen-Nürnberg, Erlangen, Germany

The pathogen *Phytophthora cinnamomi* is considered a main driver of Iberian oak decline (IOD), a forest disease which decimates holm oaks (*Quercus ilex*) and cork oaks (*Quercus suber*) in a multipurpose, silvo-pastoral and semi-natural ecosystem of 3.1 million hectares in the south-west of Europe. Little is known about the spatial dynamics of *Phytophthora cinnamomi* and how forest stand characteristics affect the IOD epidemic. Here, we analyse IOD spread over several decades in one such ecosystem by means of a multilevel approach [1] based on (a) identification of diseased sites via repeated aerial imagery at landscape scale, (b) confirmation by subsampling of soil and roots, and iii) an epidemic model accounting for host population heterogeneities. We use a 'self-exciting' spatiotemporal point process with two additive risk components: a distance-dependent epidemic component represents the inoculum pressure from nearby disease foci, and a background component describes sporadic disease transmission over larger distances or from unobserved sources.

A lagged power-law spatial kernel provides the best fit for the observed disease pattern. We estimate that 49 % of the secondary infections triggered by a primary source occur within a distance of 250 m. The color code in Fig. 1 shows the strong differences in disease intensity within the area under study.

Our results also highlight the role of density and diversity of the host population; we find that the rate of sporadic infections in silvo-pastoral systems (*dehesas*) is lower than in forests, and higher in mixed stands and shrub encroached oak lands than in pure stands.

The above findings have direct implications for IOD management, for example the estimated spatial kernel may guide the definition of suitable target areas for localized control measures and help to quantify their success. Our results also suggest that silviculture treatments aimed at controlling the density and species composition of oak stands, as well as the abundance of shrubs, are crucial to the containment of IOD.

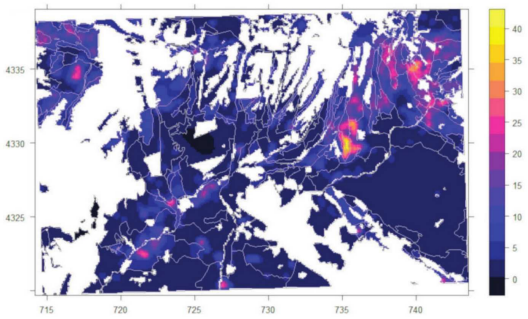

Fig. 1. Model-based estimation of the IOD disease intensity (=accumulated number of foci / km^2 during the reference period) in the area of study. UTM coordinates in km referenced to the WGS-84 system.

[1] E. Cardillo, E. Abad, and S. Meyer, Forest Pathology **51**, e12667 (2021).

Dynamics of hard particles confined by an isotropic harmonic potential

P. Maynar[1,2], M. I. García de Soria[1,2], E. Trizac[3], and D. Guéry-Odelin[4]
[1]Física Teórica, Universidad de Sevilla, Apartado de Correos 1065, E-41080, Sevilla, Spain
[2]Institute for Theoretical and Computational Physics. Universidad de Granada, E-18071, Granada, Spain
[3]Université Paris-Saclay, CNRS, LPTMS, 91405, Orsay, France
[4]Laboratoire Collisions, Agrégats, Réactivité, IRSAMC, Université de Toulouse, CNRS, UPS, France

The dynamics of a system composed of elastic hard particles confined by an isotropic harmonic potential is studied. In the low-density limit, the dynamics is described by the Boltzmann equation and the system does not reach equilibrium except for some particular class of initial conditions. On the contrary, the system reaches a periodic in time state in which the velocity distribution function is Gaussian, but with the hydrodynamic fields oscillating in time with some specific profiles. It is shown that this so-called *breather* state is completely specified by the constants of the motion, the mean square displacement, $\langle r^2 \rangle$, at the initial time and its derivative with respect to time also at the initial time. This is due to the fact that, at this level of description, $\langle r^2 \rangle$ verifies a closed second order differential equation. For low but finite densities, the dynamics of the system is analyzed by taking into account the finite size of the particles. Under well-controlled approximations, a closed evolution equation for $\langle r^2 \rangle$ is derived, obtaining that it decays to its equilibrium value, oscillating with a frequency slightly modified with respect to the Boltzmann values. The time average of the oscillations is also renormalized. An excellent agreement is found between Molecular Dynamics simulation results and the theoretical predictions for the frequency and the time average of the oscillations. For the relaxation time, the agreement is not as good as for the two previous quantities and the origin of the discrepancies is discussed.

Microrheology of isotropic and anisotropic colloidal suspensions via dynamic Monte Carlo simulations

Fabián A. García Daza[1], Antonio M. Puertas[2], Alejandro Cuetos[3], and Alessandro Patti[1,4]
[1]Department of Chemical Engineering, The University of Manchester, Manchester, M13 9PL, UK
[2]Department of Chemistry and Physics, University of Almería, 04120, Almería, Spain
[3]Department of Physical, Chemical and Natural Systems, Pablo de Olavide University, 41013, Sevilla, Spain
[4]Department of Applied Physics, University of Granada, Campus Fuentenueva s/n, 18071 Granada, Spain

The study of the rheological properties of colloidal suspensions is of key relevance in a variety of systems involved in technological applications, including polymers, micelles, emulsions, and electrorheological fluids, among others. Over the last years, microrheology (MR) has emerged as a new methodology to investigate the rheological properties of these soft materials at the particle scale [1]. In particular, MR allows one to link the bulk rheology of fluids to the microscopic dynamics of probe particles (tracers) that freely diffuse in the host medium (passive MR) or are subjected to external forces (active MR).

In this work, we have applied and modified our dynamic Monte Carlo (DMC) simulation technique to investigate passive and active MR in isotropic and liquid-crystalline colloidal suspensions. As a preliminary step, the original DMC methodology [2, 3] has been adapted to investigate the Brownian motion of a tracer particle in a bath of colloidal particles (passive MR) and to describe the impact of an external force pulling a tracer across a colloidal suspension (active MR) [4]. While in passive MR the elastic (G') and viscous (G'') moduli of the host phase are derived from the tracer's mean squared displacement, in active MR the response of the tracer to the external force provides the possibility of exploring the nonlinear viscoelastic properties of the material. We simulate the dynamics of a spherical tracer in a bath of rod-like particles in isotropic, nematic and smectic phases to explore, from the point of view of passive MR, the effect of order of the host phase and the size of the tracer on microviscosity and on G' and G''. According to our results, the computation of the loss factor (G''/G') suggests that dissipation dominates over elasticity for both isotropic and liquid-crystalline phases. Additionally, we observe a progressive increase in the effective viscosity experienced by the tracer which depends on the tracer's size. Nevertheless, the results also suggest that significantly increasing the size of the tracer reduces its ability to recognise the local structure of the surrounding medium thus perceiving it as a continuous fluid with no apparent short- or long-range order. We also investigate through active MR the linear and non-linear response regimes in a bath of spheres and rod-like particles at different densities by evaluating the effect of a constant force acting on the tracer particle. The calculated effective friction coefficients exhibit a plateau at small and large values of the external force, while a non-linear regime is observed at intermediate forces which is caused by the appearance of force-thinning. Our DMC results are benchmarked against earlier Langevin dynamics simulations [1, 5] and, where possible, also against theoretical models [6].

[1] A. M. Puertas and T. Voigtmann, *Microrheology of colloidal systems*, J. Phys. Condens. Matter, **26**, 243101 (2014).

[2] A. Patti and A. Cuetos, *Brownian dynamics and dynamic Monte Carlo simulations of isotropic and liquid crystal phases of anisotropic colloidal particles: A comparative study*, Phys. Rev. E, **86**, 011403 (2012).

[3] A. Cuetos and A. Patti, *Equivalence of Brownian dynamics and dynamic Monte Carlo simulations in multicomponent colloidal suspensions*, Phys. Rev. E, **92**, 022302 (2015).

[4] F. A. Garca Daza, A. M. Puertas, A. Cuetos and A. Patti, *Microrheology of colloidal suspensions via dynamic Monte Carlo simulations*, J. Colloid Interface Sci. **605**, 182 (2022).

[5] I. Gazuz et al., *Active and Nonlinear Microrheology in dense colloidal suspensions*, Phys. Rev. Lett., **102**, 248302 (2009).

[6] T. M. Squires and J. F. Brady, *A simple paradigm for active and nonlinear microrheology*, Phys. Fluids, **17**, 073101 (2005).

Universal patterns in information ecosystems

Violeta Calleja-Solanas[1],
María J. Palazzi[2], Carlos A. Plata[3], Albert Solé-Ribalta[2,4], Javier Borge-Holthoefer[2], Samir Suweis[5] and Sandro Meloni[1]
[1]Institute for Cross-Disciplinary Physics and Complex Systems (IFISC, UIB-CSIC), Palma de Mallorca, Spain
[2]Internet Interdisciplinary Institute (IN3), Universitat Oberta de Catalunya, Barcelona, Spain
[3]Física Teórica, Universidad de Sevilla, Sevilla, Spain
[4]URPP Social Networks, University of Zurich, Zurich, Switzerland
[5]Dipartimento di Fisica e Astronomia G. Galilei, Università di Padova, Padova, Italy.

Humans are generating data through communication networks as never before. This causes a bottleneck in our ability to tackle pieces of information, the so-called memes. As a consequence, online communication systems become an environment where memes compete for users' attention. Thus, it is crucial to understand the complex dynamics taking place in these information ecosystems because our vision of the world is partially obtained through the lens of these digital environments. All this depict a complex scenario that cannot be easily understood with classical tools. If we want to characterise the mechanisms that shape our social ecosystems, a starting approach is to study the statistical regularities or organisational patterns that arise in them. Although some statistical relationships already exist in social networks but it is in ecology where emergent patterns have been exploited for a long time and proven to be universal [1, 2].

Exploiting the similarities between natural and information ecosystems –competition for resources/attention, maximisation of abundance/visibility, etc... – we can map the quantitative characterisation of information systems into the study of variation in ecological communities. In recent years, several works [3, 4, 5] have applied this approach to disentangle a particular macroscopical property of a social system. However, they have focused only on specific aspects. On the contrary, to gain a fulfilling insight, we need an integrated view that characterise our system as a whole. Thankfully, during the last decade, researchers in theoretical ecology have developed a wide range of analytical tools that can be applied to social systems with the proposed bridge: representing users and memes in online social networks as species of an ecological community, the attention problem turns to species competition for resources.

Here, we have systematically analysed 7 major macroecological patterns [2] in the online platform Twitter: the relative species abundance (RSA), species area and time curves, daily abundance changes, distribution of abundances across communities, distribution of mean abundances across species (MAD), Taylor's Law and the variation of the mean number of species against the innovation rate. These patterns exhibit similar characteristics in very different communities. For example, the RSA reflects how the species are distributed in a given region. We have analysed Twitter streams relative to 11 different events, and we have found that the same functional forms predicted for ecological communities [1, 6] hold for online social systems. This universality suggests that, although inherent differences, the dynamics of information and natural ecosystems may be shaped by similar main drivers.The fact that as many as seven patterns coincide between the systems gives us robust support for a stable bridge and pave the way for a fruitful co-fertilisation of the two fields.

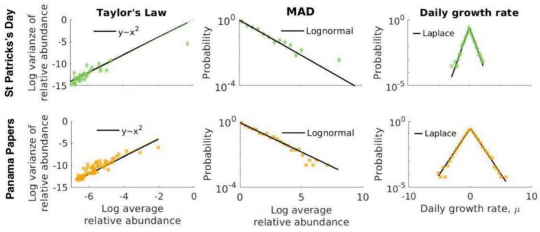

Fig. 1. Three of the patterns for two datasets. Solid lines represent fits to the data.

[1] Grilli, J. Macroecological laws describe variation and diversity in microbial communities. *Nature Communications*. **11**, 1-11 (2020)

[2] Azaele, S., Suweis, S., Grilli, J., Volkov, I., Banavar, J. & Maritan, A. Statistical mechanics of ecological systems: Neutral theory and beyond. *Reviews Of Modern Physics*. **88**, 035003 (2016)

[3] Plata, C., Pigani, E., Azaele, S., Calleja-Solanas, V., Palazzi, M., Solé-Ribalta, A., Borge-Holthoefer, J., Meloni, S. & Suweis, S. Neutral theory for competing attention in social networks. *Physical Review Research*. **3**, 013070 (2021)

[4] Palazzi, M., Solé-Ribalta, A., Calleja-Solanas, V., Meloni, S., Plata, C., Suweis, S. & Borge-Holthoefer, J. An ecological approach to structural flexibility in online communication systems. *Nature Communications*. **12**, 1-11 (2021)

[5] Calleja-Solanas, V., Pigani, E., Palazzi, M., Solé-Ribalta, A., Suweis, S., Borge-Holthoefer, J. & Meloni, S. Quantifying the drivers behind collective attention in information ecosystems. *Journal Of Physics: Complexity*. **2**, 045014 (2021)

[6] Ji, B., Sheth, R., Dixit, P., Tchourine, K. & Vitkup, D. Macroecological dynamics of gut microbiota. *Nature Microbiology*. **5**, 768-775 (2020)

Finite-time scaling for epidemic processes with power-law superspreading events

Carles Falcó[1], Álvaro Corral[2,3,4],
[1]Mathematical Institute, University of Oxford, OX2 6GG Oxford, United Kingdom
[2] Centre de Recerca Matemàtica, Edifici C, Campus Bellaterra, E-08193 Barcelona, Spain
[3] Departament de Matemàtiques, Facultat de Ciències, Universitat Autònoma de Barcelona, E-08193 Barcelona, Spain
[4] Complexity Science Hub Vienna, Josefstädter Straβe 39, 1080 Vienna, Austria

Epidemics unfold by means of a spreading process from each infected individual to a random number of secondary cases. It has been claimed that the so-called superspreading events in COVID- 19 are governed by a power-law tailed distribution of secondary cases, with no finite variance. Using a continuous-time branching process, we show that for such power-law superspreading the survival probability of an outbreak as a function of time and the basic reproductive number fulfills a finite- time scaling law (analogous to finite-size scaling) with universal-like characteristics only dependent on the power-law exponent. This clearly shows how the phase transition separating a subcritical and a supercritical phase emerges in the infinite-time limit (analogous to the thermodynamic limit). We quantify the counterintuitive hazards infinite-variance superspreading poses and conclude that superspreading only leads to new phenomenology in the infinite-variance case.

This work builds on existing literature studying branching process models and their universality [1, 2, 3]. We focus on offspring distributions with power-law decay with an exponent γ between 2 and 3, which makes the variance of the distribution divergent. In this context, the mean of the offspring distribution R_0 becomes of limited utility as we cannot define an associated standard error to it. While the average dynamics of the branching process are independent on higher moments of the offspring distribution, its variance does play an important role in the dynamics of the process. More, and in contrast with the finite variance case studied in previous works, a new universality class appears for every value of the exponent of the power-law. We focus on the study of the survival probability of the process $q(t)$, which gives direct insights in quantities such as the expected duration of an outbreak, and the total number of contagions. In particular, and as mentioned above, we find that near criticality (R_0 close to 1) a finite-time scaling law (analogously to finite-size scaling in the theory of phase transitions) emerges making explicit the dependency on time of the process. Such scaling law reads

$$q(t) \propto \frac{G_\gamma(z)}{t^{1/(\gamma-2)}} \tag{1}$$

with the $\gamma-$dependent scaling function

$$G_\gamma(z) = \left(\frac{ze^z}{e^z-1}\right)^{\frac{1}{\gamma-2}}, \tag{2}$$

and $z \propto (R_0-1)t$, a rescaled distance to the critical point.

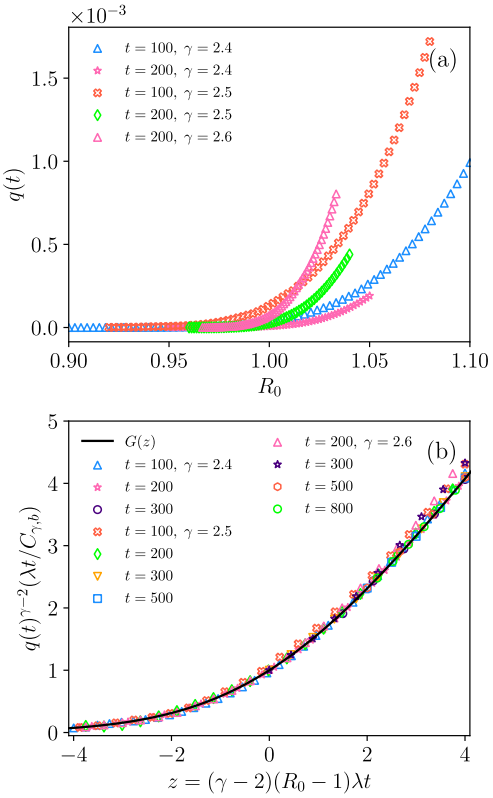

Fig. 1. (a) Survival probabilities $q(t)$ versus R_0. (b) General rescaling of $q(t)^{\gamma-2}$ given by Eq. (1).

[1] R. Garcia-Millan, F. Font-Clos, and A. Corral. *Finite-size scaling of survival probability in branching processes*, Phys. Rev. E, 91:042122, 2015.

[2] N. Wei and G. Pruessner. *Comment on "Finite-size scaling of survival probability in branching processes"*, Phys. Rev. E, 94:066101, 2016.

[3] R. Garcia-Millan, J. Pausch, B. Walter, and G. Pruessner. *Field-theoretic approach to the universality of branching processes*, Phys. Rev. E, 98:062107, 2018.

An improved estimator of Shannon entropy with applications to systems with memory

Juan De Gregorio, David Sánchez and Raúl Toral
IFISC (CSIC-UIB), Instituto de Fsica Interdisciplinar y Sistemas Complejos, Campus Universitat de les Illes Balears, E-07122 Palma de Mallorca, Spain

Many systems can be described with Markovian models in which the future state of the system only depends on its present state. While in some cases this is enough to predict the evolution of the system, in other cases it is necessary to take into account also the past states of the system. Which is the minimum number of past states needed in order to faithfully determine the probability of a future state? We call this number the memory (or order) m. To find m is not a simple task given that it depends on a large number of conditional probabilities but it turns out that a simpler answer to this question can be found from an analysis of the Shannon entropy.

Estimating the Shannon entropy of a given sample is still an open problem. The naive estimator, which is calculated simply replacing the probabilities by their respective frequencies, is biased and this can result in an extreme underestimation of the entropy [1], especially in the undersampled regime where the number of possible outcomes is similar or larger than the number of observations. There have been many attempts to improve this estimator [2]. Here, I will present an estimator that generally improves the one proposed by Chao-Shen [3] using a combination of a Horvitz-Thompson adjustment [4] and a correction to the probabilities to account for missing elements in the sample. Our estimator allows us to address strong correlations and is particularly useful to study systems with memory. As an example, in figure 1 we show a plot of Shannon entropy per block of size n for a particular case of a Markovian, binary system with transition probabilities chosen randomly, alongside the results obtained with the naive estimator (green), Chao-Shen's (blue) and our proposed estimator (red), calculated from a sequence of 10^4 realizations generated numerically. It can be seen that our estimator overlaps the exact one.

Using an ordinal pattern approach, we have applied this method to the determination of the minimum memory required to describe lexical statistics of texts in different languages and we have seen that, despite the different characteristics of each language, all of them can be described with a model of memory $m = 2$. We have also applied our method to the study of daily precipitation in different worldwide locations.

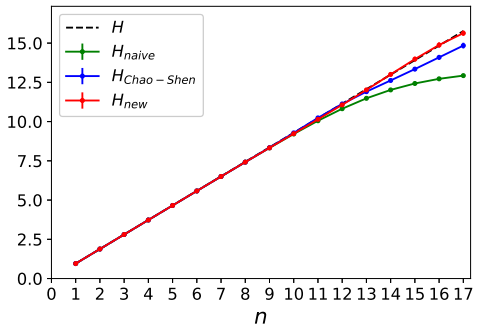

Fig. 1. Exact Shannon entropy per block of size n (dotted line) for a particular case of a Markovian, binary system with transition probabilities chosen randomly. From this setting, a sequence of 10^4 realizations is generated numerically from which we calculate the naive entropy estimator (green), Chao-Shen's (blue) and our proposed estimator (red).

[1] L. Paninski, *Estimation of entropy and mutual information*, Neural Comput. **15**, 11911253 (2003).

[2] J. Hausser, K. Strimmer *Entropy inference and the James-Stein estimator, with application to nonlinear gene association networks*, J. Mach. Learn. Res. **10**, 14691484 (2009).

[3] A. Chao, T. J. Shen *Nonparametric estimation of Shannons index of diversity when there are unseen species in the sample*, Environ. Ecol. Stat. **10**, 429443 (2003).

[4] D. G. Horvitz, D. J. Thompson *A generalization of sampling without replacement from a finite universe*, Journal of the American Stat. Assoc. **47**, 66385 (1952).

Sincronización de dos conjuntos de osciladores químicos diferentes, diagrama de fases.

Martín Saavedra[1] and Alberto P. Muñuzuri[1],
[1]Group of Nonlinear Physics, Faculty of Physics, University of Santiago de Compostela, 15782 Santiago de Compostela, Spain
CITMAGA, 15782 Santiago de Compostela, Spain

Los sistemas de osciladores químicos no lineales son capaces de presentar infinidad de comportamientos interesantes en función de los parámetros que los caractericen. De entre todos ellos, el fenómeno de sincronización es de especial interés dada su relación directa con muchos procesos de la naturaleza. La sincronización espontánea entre osciladores químicos independientes ha sido reportada con anterioridad en varias ocasiones [1, 2]

En este trabajo estudiamos y representamos, mediante métodos de simulación numérica, una región del diagrama de fases (Fig. 1 y 2) de un sistema de osciladores químicos inmersos en una disolución de tipo Belousov-Zhabotinsky. Se modeló una población de 1000 osciladores químicos, divididos en dos grupos según sus parámetros característicos. El modelo matemático utilizado fue el oregonator de tres variables modificado [2], al que se le añade un término que caracteriza las interacciones entre los osciladores, basado en una aproximación de campo medio.

Documentamos la aparición de diferentes tipos (estados) de sincronización en función de los parámetros que caracterizan a la disolución (Fig. 1). Junto a esto, mostramos que en las regiones de interfase el sistema experimenta dinámicas estables de intermitencia entre los diferentes estados de sincronización y en las que se producen interesantes fenómenos como la "escalera del diablo" (Fig. 3).

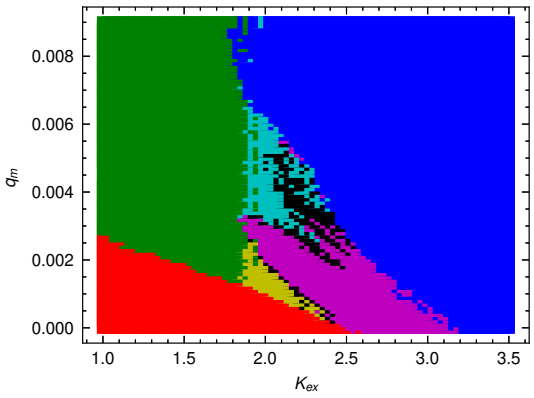

Fig. 1. Representación del diagrama de fases del sistema estudiado a través de la realización de múltiples simulaciones junto con su posterior clasificación.

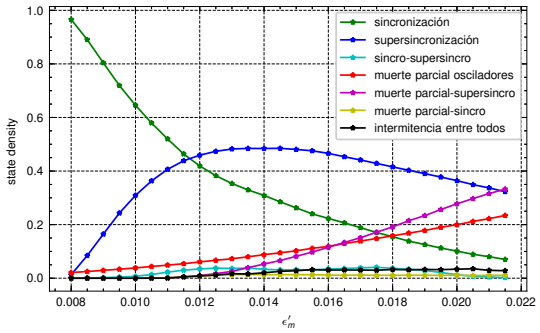

Fig. 2. Gráfica que muestra la evolución del diagrama de fases del sistema en función del parámetro ϵ'_m.

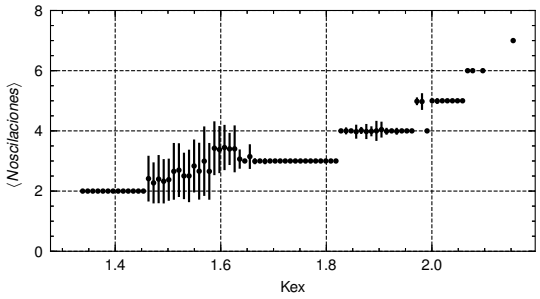

Fig. 3. Representación de la transición entre un estado de muerte parcial de osciladores y el estado de supersincronización. Se puede observar como durante esta transición emerge la conocida función de Cantor o "escalera del diablo".

[1] Tinsley MR, Taylor AF, Huang Z, Wang F, Showalter K. Dynamical quorum sensing and synchronization in collections of excitable and oscillatory catalytic particles. Physica D: Nonlinear Phenomena. 2010 jun;239(11):785-90.

[2] Ghoshal G, Muñuzuri AP, Pérez-Mercader J. Emergence of a super-synchronized mobbing state in a large population of coupled chemical oscillators. Scientific Reports. 2016 jan;6(1).

Complex dynamics in seagrass meadows in the Mediterranean Sea in a global warming scenario

Eva Llabrés[1], and Tomás Sintes[1],
[1]Instituto de Física Interdisciplinar y Sistemas Complejos IFISC (UIB-CSIC)
Campus UIB, 07122 Palma. Spain

Seagrasses are a key element in the Mediterranean Sea, and the drastic demise of its population in the last decades has worrying implications for marine ecosystems. Temperature anomalies in the coastal water are expected to be intensified in the next years due to the global climate change. Temperature elevation has been observed to strongly affect the ecosystems of seagrass meadows worldwide, decreasing the shoot density, biomass and leaf productivity. This effect will be particularly relevant in the Mediterranean Sea in which endemic seagrasses (mainly *P. oceanica* and *C. nodosa*) and seaweeds (*C. prolifera*) compete. The different response to the thermal stress by the different species will alter the growth dynamics, their spatial distribution and, consequently, the ecosystem functionality.

In this study we present an individual based model able to develop complex spatial patterns from the application of elementary clonal growth rules. We monitor the change in the seagrass demography, the emergence of collective behaviour, and evaluate the resilience of these ecosystems in the Mediterranean, when the growth parameters (i.e. the shoot mortality and branching rates) and the interaction among species are triggered by the raise of the sea water temperature. [1]

[1] E. Llabrés, E. Mayol, N. Marbà and T. Sintes, *A mathematical model for inter-specific seagrass interactions: reproducing field observations for C. nodosa and C. prolifera*, Quantitative Biology, Populations and Evolution. arXiv:2202.03096 (2022).

Long-lived non-equilibrium state in a molecular fluid with non-linear drag

A. Patrón[1], B. Sánchez-Rey[2], and A. Prados[1]
[1]*Física Teórica, Universidad de Sevilla, Apartado de Correos 1065, E-41080 Sevilla, Spain*
[2]*Departamento de Física Aplicada I, E.P.S., Universidad de Sevilla, Virgen de África 7, E-41011 Sevilla, Spain*

Glassy behaviour is typically associated with systems with many distinctly interacting units, which give rise to a complex energy landscape with multiple minima separated by barriers. The typical phenomenology of glassy systems includes, among other aspects, strongly non-exponential relaxation. Here, we study the dynamical evolution of a fluid with non-linear drag, for which binary collisions are elastic, described at the kinetic level by the Enskog-Fokker-Planck (EFP) equation

$$\partial_t f = \frac{\partial}{\partial \mathbf{v}} \cdot \left[\zeta(v) \left(\mathbf{v} + \frac{k_B T_s}{m} \frac{\partial}{\partial \mathbf{v}} \right) f \right] + J[\mathbf{v}|f,f]. \quad (1)$$

In the above, $f = f(\mathbf{v},t)$ is the one-particle velocity distribution function (VDF), k_B the Boltzmann's constant, T_s the bath temperature, m the mass of the fluid particles, $J[\mathbf{v}|f,f]$ the Enskog collision operator, and

$$\zeta(v) = \zeta_0 \left(1 + \gamma \frac{m v^2}{k_B T_s} \right) \quad (2)$$

the non-linear drag coefficient [1]. In the latter, γ measures the degree of non-linearity of the drag force.

The dynamical state of the system is determined via the physical variables $(T, \{a_l\}_{l=2}^{\infty})$, where $T(t)$ is the kinetic temperature, and $a_l(t)$ are the so-called Sonine coefficients, which measure deviations from the local equilibrium Maxwellian distribution

$$f_{\text{LE}}(\mathbf{v}, T(t)) = \left(\frac{m}{2k_B T(t)} \right)^{\frac{d}{2}} e^{-\frac{mv^2}{2k_B T(t)}}, \quad (3)$$

i.e. $a_l(t) = 0$, for all l, if $f = f_{\text{LE}}$.

We observe that a non-exponential relaxation function for the kinetic temperature appears when the system is quenched to low enough temperatures, such that $\theta_i \equiv T_i/T_s \gg 1$, with θ_i being the ratio between the initial and final temperatures. This relaxation is universal in the sense that, after a suitable rescaling of the variables, it does not depend on the initial and final temperatures, nor on the degree of non-linearity, nor on the relevance of the collision term. This phenomenon is related to the existence of a long-lived non-equilibrium state (LLNES), in which the Sonine coefficients approach large stationary values a_l^r. In such state, the temperature decays algebraically, specifically

$$T(s) = \frac{T_i}{1 + 2(d+2)(1+a_2^r)s}, \quad (4)$$

with $s \equiv \gamma \theta_i t$ being a new timescale. Figure 1 shows the comparison between our theoretical prediction for the relaxation function and different sets of data obtained through *Direct Simulation Monte Carlo* (DSMC), which allows to solve the EFP equation numerically. As one may observe, the agreement between simulations and theory is excellent.

The physical picture behind the LLNES is appealing. The limit $\theta_i \gg 1$ is roughly equivalent to setting $T_s \to 0$, which removes the diffusion, stochastic term from the EFP equation. Thus, in the absence of collisions, the system behaviour is purely governed by the non-linear drag, and the dynamics of the particles become deterministic. In fact, we show that the VDF at the LLNES becomes a Dirac delta function in velocity space,

$$f_{\text{LLNES}}(\mathbf{v},t) \propto \delta\left(v^2 - \frac{d k_B T(t)}{m} \right), \quad (5)$$

where we may identify $v_T(t) \equiv \sqrt{2k_B T(t)/m}$ as the thermal velocity. Thus, in this regime, the motion of the particles is completely determined by the kinetic temperature.

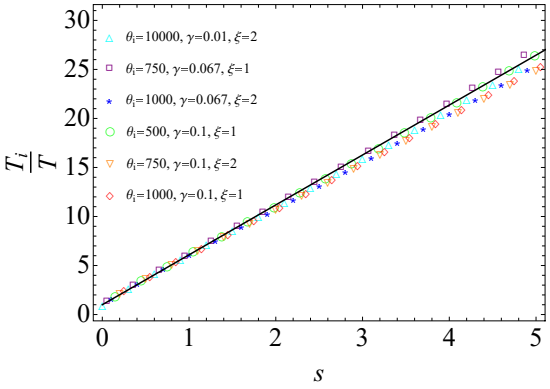

Fig. 1. Relaxation after a quench to a low temperature. Specifically, we plot T_i/T as a function of the scaled time $s = \gamma \theta_i t$. Data from DSMC correspond to parameters (θ_i, γ, ξ), as specified in the legend, and $d = 2$. In the above, ξ stands for the inverse collision rate ($\xi \to +\infty$ corresponds to the collisionless case). The linear behaviour in T_i/T implies that the temperature relaxes algebraically, basically as t^{-1}, as theoretically predicted by Eq. (4) (solid line).

[1] A. Patrón, B. Sánchez-Rey, and A. Prados, *Strong non-exponential relaxation and memory effects in a fluid with non-linear drag*, Phys. Rev. E **104**, 064127 (2021).

Lagrangian descriptors and regular motion

J Montes[1,2,3], F Revuelta[1], and F Borondo[2,3]
[1]Grupo de Sistemas Complejos, Universidad Politécnica de Madrid, 28040 Madrid, Spain
[2]Departamento de Química, Universidad Autónoma de Madrid, Cantoblanco–28049 Madrid, Spain
[3]Instituto de Ciencias Matemáticas (ICMAT), Cantoblanco–28049 Madrid, Spain

Lagrangian descriptors introduced a decade ago have revealed as a powerful tool to unveil the intricacies of the phase space of dynamical systems in a very easy way [1]. They have been extensively used to study chaotic motion in a variety of different situations [2, 3, 7], but much less attention has been paid to applications to the regular regions of phase space. Recently J. Curbelo *et al.* have provided a way to locate the regular zones (invariant tori) [5, 6]. In this contribution, we show the potential of this recent mathematical tool, when suitably manipulated, to compute and fully characterize invariant tori of generic systems [8]. To illustrate the method, we present an application to the well known Hénon-Heiles Hamiltonian, a paradigmatic example in nonlinear science [4]. In particular, we demonstrate that the Lagrangian descriptors associated with regular orbits oscillate around an asymptotic value when divided over the integration time, which enables the computation of the frequencies of invariant tori.

[1] C. Mendoza, AM. Mancho Hidden geometry of ocean flows. Phys. Rev. Lett. 2010; 105:038501-038501.

[2] F. Revuelta, RM. Benito, F. Borondo Unveiling the chaotic structure in phase space of molecular systems using Lagrangian descriptors. Phys. Rev. E 2019; 99:032221-032221.

[3] GG. Carlo, F. Borondo Lagrangian descriptors for open maps. Phys. Rev. E 2020; 101:022208-022208.

[4] M. Hénon , C. Heiles The applicability of the third integral of motion: Some numerical experiments. Astron. J. 1964; 69:73-79.

[5] J. Curbelo, C.R. Mechoso, A.M. Mancho, S. Wiggins Lagrangian study of the final warming in the southern stratosphere during 2002: Part I. The vortex splitting at upper levels. Clim Dyn 53, 27792792 (2019).

[6] V.J. García-Garrido, J. Curbelo, A.M. Mancho, S. Wiggins, C.R. Mechoso The Application of Lagrangian Descriptors to 3D Vector Fields. Regul. Chaot. Dyn. 23, 551568 (2018).

[7] GG. Carlo, J. Montes, F. Borondo Lagrangian descriptors for the Bunimovich stadium billiard. Phys. Rev. E 2022; 105:014208.

[8] J. Montes, F. Revuelta, F. Borondo Lagrangian descriptors and regular motion. Communications in Nonlinear Science and Numerical Simulation Volume 102, November 2021, 105860.

Aging effects in complex contagion

David Abella-Bujalance[1], Maxi San Miguel[1] and José Javier Ramasco[1]
[1] Instituto de Física Interdisciplinar y Sistemas Complejos IFISC (CSIC - UIB), Campus UIB, 07122 Palma de Mallorca, Spain

We study the effects of heterogeneous timing interactions in processes of complex contagion, focusing on the threshold model [1] with exogenous and endogenous aging. For the threshold model, the binary state variable indicates if either the agent has adopted a technology or not. Endogenous aging is considered as the property of agents in the system to be less prone to change state the longer they have been in the current state. On the other hand, in exogenous aging, memory is lost after failed attempts to change state [2].

In both cases, numerical simulations show that aging slows the cascade dynamics towards the fully adopted state. The exponential increase of the fraction of adopted agents $\rho(t)$ exhibited by the original threshold model is replaced by a stretched exponential or power-law increase when aging mechanism is exogenous or endogenous, respectively (see Fig.1). This behaviour is universal for different system sizes, networks and values of the control parameters (average degree z and threshold T).

The memory dependent dynamics induced by aging cannot be treated with standard methods for binary-state dynamics in networks [3]. We derive an approximate master equation (AME) reducing the non-Markovian dynamics to Markovian by enlarging the number of variables [4]. Our AME describe binary state dynamics with timing interactions for any network generated with the configuration model. For the threshold model with aging, the numerically integrated solutions give a good agreement with numerical simulations (Fig. 1).

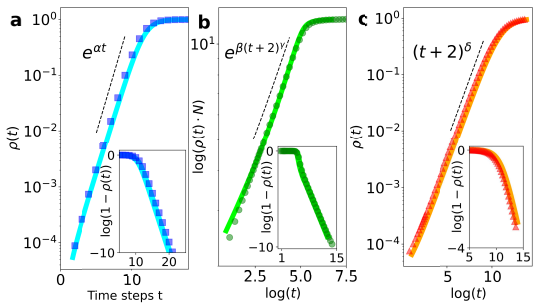

Fig. 1. Cascade dynamics and fall to the adopted state $\rho = 1$ of the Watts threshold model (a) and the versions with exogenous (b) and endogenous (c) aging effects. The underlying network is a 3-regular random graph and the homogeneous threshold is $T = 0.2$. The exponent values are $\alpha \simeq 1.0$, $\beta \simeq 1.14$, $\gamma \simeq 0.38$ and $\delta \simeq 1.0$. AME solutions (solid lines) describe accurately the numerical results.

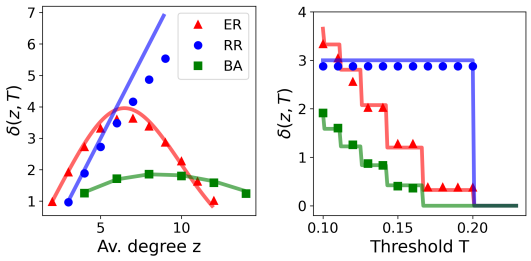

Fig. 2. Exponent δ dependence on the average degree z ($T = 0.1$) (left) and the T (right) for the threshold model with endogenous aging. Different markers indicate results from numerical simulations with different topology: red triangles indicates an Erds-Renyi (ER), blue circles indicate a Random Regular (RR) and green squares indicate a Barabasi-Albert (BA) graphs. In (b), average degree is fixed $z = 5$ for ER and RR, and $z = 8$ for the BA. Predicted values by Eq.1 (solid lines) fit the results for each topology. System size is fixed at $N = 160000$.

We reduce the AME for the threshold model with aging to a set of two coupled differential equations. The equations are linearized to find an analytical solution of the fraction of adopted agents $\rho(t)$. The exponential increase for the original model and the power law dynamics for the version with endogenous aging are predicted. In fact, the exponent is found to coincide:

$$\delta(Z,T) = \alpha(z,T) = \sum_{k=0}^{1/T} \frac{k(k-1)}{z} p_k - 1. \qquad (1)$$

This exponent dependence is shown to be different according to the degree distribution of the underlying network p_k. Values computed from numerical simulations are in good agreement with analytical predictions (see Fig.2).

[1] Watts, D. J. *A simple model of global cascades on ran- dom networks,* Proceedings of the National Academy of Sciences **99**, 5766 (2002).).

[2] J. Fernndez-Gracia, V. M. Eguiluz, and M. San Miguel, *Update rules and interevent time distributions: Slow or- dering versus no ordering in the voter model,* Physical Review E **84**, 10.1103/physreve.84.015103 (2011).

[3] Gleeson, J. P. *Binary-State Dynamics on Complex Networks: Pair Approximation and Beyond.*, Physical Review X, **3**(2), (2013).

[4] Peralta, A. F., Khalil, N., and Toral, R. *Reduction from non-Markovian to Markovian dynamics: the case of aging in the noisy-voter model.* Journal of Statistical Mechanics: Theory and Experiment, **2** 024004 (2020)

Bifurcation structure of traveling pulses in Type-I excitable media

Pablo Moreno-Spiegelberg[1], Andreu Arinyo-i-Prats[2], Daniel Ruiz-Reynés[3], Manuel A. Matías[1], and Damià Gomila[1]
[1]IFISC (CSIC-UIB), Instituto de Física Interdisciplinar y Sistemas Complejos, E-07122 Palma de Mallorca, Spain
[2]Institute of Computer Science, Czech Academy of Sciences, 182 07 Prague 8, Czech Republic
[3]Katholieke Universiteit, Leuven, Belgium

Excitability is a property of certain nonlinear dynamical systems concerning their response to external perturbations. Excitable systems can be classified into two classes, Type-I and II, with differentiated dynamical properties and obtained through different bifurcations [1]. Excitable media, locally excitable spatial extended systems, show different regimes in which local perturbation, exceeding a threshold, can propagate across the medium. There are many studies considering Type-II excitable media, but much less is known about pulse propagation in the Type-I case. Recently, several vegetation systems compatible with Type-I excitability have shown traveling pulses [2, 3, 4], renewing interest in their study.

We have studied the existence of traveling pulses in a general Type-I excitable 1-dimensional media. We have obtained the stability region and characterized the different bifurcations behind either the destruction or loss of stability of the pulses. In particular, some of the bifurcations delimiting the stability region have been connected, using singular limits, with the two different scenarios that mediated the Type-I local excitability, i.e. homoclinic (saddle-loop) and SNIC (Saddle-Node on the Invariant Circle) bifurcations. This connection explain the similarities between the pulses profile and excitable trajectories pointed out in [5]. Finally, the existence of these pulses has been tracked, outside the stability region, to a drift pitchfork instability of localized steady structures.

[1] E. M. Izhikevich, *Dynamical Systems in Neuroscience* (MIT Press, Cambridge (MA), 2007).

[2] A. Iuorio and F. Veerman *The influence of autotoxicity on the dynamics of vegetation spots*, Physica D 427, 133015 (2021).

[3] Li-Xia Zhao, Kang Zhang, Koen Siteur, Xiu-Zhen Li, Quan-Xing Liu, and Johan van de Koppel, *Fairy circles reveal the resilience of self-organized salt marshes*, Science Advances **7**(6), (2021).

[4] C. Fernandez-Oto, D. Escaff and J. Cisternas, *Spiral vegetation patterns in high-altitude wetlands*, Ecological Complexity **37**, 38-46 (2019).

[5] A. Arinyo-i-Prats, P. Moreno-Spiegelberg, M.A. Matias and D. Gomila, *Traveling pulses in type-I excitable media*, Phys. Rev. E 104, L052203 (2021).

Use of probability distributions and mathematical models in the understanding of the spreading of SARS-CoV-2 inside schools

Sergio Alonso[1], Marti Catala [1], Enric Alvarez-Lacalle [1], Daniel Lopez-Codina [1] and Clara Prats [1]
[1]Department of Physics, Universitat Politecnica de Catalunya

The opening of the schools during the pandemicl of SARS-CoV-2 was a question of debate in Spain at the begining of the curs 2020-2021 after a long time of closing. The same question appeared around the world and very differnt meassures were employed for the different countries, while Sweden left open the schools with very minor restrictions, Peru closed all the type of schools during the next two years.

Before the beginning of the course and to consider the possible dynamics we ellaborate scenarios and performed numerical simulations to calibrate the different measures considered for the begining of the curs. We found that some of the measures like for example the reduction of the class rate would produce marginal effects whoile other measures like the length of quarentine has larger effects [1].

During the reopening of the schools in Catalonia, there was a control of the cases in the schools and the formation of stable convivence groups permited the study of the propagation of the infection when an index case entered in the group. We had accessed to the individual anonimized data to perform such study and we analyzed the resulting propagation rates inside of the bubble groups.

The resulting dynamics were interpreted in colaboration with pediatric epidemiologists to quantify the spreading of SARS-CoV-2 inside the scholar groups [2]. We have fitted a negative binomial distribution to the children infected by a index case inside the bublbe groups, and characterize the average number of infected children per index case for the different school levels see Fig.1.

The low rate of progation found in our analysis agrees with other similar results in the analysis of scholar propoagation and with the fact that the capacity of infection from children to adult is smaller than the capacity of infection

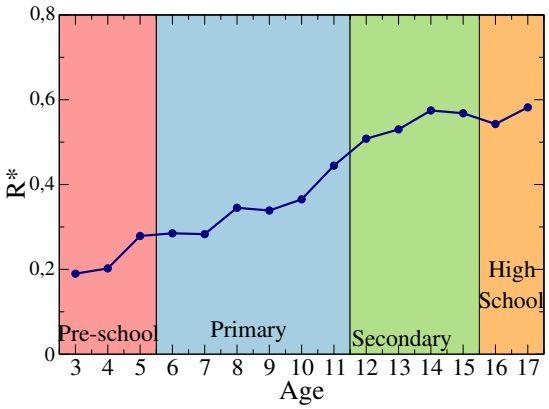

Fig. 1. Dependence of the average number of infected children on the age of the bubble group in the school.

[1] S. Alonso, et al. *Individual prevention and containment measures in schools in Catalonia, Spain, and impact of this strategy on community transmission of SARS-CoV-2 after school reopening* to be published in PLoS one (2022)

[2] S. Alonso, et al. *Age-dependency of the propagation rate of coronavirus disease 2019 inside school bubble groups in Catalonia, Spain*. The Pediatric infectious disease journal, **40**, 955 (2021).

Machine learning algorithms for coronary artery segmentation

Belén Serrano-Antón[1,2], Alberto Otero-Cacho[1,2,3], Alberto P. Muñuzuri[2,3], Vicente Pérez-Muñuzuri[4], Diego López-Otero[5,6], María Bastos-Fernández[5,6], Brais Díaz-Fernández[5,6], and J.R. González-Juanatey[5,6]

[1]FlowReserve Labs S.L., Edificio Emprendia, 15782 Santiago de Compostela, Spain

[2]Group of Nonlinear Physics. University of Santiago de Compostela, 15782 Santiago de Compostela, Spain

[3]CITMAga, Santiago de Compostela, Spain

[4]Institute CRETUS, Group of Nonlinear Physics, University of Santiago de Compostela, Santiago de Compostela, Spain

[5]Cardiology and Intensive Cardiac Care Department, University Hospital of Santiago de Compostela, Santiago de Compostela, Spain

[6]Centro de Investigación Biomédica en Red de Enfermedades Cardiovasculares (CIBERCV), Madrid, Spain

Coronary artery disease (CAD) is one of the leading causes of death worldwide [1, 2]. CADs are caused primarily by vessel narrowing (stenosis). The visual detection of stenosis, which is a tedious, subjective and time-consuming process, relies on the evaluation of CT images by specialists. Another complementary method consists on the reconstruction of the vessels from the image, thus obtaining the coronary tree geometry. This model, if it is precise enough, is particularly compelling, as it can be used to non-invasively calculated clinical parameters such as the Fractional Flow Reserve (FFR) [1].

The segmentation of images requires a classification of each pixel of the image. Again, performing this task manually is time-consuming and prone to mistakes. Therefore, the need for automatic segmentation techniques that have the precision necessary for clinical evaluation has increased in the last few years. Among the most used techniques we find methods based on neural networks, in particular convolutional neural networks (CNNs) [2, 3, 4, 5].

Different parameters will be presented to measure the goodness of the methods used.

[1] Otero-Cacho, A., López-Otero, D., Insúa-Villa, M., Díaz-Fernández, B., Bastos-Fernández, M., García-Campos, A., Pérez-Muñuzuri V., P. Muñuzuri, A., González-Juanatey, J.R. Non-invasive assessment of coronary lesions by computer tomography fractional flow reserve compared to the invasive technique under hyperaemic and basal conditions. PLOS ONE. SUBMITTED (2022)

[2] Cheung, W., Bell, R., Nair, A., Menezies, L., Patel, R., Wan, S., Chou, K., Chen, J., Torii, R., Davies, R. & Others A computationally efficient approach to segmentation of the aorta and coronary arteries using deep learning. *MedRxiv*. (2021)

[3] Pan, L., Li, C., Su, S., Tay, S., Tran, Q. & Chan, W. Coronary artery segmentation under class imbalance using a U-Net based architecture on computed tomography angiography images. *Scientific Reports*. **11**, 1-7 (2021)

[4] Shin, S., Lee, S., Yun, I. & Lee, K. Deep vessel segmentation by learning graphical connectivity. *Medical Image Analysis*. **58** pp. 101556 (2019)

[5] Jurdi, R., Petitjean, C., Honeine, P., Cheplygina, V. & Abdallah, F. A Surprisingly Effective Perimeter-based Loss for Medical Image Segmentation. *Medical Imaging With Deep Learning*. (2021)

Splitting-thermostat-engineered protocol for Mpemba effect in granular gases of inelastic and rough hard disks

Alberto Megías[1] and Andrés Santos[1,2]
[1]Departamento de Física, Universidad de Extremadura, E-06006 Badajoz, Spain
[2]Instituto de Computación Científica Avanzada (ICCAEx), Universidad de Extremadura, E-06006 Badajoz, Spain

In the last few years, Mpemba effect (an initially further from equilibrium system may relax faster than that initially closer) has attracted much attention in statistical physics and complex systems, specifically in granular gas dynamics phenomenology [1].

In this work, we consider a monodisperse dilute granular gas of inelastic and rough hard disks of mass m, diameter σ, and moment of inertia $\frac{m\sigma^2}{4}\kappa$. We adopt the simplest two-parameter model with a constant coefficient of normal restitution ($0 < \alpha < 1$), parameterizing the inelasticity, and a constant coefficient of tangential restitution ($-1 < \beta < 1$), accounting for the roughness of the particles.

To compensate for the dissipation of energy (translational and rotational contributions), we assume thermalization through heating from a stochastic thermostat that could act directly on both, rotational and translational, classes of degrees of freedom. That is, the system relaxes by means of the action of a homogeneous stochastic volume force ($\mathbf{F}^{\mathrm{n}}$) and torque (τ^{n}) with the properties of a Gaussian noise,

$$\langle \mathbf{F}_i^{\mathrm{n}}(t)\rangle = \mathbf{0},\ \langle \mathbf{F}_i^{\mathrm{n}}(t)\mathbf{F}_j^{\mathrm{n}}(t')\rangle = \mathsf{I} m^2(1-\varepsilon)\chi_0^2\delta_{ij}\delta(t-t'), \tag{1}$$

$$\langle \tau_i^{\mathrm{n}}(t)\rangle = 0,\ \langle \tau_i^{\mathrm{n}}(t)\tau_j^{\mathrm{n}}(t')\rangle = \frac{m^2\sigma^2}{2}\kappa\varepsilon\chi_0^2\delta_{ij}\delta(t-t'), \tag{2}$$

where i, j are particle indices, I is the 2×2 unit matrix, χ_0^2 refers to the total intensity of the thermostat, and ε is the *fraction* split up from the total intensity acting on the particles spinning. This class of thermostats allows us to design a controlled protocol for observing Mpemba effect in a kinetic-theoretical context. Dimensional analysis suggests to define the reference temperature $T^{\mathrm{n}} \equiv m(\chi_0^2/n\sigma)^{2/3}$, where n is the number density, as a measure of the total intensity of the thermostat

In a recent work [2], the Mpemba effect was described for hard spheres (i.e., not disks) and $\varepsilon = 0$, concluding that an initially hotter system A would need initially a smaller rotational-to-translational temperatures ratio, θ, with respect to an initially colder system B to ensure a crossover between the granular temperature curves, $T(t)$. These initial conditions are here extrapolated to any splitting $0 \le \varepsilon \le 1$ and to a two-dimensional granular gas.

Assuming that the nonequilibrium velocity distribution function of the gas can be approximated by a time-dependent, two-temperature Maxwellian distribution, the dynamics of the system (at given T^{n} and ε) is described by a coupled set of equations for the quantities θ and T. As physically expected, the rotational-to-translational temperature ratio in the steady state (θ^{st}) increases monotonically as the fraction of the total intensity of the thermostat applied to the rotational degrees of freedom (ε) increases. Moreover, the steady-state granular temperature (T^{st}) is proportional to the reference temperature (T^{n}) associated with the total intensity of the noise.

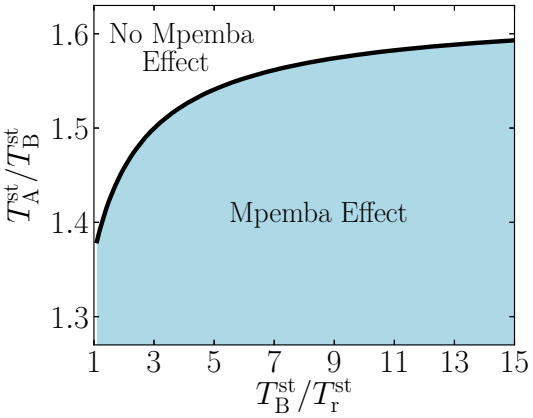

Fig. 1. Phase diagram of the Mpemba effect for $\alpha = 0.9$, $\beta = 0$, and $\kappa = \frac{1}{2}$ resulting from the protocol described in the text.

This leads us to define a protocol for the initialization of a pair of identical samples of a dilute granular gas of inelastic and rough hard disks at arbitrary initial states, from which Mpemba effect is expected to occur for a thermal reservoir with ε_{r} and $T_{\mathrm{r}}^{\mathrm{n}}$, such that the steady state is given by $(\theta_{\mathrm{r}}^{\mathrm{st}}, T_{\mathrm{r}}^{\mathrm{st}})$. The protocol can be summarized as follows: one sample, say A, is put in contact with a thermostat with $\varepsilon_{\mathrm{A}} = 0$ and $T_{\mathrm{A}}^{\mathrm{n}} > T_{\mathrm{r}}^{\mathrm{n}}$, whereas the other system, B, is put in contact with a bath characterized by $\varepsilon_{\mathrm{B}} = 1$ and $T_{\mathrm{A}}^{\mathrm{n}} > T_{\mathrm{B}}^{\mathrm{n}} > T_{\mathrm{r}}^{\mathrm{n}}$, so that $\theta_{\mathrm{B}}^{\mathrm{st}} > \theta_{\mathrm{r}}^{\mathrm{st}} > \theta_{\mathrm{A}}^{\mathrm{st}}$ and $T_{\mathrm{A}}^{\mathrm{st}} > T_{\mathrm{B}}^{\mathrm{st}} > T_{\mathrm{r}}^{\mathrm{st}}$ once the systems are thermalized. These steady-state pairs of values, $(\theta_{\mathrm{A}}^{\mathrm{st}}, T_{\mathrm{A}}^{\mathrm{st}})$ and $(\theta_{\mathrm{A}}^{\mathrm{st}}, T_{\mathrm{B}}^{\mathrm{st}})$, define a set of *initial* states candidate for observing Mpemba effect when the reservoirs of both samples are changed to have *common* $T_{\mathrm{r}}^{\mathrm{n}}$ and ε_{r}. The latter parameter is conveniently chosen as

$$\varepsilon_{\mathrm{r}} = \frac{1-\beta+2\kappa}{1-\beta+2\kappa+\kappa(1+\beta)}, \tag{3}$$

so that, according to our theoretical description, $\theta_{\mathrm{r}}^{\mathrm{st}} = \frac{1}{2}\left(\theta_{\mathrm{A}}^{\mathrm{st}} + \theta_{\mathrm{B}}^{\mathrm{st}}\right)$.

Figure 1 shows the phase diagram in the plane $T_{\mathrm{A}}^{\mathrm{st}}/T_{\mathrm{B}}^{\mathrm{st}}$ vs $T_{\mathrm{B}}^{\mathrm{st}}/T_{\mathrm{r}}^{\mathrm{st}}$, indicating the region where Mpemba effect is present for the case $\alpha = 0.9$, $\beta = 0$, and $\kappa = \frac{1}{2}$.

We will validate such theoretical description via direct simulation Monte Carlo method and event-driven molecular dynamics simulations.

[1] A. Lasanta, F. Vega-Reyes, A. Prados, and A. Santos, Phys. Rev. Lett. **119**, 148001 (2017).

[2] A. Torrente, M. A. López-Castaño, A. Lasanta, F. Vega Reyes, A. Prados, and A. Santos, Phys. Rev. E. **99**, 060901(R) (2019).

Analytic exact solution of the one-dimensional triangle-well and ramp fluids

Ana M. Montero[1] and Andrés Santos[1,2]
[1]Departamento de Física, Universidad de Extremadura, E-06006 Badajoz, Spain
[2]Instituto de Computación Científica Avanzada (ICCAEx), Universidad de Extremadura, E-06006 Badajoz, Spain

We present a comprehensive study on the thermophysical and structural properties of two prototypical classes of fluids confined in a one-dimensional line, namely the triangle-well and the ramp potentials. Both potentials are finite-ranged and have an impenetrable core of diameter σ plus a continuous linear part between $r = \sigma$ and $r = \lambda$ (see Fig. 1). While the mathematical form of that additional part is analogous in both cases, the physical meaning is not. In the triangle-well potential the tail is attractive and, apart from its own physical interest, the main importance of the potential resides in representing the effective colloid-colloid interaction in the Asakura–Oosawa mixture. On the other hand, the ramp potential is purely repulsive with a softened core between $r = \sigma$ and $r = \lambda$.

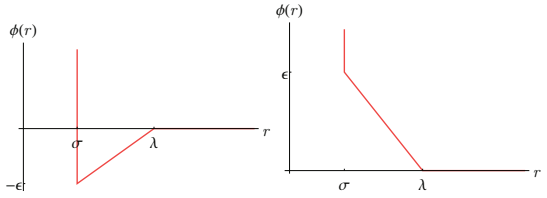

Fig. 1. Sketch of the triangle-well potential (left) and the ramp potential (right).

The exact statistical-mechanical solution in the isothermal-isobaric ensemble for general nearest-neighbor interactions [1] is applied to the study of equilibrium properties of these two classes of fluids, such as the equation of state, the excess internal energy per particle, the structure factor $S(k)$, the direct correlation function $c(r)$, and the radial distribution function $g(r)$. In the latter case, in contrast to previous studies where $g(r)$ was obtained numerically from $S(k)$ by Fourier inversion [2], a fully analytic representation for $g(r)$ is derived in terms of a finite number of coordination-shell terms for any finite r [3]. As an illustration, Fig. 2 shows $g(r)$ at some representative states.

In addition, scatter plots of the bridge function $B(r)$ versus the indirect correlation function $\gamma(r) \equiv g(r) - 1 - c(r)$ are used to gauge the reliability of the hypernetted-chain, Percus–Yevick, and Martynov–Sarkisov closures.

Lastly, the Fisher–Widom line (separating a repulsive-dominated region from an attractive-dominated one) and the Widom line (marking the states with a maximum correlation length at a given temperature) are obtained from the poles of the Laplace transform of $g(r)$ in the case of the triangle-well model. In the ramp potential, being purely repulsive, the decay of the total correlation function is always oscillatory.

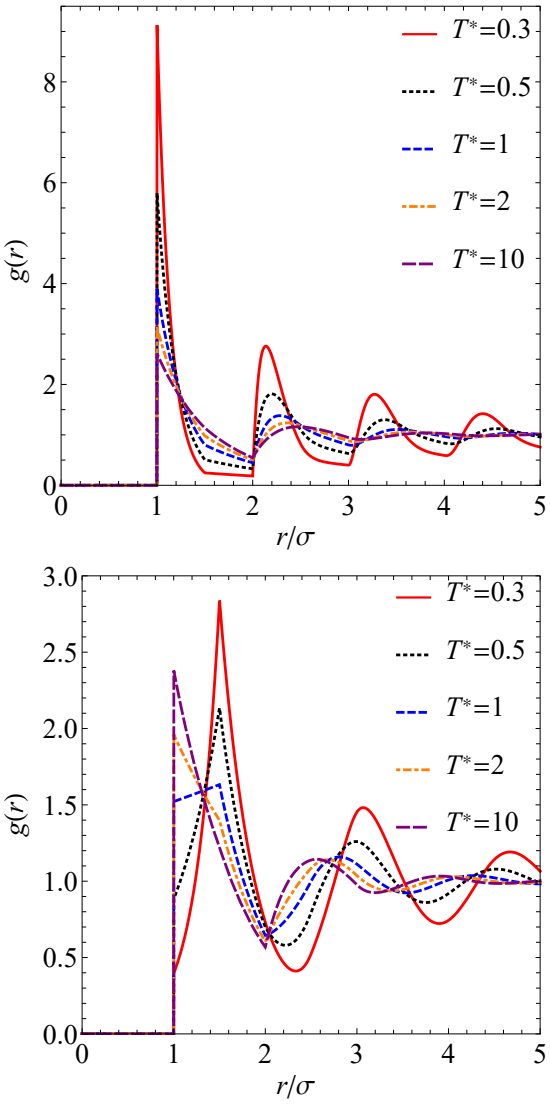

Fig. 2. Radial distribution function $g(r)$ at several representative temperatures for a reduced density $n^* = 0.6$ for the triangle-well potential (top) and the ramp potential (bottom).

[1] A. Santos, *A Concise Course on the Theory of Classical Liquids. Basics and Selected Topics*, Lecture Notes in Physics, vol. 923 (Springer, New York, 2016).

[2] A. J. Archer, B. Chacko, and R. Evans, J. Chem. Phys. **147**, 034501 (2017).

[3] A. M. Montero and A. Santos, J. Stat. Phys. **175**, 269 (2019).

Phase behaviour of hard circular arcs: purely entropy-driven cluster phases

Juan Pedro Ramírez González[1], and Giorgio Cinacchi[1,2,3]
[1]Departamento de Física Teórica de la Materia Condensada
[2]Instituto de Física de la Materia Condensada (IFIMAC)
[3]Instituto de Ciencias de Materiales "Nicolás Cabrera",
Universidad Autónoma de Madrid, Ciudad Universitaria de Cantoblanco,
E-28049 Madrid, Spain

By using Monte Carlo numerical simulations we have investigated the complete phase behavior of systems of hard infinitesimally-thin circular arcs in two dimensions and sketched their phase diagram (Fig.1) in the plane subtended angle, θ, versus the inverse of the number density, $1/\rho$ [1]. Despite their simplicity, systems of hard infinitesimally-thin circular arcs manifest a rich auto-assembly phenomenology driven by the sole entropy. In particular, these systems form a filamentary phase (Fig.3) for arcs denotable as minor ($\theta < \pi$) and a hexagonal cluster phase (Fig.2) for arcs denotable as major ($\theta > \pi$) [2]. Interestingly, in the latter phase, hard circular arcs intertwine and pack on the same parent circle, forming circular clusters which, in turn, arrange on a triangular lattice. These circular clusters are naturally chiral structures but the cluster hexagonal phase is globally non-chiral.

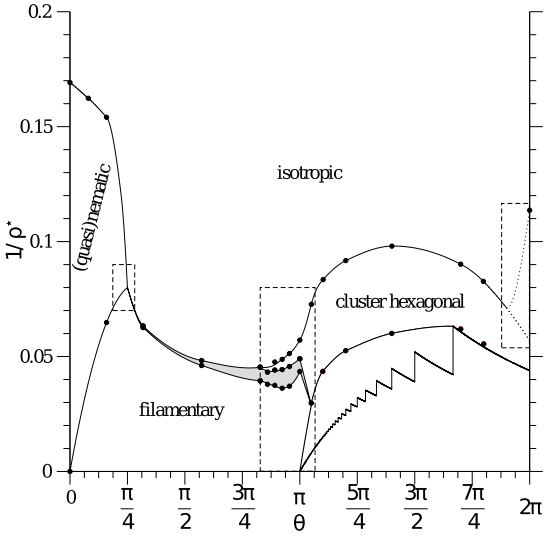

Fig. 1. Phase diagram of systems of hard circular arcs in the plane aperture angle θ versus inverse of number density $1/\rho$.

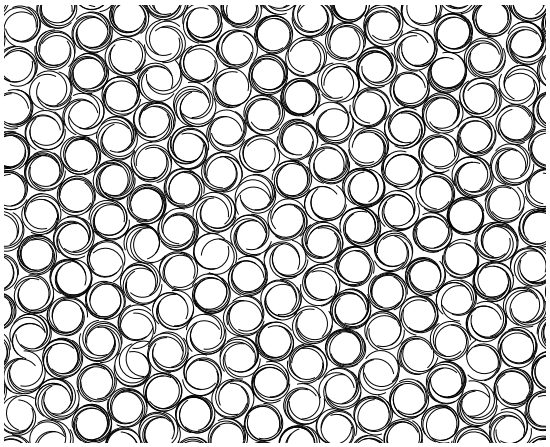

Fig. 2. Example of a hexagonal cluster phase for major arcs subtending an angle $\theta = 1.1\pi$.

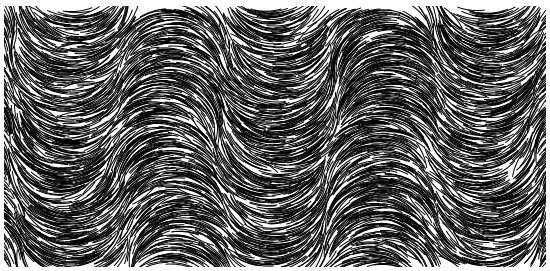

Fig. 3. Example of a filamentary phase for minor arcs subtending an angle $\theta = 0.5$.

[1] J.P. Ramrez Gonzlez and, G. Cinacchi, *Phase behavior of hard circular arcs*, Phys. Rev. E **104**, 054604 (2021).

[2] J.P. Ramrez Gonzlez and, G. Cinacchi, *Dense packings of hard circular arcs*, Phys. Rev. E **102**, 042903 (2020).

Farey graphs: a real number exotic representation

Jorge Calero-Sanz[1,3], Bartolomé Luque,[1], and Lucas Lacasa[2]
[1]Departamento de Matemática Aplicada, ETSIAE, Universidad Politécnica de Madrid, Plaza Cardenal Cisneros, 3 28040 Madrid (Spain).
[2]Institute for Cross-Disciplinary Physics and Complex Systems IFISC (CSIC-UIB), Palma de Mallorca, (Spain).
[3] Signal and Communications Theory and Telematic Systems and Computing, Rey Juan Carlos University, Madrid, (Spain).

This research aims to study some properties of real numbers through the *Farey graphs*, a graph set built recursively using a concatenation operator. The graph structure, especially the connectivity distribution, allows analysing the inherent classification into family of real numbers.

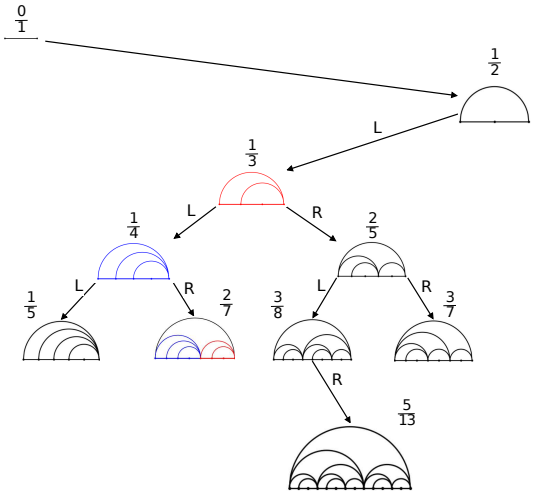

Fig. 1. The first six layers of Farey Graph Tree in $[0, 1/2]$. The rational associated is $P(2)$,the proportion of nodes with degree $k = 2$.

The Farey graph set is constructed using a initial graph (two nodes joined by a link) and an inner operation (see Fig. 2). We prove that there exists a one-to-one correspondance between the Farey graphs and Farey sequences, that are defined as $\mathcal{F}_n = \left\{ \frac{p}{q} \in [0,1] : \ 0 \leq p \leq q \leq n, \ (p,q) = 1 \right\}$ [1]. Passing to the limit, each real number in $[0, 1]$ can be associated with a Farey graph.

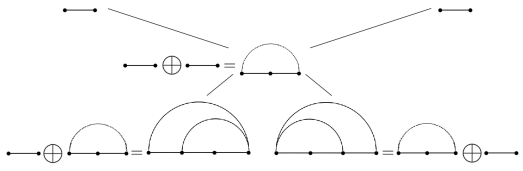

Fig. 2. An illustration of the concatenation operation, that consists on merging two extreme nodes and join the first and last nodes of the new graph with a new link

We are interested in a particular graph entropy over the degree distribution $P(k)$ [2, 3]. We compute this entropy $S(x)$ for all graphs with at least 1000 nodes (see Fig. 3). We show that $S(x)$ is a fractal function where the maximum entropy is associated with the reciprocal of Golden number. The local maximums entropy are the noble numbers, a subfamily of quadratic irrationals having a continued fraction with an infinite sequence of 1. Moreover, the local minimums entropy are the rational numbers.

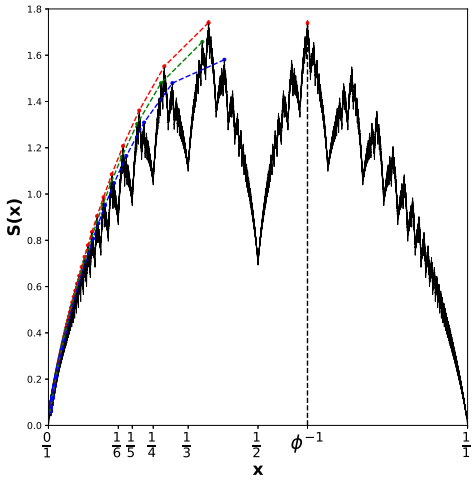

Fig. 3. Number entropy function $S(x)$ computed for all Farey graphs G_x with $x \in \mathcal{F}_{1000}$. In this figure, red dots and dashed lines are the local maxima $\mathcal{C}_1(n) = \frac{1}{n+\phi^{-1}}$ for $n \geq 2$. The global maxima are $\mathcal{C}_1(2) = 1 - \phi^{-1}$ and the reflected ϕ^{-1} (represented as a single red dot). The green and blue dots and dashed lines represent other families of noble numbers.

[1] R. L. Graham, D. E. Knuth, and O. Patashnik. Concrete Mathematics. Addison-Wesley, 1989/1994.

[2] B.Luque and L.Lacasa, *Canonical horizontal visibility graphs are uniquely determined by their degree sequence*, The European Physical Journal Special Topics, vol. 226, pp. 383-389 **3** (2017).

[3] B.Luque, L.Lacasa, F.J.Ballesteros and A.Robledo, *Analytical properties of horizontal visibility graphs in the Feigenbaum scenario*, Chaos: An Interdisciplinary Journal of Nonlinear Science, vol. 22,**1** (2012).

A bounded confidence model of emotionally aroused integrate and fire oscillators

Irene Ferri[1], Emanuele Cozzo[1,2], Albert Díaz-Guilera[1] and Luce prignano[1]
[1]Universitat de Barcelona, UBICS, Barcelona 08028, Spain
[2]Universitat Oberta de Catalunya, Internet Interdisciplinary Institute, Castelldefels 08060, Barcelona, Spain

Introduction

The bounded confidence model introduced by Deffuant et al. [1] is a popular model of opinion dynamics in which actors have a $[0, 1]$-valued opinion and interact only if their opinions differ by at most a deviation threshold, then both move closer in barycentric fashion governed by a confidence factor. A number of extensions have been proposed in order to go beyond mean-field approximation [2] or to include emotional dynamics [3, 4].
Here, we propose a framework in which actors are prevented from interacting with those that differ in opinion (O) more than a deviation threshold determined by a decreasing function of their emotional arousal (EA). The higher the emotional arousal, the smaller the deviation threshold. Additionally, by interacting, they also influence each other's activity's timing.

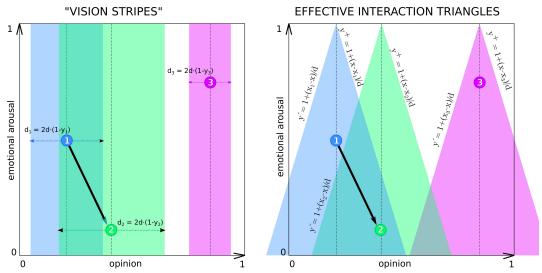

Fig. 1. Range of interaction for the oscillators. The stripes in the left panel correspond to the confidence area an emitter must be within in order to a receiver in a given opinion position O_j listens to his message. The cones in right panel correspond to the affectation area; receivers within the affectation area will be affected by emitters in a given opinion position O_i.

Results

We consider a two-dimensional continuous space, a square box with sides normalized to 1. Initially the agents are uniformly distributed in this area, their coordinates are given by their opinion position (O) in the abscissa axis and their level of emotional arousal (EA) in the ordinate axis. Additionally each agent has a phase ϕ, that increases uniformly with period T until it reaches a maximum value of 1, when a firing event - here understood as a communication action - occurs, after this the emitter's phase is reset to zero. In a firing event every emitter i broadcast a message that will be listened by any agent within the confidence cone of the emitter (see Fig. 1, right panel), and dismissed by agents situated outside this area. Each listener j (simultaneously) affected by a number of emitters n will update his phase by a factor $(1 + \epsilon)^n$ and will take a step in the O-EA plane, with a maximum longitude $d\bar{s} = \alpha$, moving towards the barycenter formed by the emitters that affected him in the current firing event as follows:

$$Q_j(t+1) = Q_j(t) + min(\alpha/d_{C_j}, 1)\frac{\sum_{i=1} n(Q_i - Q_j)}{n+1}; \quad Q \in \{O, EA\}\,, \tag{1}$$

where d_{C_j} is the distance between the j^{th} oscillator and the barycenter formed by the emitters.
The system evolves until all the oscillators remain immobile within a tolerance threshold we called μ ($\mu \ll \alpha$). At the end of the process all agents belonging to the same cluster - here defined as a weakly connected component in the interaction graph - have collapsed into a single point in the plane (except for deviations of order μ) and synchronized their phases $\forall\, \epsilon > 0$.
We find that, in general, the stationary state is characterized by an increase of the average EA and the final number of clusters is larger than the initial number of connected components of the interaction graph. Fig. 2 shows the evolution of the EA for a group of 100 agents which start forming one single (red) cluster and have $\langle EA \rangle \sim 0.5$. As the system evolves the initial cluster breaks into several components denoted by different colors, and the average level of EA increases. However, in panel A, corresponding to non-synchronized oscillators with $\epsilon = 0$ (i.e. they never synchronize), the number of final components is larger that in panel B, which corresponds to the opposite limit where all agents have the same phase from the beginning of the simulation.

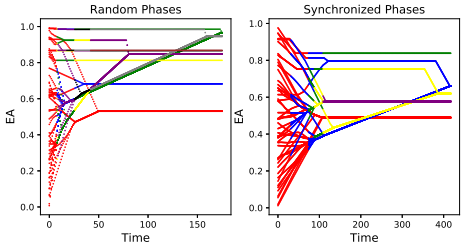

Fig. 2. Panel A. Evolution of the EA coordinates in a system of 50 oscillators with $d = 0.2$, $\alpha = 0.05$ using random initial conditions and $\epsilon = 0$. Panel B: The same as in Panel A, but in the opposite scenario of synchronized initial phases. Colors denote different weakly connected components.

[1] G. Deffuant, D. Neau, F. Amblard and G. Weisbuch, , Adv. Complex Syst. **3(4)**, 87-89 (2000).

[2] G. Weisbuch, , Eur. Phys. J. B **38(2)**, 339-343 (2004).

[3] P. Sobkowicz, , Front. Phys. **3**, 17 (2015).

[4] F. Schweitzer, T. Krivachy and D. Garcia, , Front. Phys. **3**, 17 (2015).

Rippled and buckled phases in a rotationally-invariant spin-string model

Gregorio García-Valladares[1], Antonio Prados[1], and Carlos A. Plata[1]
[1]Física Teórica, Universidad de Sevilla, Apartado de Correos 1065, E-41080 Seville, Spain

The study of rippled and buckled phases in low-dimensional system like graphene is an active research field [1, 2]. When the system is heated in STM experiments [3], there appear transitions from a rippled to a buckled state that have been qualitatively described by spin-string (in the one-dimensional case) [4] or spin-membrane (in the two-dimensional case) [5, 6] models. However, these latter models are not consistent with the classical theory of elasticity [7]—they break rotational symmetry, even though there are not any external forces.

We propose a variant of the models in Refs. [4, 5] that preserves rotational invariance. Interestingly, the phase diagram of the rotationally-invariant model has strong similarities with that found in [4]. Buckled phases emerge for low enough temperature. Their relative stability to the rippled (flat) phase depends on the strength of the antiferromagnetic interaction between the pseudospins—in the case of graphene, this mimics the electrostatic repulsion between out-of-plane electrons.

In our model, the interactions involve exclusively the curvature of the string and the internal, pseudospin, degrees of freedom. In the continuum limit, the equilibrium probability density of finding the system with a string profile $u(x)$ at temperature T can be written as $\mathcal{P}[u'';\theta,\kappa] \propto \exp\left(-F[u'';\theta,\kappa]/\theta\right)$, where θ and κ are the dimensionless temperature and coupling constant, respectively. The functional

$$F[u'';\theta,\kappa] = N\int_0^1 \mathrm{d}x\; f(u'';\kappa,\theta) \tag{1}$$

is the free energy of the string, and its minimisation provides us with its most probable configuration. Thus, the equilibrium profile obeys the Euler-Lagrange equation

$$\partial_{xx}\left(\frac{\partial f}{\partial u''}\right) = 0, \tag{2}$$

which is complemented with suitable boundary conditions.

This spin-string system exhibits different kinds of phase transitions between flat and buckled profiles. The profiles have been computed solving Eq. (2) both analytically, using bifurcation theory and the Landau theory of phase transitions, and numerically. Our study allows us to obtain the complete phase diagram, see Figure 1, where the free energy of the most stable buckled profile with respect to the flat profile is shown. (If only the flat profile exists, we set $\Delta F = 0$.) Above the tricritical point K, the black solid curve defines a second order transition line. Below the tricritical point, the order of the transition changes to first order, with the dotted line marking the change of stability between the flat and the locally stable buckled phase—there is also a unstable buckled phase. The dashed line to its right (solid line to its left) marks where the buckled phase (flat phase) disappears.

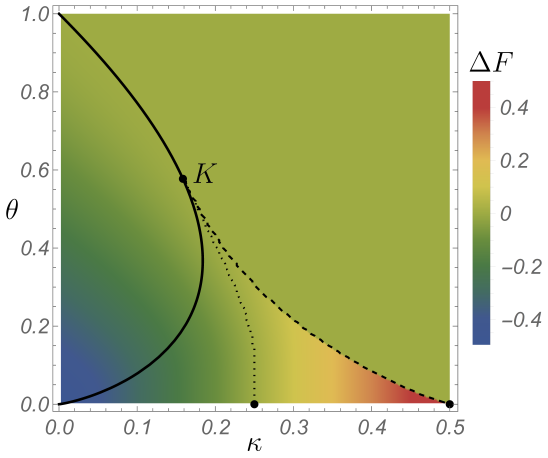

Fig. 1. Density plot of the free energy difference ΔF of the locally stable buckled state respect to the flat profile. The lines represent different kinds of phase transitions and the point where all of them intersect is the tricritical point K.

[1] P. Z. Hanakata, S. S. Bhabesh, M. J. Bowick, D. R. Nelson and D. Yllanes, Extreme Mech. Lett. **44**, 101270 (2021).

[2] A. Morshedifard, M. Ruiz-García, M. Javad and A. Komrlj, J. Mech. Phys. Solids **149**, 104296 (2021).

[3] J. Schoelz, P. Xu, V. Meunier, P. Kumar, M. Neek-Amal, P. Thibado and F. Peeters, Phys. Rev. B. **91**, 045413 (2015).

[4] M. Ruiz-García, L. L. Bonilla, and A. Prados, Phys. Rev. E. **94**, 062147 (2017).

[5] M. Ruiz-García, L. L. Bonilla, and A. Prados, J. Stat. Mech. P05015 (2015).

[6] M. Ruiz-García, L. L. Bonilla, and A. Prados, Phys. Rev. B. **94**, 205404 (2016).

[7] L. Landau and E. B. Lifshitz, *Course of Theoretical Physics Volume 7* (Butterworth-Heinemann, Oxford, 1986).

Modeling brain reorganization after hemispherectomy

Seoane LF[1,2,3], Solé R[4,5,6]
[1]Departamento de Biología de Sistemas, Centro Nacional de Biotecnología (CSIC), C/ Darwin 3, 28049 Madrid, Spain.
[2]Grupo Interdisciplinar de Sistemas Complejos (GISC), Madrid, Spain.
[3]Instituto de Física Interdisciplinar y Sistemas Complejos IFISC (CSIC-UIB), Palma de Mallorca, Spain.
[4]ICREA-Complex Systems Lab, Universitat Pompeu Fabra (GRIB), Dr Aiguader 80, 08003 Barcelona, Spain.
[5]Institut de Biologia Evolutiva, CSIC-UPF, Pg Maritim de la Barceloneta 37, 08003 Barcelona, Spain.
[6]Santa Fe Institute, 1399 Hyde Park Road, Santa Fe NM 87501, USA.

Hemispherectomy is a last-resource treatment for some neurological disorders. This radical intervention allows some patients to live normally, with better odds the earlier in life it happens. Somehow, the remaining hemisphere takes on the outstanding computational burden.

Brain plasticity at smaller scales shows how functionality is adopted by adjacent tissue. In models of brain rewiring after stroke, circuits accepting new workload are close and similar to the damaged ones. Hemispherectomy demands more drastic changes, mixing far and functionally diverse regions. We lack mathematical models of this.

We introduce a simple model of brain reorganization after hemispherectomy [1] based on Self-Organized Maps (SOMs). We show how emerging representations in SOMs constrain brain reorganization after simulated hemispherectomy, resulting in some forbidden and some other favored rearrangement pathways, each with distinct symmetries and properties (Figure 1**a-c**). We discuss what the enabled paths imply for the recovery of topographic maps and language functionality after hemispherectomy.

We find how too much symmetry can be detrimental for the proper formation of representation systems (Figure 1**d**). We also obtain results regarding the existence of window periods – a critical age after which hemispherectomy causes irreversible function loss (Figure 1**e-f**). These findings illuminate various (hitherto unexplained) clinical facts about window periods for language recovery.

Our model offers a powerful thinking tool and suggests simple guiding principles for large-scale brain plasticity notably, that the geometry of emerging representations turn into topological constraints for large-scale brain rearrangement. This offers insights about why such an aggressive intervention results in highly functional brains nevertheless, and suggests specific treatments for simulated, pathological disorders observed in our SOM models.

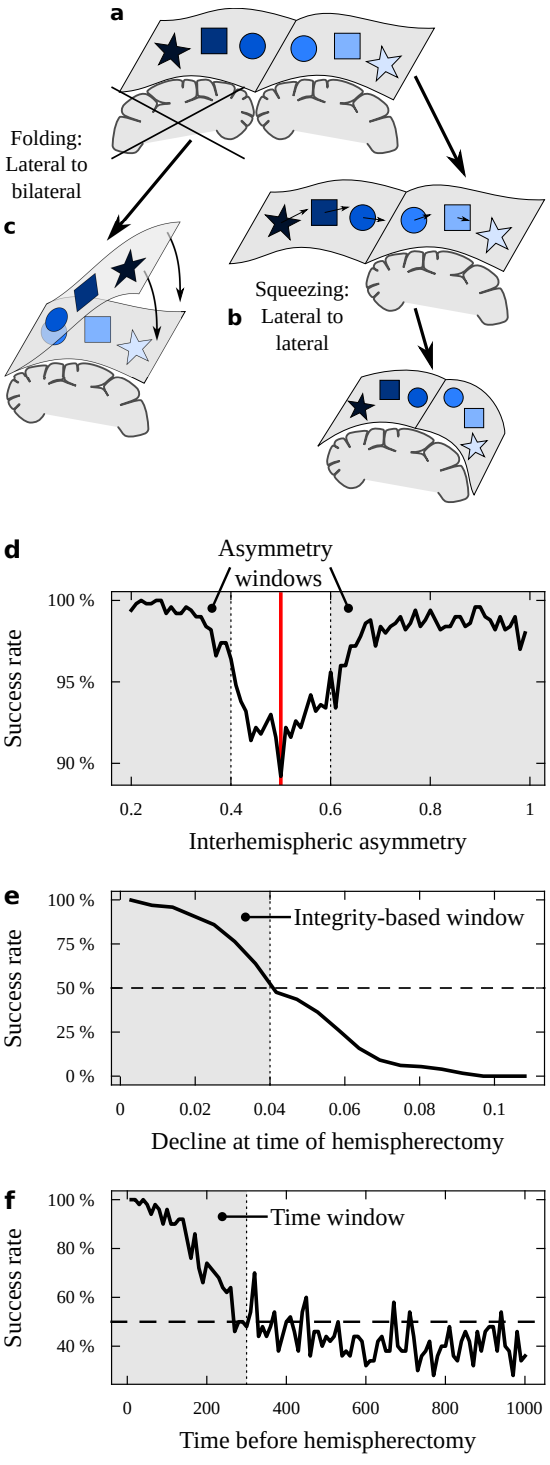

[1] L.F. Seoane and R. Sol. *Modeling brain reorganization after hemispherectomy*, https://www.biorxiv.org/content/10.1101/2020.12.25.424412v1 (2020).

Random walkers on deformable media

Carlos Lajusticia Costán[1], Silvia N. Santalla[2], Javier Rodríguez-Laguna[1], and Elka Korutcheva[1]
[1]Universidad Nacional de Educación a Distancia (UNED), Madrid, Spain
[2]Dpto. Física & GISC, Universidad Carlos III de Madrid, Spain

We consider random walkers that deform the medium as they move, enabling a faster motion in regions which have been recently visited. This induces an effective interaction between walkers mediated by the medium, which can be regarded as a space metric. Such an effect gives rise to a statistical mechanics toy model for gravity, motion through deformable matter or adaptable geometry. In the strong-deformability regime, we find that diffusion is ruled by the *porous medium equation*, thus yielding subdiffusive behavior of an initially localized cloud of particles, whose global width will grow like $\sigma \sim t^{1/3}$, though the sample-to-sample width average will sustain a $\sigma \sim t^{1/4}$ or $t^{1/2}$ growth. Indeed, random walkers present anti-persistence and strong memory effects, which we explore indirectly through the fluctuations of the center of mass of the cloud.

Our model of *random walkers on a deformable metric* (RWDM), is built from of N_p random walkers on a chain. Any particle standing on site i has a certain probability per unit time $J_{i,i-1}$ of hopping to site $i-1$, and $J_{i,i+1}$ of hopping to site $i+1$. We will assume these probabilities are symmetric and the system starts with uniform hopping rates, $J_i = J_0$ for all i. Furthermore, whenever a particle jumps across a link $(i, i+1)$ the hopping probability is updated, $J_i \to J_1 \geq J_0$. If no walker crosses the link during the subsequent time-steps, its hopping probability will decay towards the relaxed value J_0 in a time of order t_0. Figure 1 provides a graphical description of our model.

On the other hand, a theoretical approach to the problem will lead us to the following equation for the probability distribution of the walkers, $P(x,t)$,

$$\partial_t P(x,t) = b(\partial_x P(x,t))^2 + (a + bP(x,t))\partial_x^2 P(x,t), \quad (1)$$

where $a = J_0$ and $b = J_1 - J_0$. We consider the physical picture provided by Eq. (1) for different values of its parameters. Notice that if $a \to 0$, Eq. (1) corresponds to the well-known *porous medium equation* [1].

In our first model [2] where initally all the walkers were located at the same point, the average over different samples differs substantially from the time-average over a single sample. Intuitively, the reason is that the walkers cloud tends to move more rigidly than expected for non-interacting random walkers. This phenomenon can be characterized by the fluctuations in the position of the center of mass of the cloud.

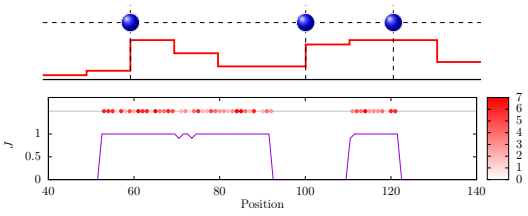

Fig. 1. Top: Illustration of our RWDM model. Walkers occupy integer positions of a chain, and hopping probabilities between neighboring sites can be different. Bottom: A configuration for $J_0 = 10^{-6}$, $J_1 = 1$, $t_0 = 10$ and $N_P = 100$ particles on $L = 200$ sites, after $T = 10^8$ time-steps. The purple line denotes the hopping probabilities, the red balls represents the positions of the particles, and the color intensity denotes the number of particles at a certain site. Notice that most hopping probabilities are near J_0 or J_1, and that the particles are neatly divided into two blocks.

Using a random initial configuration leads to a substantially different evolution of the system, where we can see some clusters start to appear after enough time has been allowed.

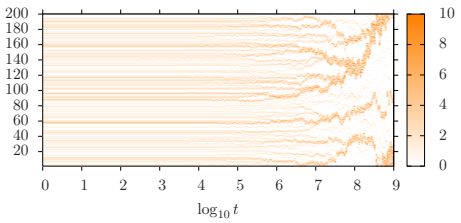

Fig. 2. The illustration shows after $T = 10^9$ time-steps the particules tend to concentrate mostly around two well-defined areas creating two prominent clusters.

[1] Juan Luis Vazquez, *The Porous Medium equation*, Clarendon Press Oxford (2007)

[2] Carlos Lajusticia-Costan et al J. Stat. Mech. (2021) 073207

Estudio de las fases del proceso de infeccin del intestino grueso por *Clostridiodies difficile* mediante el simulador de modelos basados en agentes, *gro*

Olga Hormigos[1], Juan Manuel Pastor[1], Rosa del Campo[2], and Javier Galeano[1]
[1]Grupo de Sistemas Complejos, ETSIAAB, UPM
[2]Servicio de microbiología, Hospital Ramón y Cajal

Clostridiodies difficile is an anaerobic gram-positive toxigenic bacterium that causes a severe infectious diarrhoea and pseudomembranous colitis. The large intestine of humans and mammals is protected by the gut microbiome, composed of approximately 400 bacterial species. Supply of broad-spectrum antibiotics in hospitals leads to disruption of the gut symbiosis, resulting in the emergence of niches that can be colonised by various pathogens such as *C. difficile*.

The first step against *C. difficile* infection is to stop giving broad-spectrum antibiotics, followed by providing certain antibiotics that have specific activity against *C. difficile* such as vancomycin. Nevertheless, in the last decade in about 20% of the cases conventional therapies are useless, because *C. difficile* has developed resistance and new virulent strains. Faecal microbiota transference is a novel approach to this complex problem, which is an experimental method with between 80% and 90% successful recovery rate. The via of administration of the transference and the bacterial composition of the donor faecal sample do not seem to be relevant, it is sufficient to restore a healthy and diverse gut microbiota.

The aim of this work is to study the *C. difficile* infection process and its treatment using the individual-based modelling programme *gro*, which is an open-source biological simulator created by Eric Klavins research group at the University of Washington. Specifically, I have used the version from Alfonso Patn's Artificial Intelligence Laboratory at the Polytechnic University of Madrid.

The results obtained agreed with real patient data, allowing the visualisation of the complete process of the 3 most abundant intestinal bacterial populations (*Enterobacterales*, *Lactobacillales* and *Fusobacteriales*) together with *C. difficile*. Bacterial growth was analysed in a state of symbiosis, followed by a state of dysbiosis in which *C. difficile* thrives, and finally, after the faecal microbiota transference, leading to the recovery of intestinal bacterial diversity.

In the first simulation of a healthy individual, bacteria grew exponentially according to their growth rate and the percentage of *C. difficile* population was low, as it could not thrive due to its condition as a bad competitor specie. In the second simulation, the supply of a generic antibiotic affected most bacterial populations but not *C. difficile*, leading to a decrease in intestinal bacterial diversity and, consequently, an increase in the *C. difficile* population. It is at this point that *C. difficile* begins to synthesise toxins and symptoms of infection may become visible. In the last simulation, the donor bacteria were added to the patient, restoring intestinal bacterial diversity, and thus decreasing the *C. difficile* population. Figure 1 shows the percentage of each bacterial population throughout the simulation after a faecal microbiota transference.

C. difficile infection is an evolving global health problem, there are on average 7 cases for every 10,000 overnight patients stays in European hospitals. The incidence in the US is similar, it is the main cause of hospital associated infection, with an estimated 14,000 deaths each year. For these reasons, the search for a treatment for this disease is a necessity, being focused on the faecal microbiota transference. However, in spite of the proven effectiveness of the faecal microbiota transference and an intuitive reasoning of its function, there are many important questions about the exact procedures and key molecules involve in the metabolic pathways of a faecal microbiota transference.

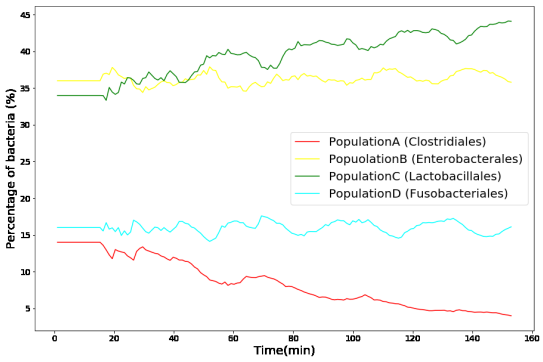

Fig. 1. Percentage of bacteria per population over time in a bacterial growth simulation of a faecal microbiota transference.

[1] S.S. Jang, K.T. Oishi, R. G. Egbert and E. Klavins *Specification and simulation of synthetic multicelled behaviors*, ACS Synthetic Biology **8**, 365-374 (2012).

[2] M. Gutierrez, P. Gregorio-Godoy, G. Prez del Pulgar, L.E.. Muoz, S. Sez and A. Rodrguez-Patn *A new improved and extended version of the multicell bacterial simulator gro*, ACS Synthetic Biology **8**, 1496-1508 (2017).

[3] "https://github.com/olgahs/" Clostridium-difficile-infection

[4] "https://www.youtube.com/" "playlist?list=PLjLAYk-Cbhr-3gYw-yvHSmS5z3UDDCGSd"}

Mathematical Model for the Vestibular System

Ismael Arán-Tapia[1,2], Andrés Soto-Varela[3], Vicente Pérez-Muñuzuri[1,4] Ismael Arán[5] & Alberto P. Muñuzuri[1,2]
[1]Group of Non-Linear Physics, Faculty of Physics, University of Santiago de Compostela, Spain.
[2] CITMAga, Santiago de Compostela, Spain.
[3] Division of Neurotology, Department of Otorhinolaryngology, Complexo Hospitalario Universitario, Santiago de Compostela, Spain.
[4] CRETUS, Santiago de Compostela, Spain.
[5] Otoneurology Unit of the Complexo Hospitalario Universitario de Pontevedra, Spain.

The diagniosis of the Vestibular System patologies is always performed following a specific procedure independently on the anatomical individualities for a given patient. This might result in an impairing diagnostic ability. Considering the personalized medicine in the development of rotational tests, there are certain optimized angular directions that maximize stimulation in a certain semicircular canal, almost completely inhibiting the other two. It is expected that this plane of rotation, known as prime direction, can provide a better response on clinical test [Furman, 2016].

Based on mathematical models of the membranous labyrinth and their simulation by means of Computational Fluid Dynamics techniques, we evaluate how different planes of rotation affect the vestibular diagnosis. Based on our results [Arán-Tapia et al., 2022], a different plane of rotation, selected following the angular relationships between the planes of the semicircular canals, helps to distinguish each cupular stimulus contribution on the nystagmus, resulting in an optimization of the rotational testing of the vestibular function.

The study of the individualities of the membranous labyrinths through numerical simulations can serve as a tool to increase the vestibular diagnosis success. In future, this technique can help to achieve personalized treatment procedures, improve knowledge about vestibular pathophysiology and implement a database for the application of data science.

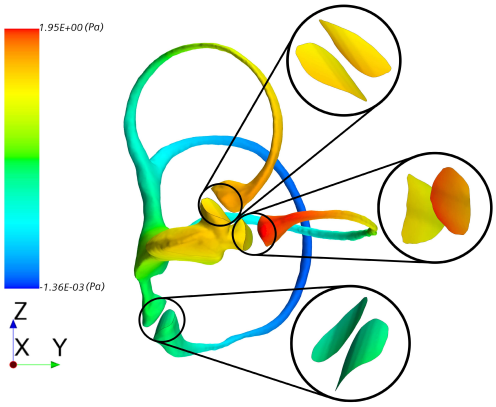

Fig. 1. The total pressure distribution for the real model of the left membranous labyrinth, under Htest angular direction for rotating reference frame. With amplified vision of cupula walls, where horizontal ones show the biggest pressure differences. The data was obtained at the end of stimulation when the head returns to the initial position (clockwise rotation).

Furman, J.M., 2016. Rotational testing. Handb Clin Neurol 137, 177186. https://doi.org/10.1016/B978-0-444-63437-5.00012-1

Arán-Tapia et al, 2022. Personalized Design for Optimal Rotational Testing of the Vestibular Function (submitted)

Dynamical anomalies and structural features of Active Brownian Particles characterised by two repulsive length scales

José Martín-Roca[1], Raúl Martínez[1,2], Fernando Martínez-Pedrero[3], Jorge Ramírez[4], and Chantal Valeriani[1,5]
[1]Dep. Est. de la Materia, Física Térmica y Electrónica, Universidad Complutense de Madrid, 28040 Madrid, Spain
[2]Dep. de Física Teórica de la Materia Condensada, Facultad de Ciencias, Universidad Autónoma de Madrid, 28049 Madrid, Spain
[3]Dep. Química-Física, Universidad Complutense de Madrid, Avda. Complutense s/n, Madrid, 28040, Spain.
[4]Dep. de Ingeniería Química, ETSI Industriales, Universidad Politécnica de Madrid, 28006 Madrid, Spain.
[5]GISC - Grupo Interdisciplinar de Sistemas Complejos 28040 Madrid, Spain

In this work we study a two-dimensional system composed by Active Brownian Particles (ABPs) interacting via a repulsive potential with two-length-scales, a soft shell and a hard-core (see Fig. 1.a).

$$V(r) = \epsilon \left(\frac{\sigma}{r}\right)^n + \frac{1}{2}\,\varepsilon_s\,\{1 - \tanh\left[k_0\,(r - \sigma_s)\right]\}, \quad (1)$$

Here, ϵ is the energy related to the hard core, ϵ_s and σ_s are the height and width of the repulsive shoulder, respectively, n affects the stiffness of the repulsive core and k_0 determines the steepness of the shoulder decay. Throughout this work, we have chosen to establish the following parameters: $n = 14$ and $k_0 = 10/\sigma$ as in ref[1], and $\sigma_s = 2.5\sigma$. In order to study the time evolution of the system we have used the open source code LAMMPS[2]; when dealing with the $N = 2^{14}$ systems, we have used a modified version of UAMMD[3] (Universally Adaptable Multiscale Molecular Dynamics). Each simulation has been reiterated until the system attains steady state, which we assume arrives when there are no further significant changes in potential energy and overall phase behaviour. The level of activity is measured via the Peclet number, defined as

$$\mathrm{Pe} \equiv \frac{3\,v_p\,\tau_r}{\sigma} = \frac{3\,|F_a|\,D_t}{k_B\,T\,D_r\,\sigma}, \quad (2)$$

where $v_p = |F_a|D_t/k_BT$ is the velocity propulsion of the active particles and $\tau_r = 1/D_r$ the reorientation time.

Depending on the ratio between the strength of the soft shell barrier, ϵ_s and the activity, we find two regimes: If this ratio is much larger or smaller than 1, the observed behaviour is comparable with ABPs interacting via a single length-scale potential. If this ratio is similar to 1, the two length-scales are relevant for both structure and dynamical properties. On the structural side, when the system exhibits a motility induced phase separation, the dense phase is characterised by new and more complex structures compared with the hexatic phase observed in single length-scale systems (see Fig 1.b). On the dynamical side, as far as we are aware, this is the first representation of an anomalous dynamics in active particles (see Fig 1.c).

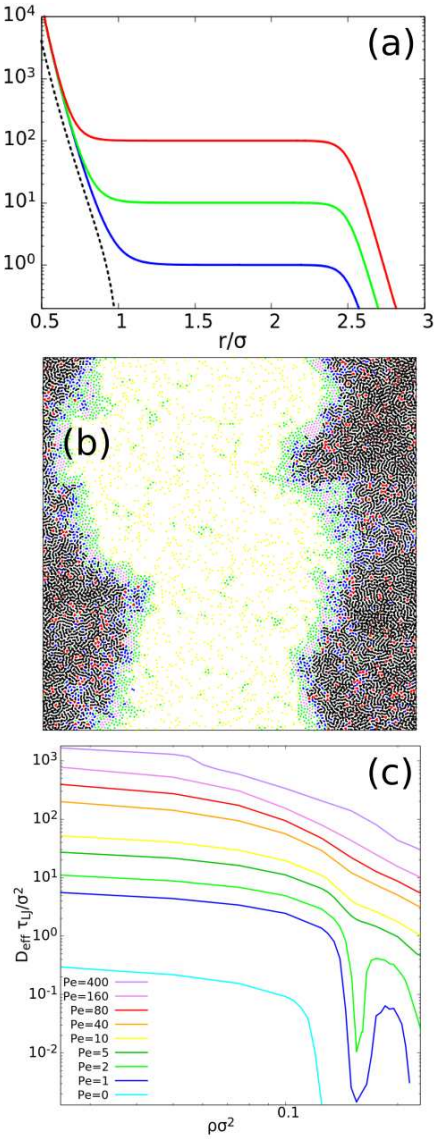

Fig. 1. (a) Shoulder interaction potential for $\epsilon_s/\epsilon = 1$ (blue), $\epsilon_s/\epsilon = 10$ (green) and $\epsilon_s/\epsilon = 100$ (red) and Weeks-Chandler-Andersen (black). (b) Snapshot for a system with $\epsilon_s/\epsilon = 10$, $\rho\,\sigma^2 = 0.150$ and $Pe = 500$. (c) Effective diffusion of the particles as a function of density for different degrees of activity.

[1] Gribova, NV and Fomin, Yu D and Frenkel, Daan and Ryzhov, *Waterlike thermodynamic anomalies in a repulsive-shoulder potential system*, Physical Review E, 79, 5, 051202 (2009).

[2] Plimpton, Steve, *Fast parallel algorithms for short-range molecular dynamics*, Journal of computational physics, 117, 1, 1–19 (1995).

[3] Ral P. Pelez, *Universally Adaptable Multiscale Molecular Dynamics (UAMMD)*, https://github.com/RaulPPelaez/UAMMD, (2021).

Time crystal oscillations in a laser system with weak periodic forcing

Jordi Tiana-Alsina[1] and Cristina Masoller[2],

[1]Department de Física Aplicada, Facultat de Física, Universitat de Barcelona, Martí i Franquès 1, 08028 Barcelona, Spain
[2]Departament de Física, Universitat Politecnica de Catalunya, Rambla Sant Nebridi 22, 08222 Terrassa, Spain

In many-particle systems, when the translation symmetry in space (in time) is spontaneously broken, the result is a space (time) crystal. Time-crystal states are characterized by highly regular oscillations that are stable over very long times, are robust under perturbations ("rigidity") and break time-translation symmetry [1]. In systems under periodic forcing, the forcing defines the discrete time translation symmetry and this symmetry is broken in the time crystal state, where the system's variable displays sub-harmonic oscillations that are rigidly locked to the driving signal.

A key requirement for observing time-crystal oscillations is that they have long-term regularity that results from the interaction of many degrees of freedom. This excludes period-doubling oscillations in low-dimensional systems, and it also excludes oscillations in mode-locked lasers, which arise from the interactions of many modes but which lack long-term regularity due to noise.

Here we address the following question: Can a time-delayed feedback loop counteract the effect of noise and generate long-term order?

Time-delayed systems (TDSs) with feedback loops, governed by equations of the form $du(t)/dt = f(u(t),t) + Ku(t-\tau)$, have an infinite phase space because the initial condition is the function $u(t)$ defined in [-τ,0], where τ is the feedback delay time. In this type of TDS, when τ is long, analogies have been found with the dynamics of one-dimensional spatially extended systems (1D SESs). Specifically, in the TDS, τ plays the role of the size, L, in a 1D SES. When τ is long enough, using the so-called space-time representation, complex spatio-temporal behavior has been found (such as pattern formation, defects and localized structures), analogous to those occurring in 1D SESs.

These analogies make periodically driven stochastic TDSs promising test benches for finding time-crystal oscillations. A semiconductor laser with optical feedback is a well-known TDS, in which feedback from a distant reflector generates a complex dynamics that, when viewed using the space-time representation, reveals spatio-temporal structures typical of 1D SES.

Near threshold and for appropriated feedback conditions the laser output intensity displays spikes that occur at irregular times (Fig. 1a). We have found [2] that a weak periodic modulation of the laser current can lock the spikes to the modulation. With a pulsed waveform we found, depending on the modulation frequency, harmonic or subharmonic locking (i.e., there is a spike every one or more modulation cycles, Fig. 1b); in contrast, with sinusoidal modulation there is no harmonic locking (Fig. 1c) but sub-harmonic locking (for a higher modulation frequency a spike is emitted every two cycles, Fig. 1d). In the locked states the spikes become periodic, but in between the spikes, the intensity fluctuations are still irregular.

When calculating the Fano factor (F, a well-known measure of the variability of a sequence of events), for particular

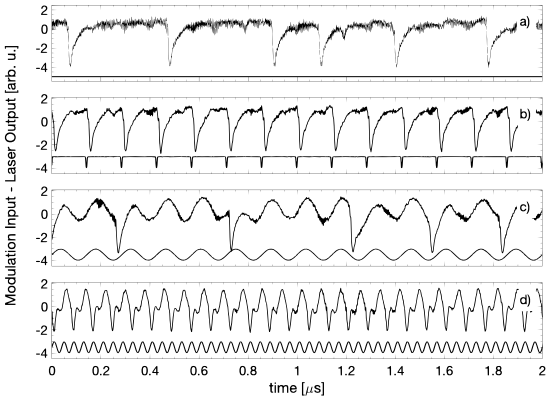

Fig. 1. Laser intensity without modulation (a) and with pulsed modulation (b) with $f_{mod} = 7$ MHz. (c), (d) laser intensity with sinusoidal modulation with $f_{mod} = 7$ MHz and 25 MHz respectively.

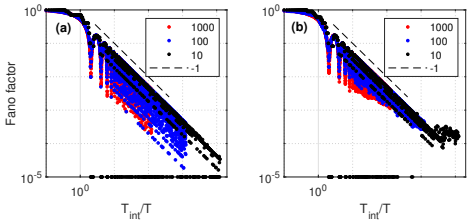

Fig. 2. Fano factor of the sequence of spikes generated by sinusoidal modulation with $f_{mod} = 25$ MHz. In (a) F is calculated from the original spike sequence and in (b) from the shuffled one, using 10, 100 or 1000 spike counting intervals. To represent $F = 0$ in log scale, we set it to $F = 10^{-5}$.

locking conditions we found [3] long-range regularity in the timing of the spikes revealed by very small F values (Fig. 2). Therefore, we conclude that we have found an experimental stochastic high-dimensional laser system where subharmonic oscillations with time-crystal characteristics are generated by sinusoidal modulation and delayed feedback.

[1] N. Y. Yao and C. Nayak, *Time crystals in periodically driven systems*, Physics Today **71**, 9, 40 (2018).

[2] J. Tiana-Alsina *et al.*, Experimental study of modulation waveforms for entraining the spikes emitted by a semiconductor laser with optical feedback. *Opt. Express* **26**, 9298 (2018).

[3] J. Tiana-Alsina and C. Masoller, Dynamics of a semiconductor laser with feedback and modulation: experiments and model comparison. *Opt. Express* in press (2022).

Non-invasive procedure to calculate Fractional Flow Reserve in patients with coronary artery disease and its comparison with the gold standard

Manuel Insúa-Villa[1] Alberto Otero-Cacho[1,2,3], Alberto P. Muñuzuri[2,3], Vicente Pérez-Muñuzuri[4], Diego López-Otero[5,6], María Bastos-Fernández[5,6], Brais Díaz-Fernández[5,6], and J.R. González-Juanatey[5,6]
[1]FlowReserve Labs S.L., Edificio Emprendia, 15782 Santiago de Compostela, Spain
[2]Group of Nonlinear Physics. University of Santiago de Compostela, 15782 Santiago de Compostela, Spain
[3]CITMAga, Santiago de Compostela, Spain
[4]Institute CRETUS, Group of Nonlinear Physics, University of Santiago de Compostela, Santiago de Compostela, Spain
[5]Cardiology and Intensive Cardiac Care Department, University Hospital of Santiago de Compostela, Santiago de Compostela, Spain
[6]Centro de Investigación Biomédica en Red de Enfermedades Cardiovasculares (CIBERCV), Madrid, Spain

Cardiovascular diseases are the leading cause of death in developing countries. The most common cause of cardiovascular disease is coronary artery disease. These are formed by the deposition of plaque on the walls of the endothelium, which produce a reduction in the blood supply and thus oxygen, increasing the risk of ischemia [1]. Fractional flow reserve (FFR) is a physiological measure that expresses the severity of a lesion caused by stenosis. It is an invasive procedure in which a pressure guidewire is introduced inside the arteries under hyperemic conditions. Numerous studies have been carried out comparing FFR, the gold standard procedure, with other procedures such as PCI (percutaneous coronary intervention). These conclude that the use of the FFR technique reduces the mortality rate and myocardial infarction [2].

Thanks to advances in technology, it is now possible to perform an FFR using CFD (computational fluid dynamics)[3]. This tool makes it feasible to simulate, in a virtual environment, the dynamics of the blood inside the heart. To do this, CT (computed Tomographic) cardiac images of individual patients and accurate boundary conditions, that simulate the normal functioning of the heart, are required [4]. This technique has been validated in studies comparing it against the invasive procedure (FFR) [5].

The main advantage of performing a FFR using CFD technology, is that it is a non-invasive test. In addition, it allows multiple variables to be measured, such as Wall Shear Stress (WSS). In particular, this variable is related to the appearance and growth of atherosclerosis plaque. Studies have shown how measuring the levels of WSS can help prevent the detachment of atherosclerosis plaques[6, 7].

In conclusion, the use of CFD techniques applied to the heart provides multiple advantages, including the elimination of the risks associated with invasive procedures, as well as broadening the spectrum of parameters that can be measured.

A comparison of the FFR calculation procedure between a coronary CFD model and its invasive counterparty will be presented.

[1] Bairey Merz, C., Pepine, C., Walsh, M., Fleg, J., Camici, P., Chilian, W., Clayton, J., Cooper, L., Crea, F., Di Carli, M. & Others Ischemia and no obstructive coronary artery disease (INOCA) developing evidence-based therapies and research agenda for the next decade. *Circulation*. **135**, 1075-1092 (2017)

[2] Pijls, N., Fearon, W., Tonino, P., Siebert, U., Ikeno, F., Bornschein, B., Veer, M., Klauss, V., Manoharan, G., Engstrm, T. & Others Fractional flow reserve versus angiography for guiding percutaneous coronary intervention in patients with multivessel coronary artery disease: 2-year follow-up of the FAME (Fractional Flow Reserve Versus Angiography for Multivessel Evaluation) study. *Journal Of The American College Of Cardiology*. **56**, 177-184 (2010)

[3] Min, J., Leipsic, J., Pencina, M., Berman, D., Koo, B., Van Mieghem, C., Erglis, A., Lin, F., Dunning, A., Apruzzese, P. & Others Diagnostic accuracy of fractional flow reserve from anatomic CT angiography. *Jama*. **308**, 1237-1245 (2012)

[4] Otero-Cacho, A., López-Otero, D., Insúa-Villa, M., Díaz-Fernández, B., Bastos-Fernández, M., García-Campos, A., Pérez-Muuzuri V., P. Muuzuri, A., González-Juanatey, J.R. Non-invasive assessment of coronary lesions by computer tomography fractional flow reserve compared to the invasive technique under hyperaemic and basal conditions. PLOS ONE. Submitted (2022)

[5] Nakazato, R., Park, H., Berman, D., Gransar, H., Koo, B., Erglis, A., Lin, F., Dunning, A., Budoff, M., Malpeso, J. & Others Noninvasive fractional flow reserve derived from computed tomography angiography for coronary lesions of intermediate stenosis severity: results from the DeFACTO study. *Circulation: Cardiovascular Imaging*. **6**, 881-889 (2013)

[6] Michel, J., Delbosc, S., Ho-Tin-Noé, B., Leseche, G., Nicoletti, A., Meilhac, O. & Martin-Ventura, J. From intraplaque haemorrhages to plaque vulnerability: biological consequences of intraplaque haemorrhages. *Journal Of Cardiovascular Medicine*. **13**, 628-634 (2012)

[7] Lee, J., Choi, G., Koo, B., Hwang, D., Park, J., Zhang, J., Kim, K., Tong, Y., Kim, H., Grady, L. & Others Identification of high-risk plaques destined to cause acute coronary syndrome using coronary computed tomographic angiography and computational fluid dynamics. *Cardiovascular Imaging*. **12**, 1032-1043 (2019)

Biased Diffusion-Advection on undirected networks

Manuel Miranda[1] and Ernesto Estrada[1]
[1] Institute of Cross-Disciplinary Physics and Complex Systems, IFISC (UIB-CSIC), 07122 Palma de Mallorca, Spain

Diffusion and advection processes are ubiquitous in natural phenomena. While advection processes show off whenever there is a privileged direction or external force affecting the process, diffusion appears when the system expands in all directions. This two effects are somehow opposite, fighting between following an specific direction and considering all of them equal. Thus, it makes interesting to study how a system evolves when both of them are present.

In the case of networks, diffusion processes are usually modeled by the Laplacian operator, a classical operator widely studied. On the other hand, advection has only been defined in directed networks, as flow orientation is naturally given by the directed edges of the graph. But, how can we generate a flow which is directly related to the graph core properties when the edges are undirected?

The answer comes together with the biased Laplacians. These operators are an extension of the classical diffusion operator and have been studied in the recent years [2]. Its main characteristic is that they their diffusion shows preference or rejects higher degree nodes, depending on whether we are referring to the hubs-attracting or the hubs-rejecting Laplacians. This difference on the diffusion probability generates an underlying bi-directed weighted graph (see fig 1) and this new configuration makes possible to define a vector field on the network, defining a new advection process.

Combining both the classical Laplacian and the new advection operator, we can model this competition between diffusion and advection in any undirected networks. In [1], we defined an Advection-Diffusion operator which depends upon two parameters, γ_{dif} and γ_{adv}, measuring how diffusive and advective is a given system.

We were able to prove that this operators have a stable state and that its convergence is faster than both the classical and the hubs-biased Laplacians alone. Moreover, for a node v_i with degree k_i, we could find an analytic expression for the node value in the final state:

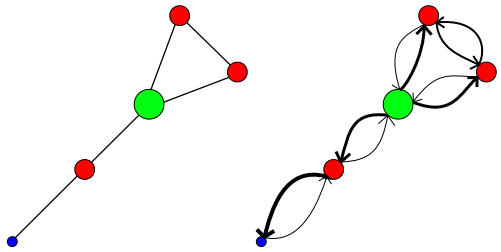

Fig. 1. Original graph (left) compared to the underlying bidirected graph induced by the Hubs-repelling Laplacian (right).

$$v_i = \sum_{T_i \in \mathcal{T}(G)} \prod_{(j,l) \in T_i} \left(\gamma_{dif} + \gamma_{adv} \left(\frac{k_l}{k_j} \right)^{\alpha} \right), \quad (1)$$

where $\mathcal{T}(G)$ is the set of all spanning trees of the graph G and T_i are each of this spanning trees rooted from node v_i.

We used this new operator to analyze the foraging of *L. catta* in a patched landscape in Southern Madagascar, so we could extract how much diffusion and how much advection there is in this situation.

[1] Miranda, M., & Estrada, E. (2021). *Degree-biased advection-diffusion on undirected graphs/networks*. Preprint: https://hal.archives-ouvertes.fr/hal-03469355

[2] Estrada, E., & Mugnolo, D. (2022). *Hubs-biased resistance distances on graphs and networks*. Journal of Mathematical Analysis and Applications, 507(1), 125728.

Vector-borne diseases with non-stationary vector populations: the case of growing and decaying populations

Àlex Giménez-Romero[1], Rosa Flaquer-Galmés[1,2], and Manuel A. Matias[1]

[1]Instituto de Física Interdisciplinar y Sistemas Complejos, IFISC (CSIC-UIB), Campus UIB, E-07122 Palma de Mallorca

[2] Grup de Física Estadística, Departament de Física, Facultat de Ciències, Universitat Autnoma de Barcelona, E-08193 Bellaterra (Barcelona)

Compartmental models have emerged as powerful tools to predict and control epidemic outbreaks, helping to mitigate its impacts. A key quantity for these models is the so-called *Basic Reproduction Number*, R_0, that measures the number of secondary infections produced by an initial infected individual in a fully susceptible population. Standard methods like the Next Generation Matrix (NGM) method [1] have been developed to allow the direct computation of R_0, provided that some conditions are fulfilled, such that the model has an initial disease-free equilibrium state. However, in vector-borne diseases, this is only accomplished when the vector population is *stationary*, this is, when the number of vector deaths are balanced with the same amount of vector births. However, many situations could lead to *non-stationary* vector populations, such as increasing or decaying populations.

Some authors have explicitly considered more general cases in which the demographic rates are not identical or even time-dependent with a given periodicity. In the first case, one obtains an asymptotic stationary vector population, but not an initial disease-free equilibrium. Nevertheless, the basic reproduction number of these models is often computed by means of the traditional methods from the asymptotic value of the population [2], i.e. the post-pandemic disease-free equilibrium. Here we show that it is not enough to study the asymptotic behaviour of the model to derive the epidemic threshold. In the case of periodic demographic rates, it has been shown that the time-averaged basic reproduction number defines the epidemic threshold under some circumstances and even a generalisation of the NGM method has been developed [3].

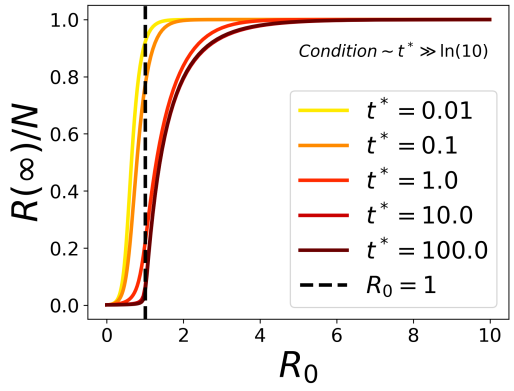

Fig. 1. Failure of the asymptotic theory to derive the epidemic threshold depending on the time-scales of the model. t^* is the time for the vector population to reach its asymptotic value.

We develop a compartmental model of vector-borne transmitted diseases that allows to describe growing and decaying vector populations. We show how and when standard methods fail to estimate the R_0 of the model and provide an alternative way to compute it. It turns out that the validity of the standard methods depends on on some time-scales of the model. Furthermore, we discuss and apply some approximations that allow to reduce the model in favour of simpler ones, with both fewer compartments and fewer parameters. In particular, we show that if some of the parameters fulfil certain conditions, it is possible to reduce the original model with 5 compartments and 4 parameters to an effective SIR model. The result is that a model in which hosts do not interact directly, but through vectors, in a certain limit yields and effective host to host interaction, what is assumed in some studies without suitable confirmation.

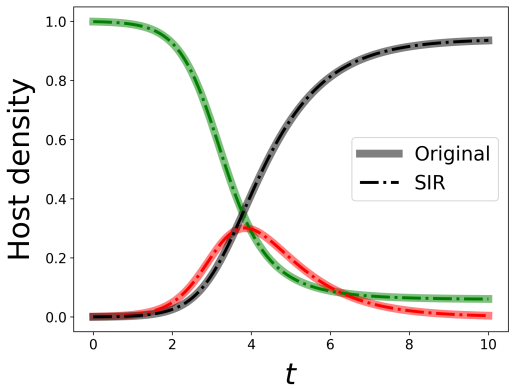

Fig. 2. Approximation to the SIR model in the suitable parameter range

[1] O. Diekmann, J. A. P. Heesterbeek, and M. G. Roberts, J. R. Soc. Interface **7**, 873-885 (2010).

[2] H.-M. Wei, X.-Z. Li, and M. Martcheva, J. Math. Anal. Appl. **342**, 895-908 (2008).

[3] N. Bacaër and S. Guernaoui, J. Math. Biol. **53**, 421-436 (2006)

A model for pattern formation in coral reefs

Miguel Álvarez-Alegra, Manuel A. Matías and Damiá Gomila
Instituto de Física Interdisciplinar y Sistemas Complejos, IFISC (CSIC-UIB), E-07122 Palma de Mallorca

Coral reefs are one of the most fascinating ecosystems in the world. The huge variety of living species they host together with the complex and colorful structures they form have made to gain for themselves the title of "rain forests of the sea". Even without considering interactions with the whole reef wildlife, corals biology is plenty of complex phenomena such as the symbiosis with microalgae named *Zooxanthellae* and emergent properties such as synchronized sexual events under very specific conditions or the self-organization of single polyps into well defined structures such as: massive, branching and table corals. Although there are some "lonely" species, coral polyps typically group into colonies of the same species forming the previously mentioned structures. Colonies living in the same region constitute a reef. Various species of these animals (corals) synthesize aragonite (a phase of calcium carbonate) during their clonal growth to build themselves a hard exoskeleton. When an entire colony dies, another new polyp can settle over the hard structure left behind by the dead colony and start a new colony on top of these remains. This process is repeated over centuries leading to the formation of large aragonite structures which display some recognizable patterns that can be spotted around the world. These include closed atolls and parallel stripes, together with large groups of closed atolls and little halos inside these big atolls (an example of self-similarity in this system).

In this work, we address the study of pattern formation in coral reefs by proposing a set of differential equations that govern the spatiotemporal evolution of some variables describing the system. Previous attempts on this direction include the work of Mistr and Bercovici [1], in which they successfully describe the formation of parallel stripes, and some models including reaction - fractional diffusion schemes [2], based on the previous work of Mistr and Bercovici. Some other authors have been proposed a model based on the chemistry of the aragonite synthesis combined with diffusion [3]. However, although these works reproduce some of the observed patterns in nature, they do not provide a whole description of the system and they do not include they key role of hydrodynamics in reef shaping.

We propose a new model to describe coral reefs by considering four fields in two spatial dimensions corresponding to: alive coral tissue P, dissolved nutrients in ocean water N, amount of accumulated aragonite A and the saturation state of aragonite in ocean water Ω. The amount of accumulated aragonite A is easily converted into the height the reef has reached at time t and we consider that at every moment live corals are settled over this hard rock structure or over the sea floor if there is no hard rock. These four fields interact following a reaction-diffusion model (plus an advective term for water flux) that includes terms representing birth, death, clonal growth and nutrients consumption for the polyps, together with some effects due to the height the reef has reached. Reef erosion and aragonite synthesis with its consequent alteration in the saturation state of aragonite in ocean water have also been included. After calibrating the parameters of the model based on real data and some reasonable assumptions, we have started to study the model's behavior in one dimension, obtaining some preliminary results that resemble the shape of closed atolls (Fig. 1).

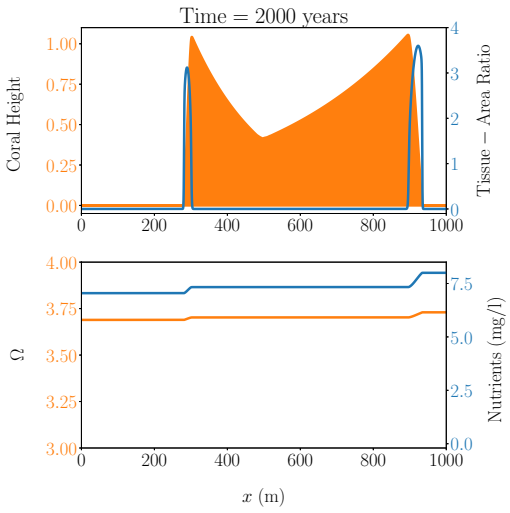

Fig. 1. Initial gaussian distribution of polyps and coral height placed at $x = 500$ m after 2000 years of evolution. Water flux coming from the right ($x = 1000$ m) flowing to the left. Blue curve at the panel above represents the ratio between alive coral tissue area respect to the sea floor area at each point. Orange shaded curve represents the height that the solid structure of aragonite rock has reached, normalized to the height of water column measured from the sea floor to the sea level. Blue and orange curves in the panel below represent nutrients concentration and aragonite saturation state, respectively.

[1] Mistr, S. and Bercovici, D. *A Theoretical Model of Pattern Formation in Coral Reefs*, Ecosystems **6** 0061-0074 (2003).

[2] Somathilake L. W. and Burrage, K. *A Space-Fractional-Reaction-Diffusion Model for Pattern Formation in Coral Reefs*, Cogent Mathematics & Statistics **5** (2018).

[3] Nakamura, T. and Nakamori, T. *A geochemical model for coral reef formation*, Coral Reefs **26**, 741755 (2007).

Experimental demonstration of relaxation asymmetry in equidistant temperature quenches

Miguel Ibáñez[1,2], Sergio Orozco[1,2], A. Lasanta[2,3] and Raúl A. Rica[1,2]
[1]Universidad de Granada, Departamento de Física Aplicada, 18071 Granada (Spain)
[2]Universidad de Granada, Nanoparticles trapping Laboratory, 18071 Granada (Spain)
[3]Departamento de Álgebra, Facultad de Educación, Economía y Tecnología de Ceuta, Universidad de Granada, Cortadura del Valle, s/n, 51001 Ceuta, Spain

The existence of asymmetries related to heating and cooling, which are paradigmatic non-equilibrium processes, are known since ancient times. The 'Mpemba effect', for instance, shows that a hot system can cool down faster than the same system initiated at a lower temperature [1]. Lapolla and Godec showed theoretically in [2] that heating a system is faster than cooling it when the equilibrium state is equidistant in energy.

In the present work we will approach experimentally the latter effect. A colloidal particle immersed in water can be trapped with optical tweezers, and its dynamics can be modelled as a Brownian particle in a parabolic potential. If we denote with κ its stiffness, the Equipartition Theorem guarantees that

$$\kappa \left\langle x^2 \right\rangle = k_B T, \tag{1}$$

where the brackets denote steady-state averaging. If a noisy external electrical field is applied, Brownian fluctuations will increase and, due to (1), so will the 'effective temperature' of the particle. Consequently, as it is suggested in [3, 4], a colloidal particle subject to an external random force with Gaussian white spectrum behaves as if it were immersed in a thermal bath whose effective temperature exceeds that of the surrounding fluid.

In order to reproduce in an accessible way the scheme proposed by Lapolla and Godec, a white-noisy external field is modulated by a periodic-squared signal of different lengths and heights [5]. We experimentally study the transient behaviour of the particle under the effect of the modulated signal, exploring the parameter space where the asymmetry can be observed in practice.

[1] A. Lasanta, F. Vega Reyes, A. Prados, and A. Santos, Phys. Rev. Lett. **119**, 148001 (2017).

[2] A. Lapolla and A. Godec, Phys. Rev. Lett. **125**, 110602 (2020).

[3] P. Mestres, I. A. Martinez, A. Ortiz-Ambriz, R. A. Rica and E. Roldan, Phys. Rev. E **90**, 032116 (2014).

[4] I. A. Martínez, E. Roldán, J. M. R. Parrondo and D. Petrov, Phys. Rev. E **87**, 032159 (2013).

[5] A. Militaru, A. Lasanta, M. Frimmer, L. L. Bonilla, L. Novotny, and R. A. Rica, Phys. Rev. Lett. **127**, 130603 (2021).

Collective decision making: From nest site selection in honeybee swarms to kilobot ensembles

David March[1], Julia Mugica[2], and Carmen Miguel[1]
[1] Departament de Fisica de la Materia Condensada, Universitat de Barcelona, Av. Diagonal 645, 08028, Barcelona, Espanya
[2] Departament de Fisica, Universitat Politecnica de Catalunya, Campus Nord, Modul B4, 08034 Barcelona, Espanya

Collective decision making is a broad and interdisciplinary field of study where statistical physics, biology and social sciences meet. In our group we study collective decision making in groups formed by social agents in complex environments. We observe these processes constantly on social groups: from humans taking part in elections, social mammals herds or schooling fish moving together or insect colonies moving to a food source or a new settlement. Information flow is crucial to the outcome of a decision making process, and the extent to which group members are able to individually explore the available options, to asses their benefit for the group or to acknowledge the information that their colleagues have gathered are some of the most relevant factors mediating this process.

The poster focuses on a particular decision making process that takes place in honeybee swarms. Come the end of spring honeybee colonies split, and around two thirds leave the nest with the queen to find a new nest site. In this process, a fraction of the swarm inspects the surroundings to gather information on the possible new sites, estimating their quality (size, food availability, distance, etc.). Scout bees return then to the nest and perform the waggle-dance (fig. 1), which is the main information exchange method. Bees that have found a good site will perform a longer, lively dance while bees that have found a poorer site will dance for shorter times [1]. Bees that have not explored its surroundings will follow another bee's waggle-dance, i.e. they will get convinced by the dancing bee choice; altogether, bees dancing for poorer sites may switch their opinion to follow a better option. During this process of exploration, waggle-dance and dance following a quorum among the swarm will be built, presumably for the best possible site. This kind decision making process is known as a decentralized decision making process, as there is no leader nor hierarchy influencing the group's decision, but every agent contributes equally to the exploration and information exchange process. It has been argued that this mechanism is the most effective for a group to reach consensus for the best possible option - a phenomena known as *wisdom of the crowds* [7].

The approach we follow is based in an agent-based model with a mean-field approximation, and it was first presented in [2]. This model is built upon the most basic features that mediate this process: the chance to discover a site α (π_α), the quality of site α (q_α) - which is directly translated to the waggle dance duration -, and the group interdependence λ - this is how much bees take individual decisions by exploring (low λ) or how much they take into account other bee's opinion (high λ). This model can be implemented into an stochastic algorithm, allowing us to simulate different environment conditions (represented by these parameters) and characterize the system outcome. Furthermore, this model can be studied analytically by terms of a master equation [3]. We make use of these tools to compare our simulations with theoretical predictions and to gain insight from some features where stochastic simulations alone are not enough.

Our results regard the 2-site decision process, already studied by other models inspired by the honeybee scenario [4, 5]. We characterize the transition from consensus for the best possible site to no consensus, aiming to acknowledge if such an agent based system suffers some kind of phase transition as seen in other models, such as the voter model. Besides, we characterize the influence of the system parameters to one another and study their relation with he accuracy of the final stationary state and the necessary time to reach it. Finally, we aim to validate our findings implementing this model to a swarm of kilobots [6], small robots specially designed to study the process of decentralized decision making in swarms, in order to asses its behavior beyond the mean filed approximation, i.e. when unavoidable spatial effects may become relevant.

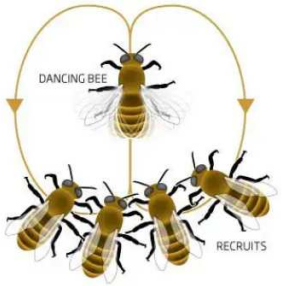

Fig. 1. Waggle dance mechanism. The dancing bee moves forward performing a lively dance and returns to the initial position. If the bee estimates that its site choice is good the dance is livelier and longer, and the return phase quicker. Other bees (recruits) may see this waggle dance and copy the bee's opinion instead of reaching out to explore.

[1] Seeley, TD and Mikheyev, AS and Pagano, GJ, J. Comparative Physiology A, **186**, 813-819 (2000)

[2] List, C. and Elsholtz, C. and Seeley, T. D, Philos. Trans. R. Soc. Lond., B, Biol. Sci. **364**, 1518, 755-762 (2009)

[3] Galla T, J. Theor. Biol., **262**, 1, 186-196 (2010)

[4] Reina, A. and Bose, T. and Trianni, V. and Marshall, J., 13th Int. Symp. on Distributed Autonomous Robotic Systems (2016)

[5] Valentini, G. and Ferrante, E. and Hamann, H. and Dorigo, M., Auton. Agents Multi-Agent Syst., **30** (2015)

[6] Rubenstein, M. and Ahler, C. and Nagpal, R., 2012 IEEE Int. Conf. on Robotics and Automation, 3293-3298

[7] Surowiecki, J. *The wisdom of crowds: Why the many are smarter than the few and how collective wisdom shapes business, economies, societies, and nations* (Doubleday Co., 2004)

Experimental study of the nonlinear dynamics of semiconductor lasers to control the coherence of the laser light

Maria Duque Gijon[1], Cristina Masoller[1], and Jordi Tiana Alsina[2]
[1]Departament de Fisica, Universitat Politecnica de Catalunya, Edifici GAIA, Rambla Sant Nebridi 22, 08222 Terrassa, Spain
[2]Departament de Fisica, Universitat de Barcelona, Carrer de Marti i Franques, 1, 11, 08028 Barcelona, Spain

Semiconductor laser diodes are widely used as illumination light sources in imaging applications because they are are low-cost, emit a stable output, and cover a wide range of wavelengths. However, illumination with coherent laser light produces a spatial interference pattern, known as speckle pattern, which degrades the image quality. The speckle pattern is a granular, noise-like structure that results from the interference of coherent waves, and which contains spectral information of the waves, and statistical information of the scattering medium that generates the pattern. When laser light propagates through a diffusive medium that creates speckle, useful information may be obtained from the analysis of the speckle pattern [1, 2, 3].

A typical measure used to quantify speckle is the speckle contrast [4], which is the ratio between the standard deviation of the patterns intensity and its average intensity, $SC = \sigma_I / \bar{I}$.

In this contribution we analyze how the laser light coherence emerges during the transition from spontaneous to stimulated emission as the laser turns on. Specifically, we perform experiments with a semiconductor laser with optical feedback from an external mirror.

The experimental control parameters are the laser pump current and the feedback strength that modify the spectral characteristics of the laser light and, consequently, its degree of coherence, which we quantify by calculating SC in the speckle images recorded with a CMOS camera.

In Fig. 1(a) we show the experimental setup, in which we are able to control the amount of light that is fed back to the laser and record the speckle images. The feedback strength is controlled by a variable attenuator that allows to regulate the amount of feedback light that passes through it. The scattering medium used to create the speckle patterns is a Multi-Mode Fiber (MMF), and speckle is created by the interference of different guided modes in the fiber. We also measure the spectrum of the light using an optical spectrum analyzer (OSA).

The effect of the feedback strength on the emergence of the coherence in the laser is shown in Fig. 1(b). We find for pump currents near $I_{th}^0 = 42.90$ mA, the transition to coherent emission varies from being smooth to being rather abrupt as the amount of feedback light increases.

The sudden transition to coherence is visualized in the speckle patterns shown in Fig. 1 (c). Both images were recorded for the same condition of feedback strength, just before and after the transition, and the change can be estimated from SC = 0.27 low coherence in the left image, to SC = 0.50 higher coherence in the right image.

For larger pump currents (above the transition) we notice in Fig. 1(b) that SC decreases in comparison to the value of the solitary laser (without feedback), revealing a partial loss of the coherence in the emitted light (due to feedback induced chaotic oscillations).

To summarize, the speckle contrast provides a non-spectral way to examine the coherence of the laser light, and we have used it to uncover an abrupt transition to coherence when the laser is subject to strong optical feedback. Ongoing work is devoted to characterize the properties of the transition, while future work will be aimed to analyze the effect of mechanical vibrations on the external mirror that provides feedback, actuated with a piezoelectric device.

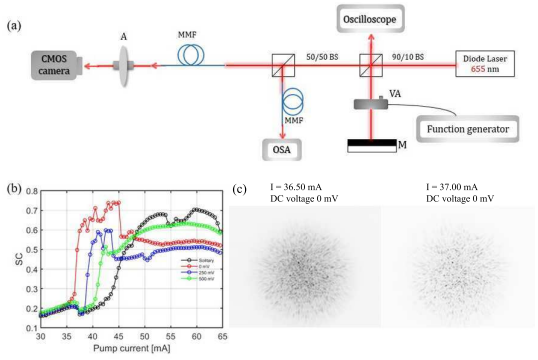

Fig. 1. (a) Experimental setup. (b) Speckle contrast as a function of the laser pump current, under different amount of feedback. (c) Speckle images before and after the sudden transition to coherence (left and right, respectively) for maximum feedback strength (i.e., with 0 voltage in the attenuator).

[1] E. Valent, Y. Silberberg, Scatterer recognition via analysis of speckle patterns, Optica **5**(2), 204 (2018).

[2] T. Ando, R. Horisaki, J. Tanida, Speckle-learning-based object recognition through scattering media, Opt. Express **23**(9), 33902 (2015).

[3] C. Barcellona, D. Halpaap, P. Amil, A. Buscarino, L. Fortuna, J. Tiana-Alsina, C. Masoller, Remote recovery of audio signals from videos of optical speckle patterns: a comparative study of signal recovery algorithms, Opt. Express **28**, 8716 (2020).

[4] J. W. Goodman, Some fundamental properties of speckle, J. Opt. Soc. Am. **66**(11), 11451150 (1976).

Liquid-Hexatic-Solid phases in active and passive Brownian particles determined by stochastic birth-death events

Alejandro Almodóvar, Tobias Galla, and Cristóbal López
IFISC, Instituto de Física Interdisciplinar y Sistemas Complejos (CSIC-UIB),
Campus Universitat de les Illes Balears, E-07122 Palma de Mallorca, Spain

We study the structural phases of a system of active or passive finite-size particles undergoing Brownian motion subject to volume exclusion. As a new ingredient we introduce stochastic reproduction and removal processes. The system of passive particles is hence also out-of-equilibrium even if forces between particles derive from a potential. The number of particles in the system at long times depends on the birth and death rates, and on the activity parameter. Thus, as these rates are varied we find liquid, hexatic or solid phases. For passive particles we find these phases to be spatially homogeneous. The system shows similar behaviour when the self-propulsion velocity is non-zero but small compared to temperature. However, for larger activity and sufficiently small birth rates motility-induced phase separation (MIPS) is observed. The solid and liquid phases then coexist. When the birth rate increases further, a hexatic phase is the only one reached; this comes from a balance of more particles filling the system, but also a larger number of defects due to demography.

Hydrodynamic interactions can induce jamming in flow-driven systems

E. Cereceda-López[1,2], D. Lips[3], A. Ortiz-Ambriz[1,2,4], A. Ryabov[5], P. Maass[3], and P. Tierno[1,2,4]

[1]Departament de Física de la Matèria Condensada, Universitat de Barcelona, 08028, Spain
[2]Institut de Nanociència i Nanotecnologia, Universitat de Barcelona (IN2UB), 08028, Barcelona, Spain
[3] Universität Osnabrück, Fachbereich Physik, Barbarastraße 7, D-49076 Osnabrück, Germany
[4] University of Barcelona Institute of Complex Systems (UBICS), 08028, Barcelona, Spain
[5] Charles University, Department of Macromolecular Physics, V Holešovičkách 2, CZ-18000 Praha 8, Czech Republic

In the present work, we experimentally study the transport of particles in a quasi-one-dimensional (q1D) periodic potential. We compare the experimental results with simulations based on the Brownian Asymmetric Simple Exclusion Process [1, 2], and we discuss the importance of hydrodynamic interactions (HI) in flow-driven particle transport.

The experimental setup consists of 27 time-shared optical tweezers, which create individual Gaussian potential wells, uniformly distributed in a ring-shape confining up to 27 colloidal particles. We rotate the optical traps at constant angular velocity to create a quasi-sinusoidal traveling potential landscape. Varying the number of particles in the potential landscape allows us to measure the fundamental diagram of the system, which is the colloidal current as a function of the particle density. We find that for different potential landscape barrier heights the particle current density decreases after reaching a maximum value.

We compare the experimental results with simulations, and we attribute the decrease of the current density relationship to the jamming produced by the HI between particles. We explain this phenomenon using the equations of motion that include HI and show that the latter enhances the potential barrier in flow-driven systems. This is opposed to previous observations in force-driven systems, which remark the fundamental difference with our flow-driven system.

[1] Dominik Lips, Artem Ryabov, and Philipp Maass, *Brownian Asymmetric Simple Exclusion Process*, Phys. Rev. Lett. **121**, 160601 (2018).

[2] Dominik Lips, Artem Ryabov, and Philipp Maass, *Single transport in periodic potentials: The Brownian asymmetric simple exclusion process* , Phys. Rev. E **100**, 052121 (2019).

Dynamic exponents for thin-film spreading

J. M. Marcos[1,2], P. Rodriguez-Lopez[3], J. J. Meléndez[1,2], R. Cuerno[4], and J. J. Ruiz-Lorenzo[1,2]

[1]Instituto de Computación Científica Avanzada de Extremadura (ICCAEx), Universidad de Extremadura, 06006 Badajoz, Spain

[2] Departamento de Física, Universidad de Extremadura, 06006 Badajoz, Spain

[3] Área de Electromagnetismo and Grupo Interdisciplinar de Sistemas Complejos (GISC), Universidad Rey Juan Carlos, 28933 Mstoles, Spain

[4] Departamento de Matemáticas and Grupo Interdisciplinar de Sistemas Complejos (GISC), Universidad Carlos III de Madrid, 28911 Leganés, Spain

In the case of complete wetting, spreading of nonvolatile liquid drops on surfaces exhibits, when examined on the atomic length scale in the direction normal to the substrate, a precursor film about one molecule thick [1]. This precursor film is expected to expand as $R \sim t^{1/2}$, where R is the drop radius, as many experiments have confirmed [2].

In Ref. [3], a quasi two-dimensional (2D) driven Ising lattice gas model was introduced to study this phenomenon. The model considers the evolution of two layers, namely the precursor (bottom) layer and the supernatant (or upper) layer. At each cell of the lattice, an occupation number n_r is defined and allowed to take only the values 1 and 0, depending on whether the cell is occupied (by only one particle) or empty. Initially, all cells are empty except those of the first column for both layers, which acts as a reservoir for particles; if, at any step, any of the cells of this column became empty, it is automatically refilled.

In this model, the energy of the system is given by

$$H = -J \sum_{\langle r,s \rangle} n_r n_s - A \sum_r \frac{n_r}{Z^3}, \qquad (1)$$

where Z takes on the values 1 or 2 (for the precursor and supernatant layers, respectively). The first term describes the interactions between the liquid particles and their nearest neighbors in terms of a coupling constant $J > 0$. The second term, whose intensity is given by the Hamaker constant $A > 0$, describes the interactions between the liquid particles and the substrate [1].

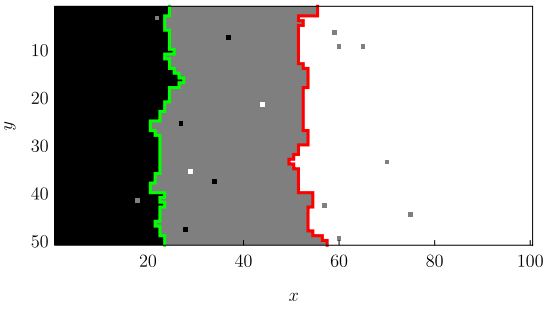

Fig. 1. Top view of a typical snapshot of the two-layers model. Occupied cells with $Z = 1$ (precursor film) and $Z = 2$ (supernatant film) appear in gray and black, respectively; uncolored cells are empty. The red (green) line denotes the edge of the precursor (the supernatant) layer, which we use to define the position of the front, $x = h(y, t)$.

The evolution of the system was simulated by a continuous-time Monte Carlo algorithm with Kawasaki dynamics for pair exchange, for large enough J to achieve a high degree of non-volatility, and for large enough A for the system to be in the complete wetting regime. Under these conditions, the system evolves according to the $R \sim t^{1/2}$ law after a short initial transient.

Very recently, this system has been simulated using Kawasaki dynamics, for a wider range of J and A values [4]. In this case, the precursor film was found to grow as $R \sim t^{\delta}$, with the scaling exponent δ greatly depending on the dynamical parameters for the system. In particular, the $\delta = 1/2$ universal value for the exponent is not recovered for any values of the J and A parameters studied in [4].

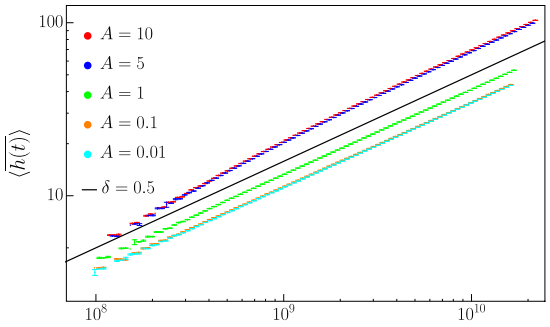

Fig. 2. Log-log plot of the average front position $\langle \bar{h}(t) \rangle$ as a function of time for $T = 1$, $L_x = 1000$, $L_y = 256$, and several values of A. The solid black line corresponds to the reference scaling $\langle \bar{h}(t) \rangle \sim t^{1/2}$. All units are arbitrary.

Thus, controversy exists about the proper description at the atomistic scale of the growth of drops on surfaces under complete wetting conditions. In this contribution, we have tried to shed light on this problem by studying the dependence of the scaling exponent δ on the dynamical parameters of the system. Our results indicate that such a dependence is very weak, with little variation from the universal value $1/2$. We additionally report calculations of correlation functions and front structure factors which, to our best knowledge, are reported for the first time. We discuss our results in the light of continuum descriptions of the process put forward in Ref. [3].

[1] D. Bonn, J. Eggers, J. Indekeu, J. Meunier, and E. Rolley. *Wetting and spreading*. Rev. Mod. Phys. **81**, 739 (2009).

[2] F. Heslot, A. M. Cazabat, and P. Levinson. *Dynamics of wetting of tiny drops: Ellipsometric study of the late stages of spreading*. Phys. Rev. Lett. **62**, 1286 (1989).

[3] D. B. Abraham, R. Cuerno, and E. Moro, *Microscopic Model for Thin Film Spreading*, Phys. Rev. Lett. **88**, 206101 (2002).

[4] M. Harel and H. Taitelbaum, *Non-universal dynamic exponents for thin-film spreading*, Eur. Phys. Lett **122**, 26002 (2018).

Congestion Phase Transitions in Urban Street Networks

Aniello Lampo [1,2], Javier Borge-Holthoefer[2], Sergio Gómez[3] and Albert Solé-Ribalta[2,4]
[1]Departamento de Matemáticas, Universidad Carlos III de Madrid, 28911 Leganés, Spain;
[2]Internet Interdisciplinary Institute (IN3), Universitat Oberta de Catalunya, Barcelona, Catalonia, Spain;
[3]Departament d'Enginyeria Informàtica i Matemàtiques, Universitat Rovira i Virgili, Tarragona, Catalonia, Spain
[4]URPP Social Networks, University of Zurich, Zurich, Switzerland

Cities exhibit different organizational patterns as a consequence of historical, political or economical circumstances, and constitute a paradigmatic example of complex system. In this context, network theory stands out as a fundamental tool facilitating the quantitative modeling of the main urban features and the analysis of the resulting dynamical processes, such as mobility and city growth.

Our work focuses on street networks, which edges represent city roads, while the nodes portray the points where such roads cross. In the literature, the topic has been addressed following different points of views according the purpose and the system characteristics. For instance, the dynamics related to inter-urban roads (also known as arterial roads or high capacity roads), characterized by long segments and limited inter-connection, has been approached employing fluids models, or the fundamental diagram of traffic flow. On the contrary, phenomenology of intra-urban streets is ruled by the underlying network structure and has been traditionally treated by means of graph models

These two types of street networks, which are usually studied independently, are increasingly entangled as cities sprawl over suburban areas. So far, only few works dealt with street networks from an intertwined perspective, and the effects induced by such an interaction have been mostly overlooked. The analysis of the spatial interplay of intra and inter roads networks is the main motivation of the current work.

We focus on monocentric cities and consider the situation in which arterial roads and urban local ones operate on separate geographic spaces. Specifically, local roads are located at the city center, and arterial ones at the urban periphery. Along this line, we introduce a family of random planar network models composed by a dense center surrounded by an arboreal periphery. Such a class of models reproduces previous results in terms of betweenness distribution and, at the same time, offers a considerable advantage in terms of analytical tractability.

In this way, we are able to unveil several unexpected properties of road networks with respect to the congestion phenomena. In particular, it evidences that cities may experience a set of multiple abrupt phase transitions in the spatial localization of congested areas. These transitions define a set of congestion regimes that correspond to the emergence of congestion in the city center, its periphery or in urban arterial roads, and regards the way in which different road classes are entangled to form a unique transportation system. In other word, traffic bottlenecks shift away from the center towards the periphery, as larger areas are incorporates in the urban setting.

The detection of congestion abrupt transition is performed both numerically and analytically and constitutes the main finding of our work. Importantly, this is validated by looking into real road networks. Empirical analysis is carried out over almost a hundred of cities worldwide, and relies on automatic and unsupervised methods. Results show that the multiple abrupt transitions exist in real cities, confirming the prediction performed with our model.

The phase transitions we detect, represents an important resource to improve the efficiency of road networks. The displacement of the traffic bottlenecks towards the peripheral zones, indeed, is crucial to reduce the pressure on the city center, and to avoid the degradation of the transportation system. Therefore, the possibility to control and manipulate such effect constitutes a notable task which has never been performed before [2].

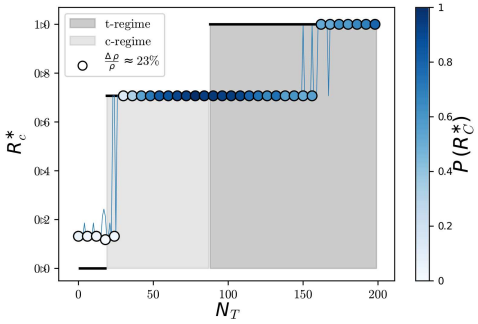

Fig. 1. Congestion radius as a function of the periphery nodes number, showing the various regimes and their transitions. Solid black lines refer to the analytical prediction. Circles represent the experimental results after the introduction of noise, implemented through the addition of random edges to the basic model skeleton till matching a density mentioned in the legend. Each circle is located at the statistical mode obtained with the distribution of R_c after 150 realizations of the model with noise. The color of the circle shows the probability of that value over the experimental R_c distribution. Details about the parameters definitions, and the calculations underlying the figures are discussed in [1].

[1] A. Lampo, J. Borge-Holthoefer, S. Gómez and A. Solé-Ribalta, *Multiple abrupt phase transitions in urban transport congestion*, Phys. Rev. Research 3, 013267 (2021).

[2] A. Lampo, J. Borge-Holthoefer, S. Gómez and A. Solé-Ribalta, *Emergence of spatial transitions in urban congestion dynamics* Journal of Applied Network Science, volume 6 (2021).

Noisy Voter Model with time-varying influencers

Annalisa Caligiuri[1] and Tobias Galla [1]
[1]Instituto de Física Interdisciplinar y Sistemas Complejos, IFISC (CSIC-UIB),
Campus Universitat Illes Balears, E-07122 Palma de Mallorca, Spain

Abstract

The noisy voter model (NVM) [1] describes emergent behavior of interacting agents choosing between two or more opinions. The adjective 'noisy' indicates that an agent can change their choice by imitating that of a neighbor. When the imitation mechanism is stronger than the noise, the stationary distribution of the fraction of agents choosing one opinion is bimodal. On the other hand, if the noise is stronger the resulting stationary distribution is unimodal.
Several variations of the NVM have been proposed; in [2], for example, the authors study how the presence of agents that never change opinion, so-called *Zealots*, affects the emergence of consensus.
In this work we enrich the analysis of external influence on the NVM by introducing a group of agents that change opinion only at random, but who are not subject to the herding process. We call these '*Influencers*'. This is motivated by *Influence marketing*, that is when a brand enrolls influencial people in order to change the buying habits of consumers. Nevertheless, a group of influencers may switch the endorsed brand. The goal of this work is to model and analyze this phenomenon and understand if the switch in the influencers may prevent consensus on a product.

If we use the notation X_A for a normal voter that chooses *A* (and similarly, X_B) and Y_A (Y_B) for an influencer that chooses *A* (*B*), the dynamics of the model results in the following reactions:

$$\begin{aligned} X_A + X_B &\xrightarrow{h} X_B + X_B \\ X_A + Y_B &\xrightarrow{h} X_B + Y_B, \\ X_B &\xrightarrow{a} X_A, \\ X_A &\xrightarrow{a} X_B \end{aligned} \tag{1}$$

Additionally, the influencers change between states A and B with rate λ. This can occur collectively (i.e., all influencers must change at once), or they can change individually or in multiple groups. For the purposes of the population of normal agents, the state of the influencers sets an 'environmental state', σ.

Assuming that there are N normal agents and that n of these are in state A, the system can be described by a master equation of the type

$$\partial_t P(n,\sigma,t) = \mathbf{M}_\sigma P(n,\sigma,t) + \lambda \mathbf{A} P(n,\sigma,t), \tag{2}$$

where the operator $\mathbf{M}_\sigma$ describes the evolution of normal agents in environment σ, and $\mathbf{A}$ effects the changes of the environmental state. The parameter λ describes the time scale separation between the dynamics of normal agents and that of the influencers.

We now assume that there are αN influencers, who change opinion collectively. The environment then has two states. In the adiabatic limit $\lambda \to \infty$ (infinitely fast switching influencers), the system reduces to a NVM with effective size $\tilde{N} = N/(1+\alpha)$, and noise constant $\tilde{a} = a(1+\alpha) + \frac{\alpha}{2}$.

In the limit of a large, but finite population ($N \gg 1$) we can use methods from [3] to reduce Eq. (2) to

$$\partial_t P(x,\sigma,t) = \mathbf{L}_\sigma P(x,\sigma,t) + \lambda \mathbf{A} P(x,\sigma,t), \tag{3}$$

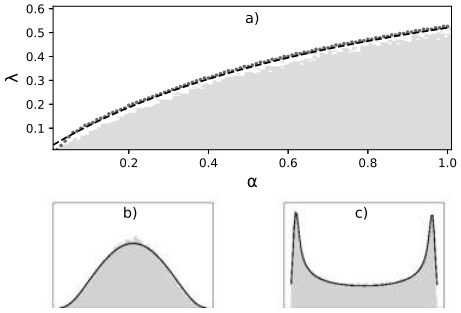

Fig. 1. **a)** is the phase diagram of the NVM with influencers. The dashed line represents the line separating the unimodal and bimodal regimes obtained from the analytical solution for the stationary distribution in the PDMP limit. The dots take into account leading order corrections in $1/N$ in the dynamics. The shaded area is from simulations of the original system. ($N = 100$, $a = 0.01$, $h = 1$).
b) and **c)** are respectively a unimodal ($\lambda = 0.5$ and $\alpha = 0.2$) and a bimodal ($\lambda = 0.2$ and $\alpha = 0.7$) stationary distribution for $N = 200$, $a = 0.01$ and $h = 1$; here the black solid line is the numerical solution that takes into account Gaussian fluctuations.

where $x = \frac{n}{N}$. The operator $\mathbf{L}_\sigma$ is now of the type as in a Fokker-Planck equation, and captures leading and subleading terms in $1/N$. Upon sending $N \to \infty$ this reduces further to a Liouville operator, resulting in a piecewise deterministic Markov process (PDMP).

From these equations the shape of the stationary distribution can be obtained analytically in the PDMP limit, and numerically when Gaussian fluctuations are taken into account. Results are shown in Fig. 1. For a fixed value of α, we observe a phase transition from a bimodal to a unimodal shape of the stationary distribution at a critical value $\lambda_c(\alpha)$. As can be seen from Fig. 1, $\lambda_c(\alpha)$ increases with α, i.e. if there are more influencers (or analogously if their influence is stronger), they need to switch opinion faster in order to prevent the reach of consensus. Indeed, the more influencers there are the faster normal consumers tend to allign with their opinion.

[1] A. Kirman, *Ants, Rationality, and Recruitment*, The Quarterly Journal of Economics **108**, 137(1993)

[2] N. Khalil, M. San Miguel, and R. Toral, *Zealots in the mean-field noisy voter model*, Phys. Rev. E **97**, 012310(2018).

[3] P. G. Hufton, Y. T. Lin, T. Galla, and A. J. McKane, *Intrinsic noise in systems with switching environments*, Physical Review E **93**, 052119 (2016).

Study of the evolution of Cellular communities through Cellular Simulation.

Alejandro Cuetos[1],
[1]Departamento de Sistemas Físicos, Químicos y Naturales, Universidad Pablo de Olavide, 41013 Seville, Spain acuemen@upo.es

Cell simulation emerges as a new perspective to simulate the growth and development of cell colonies, and thus study their properties. In cell simulation, ideas and techniques already developed in the field of molecular or colloidal simulation are used. In this way, starting from the defining characteristics of the basic agents of the system, the cells in this case, an attempt is made to obtain information on the emerging properties of the cell colonies. In this approach, in addition to being necessary to have an adequate description of the interaction between cells and their dynamics, it is important to model the process of cell growth and division, which converts developing cell colonies into systems out of equilibrium. We will present a summary of recent research using cell simulation strategies. Results of studies on the development of bacterial colonies will be shown, discussing the consequences of competition between growth/division processes and cell diffusion [1]. We will also present results on the influence of high concentrations of polymers in the medium on the structure of growing bacterial colonies[2]. Finally, we will show how these techniques can also be applied to the study of organ development [2].

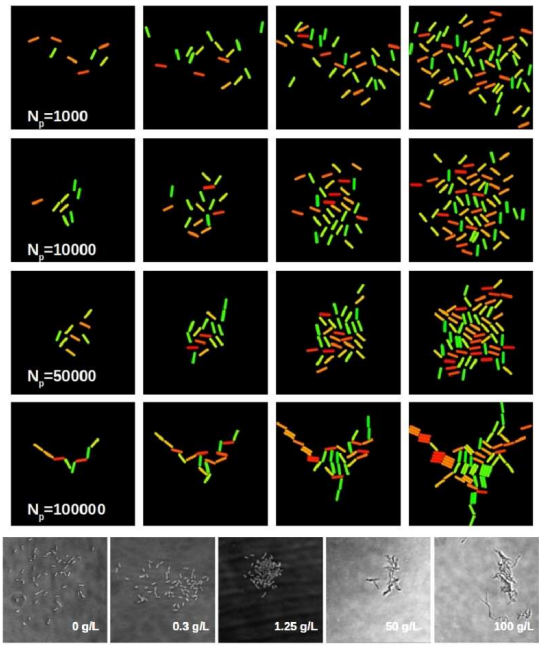

Fig. 1. Top rows:Simulation of bacterial biofilm evolution growing in media with different numbers of polymeric particles N_p. Bottom row:Micrographs of microcolonies containing 40 cells of Δ*fle*Q *P. putida* strain MRB52 at different dextran sulfate concentration. [2]

[1] R. D. Acemel, F. Govantes y A. Cuetos. *Computer simulation study of early bacterial biofilm development*. Scientific Reports, **8**, 5340 (2018).

[2] F. J. Lobo-Cabrera, A. Patti, F. Govantes, and A. Cuetos, *Polymer-induced microcolony compaction in early biofilms: A computer simulation study*. Phys. Rev. E **103**, 052407 (2021).

[3] F. J. Lobo-Cabrera, T. Navarro, A. Iannini, F. Casares and A. Cuetos. *Quantitative relationships between growth, differentiation, and shape that control drosophila eye development and its variation*. Front. Cell Dev. Biol. **9**, 68193 (2021).

Resonant Behavior in a Periodically Forced Non-Isothermal Oregonator

David García-Selfa[1,2,3], Alberto P. Muñuzuri[1,2,4], David S. A. Simakov[6] and Juan Pérez-Marcader[4,5]
[1]CITMAga, 15782 Santiago de Compostela, Spain
[2]Group of Nonlinear Physics, Universidade de Santiago de Compostela, Campus Sur, 15782 Santiago de Compostela, Spain
[3]CESGA (Supercomputing Center of Galicia), Avd. de Vigo s/n, Campus Sur, 15705 Santiago de Compostela, Spain
[4]Department of Earth and Planetary Sciences, Origins of Life Initiative, Harvard University, Cambridge, Massachusetts 02138, United States
[5]Santa Fe Institute, Santa Fe, New Mexico 87501, United States
[6]Department of Chemical Engineering, University of Waterloo, Waterloo, Ontario N2L 3G1,Canada

Oscillatory phenomena are common in Nature and observed in a great variety of biological processes such as the Krebs cycle, the circadian clock, and the cell cycle[1]. A classic example of a chemical oscillator is the Belousov-Zhabotinsky reaction[2, 3], which has become a prime example for non-linear, out-of-equilibrium chemical dynamics. Natural oscillators are normally subject to both periodic and stochastic external perturbations in the values of environmental physical variables, such as light irradiation and temperature. Such fluctuations are expected to modulate, modify, or even determine and entrain the behavior of nonlinear systems[4].

Nonisothermal chemical oscillators are poorly studied systems because chemical oscillations are conventionally studied under isothermal conditions. Coupling chemical reactions with heat generation and consumption in a nonisothermal oscillatory system can lead to a highly nontrivial nonlinear dynamic behavior. For this study we considered the three-variable Oregonator model with the temperature incorporated as a variable (not a parameter) thus adding an energy balance to the set of equations. The effect of the temperature on reaction rates is included through the temperature-dependent reaction rate coefficients (Arrhenius law). To model a continuous operation in a lab environment, the system was subjected to external forcing through the coolant temperature and infrared irradiation. By conducting numerical simulations and parametric studies, we have found that the system is capable of resonant behavior exhibiting induced oscillations. Our findings indicate that an external source of heat (e.g., via an infrared light emission diode) can be used to induce a Hopf bifurcation under resonant conditions in an experimental BelousovZhabotinsky reactor [5].

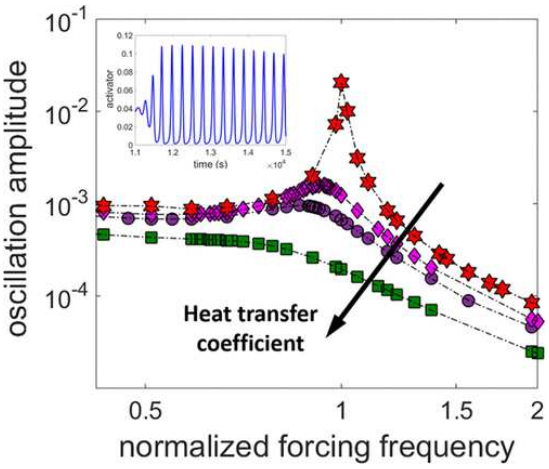

Fig. 1. Resonant curves for some values of the heat transfer coeffiecient.

[1] Murray, J. D., *Mathematical Biology*. (Springer, 1989).

[2] Belousov, B. P., *A periodic reaction and its mechanism*. Ref. Radiats. Med. Medgiz, 145. Moscow (1959).

[3] Zhabotinskii, A. M., *Periodical oxidation of malonic acid in solution (A study of the Belousov reaction kinetics)*. Biofizika, **9**, 306-311 (1964).

[4] Simakov, D. S.; Prez-Mercader, J., *Noise induced oscillations and coherence resonance in a generic model of the nonisothermal chemical oscillator*. Sci. Rep. **3**, 2404 (2013).

[5] García-Selfa, D.; Muñuzuri, A. P.; Pérez-Mercader, J. and Simakov, D. S. A., *Resonant Behavior in a Periodically Forced Nonisothermal Oregonator*. J. Phys. Chem. A, **123**, 38, 8083-8088 (2019).

Using batteries for frequency control in power grids with renewable sources

Giulia Ruzzene[1], Damià Gomila[1], and Pere Colet[1]
[1]IFISC, Institute for Physics of Complex Systems (CSIC-UIB), Campus Universitat Illes Balears, 07122 Palma de Mallorca, Spain

The ambitious decarbonisation goals that many countries are pursuing to fight climate change present various challenges for the operation of power grids. In particular, the stability of the grid may be affected by the intermittent nature of renewable energy resources, such as wind and solar power. A way to assess grid stability is to study frequency fluctuations. The frequency of the alternating current produced by the generators has a fixed reference value of 50 Hz, but it is subject of random fluctuations due to the imbalance between production and demand.

A possible way to reduce frequency fluctuations is to introduce in the grid energy storage systems that can store the excess of energy produced by renewable sources and use it to balance demand peaks. In this work we analyse the effects of introducing a battery in a power system with conventional and wind generation and we compare two algorithms for the battery operation. The first battery control method responds only to wind fluctuations, while the second one is sensitive to both wind and demand fluctuations.

We use a simple model with just one conventional generator with conventional primary and secondary control [2, 3]. The model includes the classical swing equation for the frequency ω, an equation for primary control which damps the frequency oscillations with a fast response time, and one for secondary control, in which the spinning reserve acts on a slower time scale to bring back the frequency to the reference value.

The first control method uses a battery that responds only to wind fluctuations and based on an optimisation technique called model predictive control. This method is aimed at smoothing wind power using a battery was introduced in [1]. It uses a model for the battery state of charge where the smoothed wind power is obtained solving an optimisation problem that minimises the oscillations of the battery state of charge. The output smoothed wind power substitutes the real wind production in the swing equation.

The second control method consists in using the battery as an additional primary and secondary control, and its equations are analogous to the ones in [3]. The battery power is added to the measured wind power in the swing equation.

As a case study, we consider the island of Gran Canaria, Spain, for which the data about wind production and consumer demand are publicly available in [4].

To assess the effectiveness of both methods we compute cumulative probability ranks $R(\Delta\omega)$ that estimate the probability of the occurrence of fluctuations bigger than a certain value $\Delta\omega$ and we also study the stress level of the battery state of charge.

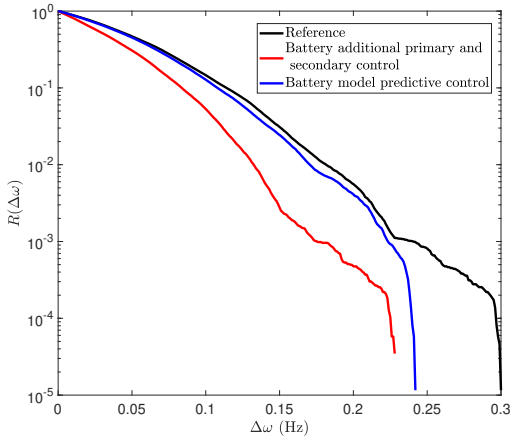

Fig. 1. Cumulative probability ranks calculated over one day (May 31st, 2021). Black line: reference case without battery. Red line: battery as additional primary and secondary control, capacity 0.5 MWh. Blue line: battery with model predictive control algorithm, capacity 5 MWh.

Our results show that both methods can reduce frequency fluctuations, although at different costs in terms of the size of battery needed. In Figure 1 we show an example of this fact for one day. In general, for the model predictive control method one needs a bigger battery to ensure that the optimisation algorithm converges. On the other hand, using the battery as an additional primary and secondary control is more effective with small batteries, in particular to reduce the part of fluctuations caused by the demand variability.

[1] M. Khalid and A. V. Savkin, *A model predictive control approach to the problem of wind power smoothing with controlled battery storage*, Renewable Energy, 25, 1520-1526 (2010)

[2] H. Saadat, *Power system analysis*, McGraw Hill (1999).

[3] E. B. Tchawou Tchuisseu and D. Gomila and D. Brunner and P. Colet, *Effects of dynamic-demand-control appliances on the power grid frequency*, Physical Review E, 96, 2, 022302 (2017).

[4] Red Electrica España
https://demanda.ree.es/visiona/canarias/gcanaria/total

Kuramoto model for populations of quadratic integrate-and-fire neurons with chemical and electrical coupling

Pau Clusella[1], Bastian Pietras[2], and Ernest Montbrió[2]
[1]Department of Experimental and Health Sciences, Universitat Pompeu Fabra, Barcelona Biomedical Research Park, 08003, Barcelona.
[2]Neuronal Dynamics Group, Department of Information and Communication Technologies, Universitat Pompeu Fabra, 08018 Barcelona.

The Kuramoto model (KM) is a minimal mathematical model for investigating the emergence of collective oscillations in populations of heterogeneous, self-sustained oscillators. Over time, it has increasingly been used to describe neuronal oscillations. Yet, the KM was not originally intended to describe any specific natural system, and it is unclear how the parameters of the KM relate to bio-physically meaningful parameters of spiking neuron models.

Here, we uncover a mathematical relation between the Quadratic Integrate-and-Fire (QIF) neuron model and a well-known variant of the KM [1]. By using a perturbation method and averaging, we reduce the population dynamics of weakly heterogeneous QIF neurons that are weakly coupled both with chemical and electrical synapses. The resulting KM readily allows for a comprehensive analysis of the collective dynamics of QIF neurons. We thus provide a rigorous footing for the use of the KM in modeling studies in computational neuroscience. We also show that the ratio of chemical to electrical coupling manifests a critical parameter determining the synchronization properties of the network.

The dynamics of N QIF neurons interacting all-to-all via both electrical and chemical synapses are given by

$$\tau \dot{V}_i = V_i^2 + \eta_i + \varepsilon \left[J\tau r(t) + \tfrac{g}{N} \textstyle\sum_{j=1}^{N} (V_j - V_i) \right], \quad (1)$$

together with the resetting rule: when the membrane potential V_i of neuron $i = 1, \ldots, N$ reaches the peak value V_p, neuron i emits a spike and its voltage is reset to V_r. With $V_p = -V_r$ and $V_p \to \infty$, the QIF model is equivalent to the "theta-neuron". We consider nearly identical external currents $\eta_i = \bar{\eta} + \epsilon\chi_i > 0$ so that, in the absence of synaptic inputs ($\varepsilon = 0$), QIF neurons are self-sustained oscillators.

Inhibitory chemical coupling (of strength $-\varepsilon J > 0$) is mediated via the population firing rate $r(t)$. Electrical synapses (of strength $\varepsilon g > 0$) diffusively couple all the neurons with each other, and have previously been shown to favor synchrony in populations of QIF neurons when g is sufficiently strong [2]. Here, however, we consider only weak synapses, $\varepsilon \ll 1$, which allows us to derive the KM for populations of QIF neurons of the form:

$$\dot{\theta}_i = \omega_i + \tfrac{K}{N} \textstyle\sum_{j=1}^{N} \left[\sin(\theta_j - \theta_i - \alpha) + \sin\alpha \right] \quad (2)$$

with natural frequencies $\omega_i = \left(2\sqrt{\bar{\eta}} + \epsilon\chi_i/\sqrt{\bar{\eta}}\right)/\tau$, coupling constant $K = \varepsilon\sqrt{(J/\pi)^2 + g^2}/\tau$, and phase lag parameter $\alpha = \arctan(J/(\pi g))$. The coupling parameters K and α satisfy a simple geometric relation with the coupling parameters of the QIF model Eq. (1), illustrated in Fig. 1.

Using well-known results for the KM [3], we can infer from this geometric relation how chemical and electrical synapses contribute to synchronization: electrical coupling is indispensable for synchrony; in interplay with inhibitory synapses, we find that synchronization depends on both α and the distribution of natural frequencies. For Lorentzian distributed natural frequencies, we can invoke the Ott-Antonsen ansatz and reduce the N-dimensional KM Eq. (2) to a two-dimensional mean field model in the thermodynamic limit $N \to \infty$, which conveniently allows for analyzing the collective dynamics of QIF neurons with both chemical and electrical synapses. To further illustrate the appropriateness of the KM, we investigate the presence of chimera states in two populations of QIF neurons, see Fig. 2, and present a relation between chimera states in spiking neuron networks with those originally uncovered in the KM.

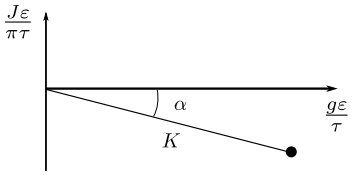

Fig. 1. Geometric relation between the coupling parameters of the QIF model (1) and the Kuramoto model (2).

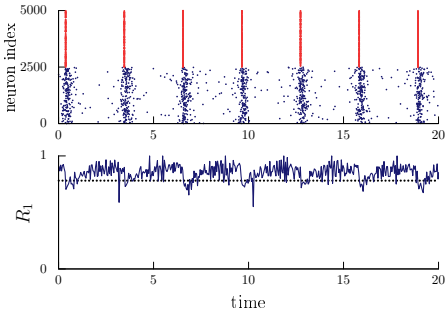

Fig. 2. Chimera state in two-population network of QIF neurons predicted by the Kuramoto model (top). The numerically obtained order parameter R_1 agrees well with theory (bottom).

[1] P. Clusella, B. Pietras, and E. Montbrió, *Kuramoto model for populations of quadratic integrate-and-fire neurons with chemical and electrical coupling*, Chaos **32**, 013105 (2022).

[2] B. Pietras, F. Devalle, A. Roxin, A. Daffertshofer, and E. Montbrió, *Exact firing rate model reveals the differential effects of chemical versus electrical synapses in spiking networks*, Phys. Rev. E **100**, 042412 (2019).

[3] H. Sakaguchi, S. Shinomoto, and Y. Kuramoto, *Mutual Entrainment in Oscillator Lattices with Nonvariational Type Interaction*, Prog. Theor. Phys. **79**, 10691079 (1988);
H. Sakaguchi and Y. Kuramoto, *A Soluble Active Rotator Model Showing Phase Transitions via Mutual Entrainment*, Prog. Theor. Phys. **76**, 576-581 (1986).

Flow of elongated particles out of a silo with rotating bottom

Tivadar Pongó[1], Tamás Börzsönyi[2], Raúl Cruz Hidalgo[1]
[1]Departamento de Física y Matemática Aplicada, Facultad de Ciencias, Universidad de Navarra, Pamplona, España
[2]Institute for Solid State Physics and Optics, Wigner Research Centre for Physics, P.O. Box 49, H-1525 Budapest, Hungary

There are several interesting procedures to avoid clogging or to enhance the particle flow rate in silo discharge processes. One possibility is introducing an additional source of external shear to the system, that is, imposing the rotation of the bottom wall. Very recently, this system was investigated experimentally [1] and numerically [2], exploring the flow of spherical particles in a cylindrical flat bottom silo, but with the bottom wall rotating around the axis of the cylinder. Examining small orifice sizes $D < 5d$, both the experimental and numerical approaches similarly found that the external shear induces that the flow rate proportionally increases with the frequency of the rotation of the bottom wall f. For large orifices $D/d > 5$, however, the flow rate depended non-monotonically on f. Starting from the static case, first the discharge rate decreased (down to 5%), and then it increased when further increasing the rotational frequency. The authors of the experimental work [1] hypothesized that in the latter case the flow field transitions from funnel flow to mass flow gradually as the rotation frequency is increased. This assumption was based on the fact that the surface of the column in the silo changed from a usual V shape to a heap when the rotation was applied. Later the discrete element modeling (DEM) and the coarse-graining post-processing analysis of the numerical data confirmed this idea [2].

In general granular materials, such as stones and pills have non-spherical shapes. Thus, another interesting question is what would be the response of this system using non-spherical particles. Last year, this was experimentally examined [3], and we found that in the large orifice regime the introduction of the rotational shear greatly reduces the flow rate by about 50% and by further increasing the rotation speed the flow rate increases only slightly. Moreover, we also take advantage of DEM simulations and modeled spherocylinder particles to mimic the behavior of the wooden rods. The analysis allows us to get insight into the dynamics of this process (Fig. 1). Our results agree very well with the experimental finding [3] that the flow rate drops significantly by introducing even a slow rotation which then increases moderately by faster rotation. Complementary, we used a coarse-graining technique, and computed all relevant macroscopic fields including the macroscopic density, momentum, and the stress tensor fields. It allows us to analyze thoroughly the spatial profiles of the macroscopic fields, which shed light on the micromechanic details of the flow process.

Fig. 1. Visualization of the numerical setup of the flat bottom, cylindrical silo with rotating bottom. Elongated particles are mimicked by spherocylinders.

[1] K. To, Y. Yen, Y.K. Mo and J.R. Huang, *Granular flow from silos with rotating orifice*, Physical Review E, **100**, 012906 (2019).

[2] D. Hernández-Delfin, T. Pongó, K. To, T. Börzsönyi, and R.C. Hidalgo, *Particle flow rate in silos under rotational shear*, Physical Review E, **102**, 042902 (2020).

[3] K. To, Y.K. Mo, T. Pongó, and T. Börzsönyi, *Discharge of elongated grains from silo with rotating bottom*, Physical Review E, **103**, 062905 (2021).

Synchronization meets non-pairwise interactions: the enlarged Kuramoto model

Iván León[1], and Diego Pazó[1]
[1]Instituto de Física de Cantabria (IFCA), Universidad de Cantabria-CSIC, 39005 Santander, Spain

The transition from incoherence to collective synchronization is a pivotal phenomenon in a wide variety of systems, from physical to biological. Seeking to understanding the synchronization transition, in 1975 Kuramoto derived his famous model [1]. Applying a perturbative technique (phase reduction) to an ensemble of globally coupled Stuart-Landau oscillators, he derived the first analytically tractable model able to describe the transition to collective synchrony. Despite its great success, the Kuramoto model is not the end of the story. The complex dynamics present in the ensemble of Stuart-Landau oscillators, Fig. 1a), is not captured by the Kuramoto model, Fig. 1b), pointing to the existence of a more complex transition to collective synchronization [2, 3].

In this work we extend the Kuramoto model to shed light on the rich dynamics of the ensemble of Stuart-Landau oscillators. Emulating Kuramoto's idea, we apply phase reduction to second order, obtaining the "enlarged Kuramoto model". The inclusion of new correction terms with non-pairwise interactions give rise to qualitative (in addition to quantitative) differences, Fig. 1 c).

Although the enlarged Kuramoto model is simpler than the ensemble of Stuart-Landau oscillators, it is still difficult to determine the different regimes due to finite size fluctuations. In order to characterize the series of bifurcation occurring in the system, we develop a numerical method that allows an efficient simulation of ensembles of phase oscillators in the thermodynamic limit. This method is based on the decomposition in Fourier-Hermite modes of the oscillator density. Truncating the number of modes, we obtain a finite dimensional system used to simulate the thermodynamic limit of the enlarged Kuramoto model.

The use of Fourier-Hermite modes allows us to analyze the rich dynamics of the model, confirming the existence of a secondary instability and collective chaos in the transition to synchrony. The modes decomposition is applicable to any ensemble of heterogeneous phase oscillators, facilitating and promoting studies of more complicated phase models, such as the ones with higher-order interactions.

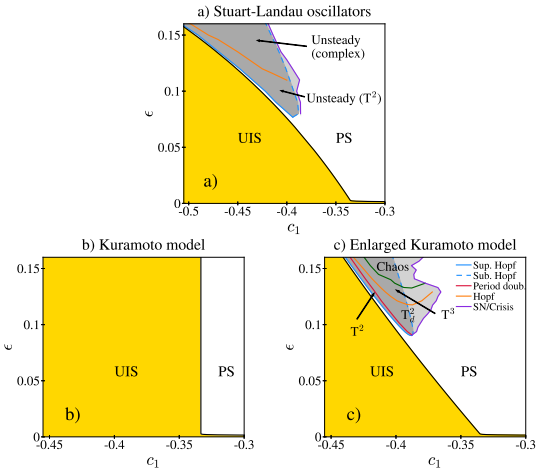

Fig. 1. Phase diagram of a) the ensemble of Stuart-Landau oscillators, b) the Kuramoto model, c) the enlarged Kuramoto model. In yellow and white regions Uniform Incoherence State and Partial Synchrony are stable respectively. The shaded gray region represents the parameters where complex dynamics are stable. Color lines are the transition between different regimes. The rich phase diagram of panel a) is only captured by the enlarged Kuramoto model depicted in panel c).

[1] Y. Kuramoto, *Self-entrainment of a population of coupled non-linear oscillators*, (International Symposium on Mathematical Problems in Theoretical Physics, Lecture Notes in Physics, Vol. 39, pp. 420-422, edited by Huzihiro Araki, Springer, Berlin, 1975)

[2] I. León and D. Pazó, *Phase reduction beyond the first order: The case of the mean-field complex Ginzburg-Landau equation* Phys. Rev. E **100**, 012211 (2019)

[3] I. León and D. Pazó, *Enlarged Kuramoto Model: Secondary Instability and Transition to Collective Chaos*, arXiv:2112.00176 (2021).

Effects of demand control on the complex dynamics of electric power system blackouts

Benjamín A. Carreras[1,2], Eder Batista Tchawou Tchuisseu,[1,3] José M. Reynolds-Barredo[2], Damià Gomila[1], and Pere Colet[1]

[1]Instituto de Física Interdisciplinar y Sistemas Complejos (IFISC, UIB-CSIC), Campus Universitat de les Illes Balears E-07122 Palma de Mallorca, Spain

[2] Departamento de Física, Universidad Carlos III de Madrid, 28911 Leganés, Madrid, Spain

[3] Institute of Thermomechanics, Academy of Science of the Czech Republic, 18200 Prague 8, Czech Republic

The propagation of failures and blackouts in electric networks is a complex problem. Typical models, such as the ORNL-PSerc-Alaska (OPA), are based on a combination of fast and slow dynamics. The first describes the cascading failures while the second describes the grid evolution through line and generation upgrades as well as demand growth, all taking place in time scales from days to years. The growing integration of renewable energy sources, whose power fluctuates in time scales from seconds to hours, together with the increase in demand, which also presents fast fluctuations, requires the incorporation of distributed methods of control in the demand side to avoid the high cost of ordinary control in conventional power plants. In this work, we extend the OPA model to include fluctuations in the demand at time scales of the order of minutes, intraday demand variations, and the effect of demand control. We find that demand control effectively reduces the number of blackouts without increasing the probability of large-scale events.

[1] B.A. Carreras, E.B. Tchawou Tchuisseu, J.M. Reynolds-Barredo, D. Gomila, and P. Colet, Chaos **30**, 113121 (2020).

Data analysis of frequency fluctuations in the Balearic grid before and after coal closure

María Martínez-Barbeito[1], Damià Gomila[1], and Pere Colet[1]
[1]Instituto de Física Interdisciplinar y Sistemas Complejos (IFISC, UIB-CSIC), Campus Universitat de les Illes Balears E-07122 Palma de Mallorca, Spain

In 2019, Es Murterar, the most polluting power station in the Balearic Islands, was partially closed down. Since then, the operation time of its remaining units has been heavily restricted. These measures were taken as a first step in the decarbonization agenda, and they marked the end of coal as the main electricity generation source in the territory.

The aim of this work is to evaluate the effect that the close down has in the frequency fluctuations statistics [1] which is a good proxy to monitor grid stability. We have used the open database [2], which includes 1-second measurements from October 2019 until December 2020. These were taken from a single location in Mallorca, and we assume that the frequency is the same in the other islands. Moreover, since the frequency is closely related to the demand-generation balance, we have also looked at the power data publicly available on the web site of Red Eléctrica de España (REE) [3]. In particular, they provide 10-minutes averaged data of the overall demand and generated power disaggregated by power plant technology, as well as the power through the High Voltage Direct Current (HVDC) line to the mainland.

Comparing the data from before and after the close down, we have seen that coal has been replaced by Combined Cycle Gas Turbine (CCGT). This has lead to a significant reduction of frequency fluctuations (see Figure 1), which indicates that the overall control capacity of the Balearic grid nowadays is significantly larger than before which indicates that CCGT power plants have a faster and more powerful control response than the coal plant.

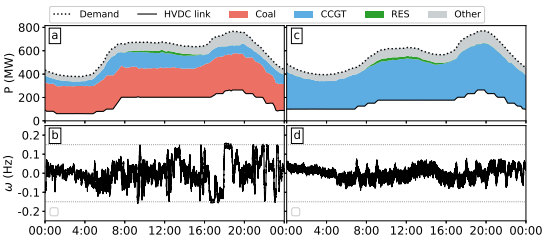

Fig. 1. Evolution of the demand and generation, and grid frequency in (a,b) a day in which coal was the main generation source compared to (c,d) a day when there was no coal generation. Generation is disaggregated by technology, including the HVDC connection to mainland. The dotted lines in the frequency plots indicate the statutory operational limits, i.e., (50.00 ± 0.15) Hz.

In order to characterize the frequency deviations, we use the rank size distribution. In Figure 2a, we show the rank of the two frequency time series from Figure 1. When CCGT is the main generation source, the shape of the curve shows a smooth decay in the probability of having large fluctuations. In other words, the frequency tends to stay close to its nominal value, and large deviations are highly unlikely. However, for the case when coal is the main generation source, we see a much slower decay of frequency deviations up to 0.15 Hz, which indicates there is a significantly larger probability, followed by a very steep drop.

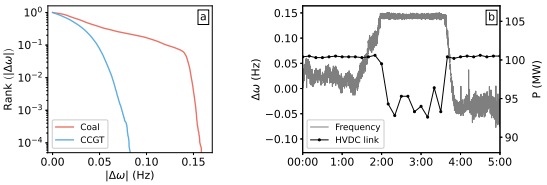

Fig. 2. (a) Rank size distribution of the absolute value of the frequency deviations for two days in which coal and CCGT were the main generation sources (Figure 1). (b) Evolution of the grid frequency and HVDC link power when frequency fluctuations reach ±0.15 Hz.

The typical frequency control mechanisms of conventional power plants act proportionally to the frequency deviation and tend to restore the frequency back to its nominal value, thus for most power grids the frequency distribution decays smoothly [4]. The existence of a threshold-like value, beyond which there is a much stronger damping of fluctuations, is a singularity in the Balearic system associated to the HVDC cable. If the frequency is within the statutory range ±0.15 Hz, the HVDC cable operates at a given set point without providing control. When the frequency deviation reaches reaches the limits then the power of the cable is continusly adjusted to avoid frequency deviations beyond that limit as shown in Figure 2b.

This control mechanism was frequenly activated when the coal power plant was the main source of generation due to the larger frequency fluctuations while its activation is quite rear since generation is dominted be combined cycle. The fact that fluctuations has reduced after the closure of the coal plant (which provided substantial inertia to the system) is a clear indication that inertia reduction is not as relevant for grid stability as having a fast flexible control.

[1] M. Martínez-Barbeito, D. Gomila, and P. Colet, *Data analysis of frequency fluctuations in the Balearic grid before and after coal closure*, ENERGY 2021, pp. 13-18 (2021).

[2] `https://power-grid-frequency.org/`

[3] `https://demanda.ree.es/visiona/home`

[4] L.R. Gorjão, R. Jumar, H. Maass, V. Hagenmeyer, G.C. Yalcin, J. Kruse, M. Timme, C. Beck, D. Witthaut, and B. Schäfer, *Open database analysis of scaling and spatio- temporal properties of power grid frequencies*, Nat. Commun., vol. 11, no. 1, pp. 111 (2020).

Assessing blackout risk in scenarios of high penetration of variable renewable energies

Benjamín A. Carreras[1,2], Pere Colet[1], José M. Reynolds-Barredo[2], and Damià Gomila[1]
[1]Instituto de Física Interdisciplinar y Sistemas Complejos (IFISC, UIB-CSIC),
Campus Universitat de les Illes Balears E-07122 Palma de Mallorca, Spain
[2] Departamento de Física, Universidad Carlos III de Madrid, 28911 Leganés, Madrid, Spain

We propose a method to analyze the risk of blackouts with high penetration of variable renewable energy sources (VRESs). We consider a model for the self-organized critical dynamics describing the long-term evolution of the power grid including propagation of cascading failures, day-to-day fluctuations of renewable generation and moderate use of storage. We analyze grid resilience and stress as VRESs are progressively incorporated. We also evaluate the VRES performance as the average fraction of daily demand covered by renewables. We find that in general, VRES intrinsic variability increases the grid stress and the blackout risk. However, if VRESs are implemented in a distributed way, the spatial spreading of the generation may have a positive effect on grid resilience. As a case study, we analyze the replacement of conventional power plants by solar photovoltaic generation combined with storage in the power grid of the Balearic Islands. We also consider the use of source redundancy and briefly discuss the potential of wind energy.

[1] B.A. Carreras, P. Colet, J.M. Reynolds-Barredo, D. Gomila, IEEE Access **9**, 132663-132674 (2021).

Effects of high penetration of wind power in the frequency fluctuations of Gran Canaria's power grid

María Martínez-Barbeito[1], Damià Gomila[1], and Pere Colet[1]
[1]Instituto de Física Interdisciplinar y Sistemas Complejos (IFISC, UIB-CSIC), Campus Universitat de les Illes Balears E-07122 Palma de Mallorca, Spain

The need to address the effects of climate change is accelerating the transition towards a more sustainable energy system. The progressive replacement of conventional power plants by variable renewable energy sources (VRES) will reduce both the inertia and the frequency control capabilities of the system, diminishing the overall flexibility of the grid as a consequence. Thus, additional control strategies will be needed to ensure stable operation.

In this work, we address this issue by simulating a power grid with different ratios of wind power. Our approach is based on the perhaps most common in the literature [1], which is the use of the swing equation and Kuramoto-like models of synchronous motors. We propose an extended dynamical model for the high voltage power grid, which includes conventional generators with primary and secondary frequency control, operation set points, fluctuations from demand and VRES, and the grid topology [2].

The first step in our study was to calibrate the model against observations. In Figure 1.a,b, we see that the model correctly captures frequency deviations in accordance to wind power ramps. In fact, it reproduces the frequency time series and the main statistical properties with a reasonable accuracy (Figure 1.c,d). However, there are some discrepancies, which we associate to simplifying assumptions of the model and lack of faster timescale data.

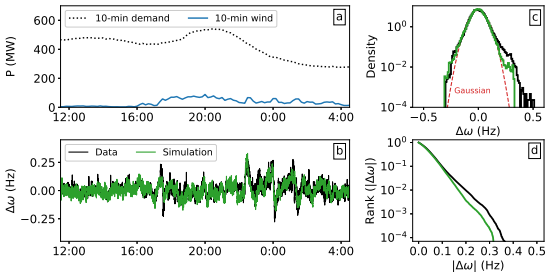

Fig. 1. (a) Evolution of demand and wind generation data [3]. (b) Time series, (c) probability density, and (d) rank size distribution of frequency fluctuations given by the model in comparison to the data [4].

After calibrating the model parameters to best fit the data, we have a model that can be used as a test bench to study the power grid under different scenarios. In this work, we focus on the effects of a high penetration of VRES. In particular, we study future scenarios with a high ratio of wind power in the Canary Islands, where wind is a major resource. We perform simulations for increasing amounts of wind in the system. Taking 2019 as our reference case, we multiply the wind generation data by a factor and we evaluate the frequency control needs.

Nowadays, wind generation covers a small fraction of the demand, and frequency deviations stay close to the statutory limits. However, increasing the wind capacity changes the size of the wind profile and magnifies wind fluctuations. In turn, frequency deviations become larger, except for the time windows where the wind generation exceeds the demand. In these cases, we only feed into the grid the demanded amount and the excess power is simply discarded. Curtailment in case of extra wind generation is another control mechanism, showing benefits to some extent.

To keep frequency fluctuations within reasonable limits, we have to increase the amount of control in the system. In our case, since we only study wind changes through the 10-minute data, we increase secondary control, which is responsible for adjusting the frequency over this timescale.

We observe that increasing secondary control reduces the size of all frequency deviations. But the key question is how much control is needed to keep fluctuations within the range 50 ± 0.2 Hz. We answer this question both by numerical simulations and by an analytical approach. As expected, the control needed to decrease fluctuations increases with wind penetration. Up to a certain point, there is a linear relationship between the secondary control gain parameter κ and the installed wind power (Figure 2). However, for bigger fractions of installed wind power, there is a plateau due to the curtailment. We obtain a good agreement between the analytical approach and the numerical simulation results for scenarios with up to 4 times the current wind capacity, but our analytical formula to estimate the needed secondary control capacity underestimates the need for secondary control for higher wind penetrations.

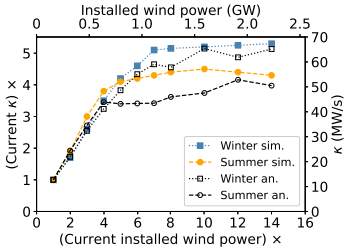

Fig. 2. Secondary control gain parameter κ needed to keep fluctuations within statutory limits as wind capacity increases.

[1] T. Nishikawa, and A.E. Motter, New J. Phys., 17(1), 015012 (2015).

[2] M. Martínez-Barbeito, D. Gomila, and P. Colet, Submitted for publication (2022).

[3] https://demanda.ree.es/visiona/home

[4] https://power-grid-frequency.org/

Analyticity constraints bound the decay of the spectral form factor

Pablo Martínez-Azcona[1], and Aurélia Chenu[1]
[1]Department of Physics and Materials Science, University of Luxembourg, L-1511 Luxembourg

Quantum mechanics and non-linear dynamics are two of the most prominent scientific triumphs of the 20th century. The connection between them, i.e. the study of chaotic behaviour of quantum systems, also known as *quantum chaos*, is an exciting field of study which gathers the high-energy, quantum-information and statistical mechanics communities.

The modern study of quantum chaos relies on dynamical quantities like the Out-of-Time-Order Correlator (OTOC) and the Spectral Form Factor. The former measures how much two operators fail to commute at different times and it allows for a definition of a *quantum lyapunov exponent*, while the latter is the Fourier transform of the two-level correlation function and characterises chaos in the *correlation hole* which serves as a signature of quantum chaotic dynamics. Recently a universal bound on the quantum Lyapunov exponent was conjectured $\lambda \leq 2\pi/(\beta\hbar)$ [1, 2, 3] which essentially states that the maximum rate at which quantum chaos can develop is proportional to the temperature of a system at equilibrium. This 'MSS-bound' on the Lyapunov exponent is inspired by black hole physics and AdS/CFT correspondence but its proof relies on a mathematical property of the OTOC, namely that it is analytic in some half-stripe of the complex plane when we consider complex times $t \to t + i\tau$.

Our main observation is that the mathematical machinery developed for proving the MSS bound is not restricted to the OTOC or even to chaos itself. Therefore it also yields universal bounds on different dynamical quantities. Particularly, we find that a dynamical quantity f_t that is (i) analytic on a half-stripe of the complex plane when $t \to t + i\tau$, (ii) normalized such that $|f_{t+i\tau}| \leq 1$ and (iii) exponentially decaying or growing, can be bounded by analyticity.

Specifically, we find that the Spectral Form Factor obeys all of these properties in its intermediate-time exponential decay $S(\beta, t) \sim e^{-\eta t}$, before the chaotic features show up in the correlation hole, therefore yielding a universal bound which does not depend on chaos. The bound we find on the *inflection exponent* η is given by

$$\eta \leq \frac{\pi}{2\beta\hbar}. \tag{1}$$

We illustrate the derived bound in systems with non-chaotic and chaotic dynamics. The former case is exemplified with the quantum harmonic oscillator while for the latter we use an ensemble from Random Matrix Theory. To bridge between the two cases we use the *quantum kicked top*, a model proposed in the original studies of quantum chaos which describes an angular momentum subject to a free precession and some periodic non-linear kicks [4]. The inflection exponent for this system shows a similar qualitative behaviour in both dynamical regimes (see Fig. 1). Furthermore, the exponent gets very close to the bound in both regimes, while the MSS bound is saturated only for *maximally chaotic* systems. This supports the idea that the derived bound is not sensitive to chaos and therefore bounds based on analyticity can apply to a wider range of quantities, not necessarily within the context of quantum chaos. Furthermore we also compare our derived universal bound with other physical bounds, like Quantum Speed Limits, and find that the derived universal bound can be tighter in some regimes than Quantum Speed Limits.

We believe that conditions (i)-(iii) are not so restrictive and could yield universal bounds in dynamical quantities throughout Quantum and Statistical Mechanics.

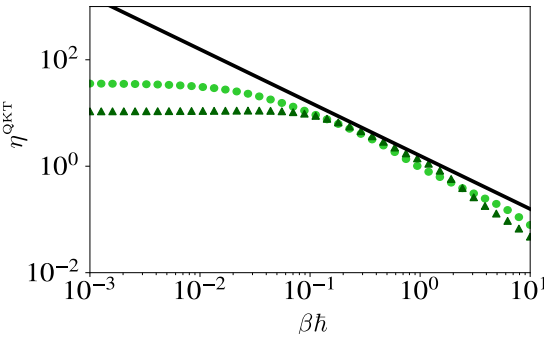

Fig. 1. **Inflection exponent for the Quantum Kicked Top** η^{QKT} for chaotic (light-green circles) and non-chaotic (dark-green triangles) dynamics along with the derived bound (1) (black solid line).

[1] Maldacena, J., Shenker, S.H. and Stanford, D. *A bound on chaos*. J. High Energy Phys. 2016, **106** (2016)

[2] Kurchan, J. *Quantum Bound to Chaos and the Semiclassical Limit*. J. Stat. Phys. **171**, 965979 (2018)

[3] Tsuji, N., Shitara, T. and Ueda, M. *Bound on the exponential growth rate of out-of-time-ordered correlators* Phys. Rev. E. **97** 012101 (2018)

[4] Haake, F., Ku, M. and Scharf, R. *Classical and quantum chaos for a kicked top*. Z. Physik B - Condensed Matter **65**, 381395 (1987)

[5] Martinez-Azcona, P. and Chenu, A. *Analyticity contraints bound the decay of the Spectral Form Factor. Submitted.*

Mixing dimensions in systems of ultracold atoms in optical traps

Tomas Sánchez-Pastor[1], Alejandro Saenz[2], and Fabio Revuelta[1]
[1]Grupo de Sistemas Complejos, E.T.S.I. Agronómica, Alimentaria y de Biosistemas, Universidad Politécnica de Madrid, Avda. Puerta de Hierro 2-4, 28040 Madrid, Spain.
[2] AG Moderne Optik, Institut fr Physik, Humboldt-Universitt zu Berlin, Newtonstrasse 15, 12489 Berlin, Germany.

Ultracold quantum atoms (UCAs) have become a topic of great interest over the last years since the experimental realization of the first Bose-Einstein Condensate [1]. Nowadays, UCAs lie among the most promising platforms for quantum information and computation due to the excellent degree of control that we have to manipulate and control them. One way to do so consists in tuning the interparticle interactions with the help of Feshbach resonances by application of external magnetic fields [2].

Moreover, quantum gases are routinely confined in optical traps of different shape and geometry (optical lattices, tweezers, dipolar traps, etc.). Changing the trapping potential enables an alternative way to manipulate the atomic sample through the so-called inelastic confinement-induced resonances (ICIRs). They were first observed in a groundbreaking experiment in Innsbruck [3]. The origin of the ICIRs lies on the coupling between the center-of-mass (CM) and the relative-motion (rm) coordinates due to the nonlinearities in the trapping potential. Consequently, they are absent in perfectly harmonic traps.

More recently, ICIRs have been observed in a 3D optical trap, demonstrating the existence of this phenomenon in more general situations. In this line, the theoretical model that reproduce the resonances has been validated in quasi-1D and refined in 3D confinements [4]. Knowing the position of the ICIRs is important due to their influence on quantum gases: sometimes, one must try to avoid them due to the losses that they cause in the atomic sample, while in other situations experimentalists make use of them to create coherent molecules [5]. The experimental developments over the last years have also enabled experiments where two interacting atomic clouds are confined in optical traps of different dimension [6]. The natural question is whether or not the dimension confinement affect the resonances.

In this communication, we try to sed light to the last question examining the ICIRs in mixed-dimensional optical traps with full CI *ab initio* simulations. For this purpose, we calculate the energy spectrum of a system of two ^{7}Li atoms confined in several settings (quasi-1Dquasi-1D), (quasi-1D–quasi-2D), (quasi-1D–3D), (quasi-2D–3D), (quasi-2D–quasi-2D) and (3D-3D) traps by solving the corresponding six-dimensional Schrdinger equation for several values of the s-wave scattering length a_0 (see for example Fig. 1). ICIRs manifest as avoided crossings in the spectrum due to the interaction between the least-bound (molecular) state and the first-trap state. Moreover, we increase the anisotropy between the longitudinal and transversal directions for the sake of breaking the degeneracy and, therefore, split the resonances in two branches. We have observed that the position of the ICIR's is strongly influenced by the trap dimensionality. The study for systems with heteronuclear species, which is experimentally more interesting [6], is currently under study.

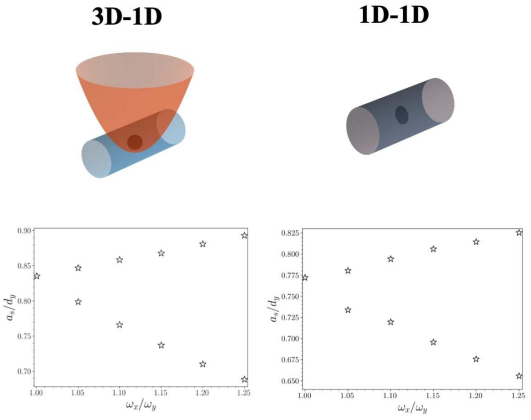

Fig. 1. Inelastic Confinement-Induced Resonances produced by two atoms of ^{7}Li in quasi-1D optical traps (right) and in mixed 3D–quasi-1D confinement (left) as a function of the anisotropy between the longitudinal (X) and transverse directions (Y, Z). Upper branch corresponds to the atomic level $(n_x, n_y, n_z) = (0, 2, 0)$ and the lower to $(n_x, n_y, n_z) = (2, 0, 0)$.

[1] Davis, Kendall B., *et al*., Phys. Rev. Lett., **75**, 3969 (1995).

[2] C. Chin, R. Grim, P. Julienne, and E. Tiesinga, Rev. Mod. Phys. **82**, 1225 (2010).

[3] E. Haller, et al., Phys. Rev. Lett., 104, 153203 (2010).

[4] T. Snchez-Pastor, A. Saenz, and F. Revuelta *On the limits of the theoretical calculation of inelastic confinement-induced resonances*. (In preparation).

[5] S. Sala, P.-I. Schneider, and A. Saenz, Phys. Rev. Lett., **109**, 073201 (2012).

[6] Lamporesi, G., et al. Phys. Rev. Lett., **104**, 153202. (2010).

Uniqueness of water compared with other liquids under nano-confinement

Giancarlo Franzese[1,2], Carles Calero[1,2]
[1] Secció de Física Estadística i Interdisciplinària, Departament de Física de la Matèria Condensada
Universitat de Barcelona, 08028 Barcelona, Spain
[2] Institut de Nanociència i Nanotecnologia (IN2UB), Universitat de Barcelona, 08028 Barcelona, Spain

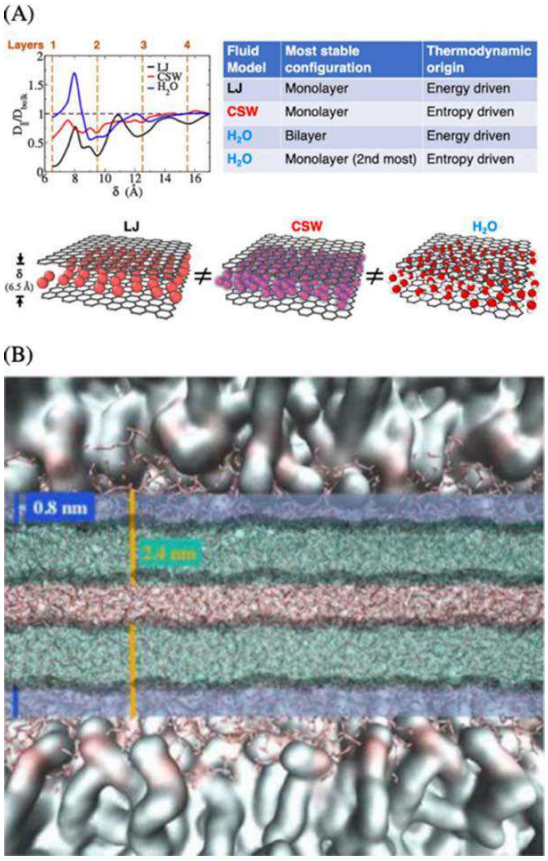

Fluid Model	Most stable configuration	Thermodynamic origin
LJ	Monolayer	Energy driven
CSW	Monolayer	Entropy driven
H_2O	Bilayer	Energy driven
H_2O	Monolayer (2nd most)	Entropy driven

Fig. 1. (A) Comparison of the diffusion of a normal fluid (LJ), an anomalous fluid (CSW), and water in a graphene nanopore. Their free energies change differently with the pore size (upper right table), and water is the only one that diffuses faster than bulk under sub-nm confinement (upper left panel). (B) Atomistic simulations of water between two membrane leaflets, Martelli et al. (2021). Away from the lipids (smooth surfaces), we schematically mark three regions: lipid-bound water (blue), unbound water (green), bulk water (red and withe the stick molecules), and the interfaces between them (dark regions). Water penetrates between the lipids and persists there even at low hydration.

Living organisms, viruses, and technological devices have water layers between their cells or parts and can die or stop working when dehydrated. But why water and not any other fluid? What makes water unique when it is in these tiny pores? We investigate why the water in a pore tinier than one-millionth of a hair moves faster than free water, while other fluids do not. We show that it all depends on the peculiar hydrogen bond interaction of water [1] (Fig. 1A). The results might be a key factor contributing to the solution of the United Nations Sustainable Development Goals about clean water and sanitation and relate to the switching behavior observed in a hydrated graphene nano-memristor proposed as a memory device that could store the data of 100 trillion flash memories in just 1 cm^3 for quantum computing [2, 3].

On the other hand, water's uniqueness is also essential in cellular membranes. We revise and extend the concept of 'hydration' or 'biological water', i.e., the nanoscopic layer of water covering the surface of biosystems. We find and discuss the existence of a bound/unbound water interface and its effect on dynamics and structure as far as 2.4 nm away from the membrane (Fig. 1B). The results might be relevant for understanding the role of water in biological activity, e.g., the efficacy of new drugs or vaccines [4, 5, 6].

[1] F. Leoni, C. Calero, and G. Franzese, *Nanoconfined Fluids: Uniqueness of Water Compared to Other Liquids*, ACS Nano **15**, 19864 (2021).

[2] H-T. Chin, et al. *Ferroelectric 2D ice under graphene confinement*, Nat. Commun. **12**, 6291 (2021).

[3] G. Franzese, *Supercomputer memories made of water*, https://doi.org/10.32388/9NTVN5.

[4] F. Martelli, J. Crain, and G. Franzese, *Network Topology in Water Nanoconfined between Phospholipid Membranes*, ACS Nano **14**, 8616 (2020).

[5] F. Martelli, C. Calero, and G. Franzese, *Redefining the concept of hydration water near soft interfaces*, Biointerphases **16**, 020801 (2021).

[6] The work has been possible thanks to the financial support of the Spanish MICIN grant PGC2018- 099277-B-C2, the ERDF (A way of making Europe), and the ICREA - Instituci Catalana de Recerca i Estudis Avanats.

Evolutionary Dynamics of The Ethereum Transaction Network

F Borondo[1,2], M Grande[3,5], and J Borondo[4,5]
[1]Instituto de Ciencias Matemáticas (ICMAT); Campus de Cantoblanco UAM; Nicolás Cabrera, 13-15; 28049 Madrid (Spain)
[2]Departamento de Química; Universidad Autónoma de Madrid; CANTOBLANCO - 28049 Madrid (Spain)
[3]Grupo de Sistemas Complejos; Universidad Politécnica de Madrid; 28035 Madrid (Spain)
[4] Departamento de Gestión Empresarial; Universidad Pontificia de comillas ICADE; Alberto Aguilera 23; 28015 Madrid (Spain)
[5]AGrowingData; Navarro Rodrigo 2 AT; 04001 Almería (Spain)

We are witnessing a revolution in the financial system, which is being replaced by the new and innovative Decentralized Finance (DeFi). DeFi projects are tackling long-standing problems and addressing inefficiencies in our current system, improving financial inclusion, increasing liquidity and reducing costs. In contrast to the traditional system, where financial applications are difficult to access, rigid, hard to use and expensive, DeFi applications are open and permissionless. Anyone can access them, all they need is an internet connection.

But what really makes this self-organized market of digital currencies attractive for the research community is that, unlike in the traditional financial system, all transactions are publicly available. This represents an unprecedented scenario that allows us to understand and explain the evolution and adoption of a financial system by capturing the complex behavior that emerges from the relationships between users.

In this work we focus on the Ethereum Blockchain, the largest decentralized computing platform in terms of users and usage. We have analyzed the transactions that occur in the network under a complex system perspective, in which nodes are the accounts that operate and links represent the transactions between them. We describe the dynamics and evolution of the system by analyzing its structure and computing its properties over time. Finally, we explore the relationships that exist between these properties and the future price of the network cryptocurrency called Ether (ETH).

Since this system is an evolving system, it is important to define dynamic intervals that capture the evolution of the system. Unlike other works that propose to create networks with an arbitrary time interval, [2], we use the method developed by Darst et al. [1], that detects evolutionary changes in the configuration of a complex system and generates intervals accordingly. In this method, the size of each interval is determined by maximizing the similarity between the sets of events within consecutive intervals.

We applied the Dynamic time-slicing method [3] on our dataset and found that the activity of the network can be measured by considering regular time intervals of 14 days. We also found a strong correlation between the similarity score obtained from the Dynamic time-slicing method and the Ethereum price.

Next, we analyzed the properties of the resulting networks and found that the degree distribution of the networks are highly heterogeneous, where a small fraction of addresses tend to trade with the vast majority, while most addresses hardly trade with others. We found that the networks are disassortative and present very low clustering.

Finally, we explored the relations between the network properties and the future price of Ethereum and found a strong negative correlation between the exponent of the degree distribution and the price. Hence, our results suggest that the transaction network contains relevant information to explain the evolution and adoption of the system.

[1] A. Darst, R. K., B. Granell, C., C. Arenas, A., D. Gmez, S., E Saramki, J., and F Fortunato, S., *Detection of timescales in evolving complex systems.* , Scientific reports **6**, 39713 (2016).

[2] A. Liang, J., B. Li, L., and C. Zeng, D. *Evolutionary dynamics of cryptocurrency transaction networks: An empirical study.*, PloS one, **13(8)** (2018).

[3] https://github.com/rkdarst/dynsnap/blob/master/doc/Manual.rs

El doble efecto de los obstáculos en la prevención de los atascos en silo 2D

Rodrigo Caitano[1], Diego Gella[1], Daichi Yanagisawa[2,3], María Victoria Ferreyra[4], and Iker Zuriguel[1]
[1]Departamento de Física y Matemática Aplicada, Facultad de Ciencias, Universidad de Navarra, Pamplona, Spain
[2]Research Center for Advanced Science and Technology, The University of Tokyo, Tokyo, Japan
[3] Department of Aeronautics and Astronautics, School of Engineering, The University of Tokyo, Tokyo, Japan
[4] Departamento de Física, Facultad de Ciencias Exactas y Naturales, Universidad Nacional de La Pampa, Santa Rosa, Argentina

La colocación de un obstáculo frente a un orificio se ha propuesto como una buena alternativa para mejorar el flujo de materiales discretos en una amplia variedad de escenarios. Sin embargo, las razones físicas detrás de este comportamiento no se comprenden completamente y la idoneidad de esta práctica ha sido cuestionada recientemente para las evacuaciones de peatones. Las explicaciones existentes que justifican el efecto de un obstáculo sobre la obstrucción están relacionadas con la dinámica del sistema. Por lo tanto, podría esperarse que si se minimiza el movimiento del grano, el impacto del obstáculo apenas sea importante. En este trabajo demostramos que esto no es así mediante la implantación de un mecanismo de extracción granular consistente en una cinta colocada debajo del orificio que permite descargar el silo de forma cuasi estática. En trabajos anteriores se ha determinado que la influencia de la velocidad de las partículas en el proceso de atasco es notable [1]. De hecho, la probabilidad de atasco p_c al descargar un silo bidimensional con velocidad constante y controlada ha sido descrita mediante la Eq. (1). Donde D es el tamaño de agujero, d_p el tamaño de la partícula, v la velocidad media de salida de los granos, y a y b son dos parámetros de ajuste. En particular, a determina la probabilidad de atasco cuando el material es extraído con una velocidad despreciable, y b determina la influencia de v en p_c.

$$p_c = (a + bv)^{(-D/d_p)^2} \tag{1}$$

Experimentalmente se comprobó que la probabilidad de detener el flujo en un silo descargado a una velocidad impuesta por la gravedad se puede reducir en un factor 100 para una determinada posición del obstáculo [2]. Un efecto similar fue también verificado en el paso de animales por una puerta [3], aunque no fue observado en el caso de evacuación de personas [4]. Un indicador que justificaría un posible origen de la reducción del atasco en el límite cuasi esttico proviene del análisis de la fracción sólida bidimensional ϕ en la región comprendida entre la salida y el obstáculo.

Para evaluar la orientación de la red de contactos, calculamos el *contact fabric tensor* de segundo orden, una magnitud capaz de caracterizar estadísticamente la microestructura de un conjunto granular. Este tensor puede medir el grado de anisotropía en las direcciones de los contactos entre los granos que componen la muestra y se define para cada partícula i con la Eq. (2),

$$f^i_{\alpha\beta} = \frac{1}{N_c} \sum_c n^c_\alpha n^c_\beta, \tag{2}$$

donde, N_c es el número de contactos de esa partícula, mientras que $\vec{n^c}$ es el vector de rama normalizado que une el centro de la partícula i con los de sus partículas en contacto.

En este trabajo demostramos experimentalmente que para el caso de la descarga de granos inertes de un silo, un obstculo por encima de la salida conduce a una reducción de la formación de atascos a través de dos mecanismos diferentes: i) una alteración de las propiedades cinemáticas en las proximidades de la salida que impide la estabilización de arcos; y ii) una introducción de una clara anisotropía en el *contact fabric tensor* que se vuelve relevante cuando se trabaja en régimen cuasi estático. Luego, ambos mecanismos se engloban en una sola formulación que podría ser inspiradora para otros sistemas más complejos [5].

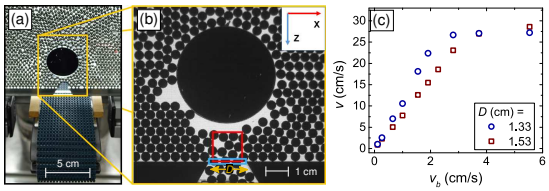

Fig. 1. **Esquema del montaje experimental. a** Fotografía de la parte inferior del silo donde se puede distinguir el obstáculo, el orificio y la cinta transportadora. **b** Fotograma tomado de una película grabada con la cámara de alta velocidad donde se define el tamaño del orificio. El cuadro azul es la región ubicada en la salida donde se promedia la velocidad de las partículas para calcular v. El cuadro rojo es el área representativa por encima del orificio y por debajo del obstáculo donde se promedian las magnitudes para obtener v_x, v_z y la fracción sólida ϕ. El sistema de coordenadas (donde, por conveniencia, los valores positivos se consideran en la dirección hacia abajo) también se muestra en esta figura. **c** Datos experimentales de la velocidad media de las partículas a la salida del silo v, frente a la velocidad de la cinta v_b, en el silo con el obstáculo, para los dos tamaños de orificio indicados en la leyenda. Las incertidumbres son más pequeñas que el tamaño del punto, ya que las velocidades provienen de promedios de una gran cantidad de datos.

[1] D. Gella, I. Zuriguel, and D. Maza, *Decoupling Geometrical and Kinematic Contributions to the Silo Clogging Process*, Phys. Rev. Lett. **121**, 138001 (2018).

[2] I. Zuriguel, A. Janda, A. Garcimartín, C. Lozano, R. Arvalo, and D. Maza, *Silo clogging reduction by the presence of an obstacle*, Phys. Rev. Lett. **107**, 278001 (2011).

[3] I. Zuriguel, J. Olivares, J.M. Pastor, C. Martín-Gómez, L.M. Ferrer, J.J. Ramos, and A. Garcimartín, *Effect of obstacle position in the flow of sheep through a narrow door*, Phys. Rev. **E 94**, 032302 (2016).

[4] A. Garcimartín, J.M. Pastor, C. Martín-Gómez, D. Parisi and I. Zuriguel, *Pedestrian collective motion in competitive room evacuation*, Sci. Rep. **7**, 10792 (2017).

[5] D. Gella, D. Yanagisawa, R. Caitano, M.V. Ferreyra and I. Zuriguel, *On the dual effect of obstacles in preventing silo clogging in 2D*, Commun Phys **5**, 4 (2022).

Collisional Reservoirs and Thermalization

Jorge Tabanera Bravo[1] and Juan M.R. Parrondo[1],
[1] Departamento de Estructura de la Materia, Física Térmica y Electrónica and GISC,
Universidad Complutense de Madrid, 28040 Madrid, Spain

Collisional reservoirs are becoming a remarkable tool in the field of Open Quantum Systems due to their capacity to simulate thermal interactions in a relatively simple way. The more common implementation of these reservoirs consists on a repeated interaction of the target quantum system, S, with identical copies of ancillary systems called units, U. These units are refreshed into a thermal state after each interaction, mimicking the action of the thermal bath. However, the continuous switching on and off of the interaction between the system and the units provides additional energy to the system. This external work prevents thermalization in certain cases [1], yielding spurious currents and the violation of the second law.

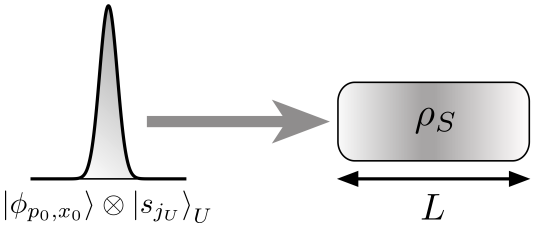

Fig. 1. Sketch of the autonomous system. The units U possess an additional kinetic degree of freedom, p, whose state is a wave packet with a random momentum distribution according to the effusion distribution. The system acts as a scatterer of the wave packets. [5]

This situation is treated in a serie of works [2, 3, 4]. There is shown how the introduction of the kinetic degree of freedom of the units, p, makes the whole setup autonomous. The unit state is then a narrow wave packet with random momentum, Fig.1. In this case, the energy to switch on and off the interaction is provided by the spatial degree of freedom of the unit. If the momentum is in equilibrium, the energy exchange is no longer work, but heat, and the system thermalizes [2, 3]. As a result, this approach captures all the essential features of a genuine thermostat.

In [5] we extend previous results by solving the complete scattering problem, and find approximations to the exact scattering map preserving microreversibility at high temperatures. The usual repeated interaction mechanism can be recovered from this solution as a high temperature limit, Fig.2.

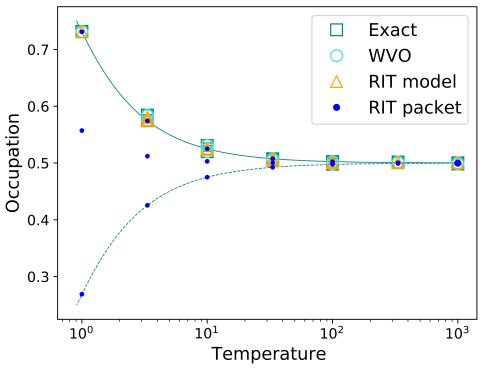

Fig. 2. Comparison between the implementation proposed in [5] (WVO) and the usual repeated interaction mechanism (RIT).

[1] Barra, F. (2015). *The thermodynamic cost of driving quantum systems by their boundaries.* Scientific reports, 5(1), 1-10.

[2] Ehrich, J., Esposito, M., Barra, F., Parrondo, J. M. (2020). *Micro-reversibility and thermalization with collisional baths. Physica A: Statistical Mechanics and its Applications*, 552, 122108.

[3] Jacob, S. L., Esposito, M., Parrondo, J. M., Barra, F. (2021). Thermalization induced by quantum scattering. PRX Quantum, 2(2), 020312.

[4] Jacob, S. L., Esposito, M., Parrondo, J. M., Barra, F. (2021). Quantum scattering as a work source. arXiv preprint arXiv:2108.13369.

[5] Tabanera, J., Luque, I., Jacob, S. L., Esposito, M., Barra, F., Parrondo, J. M. (2022). Quantum collisional thermostats. New Journal of Physics.

The microscopic mechanism of ice friction

Lukasz Baran[1], Pablo Llombart[2] y Luis G. MacDowell[3].
[1]Institute of Chemical Sciences, Maria Curie-Sklodowska University in Lublin, Poland.
[2] Facultad de Ciencias, Universidad Autónoma de Madrid, Spain.
[3]Departamento de Química Física, Universidad Complutense de Madrid, Spain.

Aunque las propiedades deslizantes del hielo nos son a todos familiares, las causas de este comportamiento tienen una larga historia de controversias sin resolver [1]. Durante más de un siglo, se ha aceptado que la razón fundamental que causa tan baja fricción es la presencia de una capa delgada de agua fundida que hace las veces de lubricante. Sinembargo, no hay consenso sobre el origen de esta capa de lubricación. Entre las hipótesis barajadas se han invocado el derretimiento por presión característico del hielo; el fenómeno de mojado superficial o 'premelting'; y la fusión por disipación de calor [1]. Mś recientemente, se ha propuesto que la lubricación no juega papel alguno, sino que la fricción del hielo a baja temperatura es principalmente adhesiva y que se puede describir en términos de propiedades meramente mecánicas a alta temperatura [2].

Desgraciadamente, ninguna de estas hipótesis es fácilmente verificable mediante experimentos macroscópicos. ¿Cual es el espesor de la capa de lubricación en condiciones estáticas? ¿Cómo cambia con la naturaleza del sustrato? ¿Aumenta significativamente con la presión o la cizalladura? ¿Es suficiente el espesor resultante para el establecimiento de un flujo de Couette?

En este trabajo usaremos herramientas desarrolladas en nuestros recientes estudios sobre la estructura superficial del hielo [3, 4, 5, 6], con el objeto de comprender los mecanismos microscópicos responsables de su bajo coeficiente de fricción.

Sliding on ice is a familiar experience, but the reason why ice has such a low friction has a long and controversial history [1]. For many years, it has been assumed that the main reason for the low friction of ice is due to the formation of a thick lubrication layer of meltwater. However, there is no consensus on the origin of the meltwater film. Among the different hypothesis enumerated are pressure melting, ice premelting and frictional heating of the surface [1]. Very recently, however, it has been suggested that lubrication plays no role whatsoever, and that ice friction is of adhesive origin at low temperature and can be explained in terms of mechanical properties at high temperature. [2].

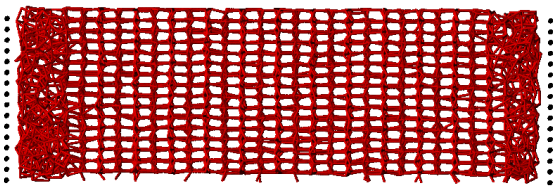

Fig. 1. Hielo confinado entre dos superficies. Se observa la formación de una capa superficial desordenada.

Unfortunately, these hypothesis cannot be easily confirmed by macroscopic experiments. What is the actual thickness of the watery lubrication film under static conditions? Does it change significantly with the nature of the substrate? Does it become thicker upon increasing the pressure or shearing? Is the resulting thickness sufficient for the stablishment of a lubricating Couette flow?

In this work we borrow tools from our recent investigations on the structure of ice premelting [3, 4, 5, 6], in order to understand better the microscopic origin of the low friction coefficient of ice.

[1] Rosenberg *Why is ice slippery?*, Phys. Today **58**, 50 (2005).

[2] Liefferink, Hsia, Weber and Bonn, *Friction on Ice*, Phys. Rev. X, **11**, 011025 (2021).

[3] Benet, Llombart, Sanz and MacDowell, *Premelting of the Ice-Vapor Interface*, Phys. Rev. Lett. **117**, 096101 (2016).

[4] Llombart, Noya, Sibley, Archer and MacDowell, *Rounded Layering Transitions on the Surface of Ice*, Phys. Rev. Lett. **124**, 065702 (2020).

[5] Llombart, Noya and MacDowell, *Surface Phase Transitions and Crystal Habits of Ice in the Atmosphere*, Sci. Adv. **6** eaay9322 (2020).

[6] Sibley, Llombart, Noya, Archer and MacDowell, *How ice grows from premelting films and liquid droplets*, Nat. Comm. **12** 239 (2021).

On the cross-over from Casimir (retarded) to London (non-retarded) van der Waals interactions

Juan Luengo[1], Fernando Izquierdo-Ruiz[1] y Luis G. MacDowell[1]
[1]Universidad Complutense de Madrid, Depto. de Química Física, Madrid.

The experimental measurement of surface forces between plates a distance L apart stands as the most important probe for the understanding of van der Waals intermolecular forces [1]. Paradoxically, experiments have had far less trouble confirming these forces in the long range (Casimir) retarded regime, where they decay as L^{-3}, than in the familiar non-retarded regime (London-Hamaker), where they decay as L^{-2}. Be as it may, in most applications in chemical-physics, from wetting to colloidal sciences, the retarded Casimir regime is completely ignored, in favor of the non-retarded London-regime [2]. The reason is that the full theoretical treatment for the interaction between two semi-infinite media across a dielectric due to Dzialoshinskii, Lifshitz and Pitaevskii (DLP) is numerically very difficult to implement, and analytically not very transparent to interpret [3, 4]. Unfortunately, using merely the pair-wise Hamaker approximation can incur in very serious errors, as the crossover from London to Casimir regimes is often accompanied by a sign reversal of the forces [3, 4].

In this communication we present simple closed forms for the distance dependent Hamaker constant, that are able to capture with great accuracy all the relevant regimes from the subnanometer length-scale to beyond the micrometer [5]. The theory uses dielectric data as only input and does not require any adjustable parameter. This allows an easy implementation of DLP theory, but more importantly, it allows us to clearly recognize the widely different L dependence that results as the distance between plates is increased. Particularly, for the finite frequency contributions to the Hamaker constant, we show how the exact treatment provides an L^{-2} regime at short distance, an L^{-3} regime at intermediate distance, but also the very much less appreciated e^{-L} exponential suppression of finite frequency contributions that can lead to sign reversal of the Hamaker constant (see Fig. 1).

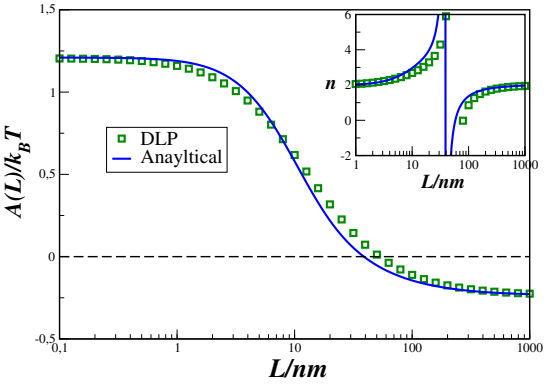

Fig. 1. Hamaker constant of an octane film adsorbed between water and air. The symbols are numerical results from DLP theory, the line is a simple analytical approximation with no adjustable parameters. The crossover from non-retarded to retarded interactions results in the sign reversal of the Hamaker constant. Inset displays the effective exponent of the power law decay.

[1] J. N. Israelachvili and D. Tabor, Proceedings of the Royal Society of London A: Mathematical, Physical and Engineering Sciences **331,** 19–38 (1972).

[2] J. N. Israelachvili, *Intermolecular and Surfaces Forces*, 3rd ed. (Academic Press, London, 1991), pp. 1–674.

[3] I. E. Dzyaloshinskii, E. M. Lifshitz, and L. P. Pitaevskii, Soviet Physics Uspekhi **4,** 153.175 (1961).

[4] V. A. Parsegian, *Van der Waals Forces* (Cambridge University Press, Cambridge, 2006), pp. 1–311.

[5] L. G. MacDowell, J. Chem. Phys. **150,** 081101 (2019).

Surface phase transitions, anomalous step free energies and crystal growth rates of ice in the atmosphere

P. Llombart[1,2], E. G. Noya[2] y Luis G. MacDowell[1]
[1]Universidad Complutense de Madrid, Dpto. de Química Física, Madrid
[1]Instituto de Química Física Rocasolano, Consejo Superior de Investigaciones Científicas, Madrid.

As the thread of global warming is confirmed, the fate of ice has become a serious concern. Unfortunately, our understanding of how ice actually grows (or melts) remains poor. The Nakaya diagram, which describes the growth forms of snow crystals in the atmosphere provides an eloquent example [1]. At low vapor saturation, ice crystallites are found as simple hexagonal prisms, but their shape changes from plates, to columns to plates and yet back to columns as temperature is cooled down below 0 C. Experiments allow to correlate empirically these shape transitions with a crossover of crystal growth rates, but the physics behind these transformations and its relation with the underlying equilibrium surface structure remains completely unknown.

In this work we exploit a methodology for the study of surface fluctuations developed in the last years in our lab [2, 3, 4, 5] to unveil the structure and dynamics of the ice surface [6, 7]. We show that in the range from -80 to 0 C, the main crystal facets of ice undergo a sequence of alternating structural surface phase transitions that result in the anomalous increase of step free energies and the crossover of crystal growth rates exactly as required to explain the Nakaya diagram [7].

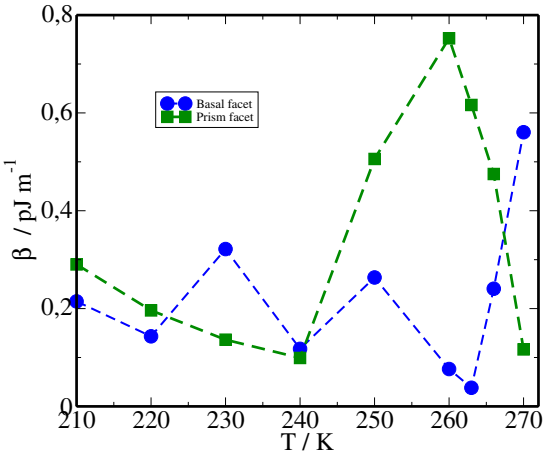

Fig. 1. Step free energies of ice below a premelting film. Results are shown for basal and prism facets as a function of temperature as calculated from the spectrum of surface fluctuations of the TIP4P/Ice water model. The free energies crossover twice, resulting in a crossover of crystal growth rates and the alternation of crystal habits from plate to column like hexagonal prisms twice.

[1] U. Nakaya, *Snow Crystals: Natural and Artificial* (Harvard University Press, Cambridge, 1954).

[2] J. Benet, P. Llombart, E. Sanz, and L. G. MacDowell, Phys. Rev. Lett. **117,** 096101 (2016).

[3] J. Benet, P. Llombart, E. Sanz, and L. G. MacDowell, Mol. Phys. **117,** 2846–2864 (2019).

[4] P. Llombart, R. M. Bergua, E. G. Noya, and L. G. MacDowell, Phys. Chem. Chem. Phys **21,** 19594–19611 (2019).

[5] P. Llombart, E. G. Noya, D. N. Sibley, A. J. Archer and L. G. MacDowell, Phys. Rev. Lett. **124**, 065702 (2020).

[6] D. Sibley, P. Llombart, E. G. Noya, A. Archer, and L. G. MacDowell, Nat. Comm. **12** 239 (2021).

[7] P. Llombart, E. G. Noya, and L. G. MacDowell, Sci. Adv. **6** eaay9322 (2020).

El principio de máxima entropía y la distribución de viajes en servicios de bicicletas compartidas

Carlos Miguel Vallez[1] and Mario Castro[1] and David Contreras[1]
[1]Instituto de Investigación Tecnológica (IIT), Universidad Pontificia Comillas, Madrid, Spain

La abundancia de datos de redes sociales ha catalizado el estudio cuantitativo de la movilidad humana. Con estos datos y otras fuentes de informacin, se han extrado diversos patrones de movilidad [1], surgiendo infinidad de modelos matemticos y estadsticos para capturar dichos modelos [2].

La mayor parte de los esfuerzos se centran en modelar las llamadas *matrices origen-destino*, T_{ij}, que miden cuntos desplazamientos tienen lugar entre una localizacin origen i y un destino j. En muchos casos, estas matrices pueden modelarse como un campo vectorial de movilidad que permite identificar las regiones que atraen ms desplazamientos [3].

En este trabajo nos centramos en el problema de la movilidad urbana en servicios bicicletas compartidas (BSS) en la ciudad de Madrid, que han ganado popularidad en los ltimos aos por su potencial para contribuir al desarrollo de ciudades sostenibles. Aunque los primeros intentos de implantar un servicio pblico de bicicletas compartidas se remontan a 1965 (msterdam), su uso generalizado lleg con el milenio, convirtindose en una vibrante actividad y en un rea de investigacin cuya actividad ha aumentado de forma constante en la ltima dcada [4].

Este problema que tiene dos particularidades. Por una parte, las bicicletas se ubican en estaciones fijas, llamadas *docks*, y estn sujetas a problemas de demanda (falta de bicicletas en la estacin de origen) y de concentracin (falta de ranuras libres para devolver la bicicleta en su destino). Por otra parte, se afronta el modelado de la matriz T_{ij} desde un punto de vista probabilstico (en lugar de describir el nmero de viajes, se describe la probabilidad de realizar un viaje a una cierta distancia d, p_d).

Para el modelado de este problema, se parte del principio de mxima entropa [5] sujeto a dos restricciones. La primera est vinculada a la distancia media, $\bar{d}$ y la percepcin de la distancia (logartmica, $\bar{L} \equiv \langle \log d \rangle$), y la segunda, ligada a la percepcin psicolgica de *esfuerzo* y postulamos que obedece la llamada ley de Weber-Fechner [6] de la percepcin logartmica. Maximizando, y usando los multiplicadores de Lagrange β y $\alpha - 1$ (por conveniencia

$$\begin{aligned} \mathcal{S} &= -\sum p_d \log p_d - \lambda(\sum p_d - 1) \\ &- \beta(\sum p_d d - \bar{d}) - (\alpha - 1)(\sum p_d \log d - \bar{L}) \end{aligned} \quad (1)$$

La solucin es una distribucin Gamma para la probabilidad de viajar a una cierta distancia d

$$p_d = \frac{\beta^\alpha}{\Gamma(\alpha)} d^{\alpha-1} e^{-\beta d} \quad (2)$$

En la figura 1 mostramos una comparacin entre los datos empricos y distintas distribuciones propuestas en la literatura [2]. Como se puede ver, el ajuste con la Ec. (2) es excelente. La distribucin exponencial corresponde al llamado **gravity model** propuesto para la movilidad entre ciudades [2].

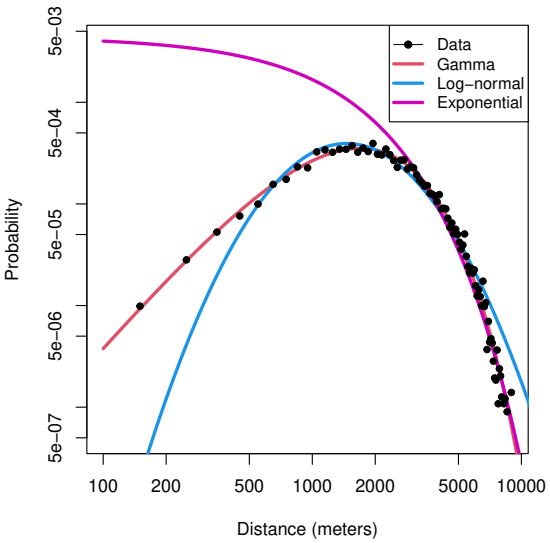

Fig. 1. Distribucin emprica de probabilidad de viajar en bicicleta compartida a una distancia d y comparacin con distribuciones propuestas en la literatura—log-normal y exponencial—, y en este trabajo, distribucin Gamma, Ec. (2).

[1] T. Louail, et al. *Uncovering the spatial structure of mobility networks*. Nature communications **6(1)**, 1 (2015).

[2] H. Barbosa, Hugo, et al. *Human mobility: Models and applications*. Physics Reports **734**, 1 (2018).

[3] M. Mazzoli, et al. *Field theory for recurrent mobility*. Nature communications **10(1)** 1, (2019).

[4] CM. Vallez, M. Castro, and D. Contreras. *Challenges and Opportunities in Dock-Based Bike-Sharing Rebalancing: A Systematic Review*. Sustainability **13(4)**, 1829 (2021).

[5] ET. Jaynes, *Information theory and statistical mechanics*. Physical Review **106(4)**, 620 (1957).

[6] S. Dehaene, *The neural basis of the WeberFechner law: a logarithmic mental number line* Trends in cognitive sciences **7(4)**, 145 (2003).

Effect of memory in a dynamic quantum Cournot duopoly game with heterogeneous players

Juan Grau-Climent[1], Luis Garcia-Perez[1], Ramon Alonso-Sanz[1], and Juan Carlos Losada[1]
[1]Complex Systems Group, Universidad Politécnica de Madrid, C. Universitaria, 28040 Madrid, Spain.

The study of Game Theory is widely developed currently and has many applications in several fields such as economics, psychology, biology, etc. The use of entangled modelling is a demonstrated way to improve the results comparing with the classic games due to the entanglement between the players, based on quantum theory. In this kind of models, also called quantum games, it is often studied how the degree of entanglement affects the equilibrium strategies of both players [1]. An interesting case is when the players are heterogeneous, so one of them follows naively the previous steps of the other rational player, since the dynamics of both players can be chaotic and not reach stable equilibria [2].

In the classic Cournots Duopoly with linear inverse demand, the profits of the two players given by:

$$u_i(t) = q_i(t)\left(p(t) - c_i\right), \tag{1}$$

where $q_i(t), i = 1, 2$ represent the output of ith player in the period t, $p(t)$ the prevailing price and c_i the marginal cost of the i player.

Now, we consider the quantization of the classical Cournot's Duopoly, according to Li-Du-Massar quantum scheme [3]. This quantum version has the following steps. First, the game starts from *initial state* $|00\rangle$. This state undergoes a *unitary operation* $\hat{J}(\gamma) = e^{-\gamma\left(\hat{a}_1^\dagger \hat{a}_2^\dagger - \hat{a}_1 \hat{a}_2\right)}$, where $a_i^\dagger(\hat{a}_i)$ represents the creation (annihilation) operator of player i and $\gamma \geq 0$ is known as the *squeezing parameter*. Next, the two players execute their *strategic movements* via unitary operation $\hat{D}_i(x_i) = e^{x_i(\hat{a}_i^\dagger - \hat{a}_i)/\sqrt{2}}, i = 1, 2..$ Finally, the two player' states are measured after *a disentanglement operation* $\hat{J}(\gamma)^\dagger$. Thus, the *final state* is carried out by $|\psi_f\rangle = \hat{J}(\gamma)^\dagger \left(\hat{D}_1(x_1) \otimes \hat{D}_2(x_2)\right) \hat{J}(\gamma)|00\rangle$. The quantity q_i is obtained by acting on the state $|\psi_f\rangle$:

$$\begin{aligned} q_1(t) &= \langle\psi_f|\hat{D}_1(x_1)|\psi_f\rangle = x_1(t)\cosh\gamma + x_2(t)\sinh\gamma, \\ q_2(t) &= \langle\psi_f|\hat{D}_2(x_2)|\psi_f\rangle = x_2(t)\cosh\gamma + x_1(t)\sinh\gamma, \end{aligned} \tag{2}$$

where x_1 and x_2 represent the strategies used by the two firms in the quantum game. When the degree of quantum entanglement is zero, i.e. $\gamma = 0$, then the quantum game turns into the original classical form.

In this study we consider two players with different expectations (heterogeneous expectations), where the first one is a boundedly rational player and the other one is a naive player.The strategy of first player, with bounded rationality, depend on the gradient of their marginal profit:

$$x_1(t+1) = x_1(t) + \alpha x_1(t)\frac{\partial u_1}{\partial x_1(t)}, \tag{3}$$

where α is a parameter which represents the speed of adjustment. The second player, the naive player, expects equal production in each period. Hence, this player will choose the level of output which maximizes the expected profit, i.e:

$$x_2(t+1) = x_2^*(t). \tag{4}$$

where $x_2^*(t)$ satisfies

$$\left|\frac{\partial u_2}{\partial x_2(t)}\right|_{x_2^*(t)} = 0. \tag{5}$$

The dynamic system obtained has the following structure:

$$\begin{aligned} x_1(t+1) =& f(x_1(t), x_2(t), \alpha, \gamma), \\ x_2(t+1) =& g(x_1(t), \alpha, \gamma) \end{aligned} \tag{6}$$

In this work we propose an evolution of quantum games with heterogeneous players that includes memory. In previous works we have explored the effect of embedded memory in chaotic dinamical systems [4]. In this case, the strategy of each player takes into account the strategies of previous time steps in a weighted way. To do this, we replace, in the f and g funtions of ecs. 6, the values x_i given by the following weighted function

$$\mu_i(t) = \frac{x_i(t) + \sum_{\tau=0}^{t-1} \beta^{t-\tau} x_i(\tau)}{1 + \sum_{\tau=0}^{t-1} \beta^{t-\tau}} \tag{7}$$

where the choice of the memory factor β simulates the long-term or remnant memory effect: the limit case $\beta = 1$ corresponds to a memory with equally weight records (*full* memory), whereas $\beta \ll 1$ intensifies the contribution of the most recent states (short-term working memory). The choice $\beta = 0$ leads to the non-memory model.

We have analytically proven and numerically verified that including memory in the dynamics, the stability of the system significantly improves without variation in the fixed points comparing with the memoryless model. Furthermore, even chaotic dynamics disappears in the case of maximum memory.

[1] L Garcia-Perez, J Grau-Climent, JC Losa, R Alonso-Sanz. Cellular automaton simulation of the quantum Hotelling game with reservation cost. Quantum Inf Process 20, 227 (2021).

[2] Zhang, X., Sun D., Ma S., Zhang S.: The dynamics of a quantum Bertrand duopoly with differentiated products and heterogeneous expectations. Phys. A 557, 124878 (2020)

[3] Hui Li, Jiangfeng Du, and Serge Massar. Continuos-Varianle Quatum Games. Physics Letters A 306, 73-78 (2002)

[4] Alonso-Sanz, R., Losada J.C., Porras, M. Bifurcation and Chaos in the Logistic Map with Memory. Int. J. Bifurcation and Chaos 27, 19 (2017).

Dynamic properties in a collisional model of a confined quasi-two-dimensional granular mixture

Ricardo Brito[1], Rodrigo Soto[2] and Vicente Garzó[3],
[1]Departamento de Estructura de la Materia, Física Térmica y Electrónica and GISC, Universidad Complutense E-28040 Madrid, Spain,
[2]Departamento de Física, Universidad de Chile, 8370449 Santiago, Chile,
[3]Departamento de Física and ICCAEx, Universidad de Extremadura, E-06006 Badajoz, Spain

Granular mixtures are usually modelled as a mixture of smooth inelastic hard spheres of masses m_i, diameters σ_i, and coefficients of normal restitution α_{ij} $(i,j = 1,2,\cdots,s)$. Here, s means the number of components or species of the mixture. Since the total kinetic energy of the mixture decreases in time, in order to maintain the system in rapid flow conditions an external energy input is needed to inject energy into the system and compensate for the energy dissipated by collisions. When both mechanisms cancel each other, the system achieves a steady nonequilibrium state. The injection of energy can be done, for instance, by vibrating walls or by bulk driving as in air-fluidized beds. However, given that this way of supplying energy develops in most cases strong spatial gradients, the theoretical description of the above situations is quite complex. Thus, to avoid this problem, it is common in theoretical and computational works to inject energy into the system by the action of external driving forces or *thermostats*. A remarkable observation is that the transport properties of granular systems depend not only on the mechanical properties of the grains but also on the thermostating method. An alternative to the use of thermostats has been proposed in the last few years: the so-called Δ-model [1] where the thermostat is a collisional one since energy is injected in every collision. To be more precise, in a binary collision between particles of species i and j, apart from the usual terms appearing in the collision rules, an extra *constant* velocity Δ_{ij} term is added to the normal component of the relative velocity of the two colliding spheres. Thus, in a binary collision, the change in kinetic energy is constituted by two terms: (i) a dissipation energy term proportional to $1-\alpha_{ij}^2$ and (ii) two energy injection terms with intensity depending on Δ_{ij}. The Δ-model has been mainly proposed to study dynamic properties of granular systems confined in quasi-two-dimensional geometries.

At a kinetic level, the relevant information on the state of the system is provided by the knowledge of the one-particle velocity distribution functions $f_i(\mathbf{r},\mathbf{v};t)$. For moderate densities and in the absence of external forces, the distributions f_i of the Δ-model verify the set of coupled Enskog kinetic equations

$$\frac{\partial}{\partial t}f_i+\mathbf{v}\cdot\nabla f_i=\sum_{j=1}^{s}J_{ij}[f_i,f_j], \tag{1}$$

where J_{ij} is the Enskog collision operator of the Δ-model [2]. Our main objective here is to solve Eq. (1) by means of the Chapman–Enskog (CE) method for states with small spatial gradients. This allow us to determine the Navier–Stokes transport coefficients of the confined quasi-two-dimensional granular mixture. Before doing it, as a first step we analyze the homogeneous state state (HSS). The study of this state is crucial since its *local* version is the reference state in the Chapman–Enskog solution. As expected, our solution shows that the partial temperatures T_i of each species (measuring its mean kinetic energy) in the HSS are different and hence, energy equipartition is broken down.

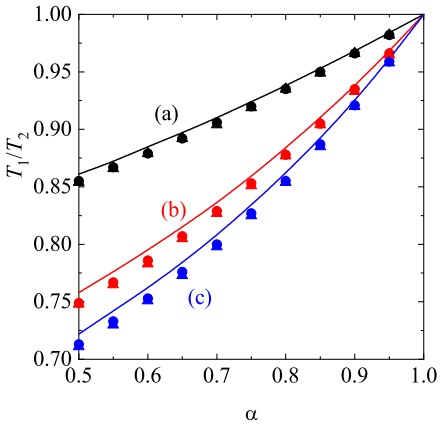

Fig. 1. Plot of T_1/T_2 versus α for $m_1/m_2=\sigma_1/\sigma_2=1$, $\Delta_{22}=\lambda\Delta_{11}$, and $\Delta_{12}=(\Delta_{11}+\Delta_{22})/2$. Here, $\lambda=2$ (a), $\lambda=5$ (b), and $\lambda=10$ (c). Circles are DSMC results while triangles refer to MD simulations for a volume fraction $\phi=0.01$.

As an illustration, Fig. 1 shows T_1/T_2 as a function of the (common) coefficient of restitution $\alpha_{ij}\equiv\alpha$ for a binary mixture ($s=2$). It is quite apparent that the temperature ratio is clearly different from 1, showing the lack of energy equipartition. We also observe a good agreement between the (approximate) theoretical results (based on the use of Maxwellian distribution to estimate the partial cooling rates) and computer simulations.

Once the HSS is characterized, the next step is to solve Eq. (1) for states near to the HSS. As said before, this solution can be obtained by the application of the CE method. Explicit forms for the diffusion transport coefficients, the shear viscosity coefficient, and the coefficients associated with the heat flux are explicitly obtained in terms of the parameter space of the system by assuming steady state conditions and by considering the leading terms in a Sonine polynomial expansion [3]. As an application, the violation of the Onsager reciprocical relations is quantified.

[1] R. Brito, D. Risso, and R. Soto, Phys. Rev. E **87**, 022209 (2013).

[2] R. Brito, R. Soto, and V. Garzó, Phys. Rev. E **102**, 052904 (2020).

[3] V. Garzó, R. Brito, and R. Soto, Phys. Fluids **33**, 023310 (2021).

Collective behaviour of energy depot repulsive particles

Juan Pablo Miranda[1,2], Demian Levis[1,3], and Chantal Valeriani[2,4]

[1] Departament de Física de la Materia Condensada, Universitat de Barcelona, Martí i Franquès 1, 08028 Barcelona, Spain
[2] Departamento de Estructura de la Materia, Física Térmica y Electrónica, Universidad Complutense de Madrid, 28040 Madrid, Spain
[3] UBICS University of Barcelona Institute of Complex Systems, Martí i Franquès 1, E08028 Barcelona, Spain
[4] GISC-Grupo Interdisciplinar de Sistemas Complejos, 28040 Madrid, Spain

In this work we consider an active particle model, that reproduces the motion of microscopic biological objects, such as cells or bacteria, that is described with Langevin dynamics. The particles are able to take energy from their environment, store it into an internal energy depot and convert it into kinetic energy [1]. This model uses a velocity dependant friction function [2]. We have studied a two dimensional suspension of repulsive particles, where the interaction between the particles is implemented with a WCA potential.

$$\dot{\mathbf{v}} = -\gamma(\mathbf{v})\mathbf{v} - \frac{1}{m}\boldsymbol{\nabla} U(\mathbf{r}) + \mathcal{F}(t)\ , \tag{1}$$

$$\gamma(\mathbf{v}) = \gamma_0 - \frac{q_0 d_2}{c + d_2 \mathbf{v}^2}. \tag{2}$$

The parameters q_0, d_2 and c express the properties of the energy depot. The pump rate of energy from the environment into the internal depot is q_0. d_2 is The rate of conversion of the internal depot energy to the particles kinetic energy, this implies that the particle is self propelling. c represents the internal dissipation, which takes into account the energy loss due to intern dissipative processes. In our study we fix the parameters d_2, and c, and we study the effect of different q_0 values.

The friction function will cancel at some velocity v_0, $\mathbf{v}_0^2 = \frac{q_0}{\gamma_0} - \frac{c}{d_2}$, this imposes two regimes onto the system; when $\mathbf{v} > \mathbf{v}_0$ the friction will be positive and the motion is damped. When $\mathbf{v} < \mathbf{v}_0$ we have negative friction, meaning that the motion of the slow particles is pumped as if the particles had an additional source of energy.

We have studied both dynamical and structural features of the system. So far we have studied the diffusion through the mean squared displacement, finding different regimes as we increase q_0 (Fig. 1). The main studied structural feature is a phase transition between an ordered an a disordered state for different volume fractions φ and values of q_0 (Fig. 2).

The interest of this model comes from the fact that its able to mimic several properties of the biological microscopic matter, as self propulsion, colective motion or out of equilibrium phase transitions. The interest in the model comes from the difference from other models such as Vicsek's or Active Brownian Particles, that address self-propulsion as a random process, while here the friction is the cause of this phenomenon.

[1] Schweitzer, F., Ebeling, W., & Tilch, B. (1998). Complex motion of Brownian particles with energy depots. Physical Review Letters, 80(23), 5044.

[2] Erdmann, U., Ebeling, W., Schimansky-Geier, L., & Schweitzer, F. (2000). Brownian particles far from equilibrium. The European Physical Journal B-Condensed Matter and Complex Systems, 15(1), 105-113.

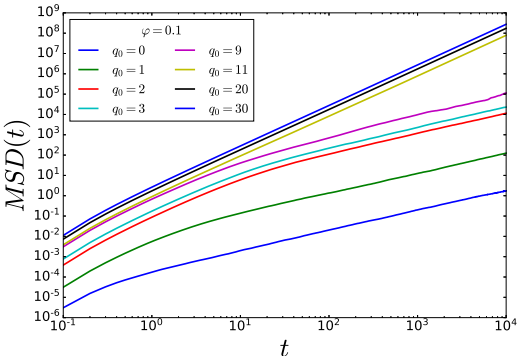

Fig. 1. Mean squared displacement over time for different systems of $\varphi = 0.1$ and different values of q_0.

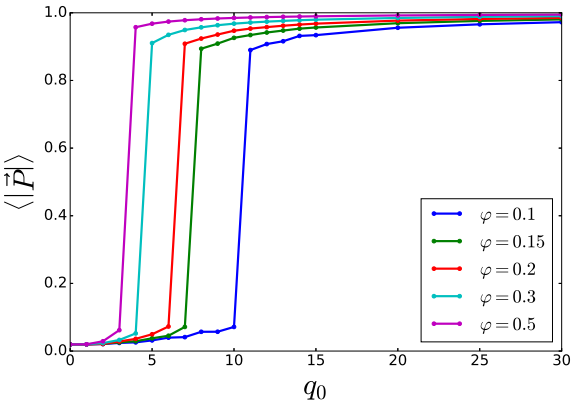

Fig. 2. a) Mean polar order parameter as a function of q_0 parameter for the studied volume fractions φ.

Lagrangian betweenness and bottlenecks in ocean flow networks

Enrico Ser-Giacomi[1], Alberto Baudena[2], Vincent Rossi[3], Mick Follows[1],
Sophie Clayton[4], Ruggero Vasile[5,6], Cristóbal López[7] and Emilio Hernández-García[7]
[1]Department of Earth, Atmospheric and Planetary Sciences, MIT, Cambridge, USA.
[2]Sorbonne Université, Institut de la Mer de Villefranche-sur-Mer, France.
[3]Mediterranean Institute of Oceanography (UM110, UMR 7294), Marseille, France. [4]Old Dominion University, Norfolk, VA, USA.
[5]UP Transfer GmbH, Potsdam, Germany. [6]GFZ German Research Centre for Geosciences, Potsdam, Germany.
[7]IFISC (CSIC-UIB), Instituto de Física Interdisciplinar y Sistemas Complejos, Palma de Mallorca, Spain.

The study of connectivity in networks has brought insights across many fields ranging from neurosciences to epidemic spreading or climate. One of the classical network measures, betweenness centrality, has demonstrated to be very effective in identifying nodes that act as focus of congestion, or bottlenecks. Outside the network framework, however, there is no obvious way to define betweenness. Nevertheless, the concept of bottleneck is equally present in dynamical systems and in fluid flows as in networks (see Fig. 2).

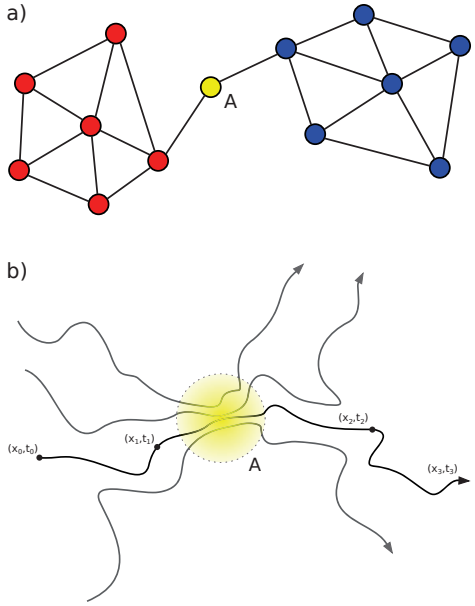

Fig. 1. Regions marked as *'A'* have large betweenness in the network of panel a), and also in the dynamical system or fluid flow in b), representing in both cases a *bottleneck*.

By using ideas that relate dynamical systems and network theory [1], we have provided a trajectory-based formulation of betweenness, called Lagrangian betweenness [2], which is computed in terms of Lyapunov exponents. This extends the concept of betweenness beyond network theory and relates hyperbolic points and heteroclinic connections in dynamical system to the structural bottlenecks of the flow network associated with it.

We illustrate the use and meaning of the Lagrangian betweenness by identifying bottlenecks in ocean surface flows in the Adriatic sea or the Kerguelen region in the Southern Ocean. Also, by analyzing plankton abundance data from the Kuroshio region in the Pacific Ocean, we find significant spatial correlations between measures of biological diversity and betweenness, suggesting that ocean bottlenecks act as ecological hot spots.

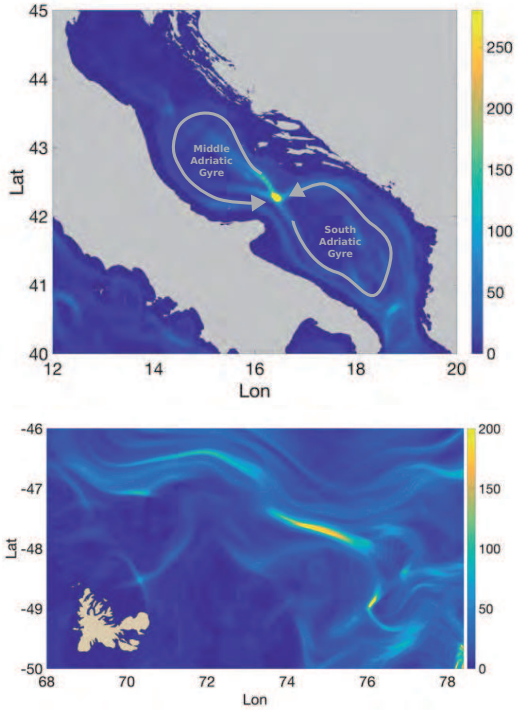

Fig. 2. Two examples of betweenness field in the Adriatic sea (upper panel) and in the Kerguelen region (lower panel). Large values (yellow color) identify flow bottlenecks.

[1] E. Ser-Giacomi, V. Rossi, C. López, and E. Hernández-García, *Flow networks: A characterization of geophysical fluid transport*, Chaos **25**, 036404 (2015).

[2] E. Ser-Giacomi,A. Baudena, V. Rossi, M. Follows, S. Clayton, R. Vasile, C. López and E. Hernández-García, *Lagrangian betweenness as a measure of bottlenecks in dynamical systems with oceanographic examples*, Nature Communications **12**, 4935 (2021).

Retirado después de la edición de este libro

Maximum in density of electrolyte solutions: learning about ion-water interactions and testing force-fields

L. Fernández-Sedano[1,2], S. Blazquez[1], E. G. Noya[2], C. Vega[1], and J. Troncoso[3]
[1]Dpto. Química Física I (Unidad Asociada de I+D+i al CSIC), Fac. Ciencias Químicas,
Universidad Complutense de Madrid, 28040 Madrid, España.
[2]Instituto de Química Física Rocasolano, Consejo Superior de Investigaciones Científicas,
(CSIC) Calle Serrano 119, 28006 Madrid, España.
[3]Dpto. Física Aplicada, Universidad de Vigo, Facultad de Ciencias del Campus de Ourense, E 32004, Ourense, España

In this work we studied the effect of Li^+, Na^+, K^+, Mg^{2+} and Ca^{2+} chlorides and sulfates on the temperature of maximum density (TMD) of aqueous solutions at room pressure. Experiments at 1 molal salt concentration were carried out to determine the TMD of the solutions. For density measurements below -15° C, the Sorensen methodology was adopted [1]. We also performed molecular dynamics simulations to estimate the TMD of these solutions at 1 m and 2 m with the Madrid-2019 force field [2], which uses the TIP4P/2005 water model [3] and scaled charges for the ions. Some of the results of this work are displayed in Fig. 1. Our experiments at room temperature are consistent with those from Laliberte [4] and the prediction of both the maximum in density and the TMD from simulations is in excellent agreement with our experimental results.

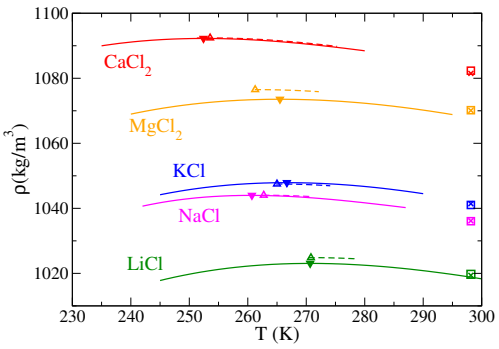

Fig. 1. Density for various chloride solutions at 1 m as a function of temperature at room pressure. Solid lines: simulations for the Madrid-2019 model. Dashed lines: experiment. Values of the TMD: empty up triangles (experimental results from this work) , filled down triangles (simulations). Density at room temperature from experiments : crosses (results from Ref. [4]) ; empty squares (results from this work).

All the salts studied in this work shift the TMD of the solution to lower temperatures and flatten the density profile (when compared to pure water) with increasing salt concentration. The shift in the TMD (Δ) depends strongly on the nature of the electrolyte. Despretz established a linear dependence of Δ with the salt concentration (in molality) as early as 1840 [5]. We hereby confirm that the Despretz law holds for all the salts considered here at least up to 1 m. In order to further explore this shift in the TMD, we have evaluated the contribution of each ion to Δ (from the experimental results), concluding that Na^+, Ca^{2+} and SO_4^{2-} seem to induce the largest changes among the studied ions. We have proved that these group contributions are able to accurately predict the shift in TMD for 1 m mixtures.

Finally, the volume of the system has been analyzed for salts with the same anion and different cation. These curves provide an insight into the effect of different ions upon the structure of water. We conclude that for those ions with a strong coordinated first layer, namely Li^+ and Mg^{2+} (where water is not just coordinating the cation but forming a complex), the remaining water molecules accommodate in an expanded structure resulting from the configurations they adopt to enable hydrogen bonding with the "rigid" water molecules from the first solvation shell. We therefore claim that the TMD of electrolyte solutions entails interesting physics regarding ion-water and water-water interactions and should then be considered as a test property when developing force fields for electrolytes. This matter has been rather unnoticed for almost a century now and we believe it is time to revisit it.

[1] D. E. Hare and C. M. Sorensen, J. Chem. Phys. **87**, 4840 (1987).

[2] I. Zeron, J. L. F. Abascal and C. Vega, J. Chem. Phys. **151**, 134504, (2019).

[3] J. L. F. Abascal and C. Vega, J. Chem. Phys. **123**, 234505, (2005).

[4] M. Laliberte and W. E. Cooper, J. Chem. Eng. Data **49**, 1141 (2004).

[5] M. C. Despretz, Ann. Chim. Phys. **70**, 49 (1839); **73**, 296 (1840).

Magnetic particles at fluid interfaces as actuated units for the construction of Stokesian and non-Stokesian carriers.

Fernando Martínez Pedrero[1], José Martín Roca[2], Chantal Valeriani[2], Francisco Ortega[1], Ramón González Rubio[1], and Carles Calero [3]

[1] Departamento de Química Física, Universidad Complutense de Madrid, Avda. Complutense s/n, Madrid 28040, Spain
[2] Departamento de Estructura de la Materia, Física Térmica y Electrónica, Universidad Complutense de Madrid, 28040 Madrid, Spain
[3] Departament de Fisica de la Matèria Condensada, Universitat de Barcelona, 08028 Barcelona, Spain

Due to the large surface energy reduction linked to the adsorption of colloids at a fluid interface, these particles are often used as stabilizing units in the formation of highly stable complex interfacial fluids, Pickering emulsions, foams and colloidosomes, as well as in the characterization of interfacial microrheological properties or in the study of different phenomena, ranging from the study of 2D phase transitions to transport in the low Reynolds number regime under confined geometries. In this presentation we will show how magnetic microparticles suspended in aqueous solutions can be used in accurate and directed transport at a fluid interface by developing Stokesian and non-Stokesian strategies. In Stokesian designs, magnetic particles are dynamically assembled on interfacial micromotors or conveyor belts, which are driven by the remotely controlled generation of local hydrodynamic flows[1], while in non-Stokesian counterparts, adsorbed and non-adsorbed particles are driven by traveling magnetic potentials generated by lattices or rails of adsorbed colloids [2]. In the last part of this talk, we will show how tracking the rotational-translational mechanism undergone by these particles, when under the influence of a rotating field, yields information on the kinetics and dynamics of particle adsorption in the presence of electrolytes or anionic and cationic surfactants.

[1] F. Martínez Pedrero, A. González-Banciella, A. Camino, A. Mateos-Maroto, F. Ortega, R.G. Rubio, I. Pagonabarraga and C. Calero, *Static and Dynamic Self-Assembly of Pearl-Like-Chains of Magnetic Colloids Confined at Fluid Interfaces*, Small **17**, 2101188 (2021).

[2] F. Martínez Pedrero, F. Ortega, R.G. Rubio, and C. Calero, *Collective Transport of Magnetic Microparticles at a Fluid Interface through Dynamic Self-Assembled Lattices*, Advanced Functional Materials **30**, 2070333 (2020).

Unraveling the Role of Node Metadata in Network Robustness: the Feature-Based Percolation Model

Oriol Artime[1], and Manlio De Domenico[2]
[1]Bruno Kessler Foundation, Via Sommarive 18, 38123 Povo, Italy
[2]Department of Physics and Astronomy, University of Padua, Via F. Marzolo 8, 35131 Padua, Italy

Percolation is an emblematic model used to understand the robustness of interconnected systems. Despite being a model broadly studied in statistical physics and mathematics, from a theoretical perspective it is usually investigated in relatively simple scenarios, such as the removal of the system's units in random order —simulating unpredictable site failures— or sequentially ordered simulating targeted attacks by specific topological descriptors, the simplest one being the number of node connections. However, in the vast majority of empirical applications, it is required to dismantle the network following more sophisticated protocols than the aforementioned ones, such as based on more convoluted topological properties or even non-topological node metadata obtained from the application domain.

In this work we propose a novel mathematical framework to fill this gap: a network is enriched with features and its nodes are then removed according to their importance in the feature space. Percolation analysis is performed, theoretically and numerically, as a function of the feature distribution, finding an excellent match between the analytical results and the simulations. Several degree-feature relations of diverse nature are explored to show the applicability of the theory. We start from ad hoc degree-feature distributions that capture the main characteristics of correlations observed in empirical systems, moving to features that arise naturally in the process of network creation and ending with the case in which features are coupled to dynamical processes running on top of the network, such as epidemics or biochemical dynamics, among others. Both synthetic and real-world networks of different nature are considered in the analysis. Moreover, we show the potential of our model by employing state-of-the-art Bayesian probability techniques that are able to give the most plausible closed-form expression for the degree-feature distribution when it cannot be computed analytically. By feeding these most plausible expressions into the equations of our model, we can study feature-based percolation in systems for which it is only known the feature and the degree of the individual nodes, instead of the entire degree-feature joint probability distribution (see Fig. 1). This considerably broadens the applicability of the theory and bridges our theory, grounded on statistical physics, with Bayesian machine learning techniques suitable for knowledge discovery.

The article has been recently published in *Percolation on feature-enriched interconnected systems*, Nature Communications, **12**(1), 1-12 (2021).

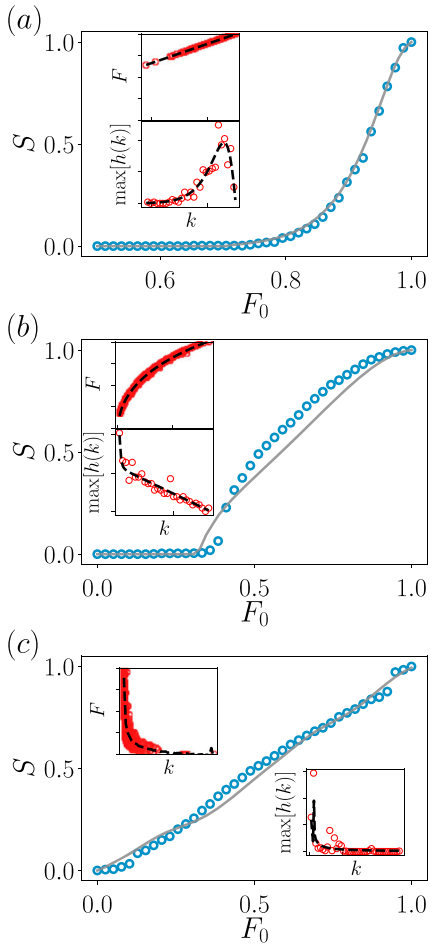

Fig. 1. Percolation curves for (a) mutualistic dynamics in symbiotic ecosystems, (b) population dynamics and (c) mass-action kinetics in biochemistry (solid lines are the theory, points are simulations). F_0 is a parameter of the feature distribution, S is the size of the giant component (order parameter of the phase transition). The insets are different variables fitted using machine-learning techniques that are necessary to compute S. The dynamical equations are not given due to space constrains. All dynamics are simulated in empirical networks.

Non-Markovian random walks characterize network robustness to non-local cascades

Angelo Valente[1], Manlio De Domenico[2], and Oriol Artime[3]
[1]Department of Mathematics, University of Trento, Via Sommarive 14, 38123 Povo, Italy
[2]Department of Physics and Astronomy, University of Padua, Via F. Marzolo 8, 35131 Padua, Italy
[3]Bruno Kessler Foundation, Via Sommarive 18, 38123 Povo, Italy

Understanding the interplay between structure and dynamics is still one of the major challenges in network science. A central question concerns the robustness of a system against perturbations, since it can advance the development of powerful analytical techniques to explain and unravel rich phenomenology, as well as it can provide a solid ground for informed interventions.

A main assumption behind the analysis of robustness is that for a system to be functional, it needs to be connected. Hence, concepts and techniques from percolation theory become useful and are frequently employed. This is a completely static approach, where a fraction of nodes (or links), either selected uniformly at random or based on topological or non-topological descriptors, is removed from the network. From a dynamical point of view, small failures placed in the network may evolve —according to some rules that depend on the phenomenon one is trying to model— causing system-wide catastrophic cascades. For the sake of mathematical tractability, cascades are assumed to spread via direct contacts. However, be it because the physical mechanisms behind the failure propagation permit far-off malfunctions, be it because the knowledge on the observed network topology is incomplete and the failure propagates through hidden or unobserved edges, real-world cascades display non-local features. From a modeling standpoint, some mechanisms like flow redistribution can lead to non-local spreading of failures but the mathematical treatment has been hitherto under-researched due to its sophistication and there is no direct way to control the underlying properties of the non-local events, seriously undermining our understanding of the phenomenon.

To better reconcile theory and observations, we propose a dynamical model of non-local failure spreading that combines local and non-local effects. We assume that the cascade unfolds in a timescale much faster than the recovery of nodes, and that a disrupted unit cannot be visited more than once by the failure. This fact causes the failure to be no longer Markovian and, for modeling purposes, a natural choice is to consider a Self-Avoiding Random Walk-like (SARW) dynamics on the network. To cope with the non-locality, we introduce a teleporting probability: at each step t the failure proceeds as in a SARW —uniformly choosing an operational neighbor and transitioning there— with probability $1-\alpha \in [0,1]$, otherwise with probability α it teleports to any operative node according to a teleporting rule $T_t(k)$, time- and degree-dependent. We name this the self-avoiding teleporting random walk (SATRW), which interpolates between percolation (purely non-local process, $\alpha = 1$) and the growing SARW (purely local process, $\alpha = 0$).

We have characterized the rich critical behavior of our model by providing analytical expressions for several quantities employed to assess the systems robustness, such as the time-dependent degree distribution $p_t(k)$, the size of the giant component in the residual network as the process evolves s_t, the cascade first-stop time distribution, and the mean value of $S^{(\mathrm{STOP})}$, the giant component at the cascade stop. These robustness descriptors display an excellent agreement with simulations in synthetic systems characterized by different types of complexity in terms of the heterogeneity of their structural connectivity. We find remarkable differences between homogeneous and heterogeneous systems, e.g., their dependence, or lack thereof, on the particular network parameters. However, we also report some hidden similarities between them, such as a dynamical version of the popular *robust-yet-fragile* feature to static attacks. It is worth noticing that, despite our framework is expected to work for locally tree-like networks lacking topological correlations, such as degree-degree ones, it still works in empirical settings as we have shown for the case of a biomolecular system, namely the interactome of the nematode *C. elegans*, and an infrastructural system, namely a national air traffic network, shown in Fig. 1.

Our findings provide a solid ground for the analytical study of network robustness, in particular, and for non-local non-Markovian processes, in general. The article is currently under review.

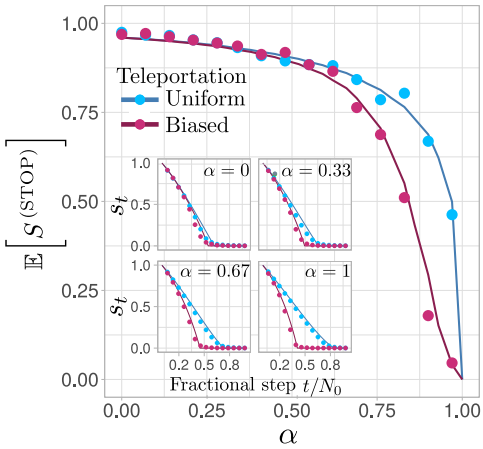

Fig. 1. Expected value of size of the giant component at the cascade stop as a function of the teleportation parameter α for the air traffic network. In the insets, evolution of s_t as a function of the fractional time t/N_0, for different values of α. Solid lines come from theory, markers from simulations. Two type of teleporting rules are shown.

A framework for self-organized explosive percolation and synchronization

S. Faci-Lázaro[1,2], L. Arola[3], P. S. Skardal[4], E. C. Boghiu[5], À. Arenas[3] and J. Gómez-Gardeñes[1,2]

[1] GOTHAM Lab, Instituto de Biocomputación y Física de Sistemas Complejos (BIFI), Universidad de Zaragoza, 50018 Zaragoza, España [2] Departamento de Física de la Materia Condensada, Universidad de Zaragoza, 50009 Zaragoza, España

[3] Departament d'Enginyeria Informática i Matemátiques, Universitat Rovira i Virgili, 43007 Tarragona, Catalonia, Spain

[4] Department of Mathematics, Trinity College, Hartford, CT 06106, USA

[5] ICFO - Institut de Ciències Fotòniques, The Barcelona Institute of Science and Technology, 08860 Castelldefels (Barcelona), Spain

Abrupt and explosive phase transitions are one of the most important results in Statistical Physics and in Complex Networks of the last few decades. They are found when the interactions between the elements of the network are coupled with their structural properties. Furthermore, these transitions exhibit drastic and unanticipated consequences that make them an emerging paradigm for modeling real-world systems ranging from social networks or epidemics to nanotubes [1].

The examples more commonly studied are the Explosive Percolation (EP) [2] and the Explosive Synchronization (ES) [3] transition. For both these transitions, the explosive or abrupt nature of the transitions arises from the delay of their critical point. This delay is achieved by introducing correlations between the links of the network and functions of its local structure. Its important to mention that, without this delay of the critical point, both these transitions are smooth and second order transitions.

Our objective in this work is the development and derivation of a rule or set of rules that allow a system to display an explosive behavior in the percolation transition as well as in the synchronization transition.

With this aim in mind, let us consider a system of N nonidentical Kuramoto oscillators running on top of a network. The equations of motion are given by

$$\dot{\theta}_i = \omega_i + \lambda \sum_{j=1}^{N} A_{ij} \cdot \sin(\theta_i - \theta_j), \qquad (1)$$

where θ_i is the phase of the i–th oscillator, ω_i is its natural frequency and is given by a distribution $g(\omega)$ such that $\langle\omega\rangle = 0$. A_{ij} are the entries of the adjacency matrix $\mathbf{A}$, capturing the interactions between oscillators and λ is the strength of their coupling. The macroscopic behavior of the system is captured by the modulus of the Kuramoto order parameter:

$$r(t) = \frac{1}{N}\left|\sum_{n=1}^{N} e^{i\cdot\theta_n(t)}\right| \text{ and } r = \langle r(t)\rangle, \qquad (2)$$

which measures the degree of synchronization of the system and is bounded between zero and one.

Now, with a series of assumptions such as: (*i*) the system tends to maximize the synchronization, (*ii*) we have limited information, *i.e.* the process is decentralized, (*iii*) the percolation is adiabatic compared to the synchronization and (*iv*) the system is closed to the synchronization attractor; we are able to derivate a rule for the order in which the links of the network have to be added (removed) that delays the critical point of the percolation and the synchronization transition. This rule is adding (removing) the link (p, q) that maximizes the magnitude

$$\Delta r_{p,q} = \frac{\pm 1}{\lambda^2 N}\left(\frac{\omega_p}{k_p} - \frac{\omega_q}{k_q}\right)\left(\frac{\omega_p}{k_p^2} - \frac{\omega_q}{k_q^2}\right). \qquad (3)$$

As we observe in Fig. 1 this rule effectively delays the critical points of both transition, allowing them to display hysteresis.

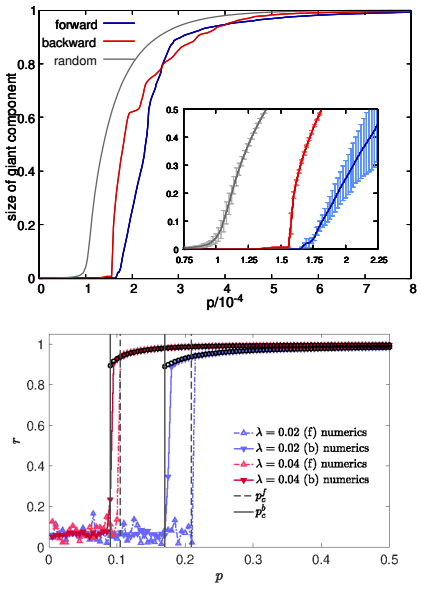

Fig. 1. Percolation and synchronization transitions for a uniform distribution of natural frequencies, $g(\omega)$. Top: Abrupt percolation transition of our system. It can be seen how the critical points of both the forward and backward process are delayed, compared to the random process. Bottom: Explosive synchronization transition of our system. It can be appreciated how the transition, well known to be of second order without any rule, now displays a discontinuity in which the parameter r jumps from $r \approx 0$ to $r \approx 1$ for the forward process and vice versa for the backward process. Black lines correspond to the theoritical predictions for the synchronization thresholds.

[1] R. M. D'Souza, J. Gmez-Gardees, . Arenas and J. Nagler *Advances in Physics* **68**, 3, 123 - 223 (2019).

[2] R. M. D'Souza and J. Nagler, *Nature Physics* **11**, 531 - 538 (2015).

[3] J. Gmez-Gardees, S. Gmez, A. Arenas and Y. Moreno *Physical Review Letters* **106**, 128701 (2011).

The Biased voter model: How persuasive a small group can be?

Agnieszka Czaplicka[1], Christos Charalambous[2],Raul Toral[2], and Maxi San Miguel[2]
[1]Centre for Humans and Machines, Max Planck Institute for Human Development, Berlin, Germany.
[2]Instituto de Fsica Interdisciplinar y Sistemas Complejos IFISC (CSIC-UIB), 07122 Palma de Mallorca, Spain

In this work, we study a variation of the classical voter model, where voters have a biased constant confidence. To have confidence, means that with a constant probability p they keep their opinion upon an interaction with their neighbor, instead of copying. We assume that the default confidence is $p = 1/2$. However for a fraction γ of these voters we assume that are biased towards a fixed opinion, in the sense that their confidence when changing from a fixed state, say $s_i = -1$ to $s_i = +1$ is given by $p = (1+v)/2$ with v being the bias parameter, while the reverse switch $s_i = +1$ to $s_i = -1$ occurs with a confidence equal to $p = (1 - v)/2$. This setup resembles that of [1], where however all voters were biased and only interactions on a complete graph (CG) were studied. We considered two distinct scenarios in our studies. First, we assumed that there was no dependence of the topology of the network on which the dynamics took place and the type of voters, in which case we studied the model on the CG as well as on an Erdős-Rényi (ER) network. Then we assumed that the topology of interactions of the two distinct type of voters was indeed dependent on their type and we examined strategies that the biased voters could follow to convince faster the rest of the voters to adopt their opinion.

For the biased-independent topology of interactions, we initially focused the study on the thermodynamic limit of the system for both the complete graph as well as the Erdős-Rényi (ER) network. In both cases, by considering the relevant Fokker-Planck equations, we showed that in general, at the long time limit, contrary to the standard voter model, the magnetization is not constant, but rather tends to $m = 1$, with an active link density $\rho = 0$. This happens at a time of the order of $\frac{1}{\gamma v}$.

Moving beyond this, we considered the finite size effects. To solve the dynamics in the case of the CG we resorted to a mean field approach, where for the ER case we made use of the pair approximation. In addition, for the ER case, we made an adiabatic approximation, i.e. we assumed that the magnetization's dynamics were slowly changing in comparison to that of the active link density and hence the latter followed the dynamics of the former. This allowed us to obtain the dependence of the active link density on the magnetization. We focused mainly on two observables, the fixation probability $P_1(\sigma)$, or probability to reach the preferred state at a finite number of steps, and the consensus time $\tau(\sigma)$ for which we derive analytical expressions. In particular for the ER case, we obtain specifically, for the fixation probability $P_1 = \frac{1}{1+e^{-\tilde{\beta}/2}}$, where $\tilde{\beta} = 2\gamma v N$ for the CG and $\tilde{\beta} = 2\gamma v \frac{\mu}{1+\mu} N$ for the ER network, with N being the number of voters. Furthermore, we find that for the special case of balanced initial condition $\sigma = 1/2$ and sufficiently large N the time to reach consensus, τ scales as $\tilde{B}\log(N)/(\gamma v)$ for both the CG and the ER network, where $\tilde{B} = 1$ for the former and $\tilde{B} = \frac{\mu-1-\gamma v}{\mu-2}$ for the latter. This is to be contrasted to the case of the classical voter model where for both the CG and the ER network scales linearly with N [2].

Finally, we also study the case where the voters lie on biased-dependent heterogeneous Erdős-Rényi networks. In this case, we defined as the parameter that quantifies our deviation from the homogeneous random network, the ratio $\delta = \frac{\mu_{BB}}{\mu_{UU}}$, where μ_{XY} represents the average degree of connections between voters of type X to voters of type Y. With this in mind we identified two candidate total average degree μ preserving strategies with which one can affect the time to consensus by varying δ. In strategy I we considered the case of varying μ_{BU} at the expense of μ_{BB} and μ_{UU}. We found that the consensus time is indifferent to this variation. On the contrary in strategy II we considered the scenario of varying μ_{BB} (and accordingly μ_{UU}) while keeping μ_{BU} constant. We found that increasing μ_{BB} resulted in a significant reduction of the consensus time τ, as well as to a significant increment to the probability of reaching consensus to the preferred state. The main conclusion of our studies is then that the more endogamous a community of biased voters is, where we define an endogamous community as one where its members have a higher average degree compared to that of the rest of the members of the ER network, the faster it can lead the rest of the society to agreement to their preferred state.

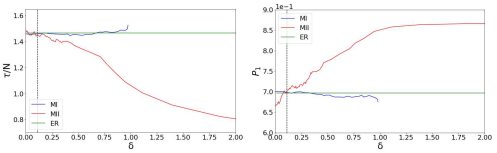

Fig. 1. In the left (right) figure, the green line represents the consensus time (fixation probability) obtained analytically for a homogeneous ER network of a given average degree μ. In both figures, the blue (red) line represents for the same μ, the scenario of the dynamics on a biased-dependent heterogeneous ER where δ varies and provokes topology changes according to model I (II). The dashed line is the value δ_{random} for the homogeneous topology scenario. The main result, is that for model II a significant decrease (increase) in consensus time (fixation probability) is observed. This is the strategy, in terms of the topology of interactions, that the small group has to follow to convince the rest of the society faster. Here $N = 1000$, $\gamma = 0.1$, $v = 0.01$ and $\sigma_0 = 0.5$

[1] N. Masuda, N. Gibert and S. Redner, *Heterogeneous voter models* (Physical Review E, 82(1):010103, 2010).

[2] F. Vazquez and V. M. Eguluz, *Analytical solution of the voter model on uncorrelated networks* (New Journal of Physics, 10(6):63011, 2008).

Translocation and degradation of repeat proteins by the protease ClpXP

Pierpaolo Bruscolini[1], Alejandro Sáinz [2]

[1]Dep. de Física Teórica & BIFI, Universidad de Zaragoza
[2]Dep. de Física de la Materia Condensada, Universidad de Zaragoza

ClpXP is a protease included in the AAA+ family in charge of the unfolding, translocation and degradation of certain tagged proteins inside cells of several organisms in the bacterial kingdom, proving fundamental in the mainteinment of equilibrium inside them [1]. This task is accomplished through the binding and subsequent hydrolization of ATP.

The protease itself is divided into two different subunits, each of them in charge of different parts of the overall degradation process: these are ClpX, an hexameric ring that leads to the unfolding and translocation of proteins it comes in contact with, and ClpP, an heptameric chamber in which the proteins are translocated to in order to be degraded back into aminoacids.

The way in which ClpXP differentiates itself from other AAA+ proteases comes in the fact that it does not present a continuous work output leading of a progressive translocation process; the protease works on a series of dwell and burst phases, the latter being characterized by sudden decreases on the length of the protein [2].

In this work we aim to build a time-discrete probabilistic model that correctly describes the dynamics of the protease, ranging from the ATP binding and hydrolization to the degradation processes observed in experiments, taking as a base the widely known WSME model [3, 4] and considering the following Hamiltonian:

$$\mathcal{H}^{(1,n)}(m_i) = -T\sum_{i=1}^{n} q_i(1-m_i) + \sum_{i<j}^{n} h_{ij}\prod_{k=i}^{j} m_k \quad (1)$$

In which n is the length of protein remaining outside ClpXP, and its characterized by enthalpic and entropic contribution to its stability, marked by h_{ij} and q_i.

The results of the model regarding ATP consumption rates and time taken for the degradation of different repeat proteins will then be compared to their experimental counterparts.

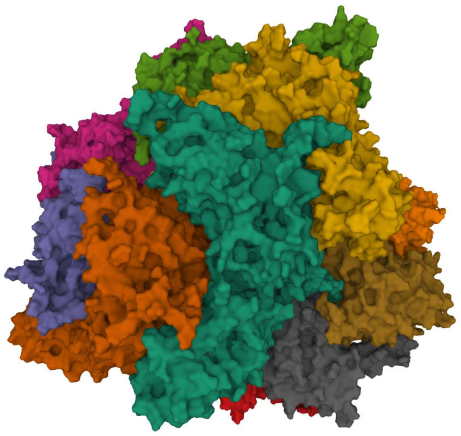

Fig. 1. ClpXP protease (6PO3).

[1] J. C. Cordova, A. O. Olivares, Y. Shin, B. M. Stinson *et al. Stochastic but highly coordinated protein unfolding and translocation by the clpxp proteolytic machine.*, Cell. **158**, 2014

[2] M. Sen, R. A. Maillard, *et al*, *The clpxp protease unfolds substrates using a constant rate of pulling but different gears.* , Cell. **155**, 2013.

[3] H. Wako and N. Sait, *Statistical mechanical theory of the protein conformation. i. general considerations and the application to homopolymers.*, JPSJ. **44**, 1931-1938, 1978

[4] A. Pelizzola and M. Zamparo, *Nonequilibrium dynamics of an exactly solvable ising-like model and protein translocation*, EPL. **102**, 2013.

Mechanochemical symmetry breaking in gastruloids

Torregrosa G.[2]*, Oriola D.[1]*, Trivedi V.[1]†, and Garcia-Ojalvo J.[2]†
[1]European Molecular Biology Laboratory (EMBL), Barcelona Biomedical Research Park (PRBB), Spain
[2]Department of Medicine and Life Sciences, Universitat Pompeu Fabra, Barcelona Biomedical Research Park (PRBB), Spain

Multicellular animals are a paradigm of self-organization, especially during their developmental stages. The sophistication of this self-organization has led to the proposal of multiple alternative mechanisms to achieve the timing, precision, and patterning required for developing their complex structures. These mechanisms range from communication through chemical components [1] to mechanical interactions [2], both with other cells and with their environment. Disentangling the spontaneous self-organization mechanisms used during development is still a challenge [1].

In recent years, gastruloids have been developed as a novel *in vitro* model to study self-organization during development [5]. In contrast with *in vitro* cell cultures, these biological models offer the possibility of studying self-organization in 3D: gastruloids are closer to the actual topology in which multicellular organisms develop. Moreover, they are easier to control experimentally than embryos.

In this work, we study theoretically and experimentally the process of symmetry breaking in the expression of a gene, specifically the mesodermal transcription factor Brachyury, in mouse gastruloids. This process establishes the initial coordinate axis that defines the anterior-posterior organization of the future embryo (head-tail). A quantitative study of single-cell RNA expression of the gastruloid cells provides information of the transcriptional paths at play during the decision. In this process, the cells start to maturate from the pluripotent state, expressing specific genetic pathways to a new fate marked by the gene Brachyury (Figure 1). This transition occurs during the initial 24h of development. We model the process by a master equation describing the jumps between metastable states:

$$\frac{dp_i}{dt} = f_i(p_i; \{p_j\}_{j\neq i}), \tag{1}$$

where $i \in 1, 2, 3$ are the metastable states defined by the transcriptomics data (Figure 1). The model considers that the transition function f_i depends on the existence of interaction between populations, supporting the idea that cell-cell communication is essential to control the proportion between cell types throughout the differentiation process.

Although the master equation approach explains the communication and proportions of cells at the different stages, additional candidate mechanisms for the observed long-range ordering are required. Candidates could be the long-range communication of diffusible chemicals, such as the ones underlying Turing patterning or wave pinning [1], or the aggregating effect of differential adhesion [2]. Lacking evidence of highly diffusible compounds and given the experimental evidence of different adhesion properties of the cell aggregates, we model the segregation with an agent-based model that takes into account differential adhesion between cells (Figure 2).

* Equal contribution.
† Equal contribution.

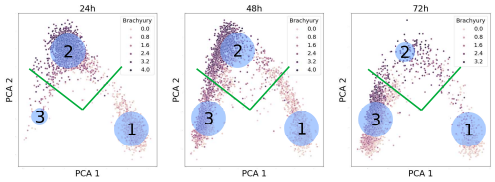

Fig. 1. Principal component projection of the single-cell RNA transcriptome. 1) Pluripotent state 2) Brachyury state 3) Posterior stages.

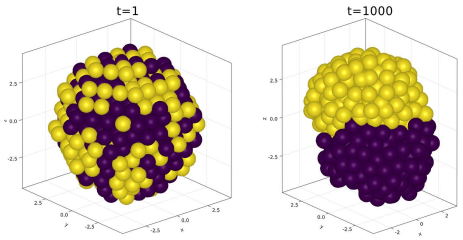

Fig. 2. Agent-based simulation exhibiting phase separation between cells in an *in silico* gastruloid, driven by active forces and differential adhesion between two populations.

The combination of the chemical communication and mechanical segregation recapitulates the generation of the Brachyury pole in gastruloids. These results pave the way towards understanding the processes underlying symmetry breaking in multicellular organisms.

[1] Green, J. B., & Sharpe, J. (2015). Development, 142(7), 1203-1211.

[2] Muncie, J. M., Ayad, N. M., Lakins, J. N., Xue, X., Fu, J., & Weaver, V. M. (2020). Developmental cell, 55(6), 679-694.

[3] Flenner, E., Janosi, L., Barz, B., Neagu, A., Forgacs, G., & Kosztin, I. (2012). Physical Review E, 85(3), 031907.

[4] Stumpf, P. S., Smith, R. C., Lenz, M., Schuppert, A., Mller, F. J., Babtie, A., ... & MacArthur, B. D. (2017). Cell Systems, 5(3), 268-282.

[5] Van den Brink, S. C., Baillie-Johnson, P., Balayo, T., Hadjantonakis, A. K., Nowotschin, S., Turner, D. A., & Martinez Arias, A. (2014). Development, 141(22), 4231-4242.

Self-diffusion of spherocylindrical particles flowing under non-uniform shear rate

D. Hernández-Delfin[1], T. Weinhart[2], and R.C. Hidalgo[3]

[1]BCAM - Basque Center for Applied Mathematics, Mazarredo, 14 E48009 Bilbao, Basque Country, Spain.
[2]Multiscale Mechanics, Department of Thermal and Fluid Engineering, Faculty of Engineering Technology, MESA+ University of Twente, P.O. Box. 217, 7500 AE Enschede, The Netherlands.
[3]Departamento de Física y Matemática Aplicada, Universidad de Navarra, P.O. Box. 177, E-31080 Navarra, Spain.

This work numerically studies the self-diffusion of spherocylindrical particles when flowing down an inclined plane. This system is challenging due to particles being non-spherical and because they are subjected to a non-uniform shear rate. We perform simulations for several aspect ratios and inclination angles, tracking the particle trajectories. Using the simulation data, we compute the diffusion coefficients D, and a coarse-graining methodology allowed accessing the shear rate spatial profiles $\dot{\gamma}(z)$. It enables us identifying the spatial regions where the diffusivity fully correlates with the local shear rate $\dot{\gamma}(z)$. Introducing an effective particle size $d_\perp$, we propose a well-reasoned scaling law between D and $\dot{\gamma}$. Our analysis also identifies specific locations where the diffusivity does not correlate with the shear rate. This observation corresponds to zones where $\dot{\gamma}(z)$ has non-linear spatial variation, and the velocity probability density distributions exhibit asymmetric shape. Moreover, examining the velocity correlations, we obtain that the correlation length l_ξ is not constant, resulting shorter l_ξ values close to the bottom plane and higher l_ξ close to the free surface. Although our scaling analysis does not involve the particle correlation length l_ξ, our finding suggests that collective movement might play a crucial role in the self-diffusive dynamics.

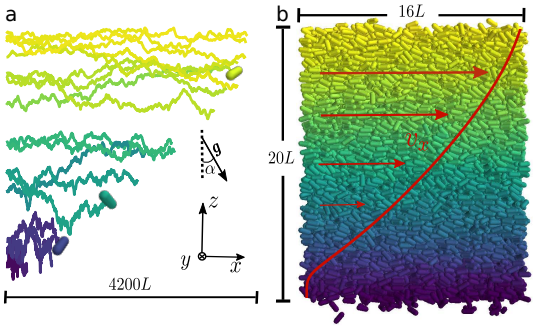

Fig. 1. a) Trajectories of twenty randomly chosen particles after reaching the steady regime. b) Snapshot of the numerical setup; the red curve indicates the mean value of the x-component of the velocity profile along the z-direction, $\bar{v}_x(z)$. The figures correspond to the case $\xi = 2.5$ and $\alpha = 31.0$ degrees. The color of the particle quantifies the magnitude of its v_x. Note that gravity has an angle α to the vertical direction, representing a slope with an angle of elevation of α degrees.

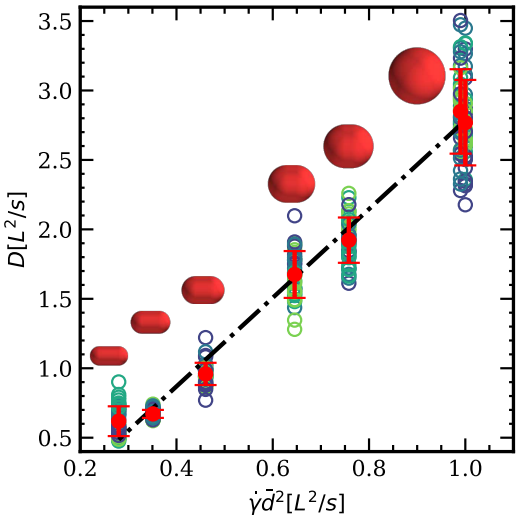

Fig. 2. Ratio of diffusion coefficient and shear rate, $D/\dot{\gamma}$, plotted against the square of the characteristic particle length $d_\perp^2$ for all inclinations α and elongations ξ. The red points are the mean values of all $D/\dot{\gamma}$ for each ξ, and the error bars indicate the standard deviation thereof. The black line represents the resultant linear fit. For all ξ values, a representation of the particle is illustrated.

[1] R. C. Hidalgo, B. Szabó, K. Gillemot, T. Börzsönyi, and T. Weinhart, "Rheological response of nonspherical granular flows down an incline" *Phys. Rev. Fluid.* 3, 074301 (2018)

[2] D. Hernández-Delfin, T. Weinhart and R.C. Hidalgo "Self-diffusion of spherocylindrical particles flowing under non-uniform shear rate" submitted to *Soft Matter*, (January 2022)

Analysis of the blackout risk reduction when segmenting large power systems using HVDC lines

Damià Gomila[1], Benjamín A. Carreras[1,2], José M. Reynolds-Barredo[2], Pere Colet[1], and Oriol Gomis-Bellmunt[3]
[1]Instituto de Física Interdisciplinar y Sistemas Complejos, IFISC (CSIC-UIB), Palma, Spain.
[2]Universidad Carlos III, Madrid, Spain
[3] Electrical Engineering Department, Universitat Politècnica de Catalunya, Barcelona, Spain.

Large electrical transmission networks are susceptible to undergo very large blackouts due to cascading failures. For instance, in 2003, a blackout in Italy produced by a cascading failure affected 55 million consumers. Despite this risk, the typical power system engineering planning approach has been for decades to build the largest possible networks. Recent studies suggest, however, that it would be beneficial to segment them [1, 2]. As a matter of fact, Ref. [1] suggests that there is an optimal size in terms of security and risk. Small power systems are more vulnerable but very large power systems can have huge blackouts with an extraordinary large associated cost. The trend to segment power systems has already started in China, where the Yunnan zone has been segmented from the main synchronous system where it was connected, to reduce the risk of a cascading blackout [3]. Several studies are considering the option of applying similar measures in Europe or North America [2]. The concept of segmentation is based on the idea of dividing a large alternate current (AC) synchronous area by introducing high voltage direct-currel (HVDC) lines to interconnect smaller asynchronous zones. HVDC allows to exchange power between the segmented zones while preventing the spread of severe disturbances thanks to active and reactive power control capability of converters.

In this work we propose a method to segment power systems using HVDC lines to reduce the risk of blackouts. The blackout risk is estimated using the ORNL-PSerc-Alaska (OPA) model [4, 5]. The OPA model is based on a combination of fast and a slow dynamics. The first describes the cascading failures while the second the grid evolution through line and generation upgrades as a respond to failures and demand growth. This way the model brings the power grid continuously to a critical state where random failures may trigger cascading blackouts. The sizes and frequency of the obtained blackouts can then be used to estimate the overall blackout risk of the network. The method to segment grids, like the one shown in Fig. 1a), consists in controlling the power flowing through HVDC lines during cascading failures in order to minimize the load shed of each blackout. As a result, the segmented grids have a substantially lower risk of blackouts than the original network (Fig. 1b). The control method is shown to work efficiently if the network is segmented in zones of similar size.

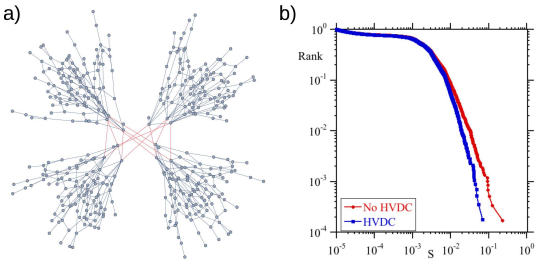

Fig. 1. a) Segmented network constructed by interconnecting four 100-nodes zones with three HVDC lines between each pair of zones (red lines). b) Rank function of the normalized size of the blackouts (S) for the 4x100 network using standard AC lines to interconnect zones (red symbols) and using controllable HVDC lines (blue symbols). A reduction in the probability of large blackouts is clearly appreciated.

[1] B. A. Carreras, D. Newman, and I. Dobson, *Does size matter?*, Chaos **24** 023104 (2014).

[2] P. Fairley, *Time to Rightsize the Grid?*, IEEE Spectrum (2014).

[3] P. Fairley, *Why Southern China Broke Up Its Power Grid*, IEEE Spectrum (2016).

[4] B. A. Carreras, V. Lynch, I. Dobson, and D. Newman, *Complex dynamics of blackouts in power transmission systems*, Chaos **14** 643–652 (2004).

[5] I. Dobson, B. A. Carreras, V. E. Lynch, and D. E. Newman, *Complex systems analysis of series of blackouts: Cascading failure, critical points, and self-organization*, Chaos **17** 026103 (2007).

Emergence, survival and segregation of competing gangs

H. Pérez-Martínez[1,2], F. J. Bauzá[2,3], D. Soriano-Paños[2,4], J. Gómez-Gardeñes[1,2,5] and L. M. Floría[1,2]
[1]Department of Condensed Matter Physics, University of Zaragoza, 50009 Zaragoza (Spain).
[2]GOTHAM lab, Institute for Biocomputation and Physics of Complex Systems (BIFI), University of Zaragoza, 50018 Zaragoza (Spain).
[3]Department of Theoretical Physics, University of Zaragoza, 50009 Zaragoza (Spain).
[4]Institute Gulbenkian of Science (IGC), 2780-156 Oeiras (Portugal).
[5]Center for Computational Social Science, University of Kobe, 657-8501 Kobe (Japan).

In this work, we approach the phenomenon of criminal activity from an infectious perspective by using compartmental agent-based models, building on a recently introduced kinetic model [1, 2] on the dynamics of norm violating (corrupt) behavior. Specifically, we focus on addressing how the existence of two competing gangs shapes the penetration of crime in society. The model, named HCCO because of their compartments' names (see Figure 1a), features a unique mechanism inherent to the social process of delation, by which the recovery of Corrupt (infected) agents is mediated by interaction with their Honest (susceptible) neighbors, reaching an Ostracism (recovered) state. Moreover, we consider that both gangs openly compete (delate each other).

The mean-field analysis of the model reveals the existence of different equilibria as a function of the delation mechanism of the honest population. While non-selective delation always leads to the extinction of the minority gang, the introduction of selective delation, reducing the probability that honest agents delate the minority gang, leads to a coexistence regime. As a result of the inter-gang delation events, the latter choice turns into a convenient strategy, resulting in a lower penetration of crime than in the former scenario.

However, the implementation of the model in networked populations with homogeneous contact patterns, both by Markov equations and Monte Carlo simulations, reveals that the evolution of crime substantially differs from that predicted by the mean-field equations (see Figure 1b). We find that the system evolves towards segregated configurations between gangs where agents' surroundings deviate from the well-mixed scenario. Moreover, in networks with spatial structure, this segregation plays a major role, leading to the emergence of two disjoint macroscopic clusters of criminals, each one associated with a gang, as seen in Figure 2. The size of these clusters, quantified with the inter-gang distances, is large enough to impair the cross-delation events resulting in a higher penetration of crime in the population, and thus explaining the important differences found with respect to the mean-field predictions.

In general terms, our analysis reveals that the interplay of the network structure, the competition between spreading units (criminal gangs) and the strategy chosen to control their diffusion (delation mechanism) crucially shapes the outcome of the dynamics. Our framework constitutes the first steps towards a formal characterization of the evolution of crime via compartmental models. In this sense, we think that this model lays the foundation for the ellaboration of a more complete formalism including more realistic features inherent to corruption such as the lack of reinsertion of certain individuals and social stigma.

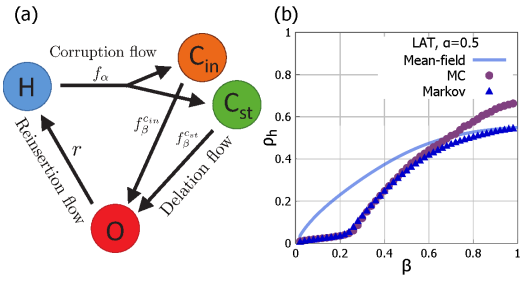

Fig. 1. (a) Compartmental scheme and flows of the HCCO model. (b) Fraction of honest population in a lattice in the gang coexistence situation, for $r = 0.5$ and corruption probability $\alpha = 0.5$, as a function of the delation probability β. We compare the mean-field, Markov and Monte Carlo (agent based) simulations. Substantial differences between the three scenarios can be seen.

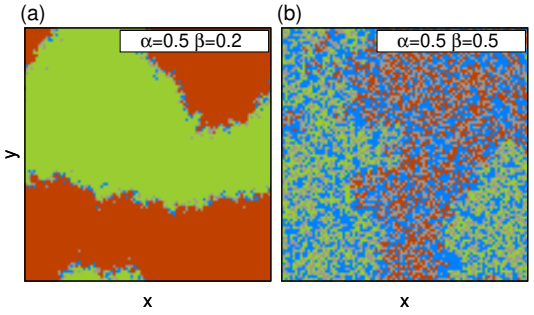

Fig. 2. Lattice configurations corresponding to Monte Carlo simulations of the HCCO model. The four species are shown: Honest (blue), C_{in} gang (green), C_{st} gang (orange) and Ostracism (grey), and segregation between both corrupt species can be clearly seen. Configurations correspond to $\alpha = 0.5$, $\beta = 0.2$ (a) and $\alpha = 0.5$, $\beta = 0.5$ (b).

[1] D. Lu, F. Bauzá, D. Soriano-Paños, J. Gómez-Gardeñes and L.M. Floría, Phys. Rev. E **101**, 022306 (2020).

[2] F. Bauzá, D. Soriano-Paños, J. Gómez-Gardeñes, and L.M. Floría, Chaos **30**, 063107 (2020).

Chirality landscape in mixtures of active spinners

Miguel Ángel López-Castaño[1], Álvaro Rodríguez-Rivas[2] and Francisco Vega Reyes[1]
[1]Departamento de Física and Instituto de Computación Científica Avanzada (ICCAEx),
Universidad de Extremadura, 06071, Badajoz, Spain
[2]Department of Physical, Chemical and Natural Systems, Pablo de Olavide University, 41013, Sevilla, Spain

In our work we study the fundamental properties of the dynamics in a binary mixture of active 3D-printed spinners. We have fabricated two sets of rotors provided with blades, these two sets are identical except for the fact that they have opposite natural spins (due to inverse blade tilt angles). The system is fluidized by a tunable air flow one clockwise, in this way, particles are provided with continuous rotation, so that one species spins clockwise (CW) and the other counter-clockwise (CCW). Moreover, turbulent streamlines generated by the upflow past the disks also provide them with Brownian-like translational motion [1].

Fig. 1. Picture of two 3D-printed particles, the natural spinning direction is indicated with arrows. We have printed them in different colors to tell them apart with our computer-vision tracking algorithms.

We performed a set of experiments with varying molar fractions of each component, at constant global density. As the first panel in Figure 2 shows, the trend of fluid vorticity vs. translational kinetic energy is opposite for each species, this confirming that fluid chirality is closely related to particle dynamical asymmetries (chirality), here substantiated by particle spin. Moreover, in close analogy with the mono-component system, we found that the system typically undergoes a regime with a complex and unstable mixture of multiple chiral vortexes as relative density approaches $1/2$. When the system achieves this kind of state, global vorticity approaches zero and the fluid flow appears as non-chiral [1]. This is very relevant since it demonstrates that a fluid of chiral particles does not necessarily develop a chiral flow.

More interestingly, a phase diagram of global vorticity vs. average kinetic energy and relative particle density shows that this kind of null global vorticity states occupy significant areas of the parameter space, as shown in the second

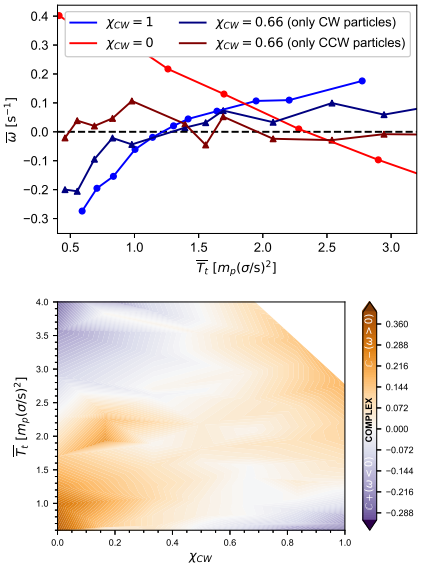

Fig. 2. First panel shows the chirality transition for the two monodisperse cases plus another set of experiments with $2/3$ of the particles having a natural CW spin and $1/3$ CCW; in that case, vorticity can be calculated for each species, displaying a different slope. The second panel is the chirality phase map. The sense of chiral motion (sign of $\overline{\omega}$) is indicated by a color gradient, orange means CW global motion ($\overline{\omega} > 0$), white, $\overline{\omega} = 0$, being the complex phase and purple meaning CCW motion. The y-axis represents mean kinetic energy (controlled by the air flow velocity) and χ_{CW} is the molar fraction of disks with CW natural spin: $\chi_{\mathrm{CW}} = N_{\mathrm{CW}}/N$

panel of Figure 2.

In our presentation, we will analyze in more detail this and other aspects of this system, such as mixing and segregation conditions.

[1] López-Castao, M. A., Seco, A. M., Seco, A. M., Rodríguez-Rivas, ., & Reyes, F. V. (2021). Chirality transitions in a system of active flat spinners. Retrieved from http://arxiv.org/abs/2105.02850

Rotations and translations are correlated in a two-dimensional chiral fluid of active particles

M. A. López-Castaño[1], A. Márquez Seco[1], A. Márquez Seco[1],
A. Rodríguez-Rivas[3] and F. Vega Reyes[1,2*]
[1]Departamento de Física, Universidad de Extremadura, 06071, Badajoz, Spain
[2] Instituto de Computación Científica Avanzada (ICCAEx), Universidad de Extremadura, 06071, Badajoz, Spain
[2]Department of Physical, Chemical and Natural Systems, Pablo de Olavide University, 41013, Sevilla, Spain
∗ email: fvega@eaphysics.xyz

Chiral fluids have recently received much attention, mainly because they are ubiquitous in important biological processes, and their dynamics is specially relevant in transport mechanisms at the cellular level (see [1] and references therein). These chiral fluids are usually composed of particles with some kind of geometric or dynamic asymmetry, which breaks the system symmetry under parity and temporal inversion, i.e., they are composed of particles whose geometrical/dynamical configuration has *chirality* [1].

Moreover, the conventional hydrodynamic theory of fluids does not describe the complex behavior observed in chiral fluids. For instance, a whole new set of transport coefficients emerges in these fluids, generically termed as *odd* (diffusion, viscosity…) [2].

We demonstrate in this work, by means of a theoretical analysis, that translations and rotations are intrinsically correlated in the experimental data we obtained. Furthermore, their correlations essentially determine the hydrodynamics of chiral fluids in such a way that the global vorticity sign (particle chirality yields chiral flow and hence global fluid vorticity can be non-null, contrary to standard fluid convection) mimics the sign of a specific cumulant of the distribution function that we named *bend coefficient*, in close analogy with glassy systems. As we will explain in our presentation, the distribution function first 4 cumulants (that characterize deviations out of the equilibrium distribution function) can be defined as

$$
\begin{aligned}
a_{20}^{(0)}(r) &= \frac{1}{2}\left(\frac{1}{2}\frac{\langle V^4\rangle}{\langle V^2\rangle^2} - 1\right), \\
a_{02}^{(0)}(r) &= \frac{1}{2}\left(\frac{1}{2}\frac{\langle W^4\rangle}{\langle W^2\rangle^2} - 1\right) \\
a_{11}^{(0)}(r) &= \frac{1}{2}\left(\frac{\langle V^2W^2\rangle}{\langle V^2\rangle\langle W^2\rangle} - 1\right), \\
a_{00}^{(b)}(r) &= \frac{3}{2}\frac{\langle(\mathbf{v}\times\mathbf{w})\cdot\hat{\mathbf{e}}_\varphi\rangle}{\sqrt{\langle V^2\rangle\langle W^2\rangle}}.
\end{aligned}
\tag{1}
$$

Where W, V denote particle angular and translational peculiar velocity (i.e., measured with respect to their corresponding average [1]), respectively, and $\hat{e}_\varphi$ the unit vector in the azimuthal direction. The bend coefficient is $a_{00}^{(b)}$. Additionally, the ratio between translational and rotational global average kinetic energies, $\overline{T}_t/\overline{T}_r^*$, also plays an important role in the chiral flow phase behavior [1].

We acknowledge funding from the Government of Spain (AEI) and Junta de Extremadura through projects No. PID2020-116567GB-C22) and GR21091 respectively. A.R.-R. also acknowledges financial support from Conserjera de Transformacin Econmica, Industria, Conocimiento y Universidades (Junta de Andalucía) through post-doctoral grant no. DC 00316 (PAIDI 2020), co-funded by the EU Fondo Social Europeo (FSE).

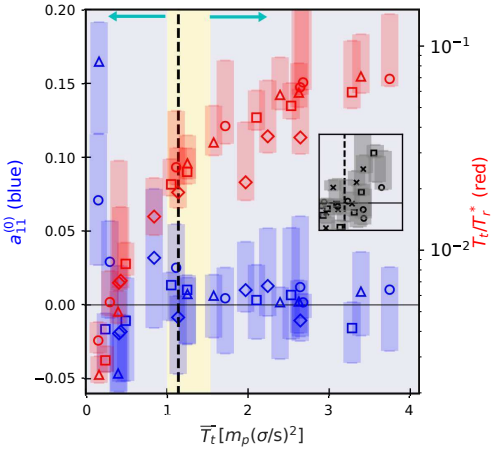

Fig. 1. (a) Particle velocity-spin correlations, vs. $\overline{T_t} \equiv \langle T_t\rangle_r$, as measured from the cumulant $a_{11}^{(0)} = \frac{1}{2}\left(\frac{\langle V^2W^2\rangle}{\langle V^2\rangle\langle W^2\rangle} - 1\right)$ (blue series, left Y axis), and the ratio $\overline{T}_t/\overline{T}_r^*$ (red series, right Y axis). Inset represents cumulant $a_{00}^{(b)}$ (dark grey color). The error bars of series of $a_{11}^{(0)}$, $\overline{T}_t/\overline{T}_r^*$ and $a_{00}^{(b)}$ points are highlighted in blueish, reddish and grey backgrounds respectively. The transition interval in $\overline{T_t}$, with complex chirality, is highlighted in yellow; a dashed line marks the chirality transition point T_c. Magnitudes are measured in different annuli of the system, each annulus marked with a different symbol: ○ : 0.49 σ, △ : 1.47 σ, : 2.45 σ, ◇ : 3.43 σ for $a_{11}^{(0)}$ and $\overline{T}_t/\overline{T}_r^*$ and ○ : 0.87 σ, : 2.62 σ, × : 4.36 σ for $a_{00}^{(b)}$; area fraction is $\phi = 0.25$. Yellow region marks the transition of the global vorticity sign (which we observed to be continuous), and as we see coincides with the sign reversal of the bend coefficient.

[1] M. A. López-Castaño and A. Márquez Seco and A. Márquez Seco and A. Rodríguez-Rivas and F. Vega Reyes (2022), Chirality transitions in a system of active flat spinners. Preprint: arXiv:2105.02850.

[2] D. Banerjee and A. Souslov and A. G. Abanov and V. Vitelli, *Nat. Commun.* **8** 1573 (2017).

Unraveling the highly non-linear dynamics of the KCN molecular system by using Lagrangian descriptors

F. Revuelta[1], F. J. Arranz[1], R. M. Benito[1], and F. Borondo[2,3]
[1]Grupo de Sistemas Complejos, Universidad Politécnica de Madrid, av. Puerta de Hierro 2-4, 28040 Madrid, Spain
[2]Departamento de Química, Universidad Autónoma de Madrid, Cantoblanco, 28049 Madrid, Spain
[3]Instituto de Ciencias Matemáticas (ICMAT), Cantoblanco, 28049 Madrid, Spain

The mathematical objects currently known as Lagrangian descriptors [1, 2] have shown their usefulness in different applications to the dynamics of non-linear systems. Particularly, their usefulness has also been shown in the study of non-linear molecular systems, as in the case of the LiCN molecule [3, 4].

For a mechanical system with $N/2$ degrees of freedom, the Lagrangian descriptors are defined as follows,

$$M_{\pm}(\mathbf{z}_0; p, \tau) = \pm \sum_{k=1}^{N} \int_0^{\pm\tau} |\dot{z}_k(t)|^p \, \mathrm{d}t, \qquad (1)$$

where $\mathbf{z} = (z_1, \ldots, z_N)$ is the vector formed by the $N/2$ position variables and their corresponding conjugate momenta, such that, Lagrangian descriptors are a function which depends on the initial condition $\mathbf{z}_0$ and two fixed parameters, the exponent p ($0 < p < 1$) and the integration time τ ($\tau > 0$). For the exponent, we have taken the value $p = 0.4$, which has been shown as adequate for other molecular systems [3, 4], whilst for the integration time, the value $\tau = 437.5$ fs has been used, which corresponds to the inverse of the stability exponent of the periodic orbit of interest. Notice that the overall Lagrangian descriptors M, as are defined in the literature [1, 2], are given by the sum of backward M_- and forward M_+ expressions in Eq. (1), namely, $M = M_- + M_+$.

In this contribution, we present the results obtained in the application of the Lagrangian descriptors to the dynamics of a remarkable system: the highly non-linear KCN molecular system. By using a suitable two-dimensional model (considering the motion of the K atom around the CN group), based on *ab initio* calculations for the potential energy function [5], it has been shown the emerging of above saddle-point regions of order in the sea of chaos [6]. Therefore, we have calculated the Lagrangian descriptors, and also the invariant manifolds, corresponding to the hyperbolic fixed point that appears on this interesting saddle-point.

First, in order to verify the optimum value of the integration time, given by the inverse of the stability exponent of the periodic orbit, we will show the Lagrangian descriptors calculated with different values of the integration time, above and below the optimum value.

Next, we will present the (optimal time) Lagrangian descriptors, as well as the invariant manifolds, both represented in a suitable Poincaré surface of section, corresponding to the hyperbolic fixed point of interest, showing a clear correspondence between both representations (see Fig. 1). In both cases, Lagrangian descriptors and invariant manifolds, we can observe the appearance of intriguing loops. We will study in detail the first discontinuity that leads to a one of these closed curves.

Last, in order to understand this interesting behavior, we will present calculations in the three-dimensional phase-space, beyond the dimension of the Poincaré surface of section, showing that the appearance of the closed curves is due to the highly non-linear dynamics of the system. This highly non-linear dynamics causes the twisting and wrinkling of the two-dimensional invariant manifolds, such that, in the crossing with the Poincaré surface, discontinuities and loops appear.

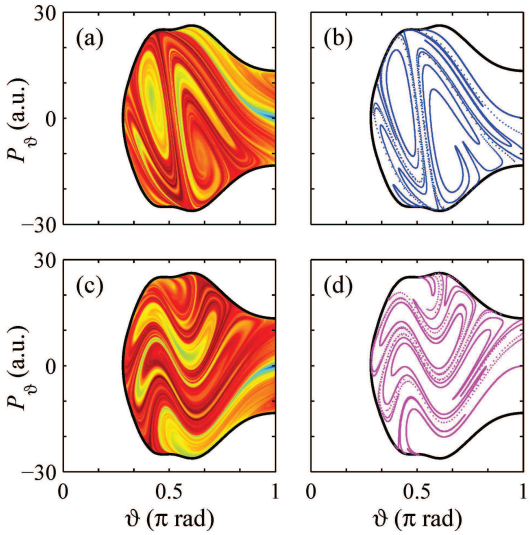

Fig. 1. Lagrangian descriptors computed forward (a) and backward (c) in time, and stable (b) and unstable (d) invariant manifolds, all of them represented in a suitable Poincaré surface of section (ϑ, P_ϑ), corresponding to a hyperbolic fixed point located at $(\vartheta, P_\vartheta) = (\pi, 0)$, with total energy $E = 1300$ cm^{-1}. Note the loops appearing in this Poincaré representation of the invariant manifolds.

[1] J. A. Jiménez-Madrid and A. M. Mancho, Chaos **19**, 013111 (2009).

[2] C. Lopesino, F. Balibrea, S. Wiggins, A. M. Mancho, Commun. Nonlinear Sci. Numer. Simulat. **27**, 40–51 (2015).

[3] F. Revuelta, R. M. Benito, and F. Borondo, Phys. Rev. E **99**, 032221 (2019).

[4] F. Revuelta, R. M. Benito, and F. Borondo, Phys. Rev. E **104**, 044210 (2021).

[5] H. Párraga, F. J. Arranz, R. M. Benito, and F. Borondo, J. Chem. Phys. **139**, 194304 (2013).

[6] H. Párraga, F. J. Arranz, R. M. Benito, and F. Borondo, J. Phys. Chem. A **122**, 3433–3441 (2018).

Isotropic to hexatic fluid transition in untilted phases of fatty acid Langmuir monolayers: a thermo-rheological study

Pablo Sánchez Puga[1], Javier Tajuelo[2], Juan Manuel Pastor[3] and Miguel A. Rubio[1]
[1]Dpto. Física Fundamental, Facultad de Ciencias, UNED, Avda. Esparta s/n, Las Rozas, Spain
[2]Dpto. Física Interdisciplinar, Facultad de Ciencias, UNED, Avda. Esparta s/n, Las Rozas, Spain
[3]Grupo de Sistemas Complejos, ETSIAAB, Universidad Politécnica de Madrid, Madrid, Spain

Two-dimensional (2D) melting is a problem that has attracted the interest of scientists for more than five decades by now. The most accepted theoretical framework is provided by the Kosterlitz-Thouless-Halperin-Nelson-Young (KTHNY) scenario [1, 2, 3] in which a second order phase transition from the crystalline solid to a hexatic phase occurs, driven by dislocation unbinding, followed by a second transition from the hexatic fluid phase to an isotropic fluid phase, driven by disclination unbinding. Interestingly, the hexatic to isotropic fluid transition can be of either first or second order [4].

Experimental confirmations of such scenario have been found in several quite different physical systems. Regarding liquid systems, probably the most detailed confirmations of such scenario have been found in few-layer freely standing films of smectic liquid crystals [5] and colloidal particle laden interfaces [6]. However, most of the experimental and numerical checks of the predictions of KTHNY framework are based on the characterization of structural properties (positional and orientational order being either short or long range). Interestingly, the KTHNY framework contains also predictions regarding the mechanical properties of the 2D system (elasticity and viscosity) and their variations across both transitions, but much less quantitative experimental and numerical investigations are available on this aspect of the problem. Pindak et al. [5] studied the mechanical properties of thin films of smectic liquid crystals and described their changes across a scenario composed of a second order solid to hexatic transition followed by a first order hexatic to isotropic fluid transition with a coexistence region that shrinks upon decreasing the number of layers in the film.

Fatty acid Langmuir monolayers at the air/water interface in condensed states can be considered as the limiting case of single layer smectic films. Langmuir monolayers are one-molecule thick films of an insoluble surfactant spread onto a fluid subphase. Fatty acids at air/water interfaces are among the simplest systems that can form Langmuir monolayers. Despite their apparent chemical simplicity, fatty acid Langmuir monolayers may show a very rich phase behaviour [7, 8].

Phase diagrams of fatty acid Langmuir monolayers obtained structural (GIXD, [7]) and mechanical (interfacial rheometry, [8]) techniques coincide nicely and draw an scenario that we will describe roughly as follows. In high pressure phases (CS, S, and LS phases) the molecules show no tilt regarding the normal to the interface, while lower pressure phases (L2, L2, and L2 phases) the molecules show a well defined tilt with respect to the normal to the interface. Structural [7] and rheological [8] measurements show that the S and LS phases behave as solid and liquid, respectively. Hence, the S-LS transition appear to be a good candidate for a study of 2D melting in fatty acid Langmuir monolayers.

We will report on an experimental study of the S-LS transition in Langmuir monolayers of eicosanoic fatty acid ($C_{20}H_{40}O_2$) at the air/water interface through the measurement of their mechanical (dynamic moduli) and thermodynamic (thermal expansion coefficient) properties under isobaric cooling. The monolayers are, first, isothermally compressed, across the L2-LS transition line, till the desired interfacial pressure is achieved. Then, the pressure is kept constant while the temperature is decreased at a slow rate (typically about 0.1 K/min). Recording the area between the Langmuir trough barriers as a function of T allows to obtain the coefficient of thermal expansion, while the dynamic moduli are measured by means of a magnetic tweezers interfacial shear rheometer [9].

The main findings can be summarized as follows: i) the LS phase response is predominantly viscous and both dynamic moduli decrease upon decreasing the temperatures, ii) in the transition to the S phase there is an abrupt increase of both dynamic moduli although the temperature range in which the viscous modulus is larger than the elastic one is not small, iii) a bump appears in the expansion coefficient for a slightly lower temperature than the transition temperature seen in the dynamic moduli measurements, iv) experiments at different cooling rates show that for a low enough cooling rate there is no hysteresis in the transition temperature. Hence, the transition from the isotropic to the hexatic fluid appears to be second order.

[1] J. M. Kosterlitz and D.J. Thouless, J. Phys. C. **6**, 1181 (1973).

[2] B.I. Halperin and D.R. Nelson, Phys. Rev. Lett. **41**, 121 (1978).

[3] A.P. Young, Phys. Rev. B. **19**, 1855 (1979).

[4] E.P. Bernard and W. Krauth, Phys. Rev. Lett. **107**, 155704 (2011). S.C. Kapfer and W. Krauth, Phys. Rev. Lett. **114**, 035702 (2015).

[5] R. Pindak, W.O. Sprenger, D.F. Bishop, D.D. Osheroff, and J.W. Goodby, Phys. Rev. Lett. **48**, 173 (1982).

[6] K. Zahn and G. Maret, Phys. Rev. Lett. **85**, 3656 (2000). H. H. von Grünberg, P. Keim, K. Zahn, and G. Maret, Phys. Rev. Lett. **93**, 255703 (2004). P. Keim, G. Maret, and H. H. von Grünberg, Phys. Rev. E **75**, 031402 (2007). S. Deutschländer, T. Horn, H. Löwen, G. Maret, and P. Keim Phys. Rev. Lett. **111**, 098301 (2011).

[7] V.M. Kaganer, H. Möhwald, and P. Dutta, Rev. Mod. Phys. **71**, 779 (1999).

[8] J. Tajuelo, E. Guzmán, F. Ortega, R.G. Rubio, and M.A. Rubio, Langmuir, **33**, 4280 (2017).

[9] J. Tajuelo, J.M. Pastor, and M.A. Rubio, J. Rheology, **60**, 1095 (2016).

A two fluid data analysis scheme for the Magnetic needle interfacial shear rheometer (MNISR): the effect of the air drag

Pablo Sánchez Puga[1], Javier Tajuelo[2], Juan Manuel Pastor[3] and Miguel A. Rubio[1]
[1]Dpto. Física Fundamental, Facultad de Ciencias, UNED, Avda. Esparta s/n, Las Rozas, Spain
[2]Dpto. Física Interdisciplinar, Facultad de Ciencias, UNED, Avda. Esparta s/n, Las Rozas, Spain
[3]Grupo de Sistemas Complejos, ETSIAAB, Universidad Politécnica de Madrid, Madrid, Spain

Interfacial shear rheometry data obtained on interfacial systems confined between two bulk fluid phases contain information on the hydrodynamic resistance of both adjacent bulk phases [1, 2]. This contribution may be relatively important depending on the actual value of the Boussinesq number (ratio of interfacial drag and bulk phases drag) [3] and the sensitivity required [4] to study the target interfacial system. Consequently, the two bulk phases contributions must be carefully separated from the total drag to obtain an accurate value of the interfacial rheological variables.

Different approximations have been used in the analysis of the experimental data of the MNISR [5]. In the first approach a linear approximation was used for the interfacial velocity profile and the contributions to the response due to the interface and the rest of the system were considered as simply additive [6]. Sophisticated data analysis schemes were proposed later [7, 8, 9, 10] that rely on an iterative solution of the hydrodynamics equations for just the subphase and the interface, coupled to the probes equation of motion.

However, the data analysis schemes that consider just the subphase and the interface are limited in two fundamental aspects: on the one hand, they cannot deal appropriately with experimental data on interfacial systems confined between two liquid bulk phases that are receiving progressively more attention, and, on the other hand, they cannot account for the drag of the air layer inherent to the most often studied case of air/water interfaces. In fact, the air layer drag must impose a lower threshold in the resolution of the conventional, single bulk phase, data analysis schemes for modern high resolution interfacial rheometers (DWR, MNISR, micro-button).

Here we report on the development of a flow field-based data analysis scheme for the MNISR geometry considering the upper bulk fluid layer. We will illustrate the performance of the data analysis scheme on two bulk fluids interfacial systems, with particular emphasis on the case of air/water interfaces in order to clarify in what conditions the contribution of the upper air phase is relevant. We will show a comparative analysis of the three levels of approximation mentioned, carried out through numerical simulations. We will discuss the different flow configurations obtained as a function of the characteristic length scales [3] and we will illustrate how the operating windows of the MNISR are affected by the air layer drag at low values of the interfacial viscosity.

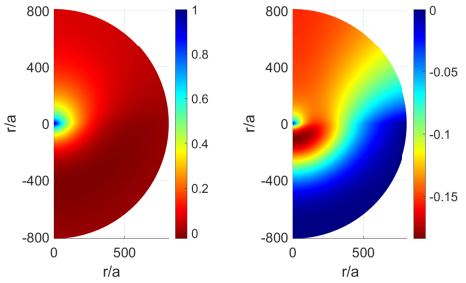

Fig. 1. Color coded graphics of the real (left) and imaginary (right) parts of the hydrodynamic velocity fields for the MNISR geometry with a microwire probe, for a purely viscous interface with interfacial viscosity, $\eta_s^* = 10^{-6}$ N·s/m at an oscillation frequency $f = 0.05$ Hz.

[1] S. Vandebril, A. Franck, G.G. Fuller, P. Moldenaers, and J. Vermant, Rheol. Acta **49**, 131 (2010).

[2] E. Guzmán, J. Tajuelo, J.M. Pastor, M.A. Rubio, F. Ortega, and R.G. Rubio, Curr. Opin. Coll. Interf. Sci. **37**, 33 (2018).

[3] S. Fitzgibbon, E.S.G. Shaqfeh, G.G. Fuller, and T.W. Walker, J. Rheol. **58**, 999 (2014).

[4] D. Renggli, A. Alicke, R.H. Ewoldt, and J. Vermant, J. Rheol. **64**, 141 (2020).

[5] P. Sánchez-Puga, J. Tajuelo, J.M. Pastor, and M.A. Rubio, Adv. Coll. Interf. Sci. **288**, 102332 (2021).

[6] C.F. Brooks, G.G. Fuller, C.W. Frank, and C. Robertson, Langmuir **15**, 2450 (1999).

[7] S. Reynaert, C.F. Brooks, P. Moldenaers, J. Vermant, and G.G. Fuller, J. Rheol. **52**, 261 (2008).

[8] T. Verwijlen, P. Moldenaers, H.A. Stone, and J. Vermant, Langmuir **27**, 9345 (2011).

[9] J. Tajuelo, J.M. Pastor, F. Martínez-Pedrero, M. Vázquez, F. Ortega, R.G. Rubio, and M.A. Rubio, Langmuir, **31**, 1410 (2015).

[10] J. Tajuelo, J.M. Pastor, and M.A. Rubio, J. Rheology, **60**, 1095 (2016).

A reaction-diffusion model for the activity of stem cell-specific transcription factors in *Arabidopsis* roots

Josep Mercadal[1,2], Isabel Betegón-Putze[3], Nadja Bosch[3], Ana I. Caño-Delgado[3], Marta Ibañes[1,2]
[1]Departament de Matèria Condensada, Facultat de Física, Universitat de Barcelona, Barcelona, Spain
[2]Universitat de Barcelona Institute of Complex Systems (UBICS), Barcelona, Spain
[3]Department of Molecular Genetics, Centre for Research in Agricultural Genomics (CRAG), CSIC-IRTA- UAB-UB, Campus UAB (Cerdanyola del Vallès), Barcelona, Spain

Stem cells are one of the fundamental features characterizing complex multicellular organisms. They are distinguished by their capacity for self-renewal, providing precursors of more specialized cell types to build the organism during development, and constitute a reservoir for tissue regeneration upon situations of damage or stress. To these ends, the size of stem cell niches is tightly regulated. Through mathematical modelling and experiments we study the spatial activity of two transcription factors involved in the division of cells within the root stem cell niche of the model plant *Arabidopsis thaliana*, and disclose the mechanisms by which their spatial activity is achieved.

The identity these cells is controlled by both positional signalling and local cues between neighbouring cells, many regulations of which are yet to be uncovered. BRAVO and WOX5 are two transcription factors specifically expressed in the stem cell niche of the primary root, and are known for their role as repressors of stem cell division [1][2]. By combining experimental analysis and mathematical modelling, we recently disclosed regulatory interactions between the two factors, finding that they interplay in a circuit involving the activation of BRAVO by WOX5 and the formation of a transcriptional complex [3]. While WOX5 is only expressed in a small group of cells (called the quiescent center), the expression of BRAVO covers both the quiescent center and part of the vasculature (Figure 1). Interestingly, in loss of function mutants of BRAVO (*bravo-2*), the activity of the BRAVO promoter expands shootwards (Figure 1). This means that in wild-type roots, BRAVO confines its own expression to the stem cell niche, in a mechanism that requires WOX5. Our aim here is to uncover the details behind these mechanisms of self-confinement.

To explain the spatial patterns observed in roots, we introduce a modelling framework based on reaction-diffusion equations, where the regulatory interactions between BRAVO and WOX5, together with diffusion of WOX5, are taken into account. The equations describing these interactions have the form [4]:

$$\frac{dB(x,t)}{dt} = P_B(B,W) - \lambda BW - d_B B$$

$$\frac{dW(x,t)}{dt} = P_W(B,W) - \lambda BW - d_W W + \nabla\left[D_W(x)\nabla W\right]$$

Where P_B and P_W are regulatory functions controlling the production of each factor, λBW represents the irreversible formation of an immobile complex, and $d_B B$, $d_W W$ represent protein degradation. The equations are implemented in a realistic root layout through the explicit spatial dependence of the diffusion coefficient $D_W(x)$, making the system spatially heterogeneous. In particular, $D_W(x)$ takes different values depending on whether the spatial position belongs to the interior of a cell or to the cell wall, thus incorporating the natural boundaries already present in the cellular structure of the root. With this model, we are able to recapitulate the spatial patterns of promoter activities in wild-type and mutant plants (Figure 1).

Altogether, our results propose a mechanism to drive self-confined expression based on the attenuation of a diffusible activator. In the case of BRAVO, attenuation happens through the formation of a complex with WOX5, which prevents its movement and subsequent activation of BRAVO. We expect our results to shed light on the regulatory principles underlying the maintenance of stem cell populations not only in plants, but in multicellular organisms on the whole.

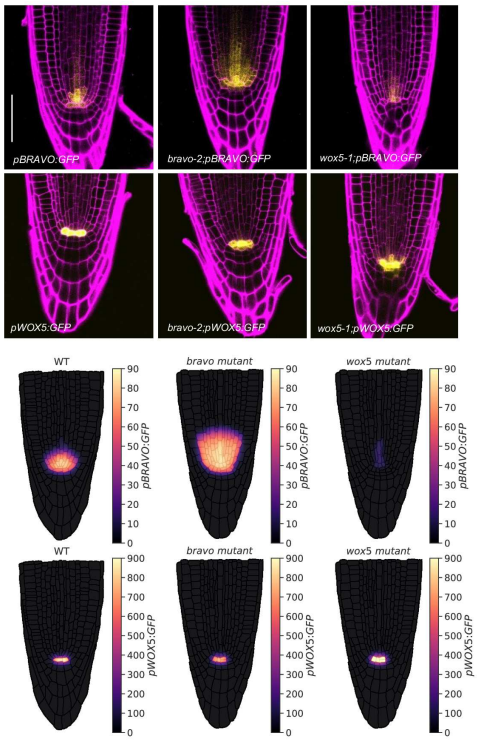

Fig. 1. **Promoter activity of BRAVO and WOX5 in the *Arabidopsis* stem cell niche.** Comparison between experiments (Top) and simulations in a realistic root layout. Images taken and adapted from [3][4].

[1] J. Vilarrasa-Blasi *et al*, Dev. Cell. **30** (1) 36-47 (2014).

[2] C. Forzani *et al*, Curr. Biol. **24** (16) 1939-1944 (2014).

[3] I. Betegón-Putze, **J. Mercadal** *et al*, Mol. Syst. Bio. **17** (6) e9864 (2021).

[4] **J. Mercadal** *et al*, bioRXiv (2021), https://doi.org/10.1101/2021.12.02.468941

High-order interactions promote diversity in productive microbial communities

Jorge Calle-Espinosa[1] and Jaime Iranzo[1]

[1]CBGP (UPM-INIA/CSIC), Campus de Montegancedo, Autopista M-40, Km 38, 28223, Pozuelo de Alarcón, Madrid (Spain)

Understanding the composition and dynamics of microbial communities associated with the human body (collectively known as the microbiome) is essential to comprehend important aspects of human physiology and health. Accordingly, the study of species interactions and their effects on the structure and stability of the microbiome has become a major topic of experimental and theoretical research. A growing body of empirical evidence has revealed that cooperative interactions are widespread across microbial communities and could be a key factor involved in species co-occurrence [1]. However, mathematical models suggest that highly diverse communities can only be stable if competition is the dominant mode of interaction. In particular, results based on generalized LotkaVolterra (gLV) equations show that mutualism destabilizes complex microbiomes, and this effect becomes stronger as the number of species increases [2].

Traditional gLV approaches have two major limitations: they (i) assume zero-growth stationary states, and (ii) exclude interactions involving more than two species (high-order interactions). The zero-growth assumption is not realistic in scenarios where there is sustained growth, such as the gut microbiome or industrial bioreactors, whereas the existence of potentially relevant high-order interactions has been increasingly acknowledged in microbiological studies. To overcome such limitations, we developed a model based on replicator equations with non-lineal fitness and conducted systematic analytical and numerical analyses to determine the effect of high-order interactions, network connectivity, and interaction spectrum (the fraction of mutualistic, exploitative, and competitive interactions) on the stationary composition of a randomly assembled community.

Our simulations show that permanence (the fraction of species that persist in the stationary state) increases with the fraction of exploitative interactions in the initial sample, as well as with the degree of mutualism (if connectivity is high) or competition (if connectivity is low). In the absence of high-order interactions, the replicator-based community dynamics purges most diversity initially present in the set of interactions and favors small clusters of mutualistic species or, if those do not exist, disjoint sets of non-interacting species. In contrast, the addition of high-order interactions allows for coexistence of species involved in a diverse range of ecological relations, which may also include order-2 interactions.

Strikingly, a theoretical examination of the stationary states shows that neither of these characteristics are the underlying determinants of high bio-diversity. In particular it can be demonstrated that for stationary states associated to high bio-diversities to exist, either the mean interactions acting on every species should be similar, or specific relations between the species abundances and the different interaction terms need to be established. Moreover, we found that the changes in the behavior of the system observed when high-order interactions are included are likely the result of a relaxation in the existence conditions for the stationary state of the replicator equations. However, when a mixture of interactions of different orders is considered, the lower order ones tends to dominate the others. Accordingly, we derived an analytical expression for the scaling factor that high-order terms must fulfil to have a qualitative impact in the dynamics of the community.

[1] A. Zelezniak, S. Andrejev, O. Ponomarova, D. R. Mende, P. Bork and K. R. Patil, *Metabolic dependencies drive species co-occurrence in diverse microbial communities*, Proc Natl Acad Sci U S A; **10**, Vol. 112: p. 6449-54. (2015).

[2] K. Z. Coyte, J. Schluter, K. R. Foster, *The ecology of the microbiome: Networks, competition, and stability*, Science **10**, 350(6261):663-6 (2015).

Vanishing protection in a vaccinated population

Michael Stich[1,2]
[1]Universidad Rey Juan Carlos, Dept. MACIMTE, C/ Tulipán s/n, 28993 Móstoles (Madrid)
[2]Aston University, Aston Triangle, Birmingham B4 7ET, Reino Unido

In this contribution, we present a simple epidemiological SIRV (Susceptible, Infected, Recovered, Vaccinated) model designed to analyze the impact of vanishing protection on a vaccinated population. Additionally to the standard processes of infection, recovery and vaccination, a recovered individual can become susceptible again with rate q_1 and a vaccinated individual can become susceptible again with rate q_2. Based on previous work [1], we focus on the study of the similarities of and the differences between the two processes, with respect to the asymptotic states (endemic or disease-free) and to transient solutions (epidemic waves). For open systems (including birth-death processes), we distinguish between vaccination at birth and vaccination of the adult population. Finally, we discuss some recent results on the entropic aspects of the model.

We acknowledge the support of Spanish research project PID2020-116846GB-C22.

[1] E. Grela, M. Stich, A.K. Chattopadhyay, *Epidemiological impact of waning immunization on a vaccinated population*, Eur. Phys. J. B **91**, 267 (2018).

Self-organization and evolution of function and structure in cultured neuronal networks.

L. M. Ballesteros-Esteban [1,2], I. Leyva[1,2], and I. Sendiña-Nadal.[1,2]
[1] Complex Systems Group and GISC, Universidad Rey Juan Carlos, Móstoles 28933, Madrid, Spain
[2] Center for Biomedical Technology, Universidad Politécnica de Madrid, Pozuelo de Alarcón 28223, Madrid, Spain

The study of cultured neuronal networks (CNN) has recently achieved a major relevance as an alternative to *in vivo* models, being a simplified version of the central nervous system while still having a complex self-organization [1,2]. CNNs are a widely used model to analyze both the topological and functional network in the nervous system, helping us to understand the complex relationship between structure and dynamics in neuronal networks and how it changes along the development process of the culture. However this understanding is often limited by the difficulties to resolve the structure of neural networks. Our experimental approach allows us to simultaneously study the detailed structure and dynamics of the cultured network and, therefore to compare the topological and functional networks through the forming process.

We grow CNNs from isolated neurons extracted from *Schistocerca gregaria* (locust) on top of microelectrode arrays (MEA), allowing the recording of their electrophysiological signal (Fig.1) for 14 days. Neurons start to developing connections among them after 3 days in vitro (DIV). We acquire large scale microscope images of the culture from which we obtain the structural networks using a homemade image segmentation algorithm. Simultaneously, we record the electrical time series (25min) from the 120 electrode channels to detect the spikes timestamps. We analyze the spikes pair-wise synchronization events along the series using cross-correlation measures to finally produce the functional network (Fig. 1).

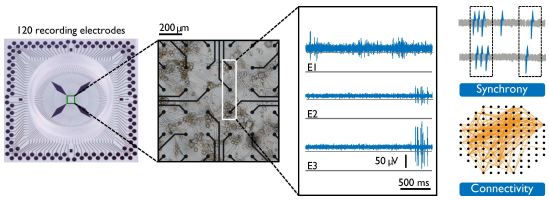

Fig. 1. Cultured Neuronal Networks are recorded on top of MEA. The signal from 120 electrodes corresponding to neuronal network activity is analyzed to study synchronization and connectivity of the functional network.

After DIV 3, the clustering coefficient in the self-organized formed structural network increases and the shortest path decreases (Fig. 2(a)), revealing small-world properties in the mature state of the network. MEA recordings of the CNN show an increase of the firing spikes activity in the active electrodes (Fig. 2(b)). As an average synchronization measure,we evaluate the mean value of the correlation matrix normalized by the number of active electrodes (Fig. 2(c)). This peak of activity and synchronization between DIV 4-6 is linked with the percolation of the topological network. A second peak, between DIV 10-12 is observed when the topological network reaches full maturity. Future work aims to a more detailed statistical analysis of the functional network and a closer comparison of the structural and functional evolution of the CNN along the developmental process.

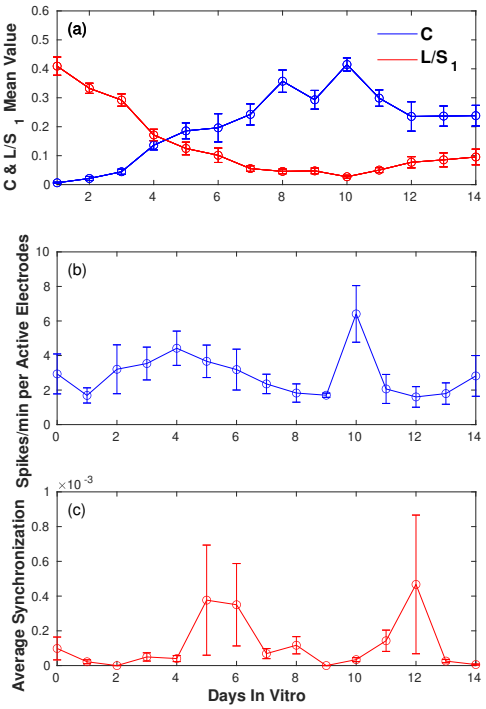

Fig. 2. (a) Clustering coefficient (C) and shortest path values (L/S_1) in the topological network analysis during 14 days in vitro. (b) Spikes/min per active electrode of MEA recordings and (c) average synchronization of the functional network.

[1] D. de Santos-Sierra, I. Sendia-Nadal, I. Leyva et al., *Emergence of small-world anatomical networks in self-organizing clustered neuronal cultures*, PLoS One 9, e85828 (2014).

[2] A. Tlaie, L. M. Ballesteros-Esteban, I. Leyva, I. Sendia-Nadal, *Statistical complexity and connectivity relationship in cultured neural networks*, Chaos 119, 284 (2019).

Fast angular velocity measurement algorithm and the correlations in a quiral fluid of active flat spinners

Miguel Ángel López-Castaño[1], Alejandro Márquez Seco[1], Alicia Márquez Seco[1], Álvaro Rodríguez-Rivas[2] and Francisco Vega Reyes[1]

[1]Departamento de Física and Instituto de Computación Científica Avanzada (ICCAEx), Universidad de Extremadura, 06071, Badajoz, Spain

[2]Departament of Physical, Chemical and Natural System, Pablo de Olavide University, 41013, Sevilla, Spain

The dynamics of chiral fluids is an emergent research field and recently our group have been displayed some relevant aspects of chiral fluids dynamics [1]. Faced with the need to understand the dynamics of these interesting fluids, we present a new technique developed by our group to carrie out the study of autocorrelations data on disk-shaped rotor systems with a high rotational speed[2].

Our experimental set-up consists in a confined system of 2D active rotors, driven by a turbulent air flow impacting from below. The experiments have been carried out at a varied range of translational kinetic energies $\bar{T}_t$ and packing fractions. To analyze the trajectories recorded by a high-speed camera, we have develop a *particle tracking velocimetry* (PTV) algorithm, based on the analysis of the particles brightness profiles from a set of digital images. An advantage of this technique has allowed us to obtain some autocorrelation function with very high accuracy.

We have studied the spin velocity field $\Omega(r) = \langle w \rangle$, and its spatial average, $\bar{\Omega} = \langle \Omega(r) \rangle_r$, where r is the distance to the center of the set-up. We see that there are two different regimes for all packing fractions: when the thermalization is low $\bar{T}_t$, the field $|\Omega(r)|$ increases monotonically versus r, and attains its maximum value at the system boundaries. However, at higher $\bar{T}_t$, particle spin profile flattens, displaying a nearly constant value across all radii, and this value is found to be proportional to $\bar{T}_t$.

We have also studied the traslational correlation fuction and the temporal ensemble spin autocorrelation function, both are dynamic properties of great interest. The latter is shown in Fig.1, by measuring the peculiar spin velocity, and the outcome of the new algorithm allows us to observe the oscillations of the autocorrelation in its high intrinsic frequency, as well as the long-term relaxation. Interesting, it is the relaxation time exchange between the external and internal regions, observed when the translational kinetic energy is increased. Process related to the changes of sign of the global vorticity[1].

We acknowledge funding from the Government of Spain (AEI) and Junta de Extremadura through projects No. PID2020-116567GB-C22) and GR21091 respectively. A.R.-R. also acknowledges financial support from Conserjería de Transformación Económica, Industria, Conocimiento y Universidades (Junta de Andalucía) through post-doctoral grant no. DC 00316 (PAIDI 2020), co-funded by the EU Fondo Social Europeo (FSE).

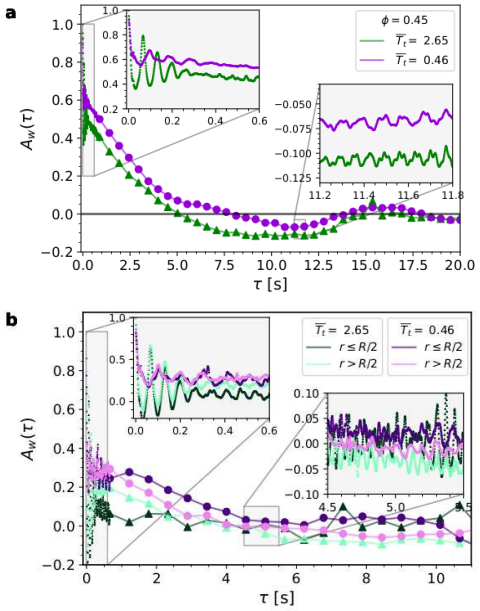

Fig. 1. (a) Spin autocorrelation function, it measures the degree of similarity between angular velocity for a single particle at two instants separated by a period τ. We compare two cases with the same density but different traslational kinetic energies ($\bar{T}_t$ in units of $m\sigma^2 s^{-2}$). (b) Our results demonstrate that spin autocorrelation is different inside the system with respect to the outer edge and that this behavior is reversed when thermalization varies, confirming a change in the total chirality observed in the system.

[1] M. Á. López-Castaño, A. Márquez-Seco, A. Márquez-Seco, Á. Rodríguez-Rivas and F. Vega Reyes (2021), *Chirality transitions in a system of active flat spinners*. Preprint: arXiv:2105.02850

[2] M. Á. López-Castaño, A. Márquez-Seco, A. Márquez-Seco, Á. Rodríguez-Rivas and F. Vega Reyes (2021), *Fast measurement of angular velocity in air-driven flat rotors with periodical features*. Preprint: arXiv:2107.14186

Thermal memory in a vibrated thin granular layer

Álvaro Rodríguez-Rivas[1],
Francisco Vega Reyes[2,3] and Miguel Ángel López-Castaño[2]
[1]Department of Physical, Chemical and Natural Systems, Pablo de Olavide University, 41013, Sevilla, Spain
[2]Departamento de Física, Universidad de Extremadura, 06071, Badajoz, Spain
[3] Instituto de Computación Científica Avanzada (ICCAEx), Universidad de Extremadura, 06071, Badajoz, Spain

In this experimental/computational study, we present the first evidence of existence of Kovacs and Mpemba effects in vibrated granular layer. Recently, it has been theoretically shown that these effects should occur, under the appropriate initial conditions, in a homogeneous granular gas [1, 2]. The Mpemba effect occurs when the system displays an anomalous cooling/heating rate, as a consequence of which, a warmer system may cool down faster, for instance. Kovacs effect consists in an anomalously non-monotonic relaxation of a macroscpic variable (granular temperature, in our case).

Under experimental conditions, however, complete homogeneity is not strictly attainable in a driven granular system (for instance, the system is not homogeneous in the vertical, in the case of a vertically vibrated layer [3], and for this and other reasons, it remained to be confirmed the existence of these effects in a realistic configuration that could be reproduced in the laboratory.

For this purpose, we have performed molecular dynamics simulations (MD) of a vertically vibrated layer, and have set-up an experiment in the laboratory. Both experiments and simulations had to be conducted however under higher density conditions, since, as we will show, the gas phase does not actually exist in this particular configuration, due to geometric restrictions and the particular features of the dynamics of inelastic particles.

The Kovacs effect is, in particular, very noticeable, as Figure 1 shows. In the presentation, we will explain in more detail the specific features of the observed memory effects and the restrictions for these to appear in our experimental configuration.

We acknowledge funding from the Government of Spain (AEI) and Junta de Extremadura through projects No. PID2020-116567GB-C22) and GR21091 respectively. A.R.-R. also acknowledges financial support from Conserjería de Transformación Económica, Industria, Conocimiento y Universidades (Junta de Andalucía) through post-doctoral grant no. DC 00316 (PAIDI 2020), co-funded by the EU Fondo Social Europeo (FSE).

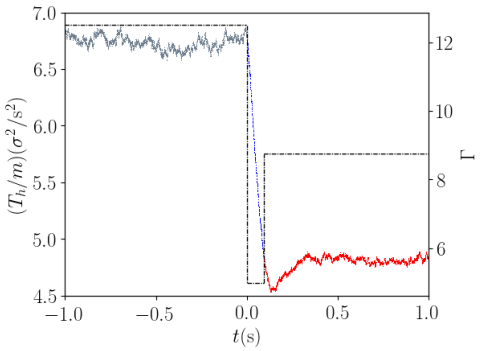

Fig. 1. Kovacs effect in a dense granular layer. σ stands for particle diameter, T_h is the XY average kinetic energy, m for particle mass Γ is the shaking acceleration (as defined in [3], in units of $g = 9.8\ \mathrm{m/s^2}$). The thermal protocol is indicated with dashed lines (the energy input). The granular temperature T_h is indicated with continuous lines, with different coloring for the different thermal protocol stages. Anomalous non-monotonic evolution of T_h occurs in the final relaxation stage (red curve), which is signaled, as it can be seen, with the presence of an absolute minimum.

[1] A. Lasanta, F. Vega Reyes, A. Prados and A. Santos, When the Hotter Cools More Quickly: Mpemba Effect in Granular Fluids, *Phys. Rev. Lett.* **119**, 148001 (2017).

[2] A. Lasanta, F. Vega Reyes, A. Prados and A. Santos, On the emergence of large and complex memory effects in nonequilibrium fluids, *New J. Phys.* **21** 033042 (2019).

[3] P. Melby, F. Vega Reyes, A. Prevost, R. Robertson, P. Kumar, D. A. Egolf and J. S. Urbach , The dynamics of thin vibrated granular layers, *J. Phys.: Condens. Matter* **17** S2689S2704 (2005).

Liquid-vapor equilibrium and critical temperature of parabolic-well fluids of variable width by Gibbs ensemble Monte Carlo simulation

Álvaro Rodríguez-Rivas[1] and Mariano López de Haro[2]
[1]Department of Physical, Chemical and Natural Systems, Pablo de Olavide University, 41013, Sevilla, Spain
[2]Instituto de Energías Renovables, Universidad Nacional Autónoma de México (U.N.A.M), Temixco, Mor. 62290, México

Systems of particles interacting via the van Hove potentials have been extensively studied by statistical mechanical methods[1]. Such interest is invariably due to the fact that these potentials are the simplest models which include the presence of attractive and repulsive forces. Nevertheless, the thermodynamic properties of fluids whose molecules interact via van Hove potentials can still offer some interesting results. In a recent paper[2], we addressed such properties for the case of parabolic-well molecular fluids. In this instance, the intermolecular potential between a pair of particles separated by a distance r is given by

$$u(x) = \begin{cases} \infty, & 0 \le x \le 1, \\ \epsilon\left[\left(\frac{x-1}{\lambda-1}\right)^2 - 1\right], & 1 < x \le \lambda, \\ 0, & x > \lambda, \end{cases} \qquad (1)$$

where $x = r/\sigma$ is the reduced distance, σ is the diameter of the hard core, $\epsilon > 0$ is the well depth and $\lambda > 1$ is the potential range, and we derived an approximate equation of state for these fluids using a second-order thermodynamic perturbation theory. The outcome of this approximation for different values of the parameters involved in the potential was tested against simulation results for various isotherms. Here we extend our previous development by further analyzing the liquid-vapor equilibrium and critical temperature of these parabolic-well fluids. By means of Monte Carlo simulation, and using a modification of the software DL_Monte from the Collaborative Computational Project *CCP5* [3, 4], Gibbs ensemble simulations have been performed for three such parabolic-well fluids in which the ranges are $\lambda = 5/4, 3/2$ and $7/4$, respectively. An advantage of the Gibbs ensemble Monte Carlo technique over other computer simulation methods is that a closer proximity to the critical point can be achieved. Finally, We compare and discuss the results with the cases of triangle-well and square-well fluids, as well as our previous estimates of the critical temperature according to the Vliegenthart and Lekkerkerker criterion[5, 2].

[1] L. van Hove, *Generalized Gradient Approximation Made Simple*, Physica **15**, 951 (1949).

[2] M. López de Haro and Á. Rodríguez-Rivas, *Thermodynamic Properties of the Parabolic-Well Fluid*, Front. Phys. **8**, 627017 (2021).

[3] A. V. Brukhno, J. Grant, T. L. Underwood, K. Stratford, S. C. Parker, J. A. Purton and N. B. Wilding, *DL_MONTE: a multipurpose code for Monte Carlo simulation* Molecular Simulation, **47**, 131 (2021)

[4] J.A. Purton, J.C. Crabtree and S.C. Parker, *DL_MONTE: a general purpose program for parallel Monte Carlo simulation* Molecular Simulation, **39**, 1240 (2013).

[5] G.A. Vliegenthart and H.N.W. Lekkerkerker, J. Chem. Phys. **112**, 5364 (2000).

Introduction of evolutionary mechanisms in the spread of epidemics

Pablo Yagüe Serrano[1], David Soriano Paños[2,3], and Jesús Gómez Gardeñes[1,3,4]
[1]Departament of Condensed Matter Physics, University of Zaragoza, 50009 Zaragoza (Spain).
[2]Instituto Gulbenkian de Ciência (IGC), 2780-156 Oeiras (Portugal).
[3]GOTHAM lab, Institute for Biocomputation and Physics of Complex Systems (BIFI), University of Zaragoza, 50018 Zaragoza (Spain).
[4]Center for Computational Social Science, University of Kobe, 657-8501 Kobe (Japan).

Contagious diseases cause millions of deaths worldwide every year. Epidemic models are compartmental models that allow us to predict their behaviour in order to take measures that help us to curb epidemic waves. In the last two years, we have suffered an historic pandemic caused by the SARS-CoV-2 virus, and in the last year variants of this virus have become very important, causing re-infections in the already recovered population. It is precisely in order to take into account the contribution of pathogen variants in the spread of an epidemic, that a new formalism has been developed.

Our equations are based on the formalism proposed in [1], in which a reinfection of the recovered individuals is included as a completely independent parameter of the system because of the social focus of the article. We adapt the reinfection mechanism proposed in that article to account for the evolutionary behaviour of a virus during an epidemic outbreak. On the one hand, that mechanism is governed in the system as a continuous variable x, which at each time step, for infected individuals, increases by a value of D, which is the parameter that models the mutation of the pathogen, the higher the value of D, the higher the mutation. On the other hand, we define the probability of reinfection of a recovered individual by contact with an infected individual as:

$$\lambda' = \lambda \left(1 - e^{-D(t-s)}\right) , \qquad (1)$$

where λ is the probability of a healthy individual becoming infected by contact with an infected individual and s is the time instant when he became infected. In this way, the more time goes by since the individual recovers, the higher the probability of reinfection tending asymptotically to λ.

After the proposal of the new formalism, a series of Monte Carlo simulations are made to compare them with the equations, as shown in the figure 1. In this graph we can see how there are 2 distinct phases, the first is a non-epidemic regime and the second leads to an endemic state

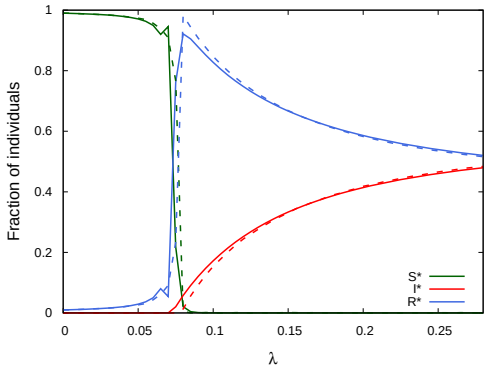

Fig. 1. In this figure, the solid lines represent the equations of our formalism, while the dashed lines represent the average of 40 Monte Carlo simulations. The parameters used are: $\mu = 0.8$ and an Erdös-Rényi lattice with $N = 10000$ and $\langle k \rangle = 10$.

in which there is a non-null fraction of infected individuals in the stationary regime.

The consequences of the endemic regime are very relevant, as the epidemic will not be curbed until external measures are introduced, such as vaccination, confinement, or other types of controls that we have seen in similar cases in the past.

[1] J. Gómez-Gardeñes, A. S. de Barros, S. T. Pinho, and R. F. Andrade, *Abrupt transitions from reinfections in social contagions*, EPL (Europhysics Letters) **110(5)**, 58006 (2015).

[2] R. M. Anderson, C. Vegvari, J. Truscott, and B. S. Collyer, *Challenges in creating herd immunity to SARS-CoV-2 infection by mass vaccination*, The Lancet **396**, 1614 (2020).

How phase resetting curves influence excitation-inhibition-based synchronization

Pau Pomés, and Ernest Montbrió
Neuronal Dynamics Group. Department of Information and Communication Technologies. Universitat Pompeu Fabra, Barcelona

The interplay between excitation (E) and inhibition (I) is a prominent mechanism of rhythmogenesis in neuronal networks [1]. Theoretical studies have shown that such E-I based rhythms —often referred to as Pyramidal-Interneuron Gamma (PING) oscillations— naturally emerge from reciprocal interactions between populations of excitatory and inhibitory neurons, when inhibition is delayed (or slower) relative to excitation [2]. In addition, recent theoretical results demonstrate that such PING rhythms can be thoroughly analyzed using a simple extension of the Kuramoto model of coupled oscillators [3].

Previous theoretical work has been made under the assumption that inhibitory cells have Type 1 *phase response curve* (PRC), that is, cells always advance their *phase* in response to excitatory pulses, see e.g. [1]. However, experimental studies show that inhibitory neurons often delay their phase in response to excitatory pulses as well, typically when the stimulus comes at the beginning of their cycle [4]. Given that PRC type critically influences synchronization, the features of PING oscillations may be altered in the presence of inhibitory neurons with PRC of Type 2.

Here we theoretically investigate the effects of the PRC-Type in the synchronization of an excitatory and an inhibitory neuron. Neurons are modeled using a variant of the Kuramoto model originally obtained in [5]. Though the Kuramoto model is ideally suited to theoretically investigate synchronization, thus far it has not been applied to investigate PING-mediated synchronization between oscillators with different PRC-Type. The Kuramoto model descriving the evolution of the phases of a pair of coupled (synaptic strengths: $K_{E,I}$) excitatory and inhibitory neurons is

$$\begin{aligned}\dot{\theta}_E &= \omega_E - K_E \sin\beta_E - K_E \sin(\theta_I - \theta_E - \beta_E),\\ \dot{\theta}_I &= \omega_I + K_I \sin\beta_I + K_I \sin(\theta_E - \theta_I - \beta_I),\end{aligned}$$

where $\omega_{E,I}$ are the natural frequencies of the neurons, and parameters $\beta_{E,I}$ control the shape of the PRC of each neuron. Specifically, for $\beta_{E,I} = \pi/2$ the PRC is of Type 1, while $\beta_{E,I} \neq \pi/2$ corresponds to different types of Type 2 PRCs. The simplicity of the Kuramoto model allows one to write the two-dimensional dynamical equations as a single equation for the phase difference, $\phi = \theta_E - \theta_I$, as

$$\dot{\phi} = \Delta\omega + 2K \sin\bar{\beta}\Big[\cos(\phi + \frac{\Delta\beta}{2}) - \cos\frac{\Delta\beta}{2}\Big],$$

where we assumed symmetric coupling $K = K_E = K_I$, and defined the new parameters $\Delta\omega = \omega_E - \omega_I$, $\bar{\beta} = (\beta_E + \beta_I)/2$, and $\Delta\beta = \beta_E - \beta_I$. The stable fixed points of this equation are created in two Saddle-Node (SN) bifurcations, and they correspond to synchronous solutions. Consistent with biophysical data, we consider that the E neuron is Type 1, $\beta_E = \pi/2$, hereafter. In Fig. 1 we show the $(\Delta\omega, \beta_I)$ phase diagram, where the SN boundaries (thick blue lines) enclose the synchronization region (shaded). Remarkably, when the PRC of the I neuron deviates from $\pi/2$, the E-I network is able to synchronize even when the I neuron is faster than the E neuron —i.e. for $\Delta\omega < 0$. Moreover, if $\beta_I \in (-\pi/2, \pi/2)$, the I neuron can precede the E neuron ($\phi^* < 0$, see red shaded region in Fig. 1).

Our findings demonstrate that E-I based oscillations broadly considered in computational neurosciences can be investigated in the powerful theoretical framework of the Kuramoto model. This allows for a systematic exploration of the effects of biologically realistic Type-2 PRCs in neuronal synchronization. Our preliminary results already indicate that broadly accepted features of EI-based rhythms may be strongly altered if inhibitory neurons have Type-2 PRCs. For example, the oscillation cycle does not always begin with a boost of (fast) excitatory activity, followed by (slow/delayed) inhibition, but this can be reversed when inhibitory neurons have PRCs with $\beta_I \in (-\pi/2, \pi/2)$.

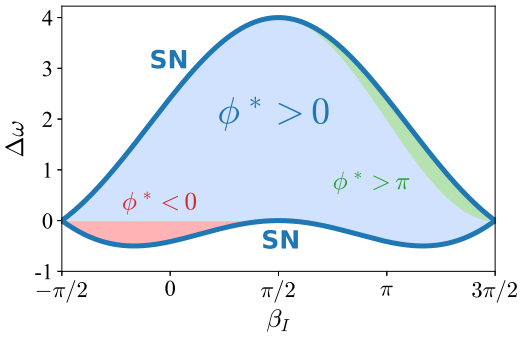

Fig. 1. Phase diagram of the Kuramoto model for a pair symmetrically coupled excitatory and inhibitory neurons. The shaded area corresponds to the synchronization region.

[1] Wang, X.J. *Neurophysiological and computational principles of cortical rhythms in cognition*, Physiol. Rev. **90**, 11951268 (2010).

[2] Wilson, H. R. and Cowan, J. D. *Excitatory and inhibitory interactions in localized populations of model neurons.*, Biophys. J. **12**, 1-24 (1972).

[3] Montbri, E. and Paz, D. *Kuramoto model for excitation-inhibition-based oscillations*, Phys. Rev. Lett. **120**, 244101 (2018).

[4] Tateno, T. and Robinson, H., *Phase resetting curves and oscillatory stability in interneurons of rat somatosensory cortex*, Biophys. J. **92**, 683695 (2007).

[5] Paz, D. and Montbri, E. *Low-dimensional dynamics of populations of pulse-coupled oscillators*, Phys. Rev. X **4**, 011009 (2014).

Experimental study of the forced silos discharge process

María Victoria Ferreyra [1], Luis A. Pugnaloni 1, and Diego Maza[2]
[1]Departamento de Física, Facultad de Ciencias Exactas y Naturales, Universidad Nacional de La Pampa.
CONICET, Uruguay 151, 6300 Santa Rosa (La Pampa), Argentina
[2]Departamento de Física y Matemática Aplicada, Facultad de Ciencias, Universidad de Navarra.
31080 Pamplona, Spain.

Hourglass discharge dynamics is a canonical example of complex granular matter behavior. The mass-flow rate independence on the height of the material remaining in the container has been profusely explored, but no theoretical approach adequately explains this phenomenon. Hoping to bring more information about this counterintuitive observation, we implement a simple experiment: a piston pushing the material discharging from a vertical silo. Under these conditions, we measure the radial distribution of the normal stress on the silo bottom and, simultaneously, the piston position and weight of material discharged. Furthermore, we investigate different piston weights and silo widths. As a result, we can correlate the influence of the stress distribution on the base with the increase in the mass flow rate reported in recent works for these forced discharge processes. Moreover, preliminary observations suggest the existence of a universal *dynamical* radial distribution function of the vertical stress on the base.

Collisional regime during the discharge of a 2D silo

Roberto Arévalo[1]
[1]Research Centre for Energy Resources and Consumption (CIRCE)
Industrial Park Dinamiza, Ranillas Ave. 3D, 1st floor 50018, Zaragoza (Spain)

A humble silo quietly discharging by gravity is a deceptively simple system that has been a benchmark for granular flow investigations for many years. An striking characteristic of the silo is that the flow can be spontaneously arrested when the exit is still as big as 4 or 5 grain diameters [1]. An arch in $2D$ or a dome in $3D$ is formed that blocks the flow.

The question of whether exists a definite orifice size separating the flowing and jammed states naturally arises. The matter has been extensively studied by means of experiments in $3D$ and $2D$. Studying the size of the avalanches as a function of the exit size one could in principle extrapolate the critical size for which the avalanche would be infinite, *i.e.*, the flow would be continuous. However, these measurements are rather difficult to carry out due to the fast growth of the avalanches of grains. As a consequence, the data can be fitted equally well to functions which present a critical value and to functions that do not. By other side, the critical exponent and the value of the critical outlet size in $2D$ turns out to be rather large to be easily interpretable. In the literature one can find opinions in favor and against the existence of a critical outlet size. In the latter case, a blocking arch can always develop but the probability decreases upon increasing the outlet size until it is unobservable whithin experimental time windows.

Looking closely at the bed of grains in the silo one can see that there are two very different regions. In the bulk of the silo grains are in permanent contact, so continuous approximations are able to yield results for velocity distributions or mass flow. Close to the exit, however, the density of the medium decreases and contacts are instantaneous. Thus, the collisional nature of the dynamics becomes significant, warranting a dedicated investigation as carried out in this work. More interesting, the vicinity of the outlet is the region where the arches that block the flow for small apertures are formed.

The present work [2] reports a novel investigation into the collisional dynamics of particles in the vicinity of the outlet of a *2D* silo using molecular dynamics simulations. It is found that the transition from the clogging regime (at small apertures) to the continuous flow regime is smooth in collisional variables. An example of this is shown in Fig. 1 where the normalized collision frequency is plotted against the aperture size. The collision frequency grows with the orifice size for small orifices until it reaches a saturating value. The transition is smooth with no hint of critical behavior. The variation of the collision frequency closely follows that of the packing fraction of the medium in the same window of observation around the orifice. This suggests a connection between the packing fraction and the probability of arch formation.

An alternative look at the collision frequency is the time between collisions or time lag. This variable also shows a smooth transition, decreasing upon increasing the size of the exit down to a saturating value. The distribution of time lags tends to a power law.

Besides the collisions frequency, the histograms of the velocities of individual particles are also studied. The horizontal histograms are gaussian, as expected, for all sizes of the exit. The histograms of the vertical velocity are nearly gaussian. The small deviations arise from the difficulty of removing the bulk velocity, which is not constant inside the observation window. However, the important observation is that these histograms are also unaffected by the transition from the clogging to the continuous flow regime and fall on top of each other when normalized. Finally, even the fluctuations of the flow around the average are observed to be gaussian for all apertures.

Our conclusion is that the collisional dynamics of particles does not show evidence of critical behaviour respect to the outlet size. Furthermore, it is worth noting that the change of behaviour (the transition to a plateau) of the collision frequency and the time lag occur at a value of D larger than that for which arches start to appear. It is difficult to harmonise this observation with the existence of a critical D which separates the continuous flow regime from the clogging regime. It is consistent, instead, with a gradual decrease in the probability to observe clogs as the size of the outlet increases.

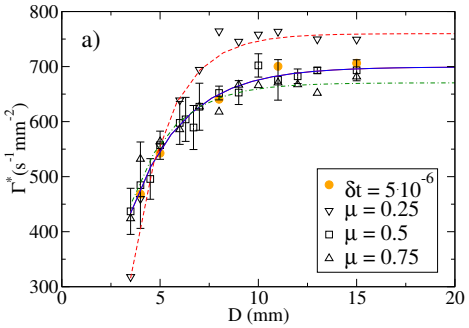

Fig. 1. Normalised collision frequency as a function of the outlet size. The empty symbols represent the main result, while the orange circles are the checking values obtained reducing the integration time step of the simulations and $\mu = 0.5$.

[1] I. Zuriguel, *Clogging of granular materials in bottlenecks*, Papers in Physics **6**, 060014 (2014).

[2] R. Arévalo, *Collisional regime during the discharge of a 2D silo*, to appear in Phys. Rev. E https://arxiv.org/abs/2202.08586

AFM pattern formation in a compliant surface

Juan J. Mazo[1,2] and Pedro J. Martínez[3,4]
[1] Departamento de Estructura de la Materia, Física Térmica y Electrónica, Universidad Complutense de Madrid, 28040 Madrid, Spain
[2] Grupo Interdisciplinar de Sistemas Complejos (GISC), Universidad Complutense de Madrid, 28040 Madrid, Spain.
[3] Instituto de Nanociencia y Materiales de Aragón, CSIC-Universidad de Zaragoza, 50009 Zaragoza, Spain
[4] Departamento de Física Aplicada, Universidad de Zaragoza, 50018 Zaragoza, Spain.

Atomic Force Microscope (AFM) is an experimental technique that has played a key role in the flowering of the new research field of nanotribology. At small forces the AFM serves as a probe of the material topography at the nanoscale. Increasing the force is able to resolve the lateral force exerted by the surface over the moving tip, allowing to characterize friction at the level of a single-contact. Remarkably, in this case an atomic stick-slip dynamics is observed in many different materials and under different experimental conditions. This dynamic can be mostly understood in terms of the Prandtl-Tomlinson model, a simple model which, however, it has been proved to be instrumental in the development of the field.

Pressing further our sample, abrasion and wear effects are typically observed in hard materials. However, a new world of interesting phenomena with promising applications have been observed in the case of compliant materials as polystyrene polymer, for instance. There, material surface is moulded by effect of the tip dragged over the surface resulting in the formation of a rippled pattern.

Thus, in 1992, Leung and Goh published a pioneering work on the orientational ordering of polymers by atomic force microscope tip-surface interaction. [1] As stated in the abstract, they observed that, by action of an atomic force microscope (AFM) tip nanometer-size structures are induced, resulting in a pattern that is periodic and is oriented perpendicular to the scan direction. Such wavy patterns, later called ripples, appear as the outcome of the tip motion, which reshapes the polymer surface locally.

Nowadays, ripples can be created in a controlled way in a given area after just one surface scan. However, these structures have been elusive to a theoretical understanding for years. This relates to the fact that the complex plowing process investigated in the aforementioned references involves concepts of physics, chemistry, and material science in a rather intermixed way which makes traditional approaches to the problem quite challenging.

In our work we have introduced a mesoscopic dynamic model which allows us to reproduce the main features of the observed patterns. The model parameters were fitted to experiments performed over polystyrene films using a commercial AFM operated in contact mode and standard silicon probes. There it was showed that the surface patterns originated from the plowing process are ultimately due to the competition between two basic mechanisms: (i) viscoplastic indentation of the tip in the polymer surface caused by a constant normal force and (ii) lateral shear of the same surface caused by the tip elastically driven (at constant velocity) along a raster scan pattern. Here, we will review here our recent results on this topic [2, 3, 4, 5].

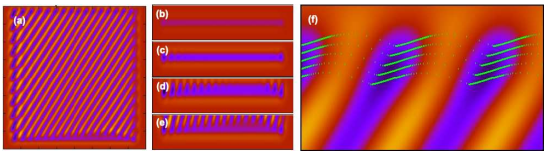

Fig. 1. (a) An example of the obtained rippled pattern. (b-e) Evolution of the same pattern after 1, 5, 10 and 20 scan lines. (f) Tip trajectories corresponding to a series of 5 consecutive scan lines (green dots) overlapped to the surface topography observed after the last one (with $y_s = 1.79\,\mu$m). Frame sizes: (a) $4\times4\ \mu$m^2, (b-e) $4\ \mu\text{m} \times 0.5\ \mu$m, (f) $0.5\ \mu\text{m} \times 0.3\ \mu$m.

[1] O. M. Leung, and M. C. Goh, *Orientational ordering of polymers by atomic force microscope tip-surface interaction*, Science **255**, 6466 (1992).

[2] J. J. Mazo, P. J. Martínez, P. Pedraz, J. Hennig, and E. Gnecco, *Plowing-induced structuring of compliant surfaces*, Phys. Rev. Lett. **122**, 256101 (2019).

[3] P. J. Martínez, E. Gnecco, and J. J. Mazo, *Surface rippling induced by periodic instabilities on a polymer Surface*, Phys. Rev. E **103** 022802 (2021).

[4] J. Hennig, A. Litschko, J. J. Mazo, and E. Gnecco, *Nucleation and detachment of polystyrene nanoparticles from plowing-induced surface wrinkling*, Appl. Surf. Sci. Adv. **6** 100148 (2021).

[5] J. Hennig, V. Feller, P. J. Martínez, Juan J. Mazo, and E. Gnecco, *Locking effects in plowing-induced nanorippling of polystyrene surfaces*, Appl. Surf. Sci. 594, 153467 (2022).

From radial to unidirectional water pumping in zeta-potential modulated Nafion nanostructures

María J. Esplandiu[1], David Reguera[2,3], Daniel Romero-Guzmán[4,5], Amparo M. Gallardo-Moreno[4,5], and Jordi Fraxedas[1]

[1]Catalan Institute of Nanoscience and Nanotechnology (ICN2), CSIC and BIST, Campus UAB, Bellaterra, 08193 Barcelona, Spain.
[2]Departament de Física de la Matèria Condensada, Universitat de Barcelona, C/Martí i Franquès 1, 08028 Barcelona, Spain.
[3]Universitat de Barcelona, Institute of Complex Systems (UBICS), C/Martí i Franquès 1, 08028 Barcelona, Spain.
[4]Department of Applied Physics and University Institute of Biomedical Research (INUBE) University of Extremadura, Badajoz, Spain.
[5]Networking Research Center on Bioengineering, Biomaterials and Nanomedicine (CIBER-BBN), Badajoz, Spain.

The development of micro/nanomachines which can move in a controlled way and perform useful tasks in a fluid environment is one of the most interesting challenges confronting nanoscience and nanotechnology today. Besides the difficulties of nanofabrication, fighting against the dominance of viscous forces and Brownian motion makes necessary the development of efficient strategies to convert chemical energy into directed motion. In this context, different methods of self-propulsion have been investigated, such as catalytic reactions or bubble propulsion. Ion exchange constitutes an interesting alternative mechanism to achieve self-propulsion, with the potential advantages of using innocuous salts as fuels and be able to work at biologically relevant conditions. In order to explore and harness the capabilities of this mechanism to drive micromotors, it is interesting to work with micrompups, which are the immobilized counterpart of micro/nanomotors, sharing the same working principle, but driving the flow of the surrounding fluid instead of self-propelling in a fluid at rest [1]. Micropumps are also promising platforms for many applications such as mass transport, accumulation, and clearance, material patterning at precise locations, or in sensing applications

We report on a new and versatile self-driven polymer micropump fueled by salt which can trigger both radial recirculating and unidirectional fluid flows [2]. The micropump is based on the ion-exchanger Nafion, which produces chemical gradients with the consequent local generation of electric fields capable to trigger interfacial electro-osmotic flows. By combining new nanofabrication strategies for Nafion structuring in microarrays with a fine tune modulation of the surface zeta potentials it was possible to redirect electro-osmotic flows into unidirectional pumping. The experimental data have been contrasted with numerical simulations accomplishing good agreement.

Nafion micropumps work in a wide range of salt concentrations covering more than four orders of magnitude, and can be regenerated for reusability. Moreover, they are activated using different cations. In particular, we demonstrate that they can work using heavy metal ions, such as the typical water-contaminant cadmium, using the own capture of the contaminant ion as fuel to drive fluid pumping. Thus, this novel system has potential for effective and fast water purification strategies for environmental remediation, where the fluid motion triggered by the contaminant ions also speeds up the ion trapping in the polymer backbone. In addition, this study constitutes a very appealing proof of concept for a new generation of wireless micro/nanofluidic networks which can autonomously propel and steer material to certain locations and be useful for different applications.

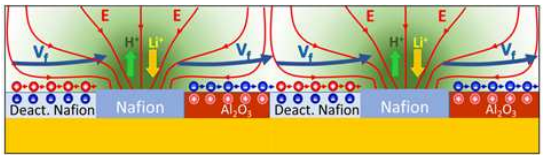

Fig. 1. **Unidirectional pumping**. Scheme of the design of a pump based on the periodic repetition of a basic unit made of alternating strips of deactivated Nafion (negative zeta potential)/Nafion/Al_2O_3 (positive zeta potential) which would lead to unidirectional fluid flow along the patterned surface. The charged interface in the Nafion has been omitted to lighten the content of the figure. The Al_2O_3 patches with positive zeta potential accumulate negative counterions that in the presence of the tangential component of the electric field generated by the ion-exchange will move also to the right, dragging the fluid along to the next repeating unit, achieving unidirectional flow.

[1] M. J. Esplandiu, K. Zhang, J. Fraxedas, B. Sepulveda, and D. Reguera, Acc. Chem. Res. **51**, 1921 (2018).

[2] M. J. Esplandiu, D. Reguera, D. Romero-Guzmn, A. M. Gallardo-Moreno, J. Fraxedas, submitted.

Effect of clustering on the orientational properties of a fluid of hard right isosceles triangles

E. Velasco[1], and Y. Martínez-Ratón[2]
[1]Departamento de Física Teórica de la Materia Condensada, Universidad Autónoma de Madrid, Madrid
[2]Departamento de Matemáticas, Universidad Carlos III de Madrid, Madrid

Recent studies [1, 2] have shown the fluid of hard right triangles to possess fourfold and quasi-eightfold (octatic) orientational symmetries. However, the standard density-functional theory for two-dimensional anisotropic fluids, based on two-body correlations, and an extension to incorporate three-body correlations, fail to describe these symmetries.

To explain the origin of octatic symmetry, we postulate strong particle clustering as a crucial ingredient. We use Scaled Particle Theory to analyze four binary mixtures of hard right triangles and squares, three of them being extreme models for a one-component fluid, where right triangles can exist as monomeric entities together with triangular dimers, square dimers or square tetramers. In some circumstances the orientational distribution function of triangles has equally high peaks at relative particle angles 0, $\pi/2$, and π, signalling fourfold, tetratic order, but also secondary peaks located at $\pi/4$ and $3\pi/4$, a feature of eightfold, octatic order.

Also, we extend the binary mixture model to a quaternary mixture, consisting of four types of clusters: monomers, triangular and square dimers, and square tetramers. This mixture is analyzed using Scaled Particle Theory under the restriction of fixed cluster fractions. Apart from the obvious tetratic phase promoted by tetramers, we found that, for certain cluster compositions, the total orientational distribution function of monomers can exhibit quasi-eightfold (octatic) symmetry [3].

The study gives evidence on the importance of clustering to explain the peculiar orientational properties of liquid-crystal phases in some two dimensional fluids.

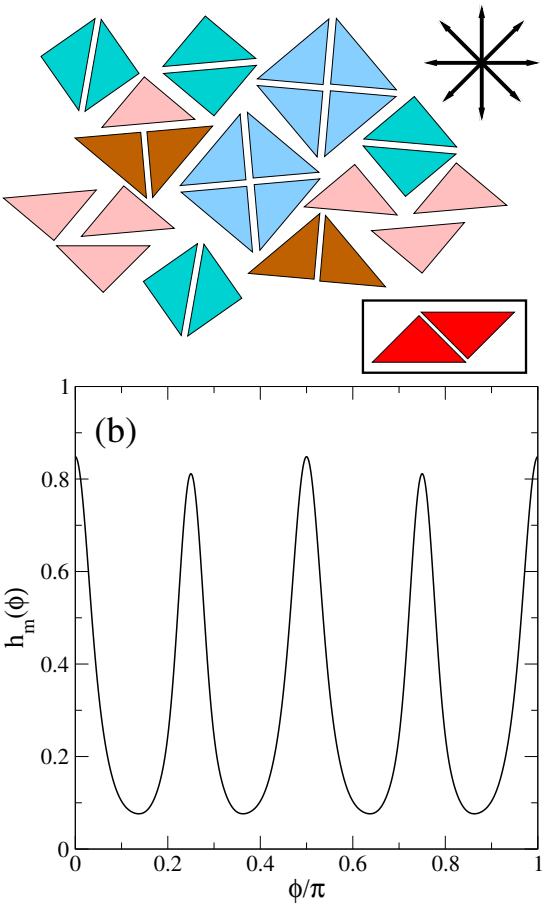

Fig. 1. (a) Sketch of clusters of triangles in the octatic phase. (b) Monomer angular distribution function.

[1] A.P. Gantapara, W. Qi and M. Dijkstra, Soft Matter **11**, 8684 (2015).

[2] Y. Martínez-Ratón and E. Velasco, Phys. Rev. E **104**, 054132 (2021).

[3] Y. Martínez-Ratón and E. Velasco, arXiv:2001.05525v2 (2022).

UAMMD: Complex fluids in the GPU era

Raul P. Pelaez[1], and Rafael Delgado-Buscalioni[1]
[1]Departamento de Física Teórica de la Materia Condensada, Universidad Autónoma de Madrid.

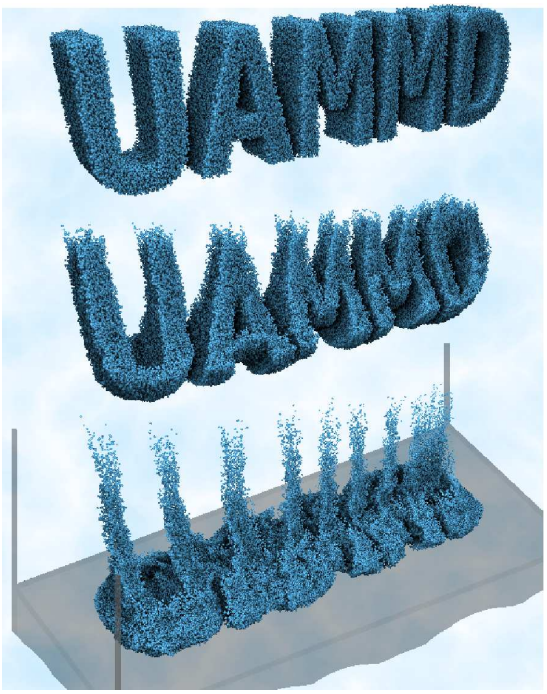

Figure 1: UAMMD logo made up of 10^6 particles sedimenting under a gravity field in a low Reynolds flow.

Complex fluids is an umbrella where solute particles and liquid phase coexist, embracing inorganic and organic soft matter, nanoparticles, polymers, colloids, membranes, interfaces, and hydrodynamics at different spatio-temporal regimes. To face this challenge, we present the "Universally Adaptable Multiscale Molecular Dynamics" code (UAMMD) [1], a novel, open-source, massive parallel, software infrastructure for soft matter simulations in Graphical Procesor Units (GPU). Starting from few nanometers up, UAMMD allows for Lagrangian simulations (MD, DPD, SPH, Brownian hydrodynamics, etc.) and also hybrid Eulerian-Lagrangian schemes.

One of the strongholds of UAMMD is to couple continuum fields with particles. Using the immersed-boundary formalism, Landau-Lifshitz fluctuating hydrodynamics are coupled to MD and this idea is generalized to other fields to model opto-hydrodynamics, charge dynamics, magnetic nanoparticles, etc. UAMMD naturally embraces coarse-grained models of proteins and any other tailored model. I will introduce UAMMD and expose my attempts to push the boundaries of numerical simulation of complex fluids, revisiting old and new schemes in the eyes of a GPU.

---

[1] |https://github.com/RaulPPelaez/UAMMD|

A Machine Learning Approach for Animal Trajectory Classification

Jorge Medina Hernández[1] J. P. Rodríguez[2], A. M. M. Sequeira[3] and Víctor M. Eguíluz[1]
[1]Institute for Cross-Disciplinary Physics and Complex Systems IFISC (CSIC-UIB), 07122 Palma de Mallorca, Spain.
[2]Instituto Mediterráneo de Estudios Avanzados IMEDEA (CSIC-UIB), 07190 Esporles, Spain.
[3]UWA Oceans Institute, Indian Ocean Marine Research Centre, University of Western Australia, Crawley, WA 6009, Australia.

Oceans are environments where a diversity of human activities threaten the marine life. Thus, knowing how, when, where and why animals move is important for their conservation. As a result of the study of marine animal movement through tracking devices during the past decades, there exists now a large database of around 13000 individual trajectories from more than 100 species, susceptible of being analyzed via data-driven methods. Since its potential remains generally unexplored under these novel techniques, our goal will be to assess their performance and adequateness through the classification of species associated with spatio-temporal points (latitude, longitude, time).

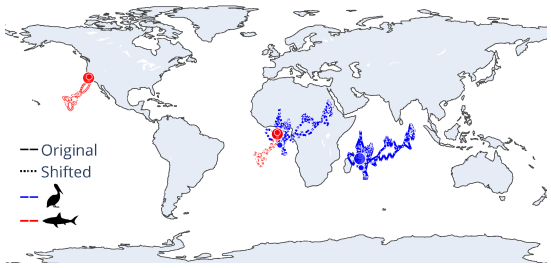

Fig. 1. Original trajectory (solid) and trajectory shifted to the origin $(\theta_0, \phi_0) = (0, 0)$ (dotted) for a wedge-tailed shearwater (blue) and a white shark (red). The initial location is plotted as the biggest point and the final one as the second biggest.

The results in terms of accuracy are shown in Table 1. We find that when trajectories are shifted to a common origin preserving distances and directions (Fig 1), the initial accuracy of 88% falls to 66%, indicating that while the initial location is a useful feature, the algorithms are also able to extract information from the shape of the trajectory. Additionally, we find that including features related to the environment can provide a slight boost in the performance. In particular, the variables with highest impact on the model output (Fig. 2) are the sea surface temperature, the sampling period dt and, in agreement with previous results [1], the bathymetry. Furthermore, these variables contain a significant portion of the information of the spatial location, since adding their values evaluated at the initial locations in the common origin setting restores most of the accuracy.

Classifier	Common origin	Accuracy	Accuracy (E)
ResNet		0.87	0.91
LSTM		0.89	0.88
InceptionTime	$\bar{x}$	0.66	0.85

Table 1. Accuracy results for several classifiers. (E) indicates the environmental variables have been added.

Lastly, we analyze the errors by computing association rules of the form $LHS \longrightarrow \mathrm{Prediction} = \mathrm{wrong}$ using the Apriori algorithm. We find that approximately 30% of the misclassifications are explained by rules with confidence $c > 0.95$ and involve very specific groups of animals (Table 2). Since the overall accuracy is high, the downfall may be explained by corrupted or inaccurate tracking of the trajectories. This can affect certain species at specific locations (blue shark, whales) and tagging systems (GLS, ARGOS) or types (PSAT, SPOT). Furthermore, the improvements in the tracking systems are reflected on the results: trajectories from 1985 to 2002 account for 1.8% of the data and 14.8% of the errors. Thus, state of the art algorithms are not only a powerful tool for analyzing animal trajectories, but provide insight to identify possible flaws in the data collection.

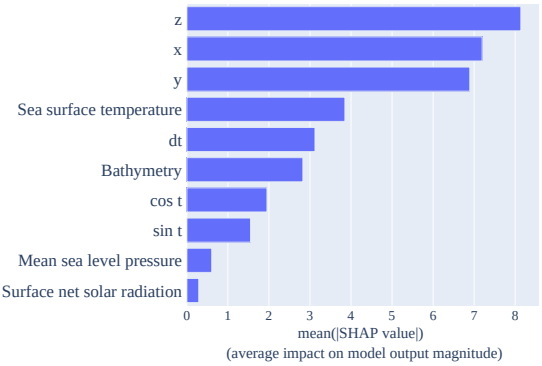

Fig. 2. Top 10 features by mean absolute SHAP [2] value, averaged across all the dataset (the union of the results for the test sets from the k-fold cross validation split ($k = 5$)).

LHS	c	count
{Blue shark, cluster ID 32 }	1	83
{Tag type PSAT, animals in data set < 54 }	1	132
{Family Lamnidae, cluster ID 42 }	1	88
{Taxa Sharks, tag GLS, years 2006-2009 }	0.97	90
{Whales, cluster ID 32}	0.97	104
{Unknown sex, tag ARGOS }	0.33	1042
{tag type SPOT }	0.4	727
{Trajectory data < 79 points }	0.34	1793
{Year < 2002 }	0.36	685
{Taxa birds, cluster ID 33 }	0.52	425

Table 2. Several association rules where the right hand side is "Prediction=wrong" for the ResNet classifier, which has an accuracy of 87% (Table 1.) Includes all the dataset (the union of the results for the test sets from the k-fold cross validation split ($k = 5$)). Some rules can provide insight about why model fails in certain trajectories. Total number of trajectories that verify the rule: count $\times$ confidence. Cluster IDs refer to the geographical location and correspond to clusters computed using HDBSCAN+DBSCAN.

[1] A.M.M. Sequeira et al., *Convergence of marine megafauna movement patterns in coastal and open oceans*, PNAS **115** (2018).

[2] S. I. Lee, and S. M. Lundberg, *A unified approach to interpreting model predictions*, Adv. Neural Inf. Process. Syst. (2018).

Mastering control of overdamped dynamics: from fast forward/backward to arbitrary connections

Carlos A. Plata[1]
[1]Física Teórica, Universidad de Sevilla, Apartado de Correos 1065, E-41080 Sevilla, España

The design and implementation of shortcut protocols able to drive physical systems from an initial state to a target state in a finite time represents a crucial problem in many fields of physics. In the last years, these protocols have been thoroughly studied and applied in quantum systems, commonly under the umbrella of the term *shortcuts to adiabaticity* [1]. More recently, some of these ideas have been adapted and/or exported to different frameworks, from isolated classical systems to statistical mechanics [2]. Still, the picture of a neat correspondence between quantum and classical shortcuts is not complete.

Herein, we present a statistical fast-forward procedure—in the spirit of its quantum counterpart [3]—for one-dimensional overdamped dynamics [4], e.g., a Brownian particle in 1D submitted to a controlled external potential $U(x,t)$. We start from the evolution equation of the probability density function $\rho(x,t)$ describing our system, which is governed by the Smoluchowski equation,

$$\gamma\partial_t\rho(x,t) = \partial_x\left[\rho(x,t)\partial_x U(x,t)\right] + \beta^{-1}\partial_x^2\rho(x,t), \quad (1)$$

where γ stands for the friction coefficient, and $\beta = (k_B T)^{-1}$, with T being the temperature of the thermal bath. From an inverse-engineered perspective, given a prescription $\rho(x,t)$, one can solve Eq. (1) for $U(x,t)$. Nonetheless, in general, the external potential obtained by this method is neither in closed-form nor suitable for applications.

We start by deriving the external potential needed to time-manipulate a certain reference process. Specifically, let us consider a solution $\rho_{\rm r}(x,t)$ of Eq. (1) with a reference potential $U_{\rm r}(x,t)$. Therefore, the prescription we would like to impose is

$$\rho(x,t) = \rho_{\rm r}(x,\Lambda(t)). \quad (2)$$

Note that $\Lambda(t)$ represents a time map between the reference and the manipulated processes. The new and the reference process are the same *film* but played at different *frame rates*, see Fig. 1. Thus, finding the driving potential that enforces the dynamical prescription given by Eq. (2) is providing us with the capability to accelerate, slow down, or even reverse time of a reference process.

Our procedure to accelerate a reference evolution can be used to build arbitrary connections between states. It suffices to use a welding protocol, which matches a fast-forward evolution and a fast-backward (i.e., time reversed) evolution to a common intermediate state. As we will show during the presentation, choosing wisely this intermediate state allows us to work out closed-form expressions for both the driving potential and the evolution itself.

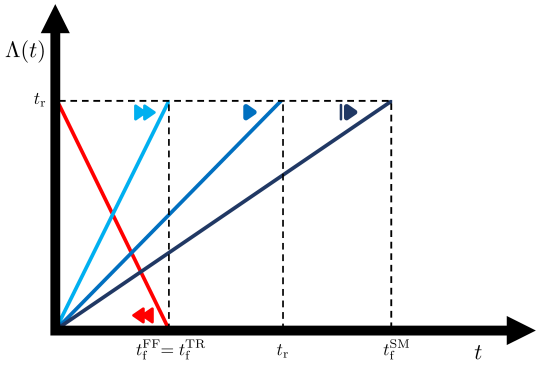

Fig. 1. Sketch of different linear instances of the time manipulation function $\Lambda(t)$. The absolute value of the slope of such function gives the acceleration ($|\dot{\Lambda}(t)| > 1$) or deceleration ($|\dot{\Lambda}(t)| < 1$) rate with respect to the reference time evolution. On the one hand, three forward processes has been plotted. Namely, a fast forward (cyan), an identity (blue), and slow motion (purple) transformations with final duration equal to $t^{\rm FF}$, $t_{\rm r}$, and $t_{\rm f}^{\rm SM}$ respectively. On the other hand, a fast time reversal (red) transformation has been displayed with the same acceleration factor than that of the fast forward example, $t_{\rm f}^{\rm TR} = t_{\rm f}^{\rm FF}$. Note that, in general, $\Lambda(t)$ does not need to be linear.

[1] D. Guéry-Odelin, A Ruschhaupt, A. Kiely, E. Torrontegui, S. Martínez-Garaot, and J. G. Muga, *Shortcuts to adiabaticity: Concepts, methods, and applications*, Rev. Mod. Phys. **91**, 045001 (2019).

[2] A. Patra and C. Jarzynski, *Shortcuts to adiabaticity using flow fields*, New J. Phys. **19**, 125009 (2017).

[3] S. Masuda and K. Nakamura, *Fast-forward problem in quantum mechanics*, Phys. Rev. A **78**, 062108 (2008).

[4] C. A. Plata, A. Prados, E. Trizac, and D. Guéry-Odelin, *Taming the Time Evolution in Overdamped Systems: Shortcuts Elaborated from Fast-Forward and Time-Reversed Protocols*, Phys. Rev. Lett. **127**, 190605 (2021).

Phase behaviour of active particles in block copolymer melts

Javier Díaz Brañas[1] and Ignacio Pagonabarraga[1,2,3]
[1] CECAM, Centre Européen de Calcul Atomique et Moléculaire, École Polytechnique Fédérale de Lausanne, Lausanne, 1015 Switzerland
[2] Departament de Física de la Matèria Condensada, Universitat de Barcelona, Martí i Franquès 1, Barcelona, 08028 Spain
[3] Universitat de Barcelona Institute of Complex Systems (UBICS), Universitat de Barcelona, Barcelona, 08028 Spain

Block copolymer(BCP) materials are perfect matrices to control the position and orientation of nanoparticles (NPs) with anisotropic shapes or chemically inhomogeneous surfaces[1] . This is due to the ordered structures that BCP melts can form in the nanoscale (e.g. lamellar, BCC spheres). On the other hand, active self-propelled particles can self-assemble into a rich phase behaviour in the bulk[2] , or in the presence of obstacles and under confinement[3].

In this work, self-propelled particles, modelled as active Brownian particles (ABPs), are guided by the BCP morphology, which in turn is deformable and reacts to the presence of active motile particles. The hybrid BCP/ABP system co-assembled into a rich phase behaviour both for interface-segregated and selective ABPs. In the presence of confinement induced by the BCP (at the interface or within compatible drop-like domains) ABPs can form train-like structures that flow continuously, as shown in figure 1. Lower activity rates and higher concentrations promote aggregation of ABPs, specially when dispersed within immiscible phases. The formation of clusters deform the BCP structure.

For higher activity rates, the ABPs and the BCP dynamics are largely decoupled, which leads to large deformations in the BCP morphology and the emergence of global polar order in the ABPs.

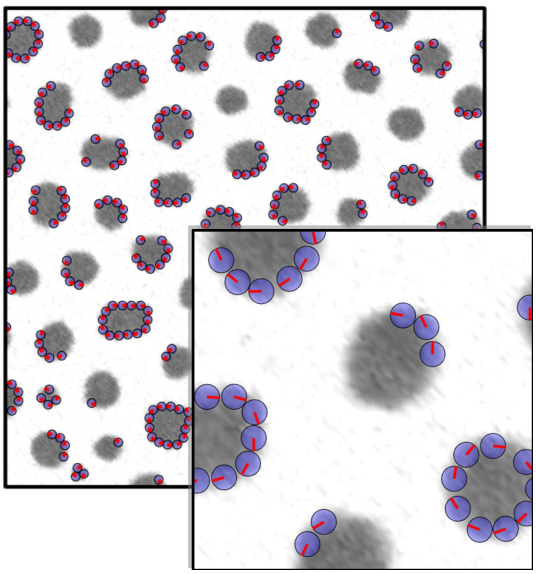

Fig. 1. ABPs (blue) organise in train-like structures with polar order when confined within the interface of circular-forming BCP domains(gray/white). The self-propulsion direction of each particle is indicated in red. This co-assembled configuration occurs for intermediate activity and intermediate ABP concentration.

[1] E. Ploshnik, A. Salant, U. Banin, and R. Shenhar. *Phys. Chem. Chem. Phys.*, **12** (2010).

[2] Telezki, V. and Klumpp, S., *Soft Matter*, **16** (2020)

[3] Bechinger, C., Di Leonardo, R., Löwen, H., Reichhardt, C., Volpe, G. and Volpe, G., *Rev. Mod. Phys.*, **88** (2016)

Dynamic Monte Carlo simulations of nanocubes in an electric field: Structure, dynamics and rheology of an electrorheological fluid.

Luca Tonti[1], Fabián A. García Daza[1], Alessandro Patti[1,2]
[1]Department of Chemical Engineering, The University of Manchester, Manchester, M13 9PL, UK
[2]Department of Applied Physics, University of Granada, Campus Fuentenueva s/n, 18071 Granada, Spain

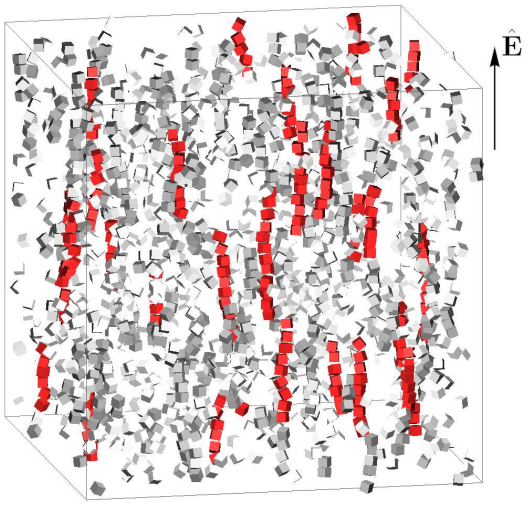

Fig. 1. Snapshot of an equilibrated suspension of cubic particles under the application of an external electric field $\hat{\mathbf{E}}$. Red particles belong to chains made of at least 6 cubes. Arrow on the top right indicates the orientation of the external field.

Colloids are biphasic systems comprising a dispersed phase and a dispersing medium. The former can consist of solid particles, liquid droplets or gas bubbles, whose size is generally between a few nanometers and a few microns. If the dispersed phase comprises solid particles and the dispersing medium is a liquid, these systems are referred to as colloidal suspensions or simply sols. Sols are especially relevant in formulation science as they form the basis for a number of products of daily usage, including detergents, paints, coatings and foods.

The phase behaviour of colloids can be altered by very mild energy changes of the order of thermal fluctuations, namely few k_BT per particle, where k_B is the Boltzmann constant and T the absolute temperature. When an external electric field is applied to a sol, the colloidal particles are polarised due to a difference in permittivity between the dispersed phase and the surrounding medium. The induced dipoles generated by external fields enhance particles attraction, which cause microscopic reorganization of the dispersed phase and the formation of oriented string-like clusters or chains. These chains, whose length strongly depends on the intensity of the applied field, have been observed in suspensions of both spherical [1] and anisotropic dielectric particles [2]. Such a directed self-assembly has relevant consequences in the rheological properties of the entire suspension. Under some specific conditions, where volume fraction, dielectric properties and field intensity play a crucial role, the viscosity of the colloidal suspension can change drastically with the overall system behaving like a Bingham plastic [3]. These very intriguing electrorheological (ER) fluids are especially attractive in technology applications where controlling viscosity is especially relevant, such as in vibration suppression and motion control of vehicles.

In this work, we report on Dynamic Monte Carlo simulations of ER colloidal suspensions of polarisable nanocubes and investigate the kinetics of formation of chain-like clusters. Our interest is estimating the response time of chain formation upon switching the field on and chain disruption upon switching the field off. Additionally, we investigate the main structural properties of the chains that are formed and how they influence the viscoelastic response of the system. More specifically, we apply passive microrheology [4] to compute the viscous and elastic moduli along the direction of the field and perpendicularly to it. Our results clarify the role of chains in determining a change in viscosity and open up a path to evaluate the viscoelastic response of ER fluids by applying efficient simulation methods.

[1] A.-P. Hynninen and M. Dijkstra, *Phase Diagram of Dipolar Hard and Soft Spheres: Manipulation of Colloidal Crystal Structures by an External Field*, Phys. Rev. Lett. **94**, 138303 (2005).

[2] H. R. Vutukuri, F. Smallenburg, S. Badaire, A. Imhof, M. Dijkstra and A. van Blaaderen, *An experimental and simulation study on the self- assembly of colloidal cubes in external electric field*, Soft Matter **10**, 9110 (2014).

[3] R. T. Bonnecaze and J. F. Brady, *Dynamic simulation of an electrorheological fluid*. J. Chem. Phys. **96**, 2183 (1992).

[4] F. A. García Daza, A. M. Puertas, A. Cuetos and A. Patti, *Microrheology of colloidal suspensions via dynamic Monte Carlo simulations*, J. Colloid Interface Sci. **605**, 182 (2022).

Long-range effects of walls in schooling fish

Andreu Puy[1], Jordi Torrents[1], M. Carmen Miguel[2,3] and Romualdo Pastor-Satorras[1]
[1]Departament de Física, Universitat Politècnica de Catalunya, Campus Nord B4, 08034 Barcelona, Spain
[2]Departament de Física de la Matèria Condensada, Universitat de Barcelona, Martí i Franquès 1, 08028 Barcelona, Spain
[3]Institute of Complex Systems (UBICS), Universitat de Barcelona, Barcelona, Spain

Collective motion occurs when a system of self-propelled units exhibit spontaneous ordered movement. It is ubiquitous in the real world, arising in systems of many different scales [1, 2, 3]. Here, we approach the topic considering fish schools.

One major challenge in the field is to capture and quantify the interactions that drive the movement, both at the individual and collective level. This includes the cooperation between individuals and the responses to external elements, such as the presence of walls in a tank. Few works have tried to address the interactions with the walls, most of them investigating schools of only one or two fish [4, 5, 6, 7], finding short-range interactions decaying exponentially.

Here we use the tracking of trajectories of freely swimming fish in an experimental tank. The school consists on 40 individuals of black neon tetra (*Hyphessobrycon herbertaxelrodi*) swimming for three segments of 10 minutes of duration (1200 frames each). We have an example of the tracking (blue arrows) overlapped with an image of the experiment in g. 1, where the tank walls are displayed as a red rectangle.

We have analysed quantitatively the experimental interactions of schooling fish with the tank walls and find that wall forces in a fish school are long-range (see fig. 2), in contrast with experiments of one or two fish. We trace back the origin of the long range interactions to the transmission of information across the school. Moreover, we employ the interactions observed to build a random walk model of schooling fish in a tank and reproduce some key features of the system.

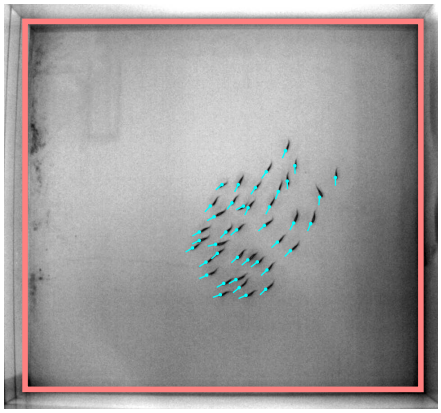

Fig. 1. The experiment consists on 40 black neon tetra free swimming in a tank. We display in blue arrows the tracking of the frame and in red the tank walls.

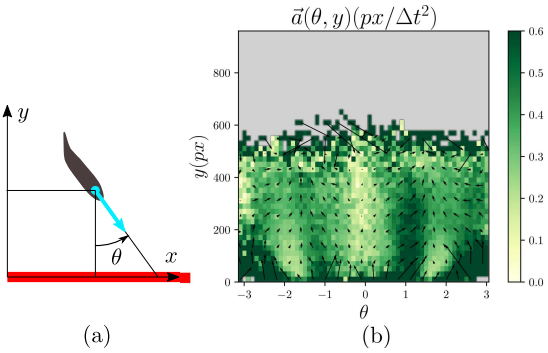

Fig. 2. (a) We analyse the dependence of the wall interactions with the fish coordinates (x, y) and orientation θ with respect to the wall. (b) We find the wall interactions (measured by the acceleration of fish $\vec{a}$) to have a relevant influence at any point in the tank.

[1] Vicsek, T. & Zafeiris, A. Collective motion. *Physics Reports*. **517**, 71-140 (2012,8).

[2] Sumpter, D. Collective animal behavior. (Princeton University Press,2010)

[3] Ramaswamy, S. The Mechanics and Statistics of Active Matter. *Annual Review Of Condensed Matter Physics*. **1** pp. 323-345 (2010,4).

[4] Calovi, D., Litchinko, A., Lecheval, V., Lopez, U., Prez Escudero, A., Chat, H., Sire, C. & Theraulaz, G. Disentangling and modeling interactions in fish with burst-and-coast swimming reveal distinct alignment and attraction behaviors. *PLoS Computational Biology*. **14**, e1005933 (2018)

[5] Zienkiewicz, A., Ladu, F., Barton, D., Porfiri, M. & Di Bernardo, M. Data-driven modelling of social forces and collective behaviour in zebrafish. *Journal Of Theoretical Biology*. **443** pp. 39-51 (2018)

[6] Gautrais, J., Jost, C., Soria, M., Campo, A., Motsch, S., Fournier, R., Blanco, S. & Theraulaz, G. Analyzing fish movement as a persistent turning walker. *Journal Of Mathematical Biology*. **58**, 429-445 (2009)

[7] Gautrais, J., Ginelli, F., Fournier, R., Blanco, S., Soria, M., Chat, H. & Theraulaz, G. Deciphering interactions in moving animal groups. (Public Library of Science San Francisco, USA,2012)

Mapas globalmente acoplados en el régimen turbulento: Convergencia no universal con el tamaño del exponente de Lyapunov

Diego Pazó, David Velasco y Juan M. López
Instituto de Física de Cantabria (IFCA), Universidad de Cantabria-CSIC, Avda. Los Castros s/n, 39005 Santander

Dentro de la teoría del caos son conocidas diversas leyes de escala. Éstas están bien fundadas para el caos de baja dimensión, pero se recurre a argumentos habitualmente heurísticos cuando tratamos con caos de muy alta dimensión (con un número de grados de libertad N muy grande). Qué cambios experimenta el caos en la convergencia al límite termodinámico ($N \to \infty$) es una cuestión habitual en la frontera entre la mecánica estadística y la teoría del caos.

Los mapas caóticos acoplados son un ejemplo paradigmático de sistemas caóticos de alta dimensión. En esta comunicación nos centramos en el caso de acoplamiento global y débil. En esa situación el sistema se encuentra en un regimen caótico extensivo, también llamado "turbulento" [1]. Hace una década Takeuchi y otros [2] llegaron a la conclusión de que para los mapas globalmente acoplados, el exponente de Lyapunov $\lambda(N)$ converge al límite termodinámico λ_∞ de forma logarítmica con el tamaño N:

$$\lambda_\infty - \lambda(N) \simeq \frac{c}{\ln N} \tag{1}$$

Esta conclusión, véase también el cap. 11 de [3], aplica por igual a mapas con multiplicadores de signo exclusivamente positivo, como aquellos con ambos signos.

En esta contribución demostramos teóricamente que la ley de escala (1) no está bien fundamentada. Para el caso con multiplicadores positivos encontramos teóricamente tres regímenes de convergencia del exponente de Lyapunov, en función del mapa usado y de la intensidad del acoplamiento:

$$\lambda_\infty - \lambda(N) \simeq \begin{cases} c/N & \\ c/N^\alpha & \text{con } 0<\alpha<1 \\ \text{más lento} & (1/\ln^\delta N?) \end{cases} \tag{2}$$

Los detalles de la teoría y las simulaciones numéricas que respaldan la ec. (2) pueden encontrarse en [4]. En la misma referencia se explica el error en el razonamiento que lleva a la ec. (1).

[1] K. Kaneko, *Clustering, coding, switching, hierarchical ordering, and control in a network of chaotic elements*, Physica D **41**, 137 (1990).

[2] K. A. Takeuchi, H. Chaté, F. Ginelli, A. Politi y A. Torcini, *Extensice and subextensive chaos in globally coupled dynamical systems*, Phys. Rev. Lett. **107**, 124101 (2011).

[3] A. Pikovsky y A. Politi, *Lyapunov Exponents* (Cambridge University Press, Cambridge, 2016).

[4] D. Velasco, J. M. López y D. Pazó, *Nonuniversal large-size asymptotics of the Lyapunov exponent in turbullent globally coupled maps*, Phys. Rev. E **104**, 034216 (2021).

Adapting reservoir computing to solve the Schrödinger equation

L.Domingo[1 2 3], J. Borondo[4 5], and F. Borondo[1 2]
[1]Instituto de Ciencias Matemáticas (ICMAT); Campus de Cantoblanco UAM; Nicolás Cabrera, 13-15; 28049 Madrid (Spain)
[2]Departamento de Química; Universidad Autónoma de Madrid; CANTOBLANCO - 28049 Madrid (Spain)
[3]Grupo de Sistemas Complejos; Universidad Politécnica de Madrid; 28035 Madrid (Spain)
[4]Departamento de Gestión Empresarial; Universidad Pontificia de Comillas ICADE; Alberto Aguilera 23; 28015 Madrid (Spain)
[5]AgrowingData; Navarro Rodrigo 2 AT; 04001 Almería (Spain)

Reservoir computing is a machine learning algorithm that excels at predicting the evolution of time series, in particular, dynamical systems. Moreover, it has also shown superb performance at solving partial differential equations such as chaotic time series prediction [1]. In the field of quantum chemistry, machine learning methods are proving to have advantages over the standard computational chemistry approaches [2, 3] , especially in the case of high-dimensional systems.

In this work, we aim to use RC to propagate wave packets with time, that is, to solve the time-dependent Schrödinger equation in continuous quantum systems. To do so, the RC model needs to be adapted to work with wavefunctions, which are complex-valued high-dimensional matrices. We adapted the regularized linear model to complex data by extending the ridge regression to the complex domain. We also propose here a new learning strategy that allows propagating wavefunctions while reducing the overfitting of the training data. Such learning strategy consists of a two-step training of the readout layer, where the reservoir is shown how predicting unseen data affects the evolution of the internal states. The learning algorithm is adapted to prevent fast error propagation during the test phase. The algorithm to train the Multi-setp RC model is schematically depicted in Fig. 1.

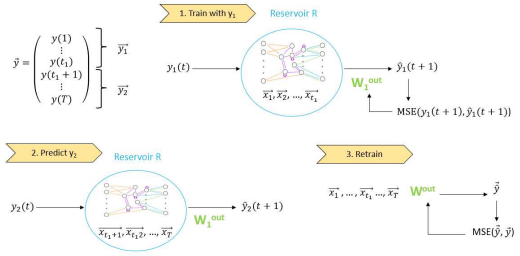

Fig. 1. Architecture of multi-step training of the reservoir computing model.

As an illustration, we have applied our method to four quantum systems: three 1D systems and one 2D system. The 1D systems include the harmonic oscillator, the Morse potential and a polynomial potential. The 2D system is a 2D harmonic oscillator. It is observed that the mean squared error of the propagated wavefunctions increases slower with time when using multi-step learning. This fact is critical in the 2D system, (see Fig. 2) which has higher-dimensional data, this leading to more overfitting. In this case, the standard RC model was not able to correctly reproduce the eigenenergies of the system, while the multi-step learning could. Moreover, the multi-step learning RC also allowed to recover the eigenfunctions of all the quantum systems, proving that the method can correctly predict the time evolution of the wavepackets and the corresponding eigenstates.

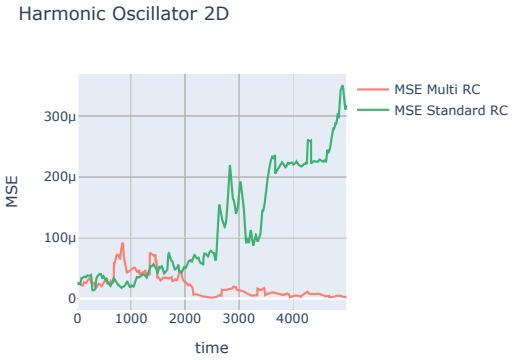

Fig. 2. Time evolution of the mean square error (MSE) of the 2D harmonic oscillator wavefunctions for the standard RC and the multi-step RC.

Once the efficiency of our multi-step RC has been proved, the present work can be extended by application to other interesting problems. This future work could include, among others, the application to more complex and realistic quantum systems, the computation of eigenstates in a high lying energy window [5], or the calculation of the so-called scarred functions [4] that play a very important role in the field of quantum chaos.

[1] J. Pathak, Z. Lu, B. Hunt, M. Girvan, and E. Ott, *Using machine learningto replicate chaotic attractors and calculate Lyapunov exponents from data*, Chaos **27**, 121102 (2017)

[2] L. Domingo and F. Borondo, *Deep learning methods for the computa-tion of vibrational wavefunctions*, Commun. Nonlinear Sci. Numer. Simul. **103**, 105989 (2021).

[3] J. Hermann, Z. Schtzle, and F. No, *Deep-neural-network solution of the electronic Schrödinger equation*, Nat. Chem. **12**, 891 (2020).

[4] F. Revuelta, E. Vergini, R. M. Benito, and F. Borondo, *Short-periodic-orbit method for excited chaotic eigenfunctions*, Phys. Rev. E **102** (2020).

[5] F. Revuelta, R. Benito, F. Borondo, and E. Vergini, *Using basis sets ofscar functions*, Phys. Rev. E **87**, 042921 (2013)

A spin-glass approach to spatial distributions in biology

Daniel Campos[1], Javier Cristín[2] and Vicenç Méndez[1]
[1]Dept de Física. Facultat de Cincies. Universitat Autónoma de Barcelona. 08193 Bellaterra
[2] Dipartimento Fisica. Nuovo Edificio Universitá La Sapienza. 00185 Roma

We propose a data-driven method, based on the framework of spin-glasses (SG), to interpret the collective dynamics of biological populations, where occupation (vacancies) of regions of a spatial domain spatial point are interpreted as up (down) states of the glass particles (Fig. 1). While tracking data from real experiments can be used in general to feed any learning algorithms, using Ising and spin-glass as reference models for this purpose has the advantages that (i) they are simple and admit a straight physical interpretation, and (ii) there is a vast amount of literature on the field to facilitate the corresponding analysis of the results. All this should help to reach sound descriptive capacity [1] to elucidate key mechanisms of interaction between individuals driving spatial occupancy.

The approach proposed solves the corresponding inverse Ising problem from the experimental occupancy patterns, and then implements an information-theoretic analysis to measure the amount of information and correlation patterns that the resulting SG model is able to capture at local and global spatial scales.

To illustrate the capacity of our approach to classify and/or interpret biological interactions, we first apply it to data generated from several lattice models. In particular, we use (i) Vicsek model, and (ii) a collective learning algorithm [2], as reference models of collective.

Then, as an experimental case study we analyze collective foraging in ants, i.e. *Aphaenogaster senilis*, exploring a large discrete arena where the food is located either at deterministic or random locations. Since the individuals of a colony adapt its movement to satisfy the colony requirements through the interaction and communication between them, it has been claimed that the colony adapts itself to the environment as a unique coordinated entity (or superorganism). This feature has been reported in several studies, where colony-level foraging strategies are shown to be adjustable to specific scenarios [1, 3].

We finally show how our spin-glass approach can be used to carry out further *in silico* experiments in order to address questions about collective search and dynamics. For this, we focus on the question of the exploration-exploitation trade-off, which is of great biological relevance. Optimal foraging

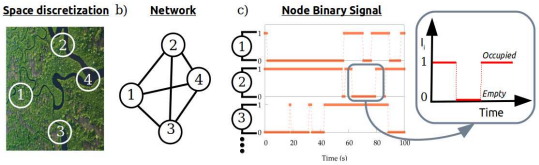

Fig. 1. Illustrative scheme of our approach to collective space use. (a) The biologically relevant regions of the space are considered as nodes of a network structure (b) The presence or absence of individuals at node i for a given time t is understood as a binary signal $I_i(t)$ representing occupancy of that region (with $I_i(t) = 1$ if occupied, and $I_i(t) = 0$ if empty).

draws from the balance between exploiting the known spots of resources and exploring new zones to obtain resources. So, uncertain scenarios (this is, when food is located randomly) would promote exploration, whereas resource exploitation plays a more prominent role in deterministic scenarios. While such exploration-exploitation trade-offs are very common across biological systems and scales but are difficult to quantify and study experimentally, even more at the collective level. So, we claim that *in silico* tools like the one proposed here can be of potential interest in order to help designing/directing adequately experiments.

[1] Cristn J., Bartumeus F., Méndez V. and Campos, D. *Occupancy patterns in superorganisms: a spin-glass approach to ant exploration.* R. Soc. Open Sci: 7201250 (2020).

[2] Falcn-Corts A, Boyer D, Ramos-Fernndez G. 2019 Collective learning from individual experiences and information transfer during group foraging. J. R. Soc. Interface 16: 20180803 (2019).

[3] Campos, D. et al. *Variability in individual activity bursts improves ant foraging success*. J. R. Soc. Interface 13: 20160856 (2016).

Estudio de la coexistencia líquido-vapor de dímeros con interacción tipo pozo cuadrado mediante simulación numérica.

Francisco Sastre[1,2], and Felipe J. Blas[1]
[1] Laboratorio de Simulación Molecular y Química Computacional,
CIQSO-Centro de Investigación en Química Sostenible y Departamento de Ciencias Integradas,
Universidad de Huelva, 21006 Huelva
[2]Departamento de Ingeniería Física de la División de Ciencias e Ingenierías,
Universidad de Guanajuato, AP E-143, C.P. 37150, León, Guanajuato, México

El estudio de sistemas compuestos por dímeros que interactúan mediante potenciales tipo pozo cuadrado [1] revierte gran interes ya que estos sistemas continen las características esenciales que se espera de fluidos reales no polares. Cada dímero consiste de dos esferas impenetrables de diametro σ unidas tangencialmente con un potencial de interacción entre los segmentos dada por

$$\phi(r) = \begin{cases} \infty & \text{if} \quad r \leq \sigma \\ -\epsilon & \text{if} \quad \sigma < r \leq \lambda\sigma \\ 0 & \text{if} \quad r > \lambda\sigma \end{cases} , \qquad (1)$$

en donde ϵ es la energía de interacción y λ es el alcance de la atracción.

En este trabajo determinamos el diagrama de coexistencia líquido-vapor y el punto crítico para alcance $\lambda = 1.5\sigma$ mediante dos técnicas de simulación numérica:

- En la vecindad del punto crĺico usamos un nuevo algoritmo que permite evaluar directamente el potencial químico basado en razones de transición, ver Fig. 1, y
- Dinámica molecular, para valores de temperatura alejadas de la región crítica.

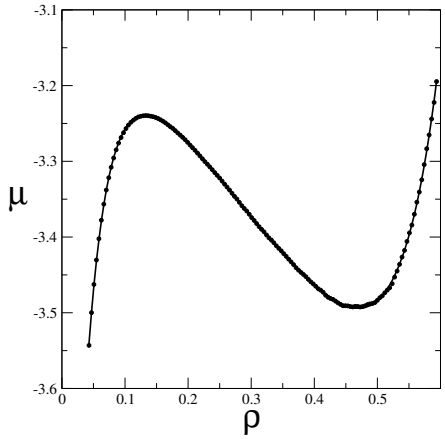

Fig. 1. Potencial químico en función de la densidad para un sitema de dímeros de alcance $\lambda = 1.5\sigma$ para una caja de simulación $L = 8\sigma$ y temperatura reducida $T = 1.49$. Los puntos son los resultados de la simulación y la línea continua es un ajuste polinomial de noveno grado.

El método de razones de transición ha sido propuesto recientemente por F. Sastre [2] y ha permitido evaluar el punto crítico de monomeros con interacción tipo pozo cuadrado con gran precisión.

Las simulaciones a bajas temperaturas se han llevado a cabo mediante la técnica de coexistencia directa haciendo uso del paquete GROMACS (versión 4.6) [3], en combinación con el potencial de pozo cuadrado continuo propuesto recientemente por Zerón y colaboradores [4].

Comparamos nuestros resultados con simulaciones numéricas obtenidas mediante aproximaciones de reweighting [5].

[1] A. Yethiraj and C. Hall, *Square-well diatomics: bulk equation of state, density profiles near walls, virial coefficients and coexistence properties*, Mol. Phys. **72**, 619 (1991).

[2] F. Sastre, *Critical temperature determination on a square-well fluid using an adaptation of the microcanonical-ensemble computer simulation method*, Mol. Phys. **118**, e1593534 (2020).

[3] D. van der Spoel, E. Lindahl, B. Hess, G. Groenhof, A. E. Mark, and H. J. Berendsen, *GROMACS: Fast, Flexible, and Free*, J. Comput. Chem., **26**, 1701 (2005).

[4] I. M. Zerón, C. Vega, and A. L. Benavides, *Continuous version of a square-well potential of variable range and its application in molecular dynamics simulations*, Mol. Phys. **116**, 3355 (2018).

[5] L. Li, K. Tang, L. Wu, W. Zhao and J. Cai, *Monte Carlo SImulation of vapor-liquid equilibrium and critical asymmetry of square-well dimer fluid*, J. Chem. Phys. **136**, 214508 (2012).

Ordering Dynamics and Path to Consensus in Multi-State Voter Models

Lucia Ramirez[1], Maxi San Miguel[1], and Tobias Galla[1]
[1]IFISC, Institute for Physics of Complex Systems (CSIC-UIB), Campus Universitat Illes Balears, 07122 Palma de Mallorca, Spain

In this work, we study the Voter Model with a general number M of opinion states, the multi-state voter model (MSVM)[1, 2], with a focus in the coarsening process. The system consists of N interacting agents placed on the nodes of a network. Agents can be in one of the M possible opinion states ($M \leq N$) and they interact with each other through an imitation process as follows: (i) a random voter is chosen; (ii) the selected voter takes the opinion of a randomly chosen neighbor; (iii) repeat until consensus is reached. We analyze the time evolution of the dynamics and the approach to consensus when the agents are placed in the nodes of a Complete Graph (CG) or in the nodes of uncorrelated networks such as the Erds Renyi (ER) or the Barabsi-Albert (BA) network. The approach to consensus is studied through the time evolution of the density of interfaces ρ, that is the fraction of links that connects the agents with different opinions.

The time evolution of the density of interfaces averaged over realizations, $< \rho >$, was analytically studied through rate equations for the MSVM on the CG and by means of the pair approximation [3, 4] for the uncorrelated networks. In both cases, $< \rho >$ has an exponential decay with a survival time τ that depends on the system size and not on the number of opinion states. It stands out that the absorbing state is only reached for finite size systems, while in the thermodynamic limit, the system stays in a metastable state. The analytical results were confirmed by numerical simulations.

The log-log plot of $< \rho >$ shows that the system stays in a plateau for a finite time before going to the absorbing state. The value of the plateaux, ξ, depends on M and on the mean degree $\overline{k}$ in the case of the ER and BA(Fig 1). The plateau value has a growing behavior with M.

Individual realizations of the MSVM show that finite systems initially fluctuates around a plateau and then ρ falls to successive intermediate plateaux as opinion states disappear, before going to the absorbing state. This behavior is not observed when the ensemble average is considered, so we performed restricted averages over realisations that only have M^* opinion states left to found intermediate plateaux (Fig 2).

After an extinction, the probability distribution of the fraction of agents in the surviving opinions states, $P(x_1, ..., x_{M^*})$, is found to be flat (this is, all $(x_1, ..., x_{M^*})$ such that $x_1 + ... + x_{M^*} = 1$ are equally likely) and the intermediate plateau value can be analytically obtained from the marginal distribution for a given M^*.

Finally, we introduced zealots (agents that do not change their opinion state during the dynamics) in order to engineer a MSVM that exhibits stable states equivalent to those intermediate plateaux of mixed opinions that were observed in the average over restricted realizations. By means of numerical simulations, we found that the addition of Z competing zealots creates stable states and, when there is one zealot of each opinion state, ρ stays in a steady state located at the same value than the intermediate plateau when only $M^* = Z$ opinion states are left (Fig 2). The correspondence between both plateaux is due to the fact that in the stationary state, when a zealot per opinion is introduced, the probability distribution of fraction of agents in each opinion is also flat.

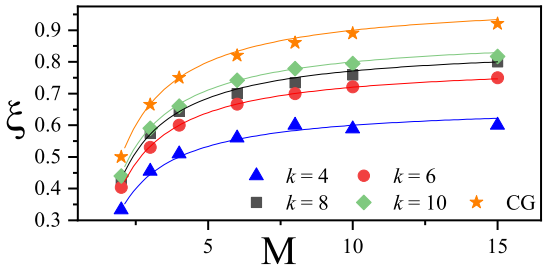

Fig. 1. Value of the plateau level ξ as function of M for the CG and networks with different mean degree $\overline{k}$. The lines are the analytical prediction. Initially, the opinions are equally distributed among the agents.

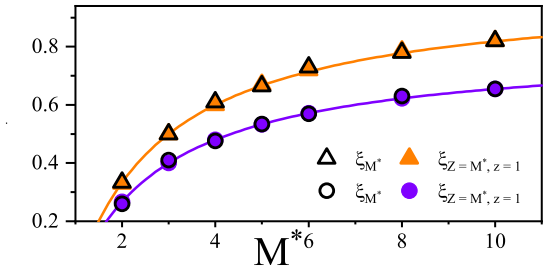

Fig. 2. Open triangles (circles) correspond to the plateau value for a MSVM on a CG (ER) when, after successive extinctions, there are M^* opinion left; full triangles (circles) correspond to the steady-state for a MSVM on a CG (ER) with a single zealot, $z_i = 1$, in each of the M^* possible opinion states. Both values are in good agreement.

[1] M. Starnini, A. Baronchelli, R. Pastor-Satorras, J. Stat. Mech. P10027 (2012).

[2] W. Pickering and C. Lim, Phys. Rev. E **93**, 032318 (2016).

[3] F. Vazquez, V. M. Eguiluz, New J. Phys.**10**, 63011 (2008).

[4] A. Carro, R. Toral, and M. San Miguel, Sci. Rep.**6**, 24775 (2016).

Predicción de las propiedades interfaciales de sustancias promotoras de hidratos usando Dinámica Molecular

C. Romero[1], J. Algaba[1], A. I. Moreno-Ventas Bravo[1], P. Gómez-Álvarez[1], J. M. Míguez[1], and F. J. Blas[1]
[1]Universidad de Huelva, Laboratorio de Simulación Molecular y Química Computacional,
CIQSO-Centro de Investigación en Química Sostenible and Departamento de Ciencias Integradas,
Facultad de Ciencias Experimentales, E21071 Huelva, Spain

Un clatrato es una red cristalina tridimensional formada por dos tipos de partículas bien diferenciadas. Por un lado, las partículas que forman la estructura cristalina, conocidas como 'host molecules', y por otro lado las partículas encerradas en las cavidades que forman estas estructuras, conocidas como 'guest molecules'. Cuando esta red cristalina está formada por moléculas de agua los clatratos se conocen con el nombre de hidratos. En la naturaleza, los hidratos se producen espontáneamente en condiciones de presión alta y de temperatura baja, muy alejadas de las condiciones ambientales, ante la presencia de un gas que ocupa sus cavidades, como por ejemplo CH_4 o CO_2. Por ello suelen aditivarse químicamente con promotores termodinámicos de hidratos, como el THF, que resulta el antecedente más importante que se tiene al desplazar la estabilidad de la fase hidrato a presión ambiental. Debido a la elevada toxicidad de esta sustancia existen otras alternativas como 1,3-dioxolano, oxano y ciclopentano. Sin embargo, los modelos moleculares disponibles para predecir el comportamiento de estas sustancias no se han testeado para comprobar su eficacia a la hora de predecir su tensión interfacial líquido-vapor. Esta es una propiedad muy sensible a los detalles moleculares, por lo que la convierte en una de las propiedades clave ya que si la tensión interfacial líquido-vapor se predice correctamente, junto con el equilibrio de fase, se obtendrán buenos candidatos para el estudio futuro de hidratos de metano, dióxido de carbono, hidrógeno, etc., en presencia de estos promotores. Así, en este trabajo se pretende disponer de modelos moleculares realistas tanto flexibles como rígidos que sean capaces de predecir con precisión el equilibrio de fase y tensión interfacial de los promotores hidratos: THF, 1,3-dioxolano, oxano y ciclopentano para posteriormente abordar su estudio en presencia de hidratos.

Interfacial properties of square-well chains using molecular dynamics

A. Morales, C. Romero, J. Algaba, P. Gómez-Álvarez, and Felipe J. Blas
Laboratorio de Simulación Molecular y Química Computacional,
CIQSO-Centro de Investigación en Química Sostenible and Departamento de Ciencias Integradas,
Universidad de Huelva, 21006 Huelva

Fully-flexible chains formed from tangentially-bonded monomeric units that interact through effective-type potentials represent perhaps the simplest option retaining the basic microscopic characteristics of molecular chains: segment connectivity, molecular flexibility, and attractive and repulsive interactions.Square-well (SW) potential is possibly the simplest interaction accounting for both attractive and repulsive interactions. However, its discontinuous functional form makes it extremely difficult to be used in molecular simulation, either Monte Carlo (MC) or Molecular Dynamics (MD) methods. Chapela and Alejandre [1] used especial techniques in MD simulations to explicitly account the impulsive forces generated in a system of SW chains with a potential range of $\lambda = 1.5\,\sigma$. The discontinuity in the interaction forces makes unfeasible to simulate this interaction potential with commercial MD programs such as GROMACS [2] or LAMMPS [3]. Very recently, Zerón *et al.* [4] have presented a parameterization of the SW potential that allows its use for simulation packages since the intermolecular potential and force are described by continuous mathematical functions. They determined the interfacial properties and the phase equilibrium of SW potentials of ranges $\lambda = 1.25$, 1.5 and $2.0\,\sigma$ using GROMACS. The excellent agreement of the obtained results with available experimental data pointed to the reliability of the reported continuous form. Since the phase equilibrium and interfacial properties of SW molecular chains with different range of interaction provide valuable information to discern whether different microscopic theories, such as those based on the density functional theory or equations of state, are capable of predicting this type of system, we extend here the study carried out by Zerón *et al.*[4] to other ranges of attractive interaction, in particular $\lambda = 1.5$ and $1.75\,\sigma$. Simulations for $\lambda = 1.5\,\sigma$ were conducted for chains of 4 monomers and the results compared with the previously reported computational predictions1 using distinct methodology. For the potential range of $\lambda = 1.75\,\sigma$, which had not yet been studied, we considered systems comprising 4, 8 and 16 monomers per molecule. Thus, the effect of the chain length is additionally assessed on the calculated properties, namely density profiles, coexistence densities, vapor pressures, temperature and critical density and surface tension. Overall, liquid-vapor interface sharpens with the increase in the chain length due to an increase in the width of the envelope of the coexistence phase, and the resulting increase in surface tension.

[1] G. A. Chapela and J. Alejandre, *Liquid-vapor interfacial properties of vibrating square well chains*, J. Chem. Fis. x **1**, 1-11 (2011).

[2] D. Van der Spoel, E. Lindahl, B. Hess, G. Groenhof, A. E. Mark, and H.J.C. Berendsen, *GROMACS: Fast, flexible, and free*, J. Comput. Chem. **26**, 1701 (2005).

[3] S. Plimpton, *Fast parallel algorithms for short-range Molecular Dynamics*, J. Comput. Phys. **117**, 1-19 (1995).

[4] I. M. Zerón, C. Vega, and A. L. Benavides, *Continuous version of a square-well potential of variable range and its application in molecular dynamics simulations*, Mol. Phys. **116**, 3355 (2018).

Air traffic flow dynamics under the lens of ordinal patterns statistics

Felipe Olivares[1] and Massimiliano Zanin[1],
[1]Institute for Cross-Disciplinary Physics and Complex Systems (IFISC), CSIC-UIB, 07122 Palma, Spain.

As true for all socio-technical systems, one key ingredient to allow an effective and efficient management of air transport is to be able to access precise, and possibly real-time information about its dynamics. It thus comes as no surprise that benchmarking airport operations is not a new topic, and many research works have appeared in the last twenty years proposing different solutions [1]. Creating and evaluating a set of measures representing airport performance is of utmost importance for multiple stakeholders, from regulatory bodies to passengers and airlines, as it allows evaluating and selecting alternative investment strategies, and monitoring aspects like the evolution of safety or environmental impact. Additionally, a well-designed benchmarking metric in principle allows to compare heterogeneous airports, e.g. independently on the available infrastructure or traffic volume. On the other hand, this task is far from trivial, as many factors may hinder the results: from how measured variables are defined, to the underlying assumptions or the methodology employed in the analysis. Consequently, no single golden solution has been proposed yet.

We here propose the use of the permutation Jensen-Shannon distance (JSD), a symbolic tool able to quantify the degree of similarity between two arbitrary time series [2]. This quantifier results from the fusion of two concepts, the Jensen-Shannon divergence and the encoding scheme based on the sequential ordering of the elements in the data series [3]. More specifically, it constitutes a measure of distinguishability between two probability distributions, the symbol composition between different sequences can be quantitatively compared through this metric.

Our goal is to measure the presence of interactions between landing flights from a macro-scale perspective. We firstly present a synthetic model of landings at an airport, showing how the JSD is able to detect interactions arising from high volumes of traffic. Secondly, we show that air trafic flow volume can be considered as a modulated noisy signal, from which the high-frequency component is an auto-regressive process of first order AR(1). Real landing data for eleven major European airports are then analysed prevouis to the COVID19 pandemic, showing that the correlation parameter of the high-frequency component is proportional to the average landing separation—see Fig. 1. Moreover, we found that restrictions impossed after March 2020 reduced the temporal correlations in the traffic flow volume, as depicted in Fig.2 for Barajas airport.

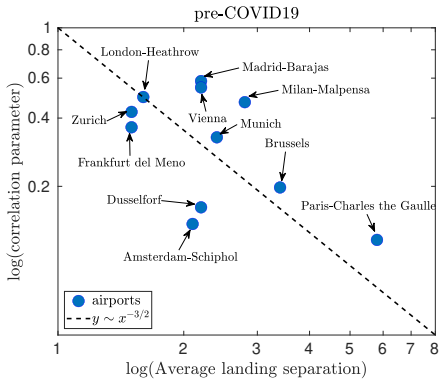

Fig. 1. Correlation parameter versus average landing separation in log-log scale for eleven major European airports pre COVID19 pandemic.

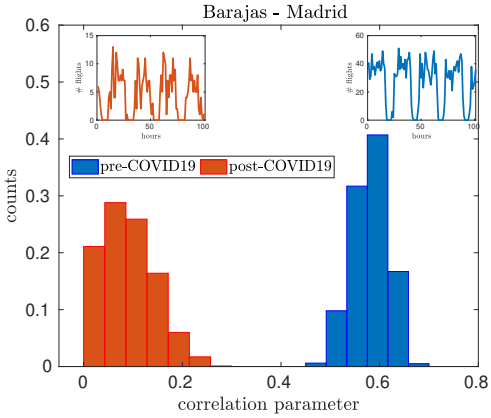

Fig. 2. Histograms of the correlation parameter pre and post COVID19 pandemic for Barajas airport. Inset left and rigth panels correspond to 4 days of operations after and before restrictions, respectively.

[1] P.L. Lai, A. Potter, M. Beynon. *The development of benchmarking techniques in airport performance evaluation research*. Transportation Journal **51**, 305337 (2012).

[2] L. Zunino, F. Olivares, H.V. Ribeiro, and O.A. Rosso. *Permutation Jensen-Shannon distance: a versatile and fast symbolic tool for complex time series analysis*. Under Review in Physical Review E (2022).

[3] C. Bandt and B. Pompe. *Permutation entropy: A natural complexity measure for time series*. Phys. Rev. Lett. **88**, 174102 (2002).

Predicción de las propiedades interfaciales de la Hidroquinona mediante Dinámica Molecular

J. M. Olmos[1], J. M. Míguez[2], A. I. Moreno-Ventas Bravo[2], M. M. Pineiro[3] and F. J. Blas[1]

[1]Universidad Autónoma de Madrid, Departamento de Química Física Aplicada, Facultad de Ciencias, Universidad Autónoma de Madrid, E28049 Madrid, Spain

[2]Universidad de Huelva, Laboratorio de Simulación Molecular y Química Computacional, CIQSO-Centro de Investigación en Química Sostenible, Departamento de Ciencias Integradas, Facultad de Ciencias Experimentales, E21071 Huelva, Spain

[3]Universidade de Vigo, Departamento de Física Aplicada, Facultad de Ciencias do Mar, Universidade de Vigo , Lagoas-Marcosende s/n, 36310 Vigo, Spain

Este trabajo presenta un detallado análisis del equilibrio de fases líquido-vapor y de las propiedades interfaciales de una sustancia química tan compleja como la hidroquinona en un rango de temperaturas comprendido entre 480K y 580K. La investigación presentada se ha llevado a cabo mediante la técnica de simulación molecular, una herramienta indispensable hoy en día en ámbitos como la Química-Física al permitir obtener propiedades estructurales y microscópicas difícilmente accesibles desde el punto de vista experimental y analizar condiciones termodinámicas inalcanzables experimentalmente. Concretamente, este trabajo se ha realizado mediante la técnica de simulación molecular denominada Dinámica Molecular, empleando el programa GROMACS (versin 4.6.5) en el colectivo canónico (NVT) y mediante el método de coexistencia directa, que consiste en poner en contacto directo en una misma caja de simulacin las distintas fases presentes en los sistemas objeto de estudio.

Los modelos moleculares seleccionados para describir el comportamiento de la hidroquinona pertenecen a la familia de campos de fuerza denominados TraPPE (Transferable Potentials for Phase Equilibria) y OPLS (Optimized Potentials for Liquid Simulations). La parametrización de los distintos grupos, así como los potenciales de enlace, torsión y flexión que forman parte de cada uno de los modelos moleculares utilizados, se han obtenido de la bibliografía a excepción del modelo Trappe-UA que es propuesto por primera vez en este trabajo a partir de la parametrización del benceno. Aunque el modelo TraPPE ya ha sido utilizado previamente por otros autores para describir el equilibrio de fases líquido-vapor y las propiedades interfaciales de la hidroquinona, los restantes modelos nunca han sido utilizados con este fin.

La simulación molecular predice correctamente la coexistencia de dos fases, una fase líquida en contacto con una fase vapor, a las condiciones termodinámicas consideradas. Los perfiles de densidad obtenidos han sido analizados en detalle en la región interfacial y han permitido calcular las densidades de coexistencia de cada fase. Finalmente, se han calculado otras propiedades como la presión de vapor y la tensión interfacial para mostrar más claramente la eficacia de los modelos moleculares propuestos en este trabajo, al comparar los resultados obtenidos con datos experimentales disponibles en la bibliografía.

Contagion-diffusion processes with recurrent mobility patterns of distinguishable agents

Pablo Valgañón[1], David Soriano-Paños[2,3], Alex Arenas[4] and Jesús Gómez-Gardeñes[1,3,5]
[1]Departament of Condensed Matter Physics, University of Zaragoza, 50009 Zaragoza (Spain).
[2]Instituto Gulbenkian de Ciência (IGC), 2780-156 Oeiras (Portugal).
[3]GOTHAM lab, Institute for Biocomputation and Physics of Complex Systems (BIFI), University of Zaragoza, 50018 Zaragoza (Spain).
[4]Departament de Matemáticas i Enginyeria Informática, Universitat Rovira i Virgili, Tarragona (Spain).
[5]Center for Computational Social Science, University of Kobe, 657-8501 Kobe (Japan).

The analysis of contagion-diffusion processes in metapopulations is a powerful theoretical tool to study how mobility influences the spread of communicable diseases. Nevertheless, many metapopulation approaches use indistinguishable agents to alleviate analytical difficulties. Here, we address the impact that recurrent mobility patterns, and the spatial distribution of distinguishable agents, have on the unfolding of epidemics in large urban areas. We incorporate the distinguishable nature of agents regarding both, their residence, and their usual destination. The proposed model allows both a fast computation of the spatio-temporal pattern of the epidemic trajectory and. the analytical calculation of the epidemic threshold. This threshold is found as the spectral radius of a mixing matrix encapsulating the residential distribution, and the specific commuting patterns of agents. By the end of this paper it will become clear that very subtle differences in the way we treat the system's agents will have very important consequences, in a similar way that the distinguishability of particles matters in statistical physics. We prove that the simplification of indistinguishable individuals overestimates the value of the epidemic threshold (Fig. 1) and show how the new formalism can be a powerful tool to assess control strategies aimed at increasing the epidemic threshold under scenarios of epidemiological risk.

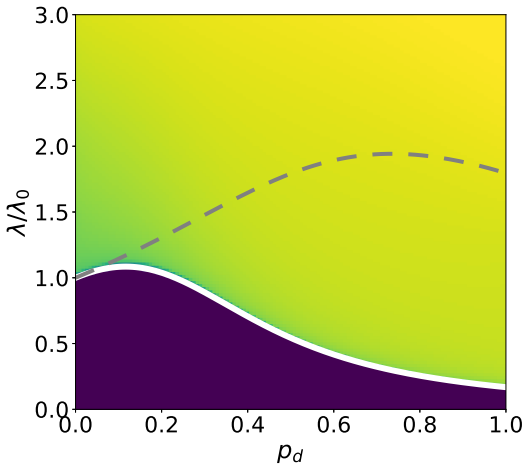

Fig. 1. Epidemic diagram with the normalized epidemic threshold (vertical axis) against the mobility parameter (horizontal axis) of the city of Miami, Florida. The dashed grey line accounts for the epidemic threshold of the indistinguishable agents, and the continuous white line shows the epidemic threshold of the distinguishable agents.

Inherent anatomic features of V1 leads to dynamical separation of neurons behaviour

Javier Galvan Fraile[1], F. Scherr[2], J.J. Ramasco[1], W. Maass[2] and C.R. Mirasso[1]
[1] Institute for Cross-Disciplinary Physics and Complex Systems (IFISC, UIB-CSIC), Palma de Mallorca, Spain
[2]Institute of Theoretical Computer Science, Graz University of Technology, Graz, Austria

Since we started to interact with the outside world, we have learned to distinguish whether the movement is coming from our own actions or from the movement of external objects. To distinguish between these experiences, it is necessary to factor out the sensory consequences of our actions from incoming sensory information. The main framework accounting for this sensorimotor integration is the **predictive coding**, which suggest that an internal representation of the world lies in the neocortex circuitry[1]. This representation, which is used to make predictions about incoming sensory input, is continuously updated using the sensed information from our surroundings. Even though the structural rules underlying this functional properties of cortical circuits are poorly understood, recent research has shed light on the computational roles played by the different neural populations[2]. Of particular interest is in this context the computational role of top-down (TD) inputs[1], which are transmitted to lower cortical areas such as the primary visual cortex (V1), during the processing of bottom-up (BU) sensory inputs. The theoretical framework suggests that the V1 circuitry is able to compute the difference between both inputs, generating prediction errors.

This findings represent a Copernican turn in the interpretation of the top-down inputs. Instead of providing sparse representations of sensory inputs, a more modern interpretation arises in the context of Reinforcement Learning models for brain learning. It should summarize all information from the present and past, including sensory experiences and internal goals, which is potentially relevant for choosing the right action in order to achieve the desired goals. This new interpretation of the **predictive coding** is at the heart of recent reviews and experimental studies [3] [5]. In addition, other experimental studies suggest that BU and TD inputs are integrated individually, without any sensorimotor expectation[6].

Therefore, understanding how the genetically encoded structure of canonical microcircuits in the neocortex implements brain computation and learning is an important open research question. The answer to this tangled question can be better elucidated from the implementation and analysis of computational models of canonical microcircuits. In this sense, the Allen Institute has developed a model for a microcircuit of area V1 in mouse that builds on a huge body of experimental work. The model is substantially more reliable than any previous model and includes the preprocessing of visual information in the thalamic lateral geniculate nucleus (LGN) [4] (see Figure 1). Hence, the detailed study of sensory input effects on the model should represent an starting point in order to shed light on these open questions.

In this work we perform extensive numerical simulations of the model introduced by the Allen Institute to analyse the effect that different visual stimuli have on the L2/3 layer excitatory neurons, which are the main candidates to behave as *prediction error neurons*. In particular, these neurons exhibit a dynamical separation in their response to perturbations of the visual flow, similarly to the behaviour of prediction error neurons (see Figure 1). Thus, we study the main factors leading to this effect, ranging from the role played by inhibitory neurons to the particular effect of visual flow features.

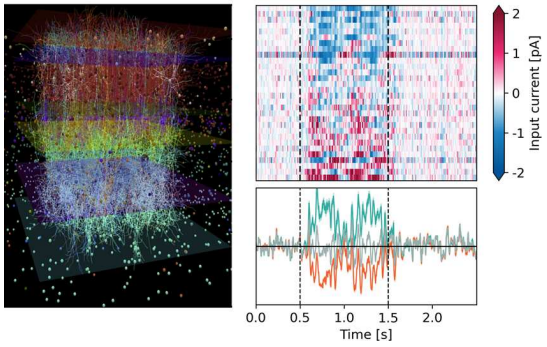

Fig. 1. Left: Visual representation of a fraction of the V1 model neurons. Right: Heatmap of average current responses for a sample of L2/3 excitatory neurons with different behaviours.

[1]Signals originated at higher order cortical areas involving actions and behavioural information.

[1] Rao, R. P., & Ballard, D. H., *Predictive coding in the visual cortex: a functional interpretation of some extra-classical receptive-field effects.*, Nature neuroscience 2.1 (1999): 79-87.

[2] Harris, K. D., & Shepherd, G. M., *The neocortical circuit: themes and variations.*, Nature neuroscience 18.2 (2015): 170-181.

[3] Keller, G. B., & Mrsic-Flogel, T. D., *Predictive processing: a canonical cortical computation.*, Neuron 100.2 (2018): 424-435.

[4] Billeh, Yazan N., et al., *Systematic integration of structural and functional data into multi-scale models of mouse primary visual cortex.*, Neuron 106.3 (2020): 388-403.

[5] Jordan, R., & Keller, G. B., *Opposing Influence of Top-down and Bottom-up Input on Excitatory Layer 2/3 Neurons in Mouse Primary Visual Cortex*, Neuron 108.6 (2020): 1194-1206.

[6] Muzzu, T., & Saleem, A. B., *Feature selectivity can explain mismatch signals in mouse visual cortex.*, Cell reports, 37(1), 109772 (2021).

Correlation lag times provide a reliable early-warning indication of approaching bifurcations in spatially extended dynamical systems

Giulio Tirabassi and Cristina Masoller
Departament de Física, Universitat Politècnica de Catalunya, Rambla Sant Nebridi 22, 08222 Terrassa, Spain

Identifying upcoming bifurcations and regime transitions from observations is a significant challenge in time series analysis. Well-known early warning indicators (EWIs) are the increase in spatial and temporal correlation. Here we propose a new indicator that takes into account both. By inspecting the distribution of lag times that maximize the cross-correlation between pairs of adjacent points, we find that the variance of the distribution consistently decreases as the bifurcation approaches. We demonstrate the reliability of this indicator using different models that exhibit different types of bifurcations [1].

Formally, we define the lag, τ_{ij}, that maximizes the absolute cross-correlation between two time series u_i and u_j, as

$$\tau_{ij} = \underset{1\leq\tau\leq\tau_{\max}}{\operatorname{argmax}_\tau} \left(\left| \sum_t u_i(t) u_j(t+\tau) \right| \right), \qquad (1)$$

where u_i and u_j are normalized to have zero mean and unitary variance. From an operational standpoint, we search for the maximum in a range of τ values from 1 up to a maximum value, $\tau_{\max}$, that is 4% of the length of the time series, and computed the cross-correlation using 96% of the time series length. Moreover, we limit the calculation only to ij nodes that are first neighbors. To test the variance of τ_{ij}, σ_τ, as a possible EWI, we simulated three different models where different types of bifurcations occur. By studying how σ_τ varies when the parameter approaches the bifurcation, we obtain integrated spatio-temporal information, and we show that it is more informative than the autocorrelation or spatial correlation.

We report in Fig. 1 an example for one of the models we studied. We consider a model that describes the evolution of a scalar field, u, in a 1D space, with diffusion, noise, and a bistable potential whose asymmetry is governed by the bifurcation parameter, α.

$$\frac{\partial u}{\partial t} = -u^3 - \alpha u^2 + u(1+\alpha) + D\frac{\partial^2 u}{\partial x^2} + \xi \qquad (2)$$

where D modulates the diffusion strength, and ξ is a gaussian noise term. Depending on α, the system has one or three fixed points. When α approaches a critical value, two fixed points collide giving rise to a transcritical bifurcation. Approaching the bifurcation point, the time series variance increases and CSD is detected through lag-1 correlation and spatial correlation (Fig. 1a). However, although both these quantities increase, their behavior does not reveal how close the system is to the bifurcation, since they grow monotonically and the bifurcation occurs way before they reach their maximum possible value. In contrast, σ_τ displays a non-monotonic behavior with respect to the bifurcation parameter (Fig. 1b). In particular, approaching the bifurcation, σ_τ slightly increases collapsing right before the transition. The variation of σ_τ is more informative than that of the mean value of τ_{ij} distribution (dashed line), as the maximum provides a condition to be fulfilled for the transition to happen. The inflection point can be explained making the hypothesis that τ_{ij} distribution is formed by two components: one localized at low τ_{ij} that dominates when close to the bifurcation, and a uniform distribution that dominates when the system is far from it. The bifurcation parameter moves the distribution towards these two extremes. The maximum represents the moment in which the localized distribution overtakes the random one.

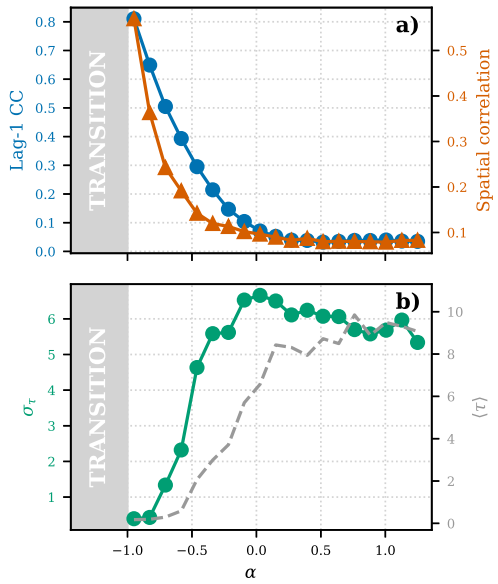

Fig. 1. **(a)** Conventional EWIs, lag-1 temporal correlation and spatial cross-correlation, as a function of the bifurcation parameter, α, for the scalar bistable 1D model. **(b)** Mean, $\langle\tau\rangle$, and standard deviation, σ_τ, of the distribution of lags that maximize the cross-correlation. One single realization of the dynamics has been used.

[1] G. Tirabassi and C. Masoller, "Correlation lags give early warning signals of approaching bifurcations", Chaos, Solitons & Fractals 155, 111720 (2022).

Temperature chaos is present in off-equilibrium spin-glass dynamics.

Javier Moreno-Gordo on behalf of the Janus Collaboration.

Spin glasses exhibit a fragile behavior in response to perturbations such as temperature changes. Specifically, arbitrary small changes in the temperature would lead to a complete reorganization of the equilibrium configurations of the spin glass. This phenomenon has been called Temperature Chaos [1, 2].

This equilibrium definition has focused the research effort on small system sizes that can be equilibrated. We have observed a phenomenon that closely mimics the Temperature Chaos in large non-equilibrium spin-glass and we provide a quantitative description [3]. By invoking the static-dynamic equivalence principle we find that the key quantity which is ruling the non-equilibrium Temperature Chaos phenomenon is the correlation length ξ . Also, a rare-event analysis is needed to deal with the strong spatial-heterogeneity of the non-equilibrium Temperature Chaos. We find a crossover between weak and strong chaos regime controlled by a crossover length ξ whose analysis reveals the close relation with its equilibrium counterpart: the chaotic-length [2].

[1] A. J. Bray and M. A. Moore, Phys. Rev. Lett. 58, 57 (1987)

[2] J. R. Banavar and A. J. Bray, Phys. Rev. B 35, 8888 (1987)

[3] Marco Baity-Jesi, Enrico Calore, Andrés Cruz, Luis Antonio Fernandez, José Miguel Gil-Narvion, Isidoro Gonzalez-Adalid Pemartin, Antonio Gordillo-Guerrero, David Iñiguez, Andrea Maiorano, Enzo Marinari, Víctor Martin-Mayor, Javier Moreno-Gordo, Antonio Muñoz-Sudupe, Denis Navarro, Ilaria Paga, Giorgio Parisi, Sergio Perez-Gaviro, Federico Ricci-Tersenghi, Juan Jesús Ruiz-Lorenzo, Sebastiano Fabio Schifano, Beatriz Seoane, Alfonso Tarancon, Raffaele Tripiccione, and David Yllanes. Communications Physics 4, 74, (2021)

Asymmetric relaxation of vibrational excitations for nitromethane in water

Arnau Jurado Romero[1], Rossend Rey Oriol[1], and Carles Calero Borrallo[2]
[1]Universitat Politècnica de Catalunya, Jordi Girona, 1-3. B5, 08034 Barcelona
[2]Universitat de Barcelona, Martí i Franquès, 1, 11, 08028 Barcelona

Energy dissipation is of interest for the accurate generation and control of movement in micro and nano-particles. Thus, studying the relaxation of molecules after a vibrational excitation has potential applications in multiple fields.

We consider the nitromethane molecule, whose energy relaxation after vibrational excitation has already been studied in argon gas and for micro-canonical excitations [1, 2]. We first test these previous works by performing individual mode excitations within the normal mode approximation. The obtained results suggests that the relaxation behaviour (shape, characteristic time, etc.) does not depend on the particular excitation in an Argon gas.

Prompted by the polar nature of the nitromethane molecule we study its relaxation in liquid water, based on the assumption that a polar solvent will present different behaviour than for a noble gas. We perform high energy excitations (200 kJ/mol) of individual modes and study their energy relaxation via all-atom molecular dynamics simulations.

Our results show that, as expected, some normal modes relax considerably faster than others. These faster modes have associated motions related to the nitro group of the nitromethane molecule, which is to be expected due to the hydrophilic nature of the functional group.

To get more insight into the relaxation mechanisms we also studied the work performed by the nitromethane molecule on the surrounding water molecules [3]. We divide surrounding molecules in two groups: the one on the nitro group side and the ones on the methyl group side.

Our main finding is that energy relaxation is remarkably asymmetric, favoring the nitro side (30% more work the work is performed to the nitro side than to the methyl side). Excitations to low frequency normal modes associated with the nitro group are significantly more asymmetric, again favoring the nitro side (between 10 and 20% more than for other excitations).

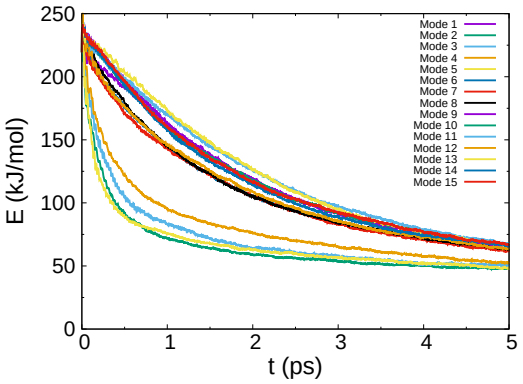

Fig. 1. Total vibrational energy (vibrational kinetic + potential energy) of a single nitromethane molecule after excitations of 200 kJ/mol in the labeled modes. Each curve represents the average of 200 realizations of the excitations in a 300 K SPC/E water system.

To our knowledge this is the smallest molecule for which a marked asymmetry has been found, irrespective of the excited mode.

[1] Rivera-Rivera, L. A., Wagner, A. F., Sewell, T. D., and Thompson, D., J. Chem. Phys. **142**, 014303 (2015).

[2] Rivera-Rivera, Luis A. and Wagner, Albert F. and Perry, Jamin W., J. Chem. Phys. **151**, 034303 (2019).

[3] Rossend Rey and James T. Hynes, PCCP **14**, 6332 (2012).

Vaccination strategies in structured populations under partial immunity and reinfection

Gabriel Rodríguez-Maroto[1,2], Iker Atienza-Diez[1,2], Saúl Ares[1,2], and Susanna Manrubia[1,2]
[1] Systems Biology Department, Centro Nacional de Biotecnología (CSIC), Madrid, Spain
[2] Grupo Interdisciplinar de Sistemas Complejos (GISC), Madrid, Spain

The enormous effects of infectious diseases in humankind through history could only be counteracted through massive vaccination campaigns. Optimal protocols of vaccine administration to minimize the effects of infectious diseases depend on several variables that admit different degrees of control: the characteristics of the disease and its impact on different groups of individuals, controlled non-pharmaceutical interventions and, critically, vaccine roll-out [1]. It is often very difficult to assess *a priori* the importance and effect of such different factors.

Here we study a compartmental model of infection propagation and analyse the effect that variations in the vaccination and reinfection rates have on the progression of the disease and on the number of fatalities [2]. The model considers five different classes: Susceptible (S), Infected (I), Reinfected (Y), Recovered (R) and Dead (D), and fulfills

$$\dot{S} = -\beta_{SI}\frac{IS}{N} - \beta_{SY}\frac{YS}{N} - v\,\Theta(S,\theta) \quad (1)$$

$$\dot{I} = \beta_{SI}\frac{IS}{N} + \beta_{SY}\frac{YS}{N} - rI - \mu_I I \quad (2)$$

$$\dot{Y} = \beta_{RI}\frac{IR}{N} + \beta_{RY}\frac{YR}{N} - rY - \mu_Y Y \quad (3)$$

$$\dot{R} = rI + rY - \beta_{RI}\frac{IR}{N} - \beta_{RY}\frac{YR}{N} + v\,\Theta(S,\theta) \quad (4)$$

$$\dot{D} = \mu_I I + \mu_Y Y, \quad (5)$$

where $\Theta(S,\theta)$ is a function taking into account the maximum fraction of population vaccinated. For simplicity, we take here a step function at 70% vaccination. Parameters refer to the infection rate (β, subindexes representing the two classes in contact), the recovery rate r and the death rate for first and secondary infections (μ_I and μ_Y, respectively). Details in estimated values can be found in [2].

As a practical example, we study COVID-19 dynamics in various countries using real demographic data and contact matrices between different groups [3]. We first divide the population into two age groups to highlight the overall effects on disease caused by vaccination rates and demographic structure. We observe, first, that the higher the fraction of reinfected individuals, the higher the likelihood that the disease becomes quasi-endemic and, second, that optimal vaccine roll-out depends on demographic structure and disease fatality. Therefore, there is no unique vaccination protocol, valid for all countries, that minimizes the effects of a specific disease.

Our second analysis focused on the dynamics of COVID-19 in Spain using nine age groups. We explored the space of all possible combinations (9!) for the order in the vaccination protocol as a function of age and evaluated its performance in terms of the number of fatalities and infections, comparing with the baseline case of vaccination in strict decreasing age order. We conclude that, at least for COVID-19 in Spain, there is no strategy significantly better than age-ordered vaccination.

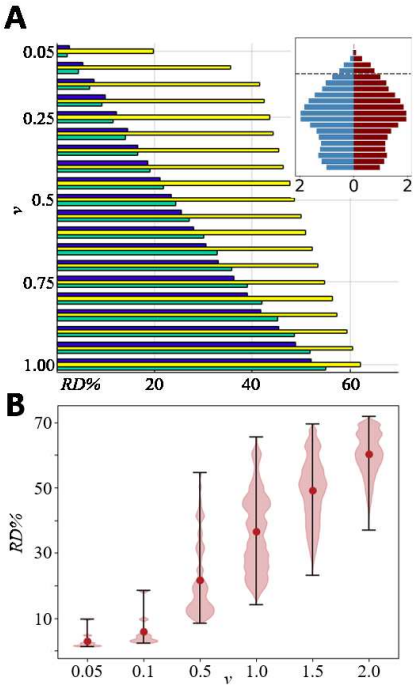

Fig. 1. Death reduction (RD%) in Spain as a function of vaccination rate (v) compared to the no vaccination scenario for (A) the 2-group model with an age threshold at 80 years considering old-first (yellow), young-first (dark blue) and simultaneous (turquoise) vaccination. (B) the extended 9-group model. Violin plots summarize the distribution of all possible permutations.

[1] J. Lavine, O. Bjornstad, and R. Antia, *Immunological characteristics govern the transition of COVID-19 to endemicity*, Science (2021).

[2] G. Rodríguez-Maroto, I. Atienza-Diez, S. Ares and S. Manrubia, *Vaccination strategies in structured populations under partial immunity and reinfection*, MedRxiv (2021).

[3] D. Mistry, M. Litvinova, AP. Piontti, M. Chinazzi, L. Fumanelli, MFC. Gomes et al., *Inferring high-resolution human mixing patterns for disease modeling*, Nature Communications (2021).

Simulating active agents with DPD hydrodynamics

C. Miguel Barriuso Gutiérrez[1], José Martín Roca[1], C. Valeriani[1], V. Bianco[2] and I. Pagonabarraga[3],

[1]Dpto. EMFTEL, Facultad de Física - Universidad Complutense de Madrid
[2] Dpto. de Química Física, Facultad de Química - Universidad Complutense de Madrid
[3] Departament de Física de la Matéria Condensada, Facultat de Física - Universitat de Barcelona

In this ongoing work we are developing a framework to simulate active agents taking into account both hydrodynamics and thermal fluctuations. Currently we are limiting our study to colloids and polymers although the framework will be applicable to agents with a wide range of structures. To achieve this we propose an extension of the widely known simulation software LAMMPS [1] that allows the implementation of hydrodynamic self-propulsion via force redistribution among solvent particles, this extension, in combination with the Dissipative Particle Dynamics (DPD) package [2], enables these kind of simulations.

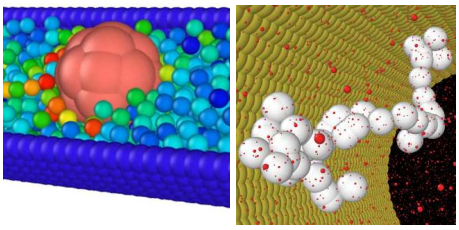

Fig. 1. Active colloid (left) and polymer (right) inside a channel full of DPD solvent.

Similar approaches using lattice Boltzmann (LB) methods [3] and Multi-Particle Collision dynamics (MPC) [4] have been already well studied. With DPD and MPC dynamics we can easily simulate agents with more complex shapes taking into account thermal fluctuations, both of which are harder to implement using LB methods. Our approach takes advantage of the versatility of the LAMMPS code, being MPI-parallelizable and allowing the combination of our implementation with the wide range of features LAMMPS offers.

We are interested in the subsets of active matter systems known as active colloids [5, 6] and active polymers [7], which have very useful and broad applications [8]. Their collective behaviour is rich and complex, and in many cases cannot be ascribed solely to the agents motion: hydrodynamic interactions need to be taken into account [9]. This is the case, for example, of many self-propelled microorganisms, or *microswimmers* [10], whose movement is an essential aspect of life. A successful model for this systems is the so-called *squirmer* [11, 12], in their simplest form these are hard spheres that take into account the propulsion induced by the beating cilia and flagella as a prescribed steady velocity of the solvent particles tangential to the surface of the sphere. This model serves as inspiration for our project.

The equations of motion of our model for the agent (i) and the solvent particles (j) read,

$$\boldsymbol{F}_i = \boldsymbol{F}_i^{\mathrm{DPD}} + \boldsymbol{F}_i^{T} \quad \text{and} \quad \boldsymbol{F}_j = \boldsymbol{F}_j^{\mathrm{DPD}} + \boldsymbol{F}_j^{H} \qquad (1)$$

where $\boldsymbol{F}^{\mathrm{DPD}} = \boldsymbol{F}^{C} + \boldsymbol{F}^{D} + \boldsymbol{F}^{R}$ represent respectively the conservative, dissipative and random forces of the DPD interaction, $\boldsymbol{F}^{T}$ corresponds to the thrust exerted by the agents propulsion, which causes a hydrodynamic reaction force, $\boldsymbol{F}^{H}$, on the solvent particles. This hydrodynamic force field results from the two first angular modes B_1 and B_2 of the surface velocity field of the squirmer model. The first mode determines the maximum velocity the swimmer can achieve, while their ratio $\beta = B_2/B_1$ captures different types of swimmers which perturb their surrounding fluid in different ways, pushers ($\beta < 0$), pullers ($\beta > 0$), neutrals ($\beta = 0$) and shakers ($\beta \to \infty$).

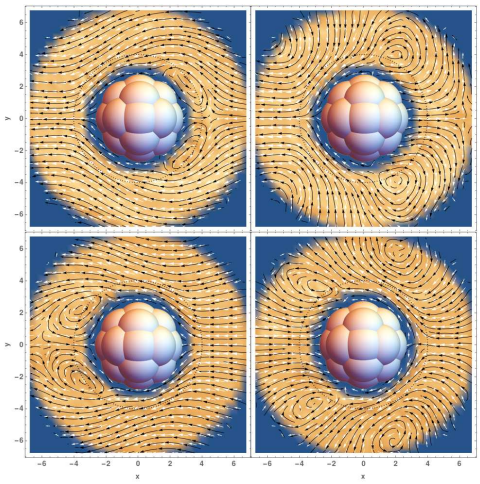

Fig. 2. Solvent velocity field around a squirmer self-propelling in the positive x-axis in the colloid (left) and laboratory (right) reference frame, for $\beta = -5$ (*pusher*, top) and $\beta = 5$ (*puller*, bottom).

[1] A. P. Thompson et al, Comp Phys Comm, **271** (2022) 10817.
[2] Groot and Warren, J Chem Phys, **107**, 4423-35 (1997)
[3] F. Alarcon, E. Navarro-Argemí, C. Valeriani, and I. Pagonabarraga, Phys. Rev. E **99**, 062602
[4] Zttl, A., Stark, H. 2018, Simulating squirmers with multiparticle collision dynamics, *Eur. Phys. J. E* **41** 61
[5] Igor S Aranson 2013 *Phys.-Usp.* **56** 79
[6] Andreas Zttl and Holger Stark 2016 *J. Phys.: Condens.Matter* **28** 253001
[7] R. Winkler and G. Gompper, J. Chem. Phys. **153**, 040901 (2020)
[8] S.J. Ebbens 2016 *Current Opinion in Colloid and Interface Science* **21** 14-23
[9] A. Scagliarini and I. Pagonabarraga, Soft Matter, 2020, **16**, 8893-8903
[10] Gerhard Gompper et al 2020 J. Phys.: *Condens. Matter* **32** 193001
[11] M.J. Lighthill 1952 *Comm. on Pure and Applied Math.*,**V** 109 118 (1052)
[12] J.R. Blake 1971 *J. Fluid Mech.* **46**, part 1, pp. 199-208

Application of a statistical inference model to the prediction of antibody affinity from sequence analysis

David Luna[1], Dr. Pierpaolo Bruscolini[2], and Dr. Sergio Pérez Gaviro[2]
[1] Dep. de Física Teórica, Universidad de Zaragoza
[2] Dep. de Física Teórica & BIFI, Universidad de Zaragoza

The interest in therapeutic antibodies has grown quickly due to their huge potential application in a large number of diseases; however they are still difficult to design. That is because they cannot be computationally designed with the necessary accuracy to reach the required affinity to the antigen and their equilibrium properties cannot be predicted precisely. Furthermore, it is not known with sufficient precision the mechanisms of antibody maturation and selection, that transform a naive antibody, generated by the random combination of copies of the V, (D), and J genes, into a specialized tool for recognizing and binding a particular antigen, without causing damages to the self.

In this work, we describe the evolution in the sequence space as a Ornstein-Uhlenbeck (OU) process, that is, a stochastic Markov process, where the sequences undergo a drift towards an attractor of high affinity, while they also diffuse randomly in sequence space. Introducing some approximation and simplifying hypotheses, we are able to perform a bayesian inference of the attractor and final variance. The objective is to model the maturation process using this OU process. In this approach, the clusters of observed sequences are considered as multivariate gaussian snapshots of the evolution. In this way, the ordinary OU process is replaced by a system of temporally linked gaussian distributions, as shown in Fig. 1, which are inferred from a sequence of sub-clusters identified in a experimental data set [1]. The attractors of this OU process are assumed to characterize the fully matured sequences cluster. It can be checked, using the MG score if the sequences of the hypermutated cluster are fully maturated or they were just maturated until their virus affinity was high enough.

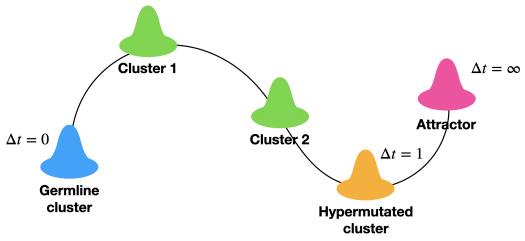

Fig. 1. Modified Ornstein-Uhlenbeck representation.

[1] Asti L, Uguzzoni G, Marcatili P, Pagnani A. Maximum-Entropy Models of Sequenced Immune Repertoires Predict Antigen-Antibody Affinity. PLoS Comput Biol 12(4): e1004870. (2016)doi:10.1371/journal.pcbi.1004870

[2] Marcou, Q., Mora, T. Walczak, A.M. High-throughput immune repertoire analysis with IGoR. Nat Commun 9, 561 (2018). doi:10.1038/s41467-018-02832-w

[3] Pilar Calvo Príncipe, Refinement of a statistical model for antibody humanization, TFM.(September 2019)

[4] Clavero-Alvarez, A., Di Mambro, T., Perez-Gaviro, S. et al. Humanization of Antibodies using a Statistical Inference Approach. Sci Rep 8, 14820. (2018) doi.10.1038/s41598-018-32986-y

Preferential orientation and interfacial anomalous energies at interfaces in aqueous liquid-liquid solutions of molecular chains

E. Feria, J. Algaba, J. M. Míguez and Felipe J. Blas
Laboratorio de Simulación Molecular y Química Computacional,
CIQSO-Centro de Investigación en Química Sostenible and Departamento de Ciencias Integradas,
Universidad de Huelva, 21006 Huelva

The behaviour of liquid-liquid equilibria systems are an object of attention due to their participation in chemical processes, specially in petroleum industry. Fatty Acid Methyl Esters (FAMEs) are very interesting compounds for being an alternative to fossil fuels, using them as biodiesel [1], and for their environmental applications, for instance, removing contaminants from water. On the other hand, hydrocarbons and alkanols produced in the industry act as contaminants because of their low solubility in water. In both cases, the interaction with water is controlled by the interfacial properties, which are the point of this investigation.

This work is focused on the comparison of the interfacial behaviour for mixtures solutions of FAMEs with water and primary alkanols with water. On one hand, binary mixtures of primary alkanols, from 1-butanol to 1-heptanol [2], with water are studied at atmospheric pressure and temperatures between 280 K and 380 K. On the other hand, aqueous solutions of methyl esters, from methyl acetate to methyl heptanoate [3], are studied at atmospheric pressure and temperatures ranged between 278.15 and 358.15K. In both cases, the interfacial properties of the systems are obtained using molecular dynamic simulations (MD) [4] in the isobaric-isothermic or NP_zT ensemble with the direct coexistence technique. Density profiles, coexistence densities, compositions, and interfacial tensions obtained from simulations are compared with experimental data taken from literature.

Agreement between simulation predictions and experiments is good, including coexistence densities and compositions, as well as interfacial tension values. Molecular models are able to predict the characteristic parabolic shape of the interfacial tension as a function of temperature. They also capture the existence of a relative maximum value for each system at a temperature that increases as the molecular weight of the organic molecule is increased. Unfortunately, the experimental values of interfacial tension are substantially overestimated by our predictions in all cases. This is probably since unlike interactions between organic molecules and water are not accounted for properly.

[1] Demirbas, M. Fatih, *Biorefineries for biofuel upgrading: a critical review.*, Applied energy **86**, 151-161 (2009).

[2] Algaba, J., Míguez, J. M., Gómez-Álvarez, P., Mejía, A., and Blas, F. J.*Preferential orientations and anomalous interfacial tensions in aqueous solutions of alcohols.*, J. Chem. Fis. **124(38)**, 8388-8401 (2020).

[3] Feria, E., Algaba, J., Míguez, J. M., Mejía, A., and Blas, F. J. *Molecular dynamics of liquidliquid equilibrium and interfacial properties of aqueous solutions of methyl esters.* Phys. Chem. Chem. Phys. **24(9)**, 5371-5382 (2022).

[4] D. Frenkel and B. Smith, *Understanding Molecular Simulation*, Academic, (2002)

Kinetic theory of a confined quasi-one-dimensional gas of hard disks

M. Mayo[1], J. Javier Brey[2], M. I. García de Soria[3], and P. Maynar[4]
[1]Universidad de Sevilla, mmayo@us.es
[2]Universidad de Sevilla, brey@us.es
[3]Universidad de Sevilla, gsoria@us.es
[4]Universidad de Sevilla, maynar@us.es

In recent years, the study of transport phenomena in gases or liquids confined in spaces whose characteristic length is comparable to the molecular size, has attracted a lot of attention. This has been prompted and stimulated by the relevant new technological applications of nanofluidics [1, 2]. The experimental advances ask for a better understanding, at a conceptual level, of the effects that strong confinement has on the non-equilibrium behavior of fluids. Because under these conditions the particles do not explore a bulklike environment, and because of the asymmetry generated by the confining boundaries, strongly confined systems exhibit inhomogeneity and anisotropy, that have both a great impact on their macroscopic properties. Kinetic theory and non-equilibrium statistical mechanics provide the appropriate context to investigate which is the right macroscopic description of transport under strong confinement, providing also the expressions for the needed transport coefficient.

In this work, a dilute gas of hard disks confined between two straight parallel lines is considered. The distance between the two boundaries is in between one and two particle diameters, so that the system is quasi-one-dimensional. A Boltzmann-like kinetic equation, that takes into account the limitation in the possible scattering angles, is derived. It is shown that the equation verifies an H-theorem implying a monotonic approach to equilibrium. The implications of this result are discussed, and when particularized for the equilibrium situation, the result agrees, in the appropriate limit, with the entropy computed by means of equilibrium statistical mechanics methods [3, 4]. Closed equations describing how the kinetic energy is transferred between the degrees of freedom parallel and perpendicular to the boundaries are derived for states that are homogeneous along the direction of the boundaries. The theoretical predictions of relaxation time of the System is:

$$\tau = \frac{3}{4\varepsilon^3}. \qquad (1)$$

Equation (1) is agree with results obtained by means of Molecular Dynamics simulations (see Fig. 1).

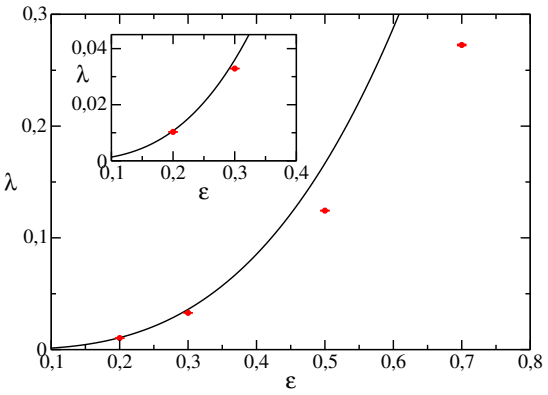

Fig. 1. Inverse of the characteristic relaxation time, λ , of the temperature parameters in a confined quasi-one-dimensional systems of hard disks, as a function of the dimensionless parameter $\varepsilon \equiv (h-\sigma)/\sigma$, that is a measure of the width of the system.

[1] Schoch, Reto B. and Han, Jongyoon and Renaud, Philippe, *Transport phenomena in nanofluidics*, Rev. Mod. Phys. **80**, 839 (2008).

[2] Bocquet, L., and Charlaix, E. *Nanofluidics, from bulk to interfaces. Chemical Society Reviews*, **39**, 1073 (2010).

[3] M. Schmidt and H. Löwen, *Freezing Between Two and Three Dimensions*, Phys. Rev. Lett. **76**, 4552 (1996).

[4] M. Schmidt and H. Löwen, *Phase diagram of hard spheres confined between two parallel plates*, Phys. Rev. E **55**, 7228 (1997).

Menzerath and Menzerath-Altmann's law as a criterion of complexity in communication

Iván G Torre [1], Łukasz Debowski[2], and Antoni Hernández-Fernández[3]
[1]Vicomtech Foundation, Basque Research and Technology Alliance (BRTA), San Sebastián, Spain
[2]Institute of Computer Science, Polish Academy of Sciences, Warszawa, Poland
[3]Complexity and Quantitative Linguistics Lab, Institut de Ciéncies de l'Educació, Universitat Politécnica de Catalunya, Barcelona, Spain,
[4]Societat Catalana de Tecnologia, Secció de Ciéncies i Tecnologia, Institut d'Estudis Catalans, Barcelona, Spain

Menzerath's law is a quantitative linguistic law which states that, on average, the longer is a linguistic construct, the shorter are its constituents. In contrast, Menzerath-Altmann's law (MAL) is a precise mathematical power-law-exponential formula which expresses the expected length of the linguistic construct conditioned on the number of its constituents:

$$y = \alpha m^{\beta} \exp(-\gamma m) \tag{1}$$

where α, β, γ are empirical parameters, being $\alpha > 0$, and usually $\beta < 0$ and $\gamma < 0$.

MAL and Menzerath's law have intensely been researched within the field of quantitative linguistics including written corpora, speech, and even music. Besides, similar analyses can be extended to any system that forms a hierarchy of units of different levels. Consequently, Menzerath's law has also been observed in genomes, protein domains, penguin vocalizations, chimpanzee gestural communication and primate vocalizations [1]. However, to fully consider whether MAL and Menzerath's law have an explanation from the point of view of compression and emerging complexity [2], we will do the exercise of studying them for so-called monkey typing models, which have previously heated the debate about other linguistic laws and brought stimulating results to the scientific community.

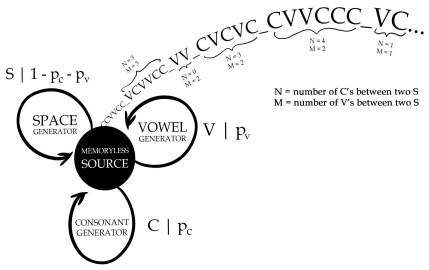

Fig. 1. The memoryless source model

Let N and M be the numbers of consonants and vowels, respectively, in a randomly generated word. Then, the mean length of a syllable equals $\frac{N+M}{M}$, if we assume that the number of syllables in the word can be approximated as the number of vowels M. Moreover p_c is the probability of emitting a C symbol in a one state memoryless source, p_v the probability of emitting V and $1-p_c-p_v$ the probability of emitting S (see Figure 1). Then, the exact form of Menzerath's law for the memoryless source is obtained:

$$E\Big(\frac{N+M}{M}\Big|M=m\Big) = \frac{a}{m} + b, \tag{2}$$

where

$$a = \frac{p_c}{1-p_c}, \quad b = 1 + \frac{p_c}{1-p_c}. \tag{3}$$

We show that this null model complies with Menzerath's law, revealing that Menzerath's law itself can hardly be a criterion of complexity in communication. This observation does not apply to the more precise Menzerath-Altmann's law, which predicts an inverted regime for sufficiently range constructs, i.e., the longer is a word, the longer are its syllables. To support this claim, we analyze MAL on data from 21 languages, consisting of texts from the Standardized Project Gutenberg. We show the presence of the inverted regime, not exhibited by the null model, and we demonstrate robustness of our results. We also report the complicated distribution of syllable sizes with respect to their position in the word, which might be related with the emerging MAL (see Figure 2). Altogether, our results indicate that Menzerath's law -in terms of correlations is a spurious observation, while complex patterns and efficiency dynamics should be rather attributed to specific forms of Menzerath-Altmann's law [3].

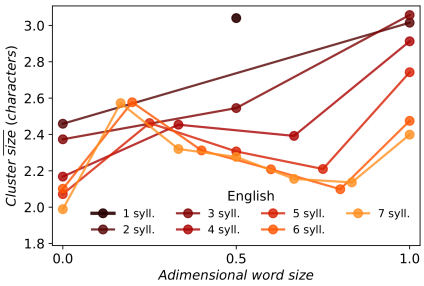

Fig. 2. Syllable sizes depending on word length and position

[1] S. Semple, R. Ferrer-i-Cancho and M. L. Gustison, *Linguistic laws in biology*, Trends in Ecology & Evolution (2021).

[2] I. G. Torre, B. Luque, L. Lacasa, C. T. Kello and A. Hernández-Fernández, *On the physical origin of linguistic laws and log-normality in speech*. R. Society open science, 6(8), 191023 (2019).

[3] I. G. Torre, Ł. Debowski and A. Hernández-Fernández, *Can Menzerath's law be a criterion of complexity in communication?*, Plos one 16(8), e0256133 (2021).

Interface Fluctuations and Intrinsic Profiles in Mobility Induced Phase Separation

Enrique Chacón[1], Francisco Alarcón[2], Jorge Ramirez[3] , Pedro Tarazona[4] and Chantal Valeriani[5]
[1]Instituto de Ciencia de Materiales de Madrid, Consejo Superior de Investigaciones Cientificas, 28049 Madrid, Spain
[3]Departamento de Ingenieria Física, División de Ciencias e Ingenierías,
Universidad de Guanajuato, Loma del Bosque 103, 37150 León
[3] Departamento de Ingenieria Química, ETSI Industriales, Universidad Politécnica de Madrid, 28006, Madrid
[4] Departamento de Física Teórica de la Materia Condensada, Universidad Autónoma de Madrid, 28049 Madrid, Spain
[4]Departamento de Estructura de la Materia, Física Térmica y Electrónica and GISC,
Universidad Complutense de Madrid 28040 Madrid, Spain

We analyse the interfacial line in two dimensions (2D) Mobility Induced Phase Separation (MIPS) of active Brownian particles, with Lennard-Jones (LJ) interactions, in the high activity regime, when the dynamics of the particles is fully dominated by a high active force, with random diffusive changes of the activity direction in each particle, but with a persistence time which becomes longer than the collision time in the dense phase of the MIPS (see general references in [1]). Simulations of a dense slab, self-maintained in contact with a low density gas, are analysed to identify the instantaneous shape of the interfacial lines, at the two edges of the slab. The accumulated statistics for the Fourier components of the lines shows independent Gaussian probabilities which may be interpreted as those of an effective thermal equilibrium interface, and used to get effective values of the line tension and bending modulus for the MIPS system.

In 2D the width of the interfacial fluctuations grows as the square root of the line length, much faster than the logarithmic effect of the capillary waves in a three dimensional liquid surface. Large MIPS simulations are required to get a good representation of dense slab, with long range structures associated to hexatic order [1], and that large size of the simulations implies a severe lost of detail in the structure of the interfacial region, when represented by the mean profiles of the density and any other property. The identification of the instantaneous interfacial lines allows to calculate intrinsic profiles for the density, the particle polarization and the interaction forces, eliminating the local wandering of the interface that smooths the mean density profile and blurs out the details of the interfacial region. The intrinsic profiles are independent of the system size (for large enough systems) and they give important clues on the physical mechanisms for the MIPS.

In normal (thermal equilibrium) liquid-vapour surfaces the intrinsic density profiles show a dense structured liquid right from the inner edge of the instantaneous interface, but in the MIPS intrinsic profiles the density raises smoothly over a thick interfacial region of $15 - 20$ particle diameters. Moreover, the shape of the intrinsic profiles is surprisingly similar over a large range of the active force, showing a perfect scaling with the density difference between the 2D quasi-crystal a the center of slab and the low density of the gas phase. The intrinsic density profiles for the local polarization of the particles and the LJ-interaction force acting on each particle show that this thick region (at the inner side of the dense slab) contains the main contribution to the 'rectification' of the active force that is at the core of the MIPS. The randomly orientation of the active force is usually interpreted as an 'exotic' kinetic effect, that shakes the particles in a different way than a thermal equilibrium, but which does not act (in average) as an external potential able to produce a pressure gradient across the interface. This view has been recently challenged [2] by Omar et al. pointing that, when the persistence time of the active force orientation becomes larger than the mean free path of the particles, the (null) averaged polarization of each particle may be 'locally rectified', i.e. it may become a non zero mean local polarization of the 'particles at a given position' at the interface. That mean local polarization implies that the (externally applied) 'active force' acts as a stationary external potential across the interface, producing a pressure difference between the two coexisting phases. The intrinsic analysis presented here not only supports that view, but it also characterizes the inner side of the interface, i.e. the thick region where the intrinsic density profile raises smoothly, as the main source for the active force rectification, and associates it to the distribution of 2D-crystal defects, as lines of dislocations anchored at the source provided by the interface.

The observed scaling of the intrinsic density profiles matches with the view that the universality class that described the MIPS (over a very broad range of the activity force) is not 'liquid-vapour like', based on a scaling length that diverges at the critical point. Instead the scaling is based on the 2D quasi-crystal lattice parameter, that sets the density in the dense slab and that reflects the balance between the particle (repulsive) interactions and the pressure generated by the active force (kinetic pressure of the gas, plus rectification effects across the interface). The closing dome, at the lower values of the activity force that produce MIPS, occurs very close to the melting of the hexatic structure in the dense slab, which implies the breaking of the 'high-activity' regime that cover most of the usual range over which MIPS has been studied.

[1] P. Digregorio, D. Levis, A. Suma L.F. Cugliandolo, G. and I. Pagonabarraga, Phys. Rev. Lett. **121**, 098003 (2018).

[2] A.K. Omar, Z-G Wang and J.F. Bradt, *Microscopic Origins of the Swim Pressure and the anomalous Surface Tension of Active Matter*, arXiv:1912.11727v1 [cond-mat.soft] (2019).

Retirado después de la edición de este libro

Técnica Mold Integration Guest Para El Cálculo De La Energía Interfacial Del Hidrato De CO_2

I. M. Zerón[1], J. M. Míguez[1], B. Mendiboure[2] y F. J. Blas[1]
[1]Laboratorio de Simulación Molecular y Química Computacional, CIQSO-Centro de Investigación en Química Sostenible y Departamento de Ciencias Integradas, Universidad de Huelva, 21007 Huelva, Spain
[2]Laboretoire des Fluides Complexes et Leurs Réservoirs, UMR5150, Université de Pau et des Pays de l'Adour, B. P. 1155, Pau Cdex 64014 (France).

En las útimas décadas, los hidratos de gas han despertado un gran interés científico, industrial y ecológico al ser estos una fuente confiable de energía futura y a su vez una alternativa viable para enclaustar gases de efecto invernadero.

Los esfuerzos científicos se han enfocado principalmente en el estudio de los hidratos de metano y de dióxido de carbono, al ser el primero una fuente prometedora de energía (se calcula la existencia de por lo menos 10 teratoneladas) repartida en todo el mundo, y el segundo, una alternativa ecológica para atrapar el gas de CO_2 cuya presencia en la atmóosfera representa aproximádamente el 64 % de los gases de efecto invernadero [1].

A pesar de los múltiples estudios, tanto experimentales como teóricos y de simulación para diversas propiedades de los hidratos de gas, pocos estudios se han enfocado en medir la energía interfacial sólido-líquido (propiedad crucial pra el entendimiento de la formación y crecimiento de los hidratos) debido a la complejidad de medir fiablemente esta cantidad. Para el caso de dióxido de carbono sólo pueden destacarse dos estudios independientes: Uchida y colaboladores [2] y el de Anderson y colaboradores [3], cuyos valores de energía interfacial reportados son: 28(6) mJ/m^2 y 30(3) mJ/m^2, en cada caso.

Cuando la exitencia de datos experimentales es escasa, las técnicas de simulación molecular se vuelven una fuente de referencia confiable. En este trabajo se ha calculado medidante dinámica molecular la energía interfacial del hidrato de CO_2 con su fase diluida en agua a condiciones de coexistencia de 287 K y 40 MPa. Los modelos moleculares usados para simular el agua y el CO_2 son el modelo TIP4P/Ice y el modelo TraPPE [4]. Debido a que la nucleación es un evento raro se ha extendido la metodología Mold Integration (MI) [5, 6] para inducir la formación de una capa delgada de hidrato mediante el uso de pozos de potencial para las moleculas de CO_2 ubicados en las posiciones de fase cristalina del hidrato. En esta contribución se combina la técnica de integración termodinámica y con la definición de la energía interfacial para su determinación.

El valor de la energía interfacial hidrato CO_2-agua obtenida en este trabajo es de 27(2) mJ/m^2, el cual concuerda con los resultado experimentales repotados por Uchida et al. y Anderson et al., siendo estos 28(6) y 30(3) mJ/m^2. Más aún, el actual resultado es acorde al obtenido por el grupo de investigación en una trabajo previo donde se utilizaron moldes para las moléculas de agua, siendo de 29(2) mJ/m^2 [7].

[1] R. Boswell and T. S. Collett, *Current perspectives on gas hydrate resources*, Energy & environmental science. **4**, pp. 1206–1215 (2011).

[2] T. Uchida, T. Ebinuma, S. Takeya, J. Nagao, H. J. Narita *Effects of pore sizes on dissociation temperatures and pressures of methane, carbon dioxide, and propane hydrates in porous media*, J. Phys. Chem. B **106**, pp. 820-826(2002).

[3] R. Anderson, M. Llamedo, B. Tohidi, R. W. Burgass, *Experimental Measurement of Methane and Carbon Dioxide Clathrate Hydrate Equilibria in Mesoporous Silica*, J. Phys. Chem. B **107**, pp. 3507–3514(2003).

[4] J. M. Míguez, M. M. Conde,1 J.-P. Torré, F. J. Blas, M. M. Piñeiro, C. Vega,*Molecular dynamics simulation of CO2 hydrates: Prediction of three phase coexistence line*, J. Chem. Phys.**142**, pp. 124505 (2015).

[5] J. R. Espinosa, C. Vega, E. Sanz, *The mold integration method for the calculation of the crystal-fluid interfacial free energy from simulations*, J. Chem. Phys. **141**, pp. 134709 (2014).

[6] J. R. Espinosa, C. Vega, E. Sanz, *Ice-Water Interfacial Free Energy for the TIP4P, TIP4P/2005, TIP4P/Ice, and mW Models As Obtained from the Mold Integration Technique*, J. Phys. Chem. C **120**, pp. 8068-8075 (2016).

[7] J. Algaba, E. Acuña, J. M. Míguez, B. Mendiboure, I. M. Zerón,and F. J. Blas *In review*.

Dynamics of Transposable Elements and Small RNA in Polyploidization Events

Esteban Meca[1], Concepción M. Díez[2], and Brandon S. Gaut[3]
[1]Departamento de Física Aplicada, Radiologa y Medicina Física, Universidad de Córdoba,
Campus Universitario de Rabanales, Edificio Albert Einstein (C2), 14014 Córdoba (Spain).
[2]Departamento de Agronomía, Universidad de Córdoba,
Campus Universitario de Rabanales, Edificio Celestino Mutis (C4), 14014 Córdoba (Spain).
[3]Department of Ecology and Evolutionary Biology, University of California, Irvine
California 92697-3875 (United States of America).

Transposable elements (TEs) are DNA sequences with the ability of independently self-replicating within a genome. They are present in the genome of most species, and can constitute a large part the genome, for plants in particular. As an example, 85% of the sequence of the maize genome derives from past transposition events [1]. Their proliferation is controlled by RNA interference, mediated by *small-interfering* RNA (siRNA), short RNA sequences (22-24nt) that can be transcribed from the TEs themselves.

The so-called "genomic shock" events can alter significantly this control mechanism, possibly enabling a burst of Transposable Elements. One of such possible events is polyploidization, by which the whole genome can be doubled. It is known that such events are common among many species, leading to very large genomes, such as the one from wheat.

In order to understand the proliferation and the epigenetic control of TEs, a model was built that accounted for the deactivation (*silencing*) of TEs, the production of different kinds of siRNA and the replication of active TEs [2] (see Fig. 1). The model compared well with experimental studies and highlighted the importance of silenced TEs as a source of siRNA.

In the case of a polyploidization event, the model needs to be extended to account for the extra copies of the genome. Here we address the development of such a model and distinguish between two cases, one in which the polyploidization event involves the same species (autopolyploid) and the case in which hybridization with a different species is present (allopolyploid).

The equilibria and stability of both cases are studied, in the general case where n copies of the genome are present (n-ploidy). The model allows to study how is siRNA partitioned among the different copies of the genome. Two cases have been considered, one in which siRNA is homogeneously distributed among the different copies and another in which siRNA is distributed according to the specific abundances of active TEs among the different copies of the genome. We study these two regimes and explore the inequivalent dynamical regimes using dynamical system theory.

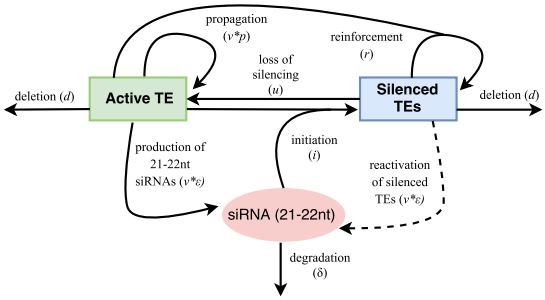

Fig. 1. Block diagram of the model from Roessler et al. [2]

This model has allowed us to uncover a very rich phenomenology, which depends very strongly on the partitioning of siRNA. This can help elucidate standing questions in hybridization dynamics, such as subgenome dominance or whether siRNA is additively expressed by the different copies of the genome.

[1] M. C. Stitzer, S. N. Anderson, N. M. Springer, and J. Ross-Ibarra, PLOS Genetics **17**(10): e1009768 (2021).

[2] K. Roessler, A. Bousios, E. Meca, and B. S. Gaut, Genome Biology and Evolution **10**, 803–815 (2018).

Trend characterisation of agri-food time series using Local Hurst exponent

L. Pérez-Sienes [1,2] , M. Grande-Toledano [1,2], J. C. Losada [1] and J.Borondo[1,2]
[1] Grupo de Sistemas Complejos, ETS Ingeniería Agronómica, Alimentaria y de Biosistemas, Universidad Politécnica de Madrid (Spain).
[2] AGrowingData S.L.

In agriculture, the sales of an horticultural product is essential for the supply chain. Depending on the commodity under study one should have into consideration certain variables. On the one hand, the volume of good, which is translated into offer in the market, will depend on the climate during the season, the crop extension, etc. On the other hand, demand will depend on consumption trends, availability of other products, period of the year (there are festivities or times along the year where certain products are more demanded). As a consequence, the analysis of price for such products is complicated, and in order to obtain more accurate predictions technical analysis should be accompanied by fundamental analysis (study of market trends, breaking news, weather history). While deep and complete analysis may require more data resources and experts in the agriculture sector, one can tackle the challenge using different methods regarding analytical techniques. Sometimes by observing the data history we can already notice patterns and cycles. Thus, knowing in advance the trend of a commodity will asses the farmer about the time to harvest.

In order to assist on harvest planning, forecasting the trend of a price commodity may result of great support. As a consequence, farmers can decide wether to collect the product or wait some days. In this scenario, time left for price median regression may be relevant.

Many studies have focused on forecasting price using various techniques with good accuracy, from ARIMA models to Neuronal Networks.

In our work, we study the relationship between the *Local Hurst* parameter (H) and the time needed for the time series to regress to the local median. Hurst exponent ranges between 0 and 1 providing information about the persistence of a series: when $H < 0.5$ the series is antipersistent, when $H = 0.5$ the series follows a random process, and when $H > 0.5$ the series is persistent. For our study we followed the methodology presented in [1] using the definition of Hurst from [2]. Then, for a time series $y : y_0, \ldots, y_N$ and for the time window τ Hurst parameter is computed as:

$$K(\tau) \propto \tau^H \quad \text{where,} \tag{1}$$

$$K(\tau) = \frac{< |y(t+\tau) - y(t)| >}{< |y(t)| >}, \tag{2}$$

Once we set a time window τ_H and assign a Hurst value for every time step i-th, we categorise days into three regimes: antipersistent when $H \in [0, 0.45]$, intermediate when $H \in (0.45, 0.55)$ and persistent $H \in [0.55, 1]$. Afterwards, for each i-th day we compute the local median of past τ_m days, $m_{\tau_m} = \text{median}(y_{i-\tau_m}, \ldots, y_i)$, and measure the time distance until the time series crosses the local median. Our time series describe daily price evolution of few horticultural commodities from the region of Almería (Spain) over 5-year period, from 2014 to 2019. They fluctuate from few cents to few euros.

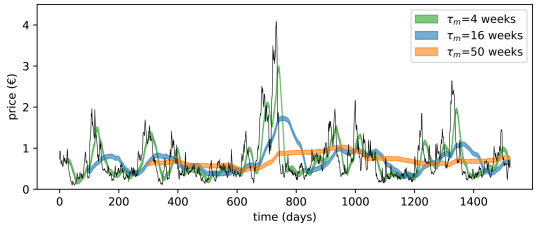

Fig. 1. Price evolution for aubergine from 2015 to 2019. Moving medians of different time windows are also represent.

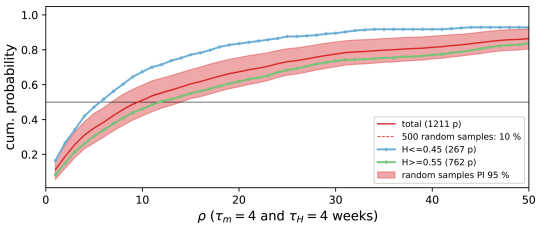

Fig. 2. Cumulative probability distribution of time for regression to local median.

Finally, we compute the cumulative distribution of time distance for next regression for the different Hurst regimes.

In Fig. 2 we have plotted the cumulative distribution of time until next regression for all days belonging to antipersistent, intermediate and persistent regime. In order to compare with a null set of data, we have also plotted the distribution of random selected sets of days from our collection. We see how persistent days (green curve) tend to regress to local median slower than rest of days. Curves suggest that for certain time scales there are significant differences between the expected time need to regress to the local median among the Hurst regimes.

[1] E. Molino-Minero-Re, F. García-Nocetti, H. Benítez-Pérez; 'Application of a Time-Scale Local Hurst Exponent analysis to time series', *Digital Signal Processing* **37**, 92-99 (2015).

[2] T. Di Matteo, T. Aste, and M. M. Dacorogna; 'Long term memories of developed and emerging markets: using the scaling analysis to characterize their stage of development', *Journal of Banking and Finance* 29, 827-851 (2005).

Numerical simulations on the Potts model using algorithms based on transition rate

Lourdes Bibiana Merino-Solís[1], and Francisco Sastre[1]
[1]División de Ciencias e Ingenieras, Campus León de la Universidad de Guanajuato,
Loma del Bosque 103, Lomas del Campestre CP 37150, León, Gto., México

In this work we implement a new algorithm based on transitions rates between order parameter levels in the two dimensional q-state Potts model without external field.

The Potts model has been widely studied and is one of the few interacting models with analytical solution, in the two dimensional case without external field [1]. Despite its simplicity it can be used to study several systems such as magnetic dominions grow [2, 3, 4], cellular behavior [5, 6] or social and demographic behavior [7, 8], for name a few.

However, the study of the phase diagram when external fields are included, has been proved to be very difficult to establish using the standard numerical methods. This is the main reason to use a new numerical method to study the Potts model, as a first step without external field.

The algorithm is based on the determination of the transition rates of between discrete macroscopic observables. This numerical method can to evaluate directly the derivative of the logarithm of the probability distribution function with respect to the order parameter [9]. Using standard finite-size scaling theory we evaluate the critical point and the correlation length critical exponent for q = 2, 3 and 4.

Our results are in good agreement with the expected theoretical value [1]. Theoretical values are as follows: $T_c = 0.9949$, $\nu = 5/6$ for $q = 3$ and $T_c = 0.9102$, $\nu = 2/3$ for $q = 4$, while the results obtained were $T_c = 0.9896 \pm 0.0075$, $\nu = 0.7735 \pm 0.0628$ for $q = 3$ and $T_c = 0.9087 \pm 0.0085$, $\nu = 0.6425 \pm 0.0458$ for $q = 4$.

[1] F. Y. Wu, *The Potts model*, Rev. Mod. Phys. **54**, 235 (1982).

[2] J. Vinals and M. Grant, *Role of activated processes and boundary conditions in the domain growth of the Potts model*, Phys. Rev. B **36**, 7036 (1987).

[3] G. S. Grest, M. P. Anderson, and D. J. Srolovitz, *Domain-growth kinetics for the Q-state Potts model in two and three dimensions*, Phys. Rev. B **38**, 4752 (1988)

[4] C. Sire and S. N. Majumdar, *Coarsening in the q-state Potts model and the Ising model with globally conserved magnetization*, Physical Review E **52**, 244254 (1995).

[5] G. J. Graner F, *Simulation of biological cell sorting using a two-dimensional extended Potts model*, Phys Rev Lett **69**, 2013 (1992).

[6] S. J. Turner S, J *Intercellular adhesion and cancer invasion: a discrete simulation using the extended Potts model*, Theor Biol **216**, 85 (2002).

[7] C. Schulze, *Potts-like model for ghetto formation in multi-cultural societies*, International Journal of Modern Physics C **16**, 351355 (2005).

[8] V. A. Traag and J. Bruggeman, *Community detection in networks with positive and negative links*, Phys. Rev. E **80**, 036115 (2009).

[9] F. Sastre, *Critical temperature determination on a square-well fluid using an adaptation of the microcanonical-ensemble computer simulation method*, Molecular Physics **118**, e1593534 (2020).

Anlisis y construcción de un modelo dinámico del sistema energético

Darío Ferreira Martínez[1,2], Ángeles López Aguera[2] y Alberto P. Muñuzuri[1,3]

[1]Grupo de Física No Lineal. Facultad de Física, Univ. Santiago de Compostela, 15782, Santiago de Compostela, España.

[2] Grupo de Aplicaciones Energéticas Sostenibles. Facultad de Física, Univ. Santiago de Compostela, 15782, Santiago de Compostela, España.

[3] CITMAga, Santiago de Compostela, España.

El acoplamiento de las energías renovables, de naturaleza fluctuante, al sistema energético, así como la seguridad de este ante las distintas fluctuaciones (distintas tecnologıas y bandas de reserva del sistema energético), es una preocupación que muchas de las herramientas ms comunmente utilizadas no pueden resolver con facilidad [1, 2]. Por este motivo, se construirá y planteará el sistema energético como una red compleja cuya evolucion viene determinada por un conjunto de ecuaciones dinámicas que atienden tanto a criterios tecnológicos y como económicos. Este modelo incluirá las conexiones entre los diferentes nodos de producción y consumo, constituyendo una red. Se utilizará este modelo para realizar análisis a cerca de los tiempos de respuesta, su comportamiento ante tales fluctuaciones y su estabilidad [3], tratando de adaptarlo al ejemplo de Galicia.

[1] M. Wlesch, P. Deane, M. Howells, B. O Gallachoir, F. Rogan, M., Bazilian y H., Rogner *Incorporating flexibility requirements into long-term energy system models A case study on high levels of renewable electricity penetration in Ireland*, Applied Energy, **135**, 600-615 (2014). doi: 10.1016/j.apenergy.2014.08.072.

[2] D. Connolly, H. Lund, B. Mathiesen y M. Leahy, *A review of computer tools for analysing the integration of renewable energy into various energy systems*, Applied Energy, **87**, 1059-1082 (2010). doi: 10.1016/j.apenergy.2009.09.026.

[3] H. Nakao y AS. Mikhailov, *Turing patterns in network-organized activator-inhibitor systems*, Nature Physics, **6**, 544-550, 1820 (2010). doi: 10.1038/nphys1651

Magnetic nanoparticles as biosensors

P. Palacios-Alonso[1,2], E. Sanz-de Diego[2], F. J. Terán[2], and R. Delgado-Buscalioni[1]
[1] Universidad Autónoma de Madrid , C. Francisco Tomás y Valiente 7, , 28049, Madrid, Spain
[2]iMdea nanociencia, C. Faraday 9, Cantoblanco, 28049, Madrid España

There are an increasing number of studies that aim to use nanoparticles to improve the current healthcare standards. In our work we are focused in using magnetic nanoparticles to detect the presence of a biomarker in a solution via their modification of the alternating current (AC) magnetization cycles. In particular, changes in the AC magnetization can be observed when the MNP are functionalized with a ligand that specifically interacts with the biomarker, affecting the magnetic and hydrodynamic response: either via surface modification (detection based on single MNPs) or via the formation of MNPs aggregates.

Most of the applications based on magnetic nanoparticle (MNP) involve liquid suspensions where the Brownian displacements of MNPs are coupled by long-ranged magnetic and hydrodynamic couplings, however at present there is no efficient computational implementation of nanoscale magneto- hydrodynamics (NMH). To carry out our study we have developed a very efficient GPU computational algorithm that integrates the magnetization dynamics of the MNP taking into account both, the Brownian Relaxation (change of the magnetization due to the rotation of the particles) and the Nel relaxation (change of the magnetization because of the internal rotation/fluctuation of the magnetic moment). Our integrator of the magnetization has been written as a module of UAMMD [1], so it trivial to include hydrodynamic interactions in our simulations.

The Brownian relaxation of the particles is solved using Brownian Dynamics to integrate the rotation and the translation of the particles taking into account the torque exerted by the magnetic field on the particles,

$$\vec{\tau} = \vec{m} \times \vec{B} \tag{1}$$

The Neel relaxation is integrated using the Landau-Lifshitz-Gilbert (LLG) equation,

$$\frac{d\vec{m}}{dt} = \frac{-\gamma_0}{1+\alpha^2}\left(\vec{m} \times \vec{B}_{eff} + \alpha \cdot \vec{m} \times \vec{m} \times \vec{B}\right) \tag{2}$$

The detection of biomarkers using the surface modification is based on the change of the hydrodynamic size of the particles when a biomarker interacts with the ligands of the particle. The change in the hydrodynamic size increase the phase-lag between the magnetic field and the magnetization changing the shape of the magnetization cycles of the particles.

Using our algorithm we can reproduce the magnetization cycles of non-interacting magnetic nanoparticles under multiple conditions of field intensity and frequency. In addition from the changes in the shape of the magnetization cycles we can detect the presence of dextran molecules on the surface of the particles and measure the new hydrodynamic size of the particles when the dextran is attached to the surface of the MNP.

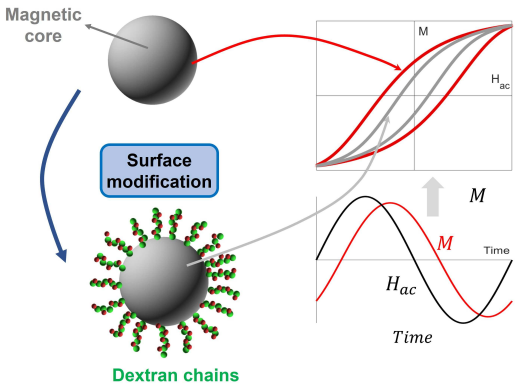

Fig. 1. The modification of the surface change the shape of the magnetization cycles.

On the other hand we have developed an algorithm to simulate the formation of MNP cross-linking structures when the biomarker can be linked to two different ligands, and we have studied multiple properties of the aggregates, in order to later simulate the response of the aggregates to an alternating current magnetic field.

[1] https://github.com/RaulPPelaez/UAMMD/

Transport coefficients of a granular gas immersed in a gas of elastic hard spheres

Rubén Gómez González[1] and Vicente Garzó[2]
[1]Departamento de Física, Universidad de Extremadura, Avda. de Elvas s/n, 06006 Badajoz (Spain)
[2] Departamento de Física, Instituto Universitario de Computación Científica Avanzada (ICCAEx), Universidad de Extremadura,, Avda. de Elvas s/n, 06006 Badajoz (Spain).

Let us consider an ensemble of inelastic hard spheres (granular gas) of mass m immersed in a gas of elastic hard spheres (molecular gas) of mass m_g. We assume that the granular gas is sufficiently rarefied and therefore the presence of the grains does not perturb the state of the surrounding molecular gas. In this situation, the molecular gas may be treated as a thermostat at a fixed temperature T_g. Nonetheless, although the number density of the grains is much smaller than that of the molecular gas, we account for the grain-grain collisions in its kinetic equation. Under these conditions, the extension of the classical kinetic theory of gases is considered as an suitable tool to model these multiphase systems.

In the low-density regime, the one-body distribution function $f(\mathbf{r},\mathbf{v},t)$ obeys the Boltzmann equation:

$$\frac{\partial f}{\partial t}+\mathbf{v}\cdot\nabla f=J[\mathbf{v}|f,f]+J_g[\mathbf{v}|f,f_g]. \qquad (1)$$

Here, the Boltzmann collision operator $J[\mathbf{v}|f,f]$ gives the rate of change of the distribution $f(\mathbf{r},\mathbf{v},t)$ due to binary *inelastic* collisions between granular particles characterized by a constant coefficient of normal restitution α. On the other hand, the Boltzmann–Lorentz operator $J_g[\mathbf{v}|f,f_g]$ accounts for the rate of change of the distribution $f(\mathbf{r},\mathbf{v},t)$ due to *elastic* collisions between granular and molecular gas particles. Since the molecular gas is assumed to be at equilibrium, its distribution function f_g is a Maxwellian distribution.

The Boltzmann–Lorentz equation Eq. (1) applies in principle for arbitrary values of the mass ratio m/m_g. However, one of the main aims of the present work is to analyze the conditions under which the transport properties derived from Eq. (1) reduce to that obtained using a Langevin-like model [1]. A careful analysis shows that both models overlap when the granular particles are much heavier than that of the interstitial gas (Brownian limit, $m/m_g\to\infty$). In this limit case, the operator $J_g[\mathbf{v}|f,f_g]$ can be approximated by the Fokker–Planck operator [2]:

$$J_g[\mathbf{v}|f,f_g]\to\gamma\frac{\partial}{\partial\mathbf{v}}\cdot\left(\mathbf{v}+\frac{T_g}{m}\frac{\partial}{\partial\mathbf{v}}\right)f(\mathbf{v}), \qquad (2)$$

where the drift or friction coefficient $\gamma\propto\sqrt{m_g/m}$ is a function of the parameters of the molecular gas [3].

On the other hand, we want to extend the results for the transport coefficients obtained in [1] to arbitrary values of the mass ratio m/m_g. To do so, the Chapman–Enskog-like expansion is applied to the Boltzmann kinetic equation. First step is to characterize the reference state in the perturbation scheme, namely the homogeneous steady state (HSS). In the HSS, the energy lost due to inelastic collisions is exactly compensated for by the energy injected by the collisions with the more rapid particles of the molecular gas. This simple situation allows us to compute the steady granular temperature T (see Fig. 1 for an example with a given value of the reduced bath temperature T_g^*) [4].

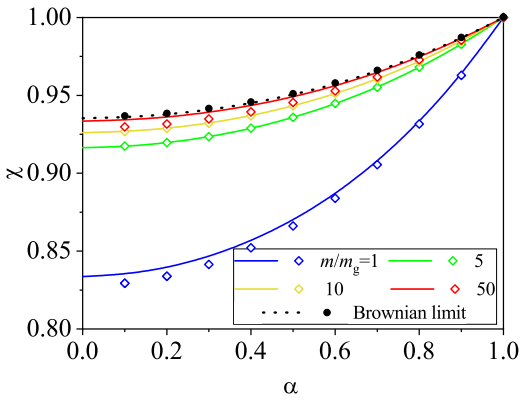

Fig. 1. Temperature ratio $\chi\equiv T/T_g$ versus the coefficient of normal restitution α for $T_g^*=1000$, and four different values of the mass ratio m/m_g. The solid lines are the theoretical results obtained by numerically solving Eq. (1) and the symbols are the Monte Carlo simulation results. The dotted line is the result obtained in [1] by using the Langevin-like suspension model (2).

Once the homogeneous state is characterized, the next step is to solve the Boltzmann equation by means of the Chapman–Enskog-like expansion to first order in spatial gradients. The Navier–Stokes–Fourier transport coefficients are explicitly determined by considering the leading terms in a Sonine polynomial expansion when steady-state conditions apply. In general, the transport coefficients show a complex dependence on the mass ratio m/m_g, the (reduced) bath temperature T_g^*, and the coefficient of restitution α. Moreover, in the Brownian limit ($m/m_g\to\infty$) we recover the results previously derived by using the Langevin-like model [1].

As an application, a linear stability analysis is performed showing that the HSS is always linearly stable regardless of the mass ratio considered.

[1] R. Gómez González and V. Garzó, *Transport coefficients for granular suspensions at moderate densities*, J. Stat. Mech. **093204**, (2019).

[2] P. Résibois and M. de Leener, *Classical Kinetic Theory of Fluids* (Wiley, New York, 1977).

[3] A. Santos, *Granular fluid thermostated by a bath of elastic hard spheres*, Phys. Rev. E **67**, 051101 (2003).

[4] R. Gómez González and V. Garzó, *Kinetic theory of granular particles immersed in a molecular gas*, arXiv:2110.15212, (2022).

Determinación de la línea de disociación del hidrato de dióxido de carbono en agua salada mediante dinámica molecular

A. Díaz Acosta, I. M. Zerón, J. M. Míguez, y F. J. Blas
Laboratorio de Simulación Molecular y Química Computacional,
CIQSO-Centro de Investigación en Química Sostenible y Departamento de Ciencias Integradas,
Universidad de Huelva, 21007 Huelva, Spain

Los hidratos de gas son estructuras cristalinas formadas por moléculas de agua las cuales se enlazan entre sí formando cajas poliédricas donde quedan retenidas moléculas gaseosas [1, 2]. El tipo de estructura del hidrato queda determinado principalmente por el tamaño de la partícula invitada, por ejemplo, el metano y el dióxido de carbono forma una estructura sI. En la naturaleza, los hidratos se producen en condiciones de presión alta y de temperatura baja como las presentes el lecho marino y zonas del permafrost.

En este trabajo se ha estimado la línea de coexistencia trifásica (hidrato- agua salada - CO_2 líquido) mediante simulaciones de dinámica molecular en el colectivo NPT, utilizando la técnica de coexistencia directa de las tres fases involucradas. La temperatura a la cuál las tres fases se encuentran en equilibrio fue determinada para diferentes presiones (10, 40 y 100 Mpa) y utilizando una concentración salina de 0.6 m en la fase acuosa. El modelo de CO_2 utilizado fue TraPPE [3], para el caso del agua se ha seleccionado el modelo TIP4P/2005 [4] y para el NaCl se usó el modelo Madrid de cargas escaladas [5].

La predicción de la línea trifásica fue comparada con los valores de simulación correspondientes al caso en ausencia de sal desarrollado por Míguez et al. [6]. En el presente estudio se encuentra un desplazamiento de la línea trifásica de 6 K hacia la izquierda debido a la presencia de sal (NaCl a 0.6 m).

[1] R. Boswell y T. S. Collett, *Current perspectives on gas hydrate resources*, Energy & environmental science **4**, 1206 (2011).

[2] E. Sloan y C. A. Koh, *Clathrate Hydrates of Natural Gases*, 3ª Edición, CRC Press (2008).

[3] J. J. Potoff y J. I. Siepmann, *Vaporliquid equilibria of mixtures containing alkanes, carbon dioxide, and nitrogen*, AIChE J. **47**, 1676 (2001)

[4] J. L. F. Abascal y C. Vega, *A general purpose model for the condensed phases of water: TIP4P/2005*, J. Chem. Phys. **123**, 234505 (2005).

[5] I. M. Zeron, J. L. F. Abascal y C. Vega, *A force field of Li^+, Na^+, K^+, Mg^{2+}, Ca^{2+}, Cl^-, and SO_4^{2-} in aqueous solution based on the TIP4P/2005 water model and scaled charges for the ions*, J. Chem. Phys. **151**, 134504 (2019).

[6] J. M. Míguez, M. M. Conde, J.-P. Torré, F. J. Blas, M. M. Piñeiro, and C. Vega *Molecular dynamics simulation of CO_2 hydrates: Prediction of three phase coexistence line*, J. Chem. Phys. **142**, 124505 (2015).

Federated Learning mediante consenso

M. Rebollo[1], C. Carrascosa[2], and J.A. Rincón[3]
Inst. Valenciano de Investigación para la IA
Universitat Politècnica de València, Camino de Vera s/n 46022 Valencia
[1]mrebollo@upv.es, [2]carrasco@dsic.upv.es, [3]jrincon@dsic.upv.es

Se conoce por *federated learning* (FL) una técnica de aprendizaje automático por la que un sistema distribuido de nodos entrena una red neuronal (RN) con subconjuntos del conjunto de entrenamiento. Una vez entrenados los modelos individuales, se envían a un nodo central que obtiene el modelo promedio y lo reenvía de vuelta a los nodos. Tras varias rondas, se ha observado que los modelos obtenidos reduciendo el número de iteraciones de entrenamiento tienen una precisión equivalente a haber entrenado una sola red [1].

Hay ocasiones en las que, por el tamaño de los conjuntos de entrenamiento, no es posible centralizar el cálculo. Otros motivos pueden ser restricciones físicas que impiden la conexión con un nodo central. En esos casos es necesario un método realmente distribuido. Este trabajo propone el uso de un protocolo de consenso [2] en el que los nodos de una red llegan al valor promedio intercambiando información con sus vecinos directos.

Supongamos que tenemos n RN idénticas. El objetivo es aprender un modelo global (W, tr) donde W son los pesos entrenados para un conjunto de entrenamiento tr. El conjunto tr se divide en n subconjuntos, uno para cada nodo $tr = \cup_i tr_i$. En cada ronda:

1. cada nodo construye su propio modelo (W_i, tr_i),
2. intercambia la matriz de pesos W_i con sus vecinos hasta que converge usando Eq 1

$$W_i(t+1) = W_i(t) + \varepsilon \sum_{j \in N_i} [W_j(t) - W_i(t)] \qquad (1)$$

Los resultados presentados corresponden con el *dataset* MNIST [3], formado por 60.000 ejemplos de dígitos manuscritos para entrenamiento y 10.000 para test. Se ha utilizado una red convolucional de cinco capas: dos conv2d, una dropout y dos lineales. Se ha estudiado el rendimiento del proceso con distintas topologias y tamaños de red: (i) grid 2d, (ii) grid triangular, (iii) una red navegable de Kleinberg, (iv) un random geometric graph (RGG), (v) una triangulación de Delaunay, y (vi) un grafo de Gabriel (una reducción de la triangulación), y con n variando entre 10 y 600 (Figura 1, superior). Teniendo en cuenta el rendimiento del proceso de consenso en cada tipo de red y otros parámetros, como sus distribuciones de grado o su eficiencia, las RGG resultan la topología más eficiente.

Con ellas se han realizado los experimentos que aparecen en la Figura 1. Se han generado 10 redes de cada tamaño y en cada una de ellas se han realizado 10 repeticiones variando las muestras asignadas a cada nodo tr_i. Se observa que la precisión aumenta cuando disminuye el tamaño de la red. Es un resultado esperable, pues el tamaño del subconjunto de entrenamiento es mayor y, por lo tanto, los pesos quese obtienen están mejor ajustados. Sin embargo, hay que balancearlo con la capacidad de cómputo de cada nodo. La precisión obtenida tras cuatro rondas del FL con consenso es equivalente a la precisión obtenida en una sola RN con diez rondas de ajuste de pesos en el escenario escogido.

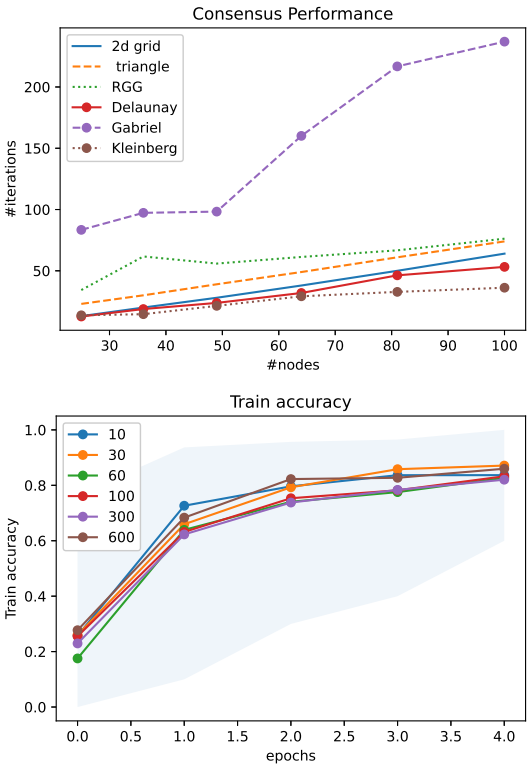

Fig. 1. (arriba) Rendimiento del proceso de consenso según la topología y el tamaño de la red (abajo) Precisión de la red entrenada para el dataset MINST [3] según su tamaño (RGG). El área sombreada señala el rango de mayor a menor precisión obtenidas

Agradecimientos Este trabajo ha sido financiado por el Ministerio de Ciencia e Innovación bajo el proyecto de código PID2021-123673OB-C31

[1] B. McMahan, E. Moore, D. Ramage, S. Hampson, & B.A. Arcas *Communication-Efficient Learning of Deep Networks from Decentralized Data*. In PMLR 54:1273-1282 (2017)

[2] R. Olfati-Saber and R.M.Murray. *Consensus problems in networks of agents with switching topology and time-delays*. IEEE TAC, 49(9):15201533, (2004)

[3] D. Li. *The MNIST database of handwrittendigit images for machine learning research*. IEEE SPM, 29(6):141142, (2012)

Estrategias de ventilación para maximizar el confort térmico

Santiago Paramés-Estévez[1], Mateo Gómez-Méndez[1], Jorge Mira[2], Alberto Otero-Cacho[1,3] and Alberto P. Muñuzuri[1,3]

[1]Facultad de Física, Univ. Santiago de Compostela, 15782, Santiago de Compostela, Spain.
[2] Departamento de Física Aplicada, Universidade de Santiago de Compostela (Spain).
[3] CITMAga, Santiago de Compostela, Spain.

Una de las consecuencias de la pandemia de COVID-19 ha sido el darse cuenta de la importancia de las condiciones de calidad de aire en los espacios interiores de trabajo, ocio y/o estudio. Ventilar aulas y locales se ha convertido, pues, en una de las principales medidas a la hora de intentar reducir los contagios de COVID-19 durante la pandemia y en una preocupación constante. La ventilación extrema, especialmente en tiempo de invierno, puede conllevar a situaciones de importante disconfort para los usuarios de las instalaciones. Por ello se hace importante establecer protocolos de ventilación que garanticen la seguridad de los espacios maximizando el grado de confort de los usuarios.

Con el fin de proponer nuevos protocolos de ventilación que mejoren considerablemente el confort en interiores, se ha desarrollado un estudio a diferentes niveles considerando distintos protocolos de ventilación y su efecto sobre la temperatura del aire y la concentración de CO_2 en diferentes entornos de la Facultad de Física de la USC.

Se mostrarán datos de medidas experimentales complementados con estudios más teóricos y simulaciones mediante técnicas de CFD (Computational Fluid Dynamics).

[1] Evaluación del riesgo de la transmisión de SARS-CoV-2 mediante aerosoles. Medidas de prevención y recomendaciones. Ministerio de Sanidad. Gobierno de España (Evaluation of risk transmision of SARS-CoV-2 through aerosols. Prevention measures and recommendations. Ministry of Heald. Government of Spain) (2020). https://www.mscbs.gob.es/profesionales/saludPublica/ccayes/alertasActual/nCov/documentos/COVID19_Aerosoles.pdf

[2] Alberto P. Munuzuri, Alberto Otero-Cacho, Jorge Mira. Ventilation time recommendation system incorporating local meteorological data. To appear in Building and Environment (2022).

Transición explosiva por recursos limitados en control de epidemias

Santiago Lamata-Otín[1], Adriana Reyna-Lara[1,2] y Jesús Gómez-Gardeñes[1,2,3]
[1]Departamento de Física de la Materia Condensada, Universidad de Zaragoza, E-50018 Zaragoza, España
[2]GOTHAM Lab-Instituto de Biocomputación y Física de Sistemas Complejos (BIFI), Universidad de Zaragoza, E-50018 Zaragoza, España
[3]Centro de Ciencias Sociales Computacionales (CCSS), Universidad de Kobe, 657-8501 Kobe, Japón

La literatura sobre epidemiología ha cubierto extensamente la caracterización del umbral epidémico, donde interviene la transición entre la fase no epidémica y la fase activa. Además, durante los últimos meses, dado el contexto de pandemia global en que nos hemos encontrado, numerosas investigaciones han tratado la implementación de estrategias de detección de infectados.

Sin embargo, en la mayoría de casos no se ha considerado un límite de recursos, a pesar de que podría llevar al colapso del sistema sanitario. Aquí mostramos que las estrategias de detección limitadas pueden ocasionar una transición adicional dentro de la fase activa de la epidemia, hacia dicha situación de colapso. Además, la nueva transición puede ser de primer orden, significando que las medidas de control tomadas han sido en vano.

Partimos de un modelo compartimental $SEPIaIsDR$ [1] ideado para modelizar la propagación y detección del COVID-19 como dos dinámicas markovianas competitivas en redes de contacto (N individuos). Previamente el mecanismo de rastreo consideraba solo la detección mediante aplicación móvil (P^{DCT}), y aquí se incluye también la manera manual (P^{MCT}) en función del número de contactos que recuerda el individuo detectado. Así, la probabilidad de detección por rastreo (P^{CT}) es la unión de ambas, y sigue siendo desencadenada por la detección de personas sintomáticas. Esto amplia la aplicabilidad del modelo inicial, ya que ambas estrategias de rastreo comparten comportamiento microscópico (pronta eliminación de los superpropagadores), y por tanto rol en la detección.

Nuestra manera de considerar que estas estrategias están limitadas por escasez de recursos es mediante una función puerta $g(t)$, que modula tanto la detección por síntomas (que pasa a tener diréctamente ese valor), como la detección por rastreo $P^{CT} \rightarrow g(t)P^{CT}$. Esta función puerta dada por la Ec. (1) pretende capturar la saturación del sistema sanitario a modo de límite inferior, y para ello se considera la población de sintomáticos $I_S(t)$ como una cantidad suficientemente representativa. De esta manera, todos los efectos de colapso observados serían aún más claros teniendo en cuenta al resto de agentes necesitados de atención sanitaria.

$$\begin{aligned} g(t) &= g_0 \qquad si \qquad I_S(t) \leq N\theta, \\ g(t) &= g_r + (g_0 - g_r)e^{-\lambda(I_S(t)-N\theta)} \quad si \quad I_S(t) > N\theta, \end{aligned} \tag{1}$$

Más allá de los posibles ratio basal $g_r \leq g_0$ y limitación del flujo en ausencia de saturación $g_0 \leq 1$, la función puerta viene descrita por los parámetros de colapso θ y λ. Consideramos que los flujos hacia el compartimento de detección ocurren con normalidad mientras la población de agentes sintomáticos es menor que cierto límite de recursos θ, pero una vez sobrepasado las transiciones se ven reducidas de acuerdo a un decaimiento exponencial regulado por la constante λ, que se puede relacionar con las características del sistema sanitario en cuanto a la optimización de recursos, además de servir como parámetro de ajuste.

El efecto en la evolución de la epidemia es que cuando se llega al límite de recursos, la población infectada crece de manera más pronunciada, tanto por el resentimiento en la propia detección como por las infecciones que siguen generando los no detectados. Esta situación apunta a que, si en algún instante se agotan los recursos, el sistema acaba con mayor fracción de la población habiendo superado la epidemia (R^{∞}). Es decir, parece existir otro punto crítico.

Para estudiar el efecto global de la epidemia con recursos limitados interesa conocer qué ocurre con el número total de recuperados en función de la infectividad del patógeno β_A (Fig. 1).

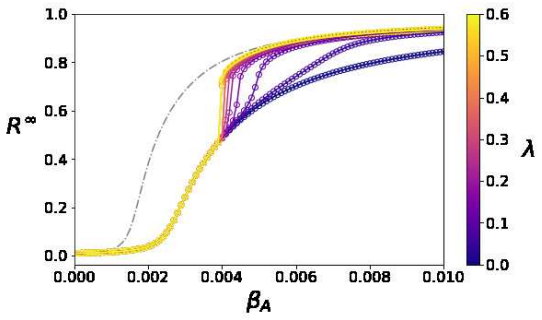

Fig. 1. Aparición de la doble transición de fase. La segunda, desencadenada por el límite de recursos, puede ser de primer orden.

Se aprecia como, además de la esperada transición en el umbral epidémico, para cierto valor $\beta^{\star}$ (determinado por el límite de recursos θ), la curva se despega de la de total detección, saltando hacia la curva de libre propagación. Es decir, aparece una segunda transición ya dentro de la fase activa de la epidemia debida a la limitación de recursos.

Esta tranisición, dependiendo de las condiciones del sistema (λ), puede pasar de segundo a primer orden. Es decir, la limitación de recursos puede llevar a una transición abrupta, implicando que en el momento en que el sistema satura, todos los esfuerzos previos por contener la epidemia habrán sido en vano.

Por último, es conveniente remarcar que, a diferencia de otras transiciones explosivas, esta no surge por un retraso en el umbral epidémico, sino que está asociada a otro punto crítico diferente.

[1] A. Reyna-Lara, D. Soriano-Paños, S. Gómez, C. Granell, J.T. Matamalas, B. Steinegger, A. Arenas y J. Gómez-Gardeñes, *Virus spread versus contact tracing: Two competing contagion processes*, Phys. Rev. Research **3** (2021).

A Nano-scale view of Protein hydration Water at Low Temperature

María Carmen Morón[1,2].
[1] Instituto de Nanociencia y Materiales de Aragón, CSIC-Universidad de Zaragoza.
[2]Departamento de Física de la Materia Condensada, Facultad de Ciencias, Universidad de Zaragoza.

Water affects every aspect of our lives. It constitutes a transversal and sustainable subject of research. With a ubiquitous character, biomolecules like nucleic acids or proteins are immersed in it. However water should not be regarded as just a solvent. The shell of water molecules in close interaction with a biomolecule surface is called *biological water*. That peculiar water is essential to biomolecule structure, dynamics and function.

In this communication, the dynamics of the hydration layer of the protein Barstar is followed at room and low temperature (300-243 K), using all-atom molecular dynamics simulations, and correlated with that of isolated water:

1. *A stretched exponential function* $exp[-(t/\tau)^{\beta}]$ describes the room and low temperature relaxation of residence times of water molecules in the protein hydration layer. The value of the stretched exponent $\beta = 0.48 \pm 0.01$, clearly departing from 1, validates the presence of remarkable temporal disorder in the system and *multiple decay time scales*. The existence of those multiple scales has been also detected at *nanoscopic level*. On the other hand as temperature goes down the relaxation time τ increases, exhibiting a divergence at a *transition temperature* $T_L = 226 \pm 4$ K.

2. A power law temporal distribution, $t_r^{-\alpha}$ (t_r stand for the residence time of water molecules at the protein surface, $\alpha = 0.63 \pm 0.07$), shows the *scale-free character of the dynamics* in the case of protein hydration water (see Fig. 1). Surprisingly, an equivalent scale-free dynamics has been also detected for isolated water ($\alpha = 0.58 \pm 0.09$). Nevertheless the *maximum residence time in the case of protein hydration water is two orders of magnitude larger than for isolated water*. Then the biomolecule but also the solvent, are responsible for the heterogeneous dynamics protein hydration water exhibits. *Biological water notices both 'scenarios' and, since the three entities must coexist at the same time, tries to accommodate them.*

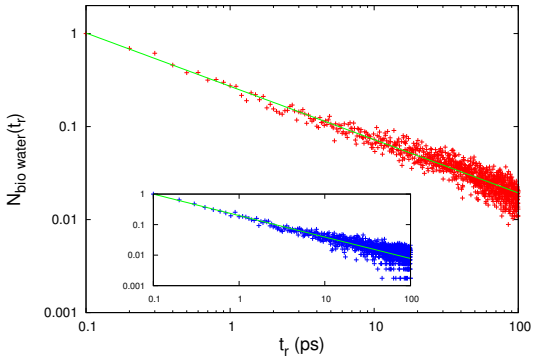

Fig. 1. Scale-free dynamics: normalized number of water molecules as a function of the time they spend within a cut-off of 0.40 nm from the protein surface at 288 K (inset at 243 K).

3. *Comparison with experimental data is presented along the work. Experimental results are quantitatively reproduced.*

[1] M.C. Morón, Journal of Molecular Liquids **272** 902-911 (2018).

Vesicle formation induced by thermal fluctuations

Andreu F. Gallen[1], and Aurora Hernandez-Machado[1,2].
[1] Universitat de Barcelona
[2] Institute of Nanoscience and Nanotechnology (IN2UB), Barcelona

Vesicles are crucial in many biological processes like transport vesicles or secretory vesicles. However, the formation of a vesicle from a membrane requires a topological transition of the membrane. This is important, as the common method to model cellular membranes is to ignore the Gaussian curvature term of the energy because it is complex to compute and is a topological invariant.

In a previous work we have developed a model that takes into account this Gaussian curvature term to study the process of vesicle formation from a membrane tube [1]. The tube geometry was chosen because is found on nature and helps in the process of vesicle formation. However, there are shapes that instead of helping the fission process hinder it, like an infinitely flat membrane.

Here we present how by adding a thermal-like noise to mimic the temperature we can make a flat membrane to vesiculate for high enough temperatures. Moreover, we have computed the phase diagram for different spontaneous curvatures where on can see the interplay between the Gaussian curvature modulus and the temperature, and depending on both we will see vesiculation or not at a given temperature.

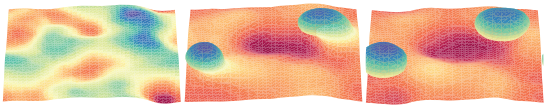

Fig. 1. Formation of two vesicles from a fluctuating flat membrane induced by thermal fluctuations.

[1] Rueda-Contreras, M. D., Gallen, A. F., Romero-Arias, J. R., Hernandez-Machado, A., & Barrio, R. A. (2021). On Gaussian curvature and membrane fission. Scientific Reports, 11(1), 1-10.

Modelling membranes in a flow with a stream function formulation

Andreu F. Gallen[1], Joan Muñoz[1], Mario Castro[2], and Aurora Hernandez-Machado[1,3].
[1] Universitat de Barcelona
[2] Instituto de Investigación Tecnológica (IIT), Universidad Pontificia Comillas, Madrid
[3] Institute of Nanoscience and Nanotechnology, Barcelona

Some existing numerical methods have successfully simulated the coupling between a fluid and membranes, with special interest in red blood cells. We introduce an alternative phase-field model formulation that solves the flow using the vorticity and stream function, which simplifies the numerical implementation. The biggest strength of this modelling is its adaptability as we can adapt it to time-dependent flows, inertial flows, and even expand the stream function formulation to a 3D system.

To prove this model we integrate red blood cell dynamics immersed in a Poiseuille flow and reproduce previously reported morphologies (slippers and parachutes). However after that we explore the morphology in different confinements.

For cells in a very wide channel, we discover a new meta-stable shape referred to as anti-parachute. This sort of meta-stable morphology may contribute to the dynamical response of the blood. We also study red blood cells in a Couette flow, where we observe cells experiencing a displacement perpendicular to the flow direction that can be modulated with the viscosity contrast.

[1] Gallen, A. F., Castro, M., & Hernandez-Machado, A. (2021). Red blood cells in low Reynolds number flow: A vorticity-based characterization of shapes in two dimensions. Soft Matter, 17(42), 9587-9594.

Spatial Scales of Population Synchrony Increase as Fluctuations Propagate through the Food Web

Miguel Ángel Fernández-Grande[1] and Francisco Javier Cao-García[1,2]
[1] Departamento de Estructura de la Materia, Física Térmica y Electrónica,
Universidad Complutense de Madrid, Parque de Ciencias, 1, 28040 Madrid, Spain.
[2] Instituto Madrileno de Estudios Avanzados en Nanociencia, IMDEA Nanociencia, Calle Faraday, 9, 28049 Madrid, Spain.

The spatial scale of population synchrony gives the characteristic size of the regions where population fluctuations are correlated, thus, of simultaneous population depletions (or even extinctions). Single-species previous results imply that the spatial scale of population synchrony is equal or greater (due to dispersion) than the spatial scale of synchrony of environmental fluctuations. Interspecies interactions are known to modify the spatial scales of population synchrony, as it is primarily found in a case-by-case computational approach. Here, we show analytically that the spatial scale of population synchrony generally increases as the fluctuations propagate through the food web, i.e., the species more directly affected by environmental fluctuations presents the smaller spatial scale of population synchrony. This result is shown here for two species ecosystems close to a stable equilibrium of their population dynamics. The relevance of the result is discussed based on previously reported observations on marine and terrestrial ecosystems.

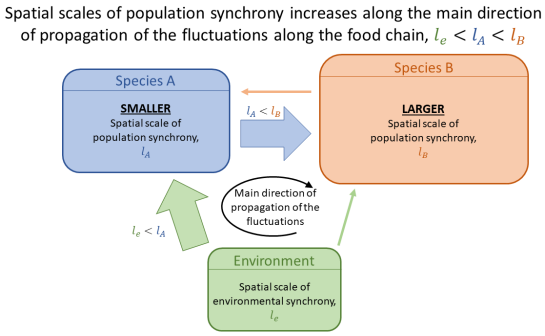

Fig. 1. Spatial scales of population synchrony increases along the main direction of propagation of the fluctuations along the food chain, $l_e < l_A < l_B$.

[1] Fernandez-Grande, M.A., Cao-Garcia, F.J. *Spatial Scales of Population Synchrony generally increases as fluctuations propagate in a Two Species Ecosystem*, https://arxiv.org/ftp/arxiv/papers/2012/2012.11043.pdf (2020).

[2] Jarillo, J., Saether, B.-E., Engen, S., Cao-Garcia, F.J. *Spatial scales of population synchrony in predator-prey systems.* Am. Nat., 195, 216-230 (2020).

[3] Jarillo, J., Saether, B.E., Engen, S., Cao, F.J. *Spatial scales of population synchrony of two competing species: effects of harvesting and strength of competition.* Oikos, 127, 1459-1470 (2018).

Cooperative kinetics of ligand binding to polymers

Juan P.G.Villaluenga[1], and Francisco Javier Cao-García[1,2]
[1]Departamento de Estructura de la Materia, Física Térmica y Electrónica, Universidad Complutense de Madrid,
[2]Instituto Madrileño de Estudios Avanzados en Nanociencia, IMDEA Nanociencia.

Ligands change the chemical and mechanical properties of polymers. In particular, single strand binding protein (SSB) non-specifically bounds to single-stranded DNA (ssDNA), modifying the ssDNA stiffness and the DNA replication rate, as recently measured with single-molecule techniques. SSB is a large ligand presenting cooperativity in some of its binding modes.

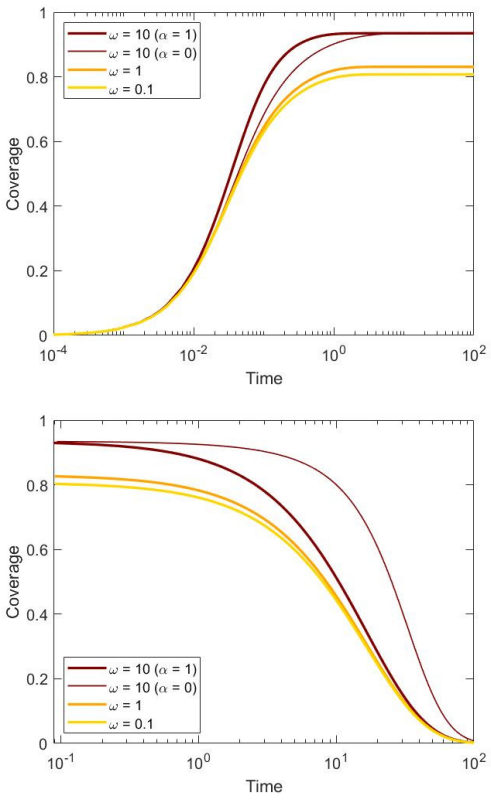

Fig. 1. Polymer coverage as a function of time compared for non-cooperative ($\omega = 1$) and cooperative ($\omega \neq 1$) cases. (Up) Starting with a naked polymer, ligands binding to 30 sites, binding rate $k_b = 0.8\,s^{-1}$, and release rate $k_r = 0.06\,s^{-1}$. (Down) Starting with the previous equilibrium coverages the detachment dynamics is induced setting $k_b = 0$. The cooperativity parameter ω is the equilibrium constant for the process of moving a bound ligand to a location with an additional neighboring bound ligand. ω is determined by the interaction energy between bound ligands. The activation state parameter α measures the impact of cooperativity on the activation energy of the binding process. In the limiting case $\alpha = 1$ cooperativity only enhances binding, while for $\alpha = 0$ only inhibits release.

We aim to develop an accurate kinetic model for the cooperative binding kinetics of large ligands [1, 2]. Cooperativity accounts for the changes in the affinity of a ligand to the polymer due to the presence of another bound ligand. Large ligands, attaching to several binding sites, require a detailed counting of the available binding possibilities. This counting has been done by McGhee and von Hippel to obtain the equilibrium state of the ligands-polymer complex. The same procedure allows to obtain the kinetic equations for the cooperative binding of ligands to long polymers, for all ligand sizes (see Fig. 1).

We also derive approximate cooperative kinetic equations in the large ligand limit, at the leading and next-to-leading orders. We found cooperativity is negligible at the leading-order, and appears at the next-to-leading order. Positive cooperativity can be originated by increased binding affinity or by decreased release affinity, implying different kinetics. Nevertheless, the equilibrium state is independent of the origin of cooperativity and only depends on the overall increase in affinity. Next-to-leading approximation is found to be accurate, particularly for small cooperativity (see Fig. 2).

These results allow to understand and characterize relevant ligand binding processes, as the binding kinetics of SSB to ssDNA, which has been reported to affect the DNA replication rate for several SSB-polymerase pairs.

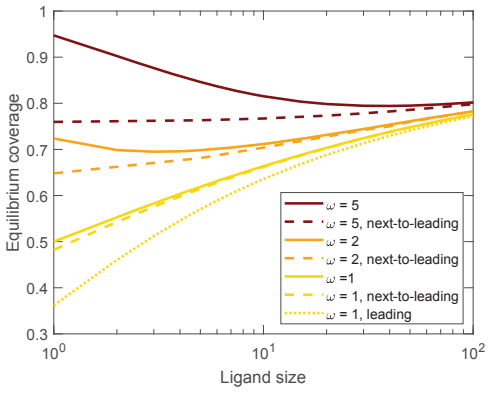

Fig. 2. Comparison of exact and large ligand-size approximation results. Equilibrium coverages as a function of the ligand size.

[1] Juan P.G. Villaluega, and Francisco Javier Cao-García, *Cooperative kinetics of ligand binding to linear polymers*, Comput. Struct. Biotechnol. J. **20**, 521 (2022).

[2] J.P.G. Villaluega, J. Vidal, and F.J. Cao-García, *Noncooperative thermodynamics and kinetic models of ligand binding to polymers: Connecting McGhee – von Hippel model with the Tonks gas model*, Phys. Rev. E **102**, 12407 (2020).

Casimir forces on curved backgrounds

Begoña Mula[1], Silvia N. Santalla[2], Javier Rodríguez-Laguna[1]
[1]Dto. Física Fundamental, UNED, Madrid, Spain
[2]Dto. Física & GISC, Universidad Carlos III de Madrid, Leganés, Spain

The quantum vacuum on a static space-time is nothing but the ground state of a certain Hamiltonian. Therefore, it is subject to quantum fluctuations which help minimize the energy. Yet, these fluctuations are clamped near the boundaries, giving rise to the celebrated *Casimir effect* [1, 2].

For fields subject to conformal invariance, the Casimir force is associated to the conformal anomaly. Using open boundary conditions on a $(1+1)D$ system with size N, the energy of the ground state can be proved to be [3]

$$E(N) = \epsilon_1 N + \epsilon_0 + \frac{cv}{6N} + O(N^{-2}), \qquad (1)$$

with ϵ_0 and ϵ_1 constants, v standing for the Fermi velocity, and c is the central charge. Let us also remark the fact that the sign of the force can be changed from attractive to repulsive by suitable choice of the boundary conditions.

We characterize Casimir forces for the Dirac vacuum on free-fermionic chains with smoothly varying hopping amplitudes, which can be seen to correspond to (1+1)D curved space-times with a static metric of optical type in the thermodinamic limit. The metrics considered are anti-de Sitter (Rainbow system), Rindler, oscillatory and random [4]. Thus, our main objective is to characterize how Eq. (1) changes in presence of a static graviational field for fermionic (1+1)D systems.

Let us consider a fermionic chain of N sites, whose dynamics is described by the Hamiltonian

$$H_N(\mathbf{J}) = -\sum_{m=1}^{N-1} J_m c_m^\dagger c_{m+1} + \text{h.c.}, \qquad (2)$$

where $\mathbf{J} = \{J_m\}_{m=1}^{N-1}$ are the *hopping amplitudes*, $J_m \in R^+$ referring to the link between sites m and $m+1$, and $c_m^\dagger$, c_{m+1} are the fermionic creation and annihilation operators on sites m and $m+1$, respectively. Hamiltonian (2), which is quadratic in the fermionic operators, is also called free fermion Hamiltonian and is solvable in terms of single-body sates. In the thermodynamic limit, if the $\mathbf{J}$ are smooth, Eq. (2) corresponds to the Dirac field on a metric of the form [5]

$$ds^2 = -J^2(x)dt^2 + dx^2. \qquad (3)$$

Moreover, when we move away from half-filling a new phenomena is observed. A depletion region appears to arise in the fermionic density and in next-neighbours correlators as well.

We have considered the continuum limit of Hamiltonian (2) with

$$\Psi = \Psi_L + \Psi_R, \qquad (4)$$

$$c_m = \sqrt{a}\left(e^{ik_F x}\Psi_L(x) + e^{-ik_F x}\Psi_R(x)\right), \qquad (5)$$

where k_F is the Fermi momenta.

Expanding the fields, $\Psi_L(x)$ and $\Psi_R(x)$, to second order we end up with a new Hamiltonian which equations of motion give rise to a Schrödinger-like expression where an effective potential could explain the depletion phenomena. It is important to say that away from half filling the theory is not conformal.

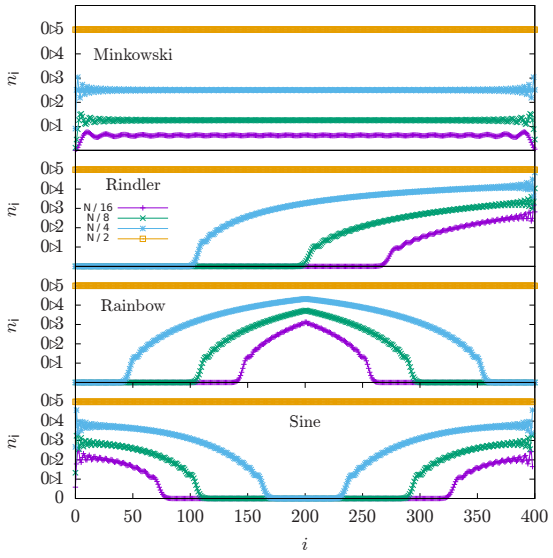

Fig. 1. Fermionic density for different filling-factors with $N = 400$ sites. Four metrics have been considered: Minkowski, Rindler, Rainbow and Sine.

[1] H.B.G. Casimir, D. Polder, Phys. Rev. **73**, 360 (1948).

[2] G.L. Klimchitskaya, V.M. Mostepanenko, Contemp. Phys. **47**, 131 (2006).

[3] P. Di Francesco, P. Matthieu, D. Sénéchal, *Conformal Field Theory*, Springer (1997).

[4] B. Mula, S. N. Santalla and J. Rodríguez-Laguna, *Casimir forces on deformed fermionic chains*, Phys. Rev. Res. **3** (2021) 013062(9).

[5] J. Rodríguez-Laguna, L. Tarruell, M. Lewenstein, A. Celi, Phys. Rev. A **95**, 013627 (2017).

LISTA DE PARTICIPANTES

1. **Enrique Abad Jarillo**
   Dpto. de Física Aplicada, Instituto de Computación Científica Avanzada, Universidad de Extremadura
   eabad@unex.es

2. **David Abella Bujalance**
   Instituto de Física Interdisciplinar y Sistemas Complejos (IFISC)
   davidabbu@gmail.com

3. **Javier Aguilar Sánchez**
   Instituto de Física Interdisciplinar y Sistemas Complejos IFISC (CSIC-UIB)
   javieraguilar@ifisc.uib-csic.es

4. **Adrian Aguirre-Tamaral**
   Centro de Astrobiología (INTA-CSIC), Madrid
   adrian.aguirre@cab.inta-csic.es

5. **Nerea Alcázar Cano**
   Departamento de Física Teórica de la Materia Condensada, Universidad Autónoma de Madrid
   nerea.alcazar@uam.es

6. **Alejandro Almodóvar Del Pozo**
   IFISC (UIB-CSIC)
   alex.adp.96@gmail.com

7. **Sergio Alonso Muñoz**
   Department of Physics, Universitat Politecnica de Catalunya
   s.alonso@upc.edu

8. **Iván Álvarez Domenech**
   Departamento de Física Matemática y de Fluidos, UNED
   iadomenech@dfmf.uned.es

9. **Ismael Aran Tapia**
   CITMAga - Grupo de Física No Lineal - Universidad de Santiago de Compostela
   ismaelaran.tapia@usc.es

10. **Alex Arenas**
    Universitat Rovira i Virgili
    alexandre.arenas@urv.cat

11. **Saúl Ares**
    Centro Nacional de Biotecnología CNB-CSIC
    saul.ares@csic.es

12. **Roberto Arévalo Turnes**
    Centro de Investigación de Recursos y Consumos energéticos
    raturnes@alumni.unav.es

13. **Lluís Arola Fernández**
    Universitat Rovira i Virgili
    lluisarolaf@gmail.com

14. **Francisco Javier Arranz Saiz**
    Grupo de Sistemas Complejos - Universidad Politécnica de Madrid
    fj.arranz@upm.es

15. **Oriol Artime**
    Bruno Kessler Foundation
    oartimevila@fbk.eu

16. **Iker Atienza Díez**
    Centro Ncional de Biotecnología (CNB-CSIC)
    iatienza@cnb.csic.es

17. **Luis Miguel Ballesteros Esteban**
    Grupo de investigación en Sistemas Complejos y Física Fundamental de la Universidad Rey Juan Carlos
    luisballesteros92@gmail.com

18. **C. Miguel Barriuso Gutiérrez**
    Universidad Complutense de Madrid - Dpto. de Estructura de la Materia, Física Térmica y Electrónica
    carbarri@ucm.es

19. **Francisco Bauzá Mingueza**
    Universidad de Zaragoza
    imrik111@hotmail.com

20. **Rosa María Benito Zafrilla**
    Universidad Politécnica de Madrid
    rosamaria.benito@upm.es

21. **Ricardo Brito**
    Universidad Complutense de Madrid
    brito@ucm.es

22. **Pierpaolo Bruscolini**
    Dep. Física Teórica y BIFI. Univ. de Zaragoza
    pier@unizar.es

23. **Javier Buceta**
    Institute for Integrative Systems Biology (I2SysBio), CSIC-UV
    javier.buceta@csic.es

24. **Giulio Burgio**
    Universitat Rovira i Virgili
    giulioburgio@gmail.com

25. **Javier Burguete**
    Departamento de Física y Matemática Aplicada, Universidad de Navarra
    javier@unav.es

26. **Rodrigo Caitano Barbosa da Silva**
    Departamento de Física y Matemática Aplicada, Facultad de Ciencias, Universidad de Navarra
    rcaitanobar@alumni.unav.es

27. **Jorge Calero Sanz**
    Universidad Politécnica de Madrid
    jorge.calero.sanz@alumnos.upm.es

28. **Annalisa Caligiuri**
    IFISC (CSIC-UIB)
    annalisa.caligiuri@gmail.com

29. **Jorge Calle Espinosa**
    CBGP (UPM-INIA/CSIC), Campus de Montegancedo
    calle.espinosa.jorge@gmail.com

30. **Violeta Calleja Solanas**
    Estudiante predoctoral en IFISC (UIB - CSIC)
    violeta@ifisc.uib-csic.es

31. **José Manuel Camacho Mateu**
    Universidad Carlos III de Madrid (UC3M), Departamento de Matemáticas
    joscamac@math.uc3m.es

32. **Daniel Campos Moreno**
Depto de Física. Universitat Autònoma de Barcelona
daniel.campos@uab.cat

33. **Francisco Javier Cao García**
Universidad Complutense de Madrid
francao@ucm.es

34. **Alejandro Carballosa Calleja**
Grupo de Física No Lineal, Facultad de Física, Universidad de Santiago de Compostela
ac.carballosa@usc.es

35. **Pau Casanova Ferrer**
Departamento de Matemáticas, Universidad Carlos III de Madrid
pcasanov@math.uc3m.es

36. **Piergiorgio Castioni**
Universidad Rovira i Virgili
piergiorgio.castioni@urv.cat

37. **Mario Castro Ponce**
Instituto de Investigación Tecnológica (IIT), Universidad Pontificia Comillas
marioc@comillas.edu

38. **Eric Cereceda López**
Departamento de Física de la Materia Condensada, Universidad de Barcelona
eric.cereceda@gmail.com

39. **Ricardo Chacón García**
Departamento de Física Aplicada, Escuela de Ingenierías Industriales, UEx e ICCAEx
rchacon@unex.es

40. **Christos Charalambous**
Instituto de Física Interdisciplinar y Sistemas Complejos (IFISC)
christos@ifisc.uib-csic.es

41. **Francisco Chinesta**
Arts et Métiers Institute of Technology
Francisco.Chinesta@ensam.eu

42. **Sara Cloux González**
CRETUS, Grupo de Física No Lineal, Facultad de Fisica, Universidad de Santiago de Compostela
s.cloux@usc.es

43. **Pau Clusella**
Dynamical Systems Biology Lab, Universitat Pompeu Fabra
pau.clusella@upf.edu

44. **Pere Colet**
Instituto de Física Interdisciplinar y Sistemas Complejos, IFISC, (CSIC-UIB)
pere@ifisc.uib-csic.es

45. **Pedro Córdoba Torres**
Departamento de Física Matemática y de Fluidos, Facultad de Ciencias, UNED
pcordoba@dfmf.uned.es

46. **Alvaro Corral**
Centre de Recerca Matematica
acorral@crm.cat

47. **Christian Camilo Cortes Garcia**
Centro Nacional de Biotecnologia
chcortes@math.uc3m.es

48. **Raul Cruz Hidalgo**
Departamento de Física y Matemática Aplicada Universidad de Navarra
raulcruz@unav.es

49. **José A. Cuesta Ruiz**
Universidad Carlos III de Madrid
cuesta@math.uc3m.es

50. **Alejandro Cuetos Menéndez**
Área de Química Física, Dpto. Sistemas Físicos, Químicos y Naturales, Universidad Pablo Olavide
acuemen@upo.es

51. **Juan Ignacio De Gregorio**
IFISC (CSIC-UIB), Instituto de Física Interdisciplinar y Sistemas Complejos
juan@ifisc.uib-csic.es

52. **Rafael Delgado Buscalioni**
Universidad Autonoma de Madrid, Deto. Fisica Teorica de la Materia Condensada
rafael.delgado@uam.es

53. **Adrián Díaz Acosta**
Centro de investigación en Química Sostenible y Fac. Ciencias Experimentales, Universidad de Huelva
adrian.diaz131@alu.uhu.es

54. **Javier Díaz Brañas**
Centre Européen de Calcul Atomique et Moléculaire, École Polytechnique Fédérale de Lausanne (EPFL)
javier.diazbranas@epfl.ch

55. **Fernando Díaz Díaz**
Instituto de Física Interdisciplinar y Sistemas Complejos (IFISC, UIB-CSIC)
fernandodiaz@ifisc.uib-csic.es

56. **Rafael Díaz Hernández Rojas**
Dipartimento di Fisica, Università di Roma "La Sapienza"
rafael.diazhernandezrojas@uniroma1.it

57. **Luis Ignacio Dinis Vizcaíno**
Dpto. de Estructura de la Materia, Física Térmica y Electrónica, Universidad Complutense de Madrid
ldinis@ucm.es

58. **Marc Domingo Cabasés**
Institut de Ciència de Materials de Barcelona (ICMAB-CSIC)
mdomingo@icmab.es

59. **Laia Domingo Colomer**
Instituto de Ciencias Matemáticas (ICMAT)
laia.d.c@hotmail.com

60. **Alvaro Domínguez**
Dpto. Física Atómica, Molecular y Nuclear, Universidad de Sevilla
dominguez@us.es

61. **María Duque Gijón**
Departament de Fisica, Universitat Politècnica de Catalunya
maria.duque.gijon@upc.edu

62. **Iñaki Echeverría Huarte**
Universidad de Navarra
iecheverria.13@unav.es

63. **Diego Escribano Gómez**
Universidad Carlos III Madrid
dieescri@math.uc3m.es

64. **Ernesto Estrada**
Instituto de Fisica Interdisciplinar y Sistemas Complejos (UIB-CSIC)
estrada@ifisc.uib-csic.es

65. **Sergio Faci Lázaro**
Departamento de Física de la Materia Condensada, Universidad de Zaragoza
sergiofacilazaro@gmail.com

66. **Carles Falcó**
Mathematical Institute, University of Oxford
falcoigandia@maths.ox.ac.uk

67. **Fernando Falo Forniés**
Universidad de Zaragoza
fff@unizar.es

68. **Esther Feria Delgado**
Centro de Investigación en Química Sostenible y Fac. Ciencias Experimentales, Universidad de Huelva
estherferia.29@gmail.com

69. **Andreu Fernández Gallen**
Universidad de Barcelona
fdzgallen@gmail.com

70. **Juan Fernandez-Gracia**
Instituto de Física Interdisciplinar y Sistemas Complejos (CSIC-UIB)
juanf@ifisc.uib-csic.es

71. **Lucía Fernández-Sedano Vázquez**
Universidad Complutense de Madrid
lufern11@ucm.es

72. **Darío Ferreira Martínez**
Grupo de Física No Lineal. Facultad de Física, Univ. Santiago de Compostela
dario.ferreira@rai.usc.es

73. **Irene Ferri**
Universitat de Barcelona, UBICS, ClabB
irene.ferri@ub.edu

74. **Alessandro Fiasconaro**
Depto de Física de la Materia Condensada - Universidad de Zaragoza
afiascon@unizar.es

75. **Rosa Flaquer Galmés**
Grup de Física Estadística. Facultat de Ciències. Universitat Autònoma de Barcelona
Rosa.Flaquer@uab.cat

76. **Mario Floria Peralta**
Depto. Física Mat. Cond. Universidad de Zaragoza
mario.floria@gmail.com

77. **Giancarlo Franzese**
Universitat de Barcelona and Institute of Nanoscience and Nanotechnology (IN2UB)
gfranzese@ub.edu

78. **Beatriz G. Barreales**
Grupo SPhinX, Universidad de Extremadura
beatrizgb@unex.es

79. **Javier Galeano**
Grupo de Sistemas Complejos, ETSIAAB, Universidad Politécnica de Madrid
javier.galeano@upm.es

80. **Javier Galván Fraile**
Institute for Cross-Disciplinary Physics and Complex Systems
jgalvan@ifisc.uib-csic.es

81. **Fabián A. García Daza**
Department of Chemical Engineering, The Universiy of Manchester
fabian.garciadaza@manchester.ac.uk

82. **María Isabel García de Soria Lucena**
Física Teórica, Universidad de Sevilla
gsoria@us.es

83. **Jordi Garcia Ojalvo**
Universitat Pompeu Fabra
jordi.g.ojalvo@upf.edu

84. **Miguel García Sánchez**
Instituto de Investigación Tecnológica
mgsanchez@comillas.edu

85. **David García Selfa**
Grupo de Física No Lineal (CITMAga - Universidade de Santiago de Compostela) y CESGA
david.garcia@usc.es

86. **Gregorio García Valladares**
Física Teórica, Universidad de Sevilla
ggvalladares@us.es

87. **Angel Garcimartín Montero**
Departamento de Física y Matemática Aplicada, Facultad de Ciencias, Universidad de Navarra
angel@unav.es

88. **Vicente Garzó**
Departamento de Física and ICCAEx, Universidad de Extremadura
vicenteg@unex.es

89. **Alex Giménez Romero**
Instituto de Física Interdisciplinar y Sistemas Complejos, IFISC, UIB-CSIC
alex@ifisc.uib-csic.es

90. **Sergio Gómez**
Universitat Rovira i Virgili
sergio.gomez@urv.cat

91. **Jesús Gomez Gardeñes**
Universidad de Zaragoza
gardenes@gmail.com

92. **Rubén Gómez González**
Departamento de Física, Universidad de Extremadura
ruben@unex.es

93. **Damia Gomila**
Instituto de Física Interdisciplinar y Sistemas Complejos, IFISC (CSIC-UIB)
damia@ifisc.uib-csic.es

94. **Eva González Noya**
Instituto de Química-Física Rocasolano, Consejo Superior de Investigaciones Científicas
eva.noya@iqfr.csic.es

95. **Ivan Gonzalez Torre**
Vicomtech
ivangonzaleztorre@gmail.com

96. **Sergi Granados Leyva**
Universitat de Barcelona, UBICS (University of Barcelona Institute of Complex Systems)
sergigraley@gmail.com

97. **Mar Grande**
Grupo de Sistemas Complejos; Universidad Politécnica de Madrid
margrande45@gmail.com

98. **Clara Granell Martorell**
Universitat Rovira i Virgili
clara.granell@urv.cat

99. **Pilar Guerrero Contreras**
Universidad Carlos III de Madrid
pilar.guerrero@uc3m.es

100. **Emilio Hernandez Garcia**
IFISC (CSIC-UIB)
emilio@ifisc.uib-csic.es

101. **Olga Hormigos de Santiago**
Grupo de Sistemas Complejos, ETSIAAB de la Universidad Politécnica de Madrid
olga.hormigos258@gmail.com

102. **Pablo Ignacio Hurtado Fernández**
Instituto Carlos I de Física Teórica y Computacional, Universidad de Granada
phurtado@onsager.ugr.es

103. **Miguel Ibáñez García**
Departamento de Física Aplicada, Universidad de Granada
miguelibaezgarcia@gmail.com

104. **Jordi Ignés Mullol**
Universitat de Barcelona, Departament de Ciència de Materials i Química Física
jignes@ub.edu

105. **Manuel Insua Villa**
FlowReserve Labs S.L., Santiago de Compostela
manuel.insua@flowreserve.es

106. **Jaime Iranzo**
Centro de Biotecnología y Genómica de Plantas, Universidad Politécnica de Madrid
jaime.iranzo@upm.es

107. **Felipe J. Blas**
Centro de Investigación en Química Sostenible y Fac. Ciencias Experimentales, Universidad de Huelva
felipe@uhu.es

108. **Arnau Jurado Romero**
Universitat Politècnica de Catalunya
arnau.jurado.romero@gmail.com

109. **Carlos Lajusticia Costan**
UNED, Ingolstadt
cajusticia@gmail.com

110. **Santiago Lamata Otín**
Departamento de Física de la Materia Condensada, Universidad de Zaragoza
santiagolaot@gmail.com

111. **Aniello Lampo**
Departamento de Matemáticas, Universidad Carlos III de Madrid
alampo@math.uc3m.es

112. **Ester Lázaro Lázaro**
Centro de Astrobiología (CSIC-INTA)
lazarole@cab.inta-csic.es

113. **Iván León Merino**
Instituto de Física de Cantabria (IFCA), Universidad de Cantabria
ivleon@ifca.unican.es

114. **Miguel Ángel López Castaño**
Universidad de Extremadura
malopez00@unex.es

115. **Javier López Pedrares**
Grupo de Física No Lineal, Universidad de Santiago de Compostela
javier.lopez.pedrares@rai.usc.es

116. **Juan Carlos Losada González**
Grupo de Sistemas Complejos. Universidad Politécnica de Madrid
juancarlos.losada@upm.es

117. **David Luna Cerralbo**
Universidad Zaragoza
luna.cerralbo.david@gmail.com

118. **Luis MacDowell**
Dpto de Química Física, Facultad de Ciencias Químicas, Universidad Complutense de Madrid
lgmac@quim.ucm.es

119. **Gonzalo Manzano Paule**
Instituto de Física Interdisciplinar y Sistemas Complejos, IFISC (UIB-CSIC)
gmanzano@ucm.es

120. **David March Pons**
Universitat de Barcelona. Institut de Sitemes Complexos
dmarchp@gmail.com

121. Jesús María Marcos Merino
Departamento de Física, Universidad de Extremadura
jesusmm@unex.es

122. José Martín-Roca
Universidad Complutense de Madrid
josema10@ucm.es

123. Pablo Martinez Azcona
Department of Physics and Materials Science, University of Luxembourg
pablo.martinez@uni.lu

124. María Martínez Barbeito
Instituto de Física Interdisciplinar y Sistemas Complejos (IFISC, UIB-CSIC)
maria@ifisc.uib-csic.es

125. Pedro J. Martínez Ovejas
Dpto. Física Aplicada, EINA, Universidad de Zaragoza
icmat1@unizar.es

126. Yuri Martínez Ratón
Departamento de Matemáticas, Escuela Politécnica Superior, Universidad Carlos III de Madrid
yuri@math.uc3m.es

127. Cristina Masoller
Departament de Física, Universitat Politècnica de Catalunya
cristina.masoller@upc.edu

128. Manuel A. Matias
Instituto de Física Interdisciplinar y Sistemas Complejos (IFISC, CSIC-UIB)
manuel@ifisc.uib-csic.es

129. Mattia Mattei
Universitat Rovira i Virgili
mattia.mattei@urv.cat

130. Pablo Maynar Blanco
Física Teórica, Universidad de Sevilla
maynar@us.es

131. Manuel Mayo León
Estudiante de doctorado por la Universidad de Sevilla
manuelmayoleon09@gmail.com

132. DIego M. Maza Ozcoidi
Dept. de Física y Mat. Aplicada. Facultad de Ciencias. Universidad de Navarra
dmaza@unav.es

133. Juan José Mazo Torres
Universidad Complutense de Madrid
jmazo@ucm.es

134. Esteban Meca Álvarez
Departamento de Física Aplicada, Radiología y Medicina Física, Universidad de Córdoba
esteban.meca@uco.es

135. Jorge Medina Hernández
IFISC (Institute for Cross-Disciplinary Physics and Complex Systems)
jorgemedina@ifisc.uib-csic.es

136. Sandro Meloni
IFISC - Institute for Cross-Disciplinary Physics and Complex Systems (CSIC-UIB)
sandro@ifisc.uib-csic.es

137. David Mendez Esteban
UNAV
dmendez.3@alumni.unav.es

138. Josep Mercadal Melià
Universitat de Barcelona, Departament de Física de la Matèria Condensada
josepmercadal@ub.edu

139. Lourdes Bibiana Merino Solís
Universidad de Guanajuato. División de Ciencias e Ingenierías
lb.merinosolis@ugto.mx

140. Ralf Metzler
Institut for Physics and Astronomy, University of Potsdam
rmetzler@uni-potsdam.de

141. M. Carmen Miguel López
Universidad de Barcelona
carmen.miguel@ub.edu

142. Jose Manuel Míguez Díaz
Centro de investigación en Química Sostenible y Fac. Ciencias Experimentales, Universidad de Huelva
jose.miguez@dfa.uhu.es

143. Manuel Miranda Barrado
Instituto de Física Interdisciplinar y Sistemas Complejos (UIB-CSIC)
m2bmanu@gmail.com

144. Juan Pablo Miranda López
Universidad Complutense de Madrid
juanpami@ucm.es

145. Carmen Molina París
Los Alamos National Laboratory, EEUU y Universidad de Leeds, UK
carmen@maths.leeds.ac.uk

146. Arturo Moncho Jordá
Dpto. de Física Aplicada. Facultad de Ciencias. Universidad de Granada
moncho@ugr.es

147. Ernest Montbrió Fairen
Department of Information and Commmunication Technologies, Universitat Pompeu Fabra
ernest.montbrio@upf.edu

148. Ana María Montero Martínez
Universidad de Extremadura
amonteron@alumnos.unex.es

149. Javier Montes Maldonado
Universidad Autónoma de Madrid y Universidad politécnica de Madrid
javier.montesm@upm.es

150. Javier Moreno Gordo
Instituto de Computación Científica Avanzada (ICCAEx), Universidad de Extremadura
jmorenogordo@gmail.com

151. Pablo Moreno Spiegelberg
IFISC (Institute for Cross-Disciplinary Physics and Complex Systems)
pablo@ifisc.uib-csic.es

152. María Carmen Morón Lafuente
INMA - Consejo Superior de Investigaciones Cientificas
nina@unizar.es

153. Felipe Olivares
Instituto de Física Interdisciplinar y Sistemas Complejos (IFISC), CSIC-UIB
felipe@ifisc.uib-csic.es

154. Juan Ozaita Corral
Grupo Interdisciplinar de Sistemas Complejos, Departamento de Matemáticas, Universidad Carlos III
jozaita@gmail.com

155. Ignacio Pagonabarraga
CECAM - EPFL, Lausanne
ipagonabarraga@ub.edu

156. Pablo Palacios Alonso
Universidad Autónoma de Madrid
pablo.pal@hotmail.com

157. Santiago Paramés Estévez
Grupo de Física No Lineal, Facultad de Física Universidade de Santiago de Compostela
santiago.parames@rai.usc.es

158. Juan MR Parrondo
Dep. Estructura de la Materia, Física Térmica y Electrónica-GISC. Universidad Complutense de Madrid
parrondo@fis.ucm.es

159. Antonio Patrón Castro
Departamento de Física Atómica, Molecular y Nuclear, Facultad de Física, Universidad de Sevilla
apatron@us.es

160. Alessandro Patti
Departamento de Ingeniería Química, Universidad de Manchester
alessandro.patti@manchester.ac.uk

161. Diego Pazó
Instituto de Física de Cantabria (IFCA), Universidad de Cantabria-CSIC
pazo@ifca.unican.es

162. Carlos Pérez Espigares
Departamento de Electromagnetismo y Física de la Materia, Universidad de Granada
carlosperez@ugr.es

163. Hugo Pérez Martínez
Universidad de Zaragoza
hugoperezmartinez@outlook.com

164. Vicente Pérez Muñuzuri
Facultad de Físicas. Universidad de Santiago de Compostela
vperezm.usc@gmail.com

165. Alberto Perez Muñuzuri
Group of Non Linear Physics Facultad de Fisicas. Univ. de Santiago de Compostela
alberto.perez.munuzuri@usc.es

166. Raul Perez Pelaez
Física Teórica de la Materia Condensada, Universidad Autónoma de Madrid
raul.perez@uam.es

167. Leticia Pérez Sienes
Grupo de Sistemas Complejos, Universidad Politécnica de Madrid
l.psienes@alumnos.upm.es

168. Bastian Pietras
Department of Information and Commmunication Technologies, Universitat Pompeu Fabra
bastian.pietras@upf.edu

169. Carlos A. Plata Ramos
Física Teórica, Universidad de Sevilla
cplata1@us.es

170. Pau Pomés Arnau
Department of Information and Communication Technologies, Universitat Pompeu Fabra
pau.pomes@upf.edu

171. Tivadar Pongó
Departamento de Física y Matemática Aplicada, Universidad de Navarra
tpongo@alumni.unav.es

172. Antonio Prados
Física Teórica, Universidad de Sevilla
prados@us.es

173. Cintia Pulido Lamas
Departamento de Química Física, Facultad de Ciencias Químicas, Universidad Complutense de Madrid
cintipul@ucm.es

174. Andreu Puy Contreras
Universitat Politècnica de Catalunya
andreu.puy@upc.edu

175. Lucia Ramirez
Instituto de Física Interdisciplinar y Sistemas Complejos
luciaramirez@ifisc.uib-csic.es

176. Juan Pedro Ramírez González
Departamento de Física Teórica de la Materia Condensada, Universidad Autónoma de Madrid
juanp.ramirez@uam.es

177. Giacomo Rapisardi
Universitat Rovira i Virgili
giacomo.rapi@gmail.com

178. Miguel Rebollo Pedruelo
Universidad Politecnica de Valencia
mrebollo@upv.es

179. David Reguera
Departament de Física de la Matèria Condensada, Universitat de Barcelona y UBICS
dreguera@ub.edu

180. Raúl Rica Alarcón
Universidad de Granada, Departamento de Física Aplicada, Nanoparticles Trapping Laboratory
rul@ugr.es

181. Miguel Angel Rodríguez Díaz
Instituto de Física de Cantabria, CSIC-UC
Rodrigma@ifca.unican.es

182. Álvaro Rodríguez Rivas
Departamento de Sistemas Físicos, Químicos y Naturales. Universidad Pablo de Olavide
arodriguezrivas@upo.es

183. José Manuel Romero Enrique
Universidad de Sevilla
enrome@us.es

184. Cristóbal Romero Guzmán
Centro de Investigación en Química Sostenible y Fac. Ciencias Experimentales, Universidad de Huelva
kristoba2010@gmail.com

185. Miguel Ángel Rubio Álvarez
Dpto. Física Fundamental, Facultad de Ciencias, UNED
mar@fisfun.uned.es

186. Miguel Ruiz Garcia
Universidad Carlos III de Madrid
m.ruizgarcia.ap@gmail.com

187. Giulia Ruzzene
IFISC, Instituto de Física Interdisciplinar y Sistemas Complejos (CSIC-UIB)
giuliaruzzene@gmail.com

188. Martín Saavedra López
Group of Nonlinear Physics, Faculty of Physics, University of Santiago de Compostela. CITMAGA
martin.saavedra.lopez@usc.es

189. Alejandro Sáinz Agost
Grupo FENOL, Universidad de Zaragoza
asainzagost@gmail.com

190. Marta Sales Pardo
Dept. Chemical Engineering, Universitat Rovira i Virgili
marta.sales@urv.cat

191. Maxi San Miguel
IFISC (UIB-CSIC)
maxi@ifisc.uib-csic.es

192. Anxo Sánchez
GISC, Departamento de Matemáticas, Universidad Carlos III de Madrid
anxo@math.uc3m.es

193. Pablo Sánchez Puga
Universidad Nacional de Educación a Distancia
p.sanchez@fisfun.uned.es

194. Bernardo Sánchez Rey
Dpto Física Aplicada I, Escuela Politécnica Superior, Universidad de Sevilla
bernardo@us.es

195. Tomás Sánchez Sánchez-Pastor
Grupo de Sistemas Complejos, Universidad Politécnica de Madrid
t.ssanchez-pastor@upm.es

196. José M. Sancho Herrero
Dep. Física Materia Condensada. Univ. de Barcelona
josemsancho@gmail.com

197. Silvia N. Santalla
Departamento de Física. Universidad Carlos III de Madrid
silvia.santalla@uc3m.es

198. Andrés Santos Reyes
Departamento de Física, Universidad de Extremadura
andres@unex.es

199. Francisco Sastre Carmona
Fac. Cs. Experimentales, Universidad de Huelva y Depto. de Ing. Física, Universidad de Guanajuato
sastre@fisica.ugto.mx

200. Luís F Seoane
Departamento de Biología de Sistemas, Centro Nacional de Biotecnología (CSIC)
brigan@gmail.com

201. Belén Serrano Antón
Grupo de Física No Lineal. Universidad de Santiago de Compostela
belen.serrano.anton@rai.usc.es

202. Tomas Sintes Olives
Instituto de Física Interdisciplinar y Sistemas Complejos IFISC (UIB-CSIC)
tomas@ifisc.uib-csic.es

203. David Soriano Paños
Instituto Gulbenkian de Ciência
sorianopanos@gmail.com

204. Benjamin Steinegger
Universitat Rovira i Virgili
benjaminsteinegger@gmail.com

205. Michael Stich
Universidad Rey Juan Carlos, Dpto MACIMTE
michael.stich@urjc.es

206. Jorge Tabanera Bravo
Departamento de Estructura de la Materia, Física Térmica y Electrónica and GISC, UCM
jorgetab@ucm.es

207. Pedro Tarazona Lafarga
Departamento de Física Teórica de la Materia Condensada, Universidad Autónoma de Madrid
pedro.tarazona@uam.es

208. Giulio Tirabassi
Universitat Politècnica de Catalunya
tirabassi.giulio@gmail.com

209. Luca Tonti
Department of Chemical Engineering, University of Manchester
luca.tonti@manchester.ac.uk

210. Raul Toral
IFISC, Instituto de Física Interdisciplinar y Sistemas Complejos, U. Illes Balears-CSIC
raul@ifisc.uib-csic.es

211. Gabriel Torregrosa Cortés
Dynamical Systems Biology Laboratory at Universitat Pompeu Fabra
gabriel.torregrosa@upf.edu

212. Pablo Valgañón Ruiz
Departamento de Física de la Materia Condensada, Universidad de Zaragoza
pablovalgaruiz@gmail.com

213. Jasper van der Kolk
Universitat de Barcelona
jasper.vanderkolk@ub.edu

214. Enrique Velasco Caravaca
Departamento de Física Teórica de la Materia Condensada, Universidad Autónoma de Madrid
enrique.velasco@uam.es

215. Guilherme Vilhena
Department of Theoretical Condensed Matter Physics
guilhermevilhena@gmail.com

216. Daniel Villarrubia Moreno
Universidad Carlos III de Madrid
dvillarr@math.uc3m.es

217. Pablo Yagüe Serrano
Departamento de física de la materia condensada, Universidad de Zaragoza
pabloyagueserrano@gmail.com

218. Iván Michael Zerón Jiménez
Centro de Investigación en Química Sostenible y Fac. Ciencias Experimentales, Universidad de Huelva
ivan.zeron@dci.uhu.es

219. Iker Zuriguel
Departamento de Física y Matemática Aplicada
iker@unav.es

Universidad Zaragoza

1542

Facultad de Medicina
Universidad Zaragoza

Real Sociedad Española de Física
R.S.E.F.

GEFENOL

Grupo especializado
en Física Estadística
y no Lineal

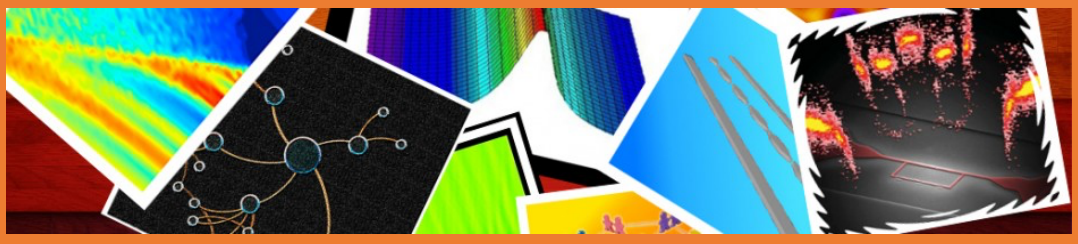

The chain-gang, Nonlinear and Statistical Physics Group
Universidad de Zaragoza